# Agronomy Research

Established in 2003 by the Faculty of Agronomy, Estonian Agricultural University

## Aims and Scope:

## Copyright:

## *Agronomy Research* online:

*Agronomy Research* is available online at: http://agronomy.emu.ee/

## Acknowledgement to Referees:

The Editors of *Agronomy Research* would like to thank the many scientists who gave so generously of their time and expertise to referee papers submitted to the Journal.

## Abstracted and indexed:

## Subscription information:

## Journal Policies:

**ISSN 1406-894X**

# CONTENTS

# Investigations about the impact of norms of the fertilisers and cultivars upon the crop capacity biomass of industrial hemp

A. Adamovics, S. Ivanovs[*] and V. Stramkale

Latvia University of Agriculture, Liela iela 2, LV 3001 Jelgava, Latvia
[*]Correspondence: semjons@apollo.lv

**Abstract.** Field trials were carried out in 2012–2014, on the Research and Study Farm 'Pēterlauki' of the Latvia University of Agriculture. Eleven sorts of industrial hemp (*Cannabis sativa* L.) – 'Bialobrzeskie', 'Futura 75', 'Fedora 17', 'Santhica 27', 'Beniko', 'Ferimon', 'Felina 32', 'Epsilon 68', 'Tygra', 'Wojko' and 'Uso 31' were sown in a sod calcareous soil (pH$_{KCl}$ 6.7, P 52 mg kg$^{-1}$, K 128 mg kg$^{-1}$, the organic matter content 21–25 g kg$^{-1}$). The total seeding rate was 50 kg ha$^{-1}$. The plots were fertilised as follows: N-120, P$_2$O$_5$- 90, K$_2$O- 150 kg ha$^{-1}$. Hemp was sown in the middle of May, in 10 m$^2$ plots, triplicate. Hemp was harvested when the first matured seeds appeared. The biometrical indices, the height and stem diameter, the harvesting time, the amount of fresh and dry biomass and the fibre content were evaluated.
Yield of dry matter on average comprised 15.06 t ha$^{-1}$, depending on the cultivars. Cultivation year and cultivar notably affected hemp biomass yield. In 2012, the highest yield of dry biomass was produced from cultivars 'Futura 75' (21.33 t ha$^{-1}$) and 'Tygra' (20.87 t ha$^{-1}$), the lowest – from 'Bialobrzeskie' (11.95 t ha$^{-1}$). Significantly higher average yield of dry biomass was obtained from cultivars 'Futura 75' (17.76 t ha$^{-1}$), 'Tygra' (16.31 t ha$^{-1}$), 'Wojko' (15.51 t ha$^{-1}$) and 'Epsilon 68' (15.28 t ha$^{-1}$), the lowest – 'Bialobrzeskie' and 'Uso 31' (13.53 t ha$^{-1}$). Meteorological conditions influenced the dry biomass yield.
The aim of this study was find productive cultivar of industrial hemp (*Cannabis sativa* L.) and clarify nitrogen fertiliser rates impact for biomass production in Latvia.

**Key words:** *Cannabis sativa*, cultivars, biomass, fertilizers.

## INTRODUCTION

Industrial hemp (*Cannabis sativa* L.) is a traditional industrial crop in many regions of Europe and of the World. For many centuries hemp has been cultivated as a source of strong stem fibre and seed oil (Ehrensing, 1998). The cultivation of industrial hemp in Europe declined in the 19th century, but recently an interest has been renewed in Germany, France, the Netherland, the United Kingdom, Spain, Italy, and also elsewhere in the world (Struik et al., 2000). Nowadays, industrial hemp has become very important as a crop for biomass production. Environmental concern and recent shortages of wood fibre have renewed an interest about hemp as a raw material for a wide range of industrial products including textiles, paper, and composite wood products (Ehrensing, 1998). Hemp is fast-growing and suitable for Latvia`s agro-climate conditions. Interest for possibilities of hemp growing in Latvia is increasing year by year (Ivanovs et al., 2015).

The hemp is considered to be one of the most promising renewable biomass sources to replace non-renewable natural resources for manufacturing of wide range of industrial products also in Latvia (Adamovics et al., 2012; Ivanovs et al., 2014; Lekavicius et al., 2015).

Nitrogen is the element that is most widely used in agriculture and it is the most important element for limiting the plant growth and development (Masclaux-Daubresse, 2010). Nitrogen fertilisation is an important environmental concern. Application of nitrogen-based fertilisers has proven very effective for increasing yields, but at the same time these fertilisers may be detrimental to the goal of sustainable agriculture and may raise the amount of nitrogen in ground water and surface water downstream of the farmland, contributing to the degradation of aquatic ecosystems (Erisman, 2011). Therefore, today the definition of fertiliser application rates is one of the major challenges that the environmentally conscious hemp growers are facing.

Industrial hemp`s need for nitrogen is high, especially during the vegetative growth period, and it should be available in the soil in sufficient quantity for a good growth and development (Ehrensing, 1998). Additional fertilisation of nitrogen stimulates hemp plant growth in field conditions (Amaducci et al., 2002; Amaducci et al., 2012). A lack of nitrogen will result in a lower yield because steps of growth will be missed and therefore will reduce the efficiency of radiation use (Struik et al., 2000). In the literature, it was found that hemp fertilisation methodology varies in different countries according to the existing soil and climatic conditions. For example, in the United States quoted nitrogen fertilisation rate is about 60 kg ha^{-1}, while in EU countries nitrogen fertilisation rates vary between 40–200 kg ha^{-1} depending on soil composition (Ehrensing, 1998). Recommendations for hemp breeding developed in EU are not considered to be suitable for Latvian climate and soil conditions. In Latvia, the recommendations for suitable nitrogen fertiliser rates for hemp breeding are not developed. Hemp is a contamination-free crop. At proper equipment support rural entrepreneurs can profitably use all the parts of the plants – fibre, sheave, leaves, seeds. Hemp is Gods' donation to mankind!

The aim of this study was find productive variety of industrial hemp (*Cannabis sativa* L.) and clarify nitrogen fertiliser rates impact for better biomass production in Latvia.

## MATERIALS AND METHODS

Field trials were carried out in 2012–2014, on the Research and Study Farm 'Pēterlauki' (56°53''N, 23°71''E) that is supervised by the Latvia University of Agriculture (Fig. 1). Eleven cultivars of industrial hemp (*Cannabis sativa* L.) cultivars – 'Bialobrzeskie', 'Futura 75', 'Fedora 17', 'Santhica 27', 'Beniko', 'Ferimon', 'Felina32', 'Epsilon 68', 'Tygra', 'Wojko' and 'Uso 31' were sown in a sod calcareous soil ($pH_{KCl}$ 6.7, containing available P 52 mg kg^{-1}, K 128 mg kg^{-1}, the organic matter content in the soil from 21 to 25 g kg^{-1}). The total seeding norm was 50 kg ha^{-1} or average 250 germinated seeds per 1 m[2]. In the field rotation, industrial hemp followed the previous crop – spring barley.

The plots with hemp cultivars were fertilised as follows: N-120, $P_2O_5$-90, $K_2O$-150 kg ha^{-1}. Industrial hemp cultivars 'Futura 75', 'Tygra' and 'Santhica 27' were tested under seven different nitrogen fertiliser application rates: control – N0P0K0; background fertiliser (next in text marked as F) – P80K112; F+N30; F+N60; F+N90; F+N120;

F+N150; F+N180 kg ha$^{-1}$. Hemp was sown by using *Wintersteiger* plot sowing machine in the middle of May, in 10 m$^2$ plots, triplicate. Hemp was harvested by a small mower 'MF-70' when first matured seeds appeared.
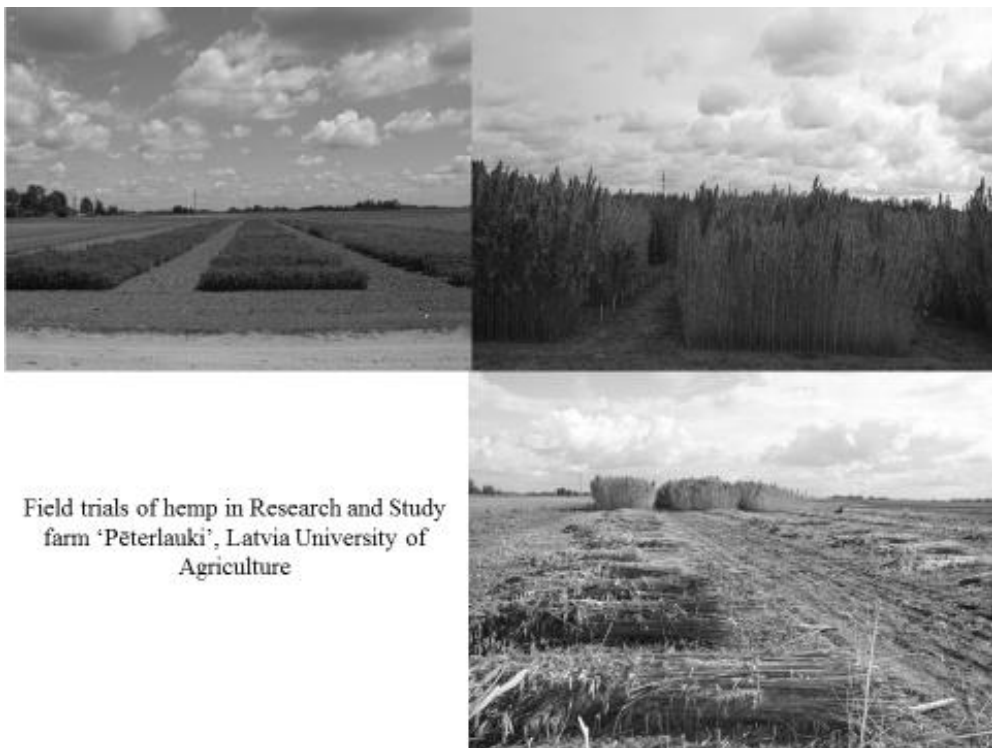


**Figure 1.** Hemp field tests in spring and in autumn.

Biometrical indices of the hemp seedlings, height and stem diameter in the middle thereof at harvesting time, amount of fresh and dry biomass, and fibre content were evaluated.

The parameters of meteorological conditions (the mean air temperature, °C and rainfall, mm) were recorded by the weather station located on the trial field. In the years 2012–2014, the period for hemp seed emergence was favourable, but in 2013 there was a lack of precipitation (the 1st ten-day period of June) (Fig. 2). In 2006, the drought and the warm weather were recorded in June, July, while in 2014 this period was much more abundant in rainfall. The rainfall in June and July is important as it strongly influences the yield. The mean air temperature in August was very similar in all the years, but the amount of rainfall differed markedly – in 2014 it was twice as high as the long-term average, and in 2013 it was approximately twice as low as the long-term average. In September and the 1st ten-day period of October the weather was still warm, later on it became cooler. In the hemp dew retting period the weather was quite dry (not favourable) in all the years.

Total height of hemp stalk was measured from the soil surface to the tip of plant. No pesticides like insecticides, herbicides, desiccants were used. The yield of fresh and dry biomass was evaluated at hemp harvesting time.
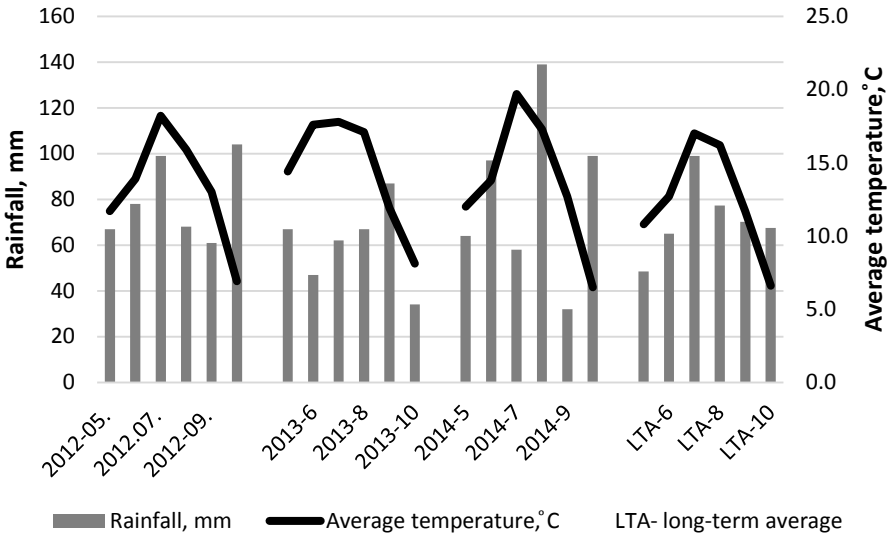


**Figure 2.** Meteorological conditions during vegetation periood.

Hemp stalk samples from each plot were taken and dried. Before starting dew retting, the technical stalk part from the hemp stalks was prepared (cutting away the top part of the plant containing panicle and leaves). The hemp stalk samples (average 2kg x 2 per cultivars) was dew retting the grassland for 2–3 weeks; then the dry straw was weighed and broken by a self-constructed tool (Fig. 3).
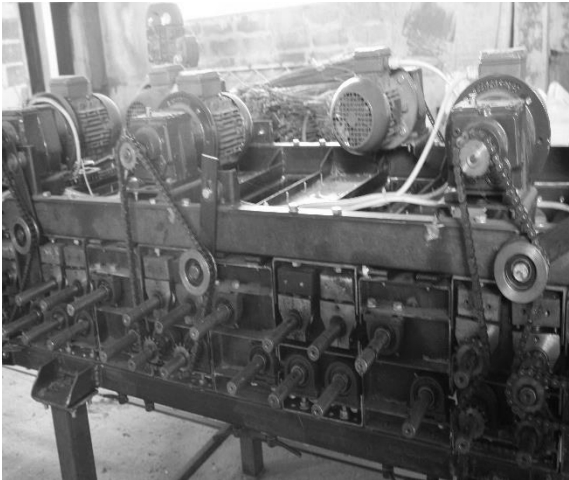


**Figure 3.** An aggregate of self-constructed tools for the production of fibre from the hemp stalks.

The obtained material was shaken manually until the sheaves were withdrawn. The obtained fibre was weighed and the fibre content in the straw was calculated by the formula:

$$F_{cs} = W_f \, 100/W_s, \tag{1}$$

where: $F_{cs}$ – the fibre content in the stalks, %; $W_f$ – the weight of the obtained $f_i$ bre, g; $W_s$ – the weight of the technical stalk, g.

The main task of research was to evaluate the biomass potential of industrial hemp cultivar 'Futura 75' under different nitrogen fertiliser rates. The yield of absolutely dry hemp biomass was calculated according to the data of fresh biomass and its moisture content at harvesting in study years. The experimental data were subjected to ANOVA analysis.

## RESULTS AND DISCUSSION

Industrial hemp biomass depends on the applied cultivar, fertiliser rates and meteorological conditions during the growing period (Ehrensing, 1998; Jankauskiene & Gruzdeviene, 2010; Ivanovs et al., 2014). Hemp grows better when an average daily temperature varies between 14 °C and 27 °C. It requires abundant moisture throughout the growing season, particularly during the first six weeks of growth (Ehrensing, 1998; Jankauskiene & Gruzdeviene, 2013).

Yield of hemp dry matter acquired within the field trials under agro-climatic conditions of Latvia on average comprised 15.06 (13.32–17.78 t ha$^{-1}$), depending on the cultivar. Cultivation year and selected cultivar notably affected hemp biomass yield (Table 1). The lowest fluctuations in the yields during the years of experiments were observed for the sort 'Futura75'.

**Table 1.** Biomass yield from different industrial hemp cultivars, 2012–2014

| Hemp variety (F$_A$) | Dry biomass, t ha$^{-1}$ | | | Average |
|---|---|---|---|---|
| | Years (F$_B$) | | | |
| | 2012 | 2013 | 2014 | |
| Bialobrzeskie | 11.95 | 12.91 | 15.56 | 13.47 |
| Futura 75 | 21.33 | 17.14 | 14.81 | 17.76 |
| Fedora 17 | 18.23 | 13.32 | 12.78 | 14.78 |
| Santhica 27 | 17.39 | 11.57 | 13.47 | 14.14 |
| Beniko | 19.27 | 13.30 | 11.96 | 14.84 |
| Ferimon | 18.59 | 13.09 | 12.93 | 14.87 |
| Epsilon 68 | 12.89 | 18.47 | 14.47 | 15.28 |
| Tygra | 20.87 | 14.66 | 13.40 | 16.31 |
| Wojko | 19.91 | 14.83 | 11.79 | 15.51 |
| Uso 31 | 17.38 | 11,40 | 11.98 | 13.59 |
| Average | 17.78 | 14.07 | 13.32 | 15.06 |
| LSD(F$_A$) $_{0,05}$ variety | 3.15 | | | |
| LSD(F$_B$) $_{0,05}$ year | 1.92 | | | |
| LSD(F$_{AB}$) $_{0,05}$ interaction between variety and year | 4.03 | | | |

In 2012, the highest yield of dry biomass was produced from cultivars 'Futura 75' (21.33 t ha$^{-1}$) and 'Tygra' (20.87 t ha$^{-1}$), while the lowest – from cultivar 'Bialobrzeskie' (11.95 t ha$^{-1}$). Significantly higher average yield of dry biomass was obtained from 'Futura 75' (17.76 t ha$^{-1}$), 'Tygra' (16.31 t ha$^{-1}$), 'Wojko' (15.51 t ha$^{-1}$) and 'Epsilon 68' (15.28 t ha$^{-1}$), whereas the lowest – from cultivars 'Bialobrzeskie' and 'Uso 31' (13.53 t ha$^{-1}$). Meteorological conditions influenced total volume of the dry biomass yield.

Hemp use is economically important for production of fiber and sheaves. Studies showed that the content of them depends on the choice of cultivars, fertiliser, seed norm and growing conditions. Depending on the growing method, the fiber content in sod calcareous soil varied from 29.8 to 45.6% of dry matter yield.
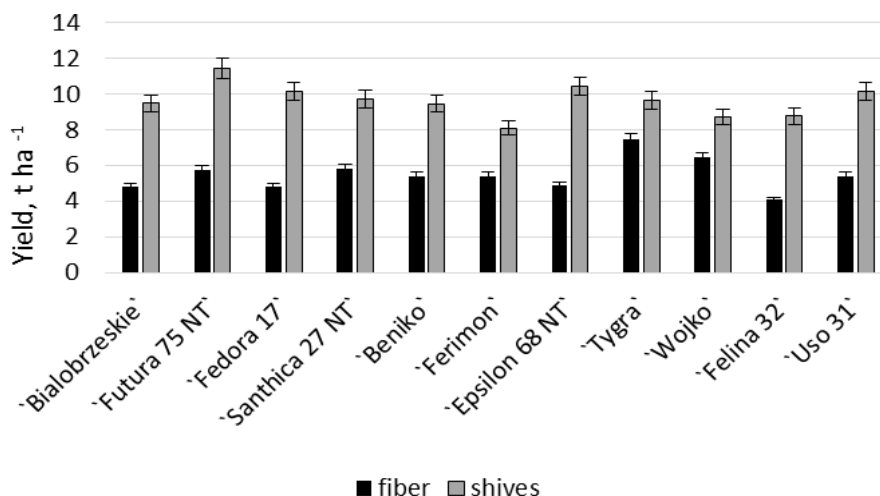


**Figure 4.** The yield of fibers and shives for hemp cultivars.

An average yield of fibre from the hemp cultivars was 4.88 t ha$^{-1}$. A higher yield during the testing years was from the cultivars 'Tygra'– 6.12 t ha$^{-1}$, 'Bialobrzeskie' – 5.67 t ha$^{-1}$ and 'Santhica 27'–5.52 t ha$^{-1}$ (Fig. 4). The nitrogen mineral fertiliser had a positive effect on the dry matter yield of hemp. This ensured also a yield of fibre. At a minimal rate of the nitrogen fertiliser F+N30 kg ha$^{-1}$ the average yield of fibre for the cultivar 'Futura75' was 4.25 t ha$^{-1}$. In contrast to the unfertilised variants N0P0K0, the average increase in the fibre yield constituted 0.87 t ha$^{-1}$, or 25.7%. Increase in the fertiliser rate to F+N150 kg ha$^{-1}$ ensured a fibre yield 6.15 t ha$^{-1}$. The increase constituted 2.72 t ha$^{-1}$, or 80.5%. Further increase in the fertiliser rates reduced a little the yield of fibre and sheaves (Fig. 5).

For biomass production, it is important to know the optimal plant density for sowing. Under the conditions of elevated plant density and the consequential interspecific competition, a part of the plants dies, the other stops growing, and only the remainder, that grows normally, contributes to the final product (Amaducci et al., 2012). In 2012, the established plant density after full emergence varied between 223–269 plants m$^{-2}$. The highest ($p < 0.05$) plant density was found in the plots where additional N fertiliser rate was not used (N0P0K0 – 259 plants m$^{-2}$) and in the plots where

fertiliser N60 rate was used (F+N60 – 262 plants m$^{-2}$). The significant (p < 0.05) lowest plant density was found where fertiliser rate N90 was used (F+N90 – 241 plants m$^{-2}$).
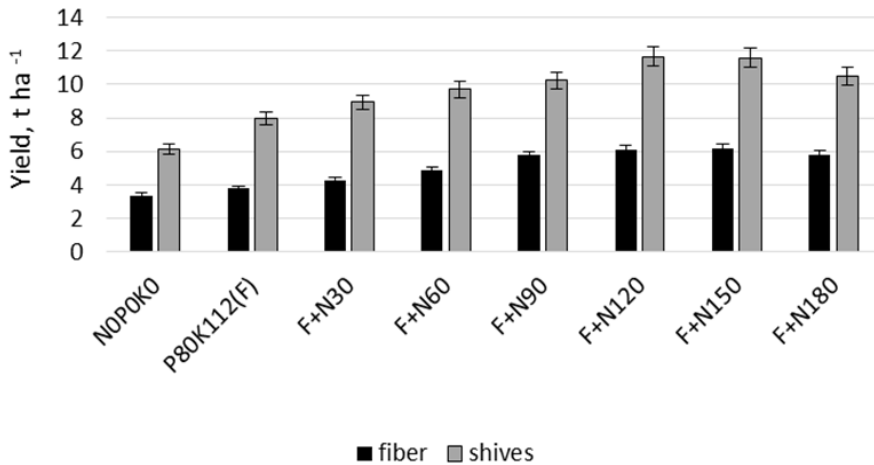


**Figure 5.** The yield of fibre and sheaves for cultivar 'Futura75', depending on fertiliser rates.

During vegetation period, the plant density decreases. At harvesting time, the highest plant density was found under N60 fertiliser rate (239 plants m$^{-2}$), but the lowest – under N180 fertiliser rate (212 plants m$^{-2}$). Some authors report that plant biomass yield decreases non-significantly if density is low (about 30–90 plants m$^{-2}$), while at high density (180–270 plants m$^{-2}$) about 50–60% of the initial stand was lost. In the other literature sources, it was found that nitrogen caused high industrial hemp plant mortality, probably due to competitive effects in the initial phase of the cycle (Amaducci et al., 2012; Ivanovs et al., 2015). Considering the average results, the influence of different nitrogen fertiliser rates on the biomass decrease was modest and non-significant (p > 0.05). On the average, during a three years' (2012–2014) period, the highest plant density was found in the plots where additional N fertiliser rate was not used (N0P0K0 – 380 plants m$^{-2}$), but the lowest plant density was found where fertiliser rates N150 and N180 were used (150 plants m$^{-2}$). On the average, the reduction in the density of fully emerged plants varied between 6.6–14.6% in the trial year. Nevertheless, the survived plants showed a high growth intensity and produced a sufficiently high biomass yield.

Industrial hemp stalk length was significantly (p < 0.05) influenced by the applied nitrogen fertiliser rate and cultivars. According to the research results, the plant height gradually increases with increasing N fertiliser rate, compared with the control (N0P0K0), but this growth increase varies between tested cultivars. The highest stalk length was observed for the cultivar 'Futura 75', 'Bialobrzeskie', 'Santhica 27' under all nitrogen fertiliser rates, compared with other tested cultivars.

The highest stalk length (318 cm) was reached under the nitrogen fertiliser rate F + N150 on the 138 growing day since sowing. The stalk length of other cultivars under the same nitrogen fertiliser rate was lower, cultivars 'Tygra' and 'Wojko' 32'–258 centimetres (Fig. 6).
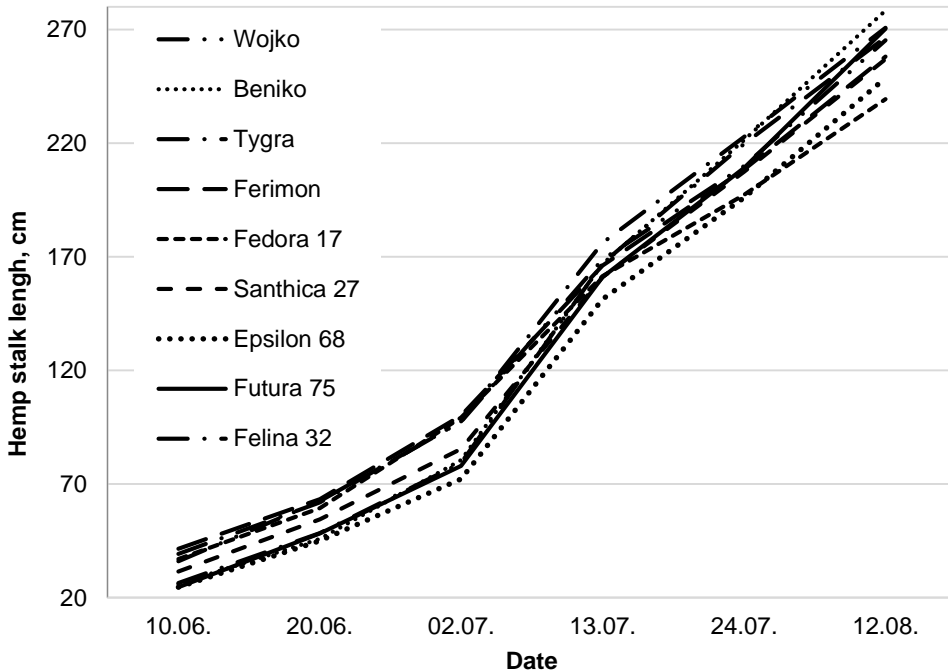
**Figure 6.** Average hemp stalk length, cm.

Analysed the relationships between hemp stalk length and biomass yield, we found out a significant (p < 0.05) close linear positive correlation (r = 0.83; n = 24) and it is reflected in the regression equation

$$y = 0.087 - 8.761,  \qquad (2)$$

In 2013, we found out a significant (p<0.05) linear positive correlation (r = 0.53; n = 24) what is reflected in the regression equation:

$$y = 0.2171x - 49.461,  \qquad (3)$$

Here we can conclude that hemp biomass yield depends not only on the nitrogen fertiliser rate, but also on such factors as plant density, meteorological conditions and other investigated factors that have not been studied.

The nitrogen fertiliser rate effect on the dry matter yield was significant (p < 0.05) for all years.

**CONCLUSIONS**

All explored hemp cultivars are productive and provide high biomass yield in Latvian agroclimatic conditions. The cultivars 'Futura 75', 'Tygra', 'Epsilon 68' and 'Santhica 27' were the most productive.

The nitrogen fertiliser rate effect was significant (p < 0.05) for biomass production. The lowest dry matter yield was observed under N0P0K0 fertiliser rate, but the highest

dry matter yield was obtained using F+N150 kg ha$^{-1}$. When N rate was increased up to 180 kg ha$^{-1}$, the decrease of hemp fresh biomass and dry matter yield was observed. Hemp biomass depends on stalk length. There were positive linear correlations found for proof of this effect.

# REFERENCES

Adamovics, A., Balodis, O., Bartusevics, J., Gaile, Z., Komlajeva, L., Poiša, L., Slepitis, J., Strikauska, S. & Visinskis, Z. 2012. Energetisko augu audzesanas un izmantosanas tehnologijas (Technologies of production and use of energy crops). *Atjaunojama energija un tas efekiva izmantosana Latvija (Renewable energy and its effective use in Latvia)*, Jelgava, LLU, pp. 38–113. (In Latvian).

Amaducci, S., Errani, M. & Venturi, G. 2012. Response of hemp to plant population and nitrogen fertilosation. *Italian Journal of Agronomy* **6**(2), 103–111.

Amaducci, S., Errani, M. & Venturi, G. 2002. Plant Population effects on fibre hemp morphology and production. *Journal of Industrial Hemp* **7**(2), 33–60.

Ehrensing, D.T. 1998. Feasibility of Industrial Hemp Production in the United States Pacific Northwest. Oregon State University. https://ir.library.oregonstate.edu/xmlui/handle/1957/

Erisman, J.W., Grinsven, H., Grizzetti, B., Bouraoui, F., Powlson, D., Sutton, M.A., Bleeker, A. & Reis, S. 2011. The European nitrogen problem in a global perspective. *European Nitrogen Assessment*, Chapter 2, 9–31.

Ivanovs, S., Adamovics, A. & Rucins, A. 2015. Investigation of the technjlogical spring harvesting variants of the industrial hemp stalk mass. *Agronomy Research* **13**(1), 73–82.

Ivanovs, S., Adamovics, A., Rucins, A. & Bulgakov, V. 2014. Investigations into losses of biological mass and quality during harvest of industrial hemp. / *Engineering for Rural Development,* Proceedings, **13**, 19–23.

Jankauskiene, Z. & Gruzdeviene, E. 2010. Evaluation of *Cannabis Sativa* in Lithuania. *Žemdirbyste=Agriculure* **97**(3), 87–96.

Jankauskiene, Z. & Gruzdeviene, E. 2013. Physical parameters of dew retted and water retted hemp(*Cannabis sativa* L.) fibres. *Zemdirbyste=Agriculture* **100**(1), 71–80.

Lekavicius, V., Shipkovs, P., Ivanovs, S. & Rucins, A. 2015. Thermo-insulation properties of hemp-based products. / *Latvian Journal of Physics and Technical Sciences* **52**(1), 38–51.

Masclaux-Daubresse, C., Daniel-Vedele, F., Dechrognat, J., Chardon, F., Gaufichon, L. & Suzuki, A. 2010. Nitrogen uptake, assimilation and remobilization in plants: challenges for sustainable and productive agriculture, *Annals of Botany* **105**(7), 1141–1157.

Struik, P.C., Amaducci, S., Bullard, M.J., Stutterheim, N.C., Venturi, G. & Cromack, H.T.H. 2000. Agronomy of fibre hemp (*Cannabis sativa* L.) in Europe. *International Journal Industrial Crops and Products* **11**, 107–118.

# Biogas potential from animal waste of Marmara Region-Turkey

## A. Ayhan

University of Uludag, Faculty of Agriculture, Department of Biosystems Engineering, TR16059, Nilüfer, Bursa, Turkey; e-mail: aayhan@uludag.edu.tr

**Abstract.** The purpose of this study was to determine the biogas production capacity from animal wastes in Marmara region of Turkey for the years 2005–2014. The wastes from the cattle and hen in the region were considered the resource for biogas production taking the number of animals and the collectability of the wastes into the account. Three scenarios were evaluated to estimate the biogas capacity by assuming that 100% (theoretical potential), 50%, and 25% of the total animal waste could be used for biogas production in the region. For theoretical biogas production from cattle wastes, the greatest potential in the year 2014 was calculated for Balıkesir province with 145.53 Mm$^3$, followed by Çanakkale, Bursa, Sakarya, and other seven provinces. Balıkesir had the highest biogas potential in 2014 from the poultry waste, too, followed by Sakarya, Kocaeli, Bursa, and other seven provinces. Biogas potential (100%) of Marmara region increased by 15% from 2005 to 2014 with 1,242.17 Mm$^3$ in 2014. The heat and electrical energy equivalents of the biogas were found to be 7,453.02 GWh and 2,608.56 GWh$_e$, respectively. In the other two scenarios, depending on the utilization rate of theoretical biogas potential: biogas amount, heat and electric power values were determined proportionally.

**Key words:** Renewable energy, biogas, animal waste, Marmara region.

## INTRODUCTION

According to International Energy Agency (2013), energy supply of the country was provided mainly by natural gas, coal, oil, hydro, biofuels/waste and geothermal/solar/wind with 32.4%, 28%, 27.3%, 4.4%, 4.2% and 3.6%, respectively (IEA, 2015a).

Total energy consumption of Turkey in 2015 was 83,633 ktoe (kilo ton of oil equivalent) and natural gas was responsible for 56% of the total energy used in the country, followed by electrical energy with 27%, and diesel fuel with 17% (Republic of Turkey ministry of energy and natural resources, 2015a, 2015b). The total electrical energy production was 259,690.3 GWh while the consumption was 264,136.8 GWh in 2015 (TETC, 2016). Clearly, Turkey has an energy market that is dependent on fossil energy sources. The instability of the costs of these sources and their environmental effects make renewable energy sources more preferable.

The fossil fuels received subsidies/incentives about 550 billion USD in 2013, four times greater than renewable energy incentives (IEA, 2015a). Despite the slow progress in Turkey, the interest and the investments in renewable energy keeps increasing. In the last decade, biogas, liquid biofuels, geothermal, solar, thermal, and wind energy production increased in Turkey. The greatest rises occurred in wind energy production with 7,557 GWh and biogas energy production with 8,511 TJ, respectively (IEA, 2015b).

Cooperatives and the agricultural industry show particular interest in biogas utilization in Turkey since storage and discharge of animal waste is one of the most important problems of agricultural enterprises (Dena, 2015). Another reason of interest to biogas is that agricultural industry is faced with high energy costs.

Biogas is renewable energy resource generated by digestion under anaerobic conditions as a result of conversion of organic wastes by the use of microorganisms, and primarily composed of methane and carbon dioxide. It is mostly used to generate electricity and heat both for urban and rural areas (Alfa et al., 2014; Li et al., 2014; Oleszek et al., 2014; Yingjian et al., 2014; Igliński et al., 2015). The animal wastes are deposited and energy costs are reduced by producing biogas in the agricultural enterprises.

A research project was undertaken to determine the biogas potential of Turkey in 2011 (DBZF, 2011). Studies were also conducted focusing on specific regions and provinces for different feedstocks to be used for biogas production in Turkey (Ediger & Kentel, 1999; Evrendilek & Ertekin, 2003; Demirel et al., 2010; Ergür & Okumuş, 2010; Ulusoy et al., 2009; DBZF, 2011; Altıkat & Çelik, 2012; Coskun et al., 2012; Onurbaş Avcıoğlu & Türker, 2012; Koçer & Kurt, 2013; Aktaş et al., 2015; Eryılmaz et al., 2015). Previous studies showed that the most appropriate feedstock are animal wastes for biogas production for Turkey in terms of costs and management aspects.

The aim of this study was to determine the biogas potential from animal wastes of Marmara region, Turkey by analysing the relevant data from 2005 to 2014. The cattle and hen wastes were considered the resource for biogas production taking the number of animals and the collectability of the wastes into the account.

## MATERIALS AND METHODS

Marmara Region is situated on the North West part of Turkey with a surface areas of 67,000 km², corresponding to 8.5% of the total land. The industry, commerce, tourism, and agriculture are strong in the region. About 30% of the land is arable and 11.5% is forestry. The region consists of 11 provinces (Balıkesir, Bilecik, Bursa, Çanakkale, Edirne, İstanbul, Kırklareli, Kocaeli, Sakarya, Tekirdağ, Yalova) and is the leading region in energy consumption in the country (Wikipedia, 2015).

The numbers of cattle and hens in Marmara region of Turkey in the period of 2005–2014 were obtained from Turkish Statistical Institute (TSI, 2015). Amount of daily produced manure varies according to animal species. Furthermore, length of stay in the shelter affects amount of collectable manure. While the manure can be almost completely collected in poultry depending on the length of stay in the shelter, amount of collectible manure is lower in feeder cattle, sheep and goats. In this study, the cattle were classified as calf and mature animal, according to the TSI data, and the corresponding manure weights were determined based on this age classification. Length of stay in the shelter for cattle was taken as 100% as the relatively larger enterprises are concentrated in western part of Turkey and the animals are kept in shelters rather than grazing in pastures. Length of stay in the shelter of some animals and solid matter contents of manures are presented in Table 1. In calculations, mean live weights were taken as 500 kg for cattle and 2 kg for hens (Alçiçek & Demiruluş, 1994; Alibaş, 1996; Karaman, 2006; Koçer et al., 2006; Eliçin et al., 2014).

**Table 1.** Time spent ratio in the shelter and solid matter content of the organic waste from various animals (Alibaş, 1996; Ekinci et al., 2010; DBZF, 2011; Kaya & Öztürk, 2012; Eliçin et al., 2014; Aktaş et al., 2015)

| Animal type | Time spent in the shelter (%) | Solid matter content (%) |
|---|---|---|
| Mature cattle | 100.00 | 15.00 |
| Calf | 100.00 | 15.00 |
| Meat hen | 99.00 | 40.00 |
| Egg hen | 99.00 | 40.00 |
| Turkey | 68.00 | 25.00 |
| Sheep, Goat | 13.00 | 25.00 |
| Horse | 29.00 | 20.00 |

The following equations were used to calculate the amount of biogas and its energy value. The total amount of manure that can be produced by the animals per day was determined by equation 1.

$$M_{Dw} = M_w \times T_S \qquad (1)$$

where $M_{Dw}$ is obtainable daily total manure per head (kg (day head)$^{-1}$), $M_w$ is wet based daily total manure per head (kg (day head)$^{-1}$), and $T_S$ is the length of stay in the shelter of animals (%). The amount of biogas that can be produced from the manure was obtained using equation 2.

$$B_A = M_{Dw} \times P_L \times C_b \times 0.365 \qquad (2)$$

where $B_A$ is annual amount of biogas (m$^3$ a$^{-1}$), $P_L$ is livestock population (number), and $C_b$ is biogas coefficient which was determined by animal type and biogas amount in m$^3$ t$^{-1}$. Dry matter contents for cattle and hen manures were assumed to be $\leq 15\%$ and $\leq 40\%$, respectively. Manure of hen has significantly higher biogas potential than cattle manure due to better feedstock qualities such as dry matter and protein content (Akbulut & Dikici, 2004; Kaya et al., 2009; FNR, 2010; Kaya & Öztürk, 2012). Equation 3 was used to calculate the calorific energy value of biogas.

$$B_T = C_c \times B_A \qquad (3)$$

where $B_T$ is equivalent calorific energy value of biogas (MJ) and $C_c$ is calorific coefficient which was determined by the rate of methane in the biogas (MJ m$^{-3}$). Although calorific value of biogas varies according to its methane content, it is approximately 20–27 MJ m$^{-3}$ (Alibaş, 1996; Banks, 2009; Eryaşar & Koçar,2009; Gümüşçü & Uyanık, 2010; Frost & Gilkinson, 2010; Kaya & Öztürk, 2012; FM Bioenergy, 2013).

Equivalent electrical energy varies according to methane content of biogas and electrical conversion efficiency (Banks, 2009; Astals & Mata, 2011; DBZF, 2011; Kaya & Öztürk, 2012; SGC, 2012). In this study, methane content and electrical conversion efficiency values were assumed to be 60% and 35%, respectively. The equivalent electrical energy value of biogas was determined using equation 4.

$$B_E = C_e \times B_A \qquad (4)$$

where $B_E$ is equivalent electrical energy value of biogas (kWh$_e$) and $C_e$ is electrical coefficient determined by the rate of methane in the biogas and conversion efficiency to electricity (kWh$_e$ m$^{-3}$).

Usually, the theoretical potential is reported in biogas potential determination studies. However, it is unlikely to use all of the theoretical potential in practice due to other uses of the animal waste in agricultural production, handling and logistics problems of the wastes, cultural preferences, etc. It might be more realistic to assume that the theoretical biogas potential can be utilized only partially. Therefore, in this study, three different scenarios were considered for biogas utilization in the evaluations: 100% (theoretical potential), 50%, and 25% use of theoretical potential of animal waste.

## RESULTS AND DISCUSSION

According to TSI data, number of mature cattle, calves and egg hens in Marmara region increased 39%, 98%, and 46%, respectively in 2014 compared to 2005. The changes in the animal populations in the region are given in Figs 1 and 2. Based on Fig. 1, both the mature cattle and calf populations kept increasing steadily from 2005 to 2013 with some reduction in 2014.
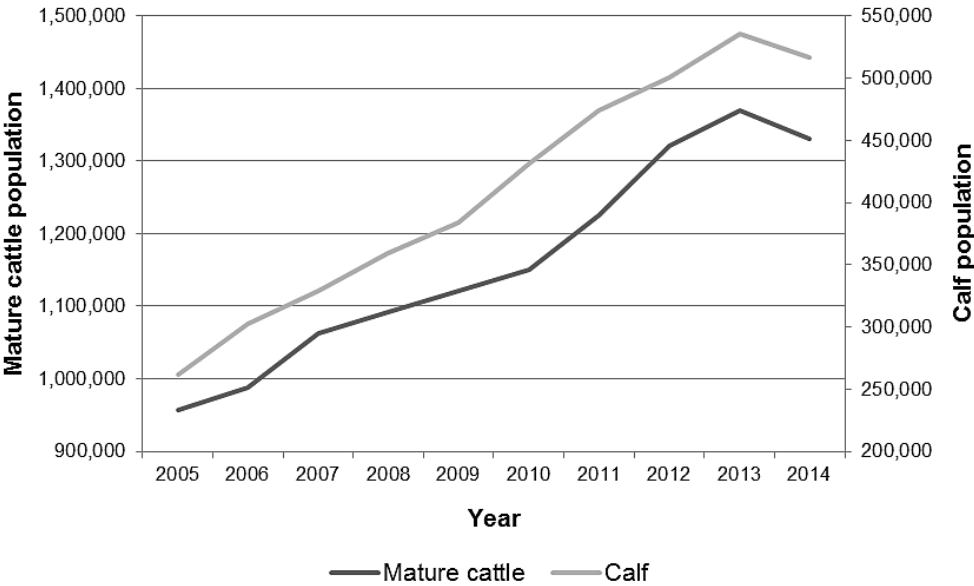


**Figure 1.** The change in cattle population in Marmara Region from 2005 to 2014.

Although the number of meat hens look similar in 2005 and 2014, there were extreme variations in the number of meat hens from 2005 to 2007, and then 2007 to 2009. Therefore, yearly variations in hen production should have serious implications in terms of accessibility to the manure when the number of hens decreases sharply as shown in Fig. 2. The production reduced further for meat hens until 2011, followed by small recovery since then. Egg hen production, on the other hand, has been increasing at a fast rate since 2010.
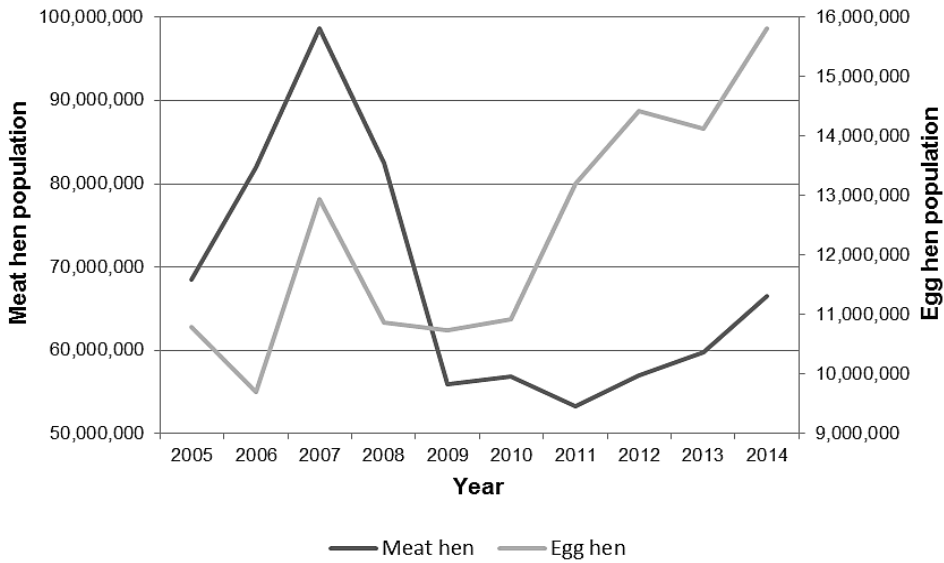
**Figure 2.** The change in hen population in Marmara Region between 2005 and 2014.

Balıkesir, Edirne, and Bursa were the first three provinces in cattle production in 2005, producing 35% of the total mature cattle in the region. The three provinces with the lowest mature cattle population were Yalova, Bursa and Kocaeli. Total number was about 81,000 cattle in these three provinces which was less than that of Bursa province. The three provinces with the highest number of animals in 2014 were Balıkesir, Çanakkale and Bursa, respectively. While the two provinces with the lowest animal numbers were the same as 2005, the third ranking province was replaced by İstanbul in 2014.

Balıkesir has the highest calf population in 2005 and 2014. Bursa and Çanakkale were the other provinces for the highest calf population in 2005 and 2014. These three provinces produced more than half of the calf population in the region in 2014 with Balıkesir 31%, Bursa 12%, and Çanakkale 10%. Yalova, Bilecik and İstanbul had the lowest calf population between 2005 and 2014.

According to TSI data, meat hen population in the Marmara region decreased about 2 million in 2014 compared to 2005. However the highest first three provinces (Kocaeli, Sakarya and Balıkesir) increased approximately 3 million in 2014 compared to 2005. The lowest provinces were Yalova, Kırklareli and Edirne in 2005. Tekirdağ had the least number of hens in 2014, followed by Yalova and Kırklareli.

In egg hen production, the greatest share belonged to Balıkesir, Bursa, and Sakarya in both 2005 and 2014 while Yalova, Bilecik and Edirne had the smallest share. In general, number of egg hens in Marmara region increased by five million during the ten years' time from 2005 to 2014.

The obtainable manure calculated based on Eq. 1 and numbers of mature cattle, calf, and egg and meat hen were given in Table 2. Although the number of animals increased 4%, the manure production increased 31.7% from 2005 to 2014. This rise resulted from greater number of cattle and egg hens in this period. As a result, manure production was more than 25 Mt in the region in 2014, 72% of which was produced from

manure cattle, 18%, 7% and 3% from meat hen manure, calf manure, and egg hen manure, respectively.

**Table 2.** Total manure production levels in Marmara region between 2005 and 2014

| | Total Manure Production (t) | | | |
|---|---|---|---|---|
| Year | Mature cattle | Calf | Meat hen | Egg hen |
| 2005 | 13,098,485.81 | 897,607.93 | 4,698,148.65 | 504,527.13 |
| 2006 | 13,526,165.44 | 1,036,844.77 | 5,630,867.45 | 453,526.32 |
| 2007 | 14,541,271.50 | 1,128,627.45 | 6,767,244.43 | 604,413.04 |
| 2008 | 14,954,250.75 | 1,234,271.37 | 5,662,799.62 | 507,397.61 |
| 2009 | 15,350,011.13 | 1,316,769.77 | 3,842,423.42 | 501,415.63 |
| 2010 | 15,755,544,38 | 1,480,256.92 | 3,899,226.85 | 510,389.28 |
| 2011 | 16,767,173.81 | 1,625,985.21 | 3,658,991.80 | 616,432.79 |
| 2012 | 18,073,262.44 | 1,718,316.85 | 3,912,185.88 | 673,491.74 |
| 2013 | 18,759,485.25 | 1,838,659.18 | 4,098,879.28 | 660,175.09 |
| 2014 | 18,207,961.13 | 1,772,372.26 | 4,565,818.42 | 738,912.21 |

Calculated theoretical biogas potential of each province for the animal types studied was given for 2005 and 2014 in Table 3. As expected from animal manure potentials, Balıkesir had the highest biogas potential both in 2005 and 2014. Kocaeli and Sakarya were the other provinces for high biogas potentials in 2005. In 2014, Bursa was the third large potential after Balıkesir and Sakarya.

**Table 3.** Theoretical biogas potential of the eleven provinces in 2005 and 2014

| | Theoretical Biogas Potential ($Mm^3$) | | | |
|---|---|---|---|---|
| | 2005 | | 2014 | |
| Province | Cattle | Hen | Cattle | Hen |
| Balıkesir | 84.82 | 166.65 | 145.53 | 288.36 |
| Bilecik | 10.11 | 18.82 | 10.68 | 11.40 |
| Bursa | 40.01 | 40.91 | 52.68 | 73.86 |
| Çanakkale | 35.91 | 110.76 | 56.99 | 48.20 |
| Edirne | 41.30 | 1.86 | 44.53 | 1.95 |
| İstanbul | 18.71 | 7.85 | 20.91 | 12.42 |
| Kırklareli | 26.32 | 2.23 | 42.49 | 2.22 |
| Kocaeli | 17.44 | 207.24 | 31.71 | 75.67 |
| Sakarya | 36.47 | 168.14 | 50.33 | 223.49 |
| Tekirdağ | 36.34 | 3.29 | 40.52 | 4.78 |
| Yalova | 2.48 | 0.64 | 3.13 | 0.31 |
| Total | 349.90 | 728.37 | 499.51 | 742.66 |

The greatest increase in biogas production from 2005 to 2014 took place in Balıkesir province with 182.42 $Mm^3$ due to high level of increases in both cattle and hen manure. Balikesir itself could provide almost one third of the biogas potential of Marmara Region in 2014. The increases in the biogas potential were high also in Kırklareli and Bursa with 56.61% and 56.38%, respectively. Serious reduction could be seen in biogas production in Kocaeli (Table 3). Çanakkale and Bilecik also experienced decreases in this period. All provinces, except three of them, increased the biogas potential from 2005 to 2014.

While Balıkesir lead the biogas production both in cattle and hens, Sakarya province also had high biogas potential coming from hen production. Balıkesir was followed by Çanakkale despite the reduction seen in this province.

Farm structure, storage capabilities for the animal wastes, and transportation might affect the utilization ratio from animal waste for biogas production. Biogas potential, calorific energy and electrical energy values of Marmara region between 2005 and 2014 were shown in Table 4.

**Table 4.** Biogas, calorific energy and electrical energy potential of Marmara region between 2005–2014 based on 100, 50, and 25% use of the total manure

| | Biogas Potential (Mm$^3$) | | | Calorific Energy of Biogas (GWh) | | | Electrical Energy of Biogas (GWh$_e$) | | |
|---|---|---|---|---|---|---|---|---|---|
| Year | 100% | 50% | 25% | 100% | 50% | 25% | 100% | 50% | 25% |
| 2005 | 1,078.28 | 539.14 | 269.57 | 6,469.66 | 3,234.83 | 1,617.42 | 2,264.38 | 1,132.19 | 566.10 |
| 2006 | 1,215.89 | 607.95 | 303.97 | 7295.34 | 3,647.67 | 1,823.84 | 2,553.37 | 1,276.68 | 638.34 |
| 2007 | 1,423.78 | 711.89 | 355.94 | 8542.68 | 4,271.34 | 2,135.67 | 2,989.94 | 1,494.97 | 747.48 |
| 2008 | 1,268.54 | 634.27 | 317.14 | 7611.24 | 3,805.62 | 1,902.81 | 2,663.94 | 1,331.97 | 665.98 |
| 2009 | 1,024.81 | 512.40 | 256.20 | 6,148.84 | 3,074.42 | 1,537.21 | 2,152.09 | 1,076.05 | 538.02 |
| 2010 | 1,048.24 | 524.12 | 262.06 | 6,289.45 | 3,144.72 | 1,572.36 | 2,201.31 | 1,100.65 | 550.33 |
| 2011 | 1,058.39 | 529.19 | 264.60 | 6,350.33 | 3,175.17 | 1,587.58 | 2,222.62 | 1,111.31 | 555.65 |
| 2012 | 1,136.78 | 568.39 | 284.20 | 6,820.71 | 3,410.35 | 1,705.18 | 2,387.25 | 1,193.62 | 596.81 |
| 2013 | 1,181.22 | 590.61 | 295.31 | 7,087.33 | 3,543.66 | 1,771.83 | 2,480.56 | 1,240.28 | 620.14 |
| 2014 | 1,242.17 | 621.09 | 310.54 | 7,453.02 | 3,726.51 | 1,863.26 | 2,608.56 | 1,304.28 | 652,14 |

Analysis of biogas production potential from animal waste in Marmara region showed that despite the fluctuations in hen production, the total manure production in Marmara region increased from 2005 to 2015. Biogas potential increased in the region significantly in 2006 and 2007. In 2007, theoretical biogas potential increased 32% compared to 2005 with 1,423.78 Mm$^3$. Then the biogas capacity reduced as a result of sharp drop in the number of hens in 2008 and 2009. However, the number of cattle was not adversely affected. A trend with gradual increase was observed in the number of hens and cattle since 2010. Biogas potential in 2014 increased %15 compared to 2005 with 1,242.17 Mm$^3$. Biogas potentials in 2014 were 621.09 Mm$^3$ and 310.54 Mm$^3$ if 50% and 25% of the theoretical potential could be used, respectively.

Calorific energy value in 2005 was 6,469.66 GWh and increased to 7,453.02 GWh in 2014. Proportional to the increase in calorific energy value, electrical energy potential of 2005 (2,264.38 GWh$_e$) increased (2,608.56 GWh$_e$) in 2014 (Table 4). In the other two scenarios, i.e. for 50% and 25% use of the theoretical biogas potential, heat and electric power values were determined proportionally.

The electrical energy produced from biogas is subsidized the Renewable Energy Law in Turkey. The Law was put into practice in 2005 for the companies that have license to produce biogas according to the subsidy policy from 2005 to 2015. The policy imposes that any company conforming to the subsidy mechanism would sell electricity at 0.133 USD kWh for ten years from the date of obtaining the license to produce biogas. According to the calculations, the theoretical biogas potential of Marmara Region is equivalent to 347 million USD in terms of electrical energy.

Although both cattle and hen rearing are developed in Marmara region, very small portion of the biogas potential is currently used. Animal waste potential of Marmara region is remarkable and farmers and investors can make benefits from biogas technologies if properly guided and supported by policy makers.

Although the exact number of biogas facilities in Turkey is not known, based on the project titled "Source Efficiency Of Animal Wastes Through Biogas And Its Climate Friendly Usage Project" the number of active biogas facilities was 36 in 2011 and the projected biogas facilities were 49 (DBZF, 2011). Even though more investments are made in Marmara region compared to the rest of the country, limited investments were made to benefit from biogas in the region (Fig 3). The main reason for this was related to the lack of appropriate incentives for biogas production. Since the theoretical biogas potential cannot be put into production, some realistic proportions of the theoretical potential should be targeted. As shown in Table 4, significant amount of electrical energy could be produced even with the 25% of the theoretical biogas potential.



**Figure 3.** Number of biogas plants in the provinces of Turkey.

The amount of manure, and hence the potential for biogas and electricity production may increase further given the trend in manure production from 2005 and 2014. Within this scope, the biogas production should be considered one of the most important means of utilizing the manure in the region. Furthermore, production and utilization of biogas is an environmentally-friendly method and is a strong candidate in meeting the rural energy need. Awareness of public institutions and private sector should be raised and investments should be further promoted to benefit from the biogas potential.

## CONCLUSIONS

In this study, biogas potential from animal wastes of Marmara region of Turkey was determined and calorific and electrical energy values of the theoretical biogas potential were calculated. It was found that manure production increased from 2005 to 2014 and will probably increase further in the near future. Although the amount of hen wastes reduced sharply in some of the provinces, the total manure production did not reduce in the region. The farmers and entrepreneurs invested in cattle production from

2005 to 2015, resulting in gradual increase in cattle population whereas significant drops were observed in the number of hens from 2007 to 2011. In recent years, the hen production has a tendency of increasing.

The animal waste produced in 2014 was about 25 Mt corresponding to a theoretical biogas volume of 1,242.17 Mm$^3$. Theoretical biogas can generate 7,453.02 GWh of calorific energy and 2,608.56 GWh$_e$ of electrical energy. Putting a small segment of the theoretical biogas production, such as 25%, into energy production would be important to meet some of the energy requirements in rural areas.

In Turkey, the number biogas plants tends to increase, but anaerobic fermentation is yet to be used efficiently. More incentives and financial support is needed for investors to take advantage of the existing biogas technology.

## REFERENCES

Akbulut, A. & Dikici, A. 2004. Biogas potential of Elazig province and cost analysis. *Doğu Anadolu Bölgesi Araştırmaları* **2**(2), 36–41. (in Turkish, English abstr.).

Aktaş, T., Özer, B., Soyak, G. & Ertürk, M.C. 2015. Determination of the electricity generation potential from animal biogas in Tekirdağ city. *Tarım Makinaları Bilimi Dergisi* **11**(1), 69–74. (in Turkish, English abstr.).

Alçiçek, A. & Demiruluş, H. 1994. Using the farm manure on biogas technology. *http://www.biyogazder.org/makaleler/mak13.pdf* Accessed 10.03.2012 (in Turkish).

Alfa, I.M., Dahunsi, S.O., Iorhemen, O.T., Okafor, C.C. & Ajayi, S.A. 2014. Comparative evaluation of biogas production from Poultry droppings, Cow dung and Lemon grass. *Bioresource Technology* **157**, 270–277.

Alibaş, K. 1996. *Determination of energy balance of fermenter and biogas production from cattle manure, chicken manure and barley by psychrophilic, mesophilic and thermophilic fermentation.* Uludağ Üniversitesi Ziraat Fakültesi Araştırma ve İncelemeler No:13, Uludağ Üniversitesi Ziraat Fakültesi, BURSA (in Turkish).

Altıkat, S. & Çelik, A. 2012. Biogas Potential from Animal Waste of Iğdır Province. *Iğdır Univ. J. Inst. Sci. & Tech.* **2**(1), 61–66. (in Turkish, English abstr.).

Astals, S. & Mata, J. 2011. Anaerobic digestion. *http://www.iperasmuseprobio.unifg.it/dwn/0.pdf* Accessed 15.11.2014.

Banks, C. 2009. Optimising anaerobic digestion. *http://www.forestry.gov.uk/pdf/rrps_AD250309_optimising_anaerobic_digestion.pdf/$FILE/rrps_AD250309_optimising_anaerobic_digestion.pdf* Accessed 15.10.2014.

Coskun, C., Bayraktar, M., Oktay, Z. & Dincer, I. 2012. Investigation of biogas and hydrogen production from waste water of milk-processing industry in Turkey. *International journal of hydrogen energy* **37**, 16498–16504.

DBZF. 2011. *Assessment of actual framework conditions and potentials for biogas investments in Turkey.* 146 pp.

Demirel, B., Onay, T.T. & Yenigün, O. 2010. Application of Biogas Technology in Turkey. *International Journal of Environmental, Chemical, Ecological, Geological and Geophysical Engineering* **4**(7), 285–289.

Dena german energy agency 2015. New studies published on french, hungarian and turkish biogas markets. *http://www.dena.de/en/news/news/new-studies-published-on-french-hungarian-and-turkish-biogas-markets.html.* Accessed 30.10.2015.

Ediger, V.Ş. & Kentel, E. 1999. Renewable energy potential as an alternative to fossil fuels in Turkey. *Energy Conversion & Management* **40**, 743–755.

Ekinci, K., Kulcu, R., Kaya, D., Yaldız, O., Ertekin, C. & Ozturk, H.H. 2010. The prospective of potential biogas plants that can utilize animal manure in Turkey. *Energy Exploration & Exploitation* **28**(3), 187–206.

Eliçin, K., Gezici, M., Tutkun, M., Şireli, H.D., Öztürk, F., Koser Eliçin, M. & Gürhan, R. 2014. Potential of biogas from animal wastes of turkey and determination of suitable reactor size. *Agriculture & Forestry* **60**(4), 189–197.

Ergür, H.S. & Okumuş, F. 2010. Cost and potential analysis of biogas in Eskisehir. *Uludağ Üniversitesi Mühendislik-Mimarlık Fakültesi Dergisi* 15(2), 155–160.

Eryaşar, A. & Koçar, G. 2009. The possibilities of biogas to be used in existing energy systems. *Mühendis ve Makina* **50**(590), 10–16. (in Turkish, English abstr.).

Eryilmaz, T., Yesilyurt, M.K., Gokdogan, O. & Yumak, B. 2015. Determination of biogas potential from animal waste in Turkey: a case study for Yozgat province. *European Journal of Science and Technology* **2**(4), 106–111.

Evrendilek, F. & Ertekin, C. 2003. Assessing the potential of renewable energy sources in Turkey. *Renewable Energy* **28**, 2303–2315.

FM Bioenergy. 2013. The practical guide to Ad. Chapter 5:Producing and using biogas. 60–77 pp. *http://adbioresources.org/wp-content/uploads/2013/06/59-80_chapter5_v4.pdf* Accessed 20.09.2014.

FNR, 2010. *Biogas guide - production from to use.* 261 pp. (in Turkish).

Frost, P. & Gilkinson, S. 2010. Interim technical report. *http://www.afbini.gov.uk* Accessed 20.09.2014.

Gümüşçü, M. & S. Uyanık. 2010. Biogas and biofertilizer production from animal waste in Southeastern Anatolia Region. *http://www.mmo.org.tr/resimler/dosya_ekler/ffcec9d25e4a0d2_ek.pdf?dergi=1045* Accessed 10.10.2014. (in Turkish, English abstr.).

Igliński, B., Buczkowski, R. & Cichosz, M. 2015. Biogas production in poland–current state, potential and perspectives. *Renewable and Sustainable Energy Reviews* **50,** 686–695.

International energy agency (IEA) 2015a. World energy outlook 2014. *https://www.iea.org/publications/freepublications/publication/WEO2014ESTurkish.pdf*. Accessed 30.10.2015 (in Turkish).

International energy agency (IEA) 2015b. Turkey renewables and waste statistics. *http://www.iea.org/countries/membercountries/turkey/statistics/* Accessed 30.10.2015.

Karaman, S. 2006. Environmental pollutions caused by animal barns and solution possibilities. *KSÜ. Fen ve Mühendislik Dergisi* **9**(2), 133–139 (in Turkish, English abstr.).

Kaya, D., Çağman, S., Eyidoğan, M., Aydoner, C., Çoban, V. & Tırıs, M. 2009. Turkey's animal waste biogas potential and economy. *Atık Teknolojileri Dergisi* **1**, 48–51. (in Turkish).

Kaya, D. & Öztürk, H. 2012. *Biogas technology-generation-use-designing*. Umuttepe Yayınları, 253 pp. (in Turkish).

Koçer, N.N., Öner, C. & Sugözü, İ. 2006. Cattle-dealing potential of turkey and biogas production. *Doğu Anadolu Bölgesi Araştırmaları* 17–20 (in Turkish, English abstr.).

Koçer, N.N. & Kurt, G. 2013. Cattle-dealing potential of Malatya and biogas production. *SAU J. Sci.* **17**(1), 1–8. (in Turkish, English abstr.).

Li, J., Wei, L., Duan, Q., Hu, G. & Zhang, G. 2014. Semi-continuous anaerobic co-digestion of dairy manure with three crop residues for biogas production. *Bioresource Technology* **156**, 307–313.

Oleszek, M., Król, A., Tys, J., Matyka, M. & Kulik, M. 2014. Comparison of biogas production from wild and cultivated varieties of reed canary grass. *Bioresource Technology* **156**, 303–306.

Onurbas¸ Avcioğlu, A. & Türker, U. 2012. Status and potential of biogas energy from animal wastes in Turkey. *Renewable and Sustainable Energy Reviews* **16**, 1557–1561.

Republic of Turkey ministry of energy and natural resources 2015a. Turkey 2013 annual energy statistics report. *http://www.enerji.gov.tr/tr-TR/EIGM-Raporlari* Accessed 01.09.2015 (in Turkish).

Republic of Turkey ministry of energy and natural resources 2015b. Monthly energy statistics report-12. *http://www.enerji.gov.tr/tr-TR/EIGM-Raporlari* Accessed 20.01.2016 (in Turkish).

Swedish Gas Centre (SGC). 2012. Basic Data on Biogas. ISBN: 978-91-85207-10-7. *http://www.sgc.se/ckfinder/userfiles/files/BasicDataonBiogas2012.pdf*

Accessed 15.08.2015.

Turkish Electricity Transmisson Company (TETC), 2016. Turkey Electrical Statistics. *http://www.teias.gov.tr/TurkiyeElektrikIstatistikleri.aspx* Accessed 15.01.2016.

Turkish Statistical Institute (TSI) 2015. Livestock Statistics. *https://biruni.tuik.gov.tr/hayvancilikapp/hayvancilik.zul* Accessed 22.10.2015 (in Turkish).

Ulusoy, Y., Ulukardeşler, A.H., Ünal, H. & Alibaş, K. 2009. Analysis of biogas production in Turkey utilising three different materials and two scenarios. African Journal of Agricultural Research **4**(10), 996–1003.

Wikipedia 2015. *https://tr.wikipedia.org/wiki/Marmara_Bölgesi*. Accessed 15.08.2015 (in Turkish).

Yingjian, L., Qi, Q., Xiangzhu, H. & Jiezhi, L. 2014. Energy balance and efficiency analysis for power generation in internal combustion engine sets using biogas. *Sustainable Energy Technologies and Assessments* **6**, 25–33.

# Material waste paper recycling for the production of substrates and briquettes

I. Balada[*], V. Altmann and P. Šařec

Czech University of Life Sciences Prague, Faculty of Engineering, Department of Machinery Utilization, Kamycka 129, CZ 165 21, Prague 6 – Suchdol, Czech Republic
[*]Correspondence: baladai@tf.czu.cz

**Abstract.** This Article is focusing on recycling waste paper, which became one of the main collecting commodities for its widespread use in many economic regions. The introduction provides an overview of the development of a segment of waste paper in the EU. The article presents information about product options, new materials from processed waste and waste paper. The first part of the article describesthe situation in the Central Bohemia region both in terms of production and in terms of processing capacities. The next part of the article contains the practical information and value gained from the process of production of briquettes from waste paper and the description and analysis of technologies as well as description and analysis of achieved physical characteristics of manufactured briquettes. Another mentioned option for using waste paper is the application in substrate production technology as an input material with excellent physical properties, which could become an indispensable component in the production of high-quality substrates. The resulting values indicate a higher absorption capacity of fluids that are substrates of biodegradable materials. In both technologies there are present variations of the different samples and their ratios used to manufacture the final products and are shown in the resulting comparison.

**Key words:** biodegradable municipal waste, material recycling, composting, production of briquettes.

## INTRODUCTION

Today the comfortable life is paid with the expressive consumption of energy in all its forms. The non-renewable energy source reserves are limited and they are to exhaust. Nevertheless, they supply about four fifths of energy consumption. In last decades, the renewable energy sources have been preferred. One of alternative forms of fuel, made from renewable sources, is the fuel on the basis of paper waste. First of all, it is recommended to recycle this raw material – to use it as a material (McKinney 1995).

From the results of works published before (Brožek 2013; Brožek & Nováková, 2013), it follows that compared to briquettes from wood waste, briquettes made from recovered paper and board are of low moisture content, high density, high mechanical durability and relatively high force is necessary for their rupture. But at the same time, they have high ash amount and low gross calorific value.

The constant industrial activity rise and world population growth are directly related to the increase of overall energy consumption, and it is estimated that in 2025, energy demand will surpass by 50% the current needs (Ragauskas et al., 2006).

Nowadays, almost 80% of the world's energy supply is provided by fossil fuels (Sims et al., 2007) with harmful impacts to the environment.

In the Czech Republic, 800,000 tons of waste paper is collected anually in average via separate sorting, but out of this amount only 315,000 tons is processed, and the rest, i.e. approx. 60% out of the mentioned total amount, is being exported abroad at the expense of the environment and the Czech economy. Although a paper consumption in the Czech Republic is estimated at 1.5 million tons, only 900,000 tons of paper is produced there. Out of this quantity, 700,000 tons is exported simultaneously, which means that it is necessary to import 1.3 mil. tons of new paper (Barták, 2010). These figures clearly confirm that 85% of the paper intended for consumption must be imported to the Czech Republic.

In recent years recorded, one of the most serious problems in the environmental field is an increased soil erosion and the associated degradation of the total agricultural land fund (Plíva et al., 2016). The paper presents two ways of secondary material recycling of waste paper in order to manufacture substrates, which are going to replace the loss of humus in the soil. Through application of produced substrates into the soil, other negative phenomenons, e.g. decreasing infiltration capacity of soil, can be prevented. Low infiltration results in poor water penetration into the deeper section and thus there is a constant destocking of groundwater.

The paper presents two ways of processing the waste paper and its consequent potential use. There are two groups of experiments that A) lead to the production of briquettes and determine their bulk density with a focus on the future use in the production of substrates as substitutes for e.g. behind wood chips, and B) lead to the production of the substrate in which the waste paper is going to be a high-quality irreplaceable commodity. During the production of the substrate, the sludge from sewage treatment plants (STP) is utilised at high extent, which brings another positive effect to recycling of problematic waste materials.

The experiments focus on the qualitative characteristics of the products produced. Both products are going to be applied to the soil in the next trial period and are going to be tested on their ability of rainwater retention in the soil profile. Based on the results, the before-mentioned primary experiments are going to be expanded with the content percentage adjustment in order to determine the optimum ratio of waste paper and added secondary waste materials that would ensure maximum dwell time of rainwater in the soil profile and would reduce risk of water erosion due to extreme precipitation.

## MATERIALS AND METHODS

The goal of the research is the confirmation of waste paper usability, especially in the view of its low apparent density and high ability to bind water. In this paper, the primary results that deal with the verification of biodegradation properties and structural transformation of waste paper after shredding and crushing are presented.

### A) Production of briquettes
The volume of shredded paper was determined using measuring cylinders of known volume and weight of the material. There were chosen 3 kinds of waste paper for the experiment:
- office paper shredded with the Fellowes MS 450Ms paper shredder,

- shredded paperboard (Fig. 3),
- shredded waste paper (a mixture of magazines, newspapers and other paper packaging), shredded using the HSM DuoShredder 5750 at WEGA recycling Ltd.

The material was scattered into a 1,000 ml measuring cylinder. The material was not compacted, just sprinkled into the measuring cylinder of the same height. Subsequently, the material was sprinkled on a scale and the weight of the material was measured in [g]. There were 10 measurements performed for each material and the mean value was determined, from which the specific weight of input shredded material was calculated.

Other devices:
- the measuring cylinder with a volume of 2,000 ml,
- laboratory scale KERN PFB 2000-2 with weighing range up to 2,000 g with a 0.01 g accuracy.

The material was inserted into the reservoir of briquetting machine BrinkStar CS25 with a matrix of 65 mm, and three types of briquettes were produced depending on a waste paper. Maximum operating pressure of the briquetting machine was 18 MPa (180 bar). Materials for pressing had to meet the following conditions: moisture content from 8 to 15%, dimensions smaller than 15 mm and bulk density of at least 70 kg m$^{-3}$. Briquette height was measured in two spots and the average value was calculated. Using the matrix diameter 65 mm, the height and the weight of the briquettes, the resulting bulk density was calculated. The briquettes were also analyzed to obtain a combustion heat and heating value according to ISO 1928. According to the manual of the briquetting machine, the briquettes should have had a shape of a cylinder of diameter 65 mm, length from 30 to up to 50 mm, and the heating value from 15 to 18 MJ kg$^{-1}$. The compression coefficient was calculated as the ratio between the density of the material prior to entering the briquetting machine and the density of the resulting briquettes.

### B) Production of substrate using waste paper

The aim of the experiment was to verify the possibility of processing raw material composed of cardboard and of sludge from sewage treatment plants in a high percentage share by technology of composting in order to verify the material degradation, and to produce a substrate.

In order to create piles for substrate production, composters showed in Fig. 1 were stocked with the raw materials listed in Table 1. Formation of raw materials was carried out according to the standard EN 14 045.



**Figure 1.** Establishment of piles of row material.

**Table 1.** The parameters of individual components and of the total

| Sample No. | Sample photo | Material used | Volume [m³] | Weight [kg] | C:N [-] |
|---|---|---|---|---|---|
| 1. |  | sludge from STP | 0.325 | 229.474 | 8.3:1 |
| | | cardboard (2x2) [cm] | 0.114 | 3.911 | 150:1 |
| | | fresh grass matter | 0.311 | 89.364 | 30:1 |
| | | **total** | **0.75** | **322.746** | **14.4:1** |
| 2. |  | sludge from STP | 0.325 | 229.474 | 8.3:1 |
| | | cardboard (10x10) [cm] | 0.114 | 3.911 | 150:1 |
| | | fresh grass matter | 0.311 | 89.364 | 30:1 |
| | | **tota**l | **0.75** | **322.746** | **14.,4:1** |
| 3. |  | sludge from STP | 0.325 | 229.474 | 8.,3:1 |
| | | cardboard (3x25) [cm] | 0.114 | 3.911 | 150:1 |
| | | fresh grass matter | 0.311 | 89.364 | 30:1 |
| | | **total** | **0.75** | **322.746** | **14.4:1** |

Due to the fact that the piles had the same weight of individual components, the speed and quality of gradual decomposition of waste paper according to its original sample size could have been observed during the prosess. In the middle of the experiment, i.e. after 30 days, observations of the decomposition were carried out according to norm ČSN EN 14045. After the decomposition assesment, substrate production was accomplished under the conditions of autumn outdoor temperatures.

The temperature during decomposition was measured using electronic thermometers Testo 175 able to record measured data (Pliva et al., 2016). Upon entering the experiment, the thermometer recorders were programmed to measure hourly the temperature at the end of the probes (inside the pile), and also ambient air temperature. Thermometers were placed in the composters for the whole duration of the experiment, with the exception of compost rearrangement.

The oxygen content was measured by an electrochemical method using the Testo 327 with a penetration probe, and an electric gas pump.

For the detection of density, a method weightigh the known volume of raw materials was used. From the weighted value, the values in desired units [kg m⁻³] were calculated. The standard scale of up to 30 kg was used for weighting as well as a vessel with calibrated volume. The procedure for determining materials' bulk density (Plíva et al., 2016) was as follows:

1) A sample of the raw material was chosen for determination of bulk density.

2) After filling the measuring vessel with a defined volume of 0.038 m³, the container with the material was weighed, and the weight of the measuring vessel was subtracted from the detected value afterwards.

3) The weighing was carried out for a total of three samples taken from the total amount of raw material.

4) The detected density in kg m$^{-3}$ was calculated with the following formula (1):

$$\overline{m_v} = k \cdot \frac{m_1 + m_2 + m_3}{3} \quad [kg\ m^{-3}] \qquad (1)$$

where: k – conversion coefficient [m$^{-3}$]; m$_n$ – sample weight [kg].

When determining the humidity of raw material, a sample of about  g was taken and was subsequently spread on a mat, and larger lumps were broken down. Dividing the sample reduced it to 500 g, and it passed then through a sieve having a mesh size of 5 mm. After this adjustment, 20 g of compost was collected from the original sample (accuracy of ± 0.05 g) into weighed dry containers and the sample was dried at 105 °C to a constant weight. After cooling in a desiccator, the sample was weighed and the moisture content was calculated in % (Plíva, et al., 2016).

The gravimetric moisture content was calculated using the formula (2):

$$x = \frac{m_1 \cdot 100}{m} \quad [\%] \qquad (2)$$

where: m$_1$ – sample weight loss by drying [g]; m – weight of the sample before drying [g].

## RESULTS AND DISCUSSION

### A) Production of briquettes

In the first part of the research, the density of selected materials was calculated, and it was found out that the cardboard had the highest density. It is due to a higher proportion of pulp after multiple recycling that the cardboard containes compared to other types of waste paper.

In the next part of the experiment, the production of briquettes of cylindrical shape with a diameter of 65 mm (Fig. 2) using a briquetting press was performed. The tested waste material was continuously inserted into the reservoir, and after the briquettes had been produced, the entire reservoir was cleaned before being used again for another tested material.
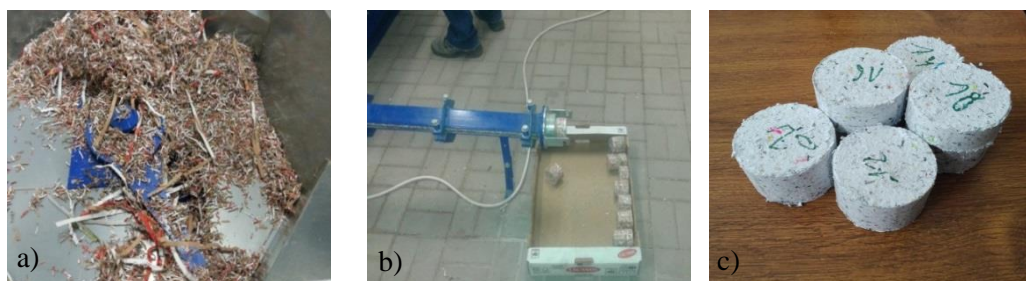


**Figure 2.** Briquette production process: a) a container with the material; b) conveyor of the briquettes; c) briquettes produced.

Twenty pieces of produced briquettes were tested for each measured type of the waste paper. Each briquette was measured at two spots to calculate the height and its average value. Furthermore, the volume of the briquettes was calculated, as was their weight and their bulk density. At the end, the compression ratio of the mentioned types of waste paper was calculated (Table 2).

**Table 2.** Calculation of compression ratio of measured types of waste paper

| Input material | Bulk density of input material [kg m$^{-3}$] | Bulk density of briquettes [kg m$^{-3}$] | Compression ratio [-] |
|---|---|---|---|
| separate paper | 66.322 | 278.343 | 4.20 |
| cardboard | 76.202 | 252.322 | 3.31 |
| office paper | 55.622 | 258.126 | 4.64 |

The briquettes were analyzed to obtain a combustion heat and heating value according to ISO 1928 (Table 3). The heating value of briquettes made of paper fell bellow the interval indicated by the manual of the briquetting machine. The cardboard briquettes demonstrated the highest heating value, probably because of the content of chemical binders.

**Table 3.** Chemical analysis, heating vaue and combustion heat of the briquettes

| Materials | Humidity | Ash | C | H | N | S | O | Combustion heat MJ kg$^{-1}$ | Heating value MJ kg$^{-1}$ |
|---|---|---|---|---|---|---|---|---|---|
| | gravimetric % | | | | | | | | |
| office paper | 4.13 | 12.628 | 36.175 | 5.107 | 0.060 | 0.041 | 44.146 | 12.941 | 11.821 |
| separate paper | 4.225 | 20.408 | 35.305 | 4.769 | 0.086 | 0.032 | 37.221 | 13.194 | 12.152 |
| cardboard | 4.820 | 11.580 | 39.348 | 5.408 | 0.135 | 0.050 | 41.183 | 14.717 | 13.535 |

The aim of the experiment where briquettes were produced by pressing three types of waste paper was to assess quality of the compression and possibility of further material use after its shredding. It is well known that there is a large amount shredded waste paper in office buildings that is according to current practice disposed of mainly together with a mixed municipal waste to a landfill. The briquettes produced can be used both in the process of energy production via combustion, and in the compost production process where they can significantly reduce the cost of transportation thanks to the compression ratio. This is going to be the subject of further reflection and experimentation. The size of manufactured briquettes is in accordance with data reporting the size of wood chip material from various wood chippers (Epstein et al., 1997), and corresponds to the commonly used sizes exploited in composting plants as mentioned by Soucek & Burg (2009).

The bulk density of the paper briquettes is up to 4 times lower than the density of briquettes made from herbaceous phytomass, and there is no problem of increased level of nitrogen that is generated by energy utilization of herbal phytomass as indicated by e.g. Theerarattananoon et al. (2011), Hutla (2012), or Zajonc & Frydrych (2012).

### B) Production of substrate using wastepaper
### Measurement of gradual decomposition of waste paper in the pile

The controlled microbial decomposition in composters was used as for a technology of substrate production. All the raw materials were measured for determining their humidity, weight and density. Table 4 showes the resulting values. During the composting process, important indicators, i.e. temperature and oxygen content, were monitored. Bulk density and humidity were measured also in the final compost. Input material and the resulting compost were subjected to chemical analysis in an accredited laboratory. The effectiveness of sanitation was assessed, and quality parameters were specified.

**Table 4.** Raw materials for the production of substrate from waste paper, and from sludge of sewage treatment plants

| Material | Weight of the samples of given volume 0.038 $m^{-3}$ [kg] | | | | Density [kg $m^{-3}$] | Humidity [%] |
|---|---|---|---|---|---|---|
| | 1 | 2 | 3 | Average | | |
| cardboard | 1.22 | 1.19 | 1.50 | 1.30 | 34.30 | 1.60 |
| grass | 10.50 | 11.20 | 10.90 | 10.87 | 286.97 | 40.51 |
| sludge (STP) | 27.60 | 26.20 | 26.80 | 26.87 | 707.02 | 79.80 |

Based on the photographs (Fig. 3), it can be stated that sample No. 3 with cardbord size of 3 x 25 cm demonstrated the fastest decomposition process. It showed signs of the highest decomposition of the superficial layer, and of disintegration into three parts. The reason seems to be the largest contact area with the other compost components, and thus absorbtion of the highest amount of moisture from the surrounding environment.



**Figure 3.** The gradual disintegration of waste paper in the compost after 30 days of composting (from left to right samples No. 1, 2, 3).

### Measurement of temperature

The temperatures in individual composters didn't show any abnormal differences, thus Fig. 4 presents the measured and recorded temperatures of only one of them. The curve of air temperature has large aberrances, because three daily measurements are plotted. Accordingly, the temperature fluctuates compared to the temperature in the compost piles where only one average value per day is charted. Eight digovers are crearly discernible in the graph. Due to autumn period, temperatures were relatively low.
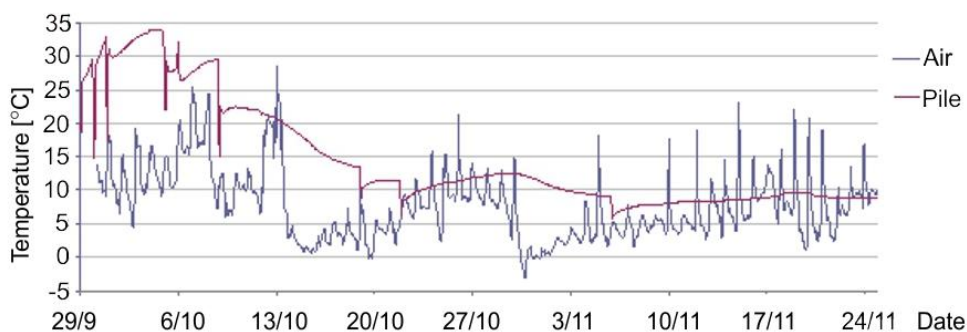
**Figure 4.** Graph of the temperature development in the composter in autumn 2015.

### Measurement of oxygen content

Concerning oxigen content, data retrieved from the composters No. 1 to 3 are shown in an abbreviated form in Fig. 5. Eight digovers were performed. After each digover, the amount of oxygen in the compost increased.



**Figure 5.** Measuremens of the average oxygen content in the piles in autumn 2015.

Aerating the substrate and securing aerobic conditions are the key requirements material decomposition through composting technology. Microorganisms that transform organic matter have high demand of aerial oxygen. The technology has to enable an exchange of gasses between the maturing substrate and its environment, so that there is enough fresh air containing oxygen in the pile. Oxygen content in the aerial pores of maturing compost should reach at least 6% (Laurik et. al., 2011; Dubský & Kaplan, 2012 etc.). As the measured values plotted in Figure 5 show, the development of the oxygen content in the piles was optimal. At the beginning of the process, it did not decrease below the threshold of 6.8%, and at the end, it continuously approached common level of aerial oxygen, i.e. 20.9%.

### Evaluation of the substrate produced

The quality of the substrate produced was evaluated from the perspective of CSN 64 5735 in an accredited laboratory. Overall characteristics and heavy metal content were assessed. Basic quality characteristics of sludge input were also established. The results are shown in Table 5.

**Table 5.** Quality parameters of the input sludge and the resulting substrate and evaluation of concentration of hazardous elements in the input sludge and in the substrate produced

| Quality parameters | Sludge | Substrate | Limits | Unit |
|---|---|---|---|---|
| humidity | 79.80 | 59.89 | min. 40.0; max. 65.0 | [%] |
| combustibles in dry sample | 54.72 | 34.5 | min. 25 | [%] |
| C* | 27.36 | 17.3 | - | [%] |
| N* | 3.30 | 1.28 | min. 0.60 | [%] |
| C:N Ratio | 8.29 | 13.5 | max. 30:1 | [-] |
| pH | - | 7.47 | from 6.0 to 8.5 | [-] |
| Cd* | 0.7 | 0.93 | max. 2 | mg kg$^{-1}$ |
| Pb* | 34 | 28 | max. 100 | mg kg$^{-1}$ |
| As* | 6.7 | 12 | max. 20 | mg kg$^{-1}$ |
| Cr* | 25 | 33 | max. 100 | mg kg$^{-1}$ |
| Cu* | 62 | 57 | max. 150 | mg kg$^{-1}$ |
| Ni* | 15 | 21 | max. 50 | mg kg$^{-1}$ |
| Hg* | 2.4 | 0.93 | max. 1 | mg kg$^{-1}$ |
| Zn* | 410 | 360 | max. 600 | mg kg$^{-1}$ |

* in dry matter

The production of substrates of sewage sludge was already covered by a number of authors, for example by Laurik et al. (2011) and Dubský & Kaplan (2012). The effect of quality of the substrate on the growth of some crops was observed by Wilson et al. (2002); Dubský & Šrámek (2008) and Carlile (2008). In the Czech Republic, the sewage sludge is added commonly into substrates, but forms generally only 20% of their weight. Sludge contains a high level of nitrogen. Therefore in the case of its higher share in the substrates, it is necessary to adjust the C:N ratio by adding the raw material with a sufficient carbon content. The fresh grass mass doesn't affect the ratio too much. Wood chips are more suitable from this respect. According to Raclavská (2008), the ratio of dewatered sewage sludge to wood chips should amount to 60:40.

The results of the experiment, where the experimental raw mix consisting of fresh grass cuttings, sewage sludge in a high share (71% of the total compost weight), and of the addition of structural material in the form of small pieces of cardboard underwent decomposition, confirmed the ability to combine these materials and showed partly favorable results. Quality characteristics of the finished substrate resulting from the conversion of the raw materials met the requirements of the standard CSN 46 5735 'Industrial substrate'. The prescribed temperature was reached during the process, though the temperature of 55 °C required by standards for the treatment of sludge from sewage treatment plants was not. Apparently, the narrow C:N ratio achieved caused this. It did not constitute a major problem, because the experiment was focused on possibility of decomposition of waste paper mixed with high amount of sewage sludge, and further utilization of the resulting substrate was not presumed in an agricultural fielda at this stage of the experiment. The fact that the decomposition was attained even at the lower

temperatures and that the temperature of the processed material increased after each digover can be assessed as positive. Chemical risk assessment of the elements contained in the compost showed below-threshold concentrations of tracked elements (Table 5).

## CONCLUSIONS

Concerning the experiment of briquette production, the cardboard waste that had undergone several recycling processes attained the lowest compression ratio, and thus pressing had the lowest effect. The highest compression ratio and therefore the highest pressing efficiency were achieved with the paper of higher quality, i.e. the paper from primary production, or once only recycled at most, which when shredded, disintegrated into smaller particles compared to shredded cardboard. Properties of the briquettes with the lower compression ratio can be exploited for example in the mentioned composting technology where it can lead to a faster decomposition of the briquettes used. The briquettes can serve as a substitute material in order to adjust the C:N ratio and moisture during composting as was reported by Souček & Burg (2009) and Plíva et al. (2016).

The results of the experiment, where the experimental raw mix consisting of fresh grass cuttings, sewage sludge in a high share (71% of the total compost weight), and of the addition of structural material in the form of small pieces of cardboard were processed, confirmed the ability to combine these materials. The tested paper waste could substitute wood chips. It demonstrates a sufficiently high percentage of carbon. If prepared at a high quality with regard to the desired particle size, it can serve also as a structural material. In the basis of the experimental substrates, only a small amount of cardboard was used (about 1.5% of the total substrate weight). Starting moisture also did not reach optimal values. Smaller water content and a more appropriate ratio of carbon to nitrogen substances would have most likely ensure better results of the process of substrate production. It is possible to continue the experiment in this area with testing higher mass loads of waste paper even with the presumption that the higher amount of waste paper will form a problem when attaining the desired substrate moisture. But this can be modified during the composting process more easily than in the case of excessive moisture.

Based on the previous, the further research is going to be focused on an analysis of physical properties of substrate made from waste paper in relation to the higher ability to retain water in the soil. This could help e.g. during intensive precipitation, and in general to protect soil against erosion.

## REFERENCES

Barták, V. 2010. Paper and paper waste. *World Press*. 4/2010.
Brožek, M. 2013a. *Properties of briquettes from paper waste*. *Manufacturing Technology*, **13**, 138–142.
Brožek, M. & Nováková, A. 2013. Briquettes from recovered paper and board. **In**: *Engineering for Rural Development*. Jelgava, Latvia University of Agriculture, 488–493.

Carlile, W.R. 2008. The use of composted materials in growing media. *Acta Horticulturae* **779**. 321–327.

Dubský M. & Kaplan L. 2012. Substrates and soil with compost and separated digestate. *Horticulture* **11**(8), 62–65.

Dubský, M. & Šrámek, F., 2008. Growing substrate with the addition of compost, their preparation and evaluation. *Applied Methodology n. 2/2008-053, the output of the research project n. MZP0002707301, VÚKOZ, v.v.i. Průhonice*, p. 24.

Epstein, E. 1997. The Science of Composting. Technomic Publishing. *Co INC*, Pensylvania, ISBN No. 1-56676-478-5.

Laurik, S., Altmann, V. & Mimra, M.2011. Composting sludge from sewage treatment plants. *Agritech. Science*, VÚZT, Prague, **5**(1), 1–6. ISSN 1802-8942.

Mckinney, R. 1995. Technology of paper recycling. New York: *Chapman & Hall*. ISBN 0751400173.

Plíva, P., Altmann, V. & Mimra, M. 2016: Composting and composter. Prague, *Profipress*, p. 140. ISBN 978-80-86726-74-8.

Raclavská, H., 2008. Technology of processing and use of sewage sludge. *VŠB Ostrava*, 171 p.

Ragauskas A.J., Williams C.K., Davison B.H., Britovsek G., Cairney J., Eckert C.A., Frederick W.J., Hallett J.P., Leak D.J. & Liotta C.L. 2006. The path forward for biofuels and biomaterials. *Science* **311**(5760), 484–489

Sims, R.E.H., Schock, R.N., Adegbululgbe, A., Fenhann, J., Konstantinaviciute, I., Moomaw, W., Nimir, H.B., Schlamadinger, B., Torres-Martínez, J., Turner, C., Uchiyama, Y., Vuori, S.J.V., Wamukonya, N., Zhang, X., Metz, B., Davidson, O.R., Bosch, P.R., Dave, R. & Meyer, L.A. 2007. Climate Change 2007. Mitigation. Contribution of Working Group III to the Fourth Assessment Report of the Intergovernmental Panel on Climate Change, *Cambridge University Press*, Cambridge, United Kingdom and New York, NY, USA (2007)

Souček, J. & Burg, P. 2009. The amount and opportunities of using material generated during maintenance of trees. *Yearbook of Lawn* **5**(1), Olomouc, Publisher Baštan, p. 89–92. ISBN 978-80-87091-08-1.

Theerarattananoon, K., Xu, F., Wilson, J., Ballard, R., Mckinney, L. & Staggenborg, S 2011. Physical properties of pellets made from sorghum stalk, corn stover, wheat straw, and big bluestem. *Industrial Crops and Products* **33**, 325–332.

Wilson, S.B., Stoffella, P.J. & Graetz, D.A., 2002. Development of compost–based media for containerized perennials. *Scientia Horticulturae* **93**, 311–320.

Zajonc, O., Frydrych, J. 2012. The Mechanical Properties of Pellets From Energy Grasses, *Agritech Science*, VÚZT, Praha, **6**(2), 1–4. ISSN 1802-8942.

# Development and analysis of a driving cycle to identify the effectiveness of the vacuum brake booster

D. Berjoza[1,*], V. Pirs[1], I. Dukulis[1] and I. Jurgena[2]

[1]Latvia University of Agriculture, Faculty of Engineering, Institute of Motor Vehicle, 5 J. Cakstes boulevard, LV-3001 Jelgava, Latvia
[2]Latvia University of Agriculture, Faculty of Economics and Social Development, Institute of Business and Management Science, 18 Svetes str., LV-3001 Jelgava, Latvia
*Correspondence: dainis.berjoza@llu.lv

**Abstract.** In electric vehicles electric vacuum pumps are used instead of traditional vacuum generation devices – the vacuum pump or the intake manifold that are specific to vehicles with internal combustion engines. A special driving cycle has to be designed to identify the effectiveness of electric vacuum pumps. The initial experiments were carried out on a real road, intensively applying the breaks and exploiting the vacuum generation devices as long and intensively as possible. Basing on these experiments brake test cycle was developed. It consists of three braking regimes that involve smooth and uninterrupted braking, interrupted and repeated braking and multiple activation of the brake pedal. Using this cycle, it is possible to conduct research on the performance of various automobile components during braking.

**Key words:** vacuum booster, brake system, brake regimes, test cycle, braking time.

## INTRODUCTION

The key purpose of the main brake system is to ensure the automobile stops within the shortest possible distance after the driver has activated the brake system. The brake system is one of the structural elements of automobiles on which focus is placed both during annual roadworthiness tests and when undergoing a certification procedure for a new automobile.

A group of scientists of the Faculty of Engineering, Latvia University of Agriculture, developed an electric automobile within an EU project. The electric automobile was built up by converting an internal combustion engine automobile – its standard internal combustion engine was removed and replaced with an electric motor. One of the elements changed in conversion was the brake vacuum generation device. Modern cars mainly use two types of engines: petrol and diesel engines. For petrol engines, vacuum is created by connecting the brake booster's vacuum hose to the intake manifold, whereas for diesel engines vacuum is provided by a special vacuum pump. In electric automobiles vacuum is provided by a special electric vacuum pump.

When reviewing the conversion design for the automobile, inspectors of the Road Traffic Safety Directorate of the Republic of Latvia raised a question about the productivity of vacuum pump in various operation regimes for the electric automobile. For this reason, it was necessary to conduct tests on a roll test bench, simulating the

driving conditions. Since no special driving cycle for testing the brake system on a roll test bench had been designed, such a cycle had to be developed. The purpose of a driving cycle is active and multiple use of the brake system under the most disadvantaged operation regimes for the brake vacuum pump.

There are two ways of developing a driving cycle. Modal or polygonal cycle is composed from various driving modes of constant acceleration, deceleration and speed, for example, New European Driving Cycle (NEDC). The other type is derived from actual driving data and is referred as 'real world' cycle. Such cycle example is the FTP-75 (Federal Test Procedure) cycle. The 'real world' cycles are more dynamic, reflecting the more rapid acceleration and deceleration patterns experienced during on road conditions (Tzirakis et al., 2006).

In this particular case the second method is most suitable. Cycle development methodology is already developed and approved at the Faculty of Engineering in previous studies investigating the use of biofuels (Dukulis & Pirs, 2009).

### Brake booster vacuum systems

A brake booster is a device that reduces the force to be applied to the brake pedal during braking by means of vacuum generation devices. Operational parameters of vacuum pumps that are powered by internal combustion engine shafts depend on the engine crankshaft's rotation frequency, while in electric automobiles the operational parameters are not affected by the main electric motor.

In the European Union, the key document that stipulates brake testing procedures is Commission Directive 98/12/EC regarding brake systems for vehicles of certain categories and their trailers (Commission Directive…, 1998). The Directive prescribes a methodology for calculating braking distances if the speed, deceleration and other parameters of a vehicle are known. Braking tests have to be performed with the engine both engaged and disengaged. Also, brakes have to be tested if their temperature is below 100 °C or exceeds it. In a test, $M_1$ category vehicles with the engine engaged have to make a deceleration of not less than 5.8 m s$^{-2}$, while with the engine disengaged it has to be not less than 5.0 m s$^{-2}$. The force applied to the brake pedal does not have to exceed 500 N (Commission Directive…, 1998). The Directive provides a methodology for determining the load on the vehicle's axles. The Directive does not provide information on how to perform tests for brake boosters.

In the Republic of Latvia, the legal act that stipulates the technical condition of vehicles is Minister Cabinet Regulation No. 466 of 29 April 2004 'Regulations Regarding Roadworthiness Tests for Vehicles and Technical Roadside Inspections' (Regulations…, 2004). Clause 405.1 stipulates that for cars the force applied to the brake pedal does not have to exceed 500 N. Nothing is mentioned regarding brake booster tests, while for defects that are evaluated with code '2' – unacceptable – the Regulation states that the amount of force applied to the brake pedal may not exceed that set by law.

There have been research studies on the optimisation and modelling of regenerative braking for electric automobiles (Yeo et al., 2004). Extensive research studies have been conducted on the effects of brake system components on braking parameters (Maciuca & Hedrick, 1995). These studies analyse the effect of vacuum brake boosters of various structures on braking and develops an algorithm for a mathematical model for reading controller parameters, which includes vehicle speed control, brake torque control, wheel brake pressure control and actuator pressure control modules.

Specific research studies and research methodologies on brake boosters are available in a limited number. A research study conducted within a doctoral dissertation at the University of Bradford can be mentioned as one of the research studies on brake system vacuum boosters. The research focused on the influence of braking system component design parameters on pedal force and displacement characteristics (Ho, 2015). This research extensively analysed vacuum booster structures as well as the brake pedal 'feeling' for various brake systems depending on their structures. The research also analysed a mathematical model for the brake vacuum booster, pointing that modern automobiles usually used such boosters at a brake booster ratio ranging from 4:1 to 6:1. Characteristics were determined for every braking system component. In the research, the brake pedal was tested at a load within a range of 49.05–245.25 N. A test was performed also for the brake pedal together with the brake cylinder. The test showed a linear increase in braking fluid pressure in the master cylinder within a range of 0–13 bar at the force applied to the brake pedal within a range of 0–600 N. The research analysed an association between change in braking pressure and the brake pedal's displacement. A brake activation robot was used to activate the brake pedal. A 0.7 bar vacuum pressure generated by an electric vacuum pump was used to operate the vacuum booster in all tests on the whole braking system. The tests on the whole braking system produced data on the effect of the brake pedal's displacement on pressure in the braking system both with and without the vacuum booster. The maximum pressure in the brake pipe ranged from 50 to 59 bar. The tests were done also on a Honda automobile, recording braking parameters. The braking was done both by the brake activation robot and by a human. The data acquired were employed in the mathematical model. A mathematical model for the vacuum booster was developed too as one of the elements of the system researched. Characteristic curves both for boosters at various brake booster ratios and for the situation with no booster were acquired by means of this model.

An analysis of available information sources leads to a conclusion that no data on brake system vacuum boosters tested on a roll test bench at various braking regimes are available, and so far no custom-adjusted driving cycles have been designed to test vacuum boosters at various braking regimes. For these reasons, it is useful to design a driving cycle for testing brake system vacuum boosters. The cycle has to ensure that a brake can be tested under the most disadvantaged regimes for the vacuum booster.

## MATERIALS AND METHODS

### Choice of regimes to research brake vacuum booster pump parameters
One of the key tasks of researching a brake vacuum booster is the choice of regimes of braking. The key criteria for choosing a braking regime are as follows:
- multiple operations of smooth braking have to be performed, so that the brake vacuum booster is engaged a number of times;
- braking regimes have to be developed in a way to be precisely simulated on a roll test bench in the regime simulating real road conditions;
- braking regimes may be repeatedly employed for all vehicles researched;
- braking regimes have to be universal and appropriate for vehicles of any kind of engine and fuel.

To select test regimes when developing the initial test programme, an approximate driving cycle algorithm was chosen (Fig. 1).
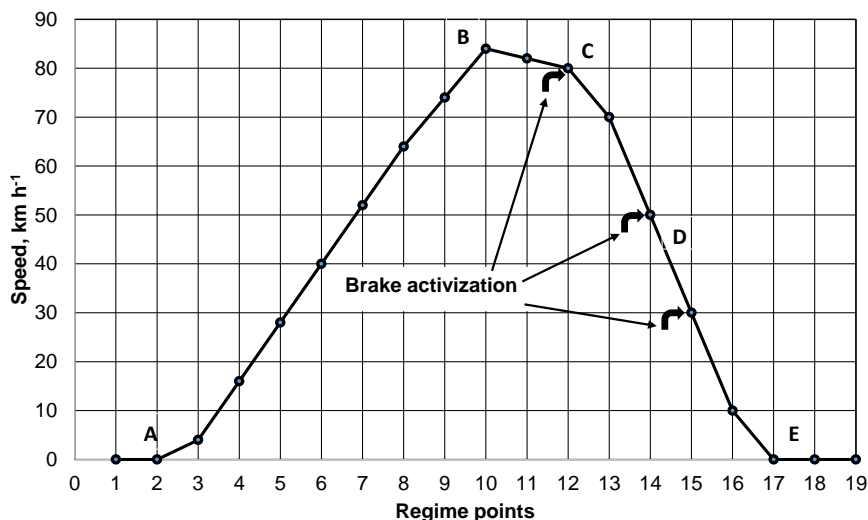


**Figure 1.** Algorithm for one regime of the driving cycle.

One stage of the driving cycle starts with an automobile being parked at point A. The automobile starts accelerating at Stage A–B. Stage B–C is characterised by depressing clutch movement at a speed of $\approx 80$ km h$^{-1}$. It starts braking at point C. Stage A–C refers to preparing the test regime, while Stage C–E directly relates to braking. At Stage C–E, the brake is activated several times. At point E, the automobile is stopped and is at a standstill. The particular stage presented in Fig. 1 is used to read speed characteristics for the driving regimes in the road tests. By choosing various maximum speed and brake activation timing and frequency regimes, different characteristic curves are acquired. A driving cycle of braking regimes is acquired by placing these different stages one behind another, which corresponds to the brake booster pump's performance characteristics. A draft regime protocol is drawn for tests, which is used during the road tests for simulating a particular regime.

The following braking regimes are envisaged in the initial test programme:

- smooth braking starting at a speed of 80 km h$^{-1}$ through to a complete stop;
- the braking regime in which the brake is activated multiple times at a specific speed of the automobile. The brake is activated to slow down from 80 to 60 km h$^{-1}$, then braking is interrupted and activated again to reach a speed of 40 km h$^{-1}$; the brake pedal is released and pushed down again to slow down to a speed of 20 km h$^{-1}$; the brake pedal is released and activated until the automobile comes to a complete stop;
- braking is started at a speed of 80 km h$^{-1}$ and the brake pedal is activated 2–3 times; when a speed of 50 km h$^{-1}$ is reached, the brake pedal is again pushed down 2–3 times.

All the mentioned driving regimes were used in the road tests.

**Devices and vehicles used for the road tests**

A compact passenger car *Renault Trafic* with a 2.0 l diesel engine was used in the road tests. The car was equipped with data reading and recording devices. The key parameters to be recorded in the road tests were speed, time, engine crankshaft frequency, brake pedal position and vacuum pressure in the brake booster pump's main pipe. The key characteristics of the devices used in experiments are given in Table 1.

**Table 1.** Technical characteristics of the devices used in experiments

| No | Characteristics | Technical parameter |
|---|---|---|
| **Automobile *Renault Trafic*** | | |
| 1. | Engine capacity, $cm^3$ | 1,995 |
| 2. | Engine power, kW | 66 |
| 3. | Gross weight, kg | 2,835 |
| 4. | Weight during road tests, kg | 2,130 |
| 5. | Maximum speed, km $h^{-1}$ | 150 |
| **Pressure sensor *Trafag 8472.77.8817*** | | |
| 1. | Measuring range, bar (accuracy) | 0...6 ($\pm$ 0.05) |
| 2. | Voltage supply, V | 10...30 |
| 3. | Output voltage, V | 0...5 |
| 4. | Output amperage, mA | 4...20 |
| 5. | Operating temperature, °C | -25...125 |
| **Data logger *DashDyno SPD*** | | |
| 1. | Speed, km $h^{-1}$ (accuracy) | 0…250 ($\pm$ 0.2) |
| 2. | Simple recording time, s | 0.2…1 |
| 3. | Engine RPM (accuracy) | 0…10000 ($\pm$ 5) |
| 4. | Accuracy of distance measuring, m | $\pm$1 |
| 5. | Ambient operating temperature, °C | -10...55 |
| **Additional adaptation unit** | | |
| 1. | Unit model | CAN Interface Module 450FT0293-01 |
| 2. | Number of analog signals | 2 |
| 3. | Number of binary signals | 13 |
| **Roll test bench MD-1750** | | |
| 1. | Maximum measured power, kW (accuracy) | 1,287 ($\pm$ 1) |
| 2. | Maximal measured speed, km $h^{-1}$ (accuracy) | 362 ($\pm$ 0.2) |
| 3. | Diameter of roller, m; | 1.27 |
| 4. | Roller face length, m | 0.71 |
| 5. | Inner track width, m | 0.71 |
| 6. | Outer track width, m | 2.13 |

A data logger *DashDyno SPD* was used to record parameters, which received signals from the automobile's CAN pipe through a modifier and directly from the OBD diagnostic socket. A signal regarding change in vacuum system pressure was received from a pressure sensor *Trafag 8472.77.8817* (Fig. 2).
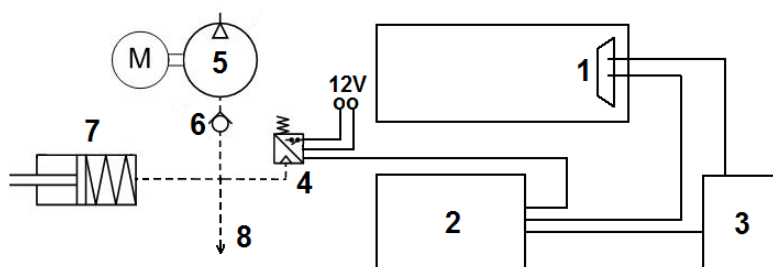
**Figure 2.** Scheme for connecting the devices to the automobile: 1 – car OBD connector; 2 – data logging system *DashDyno SPD*; 3 – CAN signal modifier for clutch and brake pedal position; 4 – pressure sensor; 5 – car vacuum pump; 6 – one way valve; 7 – vacuum booster; 8 – turbine pressure control valve line.

### Methodology for the road tests

The tests were performed in December 2015 at an ambient temperature of +6 °C on a general purpose road between Tuski and Kalnciems. Before the tests, the devices were mounted on the automobile and checked for their functionality. Air pressure in tyres was also checked and adjusted to the nominal tire inflation pressure. Driving the automobile, its engine was warmed up to operating temperature. The data recording devices were turned on and test braking was done before starting the tests. After the data were saved, the data were checked for their consistency with the regime chosen.

The driving regimes were chosen according to the description given above. Measurements were done by two operators: a driving regime operator or the driver of the automobile and a data recording operator. The driver, taking into consideration the road conditions, gave a signal about his readiness, and the data recording operator activated the recording devices.

As an example Fig. 3 shows one of the acceleration and braking regimes. The automobile was accelerated from its initial speed to the speed of the chosen regime, which was 10 km h$^{-1}$ greater than the initial braking speed (Fig. 3, a period from the 18th to the 47th second). Braking was done with the engine disengaged. The transmission was shifted to neutral or the clutch pedal was pushed down and braking was done according the regime chosen (a period from the 48th to the 55th second). The data recording device was stopped after the automobile came to a full stop.

Each test was repeated five times. When processing the data, three data series with the highest correlation were selected. The speed change in time and moments of the activation and deactivation of the brake pedal were selected as the key data.
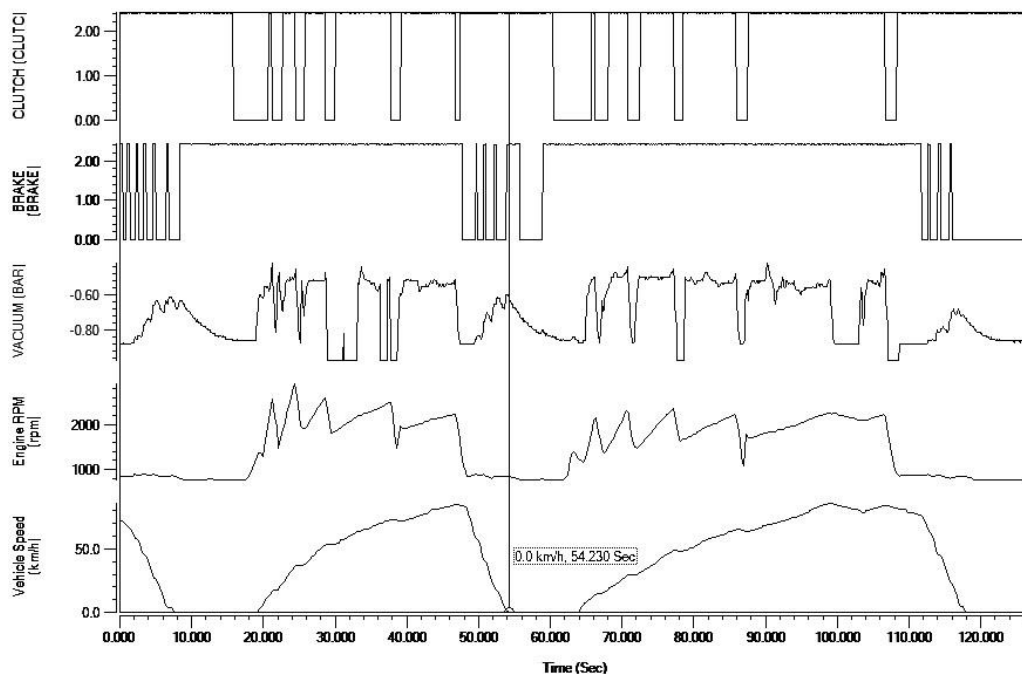
**Figure 3.** Screenshot of the test data from the logger.

## RESULTS AND DISCUSSION

In developing the cycle, the following principles that could differ from the real driving conditions in road tests were taken into account:

- the roll test bench *Mustang* has not been designed for brake system tests in particular; therefore, no hard braking was allowed, which could cause poorer traction for the test automobile;
- no too fast acceleration was allowed for an automobile during the acceleration phase in order to test automobiles of all kinds.

As an example of the cycle development the second braking mode when the brake is activated multiple times at a specific speed is discussed. Fig. 4 shows the time-speed curve of three repetitions. Correlation between these data series of more than 99%.

For each second an average speed was calculated. Extreme phases were removed, and minor adjustments to speed curves' displacement were made. As the result a theoretical speed curve for a 140 second cycle was built (Fig. 5).

678
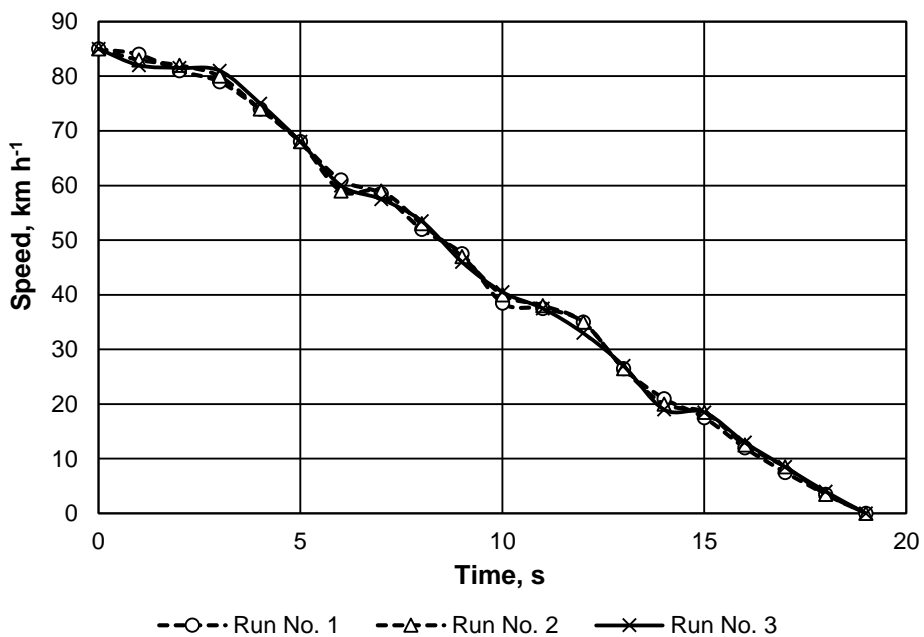
**Figure 4.** Experimental velocity curves of the second braking mode.
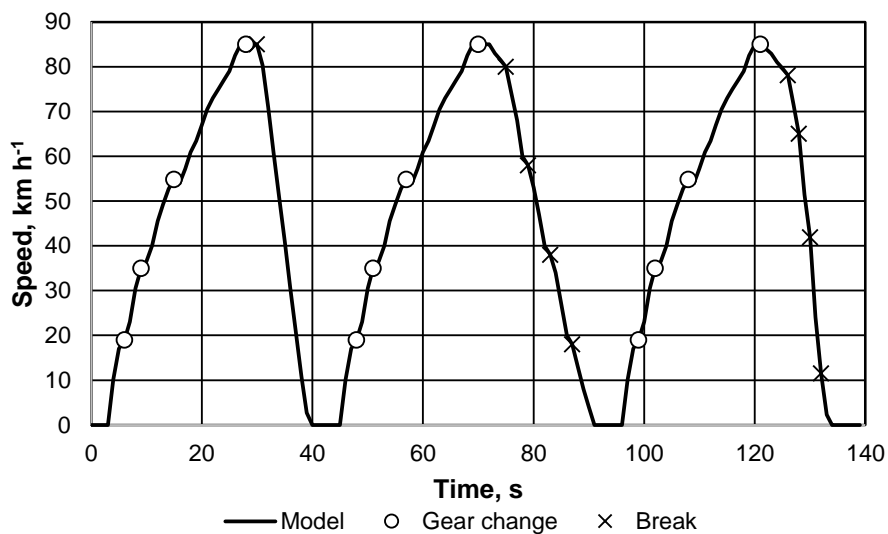


**Figure 5.** Cycle speed curves, gear changing and braking points.

Since the *Mustang* software interface and menu did not provide an option to add a new driving cycle, then the system software core was investigated, variables were identified and the current cycle parameter files were analysed, while the self-made cycle was programmed. Its fragments are given in Table 2.

**Table 2.** Program code fragments

| Cycle general information | Speed points | Gear switching points |
|---|---|---|
| [General] | [SpeedPoints] | [ShiftPoint1] |
| Name=Break test | Point1 = 0 | TimeIntoTest=7 |
| RunningTime=140 | Point2 = 0 | FromGear=1 |
| MaxSpeedToShow=60 | Point3 = 0 | ToGear=2 |
| SpeedErrorLimit=2 | Point4 = 0 | [ShiftPoint2] |
| SpeedErrorTimeRange=1 | Point5 = 6.27586464 | TimeIntoTest=9 |
| WarningToViolationTime=2 | Point6 = 10.56333652 | FromGear=2 |
| MaxDistanceError=0.05 | Point7 = 11.806082 | ToGear=3 |
| HPIntegrationWindow1Start=55 | Point8 = 14.29157294 | [ShiftPoint3] |
| HPIntegrationWindow1End=81 | Point9 = 18.95186847 | TimeIntoTest=15 |
| HPIntegrationWindow1Tolerance=0.5 | Point10 = 21.74804578 | FromGear=3 |
| HPIntegrationWindow2Start=189 | Point11 = 22.68010489 | ToGear=4 |
| HPIntegrationWindow2End=201 | … | … |
| HPIntegrationWindow2Tolerance=0.5 | … | … |
| LR_MinSE=0 | … | … |
| LR_MaxSE=2 | Point131 = 26.03551767 | … |
| LR_Minm=0.96 | Point132 = 14.97508295 | [ShiftPoint20] |
| LR_Maxm=1.01 | Point133 = 7.145786471 | TimeIntoTest=131 |
| LR_MinR2=0.97 | Point134 = 1.429157294 | FromGear=0 |
| LR_MaxR2=1 | Point135 = 0 | ToGear=0 |
| LR_Minb=-2 | Point136 = 0 | [ShiftPoint21] |
| LR_Maxb=2 | Point138 = 0 | TimeIntoTest=133 |
| MaxISEPercent=1 | Point139 = 0 | FromGear=0 |
| MinPurgeFlow=1 | Point140 = 0 | ToGear=0 |

A screenshot of the developed cycle in the test mode is shown in Fig. 6. The figure shows the test bench's monitor screenshot for the cycle at the moment when the automobile accelerates. Lines around the central curve indicate considerable deviations in the speed and time curve. In case a significant deviation from the programmed curve was observed during the cycle, the cycle had to be repeated.
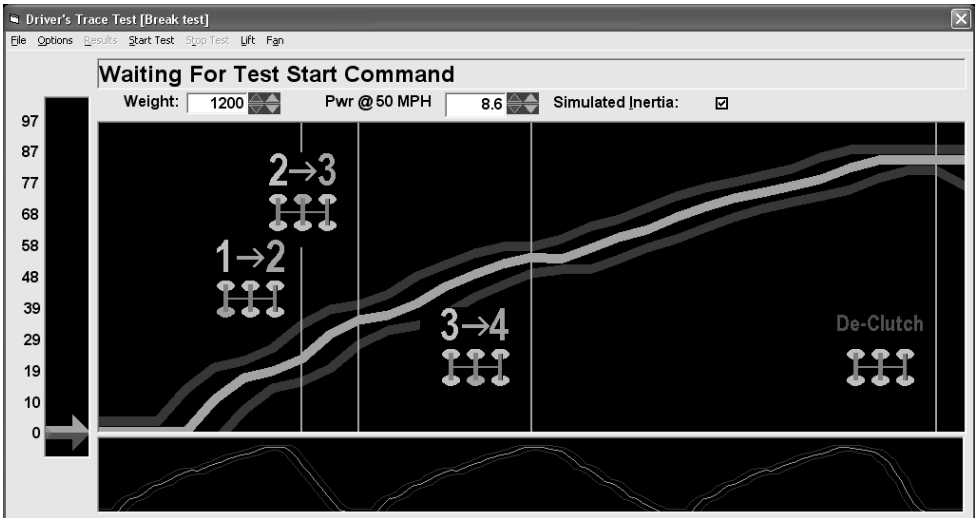


**Figure 6.** Screenshot of the developed cycle in the test mode.

The key characteristics of any driving cycle are maximum speed, average speed and cycle duration. The mentioned characteristics for the developed cycle are summarised in Table 3.

**Table 3.** Key characteristics of the brake vacuum booster for the test cycle

| No | Parameter | Measurement unit | Value |
|---|---|---|---|
| 1. | Distance covered | km | 1.727 |
| 2. | Total duration of the cycle | s | 140 |
| 3. | Maximum speed | km h$^{-1}$ | 85 |
| 4. | Average speed | km h$^{-1}$ | 44.41 |
| 5. | Movement duration in the cycle | s | 118 |
| 6. | Stopping duration in the cycle | s | 22 |

After the experimental cycle was developed, its quality was tested on a chassis dynamometer – roll test bench *Mustang MD1750*. Initially insignificant corrections were made in gear-shifting duration.

To determine whether a model (developed cycle) corresponds to the real driving, three test repetitions were made on the chassis dynamometer. Typically in such evaluation a comparison of the total cycle distance and average speed is performed. On the chassis dynamometer these parameters can be determined directly from the bench software. Real driving data were obtained by cutting out the corresponding data (acceleration and all braking modes) from the logger raw data. The results are summarized in the Table 4.

**Table 4.** Model quality verification results

| No | Parameter | Road tests | Laboratory tests | Difference, % |
|---|---|---|---|---|
| 1. | Distance covered, km | 1.75 | 1.73 | 1.14 |
| 2. | Average speed, km h$^{-1}$ | 44.10 | 44.40 | 0.68 |

These results qualify as a high rating and developed cycle can be used in future experimental studies.

## CONCLUSIONS

Brake tests in road tests on general purpose roads are dangerous, as the hard braking regime can negatively influence the smooth flow of other vehicles on the road. For this reason, it is useful to perform such experiments on a test bench or special testing grounds.

With regard to the effectiveness of brake system vacuum boosters, the EU legislation stipulates standards only for the force to be applied to the brake pedal at 500 N. No other parameters of this system are set.

The purpose of the road tests was to examine change in brake system vacuum pressure depending on the driving regime chosen and to identify an appropriate speed and time regime for the movement of an automobile. During the experiment, the vacuum pressure of the brake pump changed from 0.24 to 0.87 bar depending on the engine's operation regime.

An original driving cycle to test brake system components was developed based on the data for various braking regimes that were obtained in the experiment.

The developed brake test cycle consists of three braking regimes that involve smooth and uninterrupted braking, interrupted and repeated braking and multiple activation of the brake pedal. The regimes developed include the majority of potential brake exploitation regimes.

Using the developed driving cycle, it is possible to conduct research on the performance of various automobile components during braking. The following parameters of brake system components may be identified on a power test bench in experimental research: change in the vacuum pressure of a vacuum generation device, change in brake system pressure and change in the force applied to activate the brake pedal.

## REFERENCES

Commission Directive 98/12/EC of 27 January 1998 adapting to technical progress Council Directive 71/320/EEC on the approximation of the laws of the Member States relating to the braking devices of certain categories of motor vehicles and their trailers. 1998. *Official Journal of the European Communities* L 81, 18 March, p. 1–146.

Dukulis I., Pirs V. 2009. Development of Driving Cycles for Dynamometer Control Software Corresponding to Peculiarities of Latvia. In: *Proceedings of the 15th International Scientific Conference 'Research for Rural Development'*. Jelgava: LUA, 2009, p. 95–102.

Ho, H.P. 2015. The influence of braking system component design parameters on pedal force and displacement characteristics. Simulation of a passenger car brake system, focusing on the prediction of brake pedal force and displacement based on the system components and their design characteristics (Doctoral dissertation, University of Bradford).

Maciuca, D.B. & Hedrick, J.K. 1995. Advanced nonlinear brake system control for vehicle platooning. In: *European Control Conference* (3rd: 1995: Rome, Italy). *Proceedings of the third European Control Conference, ECC* **95**(3), 2402–2407.

Regulations Regarding Roadworthiness Tests for Vehicles and Technical Roadside Inspections (Noteikumi par transportlīdzekļu valsts tehnisko apskati un tehnisko kontroli uz ceļiem) (2004). Minister Cabinet Regulation No. 466 of 29 April 2004. Riga: *Latvijas vestnesis* **69**(3017) (in Latvian).

Tzirakis E., Pitsas K., Zannikos F., Stournas S. 2006. Vehicle emissions and driving cycles: comparison of the Athens driving cycle (ADC) with ECE-15 and European driving cycle (EDC). Global NEST Journal, Vol 8, No 3, p. 282–290.

Yeo, H., Kim, D., Hwang, S. & Kim, H. 2004. Regenerative braking algorithm for a HEV with CVT ratio control during deceleration. SAE Technical Paper 2004-40-0041, 7 p.

# Mechanical harvesting in traditional olive orchards: oli-picker case study

B. Bernardi, S. Benalia[*], A. Fazari, G. Zimbalatti, T. Stillitano and
A.I. De Luca

[1]University of Reggio Calabria, Department of Agraria, Feo di Vito, IT 89122 Reggio
Calabria, Italy; [*]Correspondence: soraya.benalia@unirc.it

**Abstract.** Olive harvesting is one of the most laborious and expensive agricultural practices. Indeed, it absorbs 50% of the product value, and this is due to the continuous increasing of labour from one hand and to the lake of labourers from the other hand. Traditional olive orchards are characterized by the presence of large, century old trees and a very low planting density. These conditions make it difficult to plan sustainable and highly productive harvesting models, and therefore require the employment of partially or fully mechanized harvesting systems. In this context, experimental trials were carried out in a traditional olive orchard, situated in Calabria (Southern Italy), in order to assess technical and economic aspects of a commonly used harvester named oli-picker. This machine allows olive harvesting from tree canopy thanks to a spiked cylindrical comb mounted on a hydraulic articulated arm. Particularly, data about operational working time as well as working productivity were collected for technical purposes, whereas economic evaluation considered harvesting cost expressed in terms of cost per hour, cost per unit of product (1 kg of olives) and average cost per hectare. The obtained results highlighted that working productivity referred to the operative time, was 0.37 trees $h^{-1}$ worker$^{-1}$, while the cost per kg of harvested olives was 0.20 € kg$^{-1}$. From the conducted study, it emerges that encouraging results may be reached by mechanizing harvesting operation even in century old orchards.

**Key words:** Olive orchard, mechanization, oli-picker, harvesting costs.

## INTRODUCTION

Olive growing represents a key sector for the entire Mediterranean Basin. It contributes to the natural landscape formation, and has been largely spread in natural systems at least from the IV millennium B.C. to the anthropic period, both as wild variety 'oleaster' *Olea europea var. sylvestris* and as cultivated one *Olea europea var. sativa* (Zohary et al., 2012). In Calabria, Southern Italy, olive orchards are spread over 188 thousand hectares and produces more than 140 thousand tons of oil per year (ISTAT, 2013). This patrimony is of a noticeable importance, however, it is characterized by a high variability, due to the co-existence of extensive orchards with few trees per hectare and intensive ones having more than 600 trees per hectare.

Most of these orchards do not enable to reach high and constant yields from qualitative and quantitative point of view due to their traditional structure. Indeed, big century old trees with irregular layouts and scaled fruit ripening characterize them. This determine a low unitary productivity, high production costs and consequently the

marginalization of extended areas with low levels of adaptation, conversion and mechanization (Sola-Guirado et al., 2014).

Due to their historical, monumental and landscaping importance, as well as to the existing regulation limitations, it is difficult to carry out the conversion of these orchards into new intensive ones (Famiani et al., 2014). Therefore, it is hard too to settle efficient and economically sustainable mechanized models for most of olive farms present in the territory.

However, it is still possible to obtain good quality olive oil from these olive trees if harvesting techniques from the canopy substitute olive harvesting from the ground (Vieri & Sarri, 2010; Castro-García et al., 2012; Deboli et al., 2014; Leone et al., 2015;). In fact, this type of olive growing belong to the latest PGI 'Oil of Calabria' for which a transitory protection regime is currently in vigour at a national level.

In this context, experimental trials were carried out in a century old olive orchard situated in Calabria, where trunk shakers are difficult to use due to trunk diameter, in view to assess technical and economic aspects of a commonly used mechanical beater (oli-picker, Mipe Viviani s.r.l.) mounted on a tractor for olive harvesting from the canopy.

## MATERIALS AND METHODS

Experimental trials were carried out on 10 trees of 'Grossa di Gerace' cultivar, which represents the typical cultivar of the Ionian versant of Reggio Calabria. It is featured by a high vigour and an assurgent growth. The trees had the same dimensional and morphological features and were planted on a 12 x 12 m layout. Dimensional features of olive trees, canopy volume determined according to C.O.I. method (International Olive Council, 2007), fruit detachment force (FDF) and total yield per tree are reported in Table 1.

**Table 1.** Parameters of olive trees (median±interquartile range)

| Trunk circumference (cm) | Trunk height (m) | Canopy diameter (m) | Tree height (m) | Branches (n) | Canopy volume (m$^3$) | FDF (N) | Total yield per tree (kg) |
|---|---|---|---|---|---|---|---|
| 340 ± 45 | 1.6 ± 0.3 | 11.3 ± 1.6 | 5.0 ± 0.4 | 4 ± 1 | 332.4 ± 114 | 4.5 ± 0.8 | 190 ± 60 |

Harvesting was carried out using the oli-picker Mipe Viviani s.r.l. having 820 kg of mass. It consists in a spiked cylindrical comb mounted on a hydraulic articulated arm of seven meters long, which can turn around its axle providing the brushing action that allow olive detachment (Fig. 1). The oli-picker was mounted in the back of a 40 kW agricultural tractor that moved only when the entire production of the tree is harvested. Two operators composed the harvesting site. The first one drived the tractor, while the second one was responsible of net handling.

In order to asses harvesting site working productivity referred to the operative time, working time of each carried out operation was measured according to CIOSTA requirements (Bolli & Scotton, 1987). The operative time includes the effective time during which the activity is carried out as well as the accessory time needed for moving and excludes the idle time.

Furthermore, technical and economic data were recorded. An estimation model based on Miyata (1980) was applied in order to calculate the machinery cost per hour (e.g., agricultural tractor cost) and the equipment cost (e.g., oli-picker), taking into account also the operator-machine labour cost.



**Figure 1.** Mipe Viviani Oli-picker Olidb08 during harvesting trials.

Fixed costs (e.g. interest, insurance and depreciation) and variable ones (e.g. fuel and oil consumption of tractor, maintenance and labour cost) were considered as operating costs. The harvesting costs expressed in terms of cost per hour, cost per unit of product (1 kg of olives) and average cost per hectare were determined.

In order to determine the harvesting cost per 1 kg of olives, the total cost per hour was divided by the harvesting yield per hour. Furthermore, the harvesting cost per kg was multiplied by the harvesting yield per hectare to calculate the average cost per hectare.

Table 2 reports the operating costs items of harvesting work site considered in the economic analysis, according to the following assumptions:
− work remuneration was evaluated in terms of opportunity cost and was equal to the employment of temporary workers for manual (net handling) and mechanical operations (Strano et al., 2015), by adopting current hourly wage (including social insurance contributions). Particularly, qualified workers were employed for mechanical operations, considering a compensation of 9.46 € h$^{-1}$, while the salary for generic workers was considered equal to 5.31 € h$^{-1}$.

- purchase price of 500 € ha$^{-1}$ and an economic life of 5 years were considered to calculate the net costs.
- machine salvage value was estimated as demolition material selling (steel and iron) equal to 10% of the initial purchase cost.
- interests on capital goods (machines and nets) were calculated by applying an interest rate equal to 2%.

**Table 2.** Operating costs of harvesting work site

| COST ITEMS | Symbol | Source |
|---|---|---|
| Machinery (tractor) value (€) | MV | Price list |
| Equipment (oli-picker) value (€) | EV | Price list |
| Total value (€) | TV | MV + EV |
| Salvage value (€) | SV | % di TV |
| Power (HP) | P | Technical manual |
| Interest rate (%) | r | Market survey |
| Economic life of machinery (years) | $EL_1$ | Technical manual |
| Average annual machine use (h year$^{-1}$) | AMU | Field survey |
| Average daily machine use (h year$^{-1}$) | DMU | Field survey |
| Fuel price (€ l$^{-1}$) | FP | Price list |
| Oil price (€ kg$^{-1}$) | OP | Price list |
| Fuel consumption (l h$^{-1}$) | FC | Field survey |
| Oil consumption (kg h$^{-1}$) | OC | Field survey |
| Area occupied by the machine (m$^2$) | A | Technical manual |
| Price per m$^2$ (€ m$^2$) | PA | Local market |
| Nets value (€) | NV | Price list |
| Economic life of nets (years) | $EL_2$ | Technical manual |
| Generic worker (n) | Wg | Field survey |
| Qualified worker (n) | Wq | Field survey |
| Average wage per hour (€ h$^{-1}$) | HWg | Collective Labour Agreement |
|  | HWq |  |
| *Variable Costs per hour* |  |  |
| Fuel consumption cost (€ h$^{-1}$) | FCC | FC*FP |
| Oil consumption cost (€ h$^{-1}$) | OCC | OC*OP |
| Maintenance (€ h$^{-1}$) | MR | Field survey |
| Worker labour cost (€ h$^{-1}$) | OMC | (HWg*Wg) + (HWq*Wq) |
| **Total variable costs per hour** | **THVC** | **FCC+OCC+MR+OMC** |
| *Annual Fixed Costs* |  |  |
| Interests on capital goods (€ year$^{-1}$) | I | ((TV+SV+NV)/2) * r |
| Depreciation (€ year$^{-1}$) | DR | (TV-SV)/EL$_1$ + NV/EL$_2$ |
| Insurance (€ year$^{-1}$) | IR | Field survey |
| Space cost (€ year$^{-1}$) | SC | A * PA * (0.03) |
| **Total fixed costs per year (€ year$^{-1}$)** | **TAFC** | **I+DR+IR+SC** |
| **Total fixed costs per hour (€ h$^{-1}$)** | **HFC** | **TAFC/AMU** |
| **TOTAL HARVESTING WORK SITE COST PER HOUR (€ h$^{-1}$)** | **THC** | **HFC + THVC** |

## RESULTS AND DISCUSSION

Elaborated data revealed a working productivity equal to 0.37 trees $h^{-1}$ worker$^{-1}$ corresponding to 80 kg $h^{-1}$ worker$^{-1}$ during the achieved trials. Harvesting efficiency expressed as the ratio between mechanically harvested olives and total olives present on the canopy exceeded 96%.

Employing the same harvesting machine, on big olive trees having a production varying between 15 to 30 kg per tree, Almeida & Peça (2012) obtained a work rate of 13 to 24 tree per hours with four workers. Whereas Famiani et al. (2014) obtained a working productivity equal to 95 kg of harvested olives $h^{-1}$ worker$^{-1}$, corresponding to 1.3 trees $h^{-1}$ worker$^{-1}$. They also obtained a productivity of 60 kg harvested olives $h^{-1}$ worker$^{-1}$ (equal to 0.6–0.7 trees $h^{-1}$ worker$^{-1}$) when olive harvesting was achieved by mean of the oli-picker and hand-held pneumatic combs, and 130 kg of harvested olives $h^{-1}$ worker$^{-1}$ (equal to 1.7 trees of $h^{-1}$ worker$^{-1}$) when the oli-picker was associated to a reversed umbrella.

Economic outputs obtained from the analysis showed a total hourly cost of harvest working site equal to 31.86 € $h^{-1}$ with a higher incidence of variable costs (27.39 € $h^{-1}$), especially due to labour costs. Fixed costs were equal to 4.47 € $h^{-1}$. The average cost per hectare was of 2.906,63 € $ha^{-1}$, while the cost per kg of harvested olives was equal to 0.20 € $kg^{-1}$. This latter is lower than the cost obtained by Almeida & Peça (2012), which ranged between 0.3–1.1 € $kg^{-1}$, as well as that obtained by Famiani et al. (2014) which was equal to 0.28 € $kg^{-1}$, using the same harvesting machinery, with different conditions of plant productivity and worker number.

From productive point of view, it emerges that encouraging results may be reached by mechanizing harvesting operation even in century old orchards that provide high yields when suitably managed considering the whole agricultural practices. This allows, to concentrate harvesting operations in a brief period and to obtain higher quality olive oil (Giuffrè, 2014) than that obtained from the harvested olives from the ground.

## CONCLUSIONS

The rising requirement to modernize olive and olive oil sector, which assisted during the recent year to the development of new growing models (Giametta & Bernardi, 2010; Tous et al., 2014), make it necessary to recover and valorise traditional orchards that still provide high yields thanks to their accurate management. The conservation of this patrimony that plays a multifunctional role is guaranteed only if a careful planning of machinery employment to accomplish the diverse agricultural practices, especially harvesting, is carried out.

*Authors contributed equally to the present work.*

# REFERENCES

Almeida, A. & Peça, J. 2012. Assessment of the oli-picker harvester in Northeast Portugal. *Acta Hortic.* **949**, 359–364.

Bolli, P. & Scotton, M., 1987. *Lineamenti di tecnica della meccanizzazione agricola*. 1ª edizione. Edagricole, Bologna. 221 pp.

Castro-García, S., Blanco Roldán, G.L., Jiménez-Jiménez, F., Gil-Ribes, J.A., Ferguson, L., Glozer, K., Krueger, W.H., Fichtner, E.J., Burns, J.K., Miles, J.A. and Rosa, U.A. 2012. Preparing Spain and California table olive industries for mechanical harvesting. *Acta Hortic.* **965**, 29–40.

Deboli, R., Calvo, A., Gambella, F., Preti, C., Dau, R. & Casu, E.C. 2014. Hand arm vibration generated by a rotary pick-up for table olives harvesting. *Agric Eng Int: CIGR Journal* **16**(1), 228–235.

Famiani, F., Farinelli, D., Rollo, S., Camposeo, S., Di Vaio, C. & Inglese, P. 2014. Evaluation of different mechanical fruit harvesting systems and oil quality in very large size olive trees. *Spanish Journal of Agricultural Research* **12**(4), 960–972.

Giametta, G. & Bernardi, B. 2010. Olive grove equipment technology. Straddling trees : mechanized olive harvests. *Advances in Horticultural Science* **24**(1), 64–70.

Giuffrè, A.M. 2014. Variation in triacylglycerols of olive oils produced in Calabria (Southern Italy) during olive ripening. *Riv. Ital. Sostanze Grasse* **91**, 221-240.

International Olive Council. (2007). *Production techniques in olive growing*. Retrieved from http://www.google.it/url?sa=t&rct=j&q=&esrc=s&source=web&cd=1&ved=0ahUKEwjR iczTs73KAhWBXQ8KHavyAmIQFggkMAA&url=http://www.internationaloliveoil.org/s tore/download/40&usg=AFQjCNFSb_anevOXJvMgkP1l4qtcThJlBw&sig2=xY7nGiGb1 8UVAI_sUbpi6A&bvm=bv.112454388,d.bGQ

ISTAT. 2013. Istituto Nazionale di Statistica. Retrieved from http://agri.istat.it/jsp/dawinci.jsp?q=plC270000030000193200&an=2012&ig=1&ct=311& id=21A|15A|32A

Leone, A., Romaniello, R., Tamborrino, A., Catalano, P. & Peri, G. 2015. Identification of vibration frequency, acceleration and duration for efficient olive harvesting using a trunk shaker. *Transactions of the ASABE* **58**(1), 19–26.

Miyata, E.S., 1980. Determining fixed and operating costs of logging equipment. *Forest Service General Technical Report*, St. Paul, MN: North Central Experiment Station. USDA, 14 pp.

Sola-Guirado, R.R., Castro-García, S., Blanco-Roldán, G.L., Jiménez-Jiménez, F., Castillo-Ruiz, FJ. & Gil-Ribes, J.A. 2014. Traditional olive tree response to oil olive harvesting technologies. *Biosystems Engineering* **118**, 186–193.

Strano, A., Stillitano, T., De Luca, A.I., Falcone, G. & Gulisano, G., 2015. Profitability Analysis of Small-Scale Beekeeping Firms by Using Life Cycle Costing (LCC) Methodology. *American Journal of Agricultural and Biological Sciences* **10**(3), 116–127.

Tous, J., Romero, A., Hermoso, J.F., Msallem, M. & Larbi, A. 2014. Olive orchard design and mechanization: Present and future. *Acta Hortic.* **1057**, 231–246.

Zohary, D., Hopf, M. & Weiss, E. 2012. *Domestication of Plants in the Old World: The Origin and Spread of Domesticated Plants in Southwest Asia, Europe, and the Mediterranean Basin*. Oxford University Press. DOI:10.1093/acprof:osobl/9780199549061.001.0001

Vieri, M. & Sarri, D. 2010. Criteria for introducing mechanical harvesting of oil olives: Results of a five-year project in Central Italy. *Advances in Horticultural Science* **24**(1), 78–90.

# Theory of vertical oscillations and dynamic stability of combined tractor-implement unit

V. Bulgakov[1], V. Adamchuk[2], M. Arak[3], V. Nadykto[4], V. Kyurchev[4] and J. Olt[3,*]

[1]National University of Life and Environmental Sciences of Ukraine, 15, Heroyiv Oborony Str., UK 03041 Kyiv, Ukraine
[2]National Scientific Centre, Institute for Agricultural Engineering and Electrification, 11, Vokzalna Str., Glevакha-1, Vasylkiv District, UK 08631 Kiev Region, Ukraine
[3]Estonian University of Life Sciences, Kreutzwaldi 56, EE51014 Tartu, Estonia
[4]Tavria State Agrotechnological University of Ukraine, Khmelnytskoho pr. 18, Melitopol, UK 72312 Zaporozhye region, Ukraine
*Correspondence: jyri.olt@emu.ee

**Abstract.** Currently, throughout the world quite extensive use is made of combined tractor-implement units, which are capable of performing several process operations in the same pass. At the same time, the state-of-the-art ploughing and general-purpose tractors that can carry as front- so rear-mounted implements and accordingly feature both the front and rear PTOs, also able to travel efficiently as forward so in reverse gear, are most suited for the performance of such operations. Authors developed and successfully tested a combined tractor-implement unit on the basis of a wheeled ploughing and general-purpose tractor, which can in one pass efficiently chop the after harvesting crop residues with a front-mounted rotary chopper and simultaneously perform tillage with a rear-mounted plough. The aim of this study is the elaboration of the theoretical basis for the process of vertical oscillation of the combined ploughing and chopping tractor-implement unit and the validation of its dynamic stability in the longitudinal and vertical plane. The research has been performed with the use of the methods of designing the analytical mathematical models of functioning of agricultural machines and machine assembly units based on the theory of tractor, the vibration theory, the theory of automatic control and dynamic stability and the methods of computer programme construction and PC-assisted numerical computation. The dynamics of the said unit have been studied basing on the analysis of the amplitude frequency characteristics of the unit as a dynamic system responding to external perturbations appearing in the form of soil surface irregularities. Following the results of the undertaken analytical study, first the equivalent schematic model of the discussed combined tractor-implement unit in the longitudinal and vertical plane was developed, the unit's characteristic points were defined, the linear and angular displacements specified and acting forces applied. Each pneumatic-tyre wheel of the unit represented by its elastically damping model had point contacts with the soil surface irregularities defined by the respective elevations. Using the original dynamic equations in the form of the Lagrange equations of the second kind, first we defined the generalised coordinates and the formulae for the kinetic and potential energy, dissipation functions and generalised forces, then, after performing the necessary transformations, we set up the system of four differential equations, which described the motion of the dynamic system under consideration. Further, we applied the Laplace transformations to the obtained differential equation system, which provided for obtaining the system of equations in the operator form and preparing them for the representation suitable for PC-assisted numerical calculations with the use of the developed

computer programme. In accordance with the numerical computation results, graphs were plotted for the amplitude and phase frequency response characteristics of the tractor's vertical oscillations at different stiffness coefficients of its steering wheels, the amplitude frequency response characteristics of the chopper's oscillations depending on its mass and its support wheel tyres' stiffness coefficient as well as the characteristics of the plough's oscillations at different stiffness coefficients of its pneumatic-tyre ground support wheel.

## INTRODUCTION

The wide application of multi-purpose combined tractor-implement units (Li et al., 2015; Xu et al., 2015) capable of performing several process operations in the same pass is stipulated by their apparent advantages as regards the significant reduction of costs, shorter running times, lower soil compacting effect, improvement of the quality indicators etc. (Nadykto et al., 2015). The most appropriate power units for such combined tractor-implement assemblies are state-of-the-art ploughing and general-purpose tractors that can carry as front- so rear-mounted implements and accordingly feature both the front and rear PTOs, also able to travel efficiently as forward so in reverse gear.

On the basis of the wheeled ploughing and general-purpose tractor we developed and then successfully tested a combined tractor-implement unit, which can in one pass efficiently capture, chop and spread after harvesting crop residues (dead and laid, up to one metre tall) using the front-mounted rotary chopper and simultaneously perform tillage with the rear-mounted plough, i.e. Plough the said residues down to the required depth. It is exactly these two process operations performed just in the described order that are used most often and feature the highest efficiency in their application.

Authors also developed another combined unit, which is also of current interest and achieves equally high efficiency in operation. It is a combined unit, which in the same pass strews mineral fertilisers over the field with the use of its front-mounted fertiliser spreader and ploughs them under with the rear-mounted plough.

At the same time, the construction and efficient operation of state-of-the-art wide-span combined tractor-implement units calls accordingly for the development of the new research and technology fundamentals of their combining. That includes first of all analysing their dynamic properties and finding the parameters that provide for their stable motion, when different work processes are performed simultaneously.

The research into the dynamics of agricultural tractor-implement units has been the subject of quite a number of studies, including the classical works by P. Vasilenko (1962; 1968; 1996), L. Gyachev (1981), M. Karkee (2009), Larson et al. (1976), Mircae & Nicolae (2014), Rabbani et al. (2011) and others. But, the objects of research in the above-mentioned works were agricultural tractor-implement units combining only one agricultural machine, either front-mounted or towed behind (rear-mounted). Meanwhile, the analytical investigation of the said tractor-implement units as dynamic systems was made in horizontal or vertical plains and the differential equations were most often derived with the use of the original dynamic equations in the form of the Lagrange equations of the second kind. The research into the dynamics of combined agricultural

tractor-implement units (featuring front-mounted and trail-behind machines) is the subject of works (Mitsuoka et al., 2008; Pădureanu et al., 2013). Nevertheless, in the mentioned works the analysis of the said units' oscillations in the longitudinal and vertical plane not always takes into consideration the case, when the support and gauge wheels of the agricultural machines have pneumatic tyres and have to be represented by elastically damping models (i.e. They have to feature the respective stiffness and damping coefficients), instead they are considered as rigid structures. Moreover, currently the up-to-date plough designs provide for the use of pneumatic-tyre wheels as the ground support wheels and also several such wheels can be installed in the rear-mounted plough. This implies the need to update the mathematical models of motion of combined tractor-implement units by developing their equivalent schematic models that are more accurate and at the same time take into account the real operating conditions to the maximum possible extent, thereafter setting up the differential equations of motion. Meanwhile, it is the research into the combined tractor-implement units that involves the examination of their oscillatory motions just in the longitudinal and vertical plane, which to a considerable extent determine the traction and operation properties of the units and quality performance of the combined implements, that is of the greatest interest.

The aim of this study is to develop the theoretical fundamentals of the vertical oscillation of the combined tractor-implement unit comprising a wheeled ploughing and general-purpose tractor, a rear-mounted plough and a front-mounted vegetation chopper and to substantiate its dynamic stability in the longitudinal and vertical plane.

## MATERIALS AND METHODS

The research has been carried out with the application of the methodology for the modelling of the functioning of agricultural implements and implement units; the theory of tractor; the higher mathematics; the theoretical mechanics, in particular, the use of the original equations in the form of the Lagrange equations of the second kind, the Laplace transformation; as well as the principles of computer programme construction and pc-assisted numerical computation.

## THEORY AND MODELLING

When the mentioned chopping and ploughing tractor-implement unit travels in operation, the front-mounted vegetation residue chopper and the rear-mounted plough impart to the carrying wheeled tractor vibration (jolts, hits) caused by the soil surface profile irregularities, the varying resistance of the tilling tool, the intermittent loads on the chopper and so on. In general, all these three segments of the tractor-implement unit are in this case subject to translational vertical and angular displacements in the longitudinal and vertical plane.

To develop the analytical mathematical model of the combined tractor-implement unit under consideration, we have first of all to devise its equivalent schematic model, taking into consideration only the motions in the longitudinal and vertical plane (Fig. 1). It is to be noted in advance that the detailed description of this equivalent schematic model will be provided step by step during the detailed discussion and modelling of the components of the tractor-implement unit.
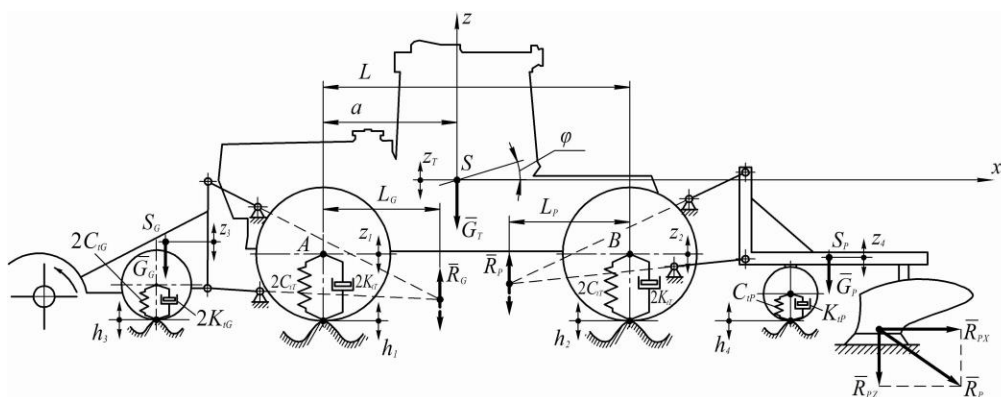
**Figure 1.** Equivalent schematic model of the combined chopping and ploughing tractor-implement unit in the longitudinal and vertical plane.

The interaction between the carrying tractor and the front- and rear-mounted agricultural implements is through the lower and central arms of the tractor's rear and front implement suspension mechanisms. When the unit travels in operation, the main (working) position of these mechanisms is floating. Therefore, when the tractor-implement unit moves performing the work process, we have every reason to ignore the angular oscillations of the front-mounted vegetation residue chopper and the rear-mounted plough. Their most notable rotation in the longitudinal and vertical plane could take place only in case the combined unit was negotiating rather high soil surface irregularities occurring at a sufficiently high rate. But, the probability of meeting such irregularities is minimal, because the macrorelief of the fields operated in the present-day agriculture is in most cases sufficiently even.

In view of the above, let's lay down the main assumptions to be used in the development of the analytical mathematical model of a combined tractor-implement unit designed on the basis of a ploughing and general-purpose tractor:

1. Since the angular oscillations of the process-related parts of the chopping and ploughing tractor-implement unit are insignificant, we assume that the sine and tangent of the small argument are approximately equal to the argument itself, while the cosine is equal to unity.

2. In order to simplify the solving of the set problem, it is most reasonable to set up the differential equations of the vertical oscillations of the chopping and ploughing tractor-implement unit individually for each of its segments (i.e. The tractor, the vegetation residue chopper and the plough). Their mutual influence on each other will be represented by forces that have equal magnitudes and opposite directions and are applied at the points of the instantaneous centres of turn of the tractor's front and rear implement suspension mechanisms.

3. The movement of the tractor as part of the chopping and ploughing unit is created by the right wheels in the furrow. Meanwhile, the inclination of the tractor in the longitudinal and transverse plane is taken into account by its positioning, with respect to the front-mounted vegetation residue chopper and the rear-mounted plough, on a horizontal plane, below the field surface by a half of the tilling depth. In that case, it is

possible to consider the vertical loads applied to the wheels on the same axle of the tractor as equal.

4. Further, we assume that during the working movement of the tractor-implement unit under consideration, the wheeled tractor retains its constant point contact with the soil surface, i.e. with the surface of the agricultural background.

5. Meanwhile, the variation of the soil surface irregularities is described by a stochastic stationary and ergodic function of the distance.

6. If the amplitude of the vertical variation of the longitudinal profile of the soil surface irregularities is insignificant, then it is possible to assume that the resisting forces in the pneumatic wheel tyres are proportionate to the variation velocity, while their resilient members have linear characteristics.

Following the made assumptions, we will first design the analytical mathematical model of vertical oscillations only for the carrying tractor. To solve this problem, we will examine a ploughing and general-purpose tractor as part of a chopping and ploughing tractor-implement unit, representing it by a separate equivalent schematic model (Fig. 2). The wheels of the tractor are represented by elastically damping models with the stiffness coefficients $C_{tT}$ of its tyres and the coefficients of resistance to deformation (damping) $K_{tT}$ of the tyres. Since the equivalent schematic model (Fig. 2) represents two wheels on each axle of the tractor, the said coefficients are doubled accordingly. Each of the tractor's wheels (front and rear ones) has a point contact with the soil surface and travels over its irregularities, the heights of which are denoted as follows: $h_1$ – for the irregularities under the front wheels of the tractor and $h_2$ – under the rear wheels of the tractor.
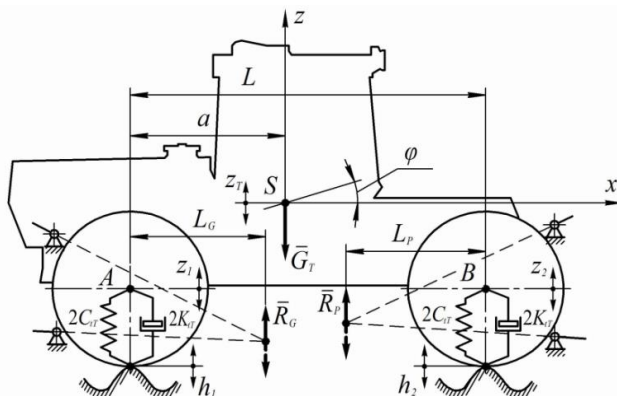


**Figure 2.** Equivalent schematic model of vertical oscillations of carrying tractor.

Now we are going to show in the equivalent schematic model all the forces that act on the tractor during its movement. In accordance with the assumptions described earlier, the action of the front-mounted vegetation residue chopper and the rear-mounted plough on the tractor will be represented by the reactions $\bar{R}_G$ and $\bar{R}_P$, localised at the points of instantaneous centre of turn of the front and rear implement suspension mechanisms of the tractor, respectively. The said reactions $\bar{R}_G$ and $\bar{R}_P$ are situated at a distance of $L_G$ and $L_P$ from the centre line of the front and rear axles of the tractor, respectively. The tractor is also subjected to the action of the force of its weight $\bar{G}_T$, localised at its centre

of mass (point S). The longitudinal base length of the tractor is denoted by $L$, while $a$ is the distance from the tractor's front axle to its centre of mass.

Let's define now the Cartesian coordinate system xSz in the equivalent schematic model, the origin of which coincides with the tractor's centre of mass (point S), the axis x is directed horizontally towards the tractor's traction wheels, the axis z – vertically upwards.

In the described representation, the analytical mathematical model of the tractor as part of the combined chopping and ploughing unit features two degrees of freedom: vertical oscillations $z_T$ of its centre of mass (point S) and angular oscillations $\varphi$ of the frame.

The differential equations of motion (oscillation) of the tractor in the longitudinal and vertical plane will be set up in the form of the Lagrange equations of the second kind as follows (Dreizler & Lüdde, 2010):

$$\frac{d}{dt}\left(\frac{\partial T_T}{\partial \dot{q}_i}\right) - \frac{\partial T_T}{\partial q_i} + \frac{\partial E_T}{\partial q_i} + \frac{\partial D_T}{\partial \dot{q}_i} = Q_i , \qquad (1)$$

where: $q_i$ – generalised coordinate ($i$ = 1, 2); $T_T$ – the tractor's kinetic energy; $E_T$ – the tractor's potential energy; $D_T$ – the tractor's energy dissipation function; $Q_i$ – generalised force.

Now we will determine the components of the expression (1).

First of all, the formula will be determined for the kinetic energy $T_T$ of the vertical oscillations of the tractor, and it will have the following form:

$$T_T = \frac{M_T \dot{z}_T^2 + J_T \dot{\varphi}^2}{2} , \qquad (2)$$

where: $M_T$ – the tractor's mass (kg); $J_T$ – the tractor's moment of inertia about the axis, which runs through its centre of mass (point S) and is normal to the longitudinal and vertical plane (kg m$^2$).

Further, let's determine the components of the expression (2). First of all, the generalised coordinates $z_T$ and $\varphi$ are in a certain manner related to the vertical displacements of the tractor's front and rear axles, i.e. to $z_1$ (point A) and $z_2$ (point B). Therefore, the said relation can be analytically represented by the following two functions:

$$z_T = \frac{z_1(L-a) + z_2 a}{L} , \qquad (3)$$

$$tan\varphi = \frac{z_2 - z_1}{L}, \qquad (4)$$

where $L$ and $a$ – longitudinal base length and longitudinal coordinate of the tractor's centre of mass (point S) (m).

Since we have $tan\varphi \approx \varphi$ for small angular displacements, which was described earlier, the expression (4) can be written down in a simplified form:

$$\varphi = \frac{z_2 - z_1}{L} , \qquad (5)$$

Further, after differentiating the expressions (3) and (5), we will obtain:

$$\dot{z}_T = \frac{\dot{z}_1(L-a) + \dot{z}_2 a}{L}, \tag{6}$$

$$\dot{\varphi} = \frac{\dot{z}_2 - \dot{z}_1}{L}. \tag{71}$$

After substituting the derivative values from (6) and (7) in expression (2), then carrying out the relevant transformations and denoting the coefficients $D_1$, $D_2$ and $D_3$, we will come to the expression for the tractor's kinetic energy in the following form:

$$T_T = \frac{D_1\dot{z}_1^2 + 2D_2\dot{z}_1\dot{z}_2 + D_3\dot{z}_2^2}{2}, \tag{8}$$

where: $D_1 = \dfrac{M_T(L-a)^2 + J_T}{L^2}$; $D_2 = \dfrac{M_T a(L-a) - J_T}{L^2}$; $D_3 = \dfrac{M_T a^2 + J_T}{L^2}$.

Now, let's perform operations in accordance with the original equation (1). As the tractor's kinetic energy $T_T$ depends only on the speed and does not depend on the generalised coordinate, so:

$$\frac{\partial T_T}{\partial q_i} = 0. \tag{9}$$

Thereafter, we will find the partial derivatives of the kinetic energy $T_T$ with respect to the velocities on the generalised coordinates, which will appear in the following form:

$$\frac{\partial T_T}{\partial \dot{z}_1} = D_1\dot{z}_1 + D_2\dot{z}_2, \tag{10}$$

$$\frac{\partial T_T}{\partial \dot{z}_2} = D_2\dot{z}_1 + D_3\dot{z}_2, \tag{11}$$

The partial time derivatives of the expressions (10) and (11) are determined as follows:

$$\frac{d}{dt}\frac{\partial T_T}{\partial \dot{z}_1} = D_1\ddot{z}_1 + D_2\ddot{z}_2, \tag{12}$$

$$\frac{d}{dt}\frac{\partial T_T}{\partial \dot{z}_2} = D_2\ddot{z}_1 + D_3\ddot{z}_2. \tag{13}$$

Further, we will find the tractor's potential energy $E_T$. It will be equal to the work of the elastic forces on the tractor's front and rear axles. The said elastic forces are functions of the deflection of the respective elastic members, i.e. the tyres of the wheeled tractor's running gear. If we denote the deflection of the front wheel by $z_{fw}$, and of the rear wheel $- z_{rw}$, measuring these values from the static state of equilibrium of the dynamic system under consideration, then their magnitudes can be determined as follows:

$$\left.\begin{array}{l} z_{fw} = z_1 - h_1, \\ z_{rw} = z_2 - h_2, \end{array}\right\} \tag{14}$$

where: $h_1$, $h_2$ – heights of the soil surface irregularities under the front and rear wheels of the tractor, respectively (m).

The time variable soil surface irregularity magnitudes $h_1$ and $h_2$ are just that perturbing factor originating from the agricultural background, which is the actual cause of the vertical oscillations of all segments of the tractor-implement unit under consideration.

The front and rear axle wheels of a ploughing and general-purpose tractor are equipped with identical wheels and also the tyres of each of the axles shown in the equivalent schematic model are in reality duplicated. Taking into account the above-said, the formula for finding the potential energy $E_T$ of the tractor will appear as follows:

$$E_T = C_{tT}\, z_{fw}^2 + C_{tT}\, z_{rw}^2 = C_{tT}\left(z_{fw}^2 + z_{rw}^2\right). \tag{15}$$

Taking into account the expressions (14), the potential energy $E_T$ of the tractor will have the following final representation:

$$E_T = C_{tT}\left(z_1^2 - 2z_1 h_1 + h_1^2 + z_2^2 - 2z_2 h_2 + h_2^2\right). \tag{16}$$

The partial derivatives of the potential energy $E_T$ will be as follows:

$$\frac{\partial E_T}{\partial z_1} = 2C_{tT}\left(z_1 - h_1\right), \tag{17}$$

$$\frac{\partial E_T}{\partial z_2} = 2C_{tT}\left(z_2 - h_2\right). \tag{18}$$

The tractor's energy dissipation function $D_T$ will be determined in terms of the resistance forces, which are proportionate to the displacement velocities. The said resistance forces are also caused by the wheel tyres of the tractor's running gear. As already mentioned for the case under consideration, i.e. for a ploughing and general-purpose tractor, the wheels on the front and rear axles have identical tyres shown doubled in the equivalent schematic model, hence the tractor's energy dissipation function $D_T$ will have the following form:

$$D_T = K_{tT}\, \dot{z}_{fw}^2 + K_{tT}\, \dot{z}_{rw}^2 = K_{tT}\left(\dot{z}_{fw}^2 + \dot{z}_{rw}^2\right). \tag{19}$$

In view of the system of equations (14), the expression (19) determining the dissipation function $D_T$ will finally appear as follows:

$$D_T = K_{tT}\left(\dot{z}_1^2 - 2\dot{z}_1 \dot{h}_1 + \dot{h}_1^2 + \dot{z}_2^2 - 2\dot{z}_2 \dot{h}_2 + \dot{h}_2^2\right). \tag{20}$$

Then, the partial derivatives for the dissipation function $D_T$ will be represented by the following expressions:

$$\frac{\partial D_T}{\partial \dot{z}_1} = 2K_{tT}\left(\dot{z}_1 - \dot{h}_1\right), \tag{21}$$

$$\frac{\partial D_T}{\partial \dot{z}_2} = 2K_{tT}\left(\dot{z}_2 - \dot{h}_2\right). \tag{22}$$

Now the only component that remains undefined in the expression (1) is the generalised forces $Q_i$. Since the analytical mathematical model of the tractor as part of the combined unit under consideration has two degrees of freedom, such generalised

forces will also be two.

In order to determine them, we are going to impart to the dynamic system the virtual displacement $\delta z_1$. At the same time, the displacement of the tractor's rear axle will be held at the zero level, hence $\delta z_2 = 0$. Then we have the following active forces that perform work on the mentioned virtual displacement of the system: $\bar{R}_G$ and $\bar{R}_P$.

Now we compute the sum of the amounts of work $\delta A$ by these forces on the virtual displacement of point A. It will be equal to:

$$\delta A = R_G \delta z_{(R_G)} + R_P \delta z_{(R_P)} - G_T \delta z_{(G_T)}, \tag{23}$$

where: $\delta z_{(R_G)}$, $\delta z_{(R_P)}$ and $\delta z_{(G_T)}$ – vertical displacements of the points of application of the forces $\bar{R}_G$, $\bar{R}_P$ and $\bar{G}_T$.

Taking into account the condition $\delta z_2 = 0$, we find from the expressions (6):

$$\delta z_{(G_T)} = \frac{\delta z_1 (L - a)}{L}. \tag{24}$$

Similar to that, we can write down:

$$\delta z_{(R_G)} = \frac{\delta z_1 (L - L_G)}{L}, \tag{25}$$

$$\delta z_{(R_P)} = \frac{\delta z_1 L_P}{L}. \tag{26}$$

As a result, the formula for determining the work by the forces $R_G$ and $R_P$ on the virtual displacement of the dynamic system $\delta z_1$ will appear as follows:

$$\delta A = \left[ \frac{R_G (L - L_G) + R_P L_P - G_T (L - a)}{L} \right] \delta z_1 \tag{27}$$

From the expression (27) we can derive the generalised force $Q_{z_1}$ causing the displacement $\delta z_1$. It will be equal to:

$$Q_{z_1} = \frac{R_G (L - L_G) + R_P L_P - G_T (L - a)}{L}. \tag{28}$$

Similarly, we determine also the second generalised force $Q_{z_2}$:

$$Q_{z_2} = \frac{R_G L_G + R_P (L - L_P) - G_T a}{L}. \tag{29}$$

Thus, we have found all components that constitute the expression (1), and it is possible to substitute them, perform the required transformations and obtain a system comprising the two differential equations of the forced oscillations of the ploughing and general-purpose tractor in the longitudinal and vertical plane, and this will just be the tractor's analytical mathematical model:

$$\left. \begin{array}{l} A_{11}\ddot{z}_1 + A_{12}\dot{z}_1 + A_{13}z_1 + A_{14}\ddot{z}_2 = f_{11}\dot{h}_1 + f_{12}h_1 + f_{13}, \\ A_{21}\ddot{z}_2 + A_{22}\dot{z}_2 + A_{23}z_2 + A_{24}\ddot{z}_1 = f_{21}\dot{h}_2 + f_{22}h_2 + f_{23}, \end{array} \right\} \tag{30}$$

where

$$A_{11} = \frac{M_T(L-a)^2 + J_T}{L^2} ; \quad A_{21} = \frac{M_T a^2 + J_T}{L^2} ; \quad A_{12} = 2K_{tT} ; \quad A_{22} = A_{12} ; \quad A_{13} = 2C_{tT} ;$$

$$A_{23} = A_{13} ; \quad A_{14} = \frac{M_T a(L-a) - J_T}{L^2} ; \quad A_{24} = A_{14} ; \quad f_{11} = f_{21} = A_{12} ; \quad f_{12} = f_{22} = A_{13} ;$$

$$f_{13} = \frac{R_G(L-L_G) + R_P L_P - G_T(L-a)}{L} ; \quad f_{23} = \frac{R_G L_G + R_P(L-L_P) - G_T a}{L} .$$

Hereafter, we are going to develop, in accordance with the earlier made assumptions, the analytical mathematical model of the vegetation residue chopper that is front-mounted on the tractor.

In order to analyse the tractor front-mounted vegetation residue chopper as a dynamic model, we will use, the same as in the previous case, its equivalent schematic model (Fig. 3). The chopper's centre of mass is represented by the point $S_G$, which is made the point of origin of the orthogonal Cartesian coordinate system $xS_Gz$, in which the axis x is directed horizontally to the right, the axis z – vertically upwards. The two support and gauge pneumatic-tyre wheels of the chopper are represented by elastically damping models shown in the equivalent schematic model as one wheel with the doubled coefficients of: stiffness $2C_{tG}$ and damping $2K_{tG}$. Now we have to denote the forces applied to the chopper in the longitudinal and vertical plane. These forces are: weight force $\bar{G}_G$ applied at the point $S_G$ and the force $\bar{R}_G$ generated by the implement-carrying tractor and applied at the point of the instantaneous centre of turn of its front implement suspension mechanism (the force has the same magnitude as the force already used in the consideration of the tractor's oscillations, but its direction is opposite). The vertical component of the force generated by the chopper's cutting unit when mowing the vegetation residues is ignored because of its insignificant magnitude.
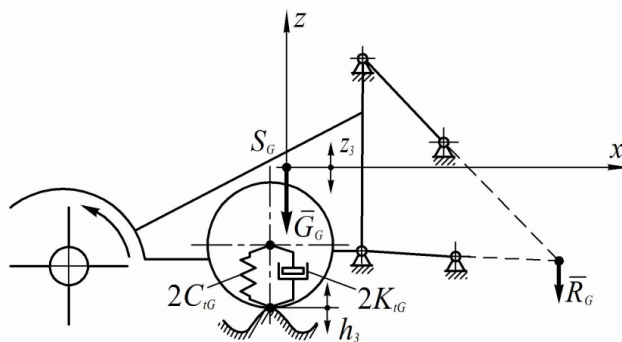


**Figure 3.** Equivalent schematic model of vertical oscillations of vegetation residue chopper front-mounted on tractor.

The chopper's gauge wheels also have point contacts with the soil surface irregularities, the height of which is denoted by $h_3$. The chopper has one degree of freedom in the longitudinal and vertical plane, which is the vertical displacement of its centre of mass (point $S_G$) – $z_3$. This vertical displacement can be regarded as the generalised coordinate $q_3$.

Using the original equations (1), we will set up the differential equations of motion (oscillation) of the vegetation residue chopper front-mounted on the carrying wheeled tractor. First of all, let's determine the chopper's kinetic energy $T_G$ and potential energy $E_G$. They are described by the following expressions:

$$T_G = \frac{M_G \dot{z}_3^2}{2},$$ (31)

$$E_G = C_{tG}\left(z_3 - h_3\right)^2,$$ (32)

where $M_G$ – mass of the vegetation residue chopper (kg).

The energy dissipation function $D_G$ for the chopper, which is directly proportional to the velocity of the vertical displacement of its centre of mass, is represented by such an expression:

$$D_T = K_{tG}\left(\dot{z}_3 - \dot{h}_3\right)^2.$$ (33)

Further, let's determine the generalised force. Since the analytical mathematical model of the vegetation residue chopper front-mounted on the tractor as part of the combined unit under consideration has one degree of freedom, we will have one generalised force $Q_{z_3}$.

First we will compute the sum of the amounts of work $\delta A$ by all active forces effective on the virtual displacement of point $S_G$. It will be equal to:

$$\delta A = -\left(R_G \delta z_3 + G_G \delta z_3\right).$$ (34)

The generalised force $Q_{z_3}$ determined by the expression (34), which causes the vertical displacements of the centre of mass (point $S_G$) of the chopper, will be equal to:

$$Q_{z_3} = -\left(R_G + G_G\right).$$ (35)

Now we will use the derived expressions (31)-(33) and (35). We will carry out the necessary transformations of them, then substitute them in the equation (1) and obtain the analytical mathematical model of the forced vertical oscillations of the vegetation residue chopper front-mounted on the carrying tractor in the following form:

$$A_{31}\ddot{z}_3 + A_{32}\dot{z}_3 + A_{33}z_3 = f_{31}\dot{h}_3 + f_{32}h_3 + f_{33},$$ (36)

where: $A_{31} = M_G$; $A_{32} = 2K_{tG}$; $A_{33} = 2C_{tG}$; $f_{31} = A_{32}$; $f_{32} = A_{33}$; $f_{33} = -\left(R_G + G_G\right)$.

Now, employing the earlier made assumptions, we are going to develop an analytical mathematical model for the rear-mounted plough.

Meanwhile, we should mention beforehand that the mounted plough as part of the combined unit can either feature a supporting ground wheel made in the form of a smooth steel wheel or it can be equipped with a supporting ground wheel that has a pneumatic tyre on its rim, the second of the options being currently widely used in the designs of state-of-the-art mounted ploughs (especially the gang / multi-furrow ones). In this latter case the rear-mounted plough of the discussed combined chopping and ploughing tractor-implement unit will during its operation have its own, independent vertical oscillations, which have to be taken into account as well. Therefore, we have developed

for the rear-mounted plough an equivalent schematic model, which contains the pneumatic-tyre ground support wheel. As in the previous cases, the wheel is represented by the elastically damping model, which is shown in the equivalent schematic model in the form of coefficients of stiffness $C_{tP}$ and damping $K_{tP}$ (Fig. 4). And again, the plough's pneumatic-tyre support wheel has point contacts with the soil surface irregularities, the height of which is denoted by $h_4$.
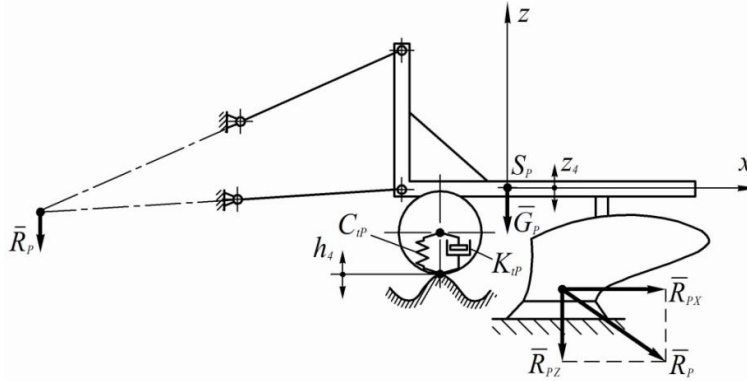


**Figure 4.** Equivalent schematic model of vertical oscillations of plough that is rear-mounted on tractor.

In the equivalent schematic model the centre of mass of the rear-mounted plough is represented by the point $S_P$, which is made the point of origin of the orthogonal Cartesian coordinate system $xS_Pz$, in which the axis x is horizontal and directed to the right, the axis z is directed upwards. The force applied at the mounted plough's centre of mass is the force of gravity $\bar{G}_P$. Another force, acting on the mounted plough in the longitudinal and vertical plane, is the force $\bar{R}_P$ – it is generated by the implement-carrying tractor and applied at the point of the instantaneous centre of turn of its rear implement suspension mechanism (the force has the same magnitude as the force already used in the consideration of the tractor's oscillations, but it has the opposite direction). Besides that, there is one more force acting in the said plane – the vertical component $\bar{R}_Z$ of the tractive resistance $\bar{R}_P$. When ploughs are tested, the horizontal component $\bar{R}_X$ of the tractive resistance is always determined. Since it is known that $\bar{R}_P = \bar{R}_X + \bar{R}_Z$ and according to the data in Macmillan (2002) $R_Z \approx 0,2R_X$.

In the longitudinal and vertical plane the rear-mounted plough also has one degree of freedom, which is the vertical displacement of its centre of mass (point $S_P$) – $z_4$. This vertical displacement of the plough's centre of mass can be regarded as the generalised coordinate $q_4$.

Now we are going to determine the plough's kinetic energy $T_P$ and potential energy $E_P$, as well as the dissipation function $D_P$ for the plough. They are described by the following expressions:

$$T_P = \frac{M_P \dot{z}_4^2}{2},\tag{37}$$

$$E_P = C_{tP}\left(z_4 - h_4\right)^2, \tag{38}$$

$$D_P = K_{tP}\left(\dot{z}_4 - \dot{h}_4\right)^2, \tag{39}$$

where $M_P$ – mass of the rear-mounted plough (kg).

To compute the generalised force $Q_{z_4}$ we will use the expressions similar to the ones presented earlier. Thus, the sum of the amounts of work $\delta A$ by all active forces effective on the virtual displacement of point $S_P$ will be equal to:

$$\delta A = -\left(R_P \delta z_4 + G_P \delta z_4 + R_{PZ} \delta z_4\right). \tag{40}$$

The generalised force $Q_{z_4}$ determined from the expression (40), which causes the vertical displacements of the plough's centre of mass (point $S_P$), will be equal to:

$$Q_{z_4} = -\left(R_P + G_P + R_{PZ}\right). \tag{41}$$

Using the derived expressions (37)-(39) and (41), after substituting them in the equation (1) and carrying out the necessary transformations, we will obtain the analytical mathematical model of the vertical oscillations of the rear-mounted plough in the following form:

$$A_{41}\ddot{z}_3 + A_{42}\dot{z}_4 + A_{43}z_4 = f_{41}\dot{h}_4 + f_{42}h_4 + f_{43}, \tag{42}$$

where

$$A_{41} = M_P; \ A_{42} = K_{tP}; \ A_{43} = C_{tP}; \ f_{41} = A_{42}; \ f_{42} = A_{43}; \ f_{43} = -\left(R_P + G_P + R_{PZ}\right).$$

The differential equation (42) describes the oscillatory motion of the rear-mounted plough in the longitudinal and vertical plane.

Hence, if we consolidate the differential equations of the vertical oscillations of the carrying tractor (30), front-mounted vegetation residue chopper (36) and rear-mounted plough (42), we will obtain the analytical mathematical model of the chopping and ploughing tractor-implement unit in the longitudinal and vertical plane:

$$\left.\begin{aligned}
A_{11}\ddot{z}_1 + A_{12}\dot{z}_1 + A_{13}z_1 + A_{14}\ddot{z}_2 &= f_{11}\dot{h}_1 + f_{12}h_1 + f_{13}, \\
A_{21}\ddot{z}_2 + A_{22}\dot{z}_2 + A_{23}z_2 + A_{24}\ddot{z}_1 &= f_{21}\dot{h}_2 + f_{22}h_2 + f_{23}, \\
A_{31}\ddot{z}_3 + A_{32}\dot{z}_3 + A_{33}z_3 &= f_{31}\dot{h}_3 + f_{32}h_3 + f_{33}, \\
A_{41}\ddot{z}_3 + A_{42}\dot{z}_4 + A_{43}z_4 &= f_{41}\dot{h}_4 + f_{42}h_4 + f_{43}.
\end{aligned}\right\} \tag{43}$$

The system of four differential equations (43) describes the process of vertical oscillations of the combined tractor-implement unit comprising a wheeled ploughing and general-purpose tractor, a rear-mounted plough and a front-mounted vegetation residue chopper, the constant coefficients of which were presented earlier.

The system of differential equations (43) in the presented form has the following input parameters:

1. Heights of the soil surface irregularities under the front $h_1$ and rear $h_2$ wheels of the carrying tractor, under the wheels of the vegetation residue chopper $h_3$ and under the wheel of the rear-mounted plough $h_4$;

2. The tractive resistance of the rear-mounted plough represented by its vertical component $R_{PZ}$;

3. Some design parameters of the combined tractor-implement unit under consideration represented by the coefficients $f_{14}$, $f_{24}$, $f_{34}$ and $f_{44}$.

The output parameters of the obtained system of differential equations (43) are the vertical displacements (amplitudes of oscillation) of the front $z_1$ and rear $z_2$ axles of the carrying tractor, the centre of mass of the front-mounted vegetation residue chopper $z_3$ and the centre of mass of the rear-mounted plough $z_4$.

If we carry out the Laplace transformation in the system of differential equations (43) by means of entering the operator $p = \dfrac{d}{dt}$, then we come to the presentation of the said system of differential equations in the operator form as follows:

$$\left.\begin{array}{l} K_{11}z_1\left(p\right) + K_{12}z_2\left(p\right) = F_{11}h_1\left(p\right) + F_{15}R_Z\left(p\right) + F_{16}, \\ K_{21}z_1\left(p\right) + K_{22}z_2\left(p\right) = F_{22}h_2\left(p\right) + F_{25}R_Z\left(p\right) + F_{26}, \\ K_{33}z_3\left(p\right) = F_{33}h_3\left(p\right) + F_{36}, \\ K_{44}z_4\left(p\right) = F_{44}h_4\left(p\right) + F_{45}R_Z\left(p\right) + F_{46}. \end{array}\right\} \tag{44}$$

where

$K_{11} = A_{11}p^2 + A_{12}p + A_{13}$;　　$K_{12} = A_{14}p^2$;　　$K_{21} = A_{24}p^2$;　　$K_{22} = A_{21}p^2 + A_{22}p + A_{23}$;

$K_{33} = A_{31}p^2 + A_{32}p + A_{33}$;　$K_{44} = A_{41}p^2 + A_{42}p + A_{43}$;　$F_{11} = f_{11}p + f_{12}$;　$F_{15} = f_{13}$;　$F_{16} = f_{14}$;

$F_{22} = f_{21}p + f_{22}$;　$F_{25} = f_{23}$;　$F_{26} = f_{24}$;　$F_{33} = f_{31}p + f_{32}$;　$K_{36} = f_{34}$;　$F_{44} = f_{41}p + f_{42}$;

$F_{45} = f_{43}$;　$F_{46} = f_{44}$.

Thus, the system of differential equations (44) in the presented form represents the analytical mathematical model of the combined chopping and ploughing tractor-implement unit.

## RESULTS AND DISCUSSIONS

The effect that the arrangement and parameters of the chopping and ploughing tractor-implement unit have on the smoothness of its movements in the longitudinal and vertical plane can be evaluated with the use of the amplitude and phase frequency characteristics that describe the response of the dynamic system under consideration to external perturbations. In this case, such perturbations are:

1. Variation of the height of soil surface irregularities under the front wheels of the tractor – $h_1$;

2. Variation of the height of soil surface irregularities under the rear wheels of the tractor – $h_2$;

3. Variation of the height of soil surface irregularities under the wheels of the chopper – $h_3$;

4. Variation of the height of soil surface irregularities under the pneumatic-tyre support wheel of the plough – $h_4$;

5. Variation of the rear-mounted plough's tractive resistance represented by its vertical component – $R_{PZ}$.

After a computer programme was developed for the PC-assisted numerical computation of the obtained system of equations in the operator form (44), calculations were carried out, the results of which allowed plotting the graphs of the amplitude frequency response and phase frequency response characteristics. Subsequently, their values were compared with the most desired values. For this purpose, similar characteristics of the ideal follow-up dynamic systems were taken as the desired ones. It is to be pointed out that, when such ideal dynamic systems respond to external perturbations, the amplitude frequency response in the operating range shall tend to zero, while their phase frequency response vice versa – to infinity. Accordingly, those amplitude frequency response and phase frequency response characteristics obtained for the unit under consideration, which are the closest to the desired ones, will be the most suitable for the evaluation of the efficiency of the dynamics and the design.

Following the data obtained from the laboratory and field experimental investigations that we carried out earlier and the PC-assisted processing of its results with the use of statistical methods, it has been determined that the main spectrum of dispersions of the soil surface profile irregularity variation is located in a sufficiently wide frequency range of $0...15$ m$^{-1}$. The argument of this normalised spectral density is the frequency $\omega$ in m$^{-1}$ (Fig. 5, a). Further, we carry out the transition to the argument $t$ (s), and as a result we obtain the normalised spectral density of the soil surface profile irregularity variation – its graph is presented in Fig. 5, b.
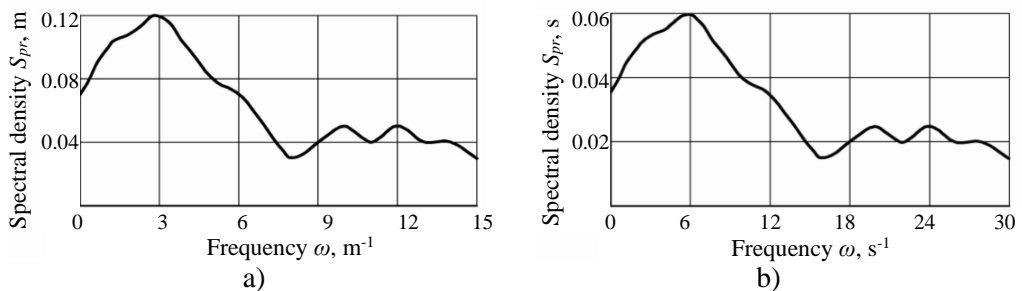


**Figure 5.** Normalised spectral density $S_{pr}$ of variation of longitudinal soil surface irregularity profile as function of frequency $\omega$ (a) and time $t$ (b).

Analysing the data in Fig. 5 b, one can see that the working range of frequencies for such an input parameter as the variation of soil surface irregularities is $0...30$ s$^{-1}$, and this is the range that we are going to use in our subsequent analytical investigations.

First of all, let's investigate the dynamics of the vertical oscillations of the front axle of the tractor during its travelling as part of the chopping and ploughing unit. Doing that, the design amplitude and phase frequency response characteristics will be analysed, as we pointed out earlier, in that frequency range, where virtually all the dispersion of the agricultural background irregularity variation is located, i.e. within $0...30$ s$^{-1}$ (Fig. 5).

The results of the PC-assisted calculations have made it possible to determine the effect the elastic properties of the pneumatic tyres on the wheels of the carrying tractor, the support and gauge wheels of the vegetation residue chopper and the ground support wheels of the rear-mounted plough have on the smoothness of the movements of the combined tractor-implement unit under consideration.

The results of the performed calculations have shown that the increase of the stiffness coefficients of the pneumatic tyres on the wheels of the components of the combined tractor-implement unit improves the unit's response to the perturbing actions. This is most evident in the graph of the amplitude frequency response characteristic for the tractor's front axle (Fig. 6).
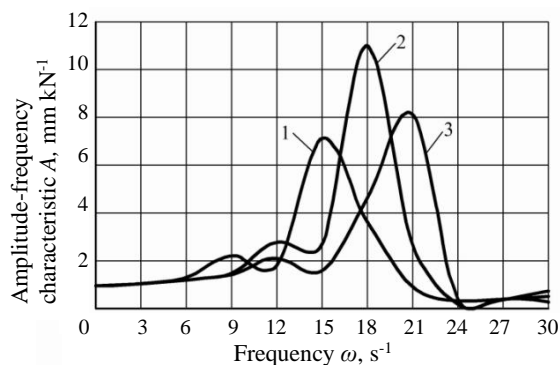


**Figure 6.** Amplitude frequency response characteristic of vertical oscillations of front axle of tractor, when it responds to variation of soil surface profile at different stiffness coefficients of tyres on its wheels $C_{tT}$: 1 – 250 kN m$^{-1}$; 2 – 350 kN m$^{-1}$; 3 – 450 kN m$^{-1}$.

It can be seen in the graphs in Fig. 6 that, when the value of $C_{tT}$ increases from 250 kN m$^{-1}$ to 450 kN m$^{-1}$, the amplitude frequency response characteristics decrease, which is the most desired effect, while the resonance peaks shift towards the higher frequencies of variation of the longitudinal soil surface profile irregularities. The effect is explained by the fact that the increase of the coefficient $C_{tT}$ is followed by the decrease of the elastic properties of the pneumatic tyres on the wheels. As a result, this dynamic segment responds to the input signal with a smaller gain. But, it is apparent that this type of behaviour of the amplitude frequency response characteristics takes place, when $\omega > 12$ s$^{-1}$ or almost 12 Hz.

The lag of the unit's response to the perturbing action depends little on the magnitudes of the stiffness coefficients of the tractor's wheel tyres. Within a perturbing action variation frequency range of $0...9$ s$^{-1}$ there is virtually no difference between the obtained phase shifts on the phase frequency response characteristics (Fig. 7).
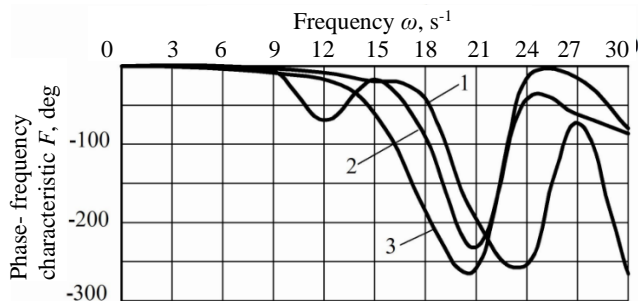


**Figure 7.** Phase frequency response characteristics of vertical oscillations of front axle of tractor, when it responds to variation of soil surface profile at different stiffness coefficients of tyres on its wheels $C_{tT}$: 1 – 250 kN m$^{-1}$; 2 – 350 kN m$^{-1}$; 3 – 450 kN m$^{-1}$.

At this point, it is also to be noted that, according to the results of our study, the stiffness coefficient $C_{tT}$ of the pneumatic tyres on the rear wheels of the carrying tractor, the same as with its front wheels, has the similar effect on the dynamics of the vertical oscillations of the power unit of the combined tractor-implement unit under consideration.

However, it has been found that, unlike the stiffness of the front and rear wheels of the carrying tractor, the coefficients of resistance to deformation $K_{tT}$ of the pneumatic tyres on its wheels have little effect on the smoothness of motion of the chopping and ploughing tractor-implement unit.

There is one very important point in the study – determination of the extent, to which the oscillations of the tractor's front and rear axles influence each other. The analytical amplitude frequency response characteristics show that the dynamics of their vertical displacements are independent. Thus, when the variation of the soil surface irregularity profile under the front wheels of the tractor stipulate the respective response of its front axle, the same variation has virtually no effect on the dynamics of the vertical displacements of the wheels on the rear axle (Fig. 8). Even in the resonance condition at $\omega = 12$ s$^{-1}$ (Fig. 8) the size of the amplitude frequency response characteristic under consideration is so small that does not exceed a value of 0.04.

The nature of the vertical displacements of the front-mounted vegetation residue chopper, while being independent of the tractor's oscillations, depends on the implement's own certain design parameters. This includes, first of all, the stiffness coefficient $C_{tG}$ of the support wheel tyres.
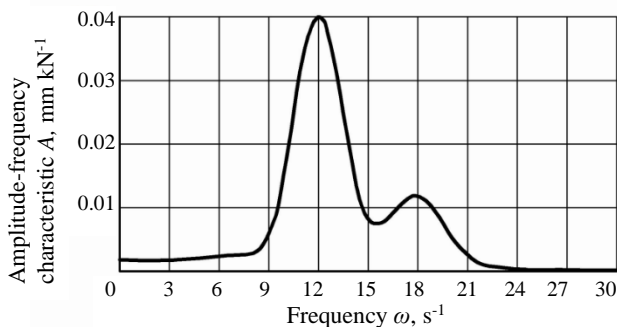


**Figure 8.** Amplitude frequency response characteristic of oscillations of tractor's rear axle, when it responds to variation of soil surface profile under tractor's front wheels.

For each examined value of this parameter, when we increase the frequency of soil surface irregularity profile variation, the amplitude frequency response characteristics of the chopper's vertical oscillations first grow, then, after reaching their maximum, they decrease, which is much desired (Fig. 9).

Within the range of frequencies $\omega = 0...16$ s$^{-1}$ (i.e. where the major share of the dispersion of soil surface profile variation is located, Fig. 5) this decrease is achieved through the increase of the coefficient $C_{tG}$ value from 100 kN m$^{-1}$ to 150 kN m$^{-1}$. In practice there is no need to apply greater values of $C_{tG}$, since the amplitude frequency response characteristic in a frequency range of $\omega = 0...16$ s$^{-1}$ decreases in that event insignificantly (curve 4, Fig. 9). At the same time, it is inexpedient to set the value of the

coefficient $C_{tG}$ below 100 kN m$^{-1}$, since in that case the respective amplitude frequency response characteristic increases, which is undesirable (curve 1, Fig. 9).



**Figure 9.** Amplitude frequency response characteristics of vertical oscillations of chopper's frame, when it responds to variation of soil surface profile at different tyre stiffness coefficients $C_{tG}$: 1 – 50 kN m$^{-1}$; 2 – 100 kN m$^{-1}$; 3 – 150 kN m$^{-1}$; 4 – 200 kN m$^{-1}$.

The second design parameter that has an effect on the dynamics of the vegetation residue chopper's vertical oscillations is its operating mass $M_G$. Its increase from 300 kg to 500 kg results in the undesirable increase of the amplitude frequency characteristic of the chopper's response to the field profile variation (curve 2, Fig. 10).
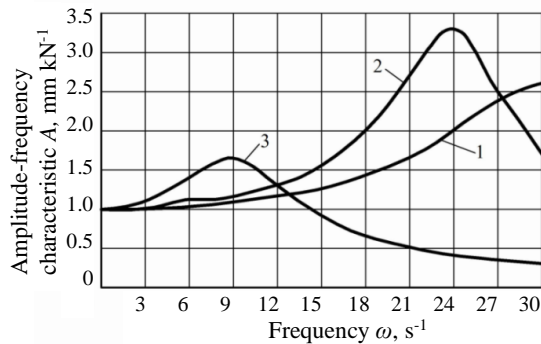


**Figure 10.** Amplitude frequency response characteristic of vertical oscillations of chopper's frame, when it responds to soil surface profile variation at different masses $M_G$ and tyre stiffness coefficients $C_{tG}$: 1 – $M_G$ = 300 kg; $C_{tG}$ = 150 kN m$^{-1}$; 2 – $M_G$ = 500 kg; $C_{tG}$ = 150 kN m$^{-1}$; 3 – $M_G$ = 300 kg; $C_{tG}$ = 25 kN m$^{-1}$.

And that result cannot be remedied even by a substantial reduction of the stiffness coefficient $C_{tG}$ of the pneumatic tyres of the front-mounted implement under consideration to a level of 25 kN m$^{-1}$. On the one hand, the amplitude frequency response characteristic decreases, at frequencies of $\omega > 14$ s$^{-1}$ it even falls below unity (curve 3, Fig. 10). But, on the other hand, at the soil surface profile variation frequencies, which are significant for the unit's operation, i.e. within $\omega = 0...9$ s$^{-1}$, the magnitude of this characteristic exceeds to a considerable extent the value that is characteristic of the vertical oscillations of the chopper with a mass $M_G$ equal to 300 kg (curve 1, Fig. 10).

Hence, we come to the conclusion that it is inadvisable to increase the operating mass $M_G$ of the front-mounted vegetation residue chopper.

The next important point in the analytical study is to determine, how the chopping and ploughing unit's motion smoothness depends on the variation of the plough's tractive resistance $\bar{R}_{PX}$. To that end, we need first of all know the underlying structure of the force $\bar{R}_{PX}$ variation process. This information, as we know, is contained in its correlation function and spectral density.

The analysis of the experimental data, which we obtained earlier, shows that the variation of the plough's tractive resistance has non-periodic and relatively high frequency nature. The average duration of the correlation dependence for the process of variation of this parameter is approximately 1.6 s (Fig. 11, a).



a)                                      b)
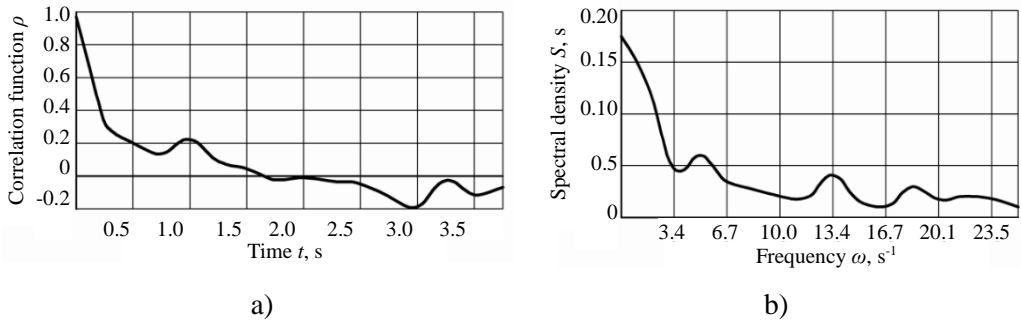
**Figure 11.** Normalised correlation function (a) and normalised spectral density (b) of variation of tractive resistance of plough as part of chopping and ploughing tractor-implement unit.

The frequency range of dispersion of the tilling tool tractive resistance variation is in this case equal to $0...25.0$ s$^{-1}$ (fig. 11, b). But, since the main part of this statistical characteristic falls within a frequency range of $0...15$ s$^{-1}$, our further analysis will be done within just that range.

We start with the assessment of how the variation of the plough's tractive resistance affects the smoothness of motion of the tractor's rear axle at different values of its tyres' stiffness coefficient $C_{tG}$. Within a frequency range of $\omega = 0...6$ s$^{-1}$ for the variation of the force $\bar{R}_{PX}$, the amplitude of the vertical displacements of the tractor's rear axle is virtually independent of the variation of the value $C_{tG}$ (Fig. 12).



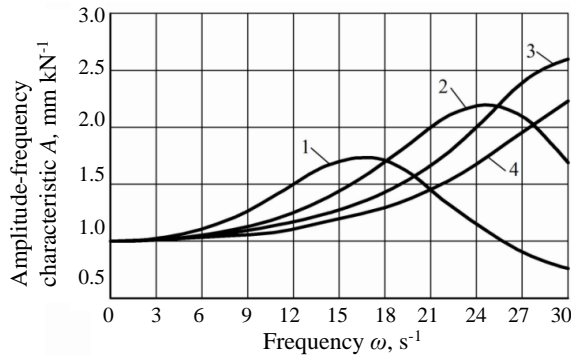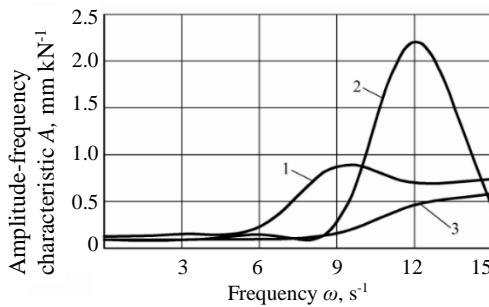**Figure 12.** Amplitude frequency response characteristic of vertical oscillations of tractor's rear axle, when it responds to variation of rear-mounted plough's tractive resistance at different coefficients $C_{tP}$: 1 – 250 kN m$^{-1}$; 2 – 350 kN m$^{-1}$; 3 – 450 kN m$^{-1}$.

Outside the said frequency range, the following trend is observed: the greater the value of the coefficient $C_{TP}$ is, the less the tractor's axle responds to the plough's tractive resistance variation. I.e. The harder the pneumatic tyre is, the lower its elastic properties are and, respectively, the lower the amplitude of its deflection in response to the impact of the perturbing factor, i.e. The variation of the force $\bar{P}_{PX}$, is.

Finally, we have investigated the response of the rear-mounted plough to the variation of its own tractive resistance. The analysis of amplitude frequency response characteristics (Fig. 13) has shown that the reduction of the stiffness $C_{tP}$ of the pneumatic tyre on its ground support wheel results in the deterioration of the tractor's motion dynamics in the longitudinal and vertical plane. This is especially noticeable, when the coefficient of stiffness $C_{tP}$ is equal to 100 kN m$^{-1}$ (curve 1, Fig. 13).
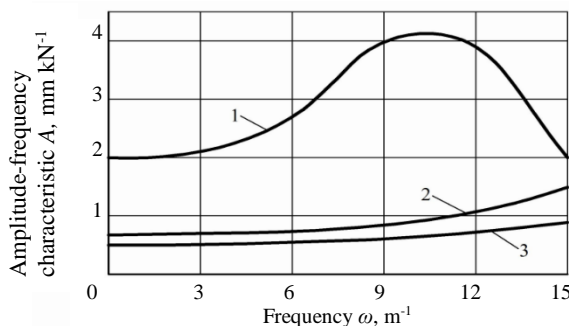


**Figure 13.** Amplitude frequency response characteristic of vertical oscillations of plough, when it responds to variation of its own tractive resistance at different coefficients of stiffness $C_{tP}$ of tyre on its ground support wheel: 1 – 100 kN m$^{-1}$; 2 – 150 kN m$^{-1}$; 3 – 200 kN m$^{-1}$.

Following the results of the analysis of Fig. 13, the coefficient $C_{tP}$ of the tyre on the plough's pneumatic-tyre support wheel shall be not less than 150 kN m$^{-1}$. At its lower values (curve 1, Fig. 13) an undesirable and, besides, considerable increase of the amplitude frequency response characteristic is observed, while this characteristic indicates the smoothness of the tractor's travel as function of its tractive resistance variation.

## CONCLUSIONS

1. An equivalent schematic model has been developed for the new design of the chopping and ploughing tractor-implement unit, including three components of the dynamic system under consideration, to which the active forces are applied as well as the perturbing actions in the form of the given soil surface irregularities. The pneumatic-tyre wheels of the running gear have been approximated by elastically damping models, the linear and angular parameters have been defined.

2. Basing on the use of the original dynamic equations in the form of the Lagrange equations of the second kind, the defined generalised coordinates and the expressions for the kinetic energy, potential energy and dissipation function, a system of differential equations has been obtained, which describes the vertical oscillations of the combined tractor-implement unit under consideration.

3. The amplitude and phase frequency response characteristics of the unit have been computed on the basis of the obtained differential equations of its vertical

oscillations. Their analysis has shown that, in order to improve the smoothness (stability) of motion of the Class 3 tractor, the coefficient of stiffness of the tyres on its running wheels has to be increased to a value of 450 kN m$^{-1}$. In that case, the amplitude frequency response characteristics representing the response of the tractor to the perturbing actions, decrease, which is desired, while their maximum values shift towards higher frequencies, which means lower dispersions of the soil surface profile variation. At the same time, the phase frequency response characteristics representing the lag in the tractor's response to the external perturbing actions change only little.

4. Within a frequency range of $\omega = 0\ldots16$ s$^{-1}$, where the main spectrum of the field profile variation frequencies is located (and that is typical for most fields), the coefficient of stiffness of the tyres on the support wheels of the vegetation residue chopper and the tyre on the support wheel of the rear-mounted plough shall be at a level of 150 kN m$^{-1}$. It follows from the analysis of the amplitude frequency response characteristics that the compliance with this requirement ensures the lowest impact made by these implements on the dynamics of the tractor's vertical oscillations during its operation as part of the combined chopping and ploughing unit under consideration.

5. In order to achieve the sufficient smoothness (stability) of the tractor's motion, the operating mass of the front-mounted vegetation residue chopper should not be increased. Otherwise, the amplitude frequency response characteristics of the carrying tractor's vertical oscillations show undesirable increase to such an extent that this cannot be remedied even by a six-fold (from 150 to 25 kN m$^{-1}$) reduction of the coefficient of stiffness of the tyres on the support wheels of the front-mounted chopper.

6. The developed methodology of generating an analytical mathematical model for the combined tractor-implement unit under consideration can be used in the research into the dynamics of other agricultural implements and tractor-implement units.

## REFERENCES

Dreizler, R.M. & Lüdde, C.S. 2010. *Theoretical Mechanics*. Springer, 402 pp.

Gyachev, L.V. 1981. Dynamic stability of agricultural implements and units. Moscow, 206 p.

Karkee, M. 2009. Modelling, identification and analysis of factor and single axle towed implement system. Graduate Theses and Dissertations. Paper 10875. Iowa State University, 246 pp.

Larson, D.L., Smith, D.W. & Liljedahl, J.B. 1976. Dynamics of three-dimensional tractor motion. *Transactions of the American Society of Agricultural Engineers* **19**(1), 195–200.

Li, Z., Mitsuoka, M., Inoue, E., Okayasu, T., Hirai, Y., & Zhu, Z. 2015. Modification of a tractor dynamic model considering the rotatable front end. *Journal of the Agriculture, Kyushu University* **60**(1), 219–224.

Macmillan, R.H. 2002. The Mechanics of Tractor – Implement Performance. Theory and Worked Examples. University of Melbourne, 165 pp.

Mircea, N. & Nicolae, I. 2014. Study on the dynamic interaction between agricultural tractor and trailer during braking using Lagrange equation. *Applied Mechanic and Materials* **659**, 515–520.

Mitsuoka, M., Fukushima, T., Okayasu, T., Ioue, E. & Okuda, Y. 2008. Investigation of nonlinear vibration characteristics of the half-track tractor. *Proceedings of the 4$^{th}$ international symposium on machinery and mechatronics for agriculture and Biosystems engineering* (ISMAB), Taichung, Taiwan.

Nadykto, V., Arak, M. & Olt, J. 2014. Theoretical research into the frictional slipping of wheel-type undercarriage taking into account the limitation of their impact on the soil. *Agronomy Research* **13**(1), 148–157.

Pădureanu, V., Lupu, M.I. & Vanja, C.M. 2013. Theoretical research to improve traction performance of wheeled tractors by using supplementary driven axle. *Proceedings of the 5th Int. Conf. 'Computational Mechanics and Virtual Engineering'*, 24-25 October, Brasov, Romania, pp. 410–415.

Rabbani, M.A., Tsujimoto, T., Mitsuoka, M., Inoue, E. & Okayasu, T. 2011. Prediction of the vibration characteristics of half-track tractor considering a three-dimensional dynamic model. *Biosystem Engineering* **110**(2), 178–188.

Vasilenko, P.M. 1996. Introduction in agricultural mechanics. Selhošobrazovanije, 252 p.

Vasilenko, P.M. 1968. On the dynamic equations of systems with non-holonomic constraints. Agricultural mechanics. Moskow, pp. 26–34.

Vasilenko, P.M. 1962. On the methods of mechanical and mathematical studies in the development of agricultural equipment. Technical Information Bulletin, Moskow: GOSNITI, 230 pp.

Xu, H., Zhang, Y., Liu, H., Qi, S., Li, W. 2015. Effects of configuration parameters on lateral dynamics of tractor-two trailer combination. *Advances in Mechanical Engineering*, **7**(11).

# Theory of the oscillations of a toothed disc opener during its movement across irregularities of the soil surface

V. Bulgakov[1], V. Adamchuk[2], V. Gorobey[2] and J. Olt[3,*]

[1]National University of Life and Environmental Sciences of Ukraine, 15, Heroyiv Oborony Str., UK 03041 Kyiv, Ukraine
[2]National Scientific Centre, Institute for Agricultural Engineering and Electrification, 11, Vokzalna Str., Glevaкha-1, Vasylkiv District, UK 08631 Kiev Region, Ukraine
[3]Estonian University of Life Sciences, Kreutzwaldi 56, EE51014 Tartu, Estonia
*Correspondence: jyri.olt@emu.ee

**Abstract.** The paper presents the main provisions of the new theory of oscillations of the versatile combined opener assembly of the breeding seed drill with a spring-suspended furrow opening toothed disc in the vertical longitudinal plane during its movement across irregularities of the soil surface. Basing on the improved design of the opener assembly, an equivalent schematic model has been developed, which takes into account the forces applied to the structural components of the opener, forces in the springs as well as the reaction of the soil acting on the toothed disc, the hoe-type seed conductor and the packing wheel. The system of differential equations has been set up, which describes the movement of the opener across irregularities of the soil surface depending on the opener's design parameters and the kinematic modes of performing the drilling work process. The derived mathematical model makes it possible to determine the amplitudes and frequencies of the translational oscillations of the device in order to assess their impact on the drilling work process. The developed theory provides also tools for the assessment and lowering of the energy characteristics of the versatile breeding seed drill related to the oscillating movements of its openers in soil.

**Key words:** seed drill, combined opener, toothed disc, oscillations, frequency.

## INTRODUCTION

The present-day intensive energy-efficient technologies of production of cereals and other agricultural crops make it necessary to carry out agronomical research studies with the use of breeding seed drills. And these studies have to be done as under the standard breeding experiment conditions so dropping the breeding material with minimal tillage or even without any preparation of the soil before drilling. This makes the application of openers with various design features, capable of performing the drilling work process with proper quality under various conditions, one of the key issues (Chaudhuri, 2001; Hasimu & Chen, 2014; Lin et al., 2014).

The SS-16 (SN-16) tractor-mounted breeding grain drill with a mechanical seed-feeding unit is widely used today, but it has some disadvantages, the main of which is the underdevelopment of its opener assemblies, which is especially notable, when the use of the drill entails the considerable consumption of power.

Thus, the development of versatile improved openers (opener assemblies) for breeding seed drills (along with general purpose seed drills), the justification of their design and kinematic parameters with the aim of reducing the power consumption and improving the quality of operation are of great theoretical and practical importance (Jingling et al., 2011; Liu & Ma, 2013).

Double-disc, runner and hoe-type openers supplied as standard equipment with the most popular breeding grain drills are widely used for various cereal drilling technologies employed in breeding experiments (Vamerali et al., 2006; Karayel & Özmerzi, 2007; Altikat et al., 2013). While more and more publications have recently been appearing about the research into the direct drilling (including the pedigree seed drilling), specifically into soil mulched with plant residues (Karayel, 2009; Bai et al., 2014; Šarauskis & Vaitauskiene, 2014).

One of the ways to extend the area of application of seed drills, including breeding ones, is the utilisation of the capabilities of different types of opener groups delivering the high quality sowing of cereals under various tillage systems. The wide application of diverse opener design features, such as solid disc coulters, turbo coulters, coulters with wavy and serrated surfaces is stipulated by the quality of tillage (Chen et al., 2004; Karayel & Özmerzi, 2007; Bianchini & Magalhães, 2008; Lian et al., 2012).

Quite a number of literary sources, starting from the first publications (Turbin et al., 1967), have been concerned with the oscillations of opener assemblies during the movement of their discs in the soil. It is obvious that the vibration processes of interaction between the implements and the soil provide, first of all, reduction of the coefficient of internal friction between the soil particles, the draught resistance of the soil to the vibrating implement is considerably reduced (Endrerud, 1999). For example, the use of oscillating digging out implements on beet harvesters reduces the draught resistance during their movement by 26–53% on the average (Prisyazhnyuk et al., 2013).

Moreover, theoretical research has been made into the operation of individual mechanisms of opener assemblies, in particular, studies have been carried out to find out the variation of the penetration force exerted by the spring suspension mechanism, depending on the position of the operating area of the opener suspension arm (Belov & Belov, 2007). Within these studies, the pattern of movements, the scheme for determining the tooth setting angle and blade shape have been developed, mathematical models have been put forth for the estimation of the optimal parameters of opener groups (Lisoviy, 2013). Nevertheless, the mentioned studies leave out of account the energy component rising from the vibration processes during the work of openers.

Reduction of the energy consumption in the work process of operation of the breeding grain drill through the utilisation of the vibration effect caused by the interaction of implements with the soil, by the theoretical justification of the rational design and kinematic parameters of the toothed disc opener assemblies.

## MATERIALS AND METHODS

The research has been carried out with the use of the analytical method of the generation of mathematical models of machines and process operations, which is based on the laws of theoretical mechanics and higher mathematics. The derived analytical dependencies can be solved on PCs with the use of the prepared computer programmes. We have developed the improved opener assembly with arm-and-spring suspension-

mounted implements, the configuration of which is composed in accordance with the pedigree seed planting technology selected for the breeding grain drill.

The developed new opener assembly (Fig. 1) has furrow opening toothed disc 1 mounted freely on the axle at the end of rod fastened at the lower end of the bracket attached to spar 2, which is pivotally connected to draw-bar 3. Meanwhile, draw-bar 3 is also attached at its front part through a cylindrical hinge to the seed drill's square beam 4. Draw-bar 3 is also linked to the seed drill's frame via pressure spring 5. Behind furrow opening toothed disc 1 (in one plane with the disc) hoe-type seed conductor 6 is installed on spar 2. At the rear end of spar 2, packing wheel 7 is installed, while its forward end is equipped with spring assembly 8 producing vibration during the motion in soil. The depth of running in soil of the opener assembly's furrow opening toothed disc 1 is adjusted by changing the position of packing wheel 7 with the use of adjustment device 9. The teeth of disc 1 in its front part are pointing upwards, i.e. they are tilted against the direction, in which disc 1 rotates due to its engagement with the soil. This tilt ensures the release of the soil and plant residues stuck to the disc, when they arrive to the rear part of disc 1, and this release is also facilitated by cleaning device 10 in the plane of disc 1.
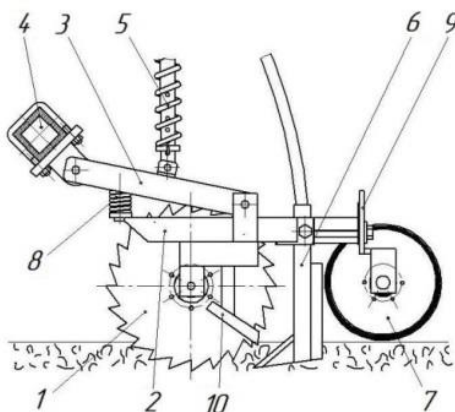


**Figure 1.** A scheme of combined opener assembly: 1 – tooted disc, 2 – spar, 3 – draw-bar, 4 – square beam, 5 – pressure spring, 6 – hoe-type seed conductor, 7 – packing wheel,  – spring assembly, 9 – adjustment device, 10 – cleaning device.

Furrow opening toothed disc 1 has a distinctive feature, which is the special V-notches equally spaced along its circumference with one side of each notch aligned radially and the other side aligned at an angle to the radius and accordingly to the radial cutting edge of the notch (Magalhães et al., 2007).

For the analytical treatment of the operation of the improved design opener assembly we have to turn from its design and process schematic model to its equivalent schematic model. In the equivalent schematic model (Fig. 2) furrow opening toothed disc 10 is situated at the end of rod 9 and mounted freely rotating on the axle. Rod 9 is fastened to spar 8, mounted on draw-bar 5 with the use of a cylindrical hinge, while this draw-bar in its turn is hinge-mounted on draw-bar beam 1 of the breeding seed drill. The draw-bar is additionally connected with the breeding seed drill's frame through spring 3 and pressure rod pivot journal 2. Also, one end of spar 8 is connected with draw-bar 5

by spring 7, while hoe-type seed conductor 11 and packing wheel 12 are attached to its other end. The teeth of furrow opening toothed disc 10 are tilted contrary to the disc's sense of rotation (caused by its engagement with the soil), which speeds up the release of plant residues from the disc.



**Figure 2.** Theoretical schematic model of the improved design toothed disc opener assembly: 1 – breeding seed drill's draw-bar beam, 2 – pressure rod pivot journal, 3 – pressure spring, 4 – pressure rod, 5 – draw-bar, 6 – vibrator rod, 7 – vibrator spring, 8 – spar, 9 – rod, 10 – toothed disc, 11 – hoe-type seed conductor, 12 – packing wheel.

To generate the differential equations describing the translational oscillating movements of the toothed disc opener assembly during its movement across irregularities of the soil surface it is necessary first to analyse and assume the pattern of forces acting on the opener assembly in the process of its movement. For this purpose we will use the approach described in (Vasilenko, 1996). To generate an equivalent schematic model, it is necessary first to decide on the necessary assumptions (Prisyazhnyuk et al., 2013). Thus, the examined movement of the toothed disc opener assembly takes place only in the vertical longitudinal plane. The seed drill, where the opener assembly is mounted, moves uniformly along a straight line. The soil surface irregularities crossed by the toothed disc in its movement can be approximated by a harmonic function. The forces applied to the components of the examined system can be represented by point forces.

Basing on the design features of the improved toothed disc opener assembly as well as the above-said assumptions, the equivalent schematic model (combined with the process layout) has the representation shown in Fig. 2.

## RESULTS

First of all, we have to designate in the equivalent schematic model the forces of weights of the main structural components in the improved design of the toothed disc opener assembly. They are:

$\bar{G}_n$ – force of weight of the draw-bar;

$\bar{G}_d$ – force of weight of the toothed disc;

$\bar{G}_л$ – force of weight of the spar;

$\bar{G}_a$ – force of weight of the hoe-type seed conductor;

$\bar{G}_к$ – force of weight of the packing wheel.

Accordingly, the masses of the listed structural components will be designated as $m_n$, $m_д$, $m_л$, $m_a$ and $m_к$. Now, the tension forces in the first and second springs are designated in the equivalent schematic model: $\bar{F}_{n1}$ and $\bar{F}_{n2}$ , respectively.

Apparently, these tension forces will have the following values:

$$F_{n1} = C_{n1}\, l_{n1},$$
$$F_{n2} = C_{n2}\, y, \tag{1}$$

where: $C_{n1}$, $C_{n2}$ – deflection rates of the first and second springs, respectively, (N m$^{-1}$); $l_{n1}$, $y$ – deflections of these springs (m). Force $\bar{F}_{n1}$ can be considered at a first approximation as having a constant value.

It is obvious that the action of the forces of weights of the opener assembly structural components and the forces exerted by the springs results in the generation of support reactions by the soil, which act on the toothed disc, hoe-type seed conductor and packing wheel.

We assume that the profile line of the travel (irregularities of the soil surface) changes by the following sinusoidal law (Macmillan, 2002):

$$h(t) = h_0 \, \sin\!\left(\frac{2\pi V t}{L}\right), \tag{2}$$

where: $V$ – constant translational velocity of the opener assembly (m s$^{-1}$); $h_0$ – maximum height of a soil surface irregularity (m); $L$ – length of a soil surface irregularity (distance between two adjacent ridges) (m); $t$ – current time (s).

We assume at a first approximation that the support reactions exerted by the soil on the teeth of the toothed disc during the movement of the opener assembly across irregularities of the soil surface change by the same sinusoidal law:

$$R_i(t) = R_0 + H \, \sin\!\left(\frac{2\pi V t}{L}\right), \quad i = 1, 2, 3, 4, \tag{3}$$

where: $R_0$ – reaction of soil during the movement of the toothed disc on the perfectly even surface of the soil (N); $H \sin\!\left(\frac{2\pi V t}{L}\right)$ – excitation component of the soil reaction caused by the irregularities of the soil surface; $H$ – amplitude of this excitation (N).

Such an assumption for a first approximation can be made following the fact that the motion of the seed drill's carrying wheels across the irregularities of the soil surface varying under law (2) causes the self-induced oscillation of the seed drill's draw-bar beam 1, draw-bar 5 itself and opener assembly spar 8 together with toothed disc 10. This results in the generation of dynamic loads imposed by the oscillating masses of the above-listed members of the opener assembly structure, which follow a law similar to (2). They are active forces giving rise to the respective reaction of the soil, therefore it is reasonable, to a first approximation, to assume that the reaction of the soil also varies under a law similar to (2), but generally with its own amplitude $H$.

Further, it is to be stressed that the deeper the penetration of toothed disc 10 into the soil is, the greater the total soil covered area of its teeth, to which the soil's reaction is applied, will be. As we can see from the schematic model in Fig. 2, when toothed disc 10 penetrates the soil down to the optimal depth, simultaneously four teeth in the disc's

front part (which is in immediate contact with the unopened part of soil) move in soil. Moreover, the tooth preceding the first of those four teeth shown in the figure is not yet in contact with the soil surface irregularity, while the tooth succeeding the fourth of the shown teeth is already out of contact with the soil, moving in the furrow that has been cut in the soil. So, the number of the teeth simultaneously making contact with the soil (effectively moving in soil) depends also on the size of those teeth. Hence, in every particular case both the size of the teeth and the depth of the disc's penetration into the soil (disc running depth) have to be taken into account. In our case we assume, according to the schematic model (Fig. 2), that only four front teeth of disc 10 are in contact with the soil.

The soil also exerts reaction $\bar{R}_a$ on the hoe-type seed conductor, which also affects, although only moderately, the movement of the opener assembly.

Lastly, when the packing wheel rolls on the opened soil, the soil's normal reaction $\bar{N}_k$ is applied to the packing wheel as well as rolling friction force $\bar{F}_k$, the value of which is:

$$F_k = \delta \frac{N_k}{r_k},\tag{4}$$

e: $\delta$ – coefficient of rolling friction (m); $r_\kappa$ – packing wheel radius (m).

The sense of the toothed disc's rotation $\omega_d$ due to its engagement with the soil is shown with an arrow. The equivalent schematic model in Fig. 2 shows the necessary linear and angular dimensions. Now we establish the system of Cartesian rectangular coordinates Oxy with the origin at point O. Axis Ox runs along the line of translational movement of the opener assembly (co-directional with translational movement velocity vector *V*), axis Oy runs upward (Fig. 2).

Now we can write down the equation of the opener assembly movement in the vector form:

$$M\,\bar{a} = \bar{F}_{n1} + \bar{F}_{n2} + \bar{G}_n + \bar{G}_d + \bar{G}_\pi + \bar{G}_a + \bar{G}_k + \bar{R}_1 + \bar{R}_2 + \bar{R}_3 + \bar{R}_4 + \\ +\bar{R}_a + \bar{N}_k + \bar{F}_k + \bar{F}_d,\tag{5}$$

where: $M$ – mass of the opener assembly (kg); $\bar{a}$ – acceleration of the opener assembly (m s$^{-2}$).

The value of the mass of the opener assembly is found as follows:

$$M = m_n + m_\partial + m_\pi + m_a + m_\kappa.\tag{6}$$

Next, we will write vector equation (5) using the projections on axes Ox and Oy. Initially we assume that the two springs (Fig. 2) are aligned parallel to axis Oy. Also we assume at a first approximation that the reactions of the soil acting on the teeth of the disc are perpendicular to the tooth surface, as shown in Fig. 2. Apparently, the adjacent teeth of the disc are spaced at an angular pitch of $\alpha = \frac{2\pi}{z}$, where $z$ – number of teeth on the disc.

Further, we designate $\varepsilon$ – angle between axis Ox and the upper side surface of the first tooth coming in contact with the soil surface, and $\beta$ – angle between side surfaces of the teeth (Fig. 1). In this case, force projections $\bar{R}_i$ on axis Oy will be as follows:

$$R_{1y} = R_1 \cos(\beta - \varepsilon);$$
$$R_{2y} = R_1 \cos(\beta - \varepsilon + \alpha) = R_1 \cos(\beta - \varepsilon + \frac{2\pi}{z});$$
$$R_{3y} = R_1 \cos(\beta - \varepsilon + 2\alpha) = R_1 \cos(\beta - \varepsilon + \frac{4\pi}{z}); \qquad (7)$$
$$R_{4y} = R_1 \cos(\beta - \varepsilon + 3\alpha) = R_1 \cos(\beta - \varepsilon + \frac{6\pi}{z}).$$

Similarly, the projections on axis Ox for the same four teeth will be:

$$R_{1x} = R_1 \sin(\beta - \varepsilon);$$
$$R_{2x} = R_1 \sin(\beta - \varepsilon + \frac{2\pi}{z});$$
$$R_{3x} = R_1 \sin(\beta - \varepsilon + \frac{4\pi}{z}); \qquad (8)$$
$$R_{4x} = R_1 \sin(\beta - \varepsilon + \frac{6\pi}{z}).$$

The force of rolling friction of the toothed disc at a first approximation can be calculated as follows:

$$F_d = \frac{4R_1}{r_d} \delta_1,$$

or, using formula (3),

$$F_d = \frac{4 \left[ R_0 + H \sin \left( \frac{2\pi V t}{L} \right) \right] \delta_1}{r_d}, \qquad (9)$$

where $\delta_1$ – coefficient of rolling friction (m); $r_d$ – disc radius (m).

The projection of force $\bar{R}_a$ (the soil's reaction acting on the hoe-type seed conductor) on coordinate axes x and y will be equal to:

$$R_{ax} = - R_a \cos\gamma , \qquad (10)$$
$$R_{ay} = - R_a \sin\gamma .$$

Angle $\gamma$ is shown in Fig. 2.

Hence, taking into account formulae (5), (7), (8) and (10), we obtain the system of differential equations of the movement of the opener assembly in the projections to axes Ox and Oy:

$$M \ddot{x} = - R_1 \left[ \sin(\beta - \varepsilon) + \sin \left( \beta - \varepsilon + \frac{2\pi}{z} \right) + \sin \left( \beta - \varepsilon + \frac{4\pi}{z} \right) \right.$$
$$\left. - \sin \left( \beta - \varepsilon + + \frac{6\pi}{z} \right) \right] - R_a \cos\gamma - F_d - F_k;$$

$$M \ddot{y} = - F_{n1} - F_{n2} - G_n - G_d - G_л - G_a - G_k \qquad (11)$$
$$+ R_1 \left[ \cos(\beta - \varepsilon) + \cos \left( \beta - \varepsilon + \frac{2\pi}{z} \right) + \cos \left( \beta - \varepsilon + \frac{4\pi}{z} \right) \right.$$
$$\left. + \cos \left( \beta - \varepsilon + \frac{6\pi}{z} \right) \right] - R_a \sin\gamma + N_k.$$

Substituting formulae (1), (3), (4), (6) and (9) into differential equation system (11), we arrive at the following system of differential equations:

$$
\left.
\begin{aligned}
M\,\ddot{x} &= -\left[R_0 + H\sin\left(\tfrac{2\pi V t}{L}\right)\right]\left[\sin(\beta-\varepsilon) + \sin\left(\beta-\varepsilon+\tfrac{2\pi}{z}\right) + \right. \\
&+ \sin\left(\beta-\varepsilon+\tfrac{4\pi}{z}\right) + +\sin\left(\beta-\varepsilon + \right. \\
&\left.\left.\tfrac{6\pi}{z}\right)\right] - R_a\cos\gamma - \frac{4\left[R_0 + H\sin\left(\tfrac{2\pi V t}{L}\right)\right]\delta_1}{R_d} - \delta\frac{N_\text{к}}{r_\text{к}}; \\
M\,\ddot{y} &= -C_{n1}\,l_{n1} - C_{n2}\,y - (m_n + m_d + m_\text{л} + m_a + m_\text{к})g + \left[R_0 + \right. \\
&\left. H\sin\left(\tfrac{2\pi V t}{L}\right)\right]\left[\cos(\beta-\varepsilon) + \cos\left(\beta-\varepsilon+\tfrac{2\pi}{z}\right) + \cos\left(\beta-\varepsilon+\tfrac{4\pi}{z}\right) + \right. \\
&\left. \cos\left(\beta-\varepsilon+\tfrac{6\pi}{z}\right)\right] - R_a\sin\gamma + N_\text{к}.
\end{aligned}
\right\} \quad (12)
$$

Differential equation system (12) characterises the process of the horizontal and vertical translational oscillations of the opener assembly (its spar) during the movement of the opener assembly across the irregularities of the soil surface. In these equations, the component $H\sin\left(\tfrac{2\pi V t}{L}\right)$ plays the role of the exciting force and the component $C_{n2}\,y$ acts as the restoring force.

To reduce the formulae of differential equation system (12), the following designations are introduced:

$$
\left[\sin(\beta-\varepsilon) + \sin\left(\beta-\varepsilon+\tfrac{2\pi}{z}\right) + \sin\left(\beta-\varepsilon+\tfrac{4\pi}{z}\right) + \sin\left(\beta-\varepsilon+\tfrac{6\pi}{z}\right)\right] = A;
$$
$$
\left[\cos(\beta-\varepsilon) + \cos\left(\beta-\varepsilon+\tfrac{2\pi}{z}\right) + \cos\left(\beta-\varepsilon+\tfrac{4\pi}{z}\right) + \cos\left(\beta-\varepsilon+\tfrac{6\pi}{z}\right)\right] = B.
$$

Then differential equation system (12) will have the following representation:

$$
\left.
\begin{aligned}
\ddot{x} &= -A\frac{R_0}{M} - \frac{A\,H}{M}\sin\left(\tfrac{2\pi V t}{L}\right) - \frac{R_a\cos\gamma}{M} - \frac{4R_0\delta_1}{M\,R_d} - 4H\frac{\sin\left(\tfrac{2\pi V t}{L}\right)\delta_1}{M\,R_d} - \frac{\delta N_k}{M\,r_k}; \\
\ddot{y} &+ \frac{C_{n2}y}{M} = -\frac{C_{n1}l_{n1}}{M} - g + \frac{R_0 B}{M} + \frac{B\,H}{M}\sin\left(\tfrac{2\pi V t}{L}\right) - \frac{R_a\sin\gamma}{M} + \frac{N_\text{к}}{M}.
\end{aligned}
\right\} \quad (13)
$$

Since the differential equations in system (13) are independent and they can be integrated separately, we start with integrating the first equation of the system. The first integral of the first equation is equal to:

$$
\dot{x} = -\left(\frac{R_0 A}{M} + \frac{R_a\cos\gamma}{M} + \frac{4R_0\delta_1}{M\,R_d} + \frac{\delta N_k}{M\,R_k}\right)t + \left(\frac{L\,AH}{2\pi V\,M} + \frac{4L\,H\delta_1}{2\pi V\,M\,R_d}\right)\cos\left(\tfrac{2\pi V t}{L}\right) + C_1. \quad (14)
$$

The second integral of the first equation is equal to:

$$
x = -\left(\frac{R_0 A}{M} + R_a\frac{\cos\gamma}{M} + 4R_0\frac{\delta_1}{M}R_d + \delta\frac{N_k}{M}R_k\right)\frac{t^2}{2} + \left(\frac{L^2\,AH}{4\pi^2 V^2\,M} + \right.
$$
$$
\left. + \frac{L^2\,H\delta_1}{\pi^2 V^2\,M\,R_d}\right)\sin\left(\tfrac{2\pi V t}{L}\right) + C_1\,t + C_2. \quad (15)
$$

Arbitrary constants $C_1$ and $C_2$ can be derived from the following initial conditions:

at $\qquad\qquad t = 0:\ x = 0,\ \dot{x} = 0,\ y = 0,\ \dot{y} = 0.$ $\qquad\qquad$ (16)

This gives the following values of the arbitrary constants:

$$C_1 = -\left(\frac{L\,AH}{2\pi\,V\,M} + \frac{2L\,H\delta_1}{\pi\,V\,M\,R_d}\right),\ C_2 = 0\,. \tag{17}$$

Thus, the first integral of the first differential equation of system (13), complying with initial conditions (16), is expressed as follows:

$$\dot{x} = -\left(\frac{R_0 A}{M} + \frac{R_a\cos\gamma}{M} + \frac{4R_0\delta_1}{M\,R_d} + \frac{\delta N_k}{M\,R_k}\right)t + \left(\frac{L\,AH}{2\pi\,V\,M} + \right.$$
$$\left. + \frac{2L\,H\delta_1}{\pi\,V\,M\,R_d}\right)\cos\left(\frac{2\pi V t}{L}\right) - \left(\frac{L\,AH}{2\pi\,V\,M} + \frac{2L\,H\delta_1}{\pi\,V\,M\,R_d}\right). \tag{18}$$

The second integral, i.e. the solution of the equation, complying with initial conditions (16), is expressed as follows:

$$x = -\left(\frac{R_0 A}{M} + \frac{R_a\cos\gamma}{M} + \frac{4R_0\delta_1}{MR_d} + \frac{\delta N_k}{MR_k}\right)\frac{t^2}{2} + \left(\frac{L^2 AH}{4\pi^2 V^2 M} + \right.$$
$$\left. \frac{L^2 H\delta_1}{\pi^2 V^2 MR_d}\right)\sin\left(\frac{2\pi V t}{L}\right) - \left(\frac{LAH}{2\pi VM} + \frac{2LH\delta_1}{\pi VMR_d}\right)t. \tag{19}$$

Formula (19) characterises the process of the translational oscillations of the opener assembly along axis Ox. The amplitude of these oscillations, as may be inferred from formula (19), is found as the multiplier at function $\left(\frac{2\pi V t}{L}\right)$. Further, we give consideration to the second differential equation of system (13). Doing this, we introduce the designation $\sqrt{\frac{C_{n2}}{M}} = k$.

Then the representation of this differential equation transforms as follows:

$$\ddot{y} + k^2 y = -\frac{C_{n1}l_{n1}}{M} - g + \frac{BR_0}{M} + \frac{BH}{M}\sin\left(\frac{2\pi V t}{L}\right) - \frac{R_a\sin\gamma}{M} + \frac{N_k}{M}. \tag{20}$$

For convenience we introduce the following designation:

$$-\frac{C_{n1}l_{n1}}{M} - g + \frac{BR_0}{M} - \frac{R_a\sin\gamma}{M} + \frac{N_\kappa}{M} = D \tag{21}$$

Then differential equation (20) obtains the following representation:

$$\ddot{y} + k^2 y = \frac{BH}{M}\sin\left(\frac{2\pi V t}{L}\right) + D\,. \tag{22}$$

Equation (22) is a linear differential equation of second order with constant coefficients and a right-hand side. Its solution is the sum of the solution of the homogeneous differential equation:

$$\ddot{y} + k^2 y = 0 \tag{23}$$

and the partial solution, which depends on the right-hand side of the equation. It is known that differential equation (23) has the following solution:

$$y_{hom} = L_1 \sin(kt) + L_2 \cos(kt) . \tag{24}$$

The partial solution of a non-homogeneous equation with a right-hand side is derived via the following expression:

$$y_{\text{part}} = R \sin \left(\frac{2\pi V t}{L}\right) + S \cos \left(\frac{2\pi V t}{L}\right) + T , \tag{25}$$

where $R, S, T$ – unknown coefficients.

These coefficients can be found using the method of undetermined coefficients. Thus:

$$\dot{y}_{\text{part}} = 2R\pi v \cos \left(\frac{2\pi V t}{L}\right)\!/ L - 2S\pi v \sin \left(\frac{2\pi V t}{L}\right)\!/ L, \tag{26}$$

$$\ddot{y}_{part} = -\frac{4R\pi^2 V^2}{L^2} \sin \left(\frac{2\pi V t}{L}\right) - \frac{4S\pi^2 V^2}{L^2} \cos \left(\frac{2\pi V t}{L}\right). \tag{27}$$

Substituting formulae (25) and (26) into equation (22), we obtain:

$$-\frac{4R\pi^2 V^2}{L^2} \sin \left(\frac{2\pi V t}{L}\right) - \frac{4S\pi^2 V^2}{L^2} \cos \left(\frac{2\pi V t}{L}\right) + k^2 R \sin \left(\frac{2\pi V t}{L}\right) +$$
$$k^2 S \cos \left(\frac{2\pi V t}{L}\right) + k^2 T = \frac{BH}{M} \sin \left(\frac{2\pi V t}{L}\right) + D . \tag{28}$$

Equating the coefficients at identical trigonometric functions in (28), we arrive at the following system of equations:

$$\left(-\frac{4\pi^2 V^2}{L^2} + k^2\right) R = \frac{BH}{M} , \quad \left(-\frac{4\pi^2 V^2}{L^2} + k^2\right) S = 0 , \quad K^2 T = D. \tag{29}$$

From system of equations (29) we find:

$$R = \frac{BH}{M\left(k^2 - \frac{4\pi^2 V^2}{L^2}\right)}, \qquad S = 0, \qquad T = \frac{D}{k^2}. \tag{30}$$

Substituting formulae (30) into formula (25), we find the needed partial solution:

$$y_{part} = \frac{BH}{M\left(k^2 - \frac{4\pi^2 V^2}{L^2}\right)} \sin \left(\frac{2\pi V t}{L}\right) + \frac{D}{k^2},$$

or, in a more convenient representation:

$$y_{part} = \frac{L^2 BH}{M(L^2 k^2 - 4\pi^2 V^2)} \sin \left(\frac{2\pi V t}{L}\right) + \frac{D}{k^2} \tag{31}$$

Thus, the general solution of differential equation (20) will be equal to:

$y = y_{hom} + y_{part},$

or, taking into account (24) and (31), we obtain the following expression:

$$y = L_1 \sin(kt) + L_2 \cos(kt) + \frac{L^2 BH}{M(L^2 k^2 - 4\pi^2 V^2)} \sin\left(\frac{2\pi Vt}{L}\right) + \frac{D}{k^2}. \quad (32)$$

Arbitrary constants $L_1$ and $L_2$ can be found from initial conditions (16). From formula (32) for $t = 0$ we obtain:

$$L_2 = -\frac{D}{k^2}.$$

To find arbitrary constant $L_1$, we differentiate expression (32) with respect to $t$:

$$y = C_1 k \cos(kt) - C_2 k \sin(kt) + \frac{2\pi VLBH}{M(L^2 k^2 - 4\pi^2 V^2)} \cos\left(\frac{2\pi Vt}{L}\right). \quad (33)$$

From formula (33) for $t = 0$ we find the value of arbitrary constant $C_1$:

$$C_1 = -\frac{2\pi VLBH}{kM(L^2 k^2 - 4\pi^2 V^2)}.$$

Hence, we obtain the solution of differential equation (22), complying with initial conditions (16):

$$y = -\frac{2\pi VLBH}{kM(L^2 k^2 - 4\pi^2 V^2)} \sin(kt) - \frac{D}{k^2} \cos(kt) + \frac{L^2 BH}{M(L^2 k^2 - 4\pi^2 V^2)} \sin\left(\frac{2\pi Vt}{L}\right) + \frac{D}{k^2}. \quad (34)$$

Formula (34) characterises the translational oscillations of the opener assembly along axis Oy in the presence of exciting force $R_0 + H\sin\left(\frac{2\pi Vt}{L}\right)$ and restoring force $C_{n2}$ $y$ of the vibrator spring.

In formula (34), the first two terms of sum characterise the natural vertical oscillations of the opener assembly, the third term – the forced vertical oscillations of the opener. Meanwhile, the amplitude of the natural oscillations, as may be inferred from formula (34), has a value of:

$$A_1 = \sqrt{\frac{4\pi^2 V^2 L^2 B^2 H^2}{k^2 M^2 (L^2 k^2 - 4\pi^2 V^2)^2} + \frac{D^2}{k^4}}, \quad (35)$$

The amplitude of forced oscillations of the opener assembly is found from the following formula:

$$B_1 = \frac{L^2 BH}{M(L^2 k^2 - 4\pi^2 V^2)}. \quad (36)$$

The frequency of the natural oscillations is determined as follows:

$$k = \sqrt{\frac{C_{n2}}{M}}, \quad (37)$$

while the frequency of the forced oscillations, as is known, equals the frequency of the exciting force:

$$k_1 = \frac{2\pi V}{L}. \quad (38)$$

Thus, the formulae have been obtained for determining the amplitude (35) and frequency of the natural oscillations (37) and the amplitude of the forced oscillations

(36) of the opener assembly depending on its main design parameters and modes of operation during its uniform movement across irregularities of the soil surface. These formulae take into account the following values: the number of teeth on the toothed disc of the opener, the deflection rates of its suspension springs and the velocity of the translational movement.

The obtained final expressions for the amplitude and frequency of vibration of the opener assembly spar provide the basis for numerical calculations with the use of a PC. The computer programme developed in the MathCAD environment has been used to carry out the numerical calculation of the amplitude of the vibration of the furrow opening toothed disc generated by the system of spring devices (two-spring suspension) comprising the pressure spring and the additional self-induced oscillation spring during the interaction between the disc and soil surface irregularities.

The results of the calculations have been used to construct the graphs of opener assembly vibration amplitudes $A(V)$ (m) for different values of spring constants $C_{\Pi1}$ and $C_{\Pi2}$ (N m$^{-1}$), depending on the translational motion velocity $V$ (m s$^{-1}$). Those graphs are presented in Fig. 3.
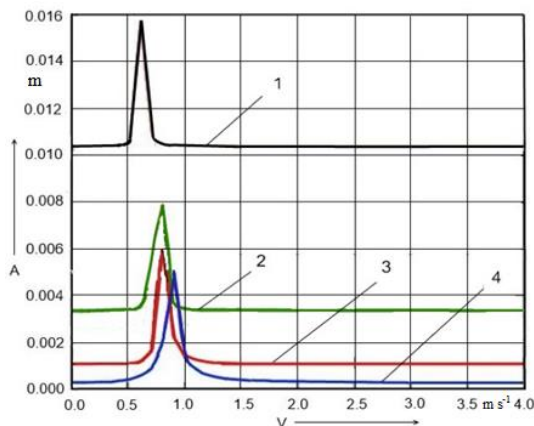


**Figure 3.** Curves of denoting the relation between the amplitude of vibration of opener assembly with a two-spring suspended toothed disc and the velocity of its motion at following deflection rates (N m$^{-1}$):
1 – $C_{\Pi1}$ = 16815, $C_{\Pi2}$ = 17150 (25% of rated deflection rate);
2 – $C_{\Pi1}$ = 33635, $C_{\Pi2}$ = 34300 (50% of rated deflection rate);
3 – $C_{\Pi1}$ = 50450, $C_{\Pi2}$ = 51450 (75% of rated deflection rate);
4 – $C_{\Pi1}$ = 67270, $C_{\Pi2}$ = 68600 (100% of rated deflection rate).

It appears from the presented graphs that resonance amplitudes of vibration are observed, when the opener assembly perturbation frequency is equal to its natural vibration frequency at velocities of 0.5 m s$^{-1}$ to 1.0 m s$^{-1}$. During the following increase of the translational motion velocity from 1.2 m s$^{-1}$ to 4 m s$^{-1}$ the amplitude values remain stable.

## CONCLUSIONS

7. The system of differential equations has been set up for the translational oscillations of the improved design opener assembly initiated by the action of the exciting force generated by the soil surface irregularities during the uniform movement of the opener assembly down the field.

8. For the mentioned differential equation system, a solution has been found that characterises the law of the oscillatory movement of the opener assembly along the axes of the Cartesian coordinate system.

9. The finite analytical expressions have been found for determining the amplitude and frequency of the mentioned oscillations depending on the design parameters and kinematic modes of operation of the opener assembly.

10. The obtained mathematical model allows to assess the conditions of the system and subsequently optimise the energy characteristics of the breeding grain drill equipped with improved design opener assemblies with toothed discs.

## REFERENCES

Altikat, S., Celik, A. & Gozubuyuk, Z. 2013. Effects of various no-till seeders and stubble conditions on sowing performance and seed emergence of common vetch. *Soil & Tillage Research* **126**, 72–77.

Bai, X., Lin, J., Lü, C. & Hu, Y. 2014. Analysis and experiment on working performance of disc coulter for no-tillage seeder. *Nongye Gongcheng Xuebao/Transactions of the Chenese Society of Agricultural Engineering* **30**(15), 1–9.

Belov, V.V. & Belov, S.V. 2007. On the operating area of the opener suspension mechanism. *Machinery in agriculture* **5**, 10–12. (in Russian).

Bianchini, A. & Magalhães, P.S.G. 2008. Evalution of coulters for cutting sugar cane residue in a soil bin. *Biosystems Engineering* **100**, 370–375.

Chaudhuri, D. 2001. Performance evaluation of various types of furrow oponers on seed drills – A review. *Journal of Agricultural Engineering Research* **79**(2), 125–137.

Chen, Y., Tessier, S. & Irvine, V. 2004. Drill and crop performances for no-till seeding. *Soil & Tillage Research* **77**, 145–155.

Hasimu, A. & Chen, Y. 2014. Soil disturbance and draft force of selected seed openers. *Soil & Tillage Research* **140**, 48–54.

Jingling, S., Zidong, Y., Shandong, Y., Guohai, Z. & Hongweng, L. 2011. Development of a new type seeder. *Intenational Agricultural Engineering Journal* **20**(2), 57–60.

Endrerud, H.C. 1999. Dynamic performance of drill coulters in a soil bin. *J. agric. Engng Res.* **74**, 391–401.

Karayel, D. 2009. Performance of a modified precision vacuum seeder for no-till sowing of maize and soybean. *Soil & Tillage Research* **104**, 121–125.

Karayel, D. & Özmerzi, A. 2007. Comparison of vertical and lateral seed distribution of furrow openers using a new criterion. *Soil & Tillage Research* **95**, 69–75.

Lin, J., Song, Y. & Li, B. 2014. Mechanical no-tillage sowing technology in ridge area of Nordheast China. *Nongye Gongcheng Xuebao/Transactions of the Chenese Society of Agricultural Engineering* **30**(9), 50–57.

Lisoviy, I.A. 2013. Justification of direct drilling opener parameters. *Kirovograd: A Thesis for applying for the degree of Doctor of Philosophy in Agricultural Engineering*.

Lian, Z., Wang, J., Yang, Z. & Shang, S. 2012. Development of plot-sowing mechanization in China. Nongye Gongcheng *Xuebao/Transactions of the Chenese Society of Agricultural Engineering* **2**8(2), 140–145.

Liu, S. & Ma, Y. 2012. Development history, status, and trends of plot seeder. *Applied Mechanics and Materials* **268**(1), 1966–1969.

Macmillan, R.H. 2002. The Mechanics of Tractor – Implement Performance. Theory and Worked Examples. *University of Melbourne*.

Magalhães, P.S.G., Bianchini, A. & Braunbeck, O.A. 2007. Simulated and experimental analyses of a toothed rolling coulter for cutting crop residues. *Biosystems Engineering* **96**(2), 193–200.

Prisyazhnyuk, N.V., Adamchuk, V.V. & Bulgakov, V.M. 2013. Theory of vibration machines in agricultural industry. *Kiev: Agricultural Science*.

Šarauskis, E. & Vaitauskiene, K. 2014. Reseach of mechanicaltraction characteristics of direct sowing equipment. *Mechanica* **20**(5), 506–511.

Turbin, B.G., Lurie, A.B. & Grigoryev, S.M. 1967. Agricultural machinery. Theory and process design. *Leningrad: Mechanical Engineering, 2nd ed. revision and updated*.

Vamerali, T., Bertocca, M. & Sartori, L. 2006. Effects of a new wide-sweep for no-till planter on seed zone properties and root establishment in maize (Zea mays, L.): A comparison with double-disk opener. *Soil & Tillage Research* **89**, 196–209.

Vasilenko, P.M. 1996. Introduction to agricultural mechanics. *Kiev: Agricultural Education*.

# Influence of biofuel moisture content on combustion and emission characteristics of stove

D. Černý[*], J. Malaťák and J. Bradna

Czech University of Life Sciences Prague, Faculty of Engineering, Department of Technological Equipment of Buildings, Kamýcká 129, CZ 165 21 Prague, Czech Republic
[*]Correspondence: david.cerny@dotacenazeleno.cz

**Abstract.** The research aim was to study the effect of moisture in solid fuel on combustion in a stove and its emissions. Analysed samples were from spruce woodchips. Four samples were prepared with different moisture contents and furthermore spruce wood was used as a reference sample. Combustion device used was a stove with a fixed fire grate. Studied parameters were ambient temperature, temperature of flue gases, coefficient of excess air, and contents of oxygen and carbon monoxide in flue gases. Laboratory measurement was performed on an analyser of flue gases whose function is based on electro-chemical converters. Measured values were first converted to a referential oxygen content in flue gases. Evaluation of these values was then made by regression analyses. The course of combustion process and its quality can be seen well in functional dependence of carbon monoxide on excess air coefficient. The area of combustion was the smallest with the least moist sample (3.2%) and increases with increasing moisture. A sample with high moisture (31.1%) was already causing the fire to gradually extinguish. Because flue gas temperature is in the same range for all samples, the overall efficiency of the stove decreases sharply with fuel moisture due to specific heat of flue gases. It has been thus confirmed that fuel moisture content has a substantial influence on combustion, especially in the chosen combustion device, which has been verified by comparison with the reference fuel.

**Key words:** Biomass, combustion, elemental and stoichiometric analyses, emissions, spruce chips.

## INTRODUCTION

Due to the decrease in fossil fuel reserves, the importance of using renewable energy sources is increasing. Production of organic waste is very significant in terms of quantity in Czech Republic, particularly in the field of agricultural and forestry activities. For energy use of these products it is very important to run combustion process under optimal conditions. If we have to decide whether the chosen biomass is suitable for combustion in a certain type of combustion device, it will be necessary to know the properties of such biofuels that characterise it sufficiently. Elemental analysis and stoichiometric calculations are essential for assessing suitability in terms of energy (Nordin, 1994; Malaťák & Passian, 2011).

Water is contained in each solid fuel. The ash as well as water are incombustible components of each fuel, which reduce the calorific value, therefore they are undesirable in the fuel. The water content in the solid fuel varies in a wide range from 0 to 60% wt. The water content in the fuel is given in weight percent (Obernbergera & Theka, 2004;

Müller et al., 2015). In many studies, the core aim is to better understand the relationship between thermal conversion processes (drying, pyrolysis, char conversion) and their interrelationship to combustor performance (efficiency, emissions, process temperatures, scale formation, and instabilities) (Demirbas, 2004; Di Blasi, 2008; Obaidullah et al., 2012). However, due to the complexity of solid fuel (particle) conversion and fuel bed behaviour, precise modelling of all aspects of biomass fixed-bed combustion is not readily achievable (Khodaei et al., 2015). One problem is the large amount of moisture content in biofuels. Higher moisture content causes operational problems for biomass combustion, as shown by the study Svoboda et al. (2009).

The aim of this study is to assess the effect of water contained in a sample of fuel on the combustion process on the grate furnace and in particular the impact on emission and combustion characteristics. To compare the quality of the combustion process a hypothesis was determined that with higher water content the quality of combustion process decreases. This hypothesis will be tested by experimental measurement and statistical evaluation of measured values. As a reduction in the quality of the combustion process can be evaluated the low efficiency of the combustion device and high CO values.

## MATERIALS AND METHODS

The method of solution to this problem is based on several methods that are based on the work progress. First of all there is a sample preparation, next is combustion process and emission concentration measurement and determinination of the combustion device operating parameters. Another extensive section is the methodology used in the analytical processing of the measured values and their statistical analysis.

### Sample preparation

Spruce wood chips were selected as a sample for combusting process. Spruce logs intended for combustion in grate furnace have been transformed into chips by wood chipper AL-KO 2500. Chips had length from 10 to 60 mm. Elemental analysis of spruce wood chips is in Table 1.

**Table 1.** Elemental analysis of reference sample, spruce wood

| Water Content (% Wt.) | Ash (% Wt.) | Gross Calorific Value (MJ kg$^{-1}$) | Net Calorific Value (MJ kg$^{-1}$) | Carbon (% Wt.) | Hydrogen (% Wt.) | Nitrogen (% Wt.) | Suplhur (% Wt.) | Oxygen (% Wt.) |
|---|---|---|---|---|---|---|---|---|
| $W$ | $A$ | $Q_s$ | $Q_i$ | $C$ | $H$ | $N$ | $S$ | $O$ |
| 14.28 | 2.8 | 18.74 | 17.16 | 43.6 | 5.88 | 0.17 | 0 | 33.3 |

Crushed chips were dipped into water, wherein the sample has reached the water content in the fuel to a value of 60%. The chips were then divided into the four sub-

samples of the same weight, which were subsequently dried in a laboratory dryer MEMMERT UFE 800 to different water contents in the samples.

An exact value of the water content was not required. For spruce chips limit water content values of 5% and over 20% are the subject of discussions. Therefore, the aim was to achieve values near to these values.

For determination of the water content, a part of each sample was removed from the drying oven and analysed by a laboratory dryer OHAUS MB 25 which measured the reference value of the water content for individual samples (Table 2). Measurement methodology is based on CSN 44 1377, drying at temperature 105 °C.

Furthermore, in Table 2 the net calorific value of examined samples is converted for the water content in the fuel based on the reference sample values according to an equation, derived from calorimetric equations:

$$Q_v = Q_s - 24{,}42 \times (W + 8{,}94 \times H_h) \tag{1}$$

where: $Q_s$ – Gross Calorific Value (J g$^{-1}$); 24,42 – coefficient corresponding to 1% water in the sample at 25 °C, J g$^{-1}$; $W$ – water content in the analysed sample, %; 8,94 – conversion coefficient for hydrogen to water; $H_h$ – hydrogen content of the analysed sample, %.

**Table 2.** Stoichiometric analysis of samples

|  | Mark | Unit | Spruce wood | Sample 1 | Sample 2 | Sample 3 | Sample 4 |
|---|---|---|---|---|---|---|---|
| Water Content | $W$ | % | 14.28 | 3.2 | 9.9 | 15.8 | 31.1 |
| Net Calorific Value | $Q_n$ | kJ kg$^{-1}$ | 17,160 | 17,211 | 17,148 | 17,092 | 16,974 |
| Theoretical amount of air necessary for complete combustion | $L_{min}$ | Nm$^3$ kg$^{-1}$ | 4.31 | 6.33 | 5.89 | 5.51 | 4.5 |
| Real amount of air necessary for complete combustion | $L_{skut}$ | Nm$^3$ kg$^{-1}$ | 9.06 | 13.29 | 12.37 | 11.56 | 9.46 |
| Theoretical mass amount of dry flue gas | $v_{sp,min}$ | Nm$^3$ kg$^{-1}$ | 4.18 | 4.72 | 4.39 | 4.1 | 3.36 |

### Combustion of samples

Measurement of the combustion process took a place in a solid fuel stove brand CALOR from the company V.J. Rousek. The stove is equipped with an internal combustion grate. As a fuel is prescribed wood or coal, fuel consumption ranged from 0.8 to 1.5 kg h$^{-1}$.

First reference sample was combusted and then the chosen individual fuel samples in the order from the lowest to the highest water content.

### Emission measurement and evaluation

To measure the combustion process and emission concentration flue gas analyzer Madur GA-60 was used, whose measuring probe was installed in the chimney. Measurement values were automatically saved each minute. The flue gas analyser uses

electro-chemical converters for the measurement of selected emission concentrations ($O_2$, $CO$) in ppm units, flue gas temperature and ambient temperature.

Emission concentrations were converted from ppm to mg m$^{-3}$ and then further converted into normal conditions, i.e. dry flue gas temperature of 273.15 K, pressure of 101.325 kPa and a reference oxygen content of 13%.

Stoichiometric calculations were performed for each sample (Table 2). It contains the calorific value of biofuels and heat of combustion, the theoretical amount of oxygen and air for complete combustion, the actual amount of air for complete combustion, the mass and volume of wet and dry flue gas and the theoretical mass and volume of dry flue gas.

The measured values were plotted against the excess of combustion air coefficient, calculated by equation:

$$n = 1 + \left( \frac{CO_{2,\max}}{CO_2} - 1 \right) \cdot \frac{V_{sp,\min}}{L_{\min}} \qquad (2)$$

where: $CO_{2,max}$ – the theoretical volume concentration of carbon dioxide in dry flue gases, %; $CO_2$ – the real (measured) volume concentration of carbon dioxide in dry flue gases, %; $V_{sp,min}$ – the theoretical mass amount of dry flue gas, Nm$^3$ kg$^{-1}$; $L_{min}$ – the theoretical amount of air necessary for complete combustion, Nm$^3$ kg$^{-1}$.

## RESULTS AND DISCUSSION

The issue of emissions is very comprehensive and important. This work primarily involves itself with the complete combustion of biomass. Among the possibilities for reducing the emissions are included in particular continuous fuel supply, temperature in the combustion chamber high enough for complete combustion, intake of secondary respectively tertiary air and choosing the optimum fuel moisture (Kjallstrand & Olsson 2004).

Low water content in the samples is a positive factor because moisture affects the combustion process and flue gas volume produced per unit of energy (Hájek & Malaťák, 2013).

The courses of the combustion process are shown in dependence of the combustion air and the flue gas temperature on time for all samples (see Fig. 1).

These dependences show the course of the entire experiment and the development of the main variables that affect the combustion process. During the measurement cycles of flaring up and burning out of samples was occurring according to the number of samples.

The flue gas temperature during the measurements fell within the interval from 410 °C to 223 °C according to the regression equation (3) at a confidence level of $R^2 = 0.74$.

The value of reliability was low, but not as significantly low as the next one.

$$T_{\text{flue gas}} = -0.086t + 362.04 \ (\degree C) \qquad (3)$$

The excess of combustion air throughout the process grew in the interval from 2 to 10,5 according to the regression equation (5) at a confidence level of $R^2 = 0.44$.
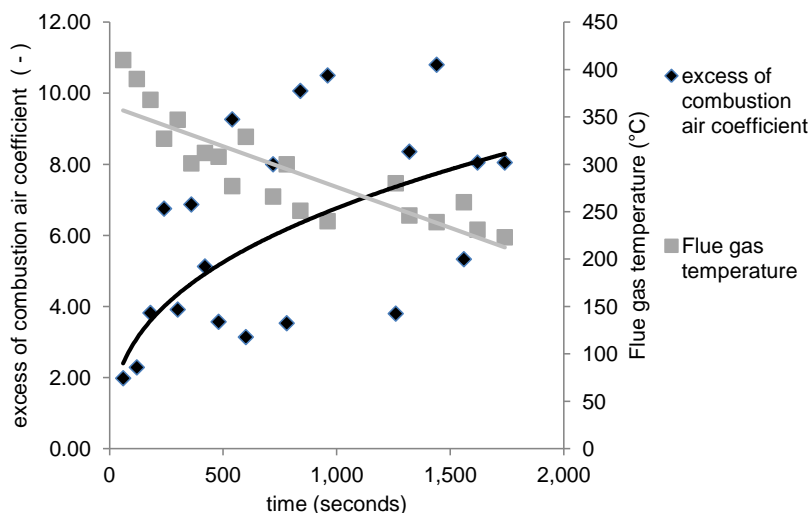
**Figure 1.** The dependence of the flue gas temperature and the excess of combustion air on time.

The value of reliability was significantly low, therefore this variable is a subject of the following sub-analysis.

$$n = 0.5312t^{0.3644} \; (\text{-}) \tag{4}$$

Fig. 2 shows the course of emission concentration of carbon monoxide in dependence upon the excess of combustion air for each sample by regression equations (5–9).
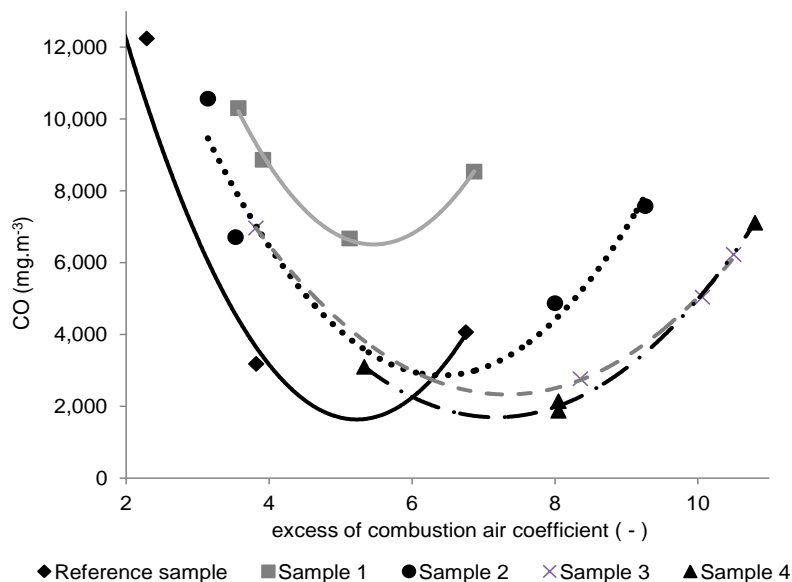


**Figure 2.** Emission CO concentration depending on the excess of combustion air for each sample.

The high level of confidence shows an appropriately selected regression equation during evaluating of the operating parameters of the combustion process also by other authors (Hájek et al., 2013; Müller et al., 2015; Skanderová et al., 2015).

Ref. Sample:

$$CO = 1{,}016.5n^2 - 10{,}625n + 29{,}394 \text{ (mg m}^{-3}\text{)}; R^2 = 0.91 \qquad (5)$$

Sample 1:

$$CO = 1{,}032.4n^2 - 11{,}284n + 37{,}339 \text{ (mg m}^{-3}\text{)}; R^2 = 0.99 \qquad (6)$$

Sample 2:

$$CO = 616.35n^2 - 7{,}908.6n + 28{,}227 \text{ (mg m}^{-3}\text{)}; R^2 = 0.81 \qquad (7)$$

Sample 3:

$$CO = 376.9n^2 - 5{,}520n + 22{,}538 \text{ (mg m}^{-3}\text{)}; R^2 = 0.99 \qquad (8)$$

Sample 4:

$$CO = 412.62n^2 - 5{,}923n + 22{,}948 \text{ (mg m}^{-3}\text{)}; R^2 = 0.99 \qquad (9)$$

Statistical assessment is based on the CSN EN 13229 by comparing the average measured values of each sample with a reference sample. Reference sample is a typical fuel for grate furnace – firewood – logs of wood, spruce. Therefore, the sample 3, spruce chips, with the same water content has a different kinetics of combustion and thus a different course in the graph. Considered samples are compared with the ideal fuel.

Change of flue gas temperature confirms the hypothesis that the effect of water content contained in the fuel has a highly significant influence on the combustion process in all examined samples (*t-test, n = 4*, P > 0.01).

For excess of combustion air the hypothesis can be also confirmed that its influence on the combustion process increases with increasing water content. For all samples this dependency can be confirmed under decreased confidence level (*t-test, n = 4*, P > 0.2).

Growth in excess of combustion air has a negative impact also on other operating parameters of the combustion process.

The excess air value is generally high during combustion in a burner furnace and this is also reflected in the high heat losses in the flue gas (chimney losses) and even in the carbon dioxide and nitrogen oxides concentrations (Jevič et al. 2007; Skanderová et al., 2015).

The course of the carbon monoxide emission concentrations is the same for all samples. An increasing amount of excess combustion air leads to better combustion and decreased emission concentration until a minimum is reached. After reaching the minimum increase of the emission values for CO occurs again due to cooling of flue gases and of the combustion chamber.

For each solid fuel, there is a maximum achievable stoichiometric proportion of carbon dioxide $CO_2$ in the flue gas, which is determined by the elemental composition of combustible fuel (Mcdonald et al., 2000; Hedberg et al., 2002).

For samples 3 and 4 low statistical significance of the influence of water content in the fuel on the combustion process can be confirmed (*t-test, n = 4*, P > 0.2). This is

caused evidently by low temperature of furnace. For samples 1 and 2 the influence of water in the fuel is significant and it is the only case of the hypothesis rejection.

The dependence of excess of combustion air and carbon monoxide emissions on the water content in the fuel is relatively low. It can be assumed that the type of combustion device has a certain influence on the deviation of the measurement. A suitable equipment for minimizing this deviation could be a combustion device with automatic feeding of fuel with a pellet burner and as a reference sample wood pellets.

## CONCLUSIONS

Based on the emission concentrations and elemental analyses we can assess the impact of the water content in the fuel on combustion process.

Increasing water content in the selected fuel leads to the following aspects:
- increasing time of combustion process;
- for wood chips reduction of the CO emission was observed;
- enlargement of the interval in which the burning process can be operated (depending on the control of excess air);
- cooling of the flue gases;
- growth of excess combustion air;
- the reduction of the combustion device efficiency;
- reducing fuel efficiency.

While increasing the duration of fuel combustion in the furnace for some devices without automatic control may be positive, in modern automatic combustion devices it is not admissible. Declining the flue gas temperature reduces the efficiency of the combustion device depending on a particular combustion device. This also reduces possibility of its use in relation to environmentally technological requirements. In the case under review the decline in overall fuel efficiency by 1.1% due to the water content, which in measured flue gas temperatures led to a reduction in the efficiency of combustion device up to 40% when considering only the chimney losses.

It can therefore be confirmed that the water content in the fuel has a significant influence on the combustion process and its high content in the fuel is inadmissible. This is also the result of many scientific publications (Hájek et al., 2013; Müller et al., 2015; Skanderová et al., 2015). The benefit of this publication is the comprehensive view of the assessed sample. In most cases, measurements are made for a reference water content in the fuel, which is not always an optimal assessment of the fuel combustion in a particular combustion device.

Relatively extensive research on the influence of water content in the fuel confirms the hypothesis that the effect of the water content affects the temperature change of flue gas and thus the efficiency of the combustion device (Bahadori et al., 2014).

From our measurements it is apparent that there may be extremes, as in the case of sample 1 with a very low water content in the fuel and very high emissions of carbon monoxide, which is operationally unacceptable as well as a high water content in the fuel and reduction of the combustion device efficiency by chimney loss.

Alternative fuels should therefore not be assessed according to the calorific value, but there should be focused attention to the water content in the fuel.

# REFERENCES

Bahadori, A., Zahedi, G., Zendehboudi, S. & Jamili, A. 2014. Estimation of the effect of biomass moisture content on the direct combustion of sugarcane bagasse in boilers. *International Journal of Sustainable Energy* **33**(2), 349–356.

Demirbas, A. 2004. Combustion characteristics of different biomass fuels. *Progress in Energy and Combustion Science* **30** (2), 219–230.

Di Blasi, C. 2008. Modeling chemical and physical processes of wood and biomass pyrolysis. *Progress in Energy and Combustion Science* **34** (1), 47–90.

ČSN EN 13229 Inset appliances including open fires fired by solid fuels – Requirements and test method. 2002.

ČSN 44 1377 Solid fuels – Determination of water content. 2004.

Hajek, D., Malatak, J. & Hajek, P. 2013. Combustion of selected biofuels types in furnace burner. *Scientia Agriculturae Bohemica* 44(1), 23–31.

Hedberg, E., Kristensson, A., Ohlsson, M., Johansson, C., Johansson, P.-A., Swietlicki, E., Vesely, V., Wideqvist, U. & Westerholm, R. 2012. Chemical and physical characterization of emissions from birch wood combustion in a wood stove. *Atmospheric Environment* **36**(30), 4823–4837.

Jevič, P., Hutla, P, Malaťák, J. & Šedivá, Z., 2007. Effciency and Gates emission with incineration of composite and one-componenet biocel briquettes in room heather. *Research in Agricultural Enginnering* **53**(3), 94–102.

Khodaei, H., Al-Abdeli, Y.M., Guzzomi, F., Yeoh, G.H. 2015. An overview of processes and considerations in the modelling of fixed-bed biomass combustion. *Energy* **88**, 946–972.

Kjällstrand, J. & Olsson, M. 2004. Chimney emissions from small-scale burning of pellets and fuelwood—examples referring to different combustion appliances. *Biomass and Bioenergy* **27**, 557–561.

Malaťák, J. & Passian, L. 2011. Heat-emission analysis of small combustion equipment's for biomass. *Research in Agricultural Engineering* **57**(2), 37–50.

Mcdonald, J.D., Zielinska, B., Fujita, E.M., Sagebiel, J.C., Chow, J.C. & Watson, J.G. 2000. Fine particle and gaseous emission rates from residential wood combustion. *Environmental Science and Technology* **34**(11), 2080–2091.

Nordin, A. 1994. Chemical elemental characteristics of biomass fuels. *Biomass and Bioenergy* **6** (5), 339–347.

Obaidullah, M., Bram, S., Verma, V.K., De Ruyck, J. 2012. A review on particle emissions from small scale biomass combustion. *International Journal of Renewable Energy Research* **2**(1), 147–159.

Obernbergera, I. & Theka, G, 2004. Physical characterisation and chemical composition of densified biomass fuels with regard to their combustion behaviour. *Biomass and Bioenergy* **27**, 653–669.

Müller, M., Horníčková, Š., Hrabě, P. & Mařík, J. 2015. Analysis of physical, mechanical and chemical properties of seeds and kernels of Jatropha curcas. *Research in Agricultural Engineering* **61**(3), pp. 99–105.

Skanderová, K, Malaťák, J. & Bradna, J. 2015. Energy use of compost pellets for small combustion plants. *Agronomy Research* **13**, 413–419.

Svoboda, K., Martinec, J., Pohořelý, M., Baxter, D. 2009. Integration of biomass drying with combustion/gasification technologies and minimization of emissions of organic compounds. *Chemical Papers* **63**(1), 15–25.

# Technical and software solutions for autonomous unmanned aerial vehicle (UAV) navigation in case of unavailable GPS signal

M. Dlouhy[1], J. Lev[2] and M. Kroulik[1,*]

[1]Czech University of Life Sciences Prague, Faculty of Engineering, Department of Agricultural Machines, Kamýcká 129, CZ165 21 Prague 6, Czech Republic
[2]Czech University of Life Sciences Prague, Faculty of Engineering, Department of Physics, Kamýcká 129, CZ165 21 Prague 6, Czech Republic
[*]Correspondence: kroulik@tf.czu.cz

**Abstract.** The article presents autonomous navigation for Unmanned Aerial Vehicles (UAV) without GPS support flying in extremely low altitudes (1.5 m – 2.5 m). Solution via visual navigation as an alternative to missing GPS position was proposed. MSER (Maximally stable extremal regions) was used as a navigation algorithm for detection of navigations objects. While GPS is useful for waypoints specification there are scenarios where GPS has unreliable signal (orchards) or is not available at all (indoor machinery halls or greenhouses). For that reason existing installed camera which is already needed for the task of inspection was used. The navigation algorithm was tested in two scenarios. The first experiment was done with dashed line marked on the floor of the hall. 8-loop testing track was created approximately 10 meters long so it was possible to fly it several times. Then outdoor experiments were performed on the university campus and park roads.

One of the discoveries was that MSER algorithm, proposed for finding correspondences between images, is possible to run in real-time. High reliability of the navigation algorithm was found during the indoor testing. The incorrect detection of the dashed line was found only in 1% of cases and those failures did not cause failure of navigation.

Although outdoor road recognition is difficult in general due to various surfaces and smoothness, MSER was able to find suitable candidates. When the UAV was fed with the parameter of road width it could verify that information with estimated distance and camera pose to accept or reject the detected pattern. The road was successfully recognized in 40% cases. Similar to the indoor algorithm in the case of navigation failure navigation along the absolute trajectory (line) was used.

**Key words:** robot, machine vision, maximally stable extremal regions, algorithm.

## INTRODUCTION

Agricultural robots can potentially take the place of manual labour, particularly in performing hazardous tasks such as protection of plants from pests, but also to improve productivity and profit-ability in farms, occupational safety and environmental sustainability. A UAV is an appropriate tool to perform multi-temporal studies for crop monitoring at low altitudes. (Torres-Sánchez et al., 2013). The application of UAVs has many advantages such as ease, rapidity, and cost of flexibility of deployment that makes

UAVs available in many land surface measurement and monitoring applications. For the UAV navigation the ground station and the predefined waypoints are usually used (Xiang, 2011; Gomez-Candon et al., 2014). On the other hand GPS technology has several critical drawbacks including insufficient accuracy for precision agriculture, interruptions in the signal and alterations of the environment which are not in the map but which need to be taken into account. This may lead to navigation failure (Santosh et al., 2014). According to Li et al. (2009) GPS and machine vision fused together or one of them fused with another auxiliary technology is becoming the trend development for agricultural vehicle guidance systems. The navigation of UAVs is still one of the most important subjects in defence research, especially in GPS-denied environments (Michaelsen & Meidow, 2014).

Autonomous navigation of field robots in an agricultural environment is a difficult task due to the inherent uncertainty of the environment (Hiremath et al., 2014). Michaelsen & Meidow (2014) summarized the related work about methods of automatic control of UAVs. Michaelsen & Meidow (2014) reported on the statistical embedding of a structural pattern recognition system into the autonomous navigation of an UAV during simulation of flight. A rule-based system is used for the recognition of visual landmarks such as bridges in aerial views. Fei et al. (2013) presented a comprehensive control, navigation, localization and mapping solution for an indoor quadrotor unmanned aerial vehicle (UAV) system. Three main sensors was used onboard the quadrotor platform, namely an inertial measurement unit, a downward-looking camera and a scanning laser range finder. The UAV, after being issued with the main navigation command, does not need to maintain any wireless link to the ground control station. Babel (2014) considered UAVs equipped with landmark-based visual navigation, a system which is less vulnerable to hostile acts than GPS or to long-term GPS outages, since it is not guided by external signals. A navigation update was obtained by matching onboard images of selected landmarks with internally stored geo-referenced images.

Methods often combine signals from multiple sensors. On the other hand, UAVs carrying capacity is limited. For this reason it is preferred to use existing equipment of the UAV without additional resource load. In the case of navigation through image analysis in real time a large amount of data is processed. According to Matas et al. (2004) the inmost images there are regions that can be detected with high repeatability since they possess some distinguishing, invariant and stable property. These regions may serve as the elements for stereo matching or object recognition. Authors presented the maximally stable extremal regions (MSER) algorithm for an efficient and practically fast detection of objects.

Main aim of this paper is presenting results of MSER algorithm utilization for autonomous UAV flight and navigation. This algorithm has not been used for the UAV navigation yet.

## MATERIALS AND METHODS

### Robot

The robot used for control algorithms was commercially available quadcopter AR.Drone 2 (AR.Drone 2.0, 2015). It is relatively cheap (approx. 300 EUR) and worldwide available unmanned aerial vehicle. This means that it is easily replaceable in

case of damage and also that other researches can simply repeat the experiments. The UAV is meant for mass market and that requires high safety for human-robot interaction.

The robot is controlled via Wi-Fi. You can operate it with FreeFlight2 application for tablets or mobile phones, but there exists also SDK (Software Development Kit) available for developers. The API (Application Programming Interface) is open to public and provides opportunities even for scientific research.

There are two cameras on the robot. The front camera has resolution 720p at 30 fps, wide angle lens 92°. The down pointing camera has lower resolution, but runs at 60 fps and it is used primarily for vehicle stabilization. They cannot be used simultaneously, but the operator/program can switch from one video stream to another anytime during the flight. The AR.Drone 2 is powered by LiPo 1,000 mAh battery (available is also bigger 1,500 mAh) which is enough for approximately 10 minutes long test flights.

The robot is equipped with three axis accelerometer, gyros and compass. Moreover it has down pointing sonar for low altitude and barometer for higher altitude control. The robot stabilization is fully handled by on-board computer and user sends only macro commands like 'take off', 'set desired pitch, roll and yaw' or 'land'. The robot responds with sensors status messages. It is possible to switch to DEBUG mode when information from all sensors and internal estimates including absolute 3D position and 3D angles are transmitted.

### Indoor experiment

There was a track created in the form of figure eight on area $5 \times 10$ m. It was in the indoor hall for the purpose of development and testing of the first algorithm. For the navigation dashed black line on light floor background was used. There were placed two wooden columns in the centre of the Fig. 8. The whole setup is sketched on Fig. 1. Note, that this test track is similar to Air Race competition, which has been part of Robot Challenge/Vienna since 2012 (RobotChallenge, 2016).

The prerequisite for presented project was implementation of framework handling communication with the ARDrone2 robot. The code was written in Python and the control program can run on any device with Wi-Fi connection. The frameworks as well as presented algorithms are freely available on GitHub (Dlouhý, 2015).

### Navigation Algorithm

The autonomous navigation code requires two processing threads. The first thread is main control loop running at 200 Hz handling communication and commands for the robot in real time. The second (working) thread is processing video stream and feeds image result data into the first control thread. The control loop simultaneously handles P-controller (proportional controller) for desired height and forward speed. The trajectory is defined by line or circular segment of given radius. Again simple P-controllers are used for angle and offset correction to navigate along the curve/line. The placement of navigation segment is updated with every processed video image.
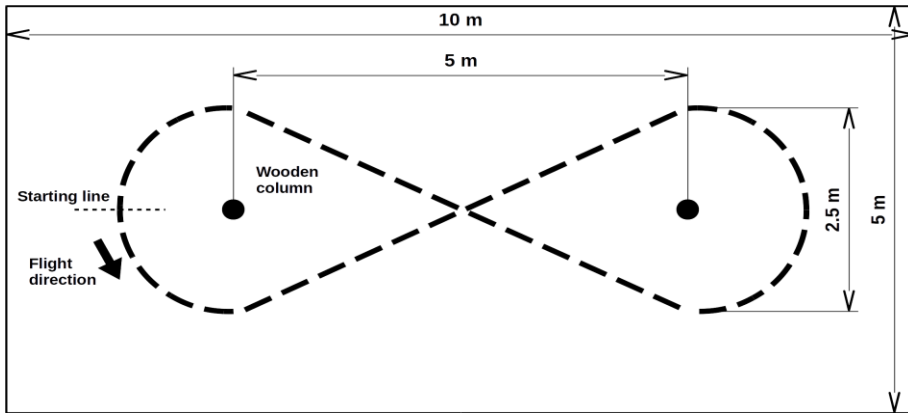
**Figure 1.** The testing track created in form of figure eight.

The image processing thread receives video stream and converts I-frames (Intra-coded picture, coded without reference to any frame except themselves, (Wiegand et al., 2003) into RGB picture. The supporting library for image processing is OpenCV 2.4.8 (package cv2) with binding to Numpy 1.8.2 (package for scientific computing with Python). The set of necessary cv2 functions was relatively small. First of all, cv2.MSER class for 'Maximally stable extremal region' extractor was created. This method was first published by Matas et al. (2002). MSER is a way how to overcome cumbersome definition of threshold for grayscale image segmentation. The basic idea is to explore all possible thresholds at once. If you imagine animation of threshold from 0 to 256 you will get white image at the beginning, then darkest features will appear and you end up with black image. On every step you could do analysis of black or white 'objects' and measure their area. The output of MSER are maximally stable objects, i.e. objects which do not change much over slight change of threshold.

There are several parameters for MSER method primarily to reduce the number of detected objects. Required is δ parameter (threshold step) and minimum and maximum size (area) of detected objects. Successful results were obtained for parameters δ = 10, minimum area = 100 pixels and maximum area = 30,000 pixels.

When objects are segmented function cv2.minAreaRect is used to find a rotated rectangle of the minimum area enclosing the input 2D point set. Rectangle was only accepted if points covered more than 70% of the area. These basic functions were then followed by several filter procedures. First of all duplicities were removed, i.e. overlapping rectangles for different threshold values. The one which was closer to desired width/height ratio was used and the other was rejected. The second filter removed the square like rectangles (when the length was less than three times the width), and width itself had to be in given limits (75 to 200 pixels, corresponding to expected height above the ground).

The result of image processing was list of filtered rectangles with their coordinates within the image, width and height, and angle orientation. These data were integrated into navigation control program with projection to 2D, where the altitude of the robot was estimated by maximal width of remaining rectangles. This pose scaling was much more robust than evaluating height for each rectangle separately.

736

The ARDrone2 has two video channels: one for quick overview with possibility of lost frames and one for video recording with extra several MB large buffers on board. It was decided to use recorded stream because otherwise it could miss some important crossing during temporary connection failure. The price for this was that the video channel was a little bit delayed (typically up to 1 second, where longer times were reported to operator as potential danger). Note, that only I-frames were used from H.264 video codec.

The delayed video stream with extra delay caused by image processing was handled with 'pose history queue'. The basic update runs on 200 Hz so it was enough to remember 200 poses for the fast history lookup. This way absolute coordinates of navigation strips were available.

The set of detected strips defined segment on which the UAV should navigate within next second (until a new image was received). A simple state machine was used to distinguish between navigation along the line, clockwise and anticlockwise circle. If there was only one segment/strip/rectangle in the processed image, then the previous state was kept. Two and more strips then defined line or circle of fixed radius.

There is one situation which requires a special care: trajectory path self-crossing. The navigation algorithm has to select subset of relevant strips/marks. In particular due to the narrow FOV (Field of View) of the down pointing camera it could see only two strips of crossing line.

First of all pairs are analysed if they define consequent line or circle. The first strip defined coordinate system and the second had to be $x$ in range 0.25 m to 0.48 m, $y$ (absolute offset to the left/right) in -0.25 m to +0.25 m and finally angle change had to be less than 50°. If there exists such a pair it was verified against current robot position. For classification as line and angle difference bigger than expected crossing angle was pair rejected.

Second, if no pair was found, only individual strips were compared against the strip poses from the last processed image. If again no suitable pair was found, then search for identical strips from the current and the previous image was performed for update path absolute position only. As the last step list of the detected strips was updated reference line or reference oriented circle was defined. One more note about speed control. The navigation pattern (number of strips on the floor defining line and arcs) was known so after state transition the control algorithm could increase the speed for given number of segments and slow down as expected line-arc or arc-line transition was approached. Moreover in case of communication problems when video was delayed for more than 2 seconds the speed was reduced to zero.

### Outdoor experiment

The goal was to present navigation on visually distinctive features like paved road. The algorithm for outdoor navigation along natural landmarks was slightly different but used the same core. The front camera was used instead of the down pointing camera for better situation overview. Because the road as the primary 'navigation line' is on the ground, only the lower parts of images were used. The road from perspective view is no longer rectangle. Individual horizontal image strips were processed via MSER where convex hull was applied on detected objects. A simple approximation via trapezoids was used.

The image trapezoid corners were projected on the ground, based on the history poses as for indoor experiments and the width of potential detected road was computed. For absolute camera position it was necessary to remember all 3 Euler angles (pitch, roll and yaw) and also estimate of UAV altitude (distance from the ground).
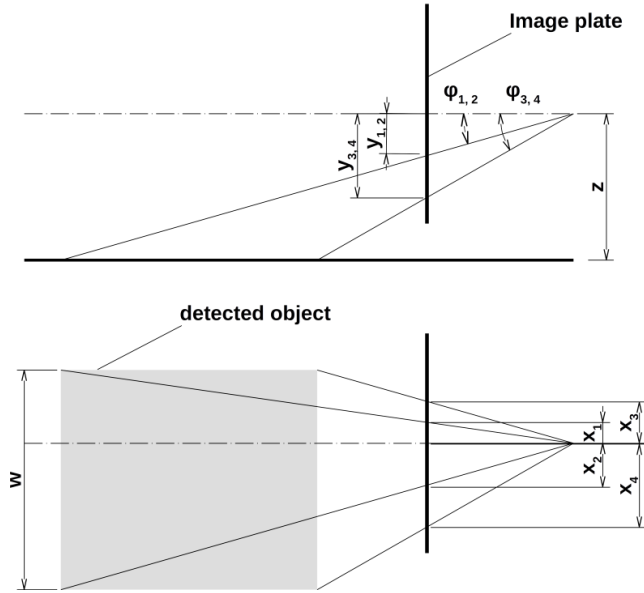


**Figure 2.** Side view and top view of simplified reverse projection from image plane to the ground. $w$ – width of the detected road, $x_i$ $y_i$ – image coordinates, $\varphi_i$ – angles between axis of robot and connecting line between robot and point on the detected object.

Fig. 2 shows simplified reverse projection of image plane points to the ground. The input parameters are estimated UAV absolute coordinates (6D, including angles) and simplified camera model defined by image centre ($x_c$, $y_c$), FOV (Field of view), and image resolution. There are four image coordinates ($x_i$, $y_i$), where I = {1, 2, 3, 4} defines boundary of trapezoid strip. Every image point is converted by following formulas. First image coordinates ($x_i$, $y_i$), are rotated along the image centre:

$$x_h = (x_i - x_c) \cdot cos(\alpha) - (y_c - y_i) \cdot sin(\alpha) \tag{1}$$

$$y_h = (x_i - x_c) \cdot sin(\alpha) + (y_c - y_i) \cdot cos(\alpha) \tag{2}$$

where: $x_h$, $y_h$ – compensated image coordinates; $\alpha$ – roll angle.

In the next step the angles for horizontally aligned coordinates were computed:

$$\psi = k \cdot x_h + \gamma \tag{3}$$

$$\varphi = k \cdot y_h + \beta \tag{4}$$

where: $k$ – ratio of FOV and resolution; $\beta$ – is pitch angle; $\gamma$ – robot heading.

Equations (3) and (4) are only simplification because proper equation should take non-circular surface and distortion into account. The ground distance from current UAV position $(x, y, z)$ is then:

$$d = \frac{z}{tan(-\varphi)} \qquad (5)$$

where: $d$ – ground distance from current robot position; $z$ – distance from the ground (UAV altitude).

The absolute coordinates of the robot can be calculated:

$$x_b = x + d \cdot cos(\psi) \qquad (6)$$

$$y_b = y + d \cdot sin(\psi) \qquad (7)$$

where: $(x_b, y_b)$ – path boundary point.

Because the four ground points do not necessarily form any regular trapezoid four different estimates were calculated (each corner against the line on opposite side). The post-processing filter of detected potential road segments was much simpler when compared to indoor experiment where exact size and dash line pattern was known. Here only expected road width was used to select the best matching object. Moreover minimum/maximum and variation limits were used for acceptance. The global navigation algorithm accepted new trajectory line if it fit within given angle (20°) and offset (2 m). The speed control for outdoor line navigation was simplified to slow down only in cases large video delays. Fig. 3 presents image processing loop for indoor and outdoor experiment.
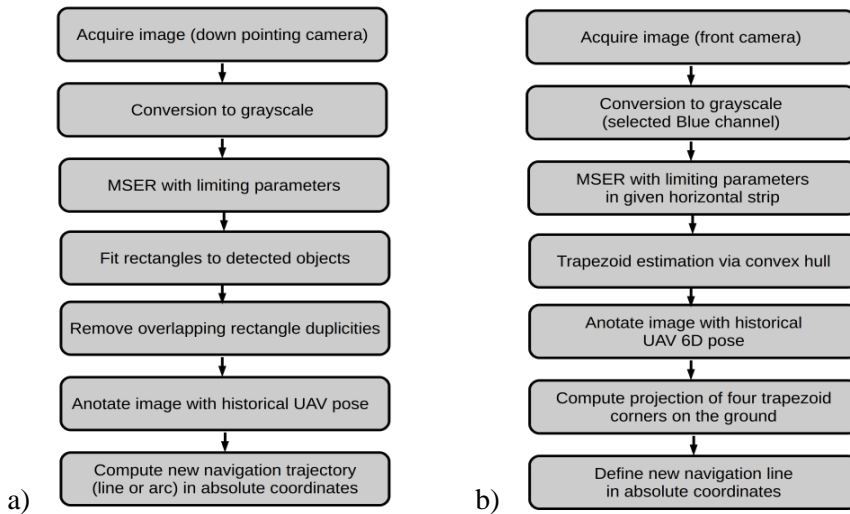


**Figure 3.** Diagram of the entire image processing: a) indoor experiment; b) outdoor experiment.

# RESULTS

**Indoor**

The final results of the indoor experiment were quite satisfactory. The robot was capable to follow marked route and the limiting factor become battery power. We can state high robustness of MSER algorithm. In particular it is suitable solution for light changing conditions. See some representative examples of problematic cases presented on Fig. 4.
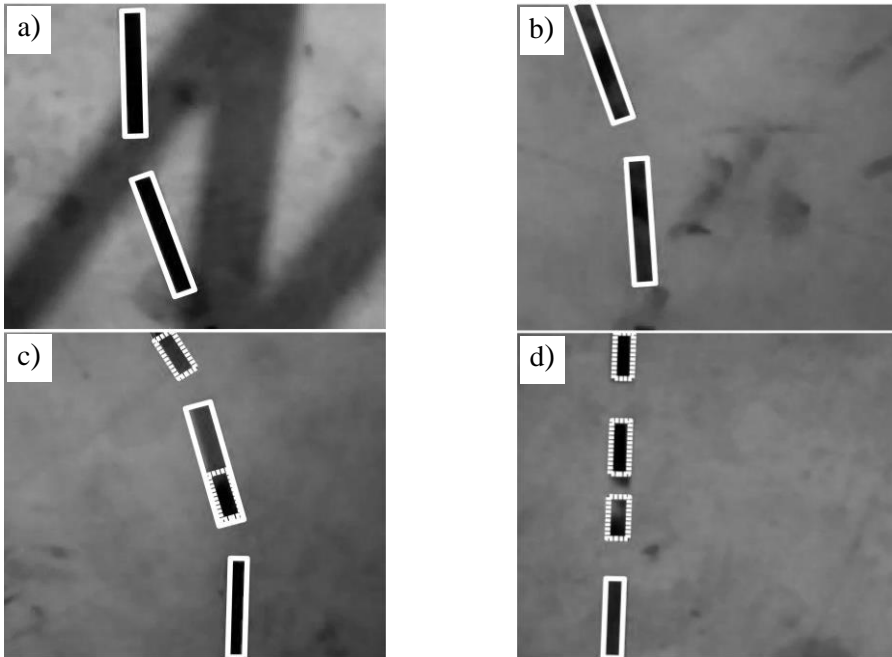


**Figure 4.** a) – example of strong sunlight and shadows; b) – dirt on the floor; c) – non-uniform colour of some marks due to light angle reflection; d) – broken mark due to strong light reflection.

The success rate was based on evaluation of three testing flights. The total length of selected flights was 20 minutes and 41 seconds. The route marked on the floor was circled in total 27 times. Fig. 5 shows histogram how many strips were typically detected in each video frame. It is apparent that mostly two strips were detected. The presented algorithm requires at least two detected strips for successful operation. This means that in 84.2% the algorithm had ideal relevant data (two or more detected mark in one image) and in 5.9% case it had to use history (no detected mark). The single mark cases (10%) can handle correction of absolute position of the navigation line or circle, but they fail to detect line-circle and circle-line transition.

Note that the robot was capable to navigate along the last defined navigation curve even in spite of detection failures in several consequent frames. This was possible thanks to reliable position estimation (for short term) using UAV inertial navigation unit integrated with optical flow (handled by on-board firmware).
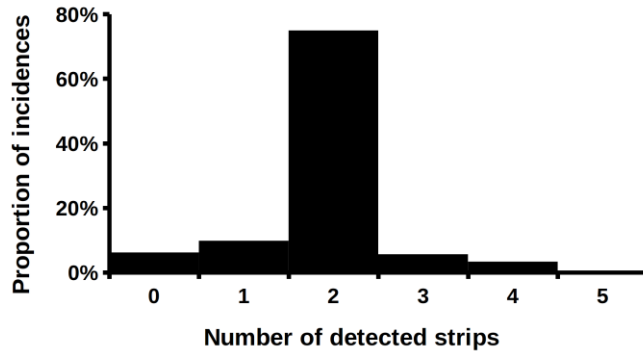
**Figure 5.** Histogram, number of strips which were typically detected in each video frame.

Important data are also incorrect detections, i.e. detection of false marks. There were only 27 wrong detections (i.e. approximately one per loop, mostly caused by dark pole holder). Correct detection was in 2,420 images i.e. there was approximately 1% failure rate. Further analysis showed that false mark detection were mostly (23 of 27) in combination with two correct marks and 3 times with one correct mark. In one case there was detected only one false mark without correct mark. All cases were successfully rejected by crossing detection procedure.

**Outdoor**

The first outdoor experiments were performed on the university campus and park roads. Although road recognition is difficult in general due to various surfaces and smoothness, MSER was able to find suitable candidates. When the UAV was fed with the parameter of road width it could verify that information with estimated distance and camera pose to accept or reject the detected pattern.
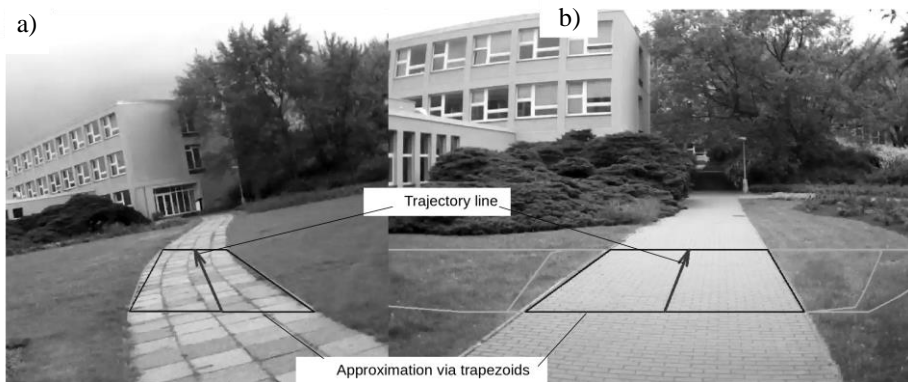


**Figure. 6.** A sample view of a) – curved and b) – straight road.

There are only relatively short road segments between junctions. The test runs were performed near the Faculty of Engineering on 42 m and 51 m long segments. The width of roads was 3 m and 2.15 m respectively. The first line was solid straight while the second has slight S-shape. The flights were short, 54 s and 106 s including take-off and

landing, and the number of processed images corresponds to number of seconds. Fig. 6 shows sample view of curved and straight road.
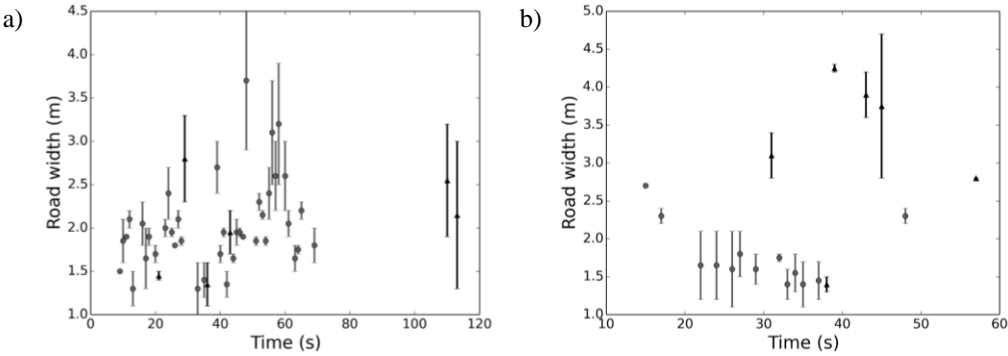


**Figure 7.** Accepted road widths with 4-corner distances variation. Correctly detected – circle, wrongly detected – triangle. (a) – curved path and (b) – straight road.

Fig. 7 shows correctly (circle) and wrongly (triangle) detected road with its minimum/maximum variation caused by distance measurement from four projected corners. In the last third the road was not visible, so failures are expected. Note that in b-case with straight road lower limit for maximal accepted road width could significantly reduce false detection.

## DISCUSSION

Control adaptation and path tracking are essential issues for moving along a crop in an autonomous way, due to the stochastic conditions inherent to crop environments (Urrea & Muñoz, 2013) and the agricultural robots must be able to adapt themselves in response to various terrain conditions (Mahadhir et al., 2014). Path detection during outdoor test was more challenging. Also Michaelsen & Meidow (2014) confirm that flying a UAV with an experimental system is expensive, risky, and legally questionable. These problems can be solved by defined marks. This was the purpose of addressing in the first phase of testing. Although the predefined marks were used for navigation, conditions were not easy for detection. It was necessary to solve the problems that represent light reflections, shadows and dirt on the floor (see Fig. 4). Advantages of the MSER algorithm were demonstrated in this case.

During the indoor experiments high algorithm reliability for navigating UAV was demonstrated. Wrong detection of individual marks ranged around 1%. However, these erroneous detection did not cause an error in navigation. Good applicability relatively inexpensive and commercially available platforms ARdrone2 was also demonstrated.

The outdoor road was successfully recognized in 40% of cases. Similarly to the indoor algorithm in case of navigation failure navigation along the absolute trajectory (line) was used, and successful detection only updated absolute coordinates of the road. The test was performed with single image strip only. The main source of failures was wind, for which the UAV had to compensate, and also angle changes of speed control. This has much bigger effect visible in front camera when compared to marks detection

of down pointing camera. Calculating the width of the road was essential for assessing the accuracy of detection. However, the accuracy of this calculation was significantly influenced by the precision determination of pitch angle (tilt of UAV). Two degrees caused width estimation change by 16% (2.68 m instead of 3.1 m). This error progressively increases depending on the pitch angle error. This error can be easily caused by slight push on UAV foam protective hull during battery exchange and would require extra self-calibration. Less restrictive post-filtering can be an alternative.

## CONCLUSIONS

This article presented experiments with UAV flying in extremely low altitudes (1.5–2.5 m). Test included outdoor and indoor environment. The first experiment was performed with artificial landmarks – dashed line marked on the floor of machinery hall. Highly reliable algorithm based on MSER image processing was demonstrated. Algorithm did not fail during the entire course of the tests and the battery power becomes the limiting factor.

In the second part the outdoor application, where the UAV were capable of following visually distinctive patterns, was demonstrated. The MSER image pre-processing was applied to horizontal image strip to recognize road on university campus. In the outdoor environment, it was necessary to distinguish between navigation failure due to an erroneous detection or weather conditions. Weather conditions play a greater role in navigation.

## REFERENCES

AR.Drone.2.0. 2015. [online]. *http://ardrone2.parrot.com.*

Babel, L. 2014. Flight path planning for unmanned aerial vehicles with landmark-based visual navigation. *Robotics and Autonomous Systems* **62**(2), 142–150.

Dlouhý, M. 2015. Heidi. GitHub repository. *https://github.com/robotika/heidi.*

Fei, W.A.N.G., Jin-Qiang, C.U.I., Ben-Mei, C.H.E.N. & Tong, H.L. 2013. A comprehensive UAV indoor navigation system based on vision optical flow and laser FastSLAM. *Acta Automatica Sinica* **39**(11), 1889–1899.

Gomez-Candon, D., Labbé, S., Virlet, N., Jolivot, A. & Regnard, J.L. 2014, High resolution thermal and multispectral UAV imagery for precision assessment of apple tree response to water stress. In: *2. International Conference on Robotics and associated High-technologies and Equipment for Agriculture and Forestry RHEA*. Madrid, Spain, pp. 283–288.

Hiremath, S., van Evert, F.K., ter Braak, C.J.F., Stein, A. & van der Heijden, G. 2014. Image-based particle filtering for navigation in a semi-structured agricultural environment. *Biosystems Engineering* **121**, 85–95.

Li, M., Imou, K., Wakabayashi, K. & Yokoyama, S. 2009. Review of research on agricultural vehicle autonomous guidance. *International Journal of Agricultural and Biological Engineering* **2**(3), 1–16.

Mahadhir, K. A., Tan, S. Ch., Low, Ch. Y., Dumitrescu, R., Amin, A.T.M. & Jaffar, A. 2014. Terrain classification for track-driven agricultural robots. *Procedia Technology* **15**, 776–783.

Matas, J., Chum, O., Urban, M. & Pajdla, T. 2002. Robust wide baseline stereo from maximally stable extremal regions. In: *Proc. of British Machine Vision Conference*. Cardiff, UK, 384–396.

Matas, J., Chum, O., Urban, M. and Pajdla, T., 2004. Robust wide-baseline stereo from maximally stable extremal regions. *Image and vision computing* **22**(10), 761–767.

Michaelsen, E. & Meidow, J. 2014. Stochastic reasoning for structural pattern recognition: An example from image-based UAV navigation. *Pattern Recognition* **47**(8), 2732–2744.

RobotChallenge. 2016. [online]. *http://www.robotchallenge.org.*

Santosh, A., van der Heijden, G.W.A.M., van Evert, F.K., Stein, A. & ter Braak, C.J.F. 2014. Laser range finder model for autonomous navigation of a robot in a maize field using a particle filter. *Computers and Electronics in Agriculture* **100**, 41–50.

Torres-Sánchez, J., López-Granados, F., De Castro, A.I. & Peña-Barragán, J.M. 2013. Configuration and specifications of an Unmanned Aerial Vehicle (UAV) for early site specific weed management. *PLoS ONE* **8**(3), e58210.

Urrea, C. & Muñoz, J. 2013. Path Tracking of Mobile Robot in Crops. *Journal of Intelligent & Robotic Systems* **80**(2), 193–205.

Wiegand, T., Sullivan, G.J., Bjøntegaard, G. & Luthra, A. 2003. Overview of the H.264/AVC Video Coding Standard. *IEEE Transactions on Circuits and Systems for Video Technology* **13**(7), 560–576.

Xiang, H. & Tian, L. 2011. Development of a low-cost agricultural remote sensing system based on an autonomous unmanned aerial vehicle (UAV). *Biosystems engineering* **108**(2), 174–190.

# Microalgae for biomethane production

V. Dubrovskis[*] and I. Plume

Latvia University of Agriculture, Faculty of Engineering, Institute of Energetics, Cakstes blvd 5, LV 3001 Jelgava, Latvia; [*]Correspondence: vilisd@inbox.lv

**Abstract.** Competition for arable land between food and energy producers has begun in Latvia. Biogas producers are seeking to use the hitherto unused land. There is a need to investigate the suitability of various biomasses for energy production. Maize is the dominating crop for biogas production in Latvia, but it is expensive to grow. The cultivation of more varied biomass with good economics and low environmental impact is thus desirable. Microalgae can be grown in pipes, basins and also in open ponds. This paper shows the results from the anaerobic digestion of microalgae *Chlorella vulgaris*, cultivated with fertilizer Varicon in open pond and harvested on 27 October and centrifuged (Study 1). The anaerobic digestion process was investigated for biogas production in sixteen 0.75 l digesters, operated in batch mode at temperature 38 ± 1.0 °C. The average methane yield per unit of dry organic matter added (DOM) from digestion of *Chlorella vulgaris* was 0.331 l $g_{DOM}^{-1}$. The second investigation (Study 2) used fresh biomass of *Chlorella vulgaris* harvested on 10–15 June with low dry matter content, as it was obtained from 4 m deep open pond without centrifugation. Anaerobic digestion process was provided in 4 digesters with volume of 5 l each. Average methane yield from the digestion of *Chlorella vulgaris* was 0.290 l $g_{DOM}^{-1}$, which is comparable to methane yield obtainable from maize silage or other energy crop silages. Microalgae *Chlorella vulgaris* can be successfully cultivated for biogas production from May to October or at least 170–180 days in a year under the agro-ecological conditions in Latvia.

**Key words:** anaerobic digestion, *Chlorella vulgaris*, biogas, methane yield.

## INTRODUCTION

According to Directive 2009/28/EC, Annex I, Part A, the goal for Latvia is to increase the share of energy produced from renewable energy sources (RES) in gross final energy consumption from 32.6% in 2005 to 40% (1918 toe) in 2020 (Ministry of Economics, 2010). Most of the biomass will come from forest products, but it should be taken into account that 1 ha of agricultural land can be used to obtain more energy than compared to forest wood biomass increment per 1 ha in a year (Dubrovskis & Adamovics, 2012). One of the most promising energy resources is biogas, which can be obtained from cogeneration plants in anaerobic fermentation process (Dubrovskis & Plume, 2015). Latvia is already running 56 biogas cogeneration plants, and maize silage is the most common biomass used as feedstock, as it gives a large quantity of biomass and a good yield of biogas (0.5–0.6 l $g_{DOM}^{-1}$). Most of the biogas plants built in Latvia are relatively large (49 of them greater than 0.5 MWel) and need a lot of raw materials for year-round running. Many of the biogas cogeneration plant owners do not have land for the cultivation of raw materials and are forced to transport raw materials even from a

great distance, therefore, the prices of biomass increase considerably (Dubrovskis & Plume, 2015).

Competition on arable land areas increases, which affects seriously those farmers who based biogas production efficiency on the cheap land rent. On the other hand, although Latvia has a lot of unused or underused land (around 360,000 ha in 2010), (Dubrovskis et al., 2011) farmers who do not own a biogas plant, put pressure on the Ministry of Agriculture and the Ministry of Economy aimed to limit the use of arable land for biogas production. Therefore, the production of raw materials from unused land would be most supported and encouraged (Dubrovskis & Plume, 2015).

Freshwater algae (*Chlorella vulgaris*) is one of the feedstock that also gives a great yield of biomass and hence could be used for biogas production. *Chlorella vulgaris* is a green algae growing in freshwater lakes. It can be used as a feed supplement for human and animal consumption also (Dubrovskis & Plume, 2015). For the cultivation of algae *Chlorella vulgaris*, the following factors should be taken into account: water, carbon dioxide, minerals and light. Optimal water temperature is 20–30 °C, as the algae grows slower at temperatures below 16°C and stops growing at temperatures above 35 °C (Chen, P.H., 1987). The following methods are used for algae cultivation:

- − cultivation in open ponds;
- − cultivation in closed basins;
- − cultivation in photobioreactors.

The cheaper and more widely used method is cultivation in open ponds. The advantages of this method are simplicity and cheapness, but its shortcomings are worse light utilisation, water evaporation losses and $CO_2$ discharge into the atmosphere, as well as the need for large land areas and partial dependence on climate (Dubrovskis & Plume, 2015).

Algae biomass yield: 150–300 tons (first year 150 t, but after adding $CO_2$ –300 t per year) of algae were obtained from 5 ha of sewage treatment pools during Bio-Crude Oil Demonstration Project activities in 2009 (Oilgae, 2016). *Chlorella vulgaris* obtainable biomass harvest was 106 t ha$^{-1}$ per year, as estimated in Ltd. Delta Riga experimental plant by owners in 2014 (Dubrovskis & Plume, 2015).

Theoretically, a large biogas yield can be obtained from algae, if all of the organic matter can be conversed. Methane yield from a unit of dry organic matter of the *Chlorella vulgaris* may be in the range 0.63–0.79 l $g_{DOM}^{-1}$ (Becker, 2004) as calculated theoretically according to Buswell equation (Symons & Buswell, 1933; Chen, 1987). However, in practice it is not possible to convert all of the organic matter into biogas. Biogas production depends on many factors and it should be taken into account that the algae cells have strong cell walls. The growing media and availability of nutrients may impose some impact on biogas yield. For example, former investigations have shown increased methane yield from algae grown in wastewater compared to algae fertilised with complex mineral fertiliser Varicon (Dubrovskis & Plume, 2015). Biogas and methane production from algae is investigated by many researchers (Symons & Buswell, 1933; Golueke et.al., 1957; Samson & LeDuy, 1986; Chen, 1987; Hernandez & Cordoba, 1993; Sanchez & Travieso, 1993; Mussgnug et al., 2010). Some of the research results on biogas and methane yield obtained from algae under different growing and treatment technologies are shown in Table 1.

**Table 1.** The methane production from algae *Chlorella sp*

| Algae | Methane (biogas) yield, l $g_{DOM}^{-1}$ | Methane content, % | Reference |
|---|---|---|---|
| *Scenedesmus sp& Chlorella sp* | 0.17–0.32 | 62–64 | Golueke et.al., 1957 |
| *Chlorella vulgaris* | 0.31–0.35 | 68–75 | Sanchez & Travieso, 1993 |
| *Chlorella sp & Scenedesmus sp* | 0.09–0.136 | 69 | Yen&Brune, 2007 |
| *Chlorella vulgaris* | 0.26–0.29 | 60–65 | Liandong Zhu,2013 |
| *Chlorella zofingiensis* | 0.06–0.1 | 52–60 | Liandong Zhu,2013 |
| *Chlorella pyrenoidosa* | 0.29 | 61–66 | Liandong Zhu,2013 |
| *Chlorella sp*+wws | (0.624) | 66.61 | Skorupskaite & Makareviciene, 2015 |
| *Chlorellasp*+cm | (0.580) | 59.63 | Skorupskaite & Makareviciene, 2015 |
| *Chlorella sp* (centrifuged) | (0.508) | 66.75 | Skorupskaite & Makareviciene, 2014 |
| *Chlorella sp* (unfreezed) | (0.652) | 67.98 | Skorupskaite & Makareviciene, 2014 |
| *Chlorella vulgaris* with Varicon as fertilizer | 0.297 | 45.95 | Dubrovskis & Plume 2015 |
| *Chlorella vulgaris* with waste water as fertilizer | 0.451 | 55.45 | Dubrovskis & Plume 2015 |

Notes: biogas yield shown in brackets; wws – waste water sludge used as fertilizer; cm – cow manure used as fertilizer.

The objective of this study was to find out how much methane and biogas can be obtained from algae Chlorela vulgaris cultivated in open ponds under conditions different from normal growing conditions (cultivated on 20–27 October, harvested on 27 October, while the average daily water temperature was 12 °C during 20–27 October) and in a deep pond (4 m), when sun radiation is smaller and insufficient, and to estimate when freshwater algae can be cultivated for biogas production in climatic conditions of Latvia.

## MATERIALS AND METHODS

### Materials, equipment and methods in Study 1
Algae from the Delta Riga experimental unit harvested on 27 October was used in Study 1. Equal quantities of algae biomass were filled in each of the 14 self-made 0.75 l volume bioreactors (30 g in R2-R15) with 500 g of inoculum, which was taken from 110 l bioreactor working with cow manure continuously. Inoculum in the amount of 500 g was filled in two of the same self-made reactors only for control sample. Each raw material sample was weighted (by electronic moisture balance Shimazy and scales Kern FKB 16KO2) carefully before it was filled in the bioreactor. Fermentation was continued in batch mode until biogas production ceased. Fermentation parameters, *e.g.*, volume, composition, pH, inside and outside temperatures, were registered every day in the experimental journal. Each sample was weighted and its composition analysed before the start and at the end of the fermentation process. Average volume of biogas released in bioreactors with inoculum (control sample) was subtracted from biogas volume obtained from each bioreactor filled with inoculum and algae biomass.

Fermentation temperature was maintained at 38 ± 1 °C inside the containers during batch mode process. Dry matter, ash and organic dry matter content was determined for every sample mixture before being filled into the bioreactor. Measuring accuracies were

the following: ± 0.2 g for inoculum and substrate weight (scales Kern FKB 16KO2), ± 0.001 g for biomass samples for dry matter, organic matter and ash weight analyses, ± 0.02 pH for pH (accessory PP-50), ± 0.05 l for gas volume, and ± 0.1 °C for temperature inside the bioreactor. Biogas composition, *e.g.*, methane, carbon dioxide, oxygen and hydrogen sulphide volume was measured with the gas analyser GA 2000. Dry matter was determined with the help of electronic moisture balance Shimazy at temperature 105°C. Dry organic matter was calculated from the weight of biomass ashes obtained in the oven Nabertherm at temperature 550°C using the standard heating program. Standard error for measurement data was calculated with the help of statistical data processing tools for each group of digesters.

### Materials, equipment and methods in Study 2

Algae *Chlorella Vulgaris* cultivated in 4 m deep open pond (from Ltd. Delta Riga experimental plant) and fertilized with Varicon, harvested on 10–15 June and having low dry matter content was used in Study 2. The algae biomass was obtained from an open pond without centrifugation.

The methodology for biogas and methane potential estimation was the same as in Study 1. The only difference was the number (4) and volume (5 l) of bioreactors used in Study 2. All 4 bioreactors were filled with 1 kg of inoculum and 2 kg of tap water. 1 kg of algae biomass was added to bioreactors B2, B3 and B4. Inoculum (finished digestate from fermented cow manure) and water only was fermented in reactor B1 for control sample.

## RESULTS AND DISCUSSION

In **Study 1**, biogas and methane data from all 16 bioreactors were used to calculate the average biogas and methane volume for each group of similar bioreactors filled in with the same sample replications. The results are summarized in Tables 2, 3, 4 and in Fig. 1, below.

The algae *Chlorella vulgaris* biomass samples investigated in the Latvia University of Agriculture Bioenergy laboratory contained the following complex substances: proteins 53.60%, lipids 18.51% and carbohydrates16.81%.

The results of raw algae biomass and inoculum analysis before fermentation are shown in Table 2.

**Table 2.** The results of the analyses of raw materials

| Bioreactor | Raw material | Substrate pH | TS, % | TS, g | Ash, % | DOM, % | DOM, g | Weight, g |
|---|---|---|---|---|---|---|---|---|
| R1, R16 | IN500 | 7.14 | 2.26 | 11.30 | 28.87 | 71.13 | 8.04 | 500.0 |
| R2-R15 | IN500 +A30 | 7.00 | 2.82 | 14.95 | 25.42 | 74.58 | 11.15 | 530.0 |
| R2-R15 | A30 | 5.95 | 12.18 | 3.65 | 14.78 | 85.22 | 3.11 | 30.0 |

Abbreviations: TS – total solids, Ash – ashes, DOM – dry organic matter, R1–R16 – bioreactors numbers; IN – inoculum, A– algae fertilised with complex fertiliser Varicon.

The algae biomass has a higher content of ashes compared to agricultural energy crops (maize silage 19–21%) (Dubrovskis et al., 2011), which can be explained by high minerals (complex fertiliser Varicon) doses used, but may be poorly utilized by algae in the growing process. This suggests that there are opportunities for the improvement of cultivation technologies and usage of optimised doses of fertilizer. Results of the analyses of finished fermented digestate are shown in Table 3.

**Table 3.** The results of the analyses of finished digestate

| Bioreactor | Raw material | Substrate pH | TS, % | TS, g | Ash, % | DOM, % | DOM, g | Weight, g |
|---|---|---|---|---|---|---|---|---|
| R1 | IN | 7.16 | 2.18 | 10.86 | 29.05 | 70.85 | 7.69 | 498.1 |
| R16 | IN | 7.15 | 2.20 | 10.96 | 29.10 | 70.90 | 7.77 | 498.2 |
| R2 | IN+A | 7.18 | 2.12 | 10.90 | 26.72 | 73.28 | 7.99 | 515.0 |
| R3 | IN+A | 7.17 | 2.18 | 11.24 | 26.57 | 73.43 | 8.25 | 515.2 |
| R4 | IN+A | 7.16 | 2.15 | 11.11 | 25.90 | 74.10 | 8.23 | 515.6 |
| R5 | IN+A | 7.18 | 2.16 | 11.14 | 26.36 | 73.64 | 8.20 | 515.0 |
| R6 | IN+A | 7.18 | 2.17 | 11.21 | 25.98 | 74.02 | 8.30 | 515.6 |
| R7 | IN+A | 7.16 | 2.17 | 11.20 | 26.13 | 73.87 | 8.27 | 516.0 |
| R8 | IN+A | 7.19 | 2.18 | 11.24 | 26.49 | 73.51 | 8.26 | 515.6 |
| R9 | IN+A | 7.20 | 2.20 | 11.36 | 26.10 | 73.90 | 8.39 | 516.4 |
| R10 | IN+A | 7.20 | 2.20 | 11.36 | 26.05 | 73.95 | 8.40 | 516.2 |
| R11 | IN+A | 7.21 | 2.22 | 11.47 | 25.88 | 74.12 | 8.50 | 516.8 |
| R12 | IN+A | 7.17 | 2.18 | 11.26 | 26.09 | 73.91 | 8.32 | 516.2 |
| R13 | IN+A | 7.21 | 2.15 | 11.08 | 26.44 | 73.56 | 8.15 | 515.0 |
| R14 | IN+A | 7.18 | 2.18 | 11.22 | 26.45 | 73.55 | 8.25 | 515.4 |
| R15 | IN+A | 7.18 | 2.17 | 11.20 | 25.89 | 74.11 | 8.30 | 516.0 |

It was calculated from Table 3 data that only a small part of inoculum's (R1, R16) dry organic matter (3.8% or 0.31 g) was biodegraded during the re-fermentation process, perhaps, due to plentiful presence of cells of microorganisms and complex humus substances persistent to biodegradation. Therefore, inoculum has little or no impact on the results of biogas production from added biomass. Algae dry organic matter was biodegraded by 82.63% during the anaerobic fermentation process. Biogas and methane yield from algae is shown in Table 4. The average volume of biogas (0.20 l) or methane (0.014 l) released in control bioreactors R1, R16 has already been subtracted from biogas volume from every bioreactor filled with inoculum and algae biomass in Table 4.

The relatively lower average methane content in biogas in bioreactors with 30 g algae biomass is explained by the fact that around 0.25 l of air remains in top of every bioreactor at beginning of anaerobic process. This air warms up and enters gas bags and was measured together with biogas during fermentation process. This effect is particularly evident in bioreactors with less added organic matter.

**Table 4.** Biogas and methane yield

| Reactor | Raw material | Biogas, l | Biogas, l $g_{DOM}^{-1}$ | Methane aver. % | Methane, l | Methane, l $g_{DOM}^{-1}$ | Methane max, % |
|---|---|---|---|---|---|---|---|
| R1 | IN | 0.2 | 0.01 | 7.3 | 0.01 | 0.01 | 7.3 |
| R2 | IN+A | 3.2 | 1.03 | 41.4 | 1.33 | 0.43 | 58.2 |
| R3 | IN+A | 2.0 | 0.64 | 49.8 | 1.00 | 0.32 | 63.2 |
| R4 | IN+A | 2.1 | 0.68 | 47.7 | 1.00 | 0.32 | 64.1 |
| R5 | IN+A | 2.3 | 0.74 | 47.4 | 1.09 | 0.35 | 64.8 |
| R6 | IN+A | 1.9 | 0.61 | 49.3 | 0.94 | 0.30 | 62.6 |
| R7 | IN+A | 1.9 | 0.61 | 49.9 | 0.95 | 0.31 | 63.2 |
| R8 | IN+A | 2.0 | 0.64 | 50.1 | 1.00 | 0.32 | 66.5 |
| R9 | IN+A | 2.3 | 0.74 | 42.5 | 0.98 | 0.31 | 65.5 |
| R10 | IN+A | 2.2 | 0.71 | 48.4 | 1.06 | 0.34 | 60.7 |
| R11 | IN+A | 1.8 | 0.58 | 50.5 | 0.91 | 0.29 | 59.7 |
| R12 | IN+A | 1.9 | 0.61 | 48.3 | 0.92 | 0.30 | 64.9 |
| R13 | IN+A | 2.7 | 0.87 | 48.7 | 1.32 | 0.42 | 65.3 |
| R14 | IN+A | 2.0 | 0.64 | 48.4 | 0.97 | 0.31 | 66.9 |
| R15 | IN+A | 1.9 | 0.61 | 48.8 | 0.93 | 0.30 | 65.3 |
| R16 | IN | 0.2 | 0.01 | 7.2 | 0.01 | 0.01 | 7.3 |
| Average (R2-15) | | 2.16± 0.38 | 0.694± 0.12 | 47.69± 2.70 | 1.027± 0.14 | 0.331± 0.04 | 63.64± 2.57 |

Biogas and methane production from algae that was fertilized by complex fertilizer Varicon and harvested on 27 October is shown in Fig. 1.
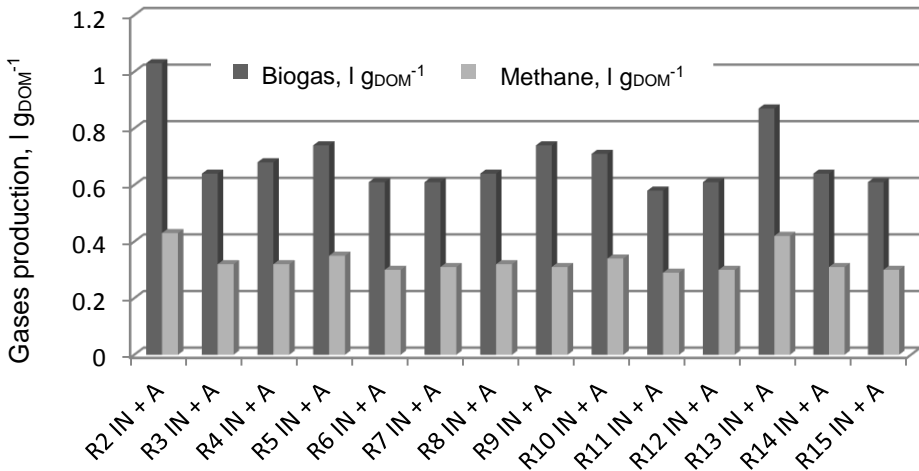


**Figure 1.** Biogas and methane production from algae; IN – inoculum; A– algae.

The results are comparable to those presented in Table 1 of the researchers who worked with *Chlorella vulgaris* results. The average methane yield is quite similar to the harvest derived from maize silage ($0.332\ l\ g_{DOM}^{-1}$), rye grass silage ($0.316\ l\ g_{DOM}^{-1}$) and perennial grass silage ($0.322\ l\ g_{DOM}^{-1}$) in our previous studies (Dubrovskis & Plume, 2015).

**Study 2** investigated the algae *Chlorella vulgaris* harvested on 10–15 June and obtained from an open pond without centrifugation (from Ltd. Delta Riga experimental plant) and fertilized with Varicon. The algae *Chlorella Vulgaris* biomass samples investigated in the LUA Bioenergy laboratory contained the following complex substances: proteins 48.7%, lipids 16.43% and carbohydrates 17.56%.The results are summarized in Tables 5, 6, 7 and in Fig. 2 below.

The results of raw biomass analysis before fermentation are shown in Table 5.

**Table 5.** The results of the analyses of raw materials

| Bioreactor | Raw material | Substrate pH | TS, % | TS, g | Ash, % | DOM, % | DOM, g | Weight, g |
|---|---|---|---|---|---|---|---|---|
| B1 | IN | 7.41 | 3.14 | 31.40 | 22.93 | 77.07 | 24.21 | 1,000.0 |
|  | Water |  |  |  |  |  |  | 2,000.0 |
| B2 | IN | 7.41 | 3.14 | 31.40 | 22.93 | 77.07 | 24.21 | 1,000.0 |
|  | Algae | 6.46 | 3.33 | 33.33 | 16.09 | 83.91 | 27.96 | 1,000.8 |
|  | Water |  |  |  |  |  |  | 2,000.0 |
| B3 | IN | 7.41 | 3.14 | 31.40 | 22.93 | 77.07 | 24.21 | 1,000.0 |
|  | Algae | 6.46 | 3.33 | 33.31 | 16.09 | 83.91 | 27.95 | 1,000.2 |
|  | Water |  |  |  |  |  |  | 2,000.0 |
| B4 | IN | 7.41 | 3.14 | 31.40 | 22.93 | 77.07 | 24.21 | 1,000.0 |
|  | Algae | 6.46 | 3.33 | 33.31 | 16.09 | 83.91 | 27.95 | 1,000.3 |
|  | Water |  |  |  |  |  |  | 2,000.0 |

The results of analyses of finished fermented digestate are shown in Table 6.

**Table 6.** The results of the analyses of digestate

| Bioreactor | Raw material | Substrate pH | TS, % | TS, g | Ashes, % | DOM, % | DOM, g | Weight, g |
|---|---|---|---|---|---|---|---|---|
| B1 | IN+w | 7.53 | 1.21 | 30.68 | 23.62 | 76.38 | 23.43 | 2536 |
| B2 | IN+w+A | 7.08 | 1.16 | 35.40 | 25.21 | 74.29 | 26.47 | 3052 |
| B3 | IN+w+A | 7.04 | 1.31 | 40.68 | 23.15 | 76.85 | 31.26 | 3105 |
| B4 | IN+w+A | 7.11 | 1.19 | 36.02 | 29.79 | 70.21 | 25.29 | 3027 |

Abbreviations: w – water; A – algae; IN – inoculum

The biogas and methane yield from the algae *Chlorella vulgaris* is shown in Table 7. The average volume of biogas (2.9 l) or methane (0.621 l) released in control bioreactor B1 has already been subtracted from biogas volume from every bioreactor filled with inoculum and algae biomass in Table 7.

**Table 7.** Biogas and methane yields

| Reactor | Raw material | Biogas, l | Biogas, l $g_{DOM}^{-1}$ | Methane aver. % | Methane l | Methane, l $g_{DOM}^{-1}$ | Methane max, % |
|---|---|---|---|---|---|---|---|
| B1 | IN+w | 2.9 | 0.12 | 21.4 | 0.62 | 0.03 | 21.4 |
| B2 | IN+w+A | 15.5 | 0.56 | 54.0 | 8.37 | 0.30 | 66.5 |
| B3 | IN+w+A | 14.2 | 0.51 | 52.0 | 7.37 | 0.26 | 65.3 |
| B4 | IN+w+A | 16.1 | 0.58 | 53.0 | 8.53 | 0.31 | 64.7 |
| Average (B2-B4) | | 15.27 ± 0.97 | 0.546 ± 0.04 | 52.95 ± 1.00 | 8.088 ± 0.63 | 0.290± 0.03 | 65.48 ± 0.92 |

The biogas and methane yields are lower compared to those obtained in Study1. Biogas and methane yield from the algae cultivated in 1 m deep pond and harvested on 27 October compared to the biogas and methane yield from the algae cultivated in 4 m deep pond and harvested on 10–15 June is higher by 27.1% for biogas and by 14.14% for methane.

This could be explained by the algae's lower content of lipids and proteins. The algae was cultivated in 4 m deep pond during 10–15 June, when sun radiation level is high, but obviously, mixing was not good enough. Another reason may be the lack of centrifugation providing some destroying of algae used in Study1.
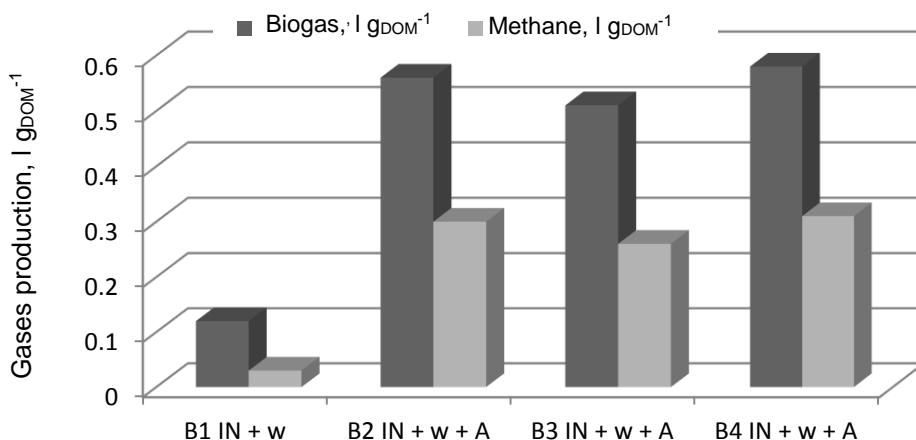


**Figure 2.** Biogas and methane production from algae; IN – inoculum; A – algae; w – water.

Further anaerobic fermentation investigations should deal with the combination of microalgae *Chlorella vulgaris* biomass having low C:N ratio of 7.53 (Skorupskaite et al., 2015) with agricultural wastes having high C:N ratio *e.g.*, straw (150), sawdust (208), etc. (Dubrovskis & Adamovics 2012). Such a combination can establish an important part of nitrogen, carbon, and other plant nutrients' life cycles, including capturing the leaching nitrogen from wastewater by algae biomass, biomethane production from combined substrates in optimised anaerobic fermentation process and returning of plant nutrients into the soil with digestate.

**CONCLUSIONS**

Biogas and methane yield obtained from algae biomass cultivated at Ltd. Delta Riga experimental plant under conditions different from normal growing conditions is comparable to that obtainable from other agricultural biomasses (maize, rye grass and perennial grasses silages) used for biogas and methane production in our previous research (Dubrovskis & Plume, 2015).

The study of methane production from algae harvested in summer or autumn period confirmed that algae can be utilised during its normal growing period from May till October or at least 170–180 days period in a year at the climatic conditions of Latvia.

The results of the investigation show that the algae *Chlorella vulgaris* is a prospective alternative biomass, suitable to replace or complement traditional feedstock, *e.g*., maize silage or energy crops in biogas and methane production.

## REFERENCES

Becker, E.W. 2004. Micro algae in human and animal nutrition. *Handbook of microalgal culture*. Oxford: Blackwell Publishing, pp. 312–351.

Chen, P.H.1987. Factors influencing methane fermentation of micro-algae. *PhD thesis*. University of California, Berkeley, CA, USA, 89 pp.

Dubrovskis, V., Plume, I., Kotelenecs, V. & Zabarovskis, E. 2011, Biogas production and biogas potential from agricultural biomass and organic residues in Latvia. In: *Proceedings of International conference Biogas in Progress*, Hohenheim, Stuttgart, pp. 80–83.

Dubrovskis, V. & Adamovics, A. 2012. *Bioenergy horizons.* Jelgava, 352 pp. (in Latvian).

Dubrovskis, V. & Plume, I. 2015. Biogas potential from freshwater algae. In: *14th International scientific conference Engineering for rural development*. Jelgava, pp. 502–509.

Ministry of Economics, 2010. Information Report: Republic of Latvia National Renewable Energy Action Plan for implementing Directive 2009/28/EC of the European Parliament and of the Council of 23 April 2009 on the promotion of the use of energy from renewable sources and amending and subsequently repealing Directives 2001/77/EC and 2003/30/EC by2020,p.103.online: http://www.ebbeu.org/legis/ActionPlanDirective2009_28/national_renewable energy action_plan_latvia_en.pdf

Golueke, C.G., Oswald, W.J. & Gotaas, H.B. 1957. Anaerobic digestion of algae. *Appl. Microbiol*. **5**, 47–55.

Hernandez, E.P.S. & Cordoba, L.T. 1993. Anaerobic digestion of chlorella vulgaris for energy production. *Resources Conservation and Recycling* **9**, 127–132.

Mussgnug, J.H., Klassen, V., Schlüter, A. & Kruse, O. 2010. Microalgae as substrates for fermentative biogas production in a combined biorefinery concept. Bielefeld University, Center for Biotechnology, *Germany Journal of Biotechnology* **150**, 51–56.

'Oilgae' 2016, Cultivation of Algae. *http://www.oilgae.com/algae/oil/biod/cult/cult.html,* Accessed 17.01.2016.

Samson, R. & LeDuy, A. 1986. Detailed study of anaerobic digestion of Spirulina max-ima algal biomass. *Biotechnology and Bioengineering* **28**, 1014–1023.

Sanchez, E.P. & Travieso, L. 1993. Anaerobic digestion of Chlorella vulgaris for energy production. *Resour. Conserv.Recycl*. **9**, 127–132.

Skorupskaite, V. & Makareviciene, V. 2015. Green energy from microalgae: usage of algae biomass for anaerobic digestion. *Journal of International Scientific Publications: Ecology and Safety* **8**, ISSN 1314-7234, *http://www.scientific-publications.net,* Accessed 10.01.2016.

Skorupskaite ,V., Makareviciene, V., Siaudinis, G. & Zajancauskaite, V. 2015. Green energy from different feedstock processed under anaerobic conditions. *Agronomy Research* **13**(2) 420–429.

Symons, G.E. & Buswell, A.M. 1933. The methane fermentation of carbohydrates. *Journal Am. Chem. Soc*. **55**, 2028–2036.

Yen, H.W. & Brune, D.E. 2007.Anaerobic co-digestion of algal sludge and waste paper to produce methane. *Bioresour. Technol*. **98**, 130–134.

# Model-based estimation of market potential for Bio-SNG in the German biomethane market until 2030 within a system dynamics approach

T. Horschig[1,*], E. Billig[2] and D. Thrän[1,2]

[1]DBFZ – Deutsches BiomasseForschungszentrum gGmbH, Department of Bioenergysystems, Torgauer Straße 116, DE 04347 Leipzig, Germany
[2]UFZ – Helmholtz Centre for Environmental Research, Department of Bioenergysystems, Permoserstraße 15, DE 04347 Leipzig, Germany
[*]Correspondence: thomas.horschig@dbfz.de

**Abstract.** One option for energy provision from renewables is the production and grid injection of synthetic natural gas from lignin-rich biomass like wood and straw. Bio-SNG (biological produced synthetic/substitute natural gas) is the product of the thermochemical production of methane via gasification and methanation of lignin-rich biomass. The first commercial bio-SNG plant went successfully into operation in the end of 2014, in Gothenburg (Sweden). Regarding the huge potential of lignin-rich biomass bio-SNG is expected to have a high potential for a sustainable and greenhouse gas reducing contribution in power, heat and fuel markets. Being a future technology with great advantages like storability and transportability within a gas grid but recently too high prices for market implementation, possible future market shares are uncertain because bio-SNG has to compete with anaerobic biomethane as well as fossil alternatives. With the combination of an extensive techno-economic evaluation for present and future costs of bio-SNG depending on the feedstock supply chain and economy of scale, Delphi-Survey and a quantitative market simulation we determined future market shares for biomethane and bio-SNG for Germany under varying scenarios like incentive schemes, economy of scale and feedstock prices. Results indicate that substantial governmental support in terms of either R&D effort to lower bio-SNG prices or direct subsidies for a further capacity development is necessary to achieve significant market shares for biogenic methane.

**Key words:** bio-SNG, System Dynamics, Bioenergy markets, biomethane.

## INTRODUCTION

Renewable Energy (RE) is a substantial part of Germanys Climate and Energy Strategy. Against the overall global trend, between 1990 and 2012 the share of Renewables increased whilst the overall energy consumption as well as the use of fossil energy carriers decreased in Germany, resulting in a 30% share of RE in Germanys power mix, a share of about 10% in the heat sector and a share of 5.4% in the mobility sector with solid, gaseous and liquid biomass ('Deutschland – Agentur für Erneuerbare Energien'). With a share of 100% in the fuels sector, 87% in the heat sector and 31% in the power sector, bioenergy is the most important RE in Germany (Thrän et al., 2015). One significant advantage of most bioenergy utilisations is the possibility to substitute

fossil fuels in already existing infrastructures. Biomethane, a biogenic gas chemically equal to natural gas, can substitute fossil gas in all scopes of application. Thus, there is a tremendous potential for biomethane to substitute fossil gas (683 TWh a$^{-1}$ in 2014 (Erdgasverbrauch von Deutschland bis 2014 | Statistik). However, due to an imperfect market situation, in most cases energy out of biomass is more expensive than its fossil alternatives (Fisher & Rothkopf, 1991; Jaffe et al., 2005). Therefore governmental support is needed if it is the political will to decarbonize the energy system and increase the use of RE. The most recent amendment of the most important support scheme for biomethane, the Renewable Energy Source Act, reduces governmental compensations. This comes along with a transformation of the biomethane market from a compensation driven market to a market-driven one. It is uncertain how the market will develop in the mid-term under these new boundary conditions. Therefore a dynamic market model was developed to simulate mid-term market development under most recent and possible new boundary conditions for already market-implemented anaerobic biomethane and not yet market-implemented thermochemical biomethane, so-called bio-SNG. If one regards the needed efforts of Germany to reach the goal of a 40% reduction of GHG emissions compared to the 1990 level (further 749 million t $CO_{2eq}$) until 2030, biomethane can be a valuable contribution to reach this goal (European Environment Agency, 2014).

### Biomethane in a nutshell

Biomethane is biogenic and renewable methane that can be produced on the one hand by anaerobic digestion (AD) of organic matter such as energy crops, manure, sewage, organic waste, and so on and on the other hand by gasification and methanation of lignin rich material such as forestry residues or energy crops (e.g. straw). Being chemically identical to natural gas it can use the already existing infrastructure and serve as a replacement in all natural gas applications. Depending on the value chain of biomethane production and the scope of application where natural gas is substituted large amounts of greenhouse gas emissions can be saved (Repele et al., 2013; Repele et al., 2014). In Germany renewable methane is primarily used in CHP plants (combined heat and power production) (Daniel-Gromke et al., 2013). Furthermore biomethane can be fed and buffered in the existing gas grid. Due to this easy storability and transportability it can be produced and consumed spatially separated and thus be an option for the upcoming task of energy plants to operate demand driven.

To start these actions support by energy and climate policies was necessary. In 2004 first stakeholders in Germany started with the production and trade of biomethane. Being a biogenic alternative to natural gas biomethane is about 2–3 times more expensive than natural gas (Dunkelberg et al., 2015). Amongst others this support led to a rapid installation of biomethane production plants and biomethane CHP plants.

However, because of the high interest on biomethane and its many advantages as fossil fuel substitute, i.e. the GHG emission saving potential, the storability, the existing industry sector but also the challenging market barriers make it worth to analyse the market structure and to derive scenario-driven forecasts on future market shares for biomethane. This is done by using a system dynamics market simulation model in combination with an extensive techno-economic analyses and involving experts via a Delphi-Survey.

**Biomethane market development and drivers in Germany**

Since 2004 the implementation of a biomethane market in Germany was promoted by a plurality of laws and regulations leading to a continuous expand of biogas plants, biogas upgrading plants and thus biomethane feed-in capacities (Fig. 1). The most important promoting law is the Renewable-Energy-Source-Act. It guarantees compensation for the production of renewable power for 20 years. Besides the application in CHP plants biomethane is a promising option for the fuel market, the heat market and the chemical industry (IEA Bioenergy, 2014). To this day the use for direct heat and transport are niche markets. With the possibility of grid feed-in biomethane could be traded within the EU, being liquefied it could be traded global. In this way a large-scale emission reduction could be achieved. Because of the recent version (2014) of the Renewable Energy Source Act support for further biomethane capacity expansion in Germany is no longer sufficient. This leads to a strong decrease of plant installations and capacity expansion.

Since the construction of the first biomethane plant in Germany in 2006 a constant biomethane plant installation was realized. Waves of plant installations occurred as a delayed reaction to supporting schemes that were highly profitable. However, big waves did not occur due to different delays in plant construction. The plant installation and biomethane producing capacity development is illustrated in Fig. 1.
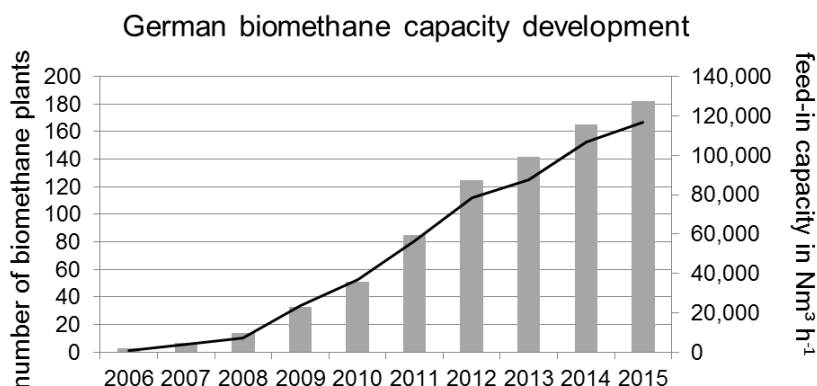


**Figure 1.** Development of biomethane capacity and plant installation in Germany (Deutsche Energie-Agentur GmbH, 2014).

Besides the above mentioned laws, regulations and support schemes further factors influenced the market development.

The competitive situation between biomethane and natural gas is determined by the price for natural gas and the profit you can make out of it. This permanent competitive situation in each scope of application is crucial for the investment decisions. The fix costs, i.e. for gas grid transport, the CHP unit, the staff or market effort can be assumed equal. But whereas natural gas can be purchased by fossil deposits, biomethane has to be produced by an expensive and complex biochemical or thermochemical conversion process out of biomass.

Another possibility to make profit out of biomethane is customers which are willing to pay a certain amount of money more for sustainable and renewable energy. This can be done via specific green power or green gas contracts. In the mobility sector pure biomethane or a mixture is available. Nevertheless this is only a niche market. Only a small fraction of potential customers are willed to pay a higher price for sustainable and climate-friendly energy.

**Production of Biomethane**

The here characterized biomethane can be produced via two conversion processes. The first one is biomethane produced via the biochemical process through digestion of biomass. The second one is the production via the thermochemical process of gasification and methanation. If produced through the thermochemical process the biomethane is often called bio-SNG (biological produced synthetic/substitute natural gas). In the following, biochemical produced methane is called biomethane and thermochemical produced methane is called bio-SNG.

The biomethane production via biochemical conversion is already a widely applied technology. The major process steps are (Kaltschmitt et al., 2009; Graf & Bajohr, 2011; FNR, 2014):

I. Pretreatment of substrate (e.g. crushing)
II. Anaerobic digestion
III. Raw biogas treatment
IV. Biogas upgrading.

Biomethane, respectively bio-SNG via the thermochemical conversion is yet barely applied in the market. A lot of research and demonstration is going on, but so far only one commercial plant is yet in operation (Kopyscinski et al., 2010). The first commercial plant has a bio-SNG capacity of 20 MW, is located in Gothenburg (Sweden) and went into operation in the end of 2014 (Goteborg Energi, 2014).

All thermochemical conversion plants and research concepts consists of the following process steps (Knoef, 2012; Seiffert & Rönsch, 2013):

I. Pretreatment of substrate (e.g. crushing, drying)
II. Gasification
III. Raw syngas treatment
IV. Methanation
V. Raw SNG upgrading.

**Current use and potentials of biomethane (biochemical and thermochemical)**

Considering economic and environmental aspects there is a reasonable potential for anaerobic biomethane in Germany of about 300 $MW_{el}$ (Scholwin et al., 2014). The bio-SNG plant in Gothenburg can be considered as the first one in commercial scale. So far there is no similar plant. However, there are research activities which concentrate on the gasification and/or methanation of lignin rich biomass to bio-SNG (e.g. in Austria (PSI, 2009), the Netherlands (ECN, 2011), Germany (Specht, 2006)).

Considering the bio-SNG potentials in Germany and Europe, there is not much data available. According to available biomass substrates there is a potential for bio-SNG out of woody biomass of around 66 and out of herbaceous biomass residues of around 6 bill. $m^3\,a^{-1}$ in Europe, according to (Thrän, 2012).

### Aims and objectives

It is the aim of this paper to show scenario-dependent possible market shares, market potentials and market behavior for bio-SNG in Germany. Therefore we analyzed the German biomethane and natural gas markets, being the markets where bio-SNG will have to compete in and transferred the results into a system dynamics market simulation model. Bio-SNG is integrated via a learning curve and market adoption concept. To validate and calibrate the model a techno-economic analysis and Delphi-Survey were conducted. Furthermore three different scenarios were implemented into the modeling approach. Thus, it is possible to derive possible future market shares for bio-SNG within the German biomethane and natural gas markets.

## MATERIALS AND METHODS

For the task of analysing the existing market structure as well as determining future market shares of biomethane and bio-SNG in the German biomethane market we decided to use the system dynamics methodology. Among a variety of approaches that are more or less capable for our demands the system dynamics methodology fits best. That`s because top-down approaches like input-output models or computable general equilibrium (CGE) models have a closer look at economic and inter-sectorial effects but lack mostly in providing technological details and development, assuming how technologies will evolve in the future, future cost-development and they violate the fundamental physical restrictions such as the conservation of matter and energy (Böhringer & Rutherford, 2006; Kretschmer & Peterson, 2010). Unlike top-down approaches, bottom-up models can describe technologies in detail, recent and prospective ones, they come usually as mathematical programming and can refer to technology changes, like efficiency standards and economy of scale. Though, bottom-up approaches are unsuitable to model economy-wide interactions and have drawbacks that come from the mathematical programming itself, i.e. the implementation of tax distortions or market failures ( Painuly, 2001; Böhringer & Rutherford, 2008).

### System dynamics methodology

Forecasts, especially for markets that were initiated by subsidies and now transferred to market-driven markets, can support decision makers. Where forecasting options are limited system dynamics (SD) is a methodology basing on the systems theory that provides decision support in dynamic and complex situations as well as capabilities to analyse, model and simulate them (Dace & Muizniece, 2015). It was first introduced by Jay W. Forrester in the 1950`s to support managers in complex business situations (Forrester, 1961). Having its foundation in business problems, SD was used in more and more disciplines to solve complex dynamic problems. The mathematical formulation of SD is made via a system of differential equations.

The basic tools of SD are causal loops diagrams, the construction of networks of stocks and flows and the analysis of the feedback structure. A special feature of SD is the high degree of learning while building the causal loops diagram and the simulation model. SD showed its suitability to fulfil modelling requirements in diverse scientific fields. In terms of energy markets SD models are predominantly used for the analysis of liberalized markets because of the advantage to model market mechanisms through differentiated mechanisms of action instead of following a single objective function that

allows those models a differentiated image of real markets. One problem that can arise during model development with SD is the need of validation of the interdependencies and the necessity of calibration. So without a real reference system the development of a SD model is not possible. The suitability to model economic and environmental interactions and feedbacks is stated by (Berka & Dobrosi, 2004). Although SD provides the necessary tools for dynamical modelling of RE policies containing energy and climate policies only little research has been done on this topic (Aslani et al., 2014).

After solving the above mentioned calibration and validation task the analysis is mostly done via experimentation, exhaustive what-if-scenarios (Forrester, 1961; Morecroft, 1988) and automatic optimization via external software (Lane & Oliva, 1994.) by trial-and-error-simulation, parameter changing or on and off switching of loops and parameters (Al-Saleh & Mahroum, 2014).

One problem arising within model building approaches is uncertainty. A lot of research was carried out determining how to reduce uncertainty in model-building. A common approach is the combination of a quantitative modelling approach with qualitative approaches. To reduce uncertainty within the presented modelling approach we combined it with an extensive techno-economic analysis on future cost development for anaerobic and thermochemical produced biomethane that was evaluated by support of external experts via a Delphi-Survey. Details of the techno-economic analysis and the associated Delphi-Survey can be found in the supplementary data file.

### Model description for the biomethane market

There are three major steps creating a SD model. The first step is the development of a conceptual model representing an abstraction of a real world problem and defining the boundaries of the model. It illustrates the fundamental principles and basic functionalities. Fig. 2 shows the conceptual model of the biomethane market simulation model (BiMaSiMo).
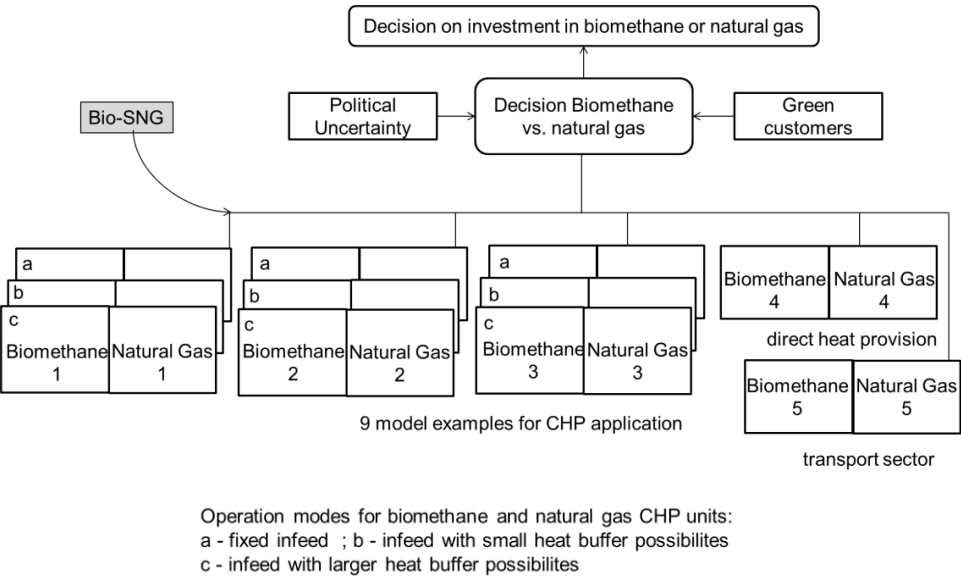


**Figure 2.** Conceptual model for BiMaSiMo.

The model is separated into the different possible applications of biogenic methane, in the same way to natural gas. For the application in CHP units the model consists of three possible applications, where biomethane and natural gas are used (hospital, swimming pool and district heating) with three different operation modes each (fixed infeed, infeed with small heat buffering possibilities and infeed with larger heat buffering possibilities and thus more flexibility). Along with the nine applications for the heat and power provision the applications for direct heat provision and in the fuel sector were modelled in a similar competitive manner. For each application a detailed sub-model was created to best possible illustrate the costs and revenues for each year in the time horizon 2000–2030. In this way the model is able to show the difference between costs and revenues for each application of biomethane respectively natural gas. In combination with a dynamic pay-off calculation it is possible to model the investment decisions. Those are affected by customers that are willing to pay a higher price for so called green products and by political uncertainty. Based on an investment rate calibrated by historical data it is possible to derive information on future investment decisions depending on future support schemes.

A detailed description of the causal loop diagrams, the stock and flow diagrams, system boundaries, and so on of BiMaSiMo can be found in (Horschig & Szarka, 2015) and the supplementary data file. Because of the already mentioned competitive situation between biogenic methane and natural gas, BiMaSiMo includes a model of the German natural gas flows, to calculate how much fossil gas can be substituted in which scope of application. Based on a large database at the German biomass research centre (DBFZ Deutsches Biomasseforschungszentrum) and the prior extensive techno-economic analyses a detailed model building process was possible, including a price formation mechanism for feedstock prices. For the biochemical conversion pathway extensive data is available and was implemented in the model. The thermochemical conversion pathway to bio-SNG for the future price and capacity development of this conversion pathway is implemented via learning curves.

Historical data of anaerobic biomethane plant installation and capacity expansion was used to calibrate the anaerobic biomethane SD model. The techno-economic analysis was used to calibrate the learning curve and market adoption model. Furthermore the price formation of biomethane is modelled separately to meet the requirements of its complexity. The availability of feedstock in form of biogas plants, which can be upgraded to biomethane plants, is limited to 10% of the installed biogas plant capacity due to calculations of (Scholwin et al., 2014). The decisions between biomethane and an alternative energy source as well as the different biomethane utilizations are based on two assumptions:

I. There is a strictly profit-based decision in which the purchaser of a certain amount of energy decides for the energy source he can receive the most payback for.
II. There is an individual and environment-based decision where there is a certain willingness to pay a higher price for a climate friendly product by direct gas consumers.

Subsequently the conceptual model was transformed to a causal-loop-diagram (CLD). In the next step the CLD is transferred into a stock and flow Diagram (SFD). SFD`s have a richer visual language than CLD`s. Variables and connections between them are defined with differential equations and therefore can be simulated. The SFD in

Fig. 3 shows the learning curve and market adoption sub-model for bio-SNG because this is not mentioned in the above mentioned reference for BiMaSiMo.
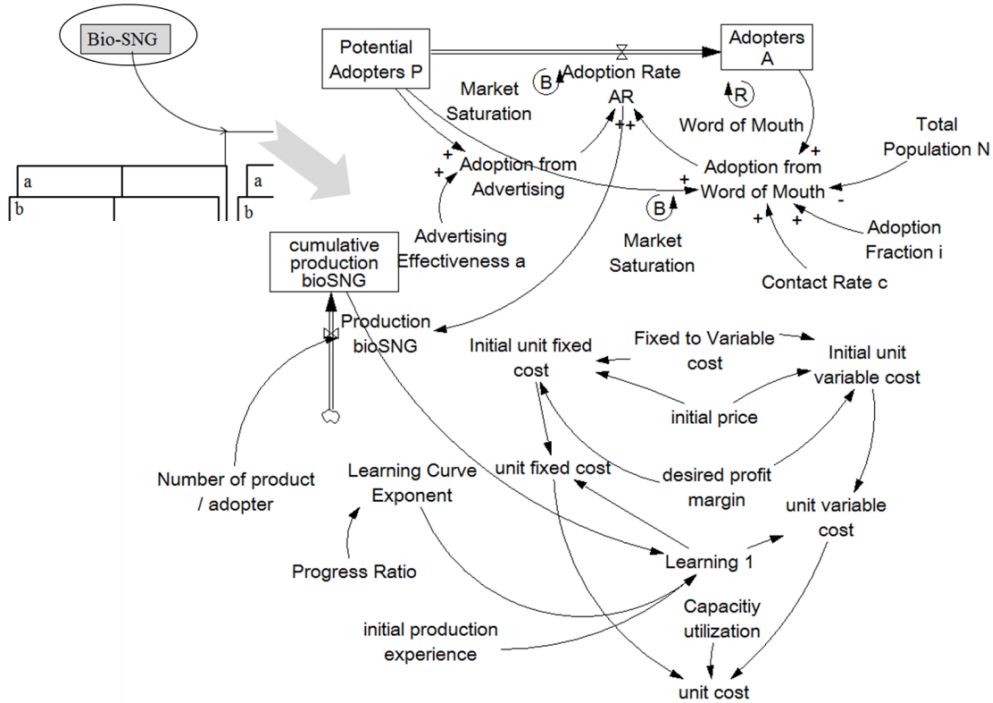


**Figure 3.** SFD of bio-SNG submodel (according to Sterman, 2009).

### Techno-economic evaluation

During a related project a comprehensive techno-economic evaluation of biochemical and thermochemical conversion technologies for biomass to biomethane was carried out. In total, 66 biochemical conversion alternatives and 33 thermochemical conversion alternatives were evaluated. The alternatives are based on different biomass feedstocks (e.g. maize, manure, straw, residual wood), different scale (1.4–16 $MW_{BioCH4}$ (AD) and 13–524 $MW_{BioCH4}$ (SNG)) and different upgrading respective gasification and methanation technologies. The alternatives were evaluated by a multi-criteria analysis.

The results of the techno-economic analyses and the Delphi-Survey show that a further reduction of the usual biomethane prices through learning processes is minimal. One reason can be seen in the cut-off of compensations for bioenergy in general and the associated decrease of funds for research and development (R&D) efforts. Being a promising future technology bio-SNG is still part of many R&D efforts and market implementation projects. With the techno-economic analyses and through further R&D activities future bio-SNG prices between 5–18.25 €ct kWh$^{-1}$ can be realised. These depend mainly on the plant concept and the feedstock mix.

### Scenario definition

Assumptions within BiMaSiMo for feedstock price development, cost development for anaerobic biomethane and gas demand are equal for all scenarios. There is no significant increase of the natural gas price (3.26 €ct kWh$^{-1}$ until 2030) and the trade with carbon emissions stays on the current level as well as the price per ton $CO_2$ (6€ t$^{-1}$ $CO_2$ (European Emission Allowances (EUA); Böhringer & Lange, 2013)). The scenarios are defined to reflect the best market possibilities in the CHP, heat and transport sector, where biogenic methane can be an alternative to fossil methane.

The *base scenario* is defined by encompassing compensation reductions for the production and use of biogenic gas in the power, heat and transport sector and thus, affects biomethane as well as bio-SNG. Whereas there are several options for the decarbonisation of the power sector, the heat sector is often called a sleeping giant. The *green heat scenario* is defined by an additional payment for green heat produced in environmental beneficial combined heat and power plants from 2016 on. The model will determine the minimum threshold for the green heat support to incite further biomethane capacity installation. This scenario shows the possibilities to partly decarbonize the heat sector with a domestic biogenic gas that can be used in all applications of natural gas. The third scenario is called *green transport scenario*. This scenario is defined by a substitution of natural gas transport through biomethane.

Each of the three scenarios is simulated with the current average anaerobic biomethane price (7.16 €ct kWh$^{-1}$) and possible future bio-SNG prices of 5, 5.5 and 6 €ct kWh$^{-1}$) derived from the techno-economic analysis and the presented learning-curve and market adoption sub-model.

### Greenhouse gas emission reduction

Values for greenhouse gas emissions (GHG) for biomethane and its fossil references are derived from (Majer, 2011) and multiplied by the amount of substituted natural gas in the particular application. Of course, GHG emission values are highly dependent on assumptions. Therefore the here presented values are more a direction than a precise value.

## RESULTS AND DISCUSSION

The results of the simulation of the *base scenario* show that there is nearly no further capacity development of anaerobic or thermochemical biomethane until 2030, except for bio-SNG with a price of 5 €ct kWh$^{-1}$. This agrees with market development predictions of (Deutsche Energie-Agentur GmbH, 2014). The main reasons for that are the insufficient support schemes that are not compensating the price difference between natural gas and biomethane. The support schemes that are in force since 2004 guarantee compensation for 20 years. According to current stand, after expiration of these compensations the biomethane plants will be taken from the grid. The model assumes that after 20 years all plant components have to be renewed and therefore new incentives are necessary for an ongoing biomethane production. The current adaptions of the main support schemes are not sufficient and consequently the biomethane plants installed in 2004 will be the first to be taken from the grid resulting in a decrease in feed-in capacity. With a future bio-SNG price of 5 €ct kWh$^{-1}$ an additional amount of 3,600 TJ a$^{-1}$ ($\approx$ 10,540 Nm³ h$^{-1}$, 1 TWh a$^{-1}$) fossil energy could be substituted by bio-SNG. This

would be natural gas in CHP plants. Environmentally seen in terms of GHG emission reduction this is the most beneficial use of biomethane.
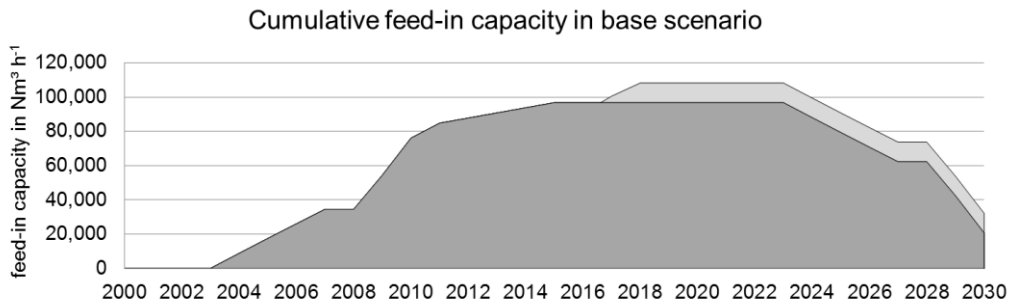


**Figure 4.** Results of base scenario simulations

Results of the *green heat scenario* show that with the current price for biomethane the additional payment for green heat must be at least 13 €ct kWh$^{-1}$ to incite further capacity installation. Decreasing prices for biomethane will lower the necessary threshold, of course. Possible future prices for bio-SNG need a threshold (additional payment) of 6 €ct kWh$^{-1}$ of green heat (bio-SNG price of 6 €ct kWh$^{-1}$) and 4 €ct kWh$^{-1}$ of green heat (bio-SNG price of 5.5 €ct kWh$^{-1}$). As shown in Figure 4 a bio-SNG price of 5 €ct kWh$^{-1}$ does not need additional support to incite further capacity installation. Implementing at least the threshold for a green heat support would incite a new capacity installation of around 2,400 TJ a$^{-1}$ ($\approx$ 7,027 Nm³ h$^{-1}$, 0.66 TWh a$^{-1}$). This is strictly tied to the assumption that the compensation for green power stays on its current level due to the fact that green energy from combined heat and power plants can receive compensation for the produced power and additional revenues from the sales of the arising heat.

Results of the *green transport scenario* show that with the current price for biomethane the additional support must be at least 6 €ct kWh$^{-1}$. This threshold is necessary to compensate the different profit opportunities of natural gas and biomethane in the current transport sector. In this way fuel stations could sell exclusively 100% biomethane instead of mixtures with natural gas. In doing so an annual natural gas demand of around 10,000 TJ a$^{-1}$ ($\approx$ 30,000 Nm³ h$^{-1}$, 2.77 TWh a$^{-1}$) could be substituted by biomethane in the transport sector only. Analog to the results of the green heat scenario the threshold gets lowered with decreasing bio-SNG prices. A bio-SNG price of 6 €ct kWh$^{-1}$ has a threshold of 5 €ct kWh$^{-1}$, a bio-SNG price of 5.5 €ct kWh$^{-1}$ has a threshold of 4 €ct kWh$^{-1}$ and a bio-SNG price of 5 €ct kWh$^{-1}$ has a threshold of 3.8 €ct kWh$^{-1}$.

The assumed future bio-SNG prices of 5, 5.5 and 6 €ct kWh$^{-1}$ can be realized by only few bio-SNG plant concepts and with ongoing R&D effort. It has to be mentioned that the different influencing variables in the system dynamics model have a different power of influence. The variables biomethane price, future bio-SNG price and natural gas price significantly influence the simulation results.

According to calculations of (Rönsch, 2010) a representative bio-SNG plant concept emits 17.9g $CO_{2eq}/MJ_{SNG}$ GHG ($\approx$ 64,5g $CO_{2eq}$ kWh$^{-1}$). Details of this concept can be found in the supplementary data file. Compared to fossil references for possible applications of bio-SNG in the power, heat and transport sector significant GHG savings can be achieved. The fossil references are 393g $CO_{2eq}$ kWh$^{-1}$ for CHP plants (average from power provision through usual power mix and heat provision by natural gas), 180g $CO_{2eq}$ kWh$^{-1}$ for direct heat provision by natural gas and 249g $CO_{2eq}$ kWh$^{-1}$ for transport with natural gas. The base scenario simulation derived a further bio-SNG capacity development of 3,600 TJ a$^{-1}$ ($\approx$ 10,540 Nm³ h$^{-1}$, 1 TWh a$^{-1}$) in the CHP sector, when a bio-SNG price of 5 €ct kWh$^{-1}$ is getting realized. This is equivalent to an emission saving of 328 kt $CO_{2eq}$ a$^{-1}$. Simulation results for the green heat scenario derived a possible capacity development for bio-SNG in the heat sector of 2,400 TJ a$^{-1}$ ($\approx$ 7,027 Nm³ h$^{-1}$, 0.66 TWh a$^{-1}$). This is equivalent to an emission saving of 76 kt $CO_{2eq}$ a$^{-1}$. The natural gas based transport in Germany could be decarbonized with 10,000 TJ a$^{-1}$ ($\approx$30,000 Nm³ h$^{-1}$, 2.77 TWh a$^{-1}$) out of bio-SNG. This is equivalent to an emission saving of 510 kt $CO_{2eq}$ a$^{-1}$. Of course, the above mentioned GHG saving values are more road signs then precise predictions. Nevertheless they show that especially investments in a further use of bio-SNG in the CHP and transport sector can achieve high GHG emission savings. In times of debates on nitrogen oxide emissions from inner-city diesel transport the substitution with biogenic gas like bio-SNG and biomethane can contribute to a decrease of nitrogen oxide emissions and thus increase air quality.

The results of the base scenario show that without further incentive schemes and funding for ongoing R&D-effort there won`t be a market penetration of bio-SNG in Germany. It has to be mentioned that our approach has limitations, of course. The model is strictly limited to the German biomethane market and trade of biomass, feedstock or the end product biomethane is not yet considered. Furthermore effects of an increased biomethane production from other bioenergy carriers are not considered like feedstock competitions. Also, due to a lack of already installed bio-SNG plants the applied bio-SNG data is mainly based on simulation and modelling, which leads to uncertainties in subsequently calculations.

## CONCLUSIONS

A system dynamics model was developed to assess the potential market share of bio-SNG in Germany until 2030. Simulation results show that a capacity development of bio-SNG in the CHP sector at current support is only possible with low bio-SNG prices of 5 €ct kWh$^{-1}$. The heat sector needs support of at least 13 €ct kWh$^{-1}$ at current support levels to foster the substitution of natural gas with biogenic methane. Lower bio-SNG prices will decrease the needed support. Results of the green transport scenario derived the necessity of an additional support of at least 6 €ct kWh$^{-1}$ at current level of support. The results of our simulation show that a further decarbonisation of natural gas supply chains in the CHP, heat and transport sector can only be achieved with additional support and further R&D effort to decrease current bio-SNG production costs. In this way it is possible to directly formulate policy proposals for decision support. Additionally the focus can be shifted respectively expended. Instead of a pure energetic focus the high potential of biomethane respective bio-SNG in the chemical sector can be included. This would also push the current evaluation to a more overall evaluation. It

could involve the consideration of further technology concepts as well as an adjustment of evaluation area and period, e.g. for whole EU till 2050. However, for a comprehensive decision support the simulation model needs to be extended and further research is necessary.

## REFERENCES

Al-Saleh, Y. & Mahroum, S. 2014. A critical review of the interplay between policy instruments and business models: greening the built environment a case in point. *Journal of Cleaner Production*. doi:10.1016/j.jclepro.2014.08.042

Aslani, A., Helo, P. & Naaranoja, M. 2014. Role of renewable energy policies in energy dependency in Finland: System dynamics approach. *Applied Energy* **113**, 758–765.

Berka, V. ja Dobrosi, L., 2004. High level handling of system dynamics models in rural development planning, in: Iron Curtain International Symposium. Wolfbauer, J., Kürzl, H. (ed), Budapest,Hungary. pp. 79–84.

Böhringer, C. & Lange, A. 2013. European Union's Emissions Trading System, in: Encyclopedia of Energy, Natural Resource, and Environmental Economics. *Elsevier*, pp. 155–160.

Böhringer, C. & Rutherford, T.F. 2008. Combining bottom-up and top-down. *Energy Economics* **30**, 574–596.

Böhringer, C. & Rutherford, T.F. 2006. Combining Top-Down and Bottom-Up in Energy Policy Analysis: A Decomposition Approach. *SSRN Electronic Journal*. doi:10.2139/ssrn.878433

Dace, E. & Muizniece, I. 2015. Modeling greenhouse gas emissions from the forestry sector – the case of Latvia. *Agronomy Research* **13**, 464–176.

Daniel-Gromke, J., Denysenko, V., Barchmann, T., Reinelt, T. & Trommler, M. 2013. *Aufbereitung von Biogas zu Biomethan und dessen Nutzung – Status quo und Perspektiven*. in: Dezentrale Energieversorgung. TK Verlag, p. 468.

Deutsche Energie-Agentur GmbH. 2014. Industry barometer biomethane. data, facts and trends of biogas feed-in. [WWW Document] URL http://www.dena.de/fileadmin/user_upload/Projekte/Erneuerbare/Bilder/Branchenbarometer_Biomethan_I_2014.pdf. (in German).

Deutschland – Agency for renewable energy [WWW Document], URL http://www.unendlich-viel-energie.de/themen/politik/deutschland (accessed 6.23.15). (in German)

Dunkelberg, E., Salecki, S., Weiß, J., Rothe, S. & Böning, G. 2015. Biomethane in the energy system – ecological and economic evaluation of upgrading technologies and utilisation options. Publication series of the institute of ecological and economic research 207/15, Berlin (in German).

ECN. 2011. MILENA – Status of Development. Online-Abfrage. Energy Research Centre of the Netherlands (ECN), Petten.

Erdgasverbrauch von Deutschland bis 2014 | Statistik [WWW Document], n.d. Statista. URL http://de.statista.com/statistik/daten/studie/41033/umfrage/deutschland---erdgasverbrauch-in-milliarden-kubikmeter/ (accessed 12.18.15).

European Emission Allowances (EUA) [WWW Document], n.d. URL https://www.eex.com/de/marktdaten/umweltprodukte/spotmarkt/european-emission-allowances#!/2016/03/30 (accessed 3.30.16).

European Environment Agency. 2014. Annual European Union greenhouse gas inventory 1990–2012 and inventory report 2014.

Fisher, A.C. & Rothkopf, M.H.. 1991. Market failure and energy policy: a rationale for selective conservation. *Energy Policy* **17**, 397–406.

FNR. 2014. Leitfaden Biogasaufbereitung und -einspeisung. Fachagentur Nachwachsende Rohstoffe e.V. (FNR), Gülzow.

Forrester, J. 1961. *Industrial Dynamics*. Productivity Press,Cambridge, MA. 482pp.

Goteborg Energi. 2014. GoBiGas – Goteborg Energi [WWW Document], URL http://www.goteborgenergi.se/English/Projects/GoBiGas__Gothenburg_Biomass_Gasification_Project

Graf, F. &, Bajohr, S. 2011. biogas – production, upgrading, feed-in. Oldenbourg Industrieverlag GmbH, München. (published in German)

Horschig, T. & Szarka, N. 2015. The German biomethane market – A policy evaluation approach using System Dynamics. Proceedings of the 33rd International Conference of the System Dynamics Society, Cambridge, Massachusetts,USA.

IEA Bioenergy. 2014. Biomethane – Status and Factors Affecting Market Development and Trade.

Jaffe, A.B., Newell, R.G. & Stavins, R.N. 2005. A tale of two market failures: Technology and environmental policy. Ecological *Economics* **54**, 164–174.

Kaltschmitt, M., Hartmann, H. & Hofbauer, H. 2009. Energy from biomass: Fundamentals, technologies and procedures, Second Edition, Springer, Berlin (in German).

Knoef, H., 2012. Handbook Biomass Gasification Second Edition, BTG Biomass Technology Group BV, Enschede, Netherlands.

Kopyscinski, J., Schildhauer, T.J. & Biollaz, S.M.A. 2010. Production of synthetic natural gas (SNG) from coal and dry biomass – A technology review from 1950 to 2009. *Fuel* **89**, 1763–1783.

Kretschmer, B. & Peterson, S. 2010. Integrating bioenergy into computable general equilibrium models — A survey. *Energy Economics* **32**, 673–686.

Lane, D.C. & Oliva, R. 1994. The greater whole: Towards a synthesis of system dynamics and soft systems methodology. *European Journal of Operational Research* **107**, 214–235.

Majer, S., 2011. Results of ecological evaluation of biogas/biomethane from exemplary biogas plants, Biogas Council e.V. Berlin (in German).

Morecroft, J.D.W. 1988. System dynamics and microworlds for policymakers. *European Jorunal of Operational Research* **59**, 9–27.

Painuly, J. 2001. Barriers to renewable energy penetration; a framework for analysis. Renewable *Energy* **24**, 73–89.

PSI. 2009. The SNG Technology Platform in Güssing, A Status report of Bio-SNG project. Paul Scherrer Institut, Villigen, Schweiz.

Repele, M., Paturska, A., Valters, K. & Bazbauers, G. 2014. Life cycle assessment of bio-methane supply system based on natural gas infrastructure. *Agronomy Research* **12**(3), 999–1006.

Repele, M., Dudko, M., Rusanova, J., Valters, K. & Bazbauers, G. 2013. Environmental aspects of substituting bio-synthetic natural gas for natural gas in the brick industry. *Agronomy Research* **11**(2), 367–372.

Rönsch, S., 2010. Technical analysis of thermo-chemical Bio-SNG production. Annual meeting of the technical committee 'energy process engineering' and 'gas cleaning'. Dortmund, Germany.

Scholwin, F., Grope, J., Schüch, A., Daniel-Gromke, J., Beil, M. &, Holzhammer, U. 2014. Actual state of biomethane use – costs – climate impact – utilisation pathways – comparison of combined heat and power production of biogas, biomethane and natural gas. Federal Ministry for Economic Affairs and Energy, Berlin, Germany.

Seiffert, M. & Rönsch, S., 2013. Biosynthetic Natural Gas, in: Encyclopedia of Sustainability Science and Technology: Springer Verlag, Berlin-Heidelberg, Germany.

Specht, M., 2006. Handout – The AER-Process. Cluster initiative 'Energy-North-East-Brandenburg'. Center for Solar Energy- and Hydrogen-Research Baden-Wuerttemberg (ZSW), Stuttgart (in German).

Sterman, J.D. 2009. Business dynamics: systems thinking and modeling for a complex world, Irwin/McGraw-Hill, Boston. pp. 982

Thrän, D., 2012. European biomethane potentials., Workshop Biomethane Trade. DBFZ, Brussels.

Thrän, D., Hennig, C., Rensberg, N., Denysenko, V., Fritsche, U. & Eppler, U. 2015. IEA Bioenergy Task 40: Country Report Germany 2014. IINAS – International Institute for Sustainability Analysis and Strategy GmbH, Darmstadt/Leipzig.

# Analysis of rapid temperature changes

M. Hromasová[*] and M. Linda

Czech University of Life Sciences in Prague, Faculty of Engineering, Department of Electrical Engineering and Automation, Kamycka 129, CZ165 21 Praha – Suchdol, Czech Republic
[*]Correspondence: hromasova@tf.czu.cz

**Abstract.** The analysis of rapid temperature changes in the dynamic system is described in the paper. Temperature changes are in range of tens of milliseconds. The sensor we used has a significant influence on the dynamic system. In these cases we need to use thermocouples that have appropriate transfer characteristics and can be manufactured with a low time constant. The time constant directly corresponds with weight and size of the sensor. The quality factor is usually in a range between 0.98 and 0.995. Information about the temperature course is particularly important in the field of dynamic systems, e.g. agricultural machines where the switching components are overloaded by pulse switching of technology systems. For the object analysis we use the thermocouples with diameter 0.012 mm with non-encapsulated finish and 0.12 mm with suppression of interference impact and comparative temperature fluctuation. For the analysis of dynamic temperature changes we conduct a measurement with a load factor change, which is the mean value of power change, expressed as ratio of the pulse duration to the delay between pulses, this way we will affect the measurement conditions. As a solution we use measurement methods for a steady state, an impulse test and a method of local measurement of temperature. Compared to a real principle of a component we do not increase temperature of the environment during experiments. The results of measurement can be applied for design and implementation of switching systems for electronic circuits with signal modulation and power load.

**Key words:** temperature, thermocouple, measurement, sensor, load factor.

## INTRODUCTION

In this part of the project we are going to look into a laboratory experiment, a set-up of laboratory environment, used equipment, and into a measurement of dynamic characteristics of a pulse-loaded object. Reference is made to the direct parameter influence of electronic components with rising temperature. In particular it shows the effect on lifetime of loaded components, which after a number of loads, change their specific parameters, and this subsequently leads to their destruction. In this case, attention is drawn to the passive components (Xu et al., 2015; Contento & Semancik, 2016; Song et al., 2016). Another reason why it is important to know the temperature waveform of electronic components are the noise characteristics, especially for circuits, where a very low voltage levels are processed. The amount of noise is influenced by the temperature of resistors and semi-conductor components. We distinguish between thermal noise, shot noise, flicker noise, crackling noise, and total noise. The thermal noise (white noise) is caused by random motion of free electrons in the crystal lattice of

the substance. Shot noise (Schottky noise) is formed by the passing of a current through the PN junction (Huesgen et al., 2008; Häb et al., 2015; Chen et al., 2015). The flicker noise occurs at the base-emitter junction, it is caused by technological impurities and applied at 0.1–10 Hz. The crackling noise again arises at the base-emitter junction, and is characterized by jumps between discrete noise levels (Milton et al., 1997; Jiao et al., 2015; Mirmanto, 2015).

## MATERIALS AND METHODS

The input signal of the pulse-loaded object is created by a pulse generator with a set power, where the load factor z is changed (can be quoted in %) (1) (O'Sullivan & Cotterell, 2001).

$$z = \frac{t_1}{T} = \frac{t_1}{t_1 + t_2} \tag{1}$$

The load factor is defined as a ratio of the pulse duration $t_1$ to the period $T = t_1 + t_2$, when $t_2$ is dwell time between pulses. The supplied medium power of periodic pulses to the loaded object is according to (2) (O'Sullivan & Cotterell, 2001), see Fig. 1.

$$\overline{P} = \frac{P_1 t_1}{T} = P_1 z , \tag{2}$$

where: $P_1$ *(W)* constant power delivered at the time $0 < t < t_1$.
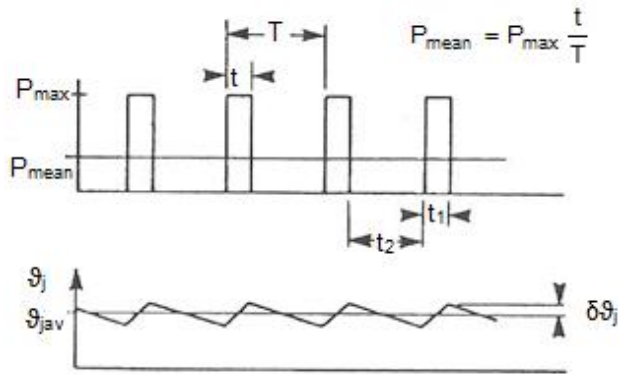


**Figure 1.** Demonstration of a medium power waveform in time, effect of the load factor ($\vartheta_j$ – an ideal temperature waveform, $\vartheta_{jav}$ – mean value of an ideal temperature waveform, $\delta\vartheta_j$ – max. temperature deviation on power pulse remission).

The established laboratory environment (see Fig. 2) for measurement of pulsed temperatures waveforms on selected power loaded objects, is comprised of:
- pulse generator, which generates a specified pulse changes of the power;
- loaded/measured object (in our case we chose resistor, which is suitable electronic element for its electrical properties, its behavior was examined by selected methods);

- measuring devices - thermocouple probe, thermoelectric voltage amplifier and a recording device (Huesgen et al., 2008; Chen et al., 2015; Sessler & Moayeri, 1990).
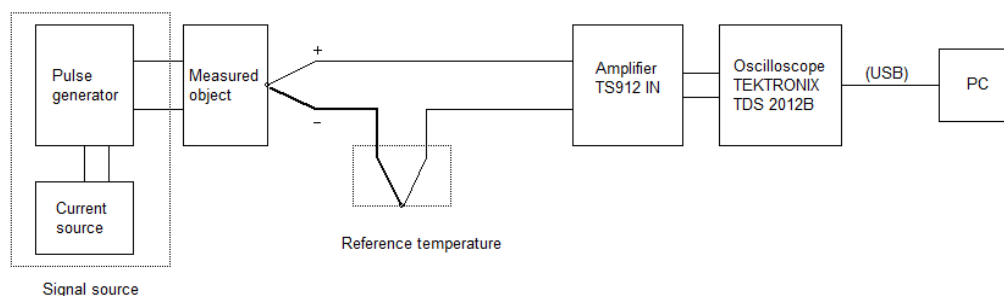


**Figure 2.** Block diagram of a measuring scheme.

We used a thermocouple with low time constant for measuring the dynamic power pulses, in order to capture the rapid temperature change with sufficient accuracy. The time constant is one of the main parameters of temperature sensors used for measurement of dynamic systems.

For measurement we used a probe 5TC – TT (PFA wire insulation, 914 mm length, wire diameter 0.12 mm). Type K thermocouple with wire diameter of 0.012 mm is designed for spot measurements with high accuracy and low heat transfer. It is suitable for measurement on small objects e.g. SMD resistors, which would not be possible to measure with other type of sensor.

Used measuring methods can be divided into three groups, where the third group complements the previous two, mainly in its functional nature.

The first method 'The measurement of a steady-state' is based on measuring surface temperature of the electric component up until its stabilization, i.e. until the input and output energy into the surroundings is balanced. This method is favorable for the possibility to observe the component's behavior at a permanent load, or up to the critical load, and subsequently concludes how many of such cycles the component is capable to endure without an evident damage, or without changing parameters °CXu et al., 2015; Song et al., 2016).

This method is showing an apparent oscillation when measured with a micro thermocouple, which is only a reaction to the measurement of the power pulses, and this change is detailed in another type of test. We can explain this phenomenon by pulse-loading the resistor layer, which is relatively less heavy than the inner layer of ceramic and coating layer. There's a sharp increase of measured surface temperature when influenced by power, without the component being warmed up, when disconnected from the power there's a sharp temperature drop, because of the heat dissipation through ceramics. This phenomenon is not as evident in the second type of thermocouple, where there is furthermore a heat dissipation through conductors that have 10 times larger diameter.

The second method 'The Pulse Test' is based on examination of the surface temperature waveform as a response to one or more pulses at the input of the system, as in our case. In this method, we can significantly increase the load factor and examine the

dynamics of the component during a critical short-term load. The result of such analysis is not only about the exact dynamics of the response, but also about the maximum transferable power of the component.

The complementary method, which is primarily used to analyze temperature distribution on the electronic component's surface, is called 'The method of measuring local temperature'. In our case, we chose it with regard to selected resistors, where because of dimensions, is convenient to know waveforms of the thermal gradient on the component's surface. This method can be extended to a surface measurement. However, an important prerequisite is an accurate matrix arrangement of sensors, see Fig. 4, which creates a basis for the method, see Fig 3. This method can detect subsurface defects in materials, where disruption of the temperature field leads to a distortion of measured temperature in one or more network nodes (Zhao et al., Yang, 2015; Ya et al., 2016).



**Figure 3.** Block diagram of the power-loaded resistor.
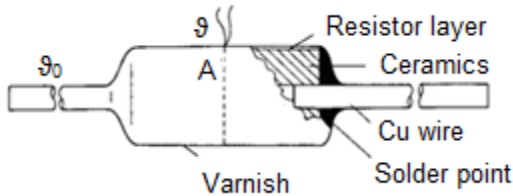


**Figure 4.** Indication of areas suitable for measuring the resistor's surface temperature.

## RESULTS AND DISCUSSION

The Fig. 5 shows the waveform for the first set of parameters, which are listed in column 1 of the Table 1. The temperature waveform during measurement with micro thermocouple reaches an average mean value in a steady-state of 220 °C, and the dispersion of the mean surface temperature of ± 26 °C. Measurement of the temperature dispersion is determined by the type and the time constant of the measuring scheme. Measurement with the second thermocouple version records the reading of stagnation temperature at 121 °C with considerably lower dispersion. This difference is caused by the sensor with higher time constant, and provided that the sensor will transfer heat, as mentioned in the theoretical analysis of the case.

At a temperature of about 150 °C a damage of the resistor's lacquer layer occurred. Measurement was carried out in the laboratory environment with an ambient temperature of 24 °C. These conditions are as close as possible to the work conditions of the analyzed component, where the component is placed inside the device, and is not significantly influenced by ambient conditions, just by the conditions inside the device. However, compared to the real function of the component, the ambient temperature was not increased during the experiment, which significantly impacts the cooling of the resistor.
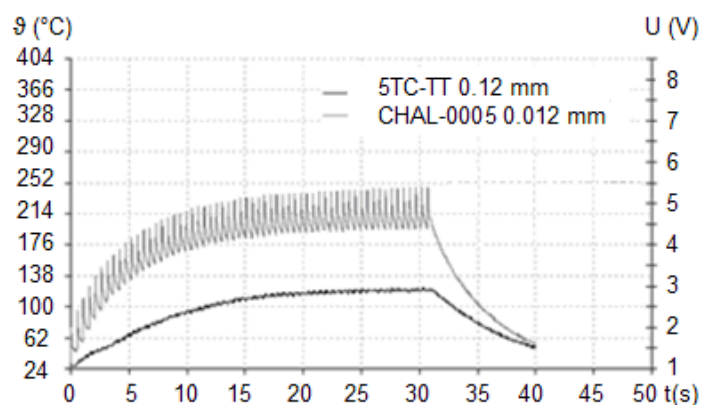
**Figure 5.** The measured waveform - case a) z = 0.0385.

**Table 1.** Load factor parameters

| Parameters/load factor | 0.0385 | 0.0566 | 0.0741 |
|---|---|---|---|
| Number of cycles $n_p$ (-) | 60 | 60 | 60 |
| Pulse duration $t_s$ (ms) | 20 | 30 | 40 |
| No pulse period $t_2$ (ms) | 500 | 500 | 500 |

Fig. 6 shows the temperature waveform when the load factor was changed to a value z = 0.0566, and the mean temperature rises to 260 °C ± 26 °C, and in the second case the temperature rises to 170 °C.
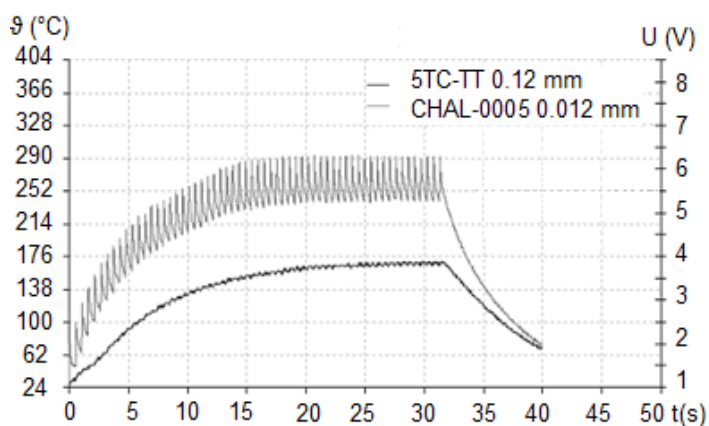


**Figure 6.** The measured waveform – case b) z = 0.0566.

The dispersion is within the same range for both cases. Overall, it can be concluded, that the measurement is within range of safe operation area, although there is damage to the component's surface layer, it is possible to run it for a certain period of time. The operating state can be considered as a critical operating state without damaging the object. However, in another case we are at the border of a physical lifetime of the object.

Fig. 7 shows the temperature waveform for $z = 0.0741$, and the mean temperature is 340 °C with ± 38 °C, and for the second case the temperature is 243 °C. In this analysis, the load factor change by 10 ms $t_1$ does not tally with temperature changes, as in previous cases. The influence is more significant in this very critical state, which damages the component by evaporating the protective layer. After this test, the component is already substantially damaged, and there is no guarantee of its further 100% activity without changing the parameters.
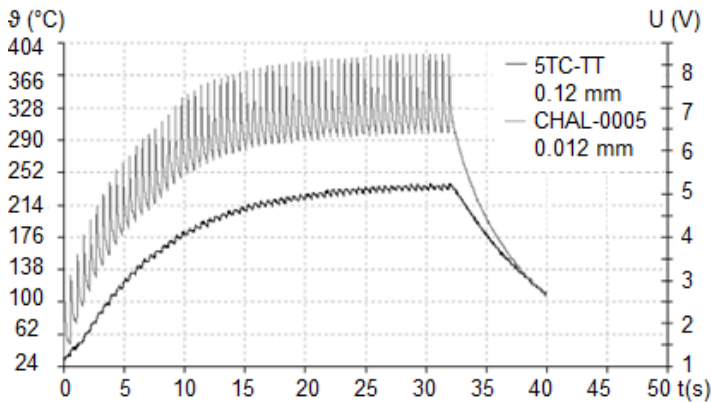


**Figure 7.** The measured waveform – case c) $z = 0.0741$.

The analysis indicates that the sensor's measuring part has a clear dependence and impact on quality of object's measured temperature, which significantly influences the use of measuring sensors with regard to measuring possibilities.

From the analysis of the second and the third case, there is a noticeable difference in a steady state of 80 °C for micro thermocouple 0.012 mm, and 73 °C for thermocouple 0.12 mm. At this stage the damage to the components is present, yet without loss of functionality and with no guarantee of maintaining characteristic parameters when an excessive overload leads to a degradation process in the component.

In the case analysis can be noted a decrease of measured surface temperature in time sphere less than 2.5 s. The decrease is caused by heat dissipation through resistor's intakes when the temperature gradient of the component is changing, and influencing significantly the heat transfer through wiring. After a certain period of time the heat dissipation by radiation begins to prevail, and to a certain extent, the heat dissipation through wiring is suppressed. This phenomenon can be observed in all performed measurements, but there is a time shift in measurement of components with higher heat capacity.

Other cases are based on the Pulse test method. The system analysis is examined when five power pulses are on the input. For comparison, two types of load factor changes were chosen when changing the time interval $t_2$ 100 ms and 50 ms.

As anticipated, from the waveforms we can determine the inertia of the system and its order. Inertia manifests itself by the temperature increase even after subsiding of the power pulse.

Fig. 8 and Fig. 9 show first examples of waveforms, where the first represents measurement with a load factor $z = 0.167$, and the second with $z = 0.286$. The figures show the influence of the measuring sensor when these rapid power changes of the surface temperature can not be captured by the second sensor.
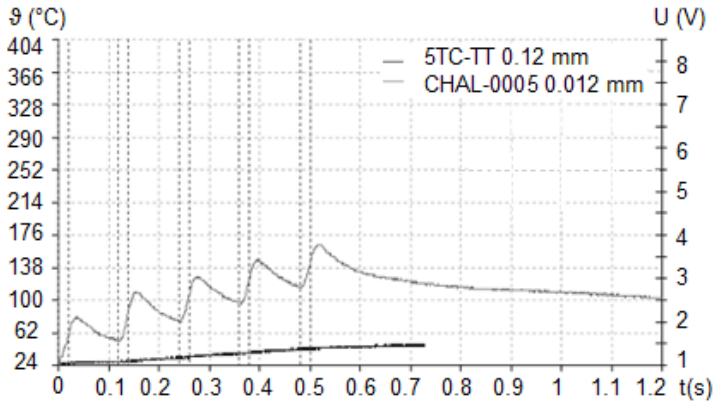


**Figure 8.** The measured waveform – case a) $z = 0.167$.

Temperature differences between the pulses can not be linear according to previous measurements. Another dependence, which is determined by inertia of the system, is the temperature increase after the pulse had subsided, this condition can be, to a certain extent, accurately simulated by created model.
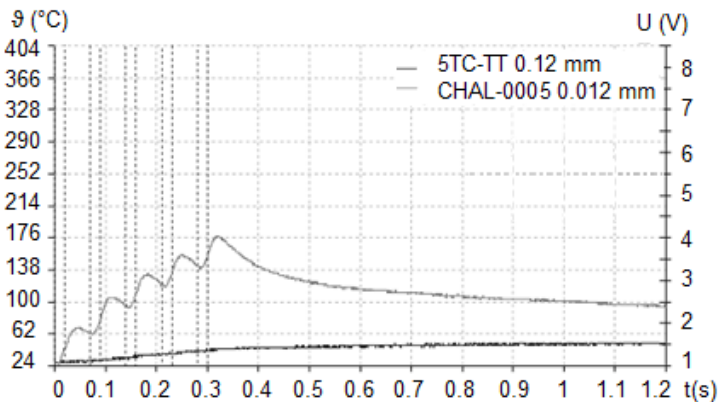


**Figure 9.** The measured waveform – case b) $z = 0.286$.

From previous cases, there is an apparent correlation of the component's warming, where the higher load factor leads to a faster warming of the component. In this setting the increase in temperature is less than in setting $t_2 = 100$ ms.

Another set of waveforms (see Fig. 10 and Fig. 11) represents a change of load factor z = 0.231 to z = 0.375. Maximum temperature of 220 °C was achieved.
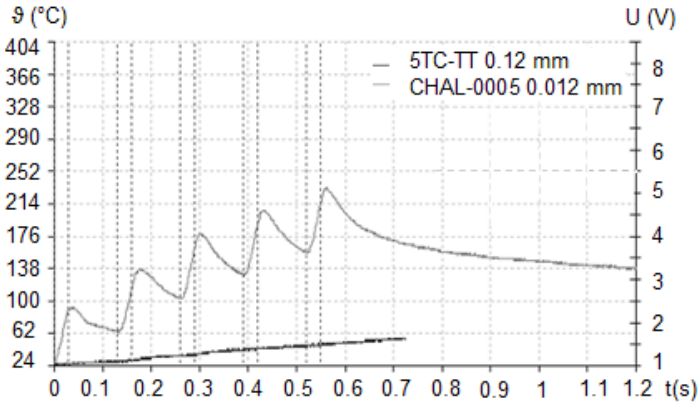


**Figure 10.** Measured waveform – case a) z = 0.231.
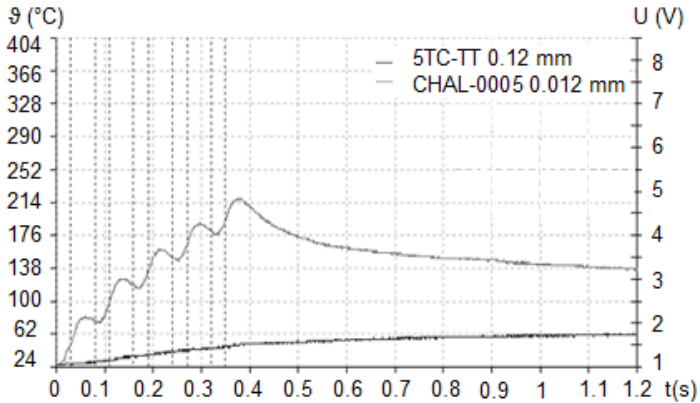


**Figure 11.** Measured waveform – case b) z = 0.375.

Established results were recorded. The analysis shows a non-linear dependence of achieved temperatures with load factor change. The result is clearly influenced by the heat dissipation through heat emission and wiring, and the temperature gradient is significantly higher when the load factor and maximum temperature are higher. Interdependence of experiments are in Tab. 2a, 2b and 2c.

**Table 2 a.** Experimental part – results – $t_1 = 20$ ms; $t_2 = 500$ ms, $n_p = 60$; z = 0.03846

| Time (s) | 5 s | 10 s | 15 s | 20 s | 25 s | 30 s |
|---|---|---|---|---|---|---|
| resistor 2.2 Ω – 0.5 W | | | | | | |
| 0.12 mm | 64 °C | 90 °C | 110 °C | 115 °C | 120 °C | 125 °C |
| 0.012 mm | 150 °C | 184 °C | 200 °C | 210 °C | 216 °C | 220 °C |
| resistor 2.2 Ω – 1 W | | | | | | |
| 0.12 mm | 35 °C | 40 °C | 50 °C | 53 °C | 55 °C | 56 °C |
| 0.012 mm | 37 °C | 46 °C | 55 °C | 57 °C | 62 °C | 64 °C |

**Table 2 b.** Experimental part – results – $t_1 = 30$ ms; $t_2 = 500$ ms, $n_p = 60$; $z = 0.0566$

| Time (s) | 5 s | 10 s | 15 s | 20 s | 25 s | 30 s |
|---|---|---|---|---|---|---|
| resistor 2.2 Ω – 0.5 W | | | | | | |
| 0.12 mm | 90 °C | 135 °C | 145 °C | 160 °C | 165 °C | 170 °C |
| 0.012 mm | 178 ° | 231 °C | 260 °C | 265 °C | 270 °C | 273 °C |
| resistor 2.2 Ω – 1W | 39 °C | 45 °C | 58 °C | 61 °C | 64 °C | 75 °C |
| 0.12 mm | | | | | | |
| 0.012 mm | 41 °C | 55 °C | 62 °C | 70 °C | 75 °C | 79 °C |

**Table 2 c.** Experimental part – results – $t_1 = 40$ ms; $t_2 = 500$ ms, $n_p = 60$; $z = 0.0741$

| Time (s) | 5 s | 10 s | 15 s | 20 s | 25 s | 30 s |
|---|---|---|---|---|---|---|
| resistor 2.2 Ω – 0.5 W | | | | | | |
| 0.12 mm | 125 °C | 180 °C | 213 °C | 220 °C | 225 °C | 230 °C |
| 0.012 mm | 234 °C | 295 °C | 328 °C | 330 °C | 340 °C | 345 °C |
| resistor 2.2 Ω – 1 W | 41 °C | 58 °C | 63 °C | 70 °C | 75 °C | 80 °C |
| 0.12 mm | | | | | | |
| 0.012 mm | 43 °C | 62 °C | 66 °C | 82 °C | 90 °C | 102 °C |

Fig. 12 shows a graphical dependence of recorded samples in Tab. 2 a, 2 b and 2 c, and represents dependence and comparison of temperature vs. load factor in time sphere. See picture for evident dependencies of used thermocouples. There is an evident flattening on the other set of pictures, that is caused by this factor.
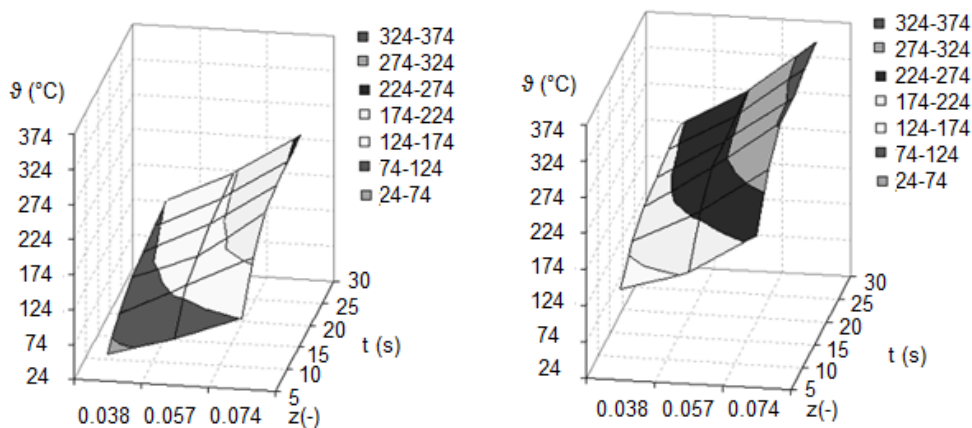


**Figure 12.** 3D dependency graph of surface temperature vs. load factor, resistor 0.5 W measured with thermocouple 0.12 mm and 0.012 mm.

## CONCLUSIONS

- Established workplace for testing temperature sensors, measurement of static and dynamic characteristics, established workplace for testing electrical components;
- models of dynamic properties of objects in rapid time changes, the suitability of using the sensors with different time constant;

- design and development of measuring methods of electrical objects according to the nature of activity, applicability of each method;
- results of surface temperature waveforms on resistors with load factor change, as per measuring methods;
- establishing the effect of load factor change on maximum warming, the evaluation of graphic dependencies between measurements.

The results recommend the contact measurement of temperature. A short term temperature rise can occur during the object analysis, which can not be detected by the sensors and therefore can not flexibly respond to a coming fault that usually manifests itself as a pulse change or as an offset of the system temperature. During the surface/contact measurements we have to take into consideration several factors, such as quality of the surface (polished, oxidized, rough), symmetry of the surface (curved) and a treatment of the surface (varnishing, laminating), the heat dissipation of the sensor, thermal conductivity at the contact, etc.

The analysis of the pulsed temperature change on the electrical object is used with regard to its possible load factor in control systems. Information about the temperature waveform, e.g. on the resistor or the semiconductor component of the power supply or the switch device, when long-term monitored, provides figures that are suitable for establishing the maximum temperature of objects, their dimensioning or diagnostics.

## REFERENCES

Contento, N.M., & Semancik, S. 2016. Thermal characteristics of temperature-controlled electrochemical microdevices. *Sensors and Actuators B: Chemical* **225**, 279–287.

Häb, K., Ruddell, B.L., & Middel, A. 2015. Sensor lag correction for mobile urban microclimate measurements. *Urban Climate* 14, 622–635.

Huesgen, T., Woias, P., & Kockmann, N. 2008. Design and fabrication of MEMS thermoelectric generators with high temperature efficiency. *Sensors and Actuators A: Physical* **145–146**(1–2), 423–429.

Chen, S., Li, H., Lu, S., Ni, R., & Dong, J. 2015. Temperature measurement and control of bobbin tool friction stir welding. *The International Journal of Advanced Manufacturing Technology*, 1–10.

Jiao, L., Wang, X., Qian, Y., Liang, Z., & Liu, Z. 2015. Modelling and analysis for the temperature field of the machined surface in the face milling of aluminium alloy. *The International Journal of Advanced Manufacturing Technology* **81**(9–12), 1797–1808.

Milton, N., Pikal, M.J., Roy, M.L., & Nail, S.L. 1997. Evaluation of manometric temperature measurement as a method of monitoring product temperature during lyophilization. *PDA Journal of Pharmaceutical Science and Technology* **51**(1), 7–16.

Mirmanto, M. 2015. Local pressure measurements and heat transfer coefficients of flow boiling in a rectangular microchannel. *Heat and Mass Transfer* **52**(1), 73–83.

O'Sullivan, D., & Cotterell, M. 2001. Temperature measurement in single point turning. *Journal of Materials Processing Technology* **118**(1–3), 301–308.

Sessler, D.I., & Moayeri, A. 1990. Skin-surface warming: heat flux and central temperature. *Anesthesiology* **73**(2), 218–224.

Song, H., Zhan, X., Li, D., Zhou, Y., Yang, B., Zeng, K., Zhong, J., Miao, X., & Tang, J. 2016. Rapid thermal evaporation of Bi2S3 layer for thin film photovoltaics. *Solar Energy Materials and Solar Cells* **146**, 1–7.

Xu, Y., Huang, Y., Wang, X., & Lin, X. 2015. Experimental study on pipeline internal corrosion based on a new kind of electrical resistance sensor. *Sensors and Actuators B: Chemical* **224**, 37–47.

Ya, W., Pathiraj, B., & Liu, S. 2016. 2D modelling of clad geometry and resulting thermal cycles during laser cladding. *Journal of Materials Processing Technology* **230**, 217–232.

Zhao, X., Yang, K., Wang, Y., Chen, Y., & Jiang, H. 2015. Stability and thermoelectric properties of ITON:Pt thin film thermocouples. *Journal of Materials Science: Materials in Electronics*.

# An approach for determination of quality in hay bale and haylage

A. Ince[1,*], Y. Vurarak[2] and S.M. Say[3]

[1]Çukurova University, Faculty of Agriculture, Agricultural Machinery and Technologies Engineering Department, TR 01330 Balcali-Adana, Turkey
[2]Eastern Mediterranean Agricultural Research Institute, P. Box: 45 Adana, Turkey
[3]Çukurova University, Faculty of Agriculture, Agricultural Machinery and Technologies Engineering Department, TR 01330 Balcali-Adana, Turkey
[*]Correspondence: aince@cu.edu.tr

**Abstract.** In this study, a new approach for faster determination of quality in hay bale and haylage was aimed. To this end, the relationships between bale densities, dry matter (DM), pH content and penetrometer values in hay bale and haylage were investigated. The mixture of caramba (*Lolium multiform cv* Caramba) and berseem clover (*Trifolium alexandrinum* L) was used as forage material. It was harvested by using two different harvesting methods and stored as dry hay and haylage. The penetrometer values were measured at four different points on bales. It was obtained that the pH content decreased with increase in bale density ($R^2 = 0.86$) and with decrease in DM content ($R^2 = 0.86$). The values measured at vertical-middle point gave higher correlation with density and pH contents.

**Key words:** Forage quality, bale density, pH, dry matter content.

## INTRODUCTION

Forage crops play an important role for on farm ruminant production. 40–90% of forage requirements are supplies as roughage. It is important to add roughage to the feeding ration at winter time for meat/milk yield and quality (Charmley, 2001). However, the storage of the roughage is one of the important problems. Whether haylage or hay bale, they must be harvested and stored with protection of nutrient elements. Since, the losses are quite high in hay bale, haylage recently comes to the fore for ruminant feeding (Wilkonson et al., 1996; Yıldız et al., 2008; Yaman, 2011).

The quality of roughage is foremost parameter for purchasing and adding to the feeding ration. Dry matter content, pH content, crude protein and relative feed value can be listed as most important quality parameters. Although there are a lot of methods for determination of quality, it is another necessity for farmers to use fastest methods. Because, chemical analysis are costly and take times. There are methods without chemical analysis but, the results of these methods can change relatively depends on the person who makes decision.

From this point of view, in this study, the relationships between bale densities, dry matter (DM), pH content and penetrometer values in hay bale and haylage were investigated. Thus, a new approach for faster determination of quality in hay bale and haylage was aimed.

## MATERIALS AND METHODS

In the research, the mixture of caramba (*Lolium multiform cv* Caramba) and berseem clover (*Trifolium alexandrinum* L) was used as forage material. Forage were harvested at the end of flowering stage of berseem clover. The harvesting and storage systems investigated in the research were given in Table 1. For haylage bales were wrapped by using PE material with 25 µ thickness in white color as four layers. The bales weight varied in between 18–20 kg for hay and 40–50 kg for haylage. Applications were left fermentation for 60 days for haylage.

**Table 1.** Harvesting and storage systems

| System code | Machines used in harvesting | Storage technique |
|---|---|---|
| S1 | Mower+round baler | Dry hay |
| S2 | Disc mower with conditioner+round baler | Dry hay |
| S3 | Mower+round baler+wrapping machine | Haylage |
| S4 | Disc mower with condationer+round baler+wrapping machine | Haylage |

The randomized block design was used for analysis the effect of systems and penetrometer values on bale densities, DM and pH content. Duncan's multiple range test was used to compare the means. Each experiment was replicated 3 times. The pH values of plants were obtained as reported by Chen et al. (1997). The dry matter (DM) content of plants was determined by drying to constant weight at 105 °C according to the ASAE standards (AOAC, 1990). The bale density was calculated as the ratio of bale mass to volume.

The penetrometers values were measured by using Shimpo mark (FGC-50B) hand penetrometer at 25 cm depth from two point of bale as shown Fig. 1.
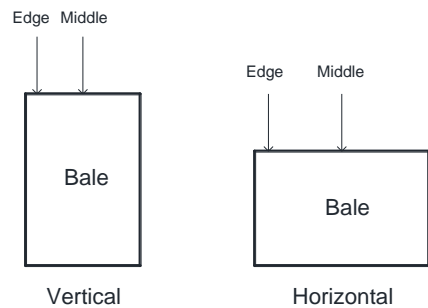


**Figure 1.** Measurements points of penetrometer values.

## RESULTS AND DISCUSSION

According to the variance analysis, it was found that storage technique (hay bale and haylage) has significant effect on bale density and pH content at 1% probability level, while the harvesting methods (mover and disc mover) have no effect statistically. Haylage has lower pH content and approximately 3 times higher bale densities comparing hay bale. DM contents ranged from 88.76% to 89.61% and from 51.38% to 48.49% for hay bale and haylage, respectively. The penetrometer values taken at vertical-middle point showed differences among the storage methods at 5% probability level according to the Duncan's Multiple Range Tests results (Table 2).

**Table 2.** Variance analysis results of Penetrometer values, bale densities, DM and pH contents

| Parameters | | Penetrometer Values (N) | | | | pH | Bale Density (kg m$^{-3}$) | DM (%) |
|---|---|---|---|---|---|---|---|---|
| | | Horizontal | | Vertical | | | | |
| | | Middle | Edge | Middle | Edge | | | |
| P values | | ns | ns | * | ns | ** | ** | ** |
| Harvesting and Storage systems | S1 | 261.08 | 317.21 | 54.33 b | 80.88 | 5.7 a | 134.37b | 88.76a |
| | S2 | 368.06 | 350.43 | 93.15 b | 94.67 | 5.7 a | 143.16b | 89.61a |
| | S3 | 205.95 | 205.94 | 138.93 a | 91.77 | 4.9 b | 305.66a | 48.49b |
| | S4 | 306.83 | 231.64 | 204.98 a | 124.67 | 5.0 b | 336.37a | 51.38b |
| P(%) | | 0.2 | 0.09 | 0.03 | 0.5 | 0.006 | 0.0001 | 0.0001 |
| LSD$_{(0.05)}$ | | - | - | 92.98 | - | 0.46 | 42.19 | 6.16 |
| CV (%) | | 30.0 | 23.3 | 37.99 | 37.50 | 3.58 | 7.3 | 3.75 |

In each column, means with the same letters are not significantly different at 0.01 level of significance using Duncan's Multiple RangeTest

There is no doubt that foremost parameter for quality is pH under any harvest and storage conditions. Kilic (2010) and Huhnke et al. (1997) reported that higher pH contents are expected in haylage (around 6.5) than conventional silage (around 3.9 and below). From this point of view, while evaluating quality in haylage, another parameters must be considered. So, the penetrometer values can be one of these parameter. According to the results, it was obtained that the pH content decreased with increase in bale density ($R^2 = 0.86$) and with decrease in DM content ($R^2 = 0.86$). The penetrometers values measured at vertical-middle point changed linearly with bale density ($R^2 = 0.59$). Moreover, it was found that it decreased with increase in DM contents ($R^2 = 0.47$) (Table 3).

**Table 3.** Correlation equations

| | x values | y values | $R^2$ | Equation |
|---|---|---|---|---|
| Horizontal-edge*density | Horizontal-Edge | Density | 0.41 | y = -0.6899x+420.63 |
| Vertical-middle*pH | Vertical-Middle | pH | 0.44 | y = -0.004x+5.8305 |
| Horizontal-edge*DM | Horizontal-Edge | DM | 0.45 | y = 0.157x+26.446 |
| Vertical-middle*DM | Horizontal-Edge | DM | 0.47 | y = -0.2061x+95.138 |
| Vertical-middle*density | Horizontal-Edge | Density | 0.59 | y = 1.0603x+99.808 |
| DM*pH | DM | pH | 0.86 | y = 0.0189x+4.0132 |
| pH*density | pH | Density | 0.86 | y = -208.83x+1343.8 |
| Density*DM | Density | DM | 0.95 | y = -0.212x+118.6 |

## CONCLUSION

Consequently, bale density in other words penetrometer values can be another parameter for determining quality. However, in this study, the values measured at vertical-middle point gave higher correlation with density and pH contents. It can be highlighted that higher penetrometer values refer to higher bale density and lower pH contents. So that, the penetrometer values measured at this point can be considered as quality indicator.

## REFERENCES

AOAC. 1990. *Official method of analysis.* Association of official analytical chemists, Washington DC., pp. 66–88.

Charmley, E. 2001. Towards improved silage quality – A review, *Can. J. Anim. Sci.*, **81**, 157–168.

Chen, V., Stoker, M.R. & Wallance, C.R. 1997. Effect of enzyme – inoculant systems on preservation and nutritive value of hay crop and corn silage. *J. Dairly* **77**, 501–505.

Huhnke, R.L., Muck, R.E. & Payton, M,E. 1997. Round Bale Silage Storage Losses of Rye Grass and Legume – Grass Forages. *Appl. Eng. Agric.* **13**, 451–457.

Kilic, A. 2010. *Silo Fodder Hand Book*. Hasad Yayıncılık, İstanbul, 200 pp. (in Turkish)

Yaman, S., 2011. Development of bale silage production technique. Project No: 105G086/03/2011. *Ministry of Agriculture*, Ankara. (in Turkish)

Yildiz, C., Ozturk, I. & Erkmen, Y. 2008. A research on determination on silage techniques and consumptions habits in Erzurum region. *J. Atatürk Univ. Agr. Fac.* **39 (1)**, 101–107.

Wilkinson, J.M., Wadephul, F. & Hill, J. 1996. *Silage in Europe – A survey of 33 countries.* Chalcombe Publications, Lincoln, UK.

# Effect of different biofuels to particulate matters production

P. Jindra[1,*], M. Kotek[1], J. Mařík[1] and M. Vojtíšek[2]

[1]Czech University of Life Science Prague, Faculty of Engineering, Department of Vehicles and Ground Transport, Kamýcká 129, CZ 16521 Prague, Czech republic
[2]Czech Technical University in Prague, Faculty of Mechanical Engineering, Center of Vehicles for Sustainable Mobility, Technická 4, CZ 16607 Prague, Czech Republic
[*]Correspondence: jindrap@tf.czu.cz

**Abstract.** In recent years the European Union has exhibited a significant interest in the reduction of crude oil usage. Biofuels can be used in conventional engines but the biofuels should reduce the emissions produced by internal combustion engines. This article deals with analysis of particulate matters (PM) production in chosen biofuels burned in internal combustion engine Zetor 1505. The conventional emission analysers are capable to detect gaseous emission components but they are not able to classify PM. Analysis of PM was performed with a TSI Engine Exhaust Particle Sizer 3090 which is able to classify particles from 5.6 nm to 560 nm. The device analysed different blends of alcohol–based biofuels tested under NRSC cycle conditions. The given size of PM can be taken as an impact on human organism's cells consequently human health. PM create an ideal medium for polyaromatic hydrocarbons (PAH), their composition and structure. Analysis of PM should become a standard component of every emission parameter assessment.

**Keywords:** biofuels, particulate matters, emissions.

## INTRODUCTION

The fast growth of the world population and industrial development is linked with an increasing consumption of fossil fuels. Fossil fuels, besides their benefits in terms of tradition and mastered processing technology, have many disadvantages as well. Among the major drawbacks include depletion and unstable price (Gumus et al., 2012). That is why all over the world are developing a new alternative fuels, with special emphasis on the renewable resources (Tashtoush et al., 2007). Diesel engines can possibly use various biofuels based on vegetable oils, fats and fatty acid esters etc. Many researches confirm the positive impact of biofuel production on harmful exhaust emission production (Altun et al., 2008; Pexa & Mařík, 2014; Obed et al., 2016). Another potential of biofuels application in diesel engines can be seen in the use of blended biofuels. In this case it brings more possibility used fuels on alcohol basis (methanol, ethanol, butanol, etc.). Many publications are showing a reduction of emissions and particulate matters (Hansen et al., 2005; Chotwichien et al., 2009). Especially in agriculture can expect significant use of biofuels through efficient access to the basic materials used for their production.

Diesel engines have dominant position in the agricultural utilisation. This is primarily due to their more advantages operating characteristics in the form of higher energy efficiency and lower production of emissions of CO, $CO_2$ and HC than gasoline

engines. On the other hand, the operation of diesel engines is accompanied by an increased production of nitrogen oxides and particulate matters. (Ozsezen et al., 2008; Karavalakis et al., 2009). Exhaust emission from diesel engines has been associated with higher risks of asthma and other pulmonary diseases, heart attack and other chronic health problems (Lewtas, 2007; McEntee & Ogneva–Himmelberger, 2008; Balmes et al., 2009).

As particulate matter (or solid particle) according to the laws of the USA is referred to any substance which is normally contained in the exhaust gas as solid particle (ash, soot) or as a liquid. They consist of elemental carbon forming particles and organic compounds (condensed water, sulphur compounds and nitrogen compounds). Solid particle itself is not toxic, but on the solid particles are adsorbed substances with high health hazards. Lwebuga–Mukasa et al. (2004) found correlation between asthma and truck traffic volumes. Most of the emitted particles have a size from one to hundreds of nanometers (nano–particles). (Chien et al., 2009; Vojtisek–Lom et al., 2015)

This article deals with the issue of blended biofuels in terms of particulate matters production depending on the type of added biofuel. The measurement was aimed not only on the total production of solid particles but on their size distribution also.

## MATERIALS AND METHODS

The tractor engine Zetor 1505 was used for measurement. This engine is a turbocharged four–cylinder engine with a volume of 4.156 dm$^3$. Detailed specifications are contained in Table 1. Engine on test bed is shown on Fig. 1. The engine falls under the classification of emission standard Tier III.

**Table 1.** Engine technical specification

| Engine Z 1505 | |
| --- | --- |
| Maximum power | 90 kW |
| Maximum torque | 525 Nm |
| Number of cylinders | 4 |
| Engine volume | 4,156 cm$^3$ |
| Bore | 105 mm |
| Stroke | 120 mm |
| Compression ratio | 17 |
| Rated speed | 2,200 rpm |
| Fuel pre–injection | 9° before TDC |
| | 1 – 3 – 4 – 2 |
| Specific fuel consumption | 255 g kWh$^{-1}$ |

Classification of particulate matters was made with the TSI analyser model EEPS 3090 whose detailed specification is shown in Table 2. The analyser enables detection of particle size and also monitors their number. The obtained data is then presented as a size range of particles produced. The measured sample is taken from the exhaust, and then is diluted by the device. Within the experiments in the production of solid particles in the diluted exhaust gas were compared only relatively with the reference fuel.
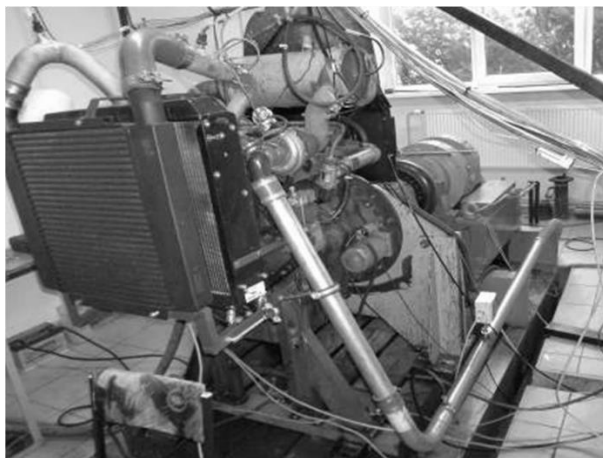
**Figure 1.** Engine on test–bed.

**Table 2.** Specification of PM analyser

| TSI EEPS 3090 | |
|---|---|
| Particle size range | 5.6–560 nm |
| Particle size resolution | 16 channels per decade (32 total) |
| Electrometer channels | 20 |
| Time resolution | 10 size distribution per second |
| Sample flow | $10 \, l \, min^{-1}$ |
| Dilution accessories | Rotation Disk thermodilution |

Production of particulate matters was measured according to 8 – point test ISO 8178 C1 that is known as Non–road Steady Cycle (NRSC). Tractor engine methodology prescribes testing at 8 steady states of speed and load. The experiment was performed in all 11 measuring points with the addition of the 12th point in the form of higher idle. Stabilization of the engine for each point of measurement was carried out for 8 minutes. The measurement then lasted 6 minutes.

The aim of experiment was to test several blended fuels containing diesel fuel and additives (in the alcohol biofuel form). Ingredients of tested fuel blends are summarized in Table 3. The reference fuel was pure diesel without biofuels which conforms to EN 590.

**Table 3.** Used fuels

| Fuel | Diesel ratio (weight, %) | Ratio of alcohol (weight, %) |
|---|---|---|
| Diesel – reference | 100 | 0 |
| Et10 | 90 | 10 ethanol |
| nBut16 | 84 | 16 n–butanol |
| iBut16 | 84 | 16 iso–butanol |

The share of individual bio–components of the reference fuel was chosen on the basis of the common shares of bio–components (in this case, bio–diesel) in commonly used fuels in the EU.

# RESULTS AND DISCUSSION

The production of PM in different size spectra for all researched fuels is shown in following figures. Operating modes of the engine were selected to see the differences in the production of particles between the individual fuels.

Fig. 2 presents the production of solid particles for full load at rated speed. Fig. 2 shows that the maximal production was achieved on diesel, the lowest production was achieved on an admixture of iso–butanol. In the case of n–butanol there is a shift of the spectrum producing particles to smaller size.
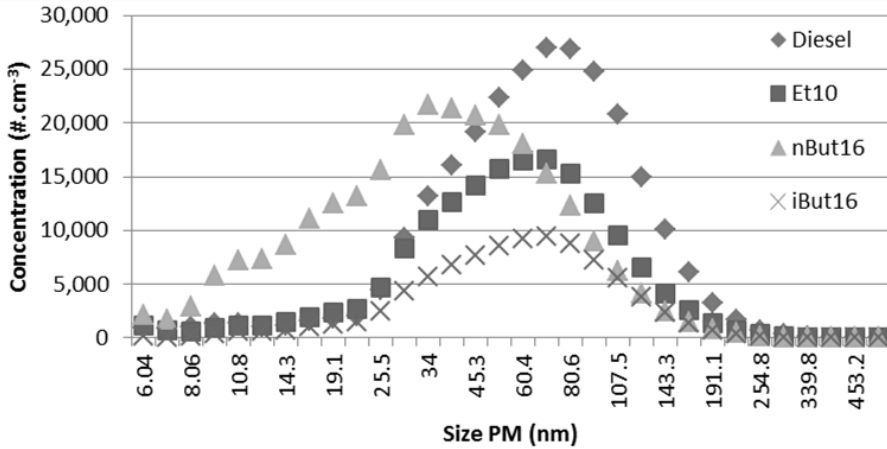


**Figure 2.** Particle concentration for point 1–100% torque, rated speed.

At 50% engine load at rated speed (see Fig. 3), it is again evident that the highest particle production was achieved when diesel fuel was used. The production of particulate matters from all monitored biofuels reached lower values than the reference fuel. The peak of all fuels has approximately the same size spectrum.
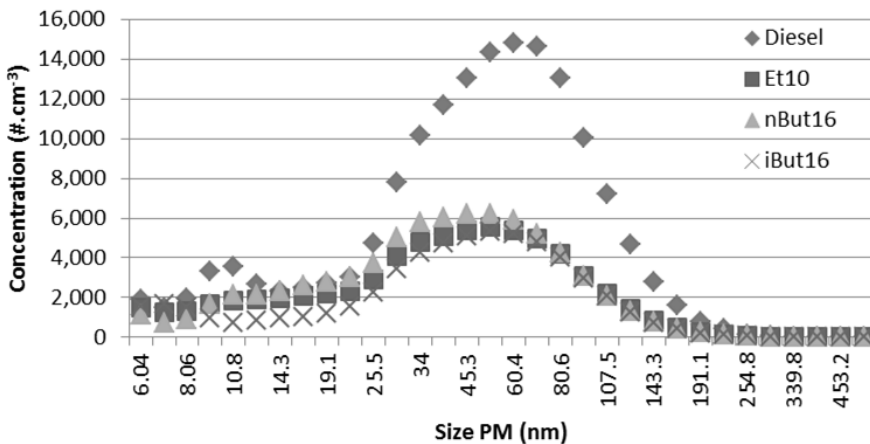


**Figure 3.** Particle concentration for point 3–50% torque, rated speed.

Fig. 4 shows the production of PM at 50% load and intermediate speed. It is evident that in most parts of the spectrum are all fuels balanced maximal particle production is shifted towards lower size spectra. The highest particle production reaches again the reference fuel.
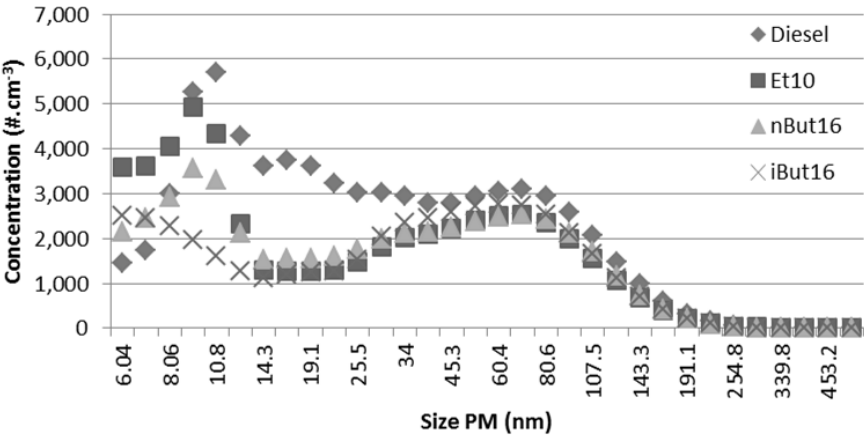


**Figure 4.** Particle concentration for point 8–50% torque, intermediate speed.

Fig. 5 shows particle production at 10% load and intermediate speed. At low loads, it is evident that the added biofuels causing increase in particle production. The highest production was achieved in the low size spectrum. The lowest total production reached the reference fuel.
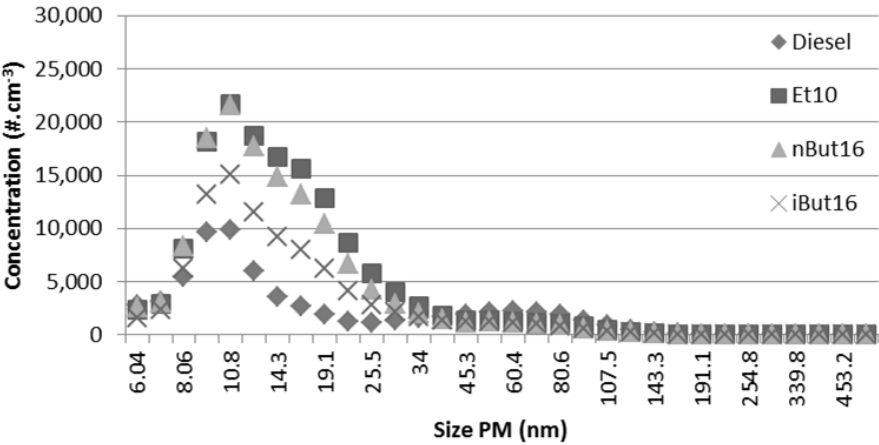


**Figure 5.** Particle concentration for point 10–10% torque, intermediate speed.

The following Fig. 6 shows the total quantity of particles produced for the entire duration of the measurement. The positive impact of added biofuels on the total production of particles is obvious.
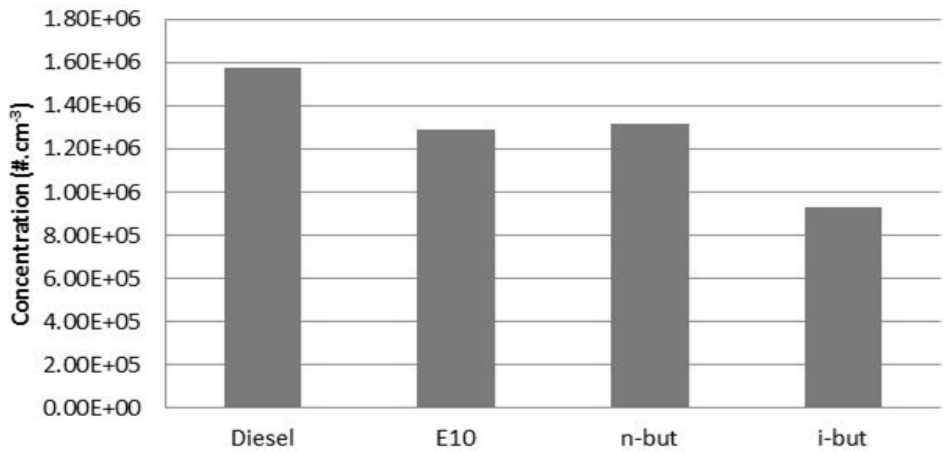


**Figure 6.** Total particle concentration for all tested fuels.

The achieved results correspond with the findings of other authors. Zhang & Balasubramanian (2014) tested several mixed fuels of similar composition and his findings confirm the positive effect of added butanol in the high engine load. Cheng et al. (2016) demonstrated the positive effect of adding butanol on engine smoke (smoke emission). Choi & Jiang (2015) highlights the positive impact of butanol in the area of higher magnitude spectra, while in the lower spectra was achieved better results to pure diesel.

**CONCLUSIONS**

Although only the production of solid particles was evaluated, the experiment's results demonstrate internal combustion engines' operability to use mixture of diesel and alcohol fuels. The engine used for tests was not additional modification specifically designed to operate with biofuels. The aim of experiment was to clearly demonstrate a different dependence of PM spectral distribution of each fuel. It can say that biofuels have a positive impact on the production of PM in the areas of higher loads and high engine speeds. Conversely, in low modes of load and speed was PM production higher than the reference fuel.

Pure alcohol biofuels using are not suitable for CI engines from their properties, because they have no optimal cetane number. The experiment results prove possibilities of appropriate use of alcohol fuels such as low blends in diesel. This can be seen a way for future in achievement to reduce a dependency on fossil fuels.

# REFERENCES

Altun, S., Bulut, H., Oner, C. 2008. The comparison of engine performance and exhaust emission characteristics of sesame oil–diesel fuel mixture with diesel fuel in a direct injection diesel engine. *Renewable Energy* **33,** pp. 1791–1795.

Balmes, J.R., Earnest, G., Katz, P.P., Yelin, E.H., Eisner, M.D., Chen, H., Trupin, L., Lurmann, F., Blanc, P.D. 2009. Exposure to traffic: lung function and health status in adults with asthma. *Journal of Allergy and Clinical Immunology* **123**, 626–631.

Cheng, X., Li, S., Yang, J., Liu, B. 2016. Investigation into partially premixed combustion fueled with N–butanol–diesel blends. *Renewable Energy* **86**. 723–732.

Chien, S.–M., Huang, Y.–J., Chuang, S.–C., Yang, H.–H. 2009. Effects of biodiesel blending on particulate and polycyclic aromatic hydrocarbon emissions in nano/ultrafine/fine/coarse ranges from diesel engine. *Aerosol and Air Quality Research* **9**, 18–31.

Choi, B., Jiang, X. 2015. Individual hydrocarbons and particulate matter emission from a turbocharged CRDI diesel engine fueled with n–butanol/diesel blends. *Fuel* **154**, 118–195.

Chotwichien, A., Luengnaruemitchai, A., Jai–ln, S. 2009. Utilization of palm oil alkyl esters as an additive in ethanol–diesel and butanol–diesel blends. *Fuel* **88**, 1618–1624.

Gumus, M., Sayin, C., Canakci, M. 2012. The impact of fuel injection pressure on the Exhaust emissions of a direct injection diesel engine fueled with biodiesel–diesel fuelblends. *Fuel* **95**, 486–94.

Hansen, A.C., Zhang, Q., Lyne, P.W.L. 2005 Ethanol–diesel fuel blends—a review. *Bioresource Technology* **96**, 277–285.

Karavalakis, G., Stournas, S., Bakeas, E. 2009. Light vehicle regulated and unregulated emissions from different biodiesels. *Science of the Total Environment* **40**7, 3338–3346.

Lewtas, J. 2007. Air pollution combustion emissions: Characterization of causative agents and mechanisms associated with cancer, reproductive, and cardiovascular effects. *Mutation Research* **636**, 95–13.

Lwebuga–Mukasa, J.S., Oyana, T., Thenappan, A., Ayirookuzhi, S.J., 2004. Association Between Traffic Volume and Health Care Use for Asthma Among Residents at a U.S.–Canadian Border Crossing Point. *Journal of Asthma* **41**, 289–304.

McEntee, J.C., Ogneva–Himmelberger, Y. 2008. Diesel particulate matter, lung cancer, and asthma incidences along major traffic corridors in MA, USA: A GIS analysis. *Health & Place* **14**, 817–828.

Obed, M.A., Mamat, R., Abdullah, N.R. 2016 Analysis of Blended Fuel Properties and Engine Performance with Palm Biodiesel–diesel Blended Fuel. *Renewable Energy* **86**, 59–67.

Ozsezen, A.N., Canakci, M., Sayin, C. 2008 Effects of biodiesel from used frying palm oil on the exhaust emissions of an indirect injection (IDI) diesel engine. *Energy and Fuels* **22**, 2796–2804.

Pexa, M. & Mařík, J. 2014. The impact of biofuels and technical engine condition to its smoke – Zetor 8641 Forterra. *Agronomy Research* **12**, 367–372.

Tashtoush, G.M., Al–Widyan, M.I., Albatayneh, A.M. 2007 .Factorial analysis of diesel engine performance using different types of biodiesel. *Journal of Environmental Management* **84**, 401–411.

Vojtisek–Lom, M., Pechout, M., Dittrich, L., Beranek, V., Kotek, M., Schwarz, J., Vodicka, P., Milcova, A., Rossnervoa, A., Ambroz, A., Topinka, J. 2015. Polycyclic aromatic hydrocarbons (PAH) and their genotoxicity in exhaust emissions from a diesel engine during extended low–load operation on diesel and biodiesel fuels. *Atmospheric Environment* **109**, 9–18.

Zhang, Z.H., Balasubramanian, R. 2014. Influence of butanol addition to diesel–biodiesel blend on engine performance and particulate emissions of a stationary diesel engine. *Applied Energy* **119**, 530–536.

# Soil compaction caused by irrigation machinery

J. Jobbágy, K. Krištof[*] and P. Findura

Slovak University of Agriculture in Nitra, Faculty of Engineering, Department of Machines and Production Systems, Tr. A. Hlinku 2, SK 94976 Nitra, Slovakia, [*]correspondence: koloman.kristof@uniag.sk

**Abstract.** This contribution is focused on the analysis of soil compaction with chassis of a wide-span irrigation machine, Valmont. The sprinkler had 12 two-wheeled chassis (size of tyre 14.9"×24"). During the evaluation of soil compaction, we monitored the values of penetration resistance and soil moisture during the operation of the sprinkler. Considering the performance parameters of the pump, the sprinkler was only half of its length (300 m) in the technological operation. In this area, also field measurements were performed in 19 monitoring points spaced both in tracks and outside the chassis tracks. The analysis showed the impact of compression with sprinkler wheels. The results of average resistance ranged from 1.20 to 3.26 MPa. The values of the maximum resistance ranged from 2.30 to 5.35 MPa. The results indicated a shallow soil compaction; however, it is not devastating.

**Key words:** penetration resistance, soil moisture, sprinkler, soil.

## INTRODUCTION

Soil compaction is a serious problem that adversely affects the productivity of crops, while crop yields are significantly reduced (Lhotský et al., 1991; Défossez & Richard, 2002). It is a process of soil particles relocation, which reduces soil porosity, thereby causing an aeration decrease and an increase in volume density and soil strength (Al-Adawi & Reeder 1996; Hillel, 1998; Brady & Weil, 1999; Hamza & Anderson, 2005). Soil compaction greatly affects the physical condition of the soil profile, especially with the pressure of agricultural machinery in cultivation and harvest (Alaoui et al., 2011; Braunack & Johnston, 2014). The result of this pressure is a technological or secondary compaction of the soil profile (Abedin & Hettiaratchi, 2002), defined with critical values of physical soil properties (Fulajtár, 2005; Carizzoni, 2007), particularly with a high volumetric density and low porosity (Keller et al., 2007).

An overview of the spatial distribution of compacted soil layers can be obtained by measuring the soil penetration resistance, which depends on volumetric density and soil moisture (Lamandé & Schjønning, 2011a). For a precise definition of the extent of compacted soil layers, it is important to determine its vertical and horizontal spatial distribution (Lamandé & Schjønning, 2011b). The critical value of soil compaction for plant growth is dependent on soil type and soil moisture (Schuler & Woods 1992). In terms of soil particle size, compacted sandy soils have little or no ability of spontaneous recovery, while for heavier soils, there are factors that allow reversible processes (regeneration of soil structure) (Mašek, 2005). Soil properties characterize the operating

conditions of tractors and influence the load of hydraulic and transmission systems. Therefore, we have to determine the soil properties in operating conditions of a tractor (Majdan et al., 2011). Interaction between the tyre and soil affects the exploitation of machinery in agriculture (Šesták et al., 1998; Rédl, 2009).

Soil compaction increases soil strength and decreases soil physical fertility through decreasing storage and supply of water and nutrients, which leads to additional fertilizer requirement and increasing production cost (Hamza & Anderson, 2005). There are environmental effects of soil compaction (Keller et al., 2013). The effect of compacted soil on the emissions released from soil into the atmosphere were observed for $N_2O$ (Šima et al., 2013) and $CO_2$ (Šima & Dubeňová, 2013).

The main objective was to investigate the effect of soil compaction with the axles of a wide-span irrigation machine and to evaluate the acquired knowledge and outcomes of the measurement.

## MATERIALS AND METHODS

To meet study objectives, field measurements were made in conditions of a farm Kovacs Agro, s.r.o., Hronovce, Slovakia (47°59'46.2"N 18°39'37.9"E). The arrangement of monitoring points was performed according to Fig. 1.

It is a very warm, dry and lowland region with following climatic conditions: Annual mean temperature 9.46 °C; Annual rainfall 620 mm; Number of rainfall days 146; Relative air humidity 77%; Depth of soil freezing from 10 to 23 cm; Annual sun light length 1817 hours; Annual Mean Cloudiness 58%).

The selected field is characterized by Haplic Chernozem and Luvi-Haplic Chernozem on loess, slope 0–1°, a plane without surface water erosion, medium (loamy) soil, according to the granularity code. The total area of the field was 181.31 ha, of which the irrigated area was 180.14 ha, which means a 99.35% coverage.
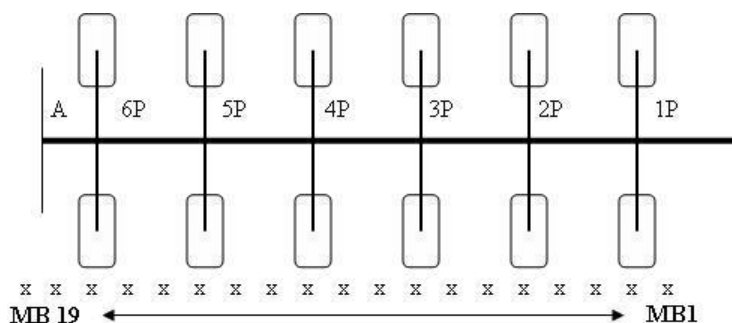


**Figure 1.** Principe of measurement of soil parameters; A – centre of wide range irrigation machine; P – tower; x – monitoring points; MB – monitoring point.

These points were located not only in tracks of the chassis but also outside them. The number of monitoring points was 19. Field experiments also included the measurement of soil moisture content (WET sensor, equipment, DELTA-T Devices Ltd., Cambridge, UK; HH2 logger, equipment, DELTA-T Devices Ltd., Cambridge, UK) and penetration resistance (Penetrologger Eijkelkamp, equipment, Eijkelkamp, Giesbeek,

Netherlands, Fig. 2). The experiments were conducted at certain soil moisture during the operation of the irrigation machine. Penetration resistance was measured simultaneously with the measurement of soil moisture. We used a conical tip with an angle of 30°, which is recommended by the ASAE Standard S313.2 (1994) for heavy and medium soils. The measurement of soil penetration resistance requires a uniform pressing of the cone into the soil (about 3 cm s$^{-1}$). The penetrologger´s measuring range is 0–10 MPa. This device allows recording the soil profile to a depth of 0.8 m, with a depth resolution of 10 mm. During the penetration, depth is sensed with an internal ultrasound sensor. When measuring the penetration resistance, each measurement consisted of three measurements. The depth of measurements was up to a 40 cm depth. Measured values of penetration resistance were corrected by obtained values of soil moisture (in percentage by weight). This was determined by a gravimetric method. Measuring the moisture with the WET sensor was carried out for each monitoring point three times.
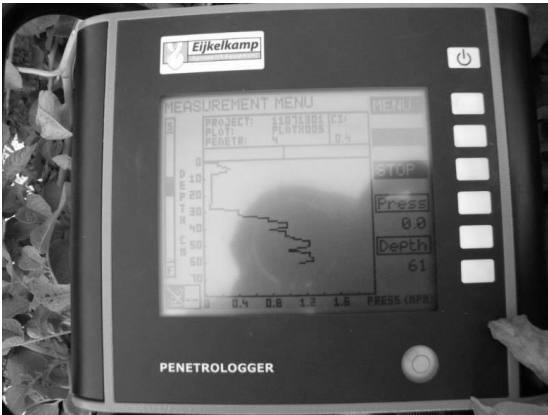


**Figure 2.** Penetrologger Eijkelkamp – measurement.



a)                                                                      b)
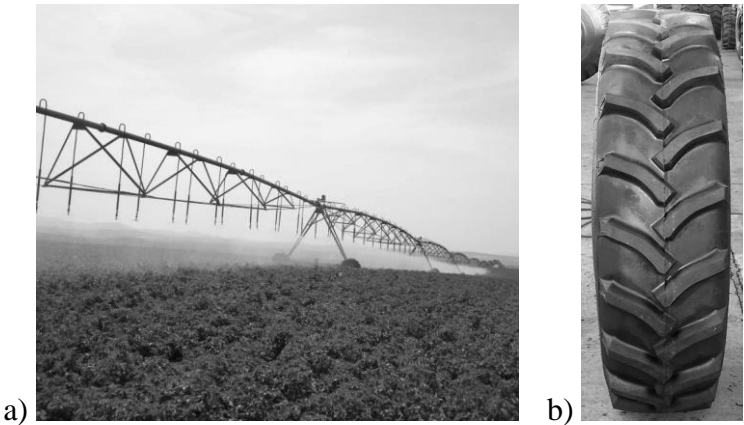
**Figure 3.** Linear irrigation machines (a) machine and (b) tyre, Valley Valmont, 600 m.

Field measurements were performed for the sprinkler Valley (Valley Irrigation, Nebraska, USA, Fig. 3), linear type, with a length of 594.59 m and the number of chassis

12 (Table 1). Besides the central tower (4 wheels), each chassis was equipped with two wheels. Only a half was always in operation (300 m, the entire irrigation machine moved, but only half sprayed water). A problem was the performance parameters of the pump, which would not cover a reliable technological operation of irrigation equipment for a length of 600 m. A water-pumping station was used as a water source.

**Table 1.** Technical characteristic of wide range irrigation machine (Valley, Valmont)

| Parameter | Value |
|---|---|
| Sprinkler spacing | 192 cm |
| Number of two-wheeled chassis | 12 |
| System length | 594.59 m |
| Type of wheels | high float 14.9" × 24" |
| Width of wheels | 37.8 cm |
| Power supply | 480 V/60 Hz |
| Maximum speed of system travel | 123.6 m h$^{-1}$ |
| Approx. weight (with water), length of section 49.12 m | 2,814 kg |
| Approx. weight (with water), length of section 54.86 m | 3,080 kg |
| Required run power | 20 kW |
| Type of guidance | below ground – shielded |
| Length of guidance cable | 5,608 m |

The effect of the sprinkler chassis on soil compaction was investigated by monitoring the compaction level in wheel tracks and outside them. Measurements were corrected and evaluated according to the Slovak Act No. 220/2004. When the soil moisture was above the correction interval, soil resistance was actually lower, and we had to add 0.25 MPa per each percentage by weight outside the interval. If soil moisture was below the correction interval, it was necessary to deduct 0.25 MPa per each percentage by weight outside the interval. In terms of our research, in clay soils this interval was 18–16% of soil moisture (percentage by weight). Therefore, data were corrected according to Lhotský et al. (1991), and the correction of the results is defined as follows:

$$PO_{KL} = (PO \pm 0.25z), \quad MPa \qquad (1)$$

where: $PO$ – measured penetration resistance (MPa); $PO_{KL}$ – corrected penetration resistance according to Lhotský et al. (1991), (MPa); $z$ – difference between the prescribed and measured moisture; its sign depends on whether it is above or below the range.

## RESULTS AND DISCUSSION

### Variability of soil moisture

Soil moisture is a key feature of the soil for crop irrigation regime. Measurements were conducted at 19 monitoring points in wheel tracks of the sprinkler and outside them. Table 2 shows the descriptive statistics of measurements before the application of irrigation rates. The average value of soil moisture was 10.11% vol. However, the value of the coefficient of variation was high (31.55%). After irrigation, values of soil moisture increased on average by 20.83% vol. The value of the coefficient of variation in

measuring the volumetric soil moisture decreased to 17.86%. In this case, there was a positive effect of irrigation and more balanced soil moisture across the whole width of the irrigation machine (Fig. 4).

**Table 2.** Measured data, soil moisture content, percentage by volume and by weight before and after irrigation

| Parameter | Soil moisture content (% wt.) | | Soil moisture content (% vol.) | |
|---|---|---|---|---|
| | before irrigation | after irrigation | before irrigation | after irrigation |
| Average | 8.44 | 25.78 | 10.11 | 30.94 |
| Median | 7.76 | 25.49 | 9.20 | 30.90 |
| Modus | 8.78 | – | 10.53 | 32.80 |
| Standard deviation | 2.66 | 4.74 | 3.19 | 5.52 |
| Variance | 7.08 | 22.49 | 10.20 | 30.52 |
| Difference max-min | 8.47 | 22.39 | 10.16 | 26.30 |
| Minimum | 5.39 | 15.82 | 6.47 | 19.30 |
| Maximum | 13.86 | 38.21 | 16.63 | 45.60 |
| Sum | 160.27 | 489.83 | 192.12 | 587.80 |
| Sample size | 19.00 | 19.00 | 19.00 | 19.00 |
| Coefficient of variation | 31.54 | 18.39 | 31.55 | 17.86 |
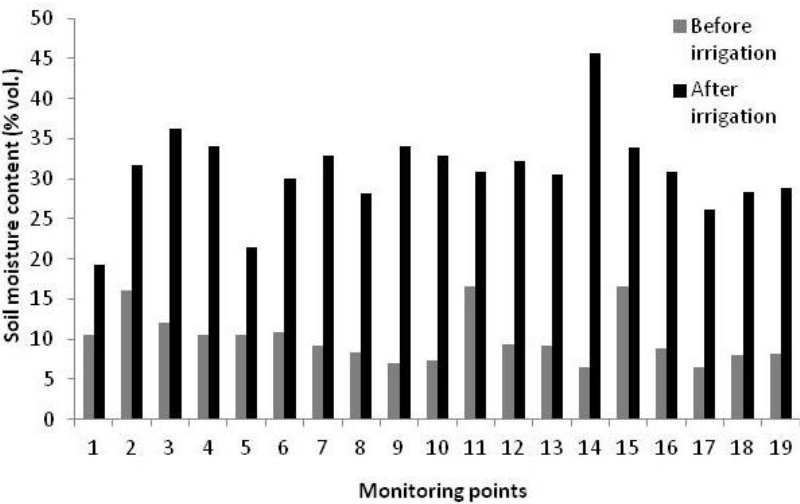


**Figure 4.** Soil moisture content before irrigation and after irrigation.

**Variability of penetration resistance**

In determining the variability of penetration resistance, measurements were performed before irrigation. After irrigation, measurements of penetration resistance were sufficiently affected by soil moisture because all values are outside of the range defined by Lhotský et al. (1991). Therefore, a correction factor of humidity was used, and all data were corrected according to the Act No. 220/2004 on the conservation and use of agricultural land. Values of penetration resistance were corrected to 18–16% vol. soil moisture.

It follows from the collected data that the farm extensively applies the principles preventing an undesired impact of agricultural machinery on the soil on the monitored

field, since the average value of penetration resistance ranged from 1.20 to 3.26 MPa (Fig. 5). The maximum values of penetration resistance ranged from 2.30 to 5.35 MPa (Fig. 6). The limit value for the maximum soil penetration resistance was exceeded at two monitoring points (P5 and P6).
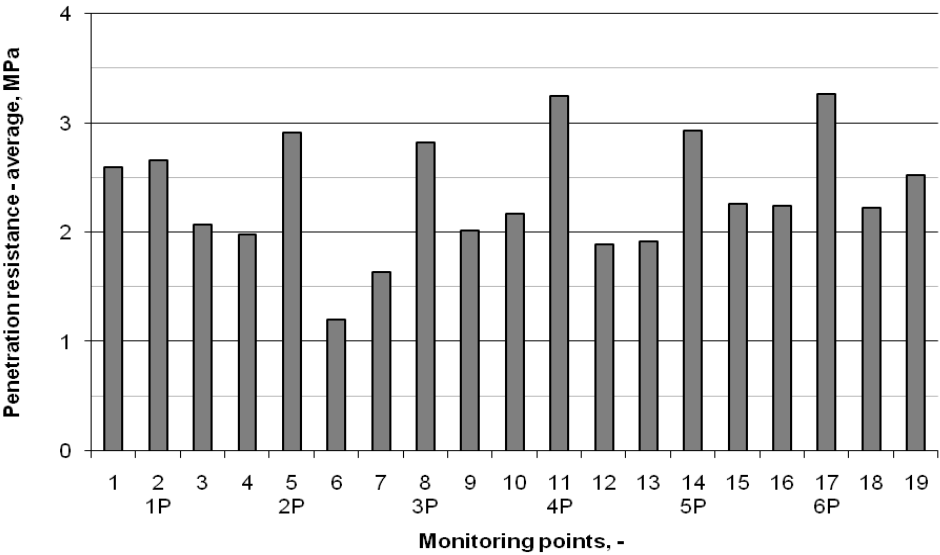


**Figure 5.** Penetration resistance of soil – average, MPa; P – tower.
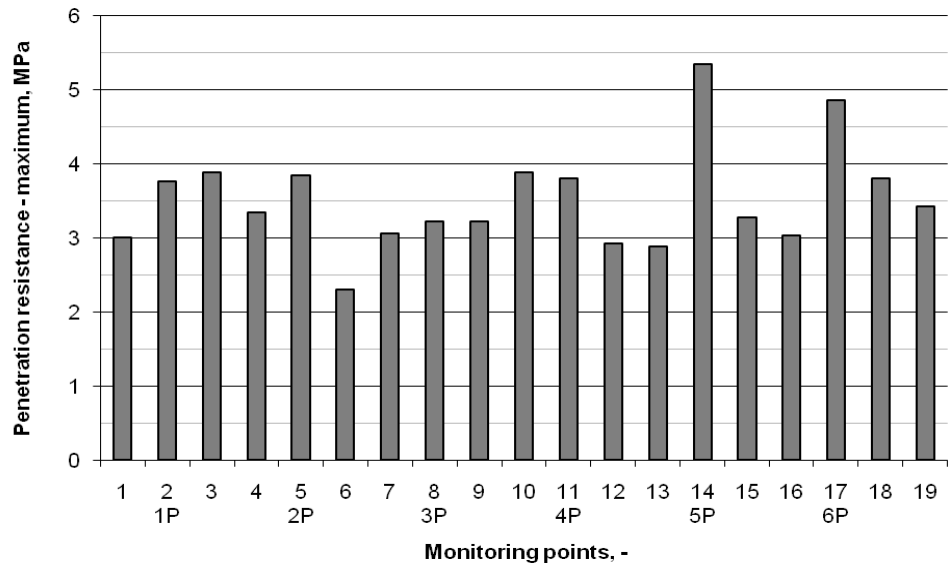


**Figure 6.** Penetration resistance of soil – maximum, MPa; P – tower.

According to the ASAE Standard EP542 (2004), 2 MPa is the value of penetration resistance which already limits the development of the root system of plants; however, this standard does not distinguish between soil types. The variability of penetration resistance is given by the variability of moisture conditions and passes of machines, too.

When comparing the data obtained, we concluded that penetration resistance increased in wheel tracks of the irrigation machine. The graphical representation shows that penetration resistance in wheel tracks after machine passes is higher than outside of tracks. Fig. 7 shows the secondary compaction which is significant especially in the depth of up to 10 cm.
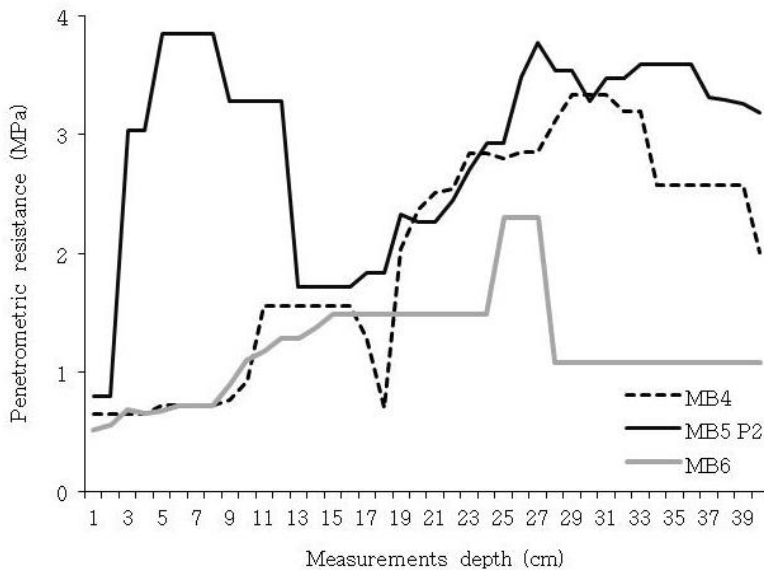


**Figure 7.** Relationship between penetration resistance and measurement depth in monitoring points: MB4, MB6 – monitoring point outside of chassis; MB5 – monitoring point within the chassis (tower 2P).

### Determining the effect of soil moisture on penetration resistance

After application of irrigation depth the value of penetration resistance decreased depending on the depth measurement (Fig. 8). Soil compaction with the impact machine passes is a specific phenomenon that is becoming even more a current topic while it was observed a clear differences in Figs 5–6.

Based on the obtained literatures (Hiller, 1998; Duiker, 2004; Fulajtár, 2005), it can be concluded that it is necessary to evaluate the soil compaction always with respect to current humidity conditions, the presence of a particular crop, soil types, and used machinery. Soil compaction is caused by effects of increasingly heavy machinery on soil as well as tillage and passes under an improper soil moisture. Increasing compaction is affected not only by tractors and harvesters but also by other self-propelled, trailer and semi-trailer machines (Keller et al., 2013). In general, shallow soil compaction is attributed to pressure in the 'tyre-soil' area, while deep soil compaction refers to the effects of the total axle load on soil (Duiker, 2004).
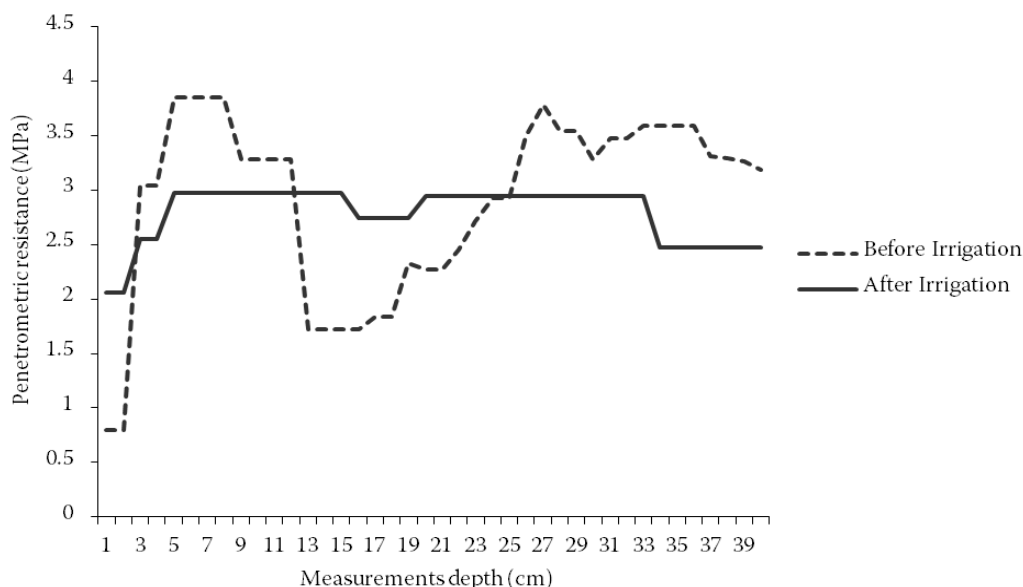
**Figure 8.** Relationship between penetration resistance and measurement depth in monitoring point MB5, tower 2, before and after irrigation.

When using the wide-span irrigation machine with selected tyres, an effect of the chassis on shallow soil compaction was confirmed. The values of penetration resistance ranged from 0 to 3.13 MPa in tracks and outside them. The highest changes were demonstrated in the tracks of the second chassis (tower). However, it is possible to state that the irrigation machine with its total mass divided into individual chassis does not cause devastating compaction. It is rather only a local and shallow soil compaction which can be removed with appropriate tillage. The soil moisture content is an important factor for passes of machines. The soil moisture content is determined from a disturbed soil sample. Another factor is the total weight of the machine and the total contact area. The number of machine passes on the soil is needed to be monitored and reduced. Joining certain operations can contribute to reducing soil compaction.

Váchal et al. (1983) recommend the reduction of passes after sub-soiling in the first year, to merge machines into aggregates, and to grow deep-rooted crops at least two years after intervention. All the performed measures must lead to creating an optimal soil structure and its protection.

Machine passes on the soil can cause its compression; they can reduce the soil porosity and create barriers to water and air movement in the soil and roots penetration in the soil (Braunack & Johnston, 2014). Soil compaction is determined by several methods. Most of them require soil sampling, time necessary for laboratory analyses, or a long period of field preparation where holes are prepared for ditch sensors.

Probably, the fastest way to determine soil compaction is the measuring of penetration resistance (Carizzoni, M. 2007). The results of penetration resistance on the monitored field confirmed a higher soil resistance in wheels tracks of the irrigation machine. Carrara et al. (2003) state that there are a lot of examples where penetration resistance is used for monitoring the soil compaction.

During the year, the soil responds to machine passes in different ways. Soil resistance to compaction decreases with increasing soil moisture. Humid and light soils have a very low resistance during seedbed preparation and sowing when passes cause compaction of the topsoil and subsoil (Kulkarni et al., 2010), which affects the crop grown during the whole growing season. Other risky periods occur during autumn field operations when loaded machines compact the soil into a high depth (Hůla, 1989). Our values were evaluated in conformance with the values introduced in the Act No. 220/2004. The results have shown a clear effect of irrigation machine wheels on compaction.

The presented act specifies the limit values of corrected penetration resistance ranging from 3.7 to 4.2 MPa at the moisture of 18–16% wt. for clayey soil. Our results have not exceeded these limit values. It means that compaction values harmful for plant growth were not exceeded. However, there was a higher compression in wheels tracks of the irrigation machine.

Solving this issue in relation to soil compaction has focused mainly on a new design of tyres and weight reduction of machines. Before new design of tyres got into production, it was recommended to use double wheels to reduce soil compaction with contact pressures. Controlled underinflated tyres of machines also appear to be suitable for driving on fields. However, new constructions of low-pressure tyres are currently dominating (Javůrek & Vach, 2008¸ Keller et al., 2013). The model of tyres used on the irrigation machine Valmont was also radial on all the axles due to a lower compaction in their tracks.

According to Abedin & Hettiaratchi (2002), the incidence of compacted layers in the soil profile is usually possible to detect only in the spring when the soil profile is evenly moistened. Measurement in summer and in autumn is unreliable because the soil profile can show large moisture differences, which are reflected in the values of soil penetration resistance.

## CONCLUSION

There was a positive effect of irrigation and more balanced soil moisture across the whole width of the irrigation machine while soil moisture coefficient of variation changed from 31.55% to 17.86%.

In examining the variability of penetration resistance in dependence on the monitoring point, we found that in wheel tracks of the irrigation machine, penetration resistance is higher than outside of tracks. It ranged from 1.20 to 2.30 MPa and from 3.26 to 5.35 MPa, respectively. Based on the results, we can say that due to a lower weight of the whole machine in comparison with other machines, there was only a shallow soil compaction which not cross 10 cm. However, penetration resistance increased with depth.

The effect of soil moisture on the penetration resistance was observed. Thererofe, irrigation has the effect on penetrometric resistance as well. However, the variability in soil condition across the field affectes the results and the final effect was different for most of the observing points which ranged from 64.1% to 91.6%.

# REFERENCES

Abedin, M.Z. & Hettiaratchi, D.R.P. 2002. State parameter interpretation of cone penetration tests in agricultural soils. *Biosystems Engineering* **83**, 469–479.

Act no. 220/2004. 2004. Act on the Conservation and Use of Agricultural Land. Online. [Available at: www.zbierka.sk/sk/predpisy/220-2004-z-z.p-7816.pdf] (accessed January 28, 2015) (in Slovak).

Al-Adawi, S.S. & Reeder, R.C. 1996. Compaction and sub-soiling effects on corn and soybean yields and soil physical properties. *Transactions of the ASABE* **39**, 1641–1649.

Alaoui, A., Lipiec, J. & Gerke, H.H. 2011. A review of the changes in the soil pore system due to soil deformation: a hydrodynamic perspective. *Soil & Tillage Research* **115–116**, 1–15.

ASAE Standards, 1994. Soil Cone Penetrometer. *ASAE Standards, Engineering Practices Data (S312.3),* St. Joseph, ASAE.

ASAE Standards, 2004. Procedures for using and reporting data obtained with the soil cone penetrometer. *ASAE Standards, 50th Ed. 2004 (EP542)*, St. Joseph, ASAE

Brady, N.C. & Weil, R.R. 1999. The Nature and Properties of Soil. Prentice Hall, New Jersey, 881 pp.

Braunack, M.V., Johnston, D.B. 2014. Changes in soil cone resistance due to cotton picker traffic during harvest on Australian cotton soils. *Soil & Tillage Research* **140**, 29–39.

Carrara, M., Comparetti, A., Febo, P., Morello, G. & Orlando, S. 2003. Mapping soil compaction measuring cone penetrometer resistance. In: *Proceedings form 4th European Conference on Precision Agriculture*, Wageningen Academic Publishers, Wageningen, 176 pp.

Carizzoni, M. 2007. Die Ausbreitung von akustischen Wellen zur Untersuchung struktureller Eigenschaften von Landwirtschaftsböden (In German with English summary). Dissertation University of Bern, Switzerland, 157 pp (in German).

Défossez, P. & Richard, G. 2002. Models of soil compaction due to traffic and their evaluation. *Soil & Tillage Research* **67**, 41–64.

Duiker, S.W. 2004. Avoiding soil compaction. On-line. [Available at: http://pubs.cas.edu/freepubs/pdfs/uc186.pdf]. (accessed February 17, 2014).

Hamza, M.A., Anderson, W.K. 2005. Soil compaction in cropping systems: A review of the nature, causes and possible solutions. *Soil and Tillage Research* **82**: 121–145.

Hillel, D. 1998. *Environmental Soil Physics*. Academic Press, Division of Harcourt Brace and Company, San Diego: 771 pp.

Hůla, J. 1989. Impact of machine passes on soil and possibilities of minimizing negative effects. In: *Impact of machinery on soil*. ČSVTS Dom techniky, Banská Bystrica, p. 54–61 (in Czech).

Fulajtár, E. 2005. *Physical properties of soil.* VÚPOP in Bratislava, Bratislava. 142pp (in Slovak).

Javůrek, M. & Vach, M. 2008. *Negative effects of soil compaction and measures for their elimination*. VURV in Prague, Prague. p. 24-36 (in Czech).

Keller, T., De´fossez, P., Weisskopf, P., Arvidsson, J. & Richard, G. 2007. SoilFlex: a model for prediction of soil stresses and soil compaction due to agricultural field traffic including a synthesis of analytical approaches. *Soil & Tillage Research* **93**, 391–411.

Keller, T., Lamandé, M., Peth, S., Berli, M., Delenne, J.-Y., Baumgarten, W., Rabbel, W., Radjaï, F., Rajchenbach, J., Selvadurai, A.P.S. & Or, D. 2013. An interdisciplinary approach towards improved understanding of soil deformation during compaction. *Soil & Tillage Research* **128**, 61–80.

Kulkarni, S.S., Bajwa, S.G. & Huitink, G. 2010. Investigation of the effects of soil compaction in cotton. *Trans. Am. Soc. Agric. Biol. Eng.* **53**(3), 667–674.

Lamandé, M. & Schjønning, P. 2011a. Transmission of vertical stress in a real soil

profile. Part II: effect of tyre size, inflation pressure and wheel load. *Soil & Tillage Research* **114**, 71–77.

Lamandé, M. & Schjønning, P. 2011b. Transmission of vertical stress in a real soil profile. Part III: effect of soil water content. *Soil & Tillage Researc,* **114**, 78–85.

Lhotský, J., Beran, P., Paris, P., Valigurská, L. 1991. Degradation of soil by increasing compression. *Soil & Tillage Research* **19**, 287–295.

Schuler, R.T. & Wood, R.K. 1992. *Soil compaction. Conservation Tillage Systems and Management.* Iowa State University, Ames: 69–76.

Mašek, J. 2005. Technology of soil cultivation. *Mechanizace zemědělství* **54**, 50–55 (in Czech).

Majdan, R., Tkáč, Z., Kosiba, J., Cvíčela, P., Drabant, Š., Tulík, J. & Stančík, B. 2011. Soil properties determination by reason of measuring the tractor operating regimes for biodegradable fluid application. In: *Engineering technology in the agricultural sector 2011*. SUA in Nitra, Nitra, p. 71–75 (in Slovak).

Šesták, J., Rédl, J. & Ryban, G. 1998. To some questions of tyred wheel rolling. In: *Quality and reliability of machinery*. SUA in Nitra, Nitra, p. 250–253 (in Slovak).

Šima, T., Nozdrovický, L., Dubeňová, M., Krištof, K. & Krupička, J. 2013. Effect of the crop residues on nitrous oxide flux in the controlled traffic farming system during the soil tillage by LEMKEN Rubin 9 disc harrow. *Agronomy Research* **11**, 103–110.

Šima, T. & Dubeňová, M. 2013. Effect of crop residues on CO2 flux in the CTF system during soil tillage by a disc harrow Lemken Rubin 9. *Research in Agricultural Engineering* **59** *(Special Issue)*, 15–21.

Rédl, J. 2009. *Mechanics of Materials*. SUA in Nitra, Nitra, 106 pp (in Slovak).

Váchal, J., Ehrlich, P., Lhotský, J., Chábera, V. & Simota, J. 1983. *Methods of improving heavy and compacted soils.* České Budějovice, Dum techniky ČSVTS: p. 31–60 (in Czech).

# Identification of worm-damaged chestnuts using impact acoustics and support vector machine

F. Kurtulmuş[1,*], S. Öztüfekçi[2] and İ. Kavdir[3]

[1]Uludag University, Faculty of Agriculture, Department of Biosystems Engineering, TR 16059 Bursa, Turkey
[2]Uludag University, Faculty of Agriculture, Department of Soil Science and Plant Nutrition, TR 16059 Bursa, Turkey
[3]Çanakkale Onsekiz Mart University, Faculty of Agriculture, Department of Agricultural Machinery and Technologies Engineering, Çanakkale, Turkey
[*]Correspondence: ferhatk@uludag.edu.tr

**Abstract.** Chestnut has both economically and nutritional values, and its production in the World is about 2 Mt. Turkey is one of the important chestnut producers with a production amount of about 60,000 t. Worm damage is one of the reasons which may reduce economical value of chestnut. Aim of this study was to reveal possibilities of distinguishing of worm-damaged chestnuts from healthy ones using impact acoustics and sound analysis methods. A Turkish local variety called 'Osmanoglu' was chosen for the study. A sound acquisition station was comprised, and acoustic emissions of worm-damaged and healthy nuts were acquired at a sampling quality of 192 kHz and 16 bit. Each sample was labelled according to worminess situation by shattering the nut after acoustic measurements. A band-pass filter between cutoff frequencies of 70 Hz and 100 kHz was designed and applied to sound samples to alleviate negative effects of unwanted noise. Various signal features such as variance, standard deviation, kurtosis, zero crossing rate, and spectral centroid were calculated. A relevant feature subset was determined using feature selection technics. An identification model was trained using Support Vector Machine and cross-validation rules. Performance of the classification system was measured on a test set. In this study, reporting the preliminary results of an ongoing and comprehensive research project[1], promising results were obtained for identification of worm-damaged chestnuts with proposed system.

**Key words:** Chestnut classification, Worm Damage, Impact Acoustics, Support Vector Machine.

## INTRODUCTION

Chestnut has both economical and nutritional values with about 2 Mt production in the World. Turkey is the second largest chestnut producer with a production about 60,000 t after China (FAO, 2011). Chestnut contains 5% protein, 40–50% carbohydrate, 40–50% moisture, and 1.5–2% clay. Additionally, 100 gr of nut contains 50 gr of vitamin C, some vitamin A, and 100 gr of nut provides 200 cal. Chestnut is also a nutritious source of energy (Gün et al., 2006).

---

Determining the quality parameters of chestnut properly is very important for producers and processers. Especially in post-harvest processes, supplying properly classified chestnuts to the consumers increases the reliability of producers and manufacturers allowing buyers to consume their products with confidence. One of the factors highly affecting the chestnut quality is existence of worm (*Cydia splendana* or *Curculio elephas*). These worms cause damage in chestnuts by directly feeding in them resulting a damage between 15% and 40%. During the growing period of a chestnut harmful larvae may dig into the peel of the nut in the hedgehog and start damaging it. In the meantime, both the hedgehog and the nut keep growing when the larvae is still active in the nut. While the growing process is still in progress the inlet hole of the larvae may be closed without leaving any trace. Generally, worms leave the fruit by piercing the nuts after harvest in storage rooms or sale stands. Damaged galleries in the nut occurred due to larvae activities may cover some parts or entire of the nut over time. Conventionally, separation of wormy chestnuts is carried out by expert employees. Chestnuts with worm-damages and closed-holes are difficult to recognize without cutting or deforming the nut. Additionally, human factor may cause errors in detecting wormy products manually. Therefore, it is extremely important to determine economic values of chestnuts effectively in evaluating raw products. Furthermore, it is advantageous to be able to classify the crops correctly and fast for the economy of the producers.

Considering the reasons explained above, auto-classification systems are needed to identify worm-damaged chestnuts by reducing labour and time. Impact acoustics (IA) method has been used for classification of some agricultural products by some researchers. IA methodology relies on both digitizing the sound obtained when a chestnut is dropped on an impact surface from a distance and also analysing it using the signal processing techniques. With this method, it is possible to conduct an identification work without peeling, deforming or damaging agricultural commodities. In an early study by Pearson (2001), an IA system was developed to distinguish uncracked pistachios from open ones. The sound signals which were created when nuts hit to an impact surface were analysed in both time and frequency domains. It was reported that closed-shell pistachios could be classified with an accuracy rate of 97%. In another study, an algorithm was developed for the same purpose using methods of speech recognition (Çetin et al., 2004). Distinguishing features consisting of Mel-Cepstrum coefficients were extracted and principal component analysis (PCA) was performed. It was reported that closed-shell nuts were successfully identified with accuracy rates over 99%. Amoodeh et al. (2006) investigated the possibility of measuring moisture content of wheat kernels based on IA. Calibration of moisture determination system was made by revealing the relation between digital sound signal and wheat moisture content. In the studies by Kalkan & Yardımcı (2006) and Kalkan et al. (2008) facilities of differentiating open-shell nuts from closed-shell nuts using IA techniques were reported. IA method was also used for identification of pistachio varieties (Omid et al. 2009). Characteristic features of sound signals were calculated using fast Fourier transform. PCA was used for reduction of feature space and a classification model was proposed using neural networks. The researchers reported an identification accuracy of 97.5% for their experiments. Another IA-based research was performed to identify walnut varieties (Khalesi et al., 2012). PCA was applied to frequency domain features and neural network

was used for the classification model. Walnut varieties could be classified with an accuracy rate of 99%.

Although some studies have been conducted involving the application of IA methods on agricultural materials, there has been a big gap in impact acoustic studies conducted on chestnuts in the literature. Automated classification systems which are able to identify worm-damaged chestnuts may provide many benefits to the producers by reducing labour and time. In this study, it was aimed to develop a prototype, an experimental classification system to identify worm-damaged chestnuts using IA method, digital sound signal processing and support vector machine. Impact acoustic method has been investigated by some researchers for the classification of agricultural crops as relatively new and immature method. In that respect, determining the impact acoustic characteristics of chestnut will also contribute to the literature as an original work.

## MATERIALS AND METHODS

### Chestnut samples

In this study, a local variety of chestnut (*Castanea Sativa* Mill.), namely 'Osmanoglu' was selected for developing and testing the identification system. A total of 904 chestnut samples were used. Of those chestnut samples, 460 were worm-damaged and 444 were of healthy samples. Some chestnut samples, which were used in this study, are shown in Fig. 1. In sound acquisition experiments, each chestnut sample was sliced and examined carefully after obtaining the sound signal. After examining internal flesh quality of each chestnut its sound signal was categorized into one of the two classes, as healthy or worm-damaged.
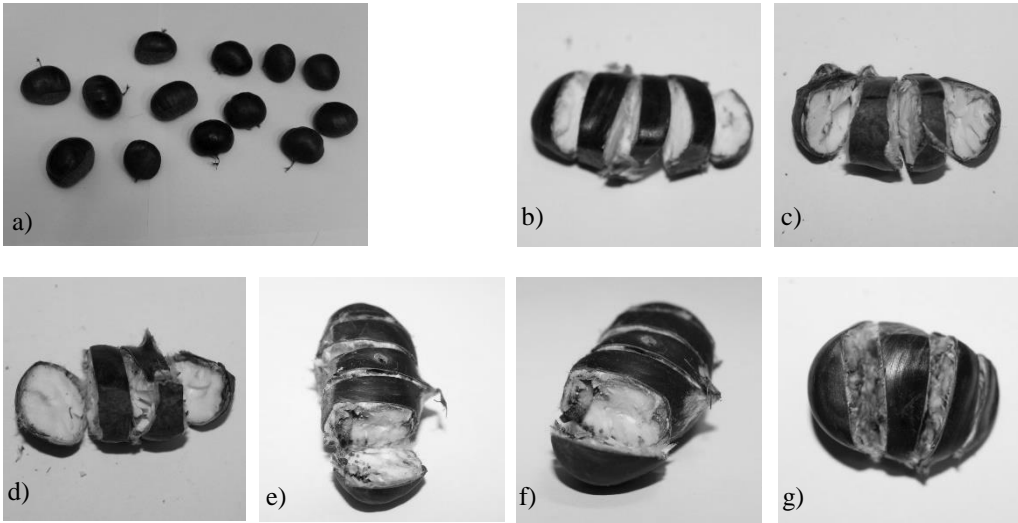


**Figure 1.** Some chestnut samples used in this study (a), healthy chestnuts (b, c, and d), worm-damaged chestnuts (e, f, and g).

### Impact conditions

IA methodology is basically performed based on digitizing of the sound obtained when a chestnut impacts on a surface after releasing from a distance using a microphone and analysing this sound signal using digital signal processing methods. In this study, a sound acquisition station, shown in Fig. 2, was comprised to capture impact signals of chestnut samples. In IA methodology, it is vitally important to convert the majority of the kinetic energy emerged from the impact itself into sound energy and to prevent any possible vibration of the platform. To determine an optimum impact plate size, preliminary tests were performed with steel plates with the dimensions of 80 x 80 x 15, 150 x 150 x15 mm, and 200 x 200 x15 mm. It was found that impact plates of 150 x 150 x15 mm and 200 x 200 x 15 mm caused unwanted vibrations and tinging at the impact moment. On the other hand, the impact plate of 80 x 80 x 15 mm was found suitable and used for impact sound acquisitions of the chestnuts studied.
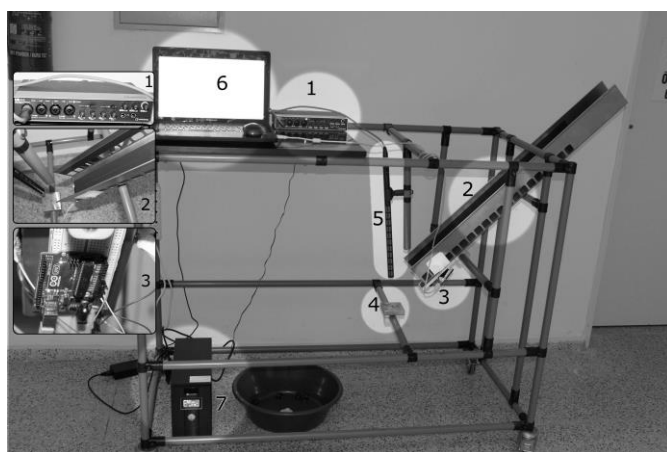


**Figure 2.** General view of impact signal acquisition station. 1 – sound card, 2 – sliding platform, 3 – triggering system, 4 – impact plate, 5 – shotgun microphone, 6 – computer, 7 – Uninterruptible power supply.

### Sliding platform

In the sound acquisition experiments, a sliding platform was used to obtain similar impact conditions for all the samples. As shown in Fig. 2, the sliding platform was made of sheet metal with a smooth surface. In preliminary tests, it was experienced that sliding platform was vibrating when chestnuts was sliding through it. Therefore, inner floor surface of the sliding platform was covered with a smooth surfaced plastic band to prevent the vibration sound to interfere with the impact itself.

### Microphone

A shot-gun microphone (ME-67 and K6 power module, Sennheiser Electronics Corporation, Old Lyme, Conn.), commonly used for broadcasting purposes, was used in this study for acquiring chestnut impact sound. This types of microphones are able to gather sound waves from a desired direction and can highly alleviate environmental noise. The microphone was placed in a location where its receiving point is 100 mm far from the impact plate.

### Triggering system

A triggering system (Fig. 2) was also designed to avoid interference of unwanted noise with the sound signals of chestnuts. With this system, sound acquisition was triggered right after a chestnut left the sliding platform. The triggering system basically consisted of light dependent resistors, laser emitters, and a microprocessor (ARDUINO, UNO R3) which was responsible for sending a command to the computer to start signal recording.

Another parameter for sound acquisition system was the angle between the sliding platform and the impact surface. It was expected that nuts hit the impact surface only once avoiding multiple impact peaks. On the other hand, it was observed that bigger angle values caused delays in the triggering system and unwanted hits to the microphone. Different angle values were tried to determine an optimum angle degree and the angle degree of 45° was determined and used in the experiments as the optimum one.

### Sound device

Most of the computer systems include a sound device with the sampling frequency of 44 kHz. To obtain more information from an impact sound signal, a sound device (UR-44, Steinberg GmbH, Germany) having 192 kHz sampling frequency was used in this study. A computer (Intel® Core™ i7-4700MQ CPU @ 2,40 GHz, 8 GB RAM) was used for signal processing and developing identification algorithms. During sound acquisition experiments, WiFi and Bluetooth devices of the computer were disabled to prevent unpredictable interferences.

### Programming environment

In this study, the algorithms of signal processing were programmed in Python 2.7 programming language using the Scipy and Numpy scientific computing libraries (Oliphant, 2007). Classification algorithms and cross-validation approaches were implemented using Scikit-learn machine learning library (Pedregosa et al., 2011). The microprocessor was programmed in C programing language.

### Signal processing

In sound acquisition, it is important to include impact signal in an appropriate time frame without skipping any important part of the signal vector. To make sure that the entire impact signal is included, sound recording was started 0.15 s before the impact moment and stopped 0.4 s after the impact moment. Thus, actual impact signal was covered by a comparatively long vector at first. On the other hand, a shorter signal frame consisting 512 peaks (about 2.7 ms for 192 kHz) was enough to represent the actual impact signal as shown in Fig. 3. Based on this approach, each recorded signal was post-processed to obtain an uniform signal length using a simple slicing algorithm. The first big extrema value of the peak values from the beginning was considered for slicing the signal vector.

Considering the signal shown in Fig. 3, a low frequency noise in the silence part before the impact moment is very distinguishable. It is unavoidable that this noise also interferes with the framed actual impact signal. It was necessary to eliminate this noise using a high-pass filter (Buerano et al., 2012). In this study, impact signals were also zoomed in and inspected carefully. So, it was observed that there was also a high frequency noise in signals due to jagged signal vector. Thus, a band-pass filter with cut-

off frequencies of 70 Hz and 100 kHz was applied to each signal sample for alleviating negative effects of the noises involved in the sound signals. Fig. 4 shows an example chestnut acoustic signal before and after filtering.
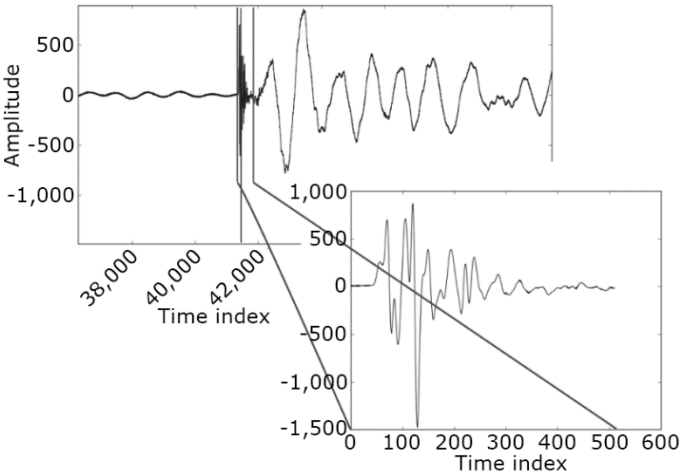


**Figure 3.** Typical acoustic signal of chestnut.
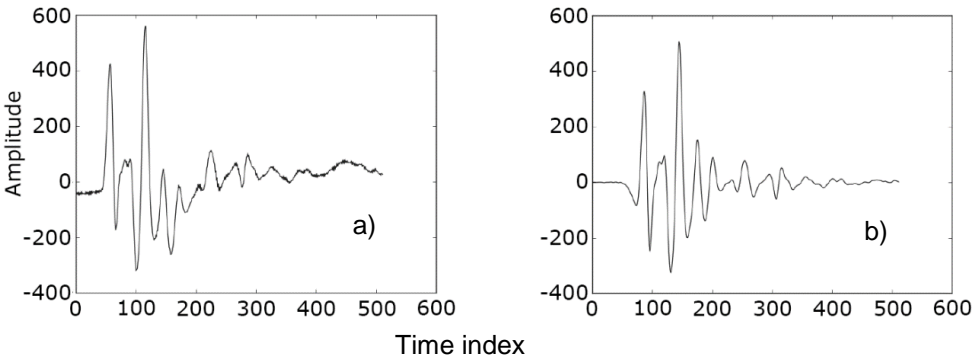


**Figure 4.** Signal vectors of chestnut sound signal before (a) and after (b) filtering.

### Feature extraction and reduction

After obtaining impact signal samples, signal features were calculated over those signals using LibXtract audio feature extraction library (Bullock, 2007). A feature vector including 36 scalar features was extracted as given in Table 1. It is beyond the scope of this paper to give all the mathematical background related with the features computed. So, the equations of those features were not included in the text due to space limitations and more details can be found in (Bullock, 2007).

In pattern classification problems, it is important to use only the features that have a discriminating power over the input samples. An optimum feature model can be defined as a subset of relevant features. Recursive feature elimination (RFE) process, which is based on feature ranking, by Guyon & Elisseeff (2003) was followed in this

work to determine the relevant features for chestnut classification. For performing RFE, a complete feature set is taken into consideration at first, and features are included as smaller sets of features recursively. A support vector machine is used as a central classifier. The SVM is trained on the initial set of features and weights are assigned to each one of them. The features are ranked based on their predictive significance at each iteration and the least significant variable is removed from the feature set. The elimination procedure is recursively reiterated on the reduced set until the desired number of features to select is reached (Pedregosa et al., 2011; Ataş et al., 2012). Desired number of features is a given parameter of the RFE and different feature numbers are also tried to reach the highest classification performance. Finally, this process yields a subset of the features used to identify worm-damaged chestnut samples.

**Table 1.** Features extracted from chestnut acoustic signals

| Features | | |
|---|---|---|
| Mean | Irregularity-k | Tonality |
| Variance | Irregularity-j | Noisiness |
| Standard deviation | Tristimulus-1 | Root mean square of amplitude |
| Average deviation | Tristimulus-2 | Spectral inharmonicity |
| Skewness | Tristimulus-3 | Spectral crest |
| Kurtosis | Smoothness | Odd to even ratio |
| Spectral mean | Spectral spread | Spectral slope |
| Spectral variance | Zero crossing rate | Lowest value |
| Spectral standard deviation | Rolloff | Highest value |
| Spectral skewness | Loudness | Sum of values |
| Spectral kurtosis | Flatness | Pitch of harmonic product spectrum |
| Spectral centroid | LOG spectral flatness | Fundamental frequency |

### Constituting an identification model using SVM

After calculating features and obtaining a relevant feature set, a classification model was needed to identify chestnut signals. A SVM model was utilized to achieve this. The SVM is a maximal margin classifier. Contrary to most of the machine learning approaches SVMs do not model probability distribution of the training vectors, instead they try to separate different classes by directly searching for adequate boundaries between them (Keuchel et al., 2003). To be able to succeed this SVM fits hyper-planes in the feature space between the classes. In this work, SVM was constructed using the training set containing positive and negative classes for classifying chestnut samples. To propose an effective classifier for identification of worm-damaged chestnuts, the parameters of SVM shown in Table 2 were tuned in this study.

**Table 2.** Tuned parameters of the SVM used in this study

| Parameter | Possible inputs |
|---|---|
| Regularization parameter | 1; 10; 100; 1,000 |
| Kernel function type | Linear, Polynomial, Radial basis |
| Kernel coefficient (for polynomial and radial basis) | 0.001; 0.0001 |
| Degree of the polynomial kernel function (for only polynomial kernel) | 1; 2; 3 |

## RESULTS AND DISCUSSION

In this work, optimum sound acquisition conditions were established as explained in the previous section. Sound acquisition experiments were performed under the same conditions for all the chestnut samples. After pre-processing the chestnut impact signals and composing relevant feature sets, cross-validated experiments were conducted with chestnut acoustic data. In creating classification models, it was desired to find an optimum model having a high generalization ability to avoid overfitting. Cross-validation routines were usually applied when performing training and testing machine learning models. In the experiments, K-fold cross validation procedure was incorporated with grid-search to determine an overfitting-safe identification system. Thus, the signal data was first split into two equal subsets; a development (75% of data) and a dedicated validation (25% of data). Training of SVM was performed on the development set with 5-fold cross validation. The development set was then again split into 5 equal sized subsets randomly. Of the 5 subsets, a single subset was assigned as the test data for testing the model, and the remaining 4 subsets were used as training data. The cross-validation process was then repeated 5 times using each of the 5 subsets once as the test data. By using grid-search with the cross-validation, this process was repeated for each combination of the tuned parameters for SVM to minimize the error and to maximize the score parameter of classification accuracy. After this training process, the model having the highest score was evaluated on the dedicated validation set which included totally unseen chestnut signal samples by the trained model.

Parameters of the SVM were tuned during the experiments using development dataset. To determine the performance of the identification experiments, performance metrics of 'precision' and 'recall', as defined in Eq. 1, were computed over confusion matrix resulted from the experiments on the dedicated validation dataset.

$$precision = \frac{tp}{tp + fp} \quad recall = \frac{tp}{tp + fn} \qquad (1)$$

where $tp$, $fp$, and $fn$ represent 'true positives', 'false positives', and 'false negatives', respectively.

The recall value was accepted as an indicator in concluding which model parameters were more successful in this study. To determine the optimum number of the features, identification experiments with RFE were conducted using desired feature numbers from 5 to 36 (all features) with the increment value of 5. Table 3 shows performance scores of the experiments.

**Table 3.** Identification performances of SVM on the dedicated validation data

| Performance scores | | | | | | | |
|---|---|---|---|---|---|---|---|
| N. of features | 5 | 10 | 15 | 20 | 25 | 30 | 36 |
| Precision | 0.75 | 0.76 | 0.76 | 0.77 | 0.77 | 0.77 | 0.77 |
| Recall | **0.71** | 0.70 | 0.69 | 0.68 | 0.69 | 0.68 | 0.68 |

Having the best identification result using only five features in the experiments was quite promising. These 5 features were 'variance', 'average deviation', 'irregularity-k', 'root mean square of amplitude' and 'highest value'. On the other hand, it was found that scores were close to each other for different number of the features. This was a good

finding because a real world application requires less processing time with lower number of the features. Grid-search results showed that the best SVM model parameters were found with linear kernel and a regularization parameter of 10. The cross-validated accuracy score for the development set during k-fold experiments was 0.88 (± 0.008).

A confusion matrix is given in Table 4 to reveal the relations between different classes and to show how errors are distributed between the negative and the positive classes. In Table 4, identification results are also shown for a total of 226 test samples at class level. According to these results, 86 healthy and 74 worm-damaged chestnuts were successfully classified by the proposed system. Within 138 samples of healthy chestnuts, 86 samples were identified correctly while 52 samples were incorrectly identified as worm-damaged. Of 88 worm-damaged samples, 74 samples were successfully identified by the system while 14 worm-damaged samples were misidentified as healthy. Therefore, class-level accuracies for healthy and worm damaged samples were found to be 62.32% and 84.01%, respectively.

**Table 4.** The confusion matrix of worm-damaged chestnut identification on the dedicated validation data for the best SVM model

|  |  | Predicted by the identification system | | |
| --- | --- | --- | --- | --- |
|  |  | Healthy chestnuts | Worm-damaged chestnuts | Recall in class level (%) |
| Ground-truth | Healthy chestnuts | 86 | 52 | 62.32 |
|  | Worm-damaged chestnuts | 14 | 74 | 84.01 |

In this study, worm-damaged chestnuts could be identified with an accuracy rate of 71% with lower number of the features (only 5 features). This study was the first effort to identify worm-damaged chestnuts using a IA based approach. Alongside of this modest identification score, it should be noted here that chestnuts do not have a hard shell compared to other nuts studied in the literature such as pistachios and hazelnuts. It was concluded that relatively softer shell of chestnut was a challenge for an IA based identification system. Still, the results obtained in this study showed that identification of worm-damaged could be achieved using IA based methods. However, more work is needed to achieve higher identification accuracies.

## CONCLUSION

Identification of chestnuts with worm damage was achieved with a promising classification success (71%) using impact acoustics, sound signal processing techniques and feature extraction and classification algorithms. Considering the difficulty in the nature of recognizing a worm defect in a chestnut covered by a perfectly healthy looking shell, these results should encourage further studies on the subject to understand chestnut impact and sound interactions and also to improve sound acquisition systems and finally the classification rates further.

# REFERENCES

Amoodeh, M.T., Khoshtaghaza, M.H. & Minaei, S. 2006. Acoustic on-line grain moisture meter. *Computers and Electronics in Agriculture* **52**, 71–78.

Ataş, M., Yardimci, Y. & Temizel, A. 2012. A new approach to aflatoxin detection in chili pepper by machine vision. *Computers and electronics in agriculture* **87**, 129–141.

Buerano, J., Zalameda, J. & Ruiz, R.S. 2012. Microphone system optimization for free fall impact acoustic method in detection of rice kernel damage. *Computers and Electronics in Agriculture* **85**, 140–148.

Bullock, J. 2007. Libxtract: A lightweight library for audio feature extraction. In: *11th International Society for Music Information Retrieval Conference.* ISMIR 2010, Utrecht.

Çetin, A.E., Pearson, T.C. & Tewfik, A.H. 2004. Classification of closed and open shell pistachio nuts using voice recognition technology. Transactions of the ASAE **47**, 659–664.

FAO, 2011. Production, yield, harvested area values of chestnut. *http://faostat3.fao.org/faostat-gateway/go/to/download/Q/QC/E*. Accessed 9.8.2015.

Guyon, I. & Elisseeff, A. 2003. An introduction to variable and feature selection. *The Journal of Machine Learning Research* **3**, 1157–1182.

Gün, A., Aşkın, A. & Kankaya, A. 2006. Research on cultivating walnut and chestnut in Buldan. In: *Buldan Conference*, Buldan, pp. 847–854.

Kalkan, H. & Yardimci, Y. 2006. Classification of hazelnuts by impact acoustics. In: *16th signal processing society workshop* on *MLSP*, IEEE, Maynooth, pp. 325–330.

Kalkan, H., Ince, N.F., Tewfik, A.H., Yardimci, Y. & Pearson, T. 2008. Classification of hazelnut kernels by using impact acoustic time-frequency patterns. *Journal on Advances in Signal Processing* **45**, 1–11.

Keuchel, J., Naumann, S., Heiler, M. & Siegmund, A. 2003. Automatic land cover analysis for Tenerife by supervised classification using remotely sensed data. *Remote sensing of environment* **86**, 530–541.

Khalesi, S., Mahmoudi, A., Hosainpour, A. & Alipour, A. 2012. Detection of Walnut Varieties Using Impact Acoustics and Artificial Neural Networks (ANNs). *Modern Applied Science* **6**, 43–49.

Oliphant, T.E. 2007. Python for scientific computing. *Computing in Science and Engineering* **9**, 10–20.

Omid, M., Mahmoudi, A. & Omid, M.H. 2009. An intelligent system for sorting pistachio nut varieties. *Expert Systems with Applications* **36**, 11528–11535.

Pearson, T.C. 2001. Detection of pistachio nuts with closed shells using impact acoustics. *Applied Engineering in Agriculture* **17**, 249–253.

Pedregosa, F., Varoquaux, G., Gramfort, A., Michel, V., Thirion, B., Grisel, O., Blondel, M., Prettenhofer, P., Weiss, R., Dubourg, V., Vanderplas, J., Passos, A, Cournapeau, D., Brucher, M., Perrot, M. & Duchesnay, É. 2011. Scikit-learn: Machine learning in python. *Journal of Machine Learning Research* **12**, 2825–2830.

# Research in farm management technologies using the expert method

A. Laurs[1*], Z. Markovics[2], J. Priekulis[1] and A. Aboltins[1]

[1]Latvia University of Agriculture, Faculty of Engineering, Institute of Agriculture Machinery, J. Čakstes bulv. 5, LV-3001 Jelgava, Latvia
[2]Riga Technical University, Faculty of Computer Science and Information Technology, Institute of Computer Control, Automation and Computer Engineering, Daugavgrīvas iela 2, LV-1048 Rīga, Latvia
*Correspondence: armins.laurs@promedia.lv

**Abstract.** The task of the research was to state the most popular peculiarities of farm management technologies depending on the size of the herd in order to use the research results in calculations of greenhouse gas emissions. The research was performed applying the expert methods based on the farm management technologies as they are closely related to the size of the herd and the kind of the obtained farm manure. The expert method can be applied for research in farm management technologies of different animal species and groups, but in the present article only milk cow management technologies will be discussed as they produce the biggest amount of greenhouse gas emissions. The practice shows that on small farms the cows are tied, on medium farms – either tied or loose, but on large farms – only loose. On the farms where the cows are tied solid litter manure is obtained, but where the cows are handled loose – liquid manure is obtained. Besides, on the farms with a small herd the cows are pastured in summer and in this period manure spread in the pastures is produced. Stating the maximal size of the herd that is pastured and the length of the pasture period as well as the marginal size at which the transition from tied to loose handling takes place and additionally using the statistical data on the total number of cows in the country and the proportion of animals according to the size of the herd, it is possible to state from which proportion of milk cows solid litter is produced and from which – liquid manure. Therefore, the experts were given the task to name the marginal values of the above mentioned technology parameters based on the value intervals stated in advance. Thereupon that the experts had to state only one chosen value, it was not possible to apply the traditional expert evaluation methods and this method had to be adapted in accordance to the existing situation. The research results showed that in Latvia the critical size of the milk cow herd at which the transition from tied to loose handling takes place is 85 cows, the herds that are not larger than 90 cows are pastured but the pasture period lasts in average for 165 days.

**Key words:** farm management technologies, size of the herd, farm manure management, the expert method.

## INTRODUCTION

Implementing the European economic zone program 'National Climate Politics' project 'Development of a Methodology for Calculating GHG Emissions in the Agricultural Sector and Modelling Tool for Data Analyses, Integrating Climate

Change'– the task was set to state what kind of farm manure in Latvia is produced from the most popular farm animal and poultry species and their groups as well as to state the proportion of this manure. It was necessary for using the research results in calculations of greenhouse gas emissions caused by farm manure management.

Considering the data of the Guidelines for National Greenhouse Gas Inventories (2006 IPCC) and statistics as well as summarising and analysing the present experience of farm management specialists the most popular species and groups of animals used in agriculture and poultry as well as the kinds of farm manure produced by each of these groups were stated in Latvia. The obtained results are summarized in Table 1.

**Table 1.** Kinds of manure produced by the most popular farm animals in Latvia

| Animal and poultry groups | Kinds of manure | | | | | |
| --- | --- | --- | --- | --- | --- | --- |
| | Pasture manure | Solid manure | Liquid manure | Deep bedding | Poultry manure with litter | Poultry and fur animal manure without litter |
| Milk cows | x | x | x | | | |
| Milk cow calves and young stock | x | x | | | | |
| Beef cattle, their calves and young stock | x | x | | | | |
| Pigs | | x | x | | | |
| Sheep | x | | | x | | |
| Goats | x | | | x | | |
| Horses | x | x | | | | |
| Laying hens | x | | | | x | x |
| Broilers | | | | | x | |
| Geese | x | | | | x | |
| Ducks | x | | | | x | |
| Turkeys | x | | | | x | |
| Rabbits | | x | | | | |
| Fur animals | | | | | | x |
| Deer | x | | | | | |

Note: technology of farm manure used in the table is coordinated with 2006 IPCC.

In order to calculate the manure proportion obtained from the corresponding farm animals a new methodology was developed (Priekulis et al., 2015) based on using of the statistical data and the farm animal zootechnical and technological parameters. Some of the zootechnical and technological parameters necessary for the calculations are given in the scientific literature and the Regulations of the Cabinet of Ministers No. 834.

But additionally it is necessary to state the marginal sizes of the herd of every group of animals at which the transition from one kind of handling to another takes place and also the length of the animal pasture (airing) period. For this reason it was not possible to trace all farms (population) that are engaged in poultry and animal breeding in Latvia as in that case information on all the working force and financial resources would be necessary. Also, it was not possible to form representative and large enough sample farms as the farms engaged in poultry and animal breeding are unevenly distributed along the whole territory of Latvia. Nevertheless, this problem can be solved applying

the expert observation method and orientating on the research in animal and poultry breeding technologies depending on the size of the herd.

In order to show the possibilities of application of the expert observation method clearly as an example only one of the farm animal groups mentioned in Table 1 will be discussed, i.e., milk cows as they produce the largest amount of the greenhouse gas emissions (National Inventory Submissions, 2014).

## MATERIALS AND METHODS

According to the scientific literature (Priekulis, 2000) and the practice it can be concluded that in Latvia on small farms (up to 50 milk cows) the animals are handled tied, on medium farms (50–200 cows) – tied or loose, but on large farms (more than 200 cows) – only loose. On farms with tied handling litter is used and solid manure is produced, but on loose handling farms litter is not used and liquid manure is produced. Besides, in summer cows from small and medium farms are usually pastured and therefore a part of manure is not collected as it stays in the pastures.

In turn, calves and young stock are usually handled loose either in individual or group enclosures (depending on the age). There litter is used that is periodically stocked up and the produced solid manure is taken to the manure storage if necessary. If milk cows are pastured, the young stock is pastured also. Therefore, it can be concluded that the obtained kind of manure is related to the kind of animal handling and the size of the herd on the farm.

One of the aims of the present research was to state the marginal value of the size of the herd at which the transition from one kind of handling to another takes place. Besides, the question about the maximal size of the herd that is pastured and the length of pasturing has also to be explained. Therefore, the experts were asked the following questions.

- What is the size of the herd (marginal value) at which the transition from tied to loose handling of cows takes place?
- What is the maximal size of the cow herd at which the cows are pastured (if there are pastures)?
- What is the average length of the pasturing period (number of days)?

The group of experts necessary for the research was completed according to the voluntary method including in it advisers from the Latvian Rural Advisory and Training Center, Latvian Milk Producer Association specialists as well as experienced animal breeding specialists and farm managers. The total number of experts was 18 people. It corresponds to the recommendations given in the scientific literature (Markovics, 2009) where 10–20 experts are recommended.

In order to get the individual opinion of the experts special enquiries or telephone enquiries were used. The task was to show the value interval in which, according to the opinion of the experts, the authentic value of the object lies.

Before the basic enquiry the pilot enquiry was performed. Its aim was to make the enquiry questions and the intervals of the researched values more precise and to state the understanding of the experts about the stated task.

Processing of the data obtained in the experiment was done in the following sequence:
- summarising of the ranging of the obtained results;
- selection of the data;
- determination of the extent of the expert agreement;
- obtaining of quantitative values from the ranged rows.

The enquiry results were ranged and summarised in a table the form of which is given in Table 2.

**Table 2.** Form of enquiry result ranging

| Experts | Objects (n) | | | | | |
|---------|-------------|------|-----|----------|-----|----------|
| (m)     | $x_1$       | $x_2$ | ... | $x_i$    | ... | $x_n$    |
| $m_1$   | $r_1$       | $r_{12}$ |  | $r_{1i}$ |     | $r_{1n}$ |
| $m_2$   |             |      |     |          |     |          |
| ...     |             |      |     |          |     |          |
| $m_j$   |             |      |     | $r_{ji}$ |     |          |
| ...     |             |      |     |          |     |          |
| $m_m$   | $r_{m1}$    | $r_{m2}$ |  | $r_{mi}$ |     | $r_{mn}$ |
| $R_i$   |             |      |     |          |     |          |

Note: in the table with *n* the objects or their values are marked, with *m* – experts, with *r* – object ranging and with *R* – the resulting value of every object.

Still, it should be mentioned that all present expert evaluation methods are meant for the tasks to evaluate many objects, respectively, to state their ranged row. Problems occur if the team of experts has to evaluate only one value or take one decision as it is in the present research. In such case the research methods need to be adapted which in this case manifests as follows.

Every expert marks only the square of the object which he/she prefers. After that the ranged row is formed using the following approach.

- If the expert chooses gradation from one or the other end of the given row, this gradation is given the first range, the next gradation will be the second range, still the next – the third range etc
- If the expert chooses some gradation from the middle of the given row, the ranging can be as follows:
  – the chosen gradation gets the range 1;
  – the proximal gradations (to the left and right from the chosen) have equal range, but theoretically they occupy the 2nd and the 3rd range in the result of what every reduced range is calculated

$$r_{red} = \frac{2+3}{2} = 2.5 \, ;$$

  – further gradations to the left or right occupy the fourth and fifth range but the reduced range between the both is 3.5 etc.

If the expert chooses gradation from the middle of the row, the version is possible that the nearest to the chosen gradation will get the ranges 2; 3 etc. only in one direction,

for instance, to the right from the first range. Besides, gradations to the left will be ranged in the furthest end of the ranged row.

With such technique of adaptation all expert ranged rows for every square of the table can be obtained and it is possible to process the results mathematically by any of the traditional methods described in literature (Voronin, 1974; Hand et al, 2001; Dunham, 2003; Tan & Steinbach, 2006; Markovics, 2009).

After ranging of the results the data were selected. In practice the situations are possible when in the data array there is an 'extraneous' number present that does not fit in the total row of numbers. Therefore, the so called data selection is necessary that is done in all columns by turn.

The expert methods have a restriction that the degree of the expert agreement and the information obtained in the enquiry can be used in further calculations only in case if the degree of agreement is bigger than the threshold value. Therefore, big choices of techniques have been developed how to evaluate the degree of expert agreement, but the method of Kendall (Markovics, 2009) that is using the concordance coefficient has become most popular.

The concordance coefficient is calculated according to formula (1) or (2). If the expert evaluation ranges do not agree, formula (1) should be used.

$$W = \frac{\sum_{i=1}^{n} \left\{ \sum_{j=1}^{m} r_{ji} - \frac{1}{2} m(n+1) \right\}^2}{\frac{1}{12} m^2 (n^3 - n)}, \tag{1}$$

where m – number of experts; n – number of objects; r – object range; i – object ordinal number; j – expert ordinal number.

If the expert evaluation ranges coincide, the concordance coefficient is calculated according to formula (2).

$$W = \frac{\sum_{i=1}^{n} \left\{ \sum_{j=1}^{m} r_{ji} - \frac{1}{2} m(n+1) \right\}^2}{\frac{1}{12} m^2 (n^3 - n) - m \sum_{j} T_j} \tag{2}$$

In formula (2) the value $T_j$ is calculated according to formula (3)

$$T_j = \frac{1}{12} \sum_{tj} \left( t_j^3 - t_j \right), \tag{3}$$

where $t_j$ – number of repeating ranges in *j-th* expert ranging.

The range of the concordance coefficient is from 0 to 1. If *W = 0*, there is no agreement among the ranging, if *W = 1*, there is complete agreement. To prove the statistic validity of the obtained result, the statistic hypothesis testing method with the Pearson coefficient $\chi^2$ is applied. It is calculated according to formula (4):

$$\chi^2 apr = m(n\text{-}1)W \tag{4}$$

From $\chi^2$ tables $\chi^2_{tab}$ is found according to the freedom degree *v = n -1*.

If $\chi^2_{tab} < \chi^2_{apr}$, then the hypothesis on expert evaluation agreement with the concordance coefficient is assumed with probability at least 0.95. It should be mentioned that by the Pearson criterion only the statistic validity of the concordance coefficient is tested. But this testing does not give information on whether the value of the concordance coefficient is high enough to judge about the agreement among the experts. Therefore, the question is open – what value of the coefficient W can be considered to be sufficient. It cannot be stated theoretically, but in practice it is assumed that the concordance coefficient is big enough if *W > 0.5* (Markovics, 2009).

If the degree of agreement is larger than the threshold value, it is possible to obtain the quantitative values from the ranged rows. It is most easy to calculate the average arithmetic values for every column, but in case of a small number of data (such are all the data given by the experts) the average arithmetic value can give a big mistake. Therefore, a method, known in literature as Voronin method, is applied (Voronin, 1974). It is based on calculation of iterative mathematical expectation for small number cases. Mathematical expectation is calculated according to formula (5).

$$
y_{ik} = \frac{\sum_{j=1}^{m} y_{ji} \exp\left[ -\frac{\left(y_{ik-1} - y_{ji}\right)^2 (m-1)}{2\sum_{j=1}^{m}\left(y_{ik-1} - y_{ji}\right)^2} \right]}{\sum_{j=1}^{m} \exp\left[ -\frac{\left(y_{ik-1} - y_{ji}\right)^2 (m-1)}{2\sum_{j=1}^{m}\left(y_{ik-1} - y_{ji}\right)^2} \right]}
\tag{5}
$$

where $y_{ik}$ – mathematical expectation in *k-th* step; $y_{ik-1}$ – mathematical expectation in the previous k-1 step; in the first step instead of $y_{ik-1}$ the average arithmetic is put; $y_{ji}$ – *i-th* object evaluation according to *j-th* expert opinion; m – number of experts.

To perform calculations using formula (5) special computer software 'MatLab' was developed in the programming media.

Considering that in the present research the experts have not to choose quantitative values but the intervals of these values, the task has to be adapted to the formal method. The values $y_{ij}$ are obtained taking the average values from the intervals that every expert has evaluated with the first range. In the result a row of numbers is formed that is obtained replacing the first ranges in the table by the average values of the corresponding interval. Therefore, only one number is obtained – mathematical expectation of the searched marginal value that can be afterwards used for explanation of the researched problems.

## RESULTS AND DISCUSSION

Ranging of the expert answers and the results of the expert agreement degree calculations related to the transition from tied handling of cows to loose handling are summarised in Table 3.

**Table 3.** Ranging of the expert answers and the results of the expert agreement degree calculations researching the question about the size of the herd at which the transition from tied handling of cows to loose handling takes place

| Expert serial No. | Average size of herd (number of cows) | | | | |
|---|---|---|---|---|---|
| | 50–60 | 61–70 | 71–80 | 81–90 | 91–100 |
| 1. | 3.5 | 2 | **1** | 3.5 | 5 |
| 2. | 3.5 | 2 | **1** | 3.5 | 5 |
| 3. | 4.5 | 3 | **1** | 2 | 4.5 |
| 4. | 4.5 | 3 | **1** | 2 | 4.5 |
| 5. | 4.5 | 3 | **1** | 2 | 4.5 |
| 6. | 4.5 | 3 | **1** | 2 | 4.5 |
| 7. | 5 | 4 | 3 | **1** | 2 |
| 8. | 5 | 4 | 3 | **1** | 2 |
| 9. | 5 | 4 | 3 | **1** | 2 |
| 10. | 5 | 3.5 | 2 | **1** | 3.5 |
| 11. | 5 | 3.5 | 2 | **1** | 3.5 |
| 12. | 5 | 4 | 3 | **1** | 2 |
| 13. | 5 | 4 | 3 | **1** | 2 |
| 14. | 5 | 4 | 3 | **1** | 2 |
| W | 0.58 | | | | |
| Concordance coefficient W statistic validity | >0.99 | | | | |

Table 3 shows that in this case the concordance coefficient $W = 0.58$, i.e., its value is higher than the sufficient value (W = 0.5) and also its statistic validity is high enough. So, the expert agreement degree is satisfactory and the value of the searched parameter can be calculated. The calculation results are shown in Table 4.

**Table 4.** Determination of the herd marginal size at which the transition from tied handling of cows to loose handling takes place

| Expert serial No. | 1 | 2 | 3 | 4 | 5 | 6 | 7 | 8 | 9 | 10 | 11 | 12 | 13 | 14 |
|---|---|---|---|---|---|---|---|---|---|---|---|---|---|---|
| Herd size interval, number of cows | 75 | 75 | 75 | 75 | 75 | 75 | 85 | 85 | 85 | 85 | 85 | 85 | 85 | 85 |
| Herd size critical size, number of cows | 85 | | | | | | | | | | | | | |

Consequently, from Table 4 it can be concluded that the critical size of the herd at which the transition from tied handling of cows to loose handling takes place is 85 cows.

In turn, Table 5 shows the research results on the maximal size of the herd which is pastured

Table 5 shows that also in this case the degree of expert agreement is satisfactory (W > 0.5), so the searched value can be calculated. In turn, the calculation results show that the maximal size of the herd that is pastured is 90 cows.

Table 6 summarises the expert enquiry results on the length of the pasture period of cows.

**Table 5.** Ranging of the expert answers, the results of the expert agreement degree and mathematical expectation calculations determining the maximal size of the herd that is pastured

| Expert serial No. | Size of herd, number of cows | | | | |
|---|---|---|---|---|---|
| | < 50 | 51–80 | 81–100 | 101–120 | 121–150 |
| 1. | 5 | **1** | 2 | 3 | 4 |
| 2. | 5 | **1** | 2 | 3 | 4 |
| 3. | 5 | **1** | 2 | 3 | 4 |
| 4. | 5 | **1** | 2 | 3 | 4 |
| 5. | 5 | **1** | 2 | 3 | 4 |
| 6. | 5 | 1.5 | **1** | 1.5 | 4 |
| 7. | 5 | 1.5 | **1** | 1.5 | 4 |
| 8. | 5 | 1.5 | **1** | 1.5 | 4 |
| 9. | 5 | 4 | 2 | **1** | 3 |
| 10. | 5 | 4 | 2 | **1** | 3 |
| 11. | 5 | 4 | 2 | **1** | 3 |
| 12. | 5 | 4 | 2 | **1** | 3 |
| 13. | 5 | 4 | 2 | **1** | 3 |
| 14. | 5 | 4 | 2 | **1** | 3 |
| **W** | 0.76 | | | | |
| Concordance coefficient W statistic validity | >0.99 | | | | |
| Maximal size of herd, number of cows | 90 | | | | |

**Table 6.** Ranging of the expert answers, the results of the expert agreement degree and mathematical expectation calculations researching in the length of the cow pasture period

| Expert serial No. | Length of the pasture period, number of days | | | | |
|---|---|---|---|---|---|
| | 145–150 | 151–160 | 161–170 | 171–180 | 181–185 |
| 1. | 4 | **1** | 2 | 3 | 5 |
| 2. | 4 | **1** | 2 | 3 | 5 |
| 3. | 4 | **1** | 2 | 3 | 5 |
| 4. | 4 | **1** | 2 | 3 | 5 |
| 5. | 4 | **1** | 2 | 3 | 5 |
| 6. | 4 | **1** | 2 | 3 | 5 |
| 7. | 4 | **1** | 2 | 3 | 5 |
| 8. | 4 | **1** | 2 | 3 | 5 |
| 9. | 4 | **1** | 2 | 3 | 5 |
| 10. | 4.5 | 1.5 | **1** | 1.5 | 4.5 |
| 11. | 5 | 3 | 2 | **1** | 4 |
| 12. | 5 | 3 | 2 | **1** | 4 |
| 13. | 5 | 3 | 2 | **1** | 4 |
| 14. | 5 | 3 | 2 | **1** | 4 |
| 15. | 5 | 3 | 2 | **1** | 4 |
| 16. | 5 | 3 | 2 | **1** | 4 |
| W | 0.78 | | | | |
| Concordance coefficient W statistic validity | >0.99 | | | | |
| Length of the pasture period, number of days | 165 | | | | |

Also for the answers summarised in Table 6 the degree of expert agreement is satisfactory, but the calculation results show that the average length of the pasture period is 165 days.

Applying the above described expert method similar research was performed also for the other farm animal groups included in Table 1 stating the length of the pasture (airing) period as well as performing research in the critical sizes of pig and laying hen herds at which transition from producing of one kind of manure to another takes place (for pigs – from solid manure to liquid manure, for laying hens – from solid manure to manure without litter).

These investigations show that application of the expert method opens wide possibilities for research in animal breeding technologies in the result of which new quantitative values are to be obtained. In the present case the change of farm animal handling depending on the size of the herd was taken as the basic principle of the research. But this method can be applied also in the research of another character where it is not possible to trace all farms (population) or form representative and quantitatively large enough sample groups.

Nevertheless, application of the expert method in the research in farm management systems can cause non-standard situations that are not described in scientific literature. For instance, in the present research the problem of determination of the expert agreement degree. It is based on comparison of ranged rows, but in the present research the experts chose only one value. Therefore, it was necessary to formalize the obtained results in accordance to the calculation methods and to adapt the initial data to calculate the mathematical expectation applying the Voronin method.

## CONCLUSIONS

In order to state the peculiarities of farm animal handling technologies for the most popular animal species and groups in Latvia it is not possible to trace all farms that are engaged in poultry or animal breeding. Also, it is not possible to form representative sample farms as the farms of the corresponding animals are unevenly scattered along the whole territory of Latvia. Still, this problem can be solved applying the expert evaluation method and basing on the changes of farm animal and poultry handling technologies depending on the size of the herd.

Applying the expert evaluation method it has been stated that the size of the milk cow herd at which the transition from tied handling to loose handling takes place as well as from producing of solid manure to liquid manure is 85 cows. Besides, the animals are pastured and manure left in pastures is obtained if the size of the herd does not exceed 90 cows, but the average length of the pasturing period is 165 days.

As the experts participating in the research had to choose only one interval of values that best suits the given question, it was not possible to apply the traditional expert evaluation methods. Therefore, it was necessary to adapt the ranging determining the expert agreement degree as well as formalising the number rows calculating the mathematical expectations.

# REFERENCES

Dunham, M.H. 2003. *Data Mining: Introductory and Advanced topics.* Pearson Education, New Jersy, 314 pp.

Hand, D.J., Heikki M., Smyth, P. 2001. *Principles of Data Mining,* MIT Press, Cambridge, 425 pp.

IPCC 2006 Guidelines for National Greenhouse Gas Inventories. Chapter 10: Emissions from Livestock and Manure Management. 2006.

Markovičs, Z. 2009. Expert Evaluation Methods. RTU, Rīga, 111 pp. (in Latvian).

National inventory Submissions. 2014. Available at http://unfccc.int/national_reports/annex_i_ghg_inventories/national_inventories_submissions/items/8108.php

Priekulis, J., Aboltins, A., Laurs, A., Melece, L. 2015. Research in manure management in Latvia. In*: Engineering for Rural Development. The 14th International Scientific Conference*, LUA, Jelgava, Latvia, pp. 88–93.

Priekulis, J. 2000. *Efficient Technologies and Mechanization in Dairy Farming.* LUA, Jelgava, Latvia.148 pp. (in Latvian).

Regulations of the Cabinet of Ministers No. 834. Regulations of water and soil protection from pollution with nitrate caused by agricultural activities. In force from 23.12.2014. (in Latvian).

Tan, P.N., Steinbach, M. 2006. *Introduction to Data Mining.* Pearson Education, Boston, 769 pp.

Voronin, A.N. 1974. *Method of Expert Evaluation Data Array Processing. Ergatic Management Systems*. Naukova dumka, Kiev, 253 pp. (in Russian).

# Natural vibrations of stepped arches with cracks

J. Lellep[1] and A. Liyvapuu[1,2,*]

[1]University of Tartu, Institute of Mathematics and Statistics, J. Liivi 2, EE50409 Tartu, Estonia
[2]Estonian University of Life Sciences, Institute of Technology, Department of Agricultural and Production Engineering, Fr.R. Kreutzwaldi 56, EE51014 Tartu, Estonia
[*]Correspondence: liyvapuu@ut.ee

**Abstract.** Natural vibrations of elastic circular arches are studied. The arches are assumed to be of constant width and piece wise constant height. It is assumed that at the re-entrant corners of steps stable surface cracks are located. The aim of the paper is to assess the sensitivity of the eigenfrequencies on the geometrical and physical parameters of the arch including the length and location of each crack.

**Key words:** elasticity, arch, natural vibrations, crack, eigenfrequency.

## INTRODUCTION

The problems of vibration and stability of beams, plates and shells have a great importance in the civil and engineering. Vibration of curved beams is studied by several researches (see Vinson & Sierakowski, 2002; Qatu, 2004; Reddy, 2004). The natural and forced vibrations of beams weakened with the crack-like defects have been investigated by Rizos at al. (1990), Dimarogonas (1996), Nandwana & Maiti (1997), Chondros et al. (1998), Kisa & Brandon (2000) and others. Lellep & Kägo (2011; 2013) investigated the influence of cracks on eigenfrequencies of elastic stretched strips and plates.

In the previous papers by Lellep & Liyvapuu (2015a; 2015b) vibrations of elastic arches made of homogeneous and laminated materials were studied.

Due to the practical needs the investigations of the free and forced vibrations of beams, arches, plates and shells are carried out by many investigators (see Qatu 2004; Soedel 2004). During last years new approach to the free vibration analysis are developed in the papers by Eroglu (2015), Wu & Chiang (2004) for the case of in-plane vibrations. While Ishaguddin et al. (2016) and Kawakami et al. (1995) accounted for the out-of-plane vibrations in their studies, Sadeghpour et al. (2016) considered the effect of debonding during the process of natural vibrations.

In the paper by Wu & Chiang (2004) the effect of both, the shear deformation and rotatory inertia are included in the analysis using finite arch elements.

Although usually the in-plane and out-of-plane vibrations of beams and bars are tackled separately the approach by Wu and Chiang admits to consider the both versions from the common point of view.

In the present paper we are interested in the evaluation of the influence of cracks on the natural frequencies of arches. That is why the simplest theory of vibration of beams is employed.

Here results of the previous study Lellep & Liyvapuu (2015b) are extended to the case of a stepped arch weakened with non-penetrated surface cracks. The cracks are assumed to be stable surface cracks. The problems of propagation of cracks are outside the scope of the present paper.

## MATERIALS AND METHODS

### Problem formulation

Let us study the free vibrations of a circular arch of radius $R$. It is assumed that the arch has rectangular cross section with dimensions $b$ (the width) and the total height $H$. The total height is assumed to be piece wise constant, e.g.

$$h = h_j, \qquad \varphi \in (\alpha_j, \alpha_{j+1}) \tag{1}$$

for $j = 0, \dots, n$.

In (1) $\varphi$ stands for the current angle (Fig. 1.) and $h_0, \dots, h_n$ and $\alpha_0, \dots, \alpha_n$ are given constants.
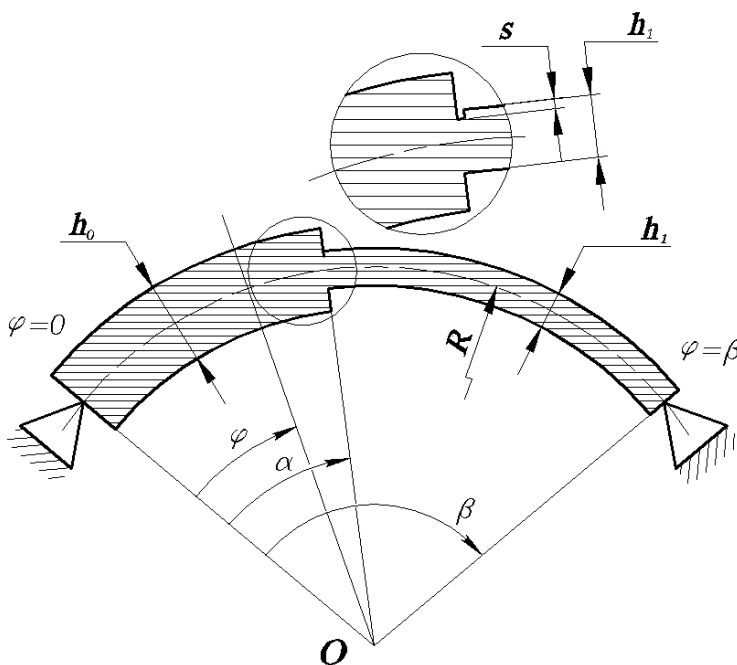


**Figure 1.** Simply supported stepped arch with a crack.

Here $\alpha_0 = 0$ and $\alpha_{n+1} = \beta$.
The arch is simply supported at $\varphi = 0$ and $\varphi = \beta$.

The arch is weakened with cracks located at the re-entrant corners of steps. It is assumed that the crack located at the position $\varphi = \alpha_j$ has the length $c_j$. Evidently, the eigenfrequencies of the arch depend on the geometry of the arch and on the geometry of the crack.

The aim of the paper is to determine the eigenfrequencies of the arch and to study the sensitivity of the eigenfrequencies on the geometrical and physical parameters of the arch.

### Basic equations and assumptions

Treating the equilibrium of an element of the vibrating arch one can conclude that (see Soedel 2004; Lellep & Liyvapuu 2015a; Lellep & Liyvapuu 2015b).

$$M'' + M - \bar\rho h_j R^2 \ddot W = 0 \tag{2}$$

for $\varphi \in (\alpha_j, \alpha_{j+1})$ $j = 0, \dots, n$. Here $M$ stands for the bending moment, $W$ is the transverse displacement (deflection) and $\bar\rho$ is the material density. In the case of a composite or laminated material the quantity $\bar\rho$ is the average of densities of the layers (see Reddy 2004; Qatu 2004).

Here and henceforth

$$M' \equiv \frac{\partial M}{\partial \varphi}, \quad \dot W \equiv \frac{\partial W}{\partial t}, \tag{3}$$

$t$ standing for time.

According to the Hook's law one has (see Lellep & Liyvapuu 2015a; Lellep & Liyvapuu 2015b)

$$M = D_j \varkappa \tag{4}$$

for $\varphi \in (\alpha_j, \alpha_{j+1})$ $j = 0, \dots, n$. Here

$$\varkappa = -\frac{1}{R^2}(W + W''). \tag{5}$$

Because we are interested in evaluation of the influence of cracks on the natural frequencies we need the simplest theory of vibration. That is why it is assumed herein that the axial extension $\varepsilon = 0$ and therefore, $U' = -W$.

Here $U$ stands for the axial displacement. Note that in the case of any homogeneous material

$$D_j = \frac{E h_j^3}{12(1 - v^2)}, \tag{6}$$

where $E$ is the Young modulus and $v$ – the Poisson ratio.

Assuming that both ends of the arch are simply supported one can present the boundary conditions as

$$W(0, t) = 0; \quad M(0, t) = 0 \tag{7}$$

and

$$W(\beta, t) = 0; \qquad M(\beta, t) = 0. \tag{8}$$

Substituting (4) and (5) in the equilibrium equation (2) leads to the equation

$$\frac{D_j}{R^2}(W^{IV} + 2W'' + W) + \bar{\rho} h_j R^2 \ddot{W} = 0 \tag{9}$$

for $\varphi \in (\alpha_j, \ \alpha_{j+1}) \ j = 0, \dots, n$.

The arch under consideration has stable surface cracks at $\varphi = \alpha_j$. It is well known that defects deteriorate the mechanical behaviour of structures. The influence of cracks on the natural vibrations of arches is modelled by the method suggested by Chondros at al. (1998) and Dimarogonas (1998). According to this method the slope of the deflection is considered as a discontinuous quantity at the cross sections with cracks. Let us denote

$$\theta_j = W'(\alpha_j + 0, t) - W'(\alpha_j - 0, t). \tag{10}$$

It was shown in Lellep & Kägo (2013) and Lellep & Liyvapuu (2015b) that on can take

$$\theta_j = p_j \varkappa(\alpha_j + 0, t), \tag{11}$$

where

$$p_j = \frac{6\pi h_j}{1 - v^2} f(s_j) \tag{12}$$

and

$$f(s_j) = 1.86 s_j^2 - 3.95 s_j^3 + 16.37 s_j^4 - 34.23 s_j^5 + 76.81 s_j^6 - \\ -126.93 s_j^7 + 172 s_j^8 - 143.97 s_j^9 + 66.56 s_j^{10}. \tag{13}$$

**Solution of governing equations**

The equation (9) is a linear fourth order equation with partial derivatives. Making use of the method of separation of variables (see Soedel 2004; Lellep & Liyvapuu 2015a; Lellep & Liyvapuu 2015b) one can look for the solution of (9) in the form

$$W(\varphi, t) = w(\varphi) \cdot \sin(\omega t). \tag{14}$$

In (14) the first term in the right hand side of the equality is assumed to be a function of the variable $\varphi$. Substituting (14) in (9) leads to the ordinary differential equation of the fourth order

$$\frac{D_j}{R^2}(w^{IV} + 2w'' + w) + \bar{\rho} h_j R^2 \omega^2 w = 0 \tag{15}$$

for $\varphi \in (\alpha_j, \ \alpha_{j+1}) \ j = 0, \dots, n$.

Evidently, the general solution of (15) can be presented as

$$w = C_{1j} \cosh(\mu_j \varphi) + C_{2j} \sinh(\mu_j \varphi) + C_{3j} \cos(\nu_j \varphi) + C_{4j} \sin(\nu_j \varphi) \quad (16)$$

where $C_{1j} - C_{4j}$ are arbitrary constants and

$$\mu_j = \sqrt{1 - \omega R^2 \sqrt{\frac{\bar{\rho} h_j}{D_j}}}, \qquad \nu_j = \sqrt{1 + \omega R^2 \sqrt{\frac{\bar{\rho} h_j}{D_j}}}. \qquad (17)$$

According to (7), (8) and (14) one can present the boundary conditions for $w(\varphi)$ as

$$w(0) = 0, \qquad w''(\beta) = 0 \qquad (18)$$

and

$$w(\beta) = 0, \qquad w''(\beta) = 0. \qquad (19)$$

The boundary conditions (18) with (16) furnish the relations

$$\begin{aligned} C_{10} + C_{30} &= 0, \\ \mu_0^2 C_{10} - \nu_0^2 C_{30} &= 0. \end{aligned} \qquad (20)$$

It immediately follows from (20) that

$$C_{10} = C_{30} = 0, \qquad (21)$$

provided $\mu_0^2 + \nu_0^2 \neq 0$.

The boundary requirements (19) lead to the equations

$$\begin{aligned} &C_{1n} \cosh(\mu_n \beta) + C_{2n} \sinh(\mu_n \beta) + C_{3n} \cos(\nu_n \beta) + C_{4n} \sin(\nu_n \beta) = 0, \\ &\mu_n^2 (C_{1n} \cosh(\mu_n \beta) + C_{2n} \sinh(\mu_n \beta)) - \nu_n^2 (C_{3n} \cos(\nu_n \beta) + \\ &+ C_{4n} \sin(\nu_n \beta)) = 0, \end{aligned} \qquad (22)$$

provided $\mu_n^2 + \nu_n^2 \neq 0$.

The particular solution of (15) must be constructed so that in each segment the solution is given by (16) and at the boundary the requirements (18), (19) are taken into account.

Moreover, at $\varphi = \alpha_j$ the quantities $W, M$ and $Q = M'$ must be continuous; the slope $W'$ must satisfy (10) — (13). Thus, $W$, $D(W'' + W)$ and $D(W''' + W')$ are continuous. Here

$$D(\alpha_j - 0) = D_j; \qquad D(\alpha_j + 0) = D_{j+1} \tag{23}$$

for each $j = 1, \dots, n$.

The continuity conditions can be presented as

$$C_{1j}\cosh(\mu_j\alpha_j) + C_{2j}\sinh(\mu_j\alpha_j) + C_{3j}\cos(\nu_j\alpha_j) + C_{4j}\sin(\nu_j\alpha_j)$$
$$= C_{1j+1}\cosh(\mu_{j+1}\alpha_j) + C_{2j+1}\sinh(\mu_{j+1}\alpha_j)$$
$$+ C_{3j+1}\cos(\nu_{j+1}\alpha_j) + C_{4j+1}\sin(\nu_{j+1}\alpha_j);$$

$$\mu_{j+1}\big(C_{1j+1}\sinh(\mu_{j+1}\alpha_j) + C_{2j+1}\cosh(\mu_{j+1}\alpha_j)\big)$$
$$+ \nu_{j+1}\big(-C_{3j+1}\sin(\nu_{j+1}\alpha_j) + C_{4j+1}\cos(\nu_{j+1}\alpha_j)\big) =$$
$$= \mu_j\big(C_{1j}\sinh(\mu_j\alpha_j) + C_{2j}\cosh(\mu_j\alpha_j)\big)$$
$$+ \nu_j\big(-C_{3j}\sin(\nu_j\alpha_j) + C_{4j}\cos(\nu_j\alpha_j)\big)$$
$$- \frac{p_j D_j}{R^2}\{C_{1j}(1 + \mu_j^2)\cosh(\mu_j\alpha_j) + C_{2j}(1 + \mu_j^2)\sinh(\mu_j\alpha_j)$$
$$+ C_{3j}(1 - \nu_j^2)\cos(\nu_j\alpha_j) + C_{4j}(1 - \nu_j^2)\sin(\nu_j\alpha_j)\};$$

$$D_j\{C_{1j}(1 + \mu_j^2)\cosh(\mu_j\alpha_j) + C_{2j}(1 + \mu_j^2)\sinh(\mu_j\alpha_j)$$
$$+ C_{3j}(1 - \nu_j^2)\cos(\nu_j\alpha_j) + C_{4j}(1 - \nu_j^2)\sin(\nu_j\alpha_j)\}$$
$$= D_{j+1}\{C_{1j+1}(1 + \mu_{j+1}^2)\cosh(\mu_{j+1}\alpha_j) \tag{24}$$
$$+ C_{2j+1}(1 + \mu_{j+1}^2)\sinh(\mu_{j+1}\alpha_j)$$
$$+ C_{3j+1}(1 - \nu_{j+1}^2)\cos(\nu_{j+1}\alpha_j)$$
$$+ C_{4j+1}(1 - \nu_{j+1}^2)\sin(\nu_{j+1}\alpha_j)\};$$

$$D_j\{C_{1j}(\mu_j + \mu_j^3)\cosh(\mu_j\alpha_j) + C_{2j}(\mu_j + \mu_j^3)\sinh(\mu_j\alpha_j)$$
$$+ C_{3j}(-\nu_j - \nu_j^3)\sin(\nu_j\alpha_j) + C_{4j}(\nu_j - \nu_j^2)\cos((\nu_j\alpha_j)\}$$
$$= D_{j+1}\{C_{1j+1}(\mu_{j+1} + \mu_{j+1}^3)\cosh(\mu_{j+1}\alpha_j)$$
$$+ C_{2j+1}(\mu_{j+1} + \mu_{j+1}^3)\sinh(\mu_{j+1}\alpha_j)$$
$$+ C_{3j+1}(-\nu_{j+1} - \nu_{j+1}^3)\sin(\nu_{j+1}\alpha_j)$$
$$+ C_{4j+1}(\nu_{j+1} - \nu_{j+1}^3)\cos(\nu_{j+1}\alpha_j)\}.$$

## NUMERICAL RESULTS AND DISCUSSION

The system of equations (24) augmented with (21) and (23) present a system of equation for determination of unknown $C_{ij}$ where $i = 1, \dots, 4$ and $j = 0, \dots, n$. This system consists of $4n + 4$ equations with the same number of unknowns. Since the system is a linear homogeneous system a non-trivial solution exists if it determinant $\Delta$ vanishes.

The solution of equation $\Delta = 0$ admits to define the eigenfrequencies. The solution procedure is implemented with the aid of the computer code MATLAB. The results of calculations are presented in Figs 2–5 for the arch with a single step ($n = 1$) and $R = 1m$, $h_0 = 0.02m$, $h_1 = 0.01m$.

The material of the arch is a mild steel with $E = 2.1 \cdot 10^{11} Pa$, $v = 0.3$.

The natural frequencies of an arch without any defects compare favorably with those obtained by the finite element method in the case of higher modes (see Zheng & Fan, 2003). For instance, according to the previous study $\omega_3 = 2160$, $\omega_5 = 6480$, whereasthe predictions obtained by the finite element method are $\bar{\omega}_3 = 3933$, $\bar{\omega}_5 = 8150$. The discrepancies between these predictions are caused by the simplified model of the present problem. Due to the hypotheses made above the comparison has no sense for the first mode. Evidently the method leads to crude approximations in the case of lower modes of deformation and deeper arches.

The influence of the first natural frequency on the location of the step is illustrated in Fig. 2 for the elastic arch with $\beta = 1$. Different curves in Fig. 2 correspond to different values of the crack depth. The upmost curve in Fig. 2 correspond s to the arch without any defects. It can be seen from Fig. 2 that the highest values of the natural frequency are obtained in the case of arch which is free of cracks.
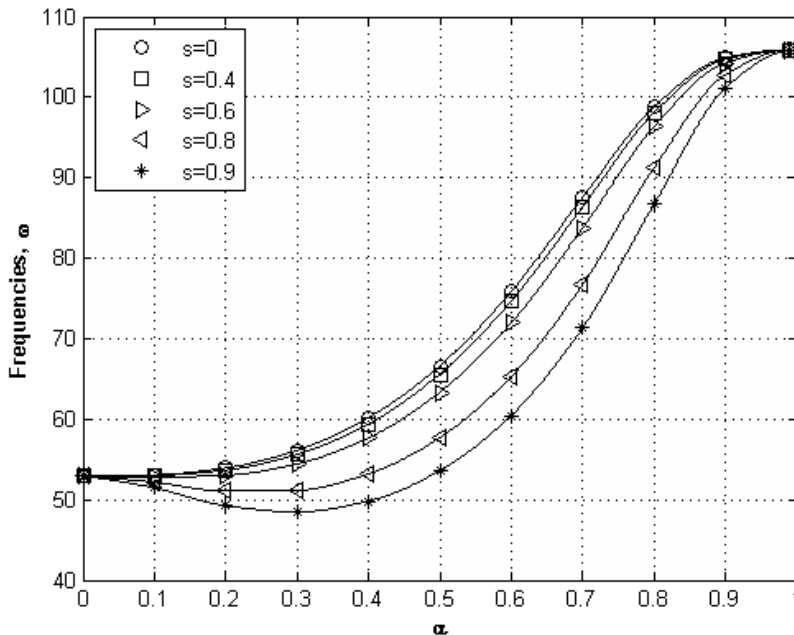


**Figure 2.** Natural frequency of the arch vs. depth of the crack.

The natural frequency versus the step location is depicted in Figs 3–5 for different values of the crack length. Different curves in Figs 3–5 correspond to the arches with the central angle $\beta = 1.0$; $\beta = 1.2$; $\beta = 1.5$; $\beta = 1.6$; $\beta = 1.7$ and $\beta = 1.8$, respectively. Note that Fig. 3 is assotiated with the arch which has no any defect. It can be seen from Fig. 3 that the larger is the central angle of the arch, the lower is the natural frequency as might be expected. Note that similar relationship between the length and

the natural frequency takes place in the case of straight beams, as well. In the case of beams it reads: the longer is the beam the lower is the natural frequency. Similar results are presented in Fig. 4 and Fig. 5 for arches with crack lengthes $c = 0.6h_1$ and $c = 0.8h_1$, respectively.
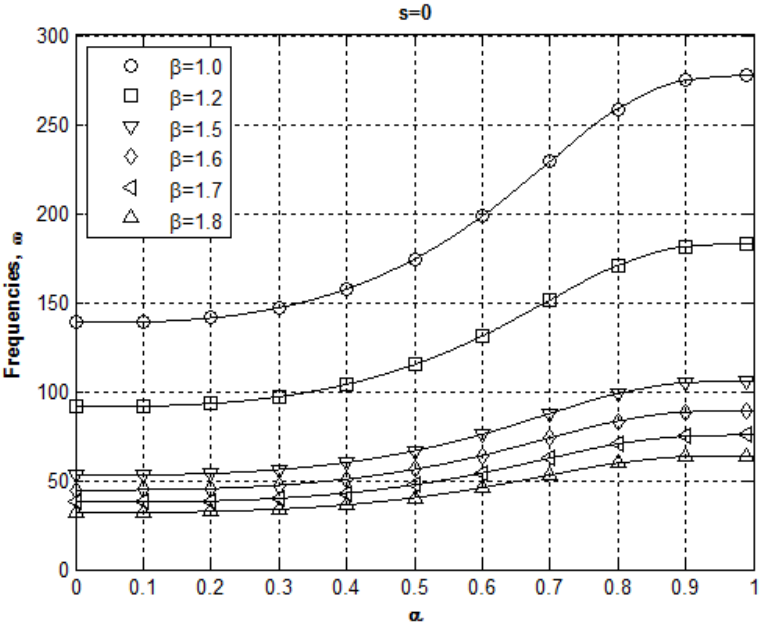


**Figure 3.** Natural frequency versus step location (s = 0).
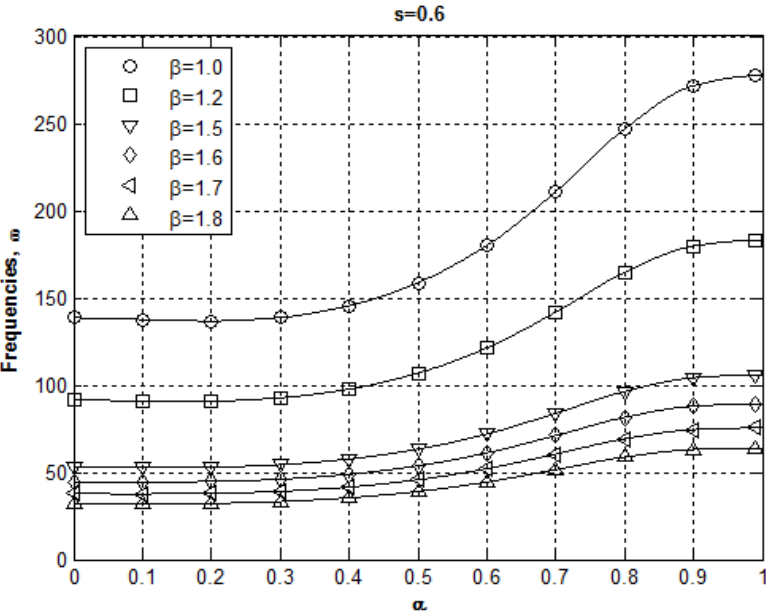


**Figure 4.** Natural frequency versus step location (s = 0.6).
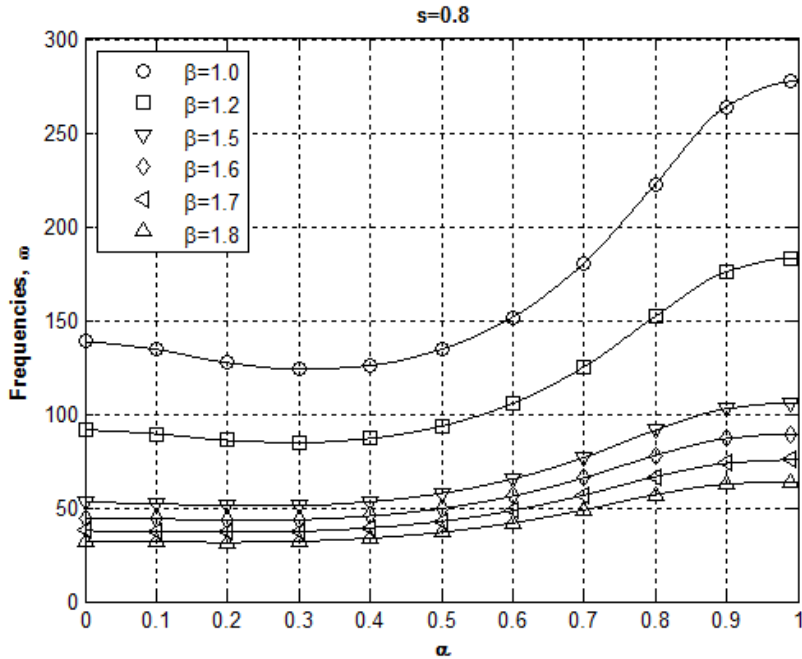
It can be seen from Fig. 5 that the upper curves associated with $\beta = 1.0$ and $\beta = 1.2$ are decreasing in the range of small values of $\alpha$. If, however, $\alpha > 0.4$ the function $\omega = \omega(\alpha)$ are increasing everywere. In the particular case if $h_0 = h_1$ the natural frequency $\omega$ decreases monotonically with increasing value of $\beta$ (see Lellep & Liyvapuu 2015a; Lellep & Liyvapuu 2015b).



**Figure 5.** Natural frequency versus step location (s = 0.8).

## CONCLUSIONS

Natural vibrations of circular arches with piece wise constant thickness have been considered. An analytical method for determination of eigenfrequencies of arches with cracks was developed. Comparison of the results of the present study with the numerical predictions shows that the present model leads to more accurate predictions in the case of higher deformation modes. It was shown that the parameters of the crack essentially influence on the vibration of the arch. The highest value of the natural frequency corresponds to the arch with any defects.

# REFERENCES

Chondros, T.J., Dimarogonas, A.D. & Yao, J. 1998. A continuous cracked beam vibration theory. *Journal of Sound and Vibration* **215**(1), 17–34.

Dimarogonas, A.D. 1996. Vibrations of cracked structures: a state of the art review. *Engineering Fracture Mechanics* **55**, 831–857.

Eroglu, U. 2015. In-plane free vibrations of circular beams made of functionally graded material in thermal environment: Beam theory approach. *Composite Structures* **122**, 217–228.

Ishaguddin, M., Raveendranath, P. & Reddy, J.N. 2016. Efficient coupled polynomial scheme for out-of-plane free vibration analysis of curved beams. *Finite Element Analysis and Design* **110**, 58–66.

Kawakami, M., Sakiyama, T. Matsuda, H. & Morita, C. 1995. In-plane and out-of-plane free vibrations of curved beams with variable sections. *Journal of Sound and Vibration* **187**, 381–401.

Kisa, M. & Brandon, J. 2000. The effect of closure cracks on the dynamics of a cracked cantilever beam. *Journal of Sound and Vibration* **238**(1), 1–18.

Kägo, E. & Lellep, J. 2013. Vibrations of elastik stretched trips with cracks. In: *Optimization and Analysis of Structures II, J.Lellep, E.Puman (Ed-s),* Tartu, 59–63.

Lellep, J. & Kägo, E. 2011. Vibrations of elastic stretched strips with cracks. *International Journal of Mechanics* **5**(1), 27–34.

Lellep, J. & Liyvapuu, A. 2015a. Free vibrations of elastic laminated arches. In: *Optimization and Analysis of Structures III, J.Lellep, E.Puman (Ed-s),* Tartu, 52–58.

Lellep, J & Liyvapuu, A. 2015b. Natural vibrations of stepped arches. *Proc. 3rd International Conference Advances in Mechanical and Automation Engineering*, Rome, 68–72.

Nandwana, B.P. & Maiti, S.K. 1997. Detection of the location and size of a crack in stepped cantilever beams based on measurements of natural frequencies. *Journal of Sound and Vibration* **203**(3), 435–446.

Qatu, M.S. 2004. *Vibrations of Laminated Shells and Plates*. Elsevier, New-York, 409 pp.

Reddy, .N. 2004. *Mechanics of Laminated Composite Plates and Shells*. CRC Press, 782 pp.

Rizos, P., Aspragathos, N. & Dimarogonas, A.D. 1990. Identification of crack location and magnitude in a cantilever beam from from the vibration modes. *Journal of Sound and Vibration* **138**(3), 381–388.

Sadeghpour, E., Sadighi, M. & Ohadi, A. 2016. Free vibration analysis of a debonded Urved sandwich beam. *European Journal of Mechanics, 1 (Solids)* **57**, 71–84.

Soedel, W. 2004. *Vibration of Shells and Plates.* Marcel Dekker, New-York, 553 pp.

Vinson, J. & Sierakowski, R.L. 2002. *The Behaviour of Structures Composed of Composite Materials*. Kluwer Academic Publishers, 435 pp.

Wu, J.S. & Chiang, L.K. 2004. A new approach for free vibration analysis of arches with effect of shear deformation and rotary inertia considered. *Journal of Sound and Vibration* **277**, 49–71.

Zheng, D.Y. & Fan, S.C. 2003. Vibration and Stability of cracked hollow-sectional beams. *Journal of Sound and Vibration* **267**, 933–954.

# Utilisation of industrial steel wastes in polymer composite design and its agricultural applications

M. Lisicins, V. Lapkovskis[*] and V. Mironovs

Riga Technical University, Scientific Laboratory of Powder Materials, Kipsalas str. 6B, LV–1048 Riga, Latvia; [*]Correspondence: lap911@gmail.com

**Abstract.** A constant development of agricultural activities is linked inherently to generation of significant amount of chemically aggressive organic wastes. This paper outlines a synergistic opportunity for industrial metalworking and plastic wastes recovery and re-use, with clear final product – composite steel-polymer material. Experimentally obtained composite polypropylene-perforated steel material is characterized by structural strength and stiffness provided by perforated steel tapes, and corrosion resistance assured by polypropylene layers, which protect steel from aggressive environment. Authors suppose that waste-based composite material could be applied for certain agricultural constructions, and namely, for boundary construction of farm animal feed lines and storage facilities for organic wastes and minerals.

**Key words:** perforated steel material, industrial wastes, polymer composites, cellular structures, feed lines, waste storage.

## INTRODUCTION

A constant development of agricultural activities is linked inherently to generation of significant amount of chemically aggressive organic wastes. Often, such chemical activity is quite harmful causing an accelerated corrosion of bearing structures, which in turn creates serious problems for waste storage and treatment. An estimate of losses related to facility corrosion is 5–10% percent of new equipment.

Circular economy assumes a resource-closed-circuit utilization oriented economy (Yin, 2011), therefore a proper recycling of industrial steel wastes for new composite materials development is in-line with modern tendencies for resource-efficient European economies. A large part of the industrial wastes composed of metallic and plastic materials. Here, one of the most interesting steel materials with great potential for use in construction and design applications are perforated steel tapes (or bands), obtaining from stamping operations in metalworking industry. At the same time, one of the largest plastic residue groups composed of polypropylenes (around 20% of all waste plastic materials) (Lisicins et al., 2015). As an example of perforated steel materials in construction can be mentioned a thin-walled cement composites. There the perforated steel wastes reinforcement performs the function of reinforcement in Portland cement-based matrix (Skudra & Skudra, 1999). The reinforcement of plastics with different metallic materials was also studied (Skudra, 1975).

In current paper, a composite material based on combination of polymer (polypropylene) and perforated steel waste materials for agricultural applications is proposed. Thus, contributing to the two large groups industrial waste materials efficient recycling for new construction materials design.
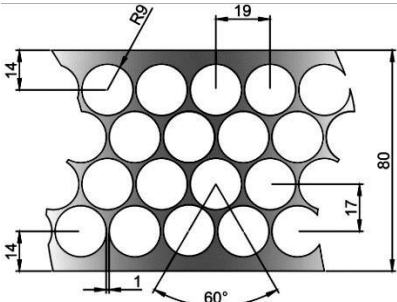
Agricultural structures suffer of the of corrosion destructive effects due to moisture content, chemicals, animal respiration, and especially fertilisers (Oki & Anawe, 2015), causing deterioration of walls and ceilings (Tubens & Brongers, 2001). Certain fertilisers are more corrosive reacting with other substances and producing aggressive gases (ammonia or hydrogen sulphide). For example, ammonium nitrate can lead to increased corrosion via hydrolysis to acids. Hygroscopic properties of many fertiliser powders are leading to corrosion due to reaction with moisture.

Most frequently applied metallic materials in agriculture are: mild steel, aluminium, galvanized steel. Mild steel is often used to contain fertilisers because it is cheap, but adequate surface cleaning, preparation and coating are necessary. The main disadvantage in this case is that regular usage of additional protective chemicals can be costly. As an alternative of carbon steel galvanized steel and stainless steel can be used for agricultural constructions. Stainless steel structures my cost 5-10 time more comparing to mild steel analogues. At the same time zinc plates mild steel rises final costs up to 25–30% (Roymech.co.uk n.d.).

## MATERIALS AND METHODS

In a framework of current paper, we offer a look at another alternative solution based on industrial wastes recycling for manufacturing of composite material suitable for agricultural construction and adjacent applications. That is a composite material based on carbon steel perforated bands (types or sheets) incorporated into polymer matrix (polypropylene or polyethylene). It is important to notice that for raw materials of both components of the composite residual (wastes) materials can be used. Perforated steel tape used in experiments is a residual material obtained from the punching process during the manufacturing of driving chain elements. Suggested material (Table 1) is characterized by good mechanical properties and moderate costs, which is about 1/3 of the price of solid steel material.

**Table 1.** Properties of sample perforated steel used in experimental works (PST-4)

| Steel | 08пс-OM-T-2-K (according to GOST 503-81) | |
|---|---|---|
| Thickness, mm | 1.25 | |
| Width, mm | 93 | |
| Permeable area, % | 66.97 | |
| Effective cross-sectional area, mm$^2$ | 16.14 | |
| Tensile load bearing capacity, N | 4,108.27 | |
| Tensile strength, N mm$^{-2}$ | 318.22 | |
| Displacement, mm | 3.27 | |
| Strain, % | 1.78 | |

Waste materials re-use efficiency is strongly related to physical and mechanical properties and materials geometry. Mechanical properties are important for load-bearing elements and constructions manufacturing, but geometrical for decorative and non-structural materials design. The most common types of polymers used in the EU is polyethylene and polypropylene, amounting to almost 55% of polymers used in various technological processes (Plastics Europe 2015). Polyethylene and polypropylene wastes have very long period of decomposition, that is important to pay more attention to polyethylene and polypropylene waste materials re-use. Polymer material residues can be combined with perforated steel material wastes, creating new composite materials suitable for construction industry. Polyethylene and polypropylene possess good weldability that allows fast and convenient materials joining for different types of structures. In present study, we have used a polypropylene as a raw material, which properties are presented in (Table 2).

**Table 2.** Properties of polypropylene used in composite material design

| | |
|---|---|
| Density, g cm$^{-3}$ | 0.91 |
| Modulus of elasticity, N mm$^{-2}$ | 1,300 |
| Tensile strength, N mm$^{-2}$ | 32.00 |
| Breaking extension, % | > 50 |
| Melting point, °C | 162–167 |

Joining of metallic and polymer materials is a difficult issue (Ochoa-Putman & Vaidya 2011). Perforated steel band has an advantage thanks to perforation slots, allowing the melted polymer to flow through the openings and ensuring mutual adhesion. There are several methods for producing of presented composite material. Main on them are pultrusion, hot pressing and polymer injection.

Hot pressing. Extrusion billet (sandwich type) heated between the press plates with a predetermined load. Disadvantage: use of template system, load, temperature parameters must be precisely defined in order to obtain the desired shape component. Advantages: The process is fast, cheap and handy for making prototypes.

## RESULTS AND DISCUSSION

In current experimental research, the composite material was produced by means of hot pressing process, using steel parts made of steel tape PST-4 sample (Fig. 1).



**Figure 1.** A composite polypropylene-perforated steel material – plane element.

Mechanical characteristics of obtained polymer-metal composite samples (a set of 5 trials) are shown in (Table 3).

**Table 3.** Mechanical characteristics of the polymer-metal composite on the basis of PST-4 sample

| Parameter | Mean value |
|---|---|
| Maximum axial tensile load, kN | $21.64 \pm 0.54$ |
| Tensile stress, N mm$^{-2}$ | $39.28 \pm 0.69$ |
| Strain, % | $4.14 \pm 0.22$ |
| Elastic modulus, GPa | $3.38 \pm 0.17$ |

Possible applications of obtained composite material are based on structural elements that can be produced using a ready-for-use components. Our solution offers an application of pre-made composite elements, such as rigid L and I shape profiles (Fig. 2, a, b, c) and reinforced composite plates to produce quickly mountable and sustainable structures protected from corrosion (Fig. 2, d, e).
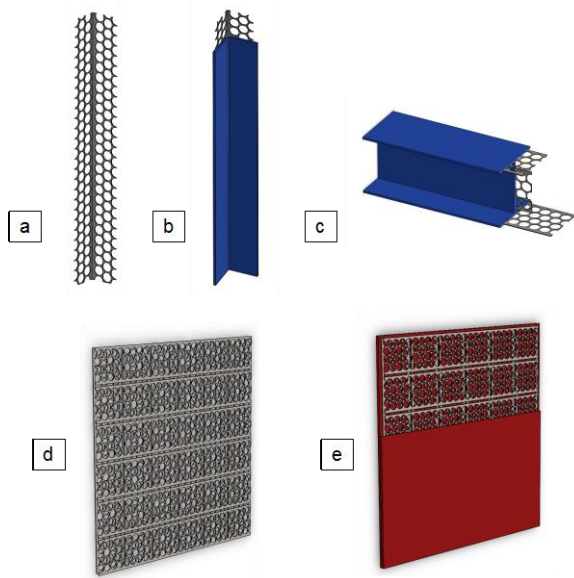


**Figure 2.** Perforated steel L and I shape profiles (a, b, c) and structures (d, e).

**Table 4.** Main benefits and disadvantages of proposed constructions

| Benefits | Disadvantages |
|---|---|
| Cheap raw materials for visually appealing structures | Less corrosion resistance than in case of stainless steel |
| Possible use waste materials (steel types and discarded polymers) | When using waste requires proper selection of raw materials |
| Fast assembling and dissembling | Time-consuming production of materials |
| Lightweight and rigid structure with need for regular anti-corrosion post-processing | Difficult to control the potential corrosion of steel |

For a number of cases the proposed solution may prove more effective, than for traditional materials. For example, if it is necessary to build a durable structure, composites walls will lasts longer than walls made of steel, meanwhile composite structures will cost less than similar structures made of galvanized or stainless steels. The following (Table 4) summarizes advantages and disadvantages of proposed solution.

## CONCLUSIONS

1. The present paper suggests a new composite material for protection of agricultural facilities against destructive effects of corrosion and based on recycled industrial wastes – perforated steel wastes and polypropylene.

2. Thanks to its mechanical properties (axial tensile load and elastic modulus), the suggested material could be used for agricultural facilities construction and repair.

3. Applications advantages of the offered material outbalance its possible limitations by following characteristics:

- corrosion resistance,
- lightweight and rigidity,
- visual appealing,
- fast assembling and dissembling.

## REFERENCES

Lisicins, M. Lapkovskis, V., Siskins, A., Mironovs, V. & Zemcenkovs, V. 2015. Conversion of Polymer and Perforated Metallic Residues into New Value-added Composite Building Materials. *Energy Procedia* **72**, 148–155.

Ochoa-Putman, C. & Vaidya, U.K. 2011. Mechanisms of interfacial adhesion in metal–polymer composites – Effect of chemical treatment. *Composites Part A: Applied Science and Manufacturing* **42**(8), 906–915.
Available at: http://www.sciencedirect.com/science/article/pii/S1359835X11000893 [Accessed October 22, 2015].

Oki, M. & Anawe, P. 2015. A Review of Corrosion in Agricultural Industries. *Physical Science International Journal* **5**(4), 216–222.
Available at: http://www.sciencedomain.org/abstract.php?iid=835&id=33&aid=7590.

PlasticsEurope. 2015. Plastics - the facts 2014/2015: An analysis of European plastics production, demand and waste data. *Plastics Europe*, pp.1–34. Available at:
http://issuu.com/plasticseuropeebook/docs/final_plastics_the_facts_2014_19122.

Roymech.co.uk, Metal Costs. Available at:
http://www.roymech.co.uk/Useful_Tables/Matter/Costs.html [Accessed January 31, 2016].

Skudra, A. 1975. Structural theory of the tensile and compressive strengths of reinforced plastics. *Polymer Mechanics* **11**(5), 844–850.

Skudra, A. & Skudra, A. 1999. Elastic Characteristics of a Cement-Based Composite Reinforced With Steel Meshed Ribbons. *Mechanics of Composite Materials* **35**(2), 119–124.

Tubens, I. & Brongers, M. 2001. Agricultural production, p.11.
Available at: http://corrosionda.com.

Yin, R. 2011. *Metallurgical process engineering*, Springer Berlin Heidelberg. Available at: https://books.google.lv/books?id=O3mb57VQhIAC.

# Measuring the mobility parameters of tree-length forwarding systems using GPS technology in the Southern Italy forestry

G. Macrì[*], G. Zimbalatti, D. Russo and A.R. Proto

Mediterranean University of Reggio Calabria, Department of AGRARIA, Feo di Vito, IT 89122 – Reggio Calabria, Italy
[*]Correspondence: giorgio.macri@unirc.it

**Abstract.** The introduction of modern forwarders to Apennines forest operations must account for the traditional forwarding units used by local logging contractors. They generally use the same machine for extraction and intermediate off-road transportation on mountain trails, inaccessible to heavy road vehicles. Conventional forwarders are not designed for fast transportation on trail and cannot replace conventional. This research set up a long-term follow-up study to determine the use pattern of three conventional tractor-trailer units (Forwarder, forestry trailer and articulated truck). The goal of this study was to gauge the potential of these machines. In particular, the study determined for both machine types: monthly usage, incidence of travelling time over total time, distance covered and travel speed. The null hypothesis was that use pattern, average travel distance and speed distribution did not differ between traditional tractor and trailer units and high-speed forwarders. For this purpose, Global Positioning System/Global System for Mobile Communications data loggers were installed for continuous real-time collection of the main work data, including position, status, speed and fuel consumption. The study showed that new forwarders could actually travel at a speed higher than 24 km h$^{-1}$, and they performed both extraction and intermediate transportation. They were capable of independent relocation, which made them suitable for small-scale forestry. Both machine types were used intensively, but the annual usage of forwarders was almost twice as large as that of tractor-trailer units. Furthermore, forwarders had a 27% higher hourly productivity and a 50% higher fuel consumption per hour, compared with tractor-trailer units.

**Key words:** GPS – Track logger, data logger, extraction, precision forestry.

## INTRODUCTION

Forests in southern Italy are an important area in terms of forest production, having the largest forest cover of all regions of the country even though the highest concentration of woodlands occurs in the northern regions of Italy. Forests cover 1,517,836 ha (NFI 2005) in southern Italy and consist mainly of mature beech, chestnut, Corsican pine, and silver fir forests (more than 300,000 ha combined). These forests account for a wooded area percentage of 31.8%. Therefore, use of these forests could certainly provide a more significant resource for the economy of the entire Mediterranean basin, an objective that could be attained with better and more efficient mechanization of forest operations, which should play a growing role (Istat, 2013). Unfortunately, the current level of mechanization is fairly low (Zimbalatti & Proto, 2009). The current increasing dynamism of the wood market has led to the development

and improvement of technologies able to extract logs more efficiently by reducing consistently the time and labour required for production (Cavalli et al., 2014; Moneti et al., 2015). Indeed, the most common work method in southern Italy, referred to as traditional, can be considered as an early stage of mechanization. It is based mainly on agricultural tractors, sometimes equipped with specific forest-related machines (winches, hydraulic cranes, log grapples, etc.); use of animals for gathering and yarding is also widespread. This level of mechanization of forest resource extraction is due to the features of the forest sites, the characteristics of the forest properties, and the small dimensions of many forest enterprises (Proto et al., 2014).

Time motion study by GPS is a key factor for the road network planning (Cavalli & Grigolato, 2010). Similar methods have recently been used in forest engineering studies dealing with wood transportation (Holzleitner et al., 2011a), forwarding units (Veal et al. 2001), mobility parameters (Suvinen & Saarilahti, 2006) and autonomous path tracking (Ringdahl et al. 2011; Spinelli et al., 2015; Russo et al., 2016). Respect to the previous studies, however, the forest features, harvesting and skidding methods are completely different in South Italy, the sites of the present research. In Calabria, where the test were conducted, the expanse of forest is 40.6% respect on average data national of 34.7%. Every year, the average increase in wood volume in this region (equal to 6–8 $m^3$ $ha^{-1}$) exceeds and sometimes doubles the estimated increase in other forests in Italy (Proto & Zimbalatti 2015,), roughness, slope, and silvicultural system affect the mobility parameters of tree-length forwarding systems. In this respect, the present research aims to develop technical and economical knowledge regarding the different use of three machinery used in Calabria (South Italy) by using GPS/GSM technology.

## MATERIALS AND METHODS

Three representative machines were selected for the study: an articulated Man Truck, model TGX 6×6 (471 kW), a forwarder, model John Deere 110 D (125 kW), and a forestry tractor-trailer (70 kW) (Table 1). All machines were road-legal and could travel at a theoretical maximum speed of 40 km $h^{-1}$. The machines were owned by separate small-scale logging contractors, which is typical of the region.

**Table 1.** Description of machines

| Machine | Articulated Truck | Forwarder | Forestry Tractor-railer |
|---|---|---|---|
| Type | MAN | John Deere | Lamborghini |
| Model | TGX 6x6 | 110 D | 1,060 |
| Trasmission | Hydrostat | Hydrostat | Mechanic |
| Axles total | 3 | 4 | 4 |
| Power (kW) | 353 | 125 | 77 |
| Weight (kg) | 33,000 | 14,600 | 8,050 |
| Width (mm) | 2,490 | 2,650 | 2,350 |
| Length (mm) | 5,200 | 5,000 | 2,350 |
| Gps Study - Months | 7 | 7 | 7 |

All these machines worked in the same valley in southern Italy and were operated by the same owner-operator. For the purpose of the study, the university researchers installed on all machines a commercial black-box GPS/GSM unit for continuous real-time collection of the main work data, including position, status (engine off, engine on, traveling), and speed (Fig. 1).

The tests were carried out at three forest sites, indicated below by the letters A, B, and C and all located in the Serre massif (VV). Table 2 gives the features and vegetation characteristics of the three test sites from surveys carried out beforehand.



**Figure 1.** Installing the GPS/GSM black-box unit.

**Table 2.** Characteristics of the two test sites

| Features | Measurement Units | Site A (Articulated truck) | Site B (Forwarder) | Site C (Forestry tractor-trailer) |
|---|---|---|---|---|
| Altitude | a.s.l. | 950 | 800 | 850 |
| Prevalent species | - | Chestnut | Corsican pine | Mediterranean pine |
| Government | - | Coppice | High forest | High forest |
| Treatment | - | Clearcuts with reservations | Thinning | Thinning |
| Stand density | n. p. ha$^{-1}$ | 2,400 | 900 | 1200 |
| Average volume per tree | m$^3$ | 0.20 | 0.65 | 0.40 |
| Total volume | m$^3$ ha$^{-1}$ | 480 | 585 | 480 |
| Average slope | % | 31 | 22.5 | 27 |
| Max gradient | | 50 | 38 | 43 |
| Min slope | | 12 | 7 | 11 |
| Roughness | - | Very rough | Moderately rough | Moderately rough |

The GPS/GSM black box collected position data at 30-second intervals and had a buffer memory to store data when GSM coverage was unavailable. Stored data were sent to the server as soon as the unit could connect again to the GSM network. The units used for the study were a commercial tracker used for truck fleet management and available at a very attractive monthly fee (www.visirun.com).

The black-box system used for the study downloaded all data at the end of each day into one spreadsheet per machine. All position data carried a time stamp, which was used to estimate speed. Data loggers were connected to the engine contact, and hence they recorded the time that the engine was on. As a consequence, each produced a daily estimate of work hours, which was downloaded together with the position points and speed graphs (Fig. 2). Data processing was rationalized by developing a new automated procedure to merge all daily spreadsheets into a single master data base per machine to convert it into a data base management system. This made it possible to select and edit all the events. Data were recorded at two records per minute more or less, which was the standard data collection rate at a 30-second pulse interval. Query views were finally converted into a spreadsheet (MS Excel) to produce suitable pivot tables. The data were then processed using the SPSS software.
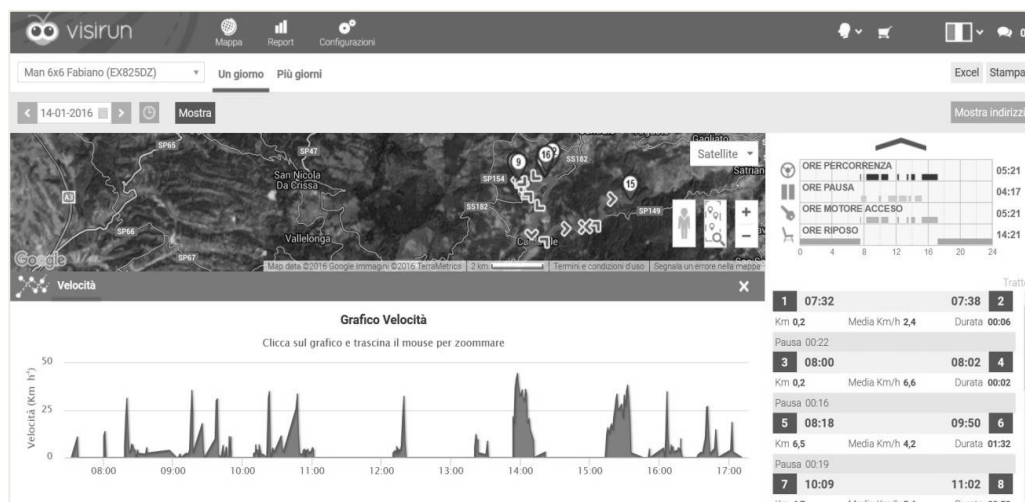


**Figure 2.** Example of machine track and speed graph for one work day.

The data considered in this preliminary study covered 7 months during the same period, from May 2015 to December 2015 inclusive. The following data were used in the analysis: duration of the working day, in hours (roughly the same as worksite time); time when the engine was running, in hours; time that the machine was moving, in hours; and total distance traveled, in km. Before analysis, the daily figures were consolidated into sums representing five working days to reduce the confounding effect of daily variability. A similar consolidation was carried out to describe the volume of wood extracted in each trip to determine the mean hourly productivity of the different machines. The total number of logs was counted and their transportation recorded to calculate the volume of each load and hence to obtain a good estimate of the total volume carried. Overall data for the periods of work and the skidding-cycle volumes on the test days were also collected.

The logs obtained during the study at the three test sites were calculated by measuring the total length and the diameter at half height (Proto & Zimbalatti, 2015; Proto et al., 2016a). At the first site (A), the full-tree harvesting method was used; the trees were delimbed, topped, and bucked on site. At the second and third sites (B and C),

the tree-length method was used. Trees were felled, then delimbed and topped at the stump. The volume of logs was calculated using the Huber formula (1):

$$V = D^2 \cdot \pi/4 \cdot L,$$ (1)

where: V = total tree volume (m$^3$); D = mid-height diameter (m); L = length (m).

The distribution of consolidated travel distance data was normalized through a logarithmic transformation. Current speed data were recorded every 30 seconds, and each record was allocated to one of the following speed classes: 0 to 2, > 2 to 5, > 5 to 10, > 10 to 20, and > 20 km h$^{-1}$. The incidence of each speed class over the total travel time was cumulated as a sum over five working days to dampen the effect of extreme daily values.

## RESULTS AND DISCUSSION

Over the seven-month period, the forwarder worked 158 days, the articulated truck 85, and the forestry tractor-trailer 75 days. The average workday lasted 8.20 hours in the forwarder, 9.40 in the articulated truck, and 8.00 with the forestry tractor-trailer. The longest workday lasted 13.4 hours with the articulated truck, 10.2 with the forwarder, and 9.25 with the forestry tractor-trailer. The total worksite time accumulated during the study period by the forwarder was 3,807 hours, 2,263 by the articulated truck, and 1865 by the forestry tractor-trailer. Engine time was 1,383 hours for the forwarder, 561 for the articulated truck, and 600 for the forestry tractor-trailer. Utilization time was about 40% for the articulated truck, subdivided into 21% for loading and unloading and 19% for time spent traveling empty and facing delays. The forwarder was used 56% of the time, with 20% of this time spent in loading and unloading. The forestry tractor-trailer was used 52% of the time, with 40% of this time used for loading and unloading. In this last machine, the greatest amount of time was spent to load and unload the wood. This high time consumption is caused by the type of mechanical grapple used, which is less powerful than the other grapples on the forwarder and the articulated truck.

Table 3 shows the average monthly data over the cumulated 7-month study period. The forwarder worked more hours per week and had a higher utilization rate than the articulated truck or the forestry tractor-trailer. However, it covered a shorter distance. The articulated truck covered a total distance of 5,063 km at an average speed of 25.5 km h$^{-1}$, the forwarder 532 km at an average speed of 2.6 km h$^{-1}$, and the forestry tractor-trailer 412 km at an average speed of 1.4 km h$^{-1}$.

**Table 3.** Worksite time, engine time, utilization rate, and travel distance (average month)

|  |  | Articulated truck | | Forwarder | | Forestry tractor - trailer | |
|---|---|---|---|---|---|---|---|
|  |  | Mean | SD | Mean | SD | Mean | SD |
| Worksite time | h | 80.1 | 72.1 | 197.6 | 38.3 | 85.7 | 29.1 |
| Engine on | h | 81.6 | 68.1 | 218.6 | 43.1 | 128.6 | 37.6 |
| Moving | h | 26.7 | 25.3 | 176.4 | 34.1 | 51 | 20.9 |
| Utilization | % | 40 | 23.9 | 75 | 14.3 | 55 | 12.1 |
| Distance | km | 723 | 710.2 | 76 | 8.9 | 58.9 | 3.9 |

Analysis of variance showed that all these differences were statistically significant except for travel distance (Table 4). Although a significant factor, machine type seldom

accounted for more than 20% of the variability in the data pool, which was consistent with the predominant effect of site variability in natural forests. The cumulative distance covered in 7months did not differ significantly among the three sites, but the hours worked during the same time did, and therefore the articulated truck covered a significantly longer distance per unit time (Table. 4).

**Table 4.** ANOVA for worksite time, engine time, utilization rate, and travel distance

| | Sum of squares | df | Mean square | F | Sig. |
|---|---|---|---|---|---|
| Between groups | 61,442.571 | 2 | 30,721.286 | 12.263 | 0.000 |
| Within groups | 45,092.000 | 18 | 2,505.111 | | |
| Total | 106,534.571 | 20 | | | |
| **Engine time** | | | | | |
| | Sum of squares | df | Mean square | F | Sig. |
| Between groups | 67,848.667 | 2 | 33,924.333 | 12.769 | 0.0004 |
| Within groups | 47,823.143 | 18 | 2,656.841 | | |
| Total | 115,671.810 | 20 | | | |
| **Move time** | | | | | |
| | Sum of squares | df | Mean square | F | Sig. |
| Between groups | 90,385.143 | 2 | 45,192.571 | 60.575 | 0.0000 |
| Within groups | 13,429.143 | 18 | 746.063 | | |
| Total | 103,814.286 | 20 | | | |
| **Distance** | | | | | |
| | Sum of squares | df | Mean square | F | Sig. |
| Between groups | 2,008,388.667 | 2 | 1,004,194.333 | 5.972 | 0.0103 |
| Within groups | 3,026,826.286 | 18 | 168,157.016 | | |
| Total | 5,035,214.952 | 20 | | | |
| **Utilization** | | | | | |
| | Sum of squares | df | Mean square | F | Sig. |
| Between groups | 6,517.460 | 2 | 3,258.730 | 10.516 | 0.0009 |
| Within groups | 5,577.778 | 18 | 309.877 | | |
| Total | 12,095.238 | 20 | | | |

These results were compatible with the distribution of moving time within predefined speed classes, as shown in Fig. 3. Almost 70% of forestry tractor-trailer moving time fell within the slowest speed class, compared to 40% for the forwarder and 5% for the articulated truck. In contrast, the percentage of moving time within the higher speed classes ($2–10 \text{ km h}^{-1}$) was twice as high for the articulated truck as for the forwarder. The percentage of moving time in which the articulated truck traveled at a speed higher than $20 \text{ km h}^{-1}$ was 66% of the total time monitored. Technically, both the

articulated truck and the forwarder were capable of traveling at speeds higher than 20 km h$^{-1}$. The database even contained rare recorded speeds greater than 30–40 km h$^{-1}$, but these could have been the result of position errors. Table 5 shows the number of hours spent moving at a given speed for the whole seven-month study period. This was obtained by multiplying total moving time by the percent incidence of each speed class. During the whole study period, the articulated truck spent much more time moving at speeds greater than 20 km h$^{-1}$. In contrast, the forestry tractor and the forwarder moved at speeds less than 20 km h$^{-1}$. This may indicate that the articulated truck reached its highest speed only when traveling unloaded during relocations, whereas the forwarder and tractor were used for road transportation over short distances.
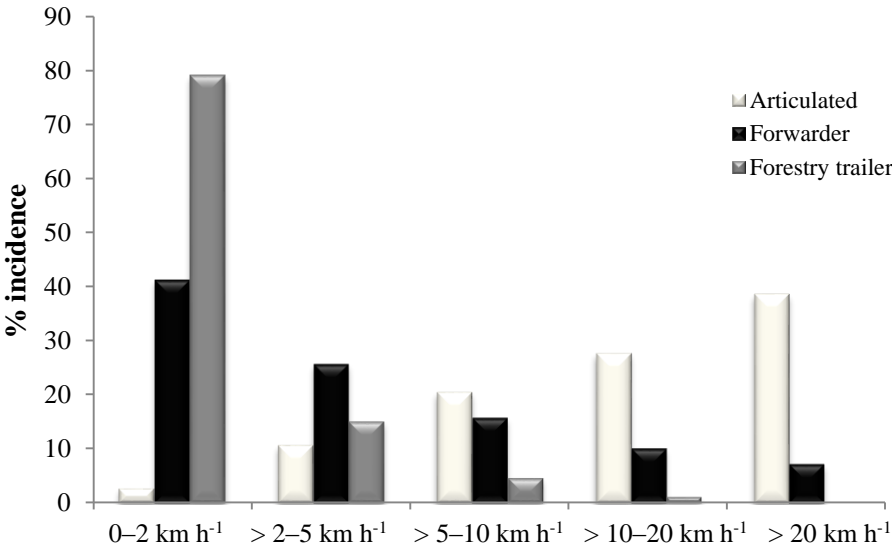


**Figure 3.** Breakdown of moving time within speed classes.

**Table 5.** Hours traveled within each speed class during the 7-month study period

| Speed Class | Articulated truck | Forwarder | Forestry trailer |
|---|---|---|---|
| 0–2 km h$^{-1}$ | 15 | 570 | 474 |
| > 2–5 km h$^{-1}$ | 60 | 355 | 91 |
| > 5–10 km h$^{-1}$ | 115 | 218 | 28 |
| > 10–20 km h$^{-1}$ | 155 | 140 | 7 |
| > 20 km h$^{-1}$ | 216 | 100 | - |
| Total hours | 561 | 1,383 | 600 |

The study showed that the three machines were used differently, which disproves the null hypothesis that the usage pattern did not change with machine type. The main difference in usage pattern was that the tractor was occasionally used for road transport, whereas the forwarder and the articulated truck were not. On the other hand, the forwarder and the forestry tractor-trailer both seemed equally capable of intermediate transport on lower-class roads, because the hours worked at speeds between 12 and 20 km h$^{-1}$ were about the same for all machines. Indeed, the articulated truck spent much more time moving over intermediate and long distances. Annual usage was substantially

higher for the forwarder and the articulated truck than for the forestry tractor-trailer, probably due to the combination of their better work capability and the need to depreciate their larger associated capital investment (Spinelli & Magagnotti, 2010). This study also highlights the substantial difference between worksite time and engine time, or hour-meter time. Differences between worksite time records and hour-meter records have already been noticed in a previous study by Spinelli & Magagnotti (2011). This is obviously related to the effect of machine utilization, which this study approximates by the ratio of engine time to worksite time (Björheden et al., 1995). The machine utilization figures obtained in this study are slightly larger than those reported by Brinker et al. (2002), and more recently by Holzleitner et al. (2011b). This may result from including non-work time within engine time, which is bound to increase utilization. For this reason, further studies are planned to compare GPS and manual records.

These studies will also aim to determine productivity, which could not be estimated from the GPS records. These machines were capable of independent relocation, which made them suitable for small-scale forestry. All machine types were used intensively, but the annual usage of the forwarder and the articulated machine was almost twice as large as that of the tractor-trailer unit. Furthermore, the forwarders had 27% higher hourly productivity and 50% higher fuel consumption per hour than the tractor-trailer units.

## CONCLUSIONS

The usefulness of articulated truck, forwarder, forestry trailer for extracting and transporting logs has attracted particular interest in the Calabrian forest industry. The transportation of timber has always been challenging, especially in mountainous environments where slopes cause processing limitations. This research has revealed that these machine types were used intensively, but that the annual usage of the forestry tractor-trailer was about half that of the other machines. The numerous observations recorded in this study confirm that the use of these different machines is influenced by the work site (Proto et al., 2016b). The forwarder is essential for efficiency in timber handling, thinning, and regeneration harvesting; the articulated truck for transport over intermediate and long distances; and the forestry tractor-trailer for extraction in gently sloping areas and transport over short distances. In terms of future road building, the position of these roads should minimize the extent of forwarding that may be economical. The models developed here provide a basis for site-specific costing of transportation operations and potentially a convenient and transparent means of negotiating contract timber extraction. Further research on extraction and transport system comparison could be based on the use of GNSS installed on carriage for supporting automatic or semi-automatic operational monitoring and for improving the quantity of acquired data reducing the engagement of the surveyor (Gallo et al., 2013).

# REFERENCES

Björheden, R., Apel, K., Shiba, M. & Thompson, M. 1995. IUFRO Forest work study nomenclature. Swedish University of Agricultural Science, Dept. of Operational Efficiency, *Garpenberg* **16** p.

Brinker, R., Kinard, J., Rummer, B. & Lanford, B. 2002. *Machine rates for selected forest harvesting machines.* Circular 296 (Revised). Alabama Agricultural Experiment Station, *Auburn University*, AL. **32** p.

Cavalli, R. & Grigolato, S. 2010. Influence of characteristics and extension of a forest road network on the supply cost of forest woodchips. *J. of Forest Research* **15**, 202–209. doi: 10.1007/s10310-009-0170-4

Cavalli, R., Grigolato, S. & Sgarbossa, A. 2014. Productivity and quality performance of an innovative firewood processor. *Journal of Agricultural Engineering* **45**, 32–36. http://doi.org/10.4081/jae.2014.228

Gallo, R., Grigolato, S., Cavalli, R. & Mazzetto, F. 2013. GNSS-based operational monitoring devices for forest logging operation chains. *Journal of Agricultural Engineering* **44**, 140–144. http://doi.org/10.4081/jae.2013.s2.e27

Holzleitner, F., Kanzian, C. & Stampfer, K. 2011a. Analizing time and fuel consumption in road transport of round wood with an onboard fleet manager. *European Journal of Forest Research* **130**, 293–301.

Holzleitner, F., Stampfer, K. & Visser, R. 2011b. Utilization rates and cost factors in timber harvesting based on long-term machine data. *Croatian Journal of Forest Engineering* **32**, 501–508.

ISTAT 2013. Wood felling and removal in forests by use and region. *National Institute of Statistics* pp **200**.

Moneti, M., Delfanti, L.M.P., Marucci, A., Bedini, R., Gambella, F., Proto, A.R. & Gallucci, F. 2015. Simulations of a plant with a fluidized bed gasifier WGS and PSA. *Contemporary Engineering Sciences* **8**, (31), 1461–1473. http://dx.doi.org/10.12988/ces.2015.56191

National Forest Inventory, 2005. Italian forests: National Forest Inventory.

Proto, A.R. & Zimbalatti, G. 2015. Firewood cable extraction in the southern Mediterranean area of Italy. *Forest Science and Technology* **3–8** http://doi.org/10.1080/21580103.2015.1018961

Proto, A.R., Grigolato, S., Mologni, O, Macrì, M., Zimbalatti, G. & Cavalli, R. 2016a. Modelling noise propagation generated by forest operations: a case study in Southern Italy. *Procedia – Social and Behavioral Sciences*, Article in press.

Proto, A.R., Macrì, G., Bernardini, V., Russo, D. & Zimbalatti, G. 2016b. Acoustic evaluation of wood quality with a non-destructive method in standing trees: A first survey in Italy. *iForest*, Article in press.

Proto, A.R., Zimbalatti, G., Abenavoli, L., Bernardi, B. & Benalia, S. 2014. *Biomass production in agroforestry systems: V.E.Ri.For Project.* Advanced Engineering Forum **11**, 58–63. Trans Tech Publications, Switzerland. doi:10.4028/www.scientific.net/AEF.11.58

Ringdahl, O., Lindroos, O., Hellström, T., Bergström, D., Athanassiadis, D. & Nordfjell, T. 2011. Path tracking in forest terrain by an autonomous forwarder. *Scandinavian Journal of Forest Research* **26**, 350–359.

Russo, D., Macrì, G., Luzzi, G. & De Rossi, A., 2016. Wood energy plants and biomass supply chain in Southern Italy. *Procedia – Social and Behavioral Sciences*. Article in press.

Spinelli, R. & Magagnotti, N. 2010. The effects of introducing modern technology on the financial, labour and energy performance of forest operations in the Italian Alps. *Forest Policy and Economics* **13**, 520–524.

Spinelli, R., Magagnotti, N, Pari, L. & De Francesco, F. 2015. A comparison of tractor – trailer units and high – speed forwarders used in Alpine forestry. *Scandinavian Journal of forestry Research* **5**, 470–477.

Spinelli, R., Magagnotti, N. & Picchi, G. 2011. Annual use, economic life and residual value of cut-to- length harvesting machines. *Journal of Forest Economics* **17**, 378–387.

Suvinen, A. & Saarilahti, M. 2006. Measuring the mobility parameters of forwarders using GPS and CAN- bus techniques. *Journal of Terra mechanics* **43**, 237–252.

Veal,,M.W., Taylor, S.E., McDonald, T.P., McLemore, D.T. & Dunn, M.R. 2001. Accuracy of Tracking Forest Machines with GPS. *Transactions of ASABE* **44**, 1903–1911.

Visirun A Fleetmatics Company 2016. *https://www.visirun.com/en/.*

Zimbalatti, G. & Proto, A.R. 2009. Cable logging opportunities for firewood in Calabrian forests. *Biosystems Engineering* **102**, 63–68. http://doi.org/10.1016/j.biosystemseng.2008.10.008

# Pulse-video method for determining the workload and energy expenditure for assessing of work environment

A. Nautras[*], B. Reppo and J. Kuzmin

Estonian University of Life Sciences, Institute of Technology, Kreutswaldi 56, EE51014 Tartu, Estonia; [*]Correspondence: arles.nautras@emu.ee

**Abstract.** Examining the humans work load and energy consumption allows us to identify the energy used for working postures and techniques and thereby create solutions how to make work technology and work environment better and altogether improve an employees work ability. There are several methods in which human energy consumption is determined by working postures, type of work and handling of loads, they all take account only the physical load factors ignoring mental or microclimate factors in the work environment. In recent times there are also used the mathematical models, in which the energy consumtion is determined on the basis of pulss frequency. The methods are complicated to realize them in the work situation because they do not allow to determine the dynamics of the work load in the work process. The aim of this research was to develop a method that enables to use a computer to determine and analyse the work process on screen at real time and that shows the employee's heart rate, work load and energy consumption momentary load values as well as their dynamics. The method is based on continuous measuring the employees pulse rate in the working process without disturbing him and at the same time also filming work process to make a video to demonstrate the results. We introduce the methodology how to measure an employees pulse rate, work load and energy consumption dynamics to make a compiled video. There are shown the fragments of research results about a farmer's and glassblower's work.

**Key words:** physical work, workload, energy expenditure, pulse-video, pigfarmer, glassblower.

## INTRODUCTION

Human physical activity has a significant impact on health. It is important to investigate energy expenditure of employees because it can help detect unhealthy working postures and to motivate and steer toward a healthier work technologies. Improper work postures or work technologies can lead to excessive gravity of the work, which would result in the bone and musculoskeletal disorders, thereby reducing work performance among employees (Priya et al., 2010). It is important to examine the energy expenditure in the field of occupational physiology and health, because it provides useful information on the work of physiological load and helps to determine the energy needs of the employee (Anjos et al., 2007).

Usually for measuring the physical load and energy expenditure it is used oxygen consumption (VO2). However, under field conditions it is a cumbersome method for measuring oxygen consumption and therefore it is taken to propose other solutions (Smolander et al., 2007). There is also used the ISO 8996-2004, standard for the assessment of person's energy consumption, which has been shown in four methods for

evaluating the metabolic rate. At level one there are mentioned two assessments: metabolic rate by occupation and the classification of metabolic rate by categories. The second assessment is based on the estimation of metabolic rate by task requirements, influence of the length of rest periods and work periods, metabolic rate for a work cycle and metabolic rate for typical activities. The third assessment is based on analysis like the estimation of metabolic rate using heart rate and the relationship between heart rate and metabolic rate. The fourth, expert level, the determination of metabolic rate measured by oxygen consumption, using double-labeled water method, which allows to characterize the metabolic rate of a mean value over a longer period of time (1–2 weeks) and direct calorimetry method. Since the heart rate and the metabolic rate are in linear relationship the third method is easier than the other methods. Heart rate is easier to measure than oxygen consumption (ISO 8996, 2004).

For the employee energetic load determination there are used more variety of methods such as Ovako Working posture Assessment System (OWAS) – which is designed for heavy work to assess and take into account the person's working positions (84 indicators), ERGOLOG – employee is tested in the workplace, VIRA – takes into account a person seated posture and movement and it is captured on video, ARBAN – takes into account the position and the movable loads of the employee while standing or walking (Tuure, 1991; 1995), Hettinger method – for measuring the energy expenditure there is used generalized tables (Hettinger et al., 1989).

The described methods take into account only the physical load of the body but does not reflect the mental and the surrounding work environment (air temperature, humidity, noise, lighting, etc.) load factors, equipment design, workflow, etc. The used methods usually do not allow to determine the workload of the working human.

Because the heart rate response is very sensitive to the work environment changes, the heart rate and energy consumption or energy expenditure are in linear relationship (Andersen et al., 1978). To analyze and evaluate the work processes and work technology the EMÜ department of Husbandry Engineering and Ergonomics developed a method (Reppo & Käämer, 1998; Reppo et al., 1999; Reppo & Lindsaar, 2001; Mikson & Reppo, 2004; Mikson et al., 2005, Kuzmin, 2014; Nautras, 2015) where the work rate of the employee and energy expenditure in the work process is determined by the person's heart rate continuous measurement. This method is easier and less disruptive to the employee but the process requires tense monitoring of the work methods used by the employee for later to show the most interesting work method with the right pulse value.

The aim was to develop a method (pulse-video method) which would allow to use the employee measured heart rate and record the work process for later to be displayed on a computer screen in sync with the employee work process and his measured heart rate, workload and energy expenditure.

## MATERIALS AND METHODS

The farmer's and glassblower's work load and energy expenditure have been demonstrated by pulse-video method. The pig farmer, 49 years old female with work experience of 5 years. The main tasks of the pig farmer are feeding and caring for animals, but also maintaining farm facilities (water pipes, hoses, fences and animal selters). When the video was taken, he was feeding the pigs. The glassblower, 31 years

old female with work experience of 7 years. A glass blower is responsible for designing, producing, decorating and finishing pieces of glass including giftware, exhibition pieces, tableware ect. Glass blowing technique involves handling molten glass, as well as a variety of tools, metals, and dyes for decoration and scientific notation. The main task of the glassblower, when the video was taken was making of glass jugs.

The pulse-video method takes into consideration both the physical, psychological risk factors and the surrounding environment to measure total impact to human energy expenditure. For determing the workload it is used Brouha and Nygard composed classification by the heart rate, which has been approved by the World Health Organization (WHO) (Tuure, 1991; 1995). The workload is classified by heart rate as shown: light (L) when the heart rate is less than 100 bpm, moderate (M) 100...124 bpm, heavy (H) 125...150 bpm and very heavy (VH) when more than 150 bpm. The energy expenditure is determined by the workload, sex and age of the employee (Andersen et al., 1978, Tuure, 1991; 1995).

The pulse-video method is based on continuous measurement of the employees pulse using the heart rate monitoring device (Suunto t6 measurement kit) at work and at the same time also filming the workprocess. Later the video is processed and based on the data of heart rate, the workload and energy expenditure are calculated (Fig. 1).
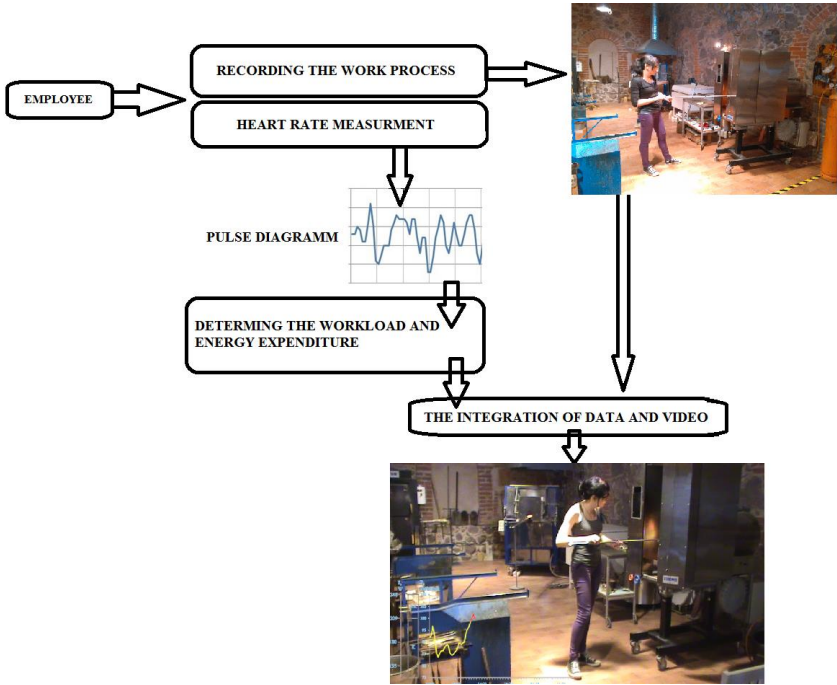


**Figure 1.** The realization of pulse-video method block diagram.

The data processing program MS Excel is used for the processing of heart rate data and creating a pulse diagram. For the integration of video and data there is used different programms like: Adobe Flash 8 Professional (Kuzmin, 2014), Photoshop and Adobe Premiere Pro (Nautras, 2015).

## ESULTS AND DISCUSSION

The pulse diagram is supplemented through data interpolation with workload and energy expenditure on the additional scales (Fig. 2) which allows to monitor the dynamics of heart rate, workload and energy expenditure during the work process.
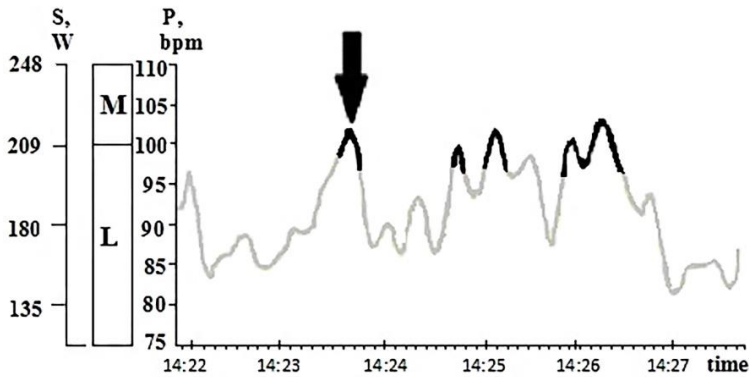


**Figure 2.** The glassblowers pulse diagram with additional scales of workload and energy expenditure: P – heart rate; L – light workload, M – moderate workload; S – energy expenditure.

Pulse-video method has been used for studing the pig farmer food distribution. The pulse-video is available on internet: https://goo.gl/zn3LG1. Fig. 3 presents a fragment from the pig farmer's pulse-video.



**Figure 3.** The fragment of pig farmer's pulse-video with additional time scales of workload and energy expenditure: S – energy expenditure (W); H – heavy workload, M – moderate workload; P – heart rate (bpm) (J. Kuzmin, 2009).

On Fig. 3 there is shown a fragment of the pig farmers pulse-video. The arrow indicates the current heart rate of the pig farmer which corresponds to 135 bpm (beats per minute), workload is heavy, and the energy expenditure is 350 W.

Fig. 4 shows a fragment about glassblowers pulse-video, where the glassblower is displayed on heating the glass mass at the furnace. Heart rate, workload and energy expenditure were measured during the exact time (see diagram in the left corner belov the figure), as displayed in Fig. 2 (indicated by the black arrow). It can be seen that the workload is moderate, because the heart rate was above 100 bpm (beats per minute) and the energy expenditure is 210 W.



**Figure 4.** The fragment of glassblower's pulse-video on heating of glassware (Nautras, 2015).

In spite of there are several methods in which human energy consumption is determined by working postures, type of work and handling of loads, they all take account only the physical load factors ignoring mental or microclimate factors in the work environment and more often using tables for measuring the work load (Tuure, 1991) and energy expenditure (Hettinger et al., 1989). Smolander and co-authors (2008) developed heart rate variability-based method (Firstbeat PRO heartbeat analysis software) for the estimation of oxygen consumption without individual calibration. There are methods like SYBAR which uses video but it is used for muscles and joints load analysis (Harlaar et al., 2000). The VIRA is another method that uses video, taking into account a person's posture and movement, but not work load and energy expenditure synchronously with the working process. Thereat, heart rate also can increase at low activity levels with high mental-strain of precision work (heating of glass detail) and additional thermal stress (Wilson & Crandall, 2011). The pulse-video method takes into account not only physical workload and energy expenditure, but indirectly demonstrates also mental and microclimate factors in the work environment, synchronously seen on a video. The glassblower's pulse-video is available online at: https://goo.gl/Z2uGcp.

## CONCLUSIONS

Since the heart rate and the person's energy expenditure or energy load are in a linear relationship the workload and energy expenditure was determined by the continuous measurement of heart rate. The developed pulse-video method allows to follow the heart rate dynamics during the workprocess and later display them on a computer screen. It is possible to measure synchronously the work process and heart rate, workload and energy expenditure. The method is easy usable and less disruptive to employee in the work process.

## REFERENCES

Andersen, L.K., Masirani, R., Rutenfranz, J. & Seliger, V. 1978. Habitual physical activity and health. *World Health Organization Regional office for Europe*. European Series no. 6.

Anjos, L.A. Ferreira, J.A. & Damiao, J.J. 2007. Heart rate and energy expenditure during garbage collection in Rio de Janeiro, Brazil. *Cad Saude Publica* **23**(11).

Harlaar, J. Redmeijer, R. Tump, P. Peters, R. & Hautus, E. 2000. The SYBAR system: integrated recording and display of video, EMG, and force plate data. *Instruments & Computers* **3**2(1), 11–16.

Hettinger, T., Müller, H. & Gebhardt, H. 1989. Ermittlung des arbeits energieumsatzes beidynamischmuskularest arbeit. *Schrifteureiche der Bundesaustalt für Arbeitsschutz.* Dortmund, pp. 22, 1–80.

International standard. 2004. Ergonomics of the thermal environment – determination of metabolic rate. ISO 8996.

Kuzmin, J. 2014. PULSAVI method of determining employee energetic workload. Estonian University of Life Sciences. Master thesis. Tartu, 55.

Mikson, B. & Reppo, B. 2004. Energetic load of herdsmen influenced by operating environment of uninsulated cowshed. Advanced technologies for energy producing and effective utilization. *Proceedings of the International Conference*. Jelgava, pp. 151–156.

Mikson, E., Reppo, B. & Luik, E. 2005. Herdsman's work load rate and ability of work in a farm with an uninsulated cowshed. *Aktualni Zadaci Mehanizacije Poljoprivrede.* Zbornik radova*.* Opatija, pp. 495–505.

Nautras, A. 2015. Glassblower work environment and work ability. Estonian University of Life Sciences. Master thesis. Tartu, 80.

Priya, V.V.S., Johnson, P., Padmavathi, R., Subhashini, A.S., Ayyappan, R. & Surianarayanan, M. 2010. Evaluation of the Relationship between Workload and Work Capacity in Petrochemical and Tannery Workers – A Pilot Study. *Life Sciences and Medicine Research* LSMR-**19**.

Reppo, B., Leola, A., Lindsaar, I. & Nurmsalu, A. 1999. Milking parlour size, capacity and milker's energy load. *Aktualni Zadaci Mehanizacije Poljoprivrede.* Zbornik radova. Opatija, pp. 231–236.

Reppo, B. & Lindsaar, I. 2001. The milkers work load and energy expenditure on milking machine. *Agricultural Academic Society* **15**, Tartu, pp. 67–70.

Reppo, B. & Käämer, J. 1998. Arbeitszeitaufwand und energetische Belastbarkeit des Viehwärters bei der Entmistung der Viehanlage. *Agricultural Machinery, Building and Energy Engineer*, 24−29.

Smolander, J., Juuti, T., Kinnunen, M.L., Laine, K., Louhevaara, V., Männikkö, K. & Rusko, H. 2008. A new heart rate variablility-based method for the estimation of oxygen consumption without individual laboratory calibration: Application example on postal workers. *Appl Ergon* **39**(3), 325–331.

Tuure, V.M. 1991. Maatilan töiden fyysisen kuormittavuuden määrittäminen. Helsinki: Työtehaseura ry. 130.

Tuure, V.M. 1995. Työympäristö kylmissä pihotaissa. Helsinki: Helsingin Yliopista. 143.

Wilson, T.E. & Crandall C.G. 2011. Effect of thermal stress on cardiac function. *Exerc Sport Sci Rev* **39**(1), 12–17.

# Intra-annual dynamics of height growth of Norway spruce in Latvia

U. Neimane[1,*], J. Katrevics[1], L. Sisenis[2], M. Purins[1], S. Luguza[2] and A. Adamovics[1]

[1]Latvian State Forest Institute 'Silava', Rigas 111, LV 2169 Salaspils, Latvia
[2]Latvia University of Agriculture, Forest Faculty, Akademijas 11, LV 3001 Jelgava, Latvia
*Correspondence: una.neimane@silava.lv

**Abstract.** Norway spruce (*Picea abies* (L.) Karst.) is a tree species with the highest economic importance in northern Europe. Therefore, it is important to improve knowledge of the potential effects of climatic changes on the growth of this tree species. An essential part of the information is the tree's intra-annual growth cycle. There are comprehensive studies describing the formation of radial increments of coniferous trees; however, information on height growth in hemiboreal forests is scarce. The aim of our study was to characterize the intra-annual height growth of Norway spruce in Latvia. The data was collected from two Norway spruce trials located in in former arable and forest land in the central part of Latvia, including 89 and 68 open-pollinated families (respectively) of plus-trees. Weekly height increment measurements of 20 trees per family were carried out during the 9th growing season. Growth intensity culminated in $10 \pm 0.2$ mm day$^{-1}$, following similar trend, but resulting consistently in significantly different values between the trials; the higher growth intensity was observed in higher trees and families, which also showed higher frequency of lammas shoots, boosting their height superiority even further. Significant family effect on all coefficients of shoot elongation curves, described by Gompertz model, was found. Both tree height and height increment at family mean level was strongly correlated with the asymptote parameter ($r_{fam} = 0.93$, $P<0.01$) and the growth rate parameter ($r_{fam} = -0.70$, $P<0.01$).

**Key words:** *Picea abies* (L.) Karst, height growth, shoot elongation, growth intensity, open-pollinated family.

## INTRODUCTION

Norway spruce (*Picea abies* (L.) Karst.) is widely planted in northern and eastern Europe for timber production. Due to its large branch biomass (Libiete-Zalite & Jansons, 2011; Libiete-Zalite et al., 2016), logging residues are often collected in spruce stands and in some regions stumps are also extracted (Lazdins & Zimelis, 2012; Zimelis et al., 2012). Biomass exploitation is expected to flourish in the future, upgrading the commercial value of spruce stands (Bardulis et al., 2012; Kaleja et al., 2013). In most of the Baltic Sea region countries, active tree breeding programs exist and hence, improved seed material is available in order to boost increment and/or improve other traits of trees (Jansson et al., 2013; Irbe et al., 2015; Jansons et al., 2015a). Furthermore, vegetative propagation and fertilization of Norway spruce is possible at a commercial scale,

providing opportunities for further increase of the stands productivity (Jansons et al., 2016). The use of improved plant material (especially clones) increases the regeneration costs, therefore it is important to assess and minimize the potential risks, i.e., ensure adaptation to climatic changes, namely, increasing length of vegetation period and increasing temperature.

Temperature has been identified as the dominant environmental signal that triggers tree phenology (Körner, 2003). However, its impact on Norway spruce growth under average conditions is not easily detected, since trees respond less strongly to climatic variation, than to extreme conditions (Mäkinen et al., 2003). Long-term trends in the temperature-height growth relationship for coniferous trees, had been analysed using annual meteorological data and information on height increments from repeated measurements or destructive sampling (Kroon et al., 2011; Jansons et al., 2013a; 2013b; 2015b). Nevertheless, such an approach does not allow the determination of the exact moments during the vegetation period bearing critical influence of meteorological conditions – for this purpose detailed information on intra-seasonal height growth intensity is required (Jansons et al., 2014). The information would also allow the evaluation of the relative importance of length of the growth period vs. the growth intensity in the total length of annual height increment and thus providing more detailed information on climate adaptation.

Numerous studies have found a great variability of climatic adaptive traits for Norway spruce, both between provenances and between families within a provenance (Krutzdch, 1974; Danusevicius, 1999; Eriksson, 2008). These differences were influencing survival and stem quality of trees, mainly due to frost damages (Persson & Persson, 1992). Also shoot growth differences between provenances (Pollard & Logan, 1974; Skrøppa & Magnussen, 1993), and more recently between families have been found (Skrøppa & Steffenrem, 2015). However, no such studies including family components had been carried out in Latvia before. The aim of our study was to characterize the intra-annual height growth of Norway spruce in Latvia. Data from this initial study could be used to design more comprehensive research work in the future for predictions of the influence of climatic changes and consideration in tree breeding.

## MATERIALS AND METHODS

The study was carried out in two Norway spruce progeny trials in central Latvia, Rembate (56°46′N, 24°48′E) and Auce (56°29′N, 22°52′E), including 89 and 68 open-pollinated families (22 families common in both sites) of plus-trees selected from different regions of the country. The trials were planted in 2005, using 3 year-old bare-rooted plants, on fertile abandoned agricultural land, corresponding to *Oxalidosa* forest type according to classification used in Latvia (Bušs, 1976), cambisol according to FAO WRB soil classification (Nikodemus et al., 2008) with 2 x 2.5 m spacing in Rembate and on forest land with fertile drained mineral soil (*Myrtillosa mel.* forest type, arenosol) with 2 x 3 m spacing in Auce. Inter-annual height increment differences in those trials had been analyzed (Neimane et al., 2015), therefore this study focuses on intra-annual height growth. Measurements were carried out during 9th growing season of trees, bud-burst date assessed (visiting the site every 2 days until approximately half of the trees had bud-burst) and weekly height increment measurements carried out for 20 randomly selected trees per family, avoiding trees with browsing damage, insect damage or broken

top. Additional assessment was carried out at the end of September, marking the trees with lammas shoots. Daily temperature and precipitation data were obtained from the closest stations of Latvian Environment, Geology, and Meteorology Centre.

The non-linear Gompertz model was fitted per tree individually and per family (1)

$$f(A) = \alpha \exp(-\beta \exp(-kA))  \qquad (1)$$

where: $\alpha$ – asymptote parameter; $\beta$ – displacement parameter; $k$ – growth rate parameter and $A$ – day since beginning of the year. This model has been advised as being sufficient for the height growth curve development, in this case, using tree age as dependent parameter A (Fekedulegn et al., 1999).

The *t*-test was used to assess differences between groups of trees stopping the height growth at different time periods, as well as to evaluate differences in tree height, length of height increment and height growth intensity between the trees forming and not forming lammas shoots at the end of vegetation period. It was also used to assess differences in height increment between groups of trees with different times of growth cessation. The Pearson correlation test was used to assess the relationship of growth intensity between the trials, links between height and height increment, relationship between proportion of trees that had stopped the growth at certain period during the season and total length of height increment, as well as link between estimated Gompertz model parameters and family mean height and individual tree height. Analyses were carried out using the statistical package R 3.0.2. (R Core Team, 2013).

## RESULTS AND DISCUSSION

The trend of Norway spruce height growth intensity was similar in both sites (Fig. 1), as indicated by the strong correlation of mean values of this trait between the trials ($r = 0.91$, $P < 0.01$). Peak of height growth intensity was reached in the first two weeks of June, when it was $10 \pm 0.2$ mm day$^{-1}$ (mean, $\pm$ 95% confidence interval) in Rembate and $8 \pm 0.4$ mm day$^{-1}$ in Auce. Differences in growth intensity could partly be explained by temperature: in 73% of days in the assessed period it was higher in Rembate than in Auce, differences in diurnal mean was on average was 0.7°C, in minimum 0.4 °C and maximum 0.8°C (Fig. 1); similar temperature differences in the year prior to measurement were observed. In the analysis of formation of radial increment (secondary growth) of 75-year-old Norway spruce, Giagli et al. (2016) found, that the monthly minimum temperature in January-April, as well as the monthly maximum temperature during the growing period was a major factor affecting the average rate of cambial cell production and amount of precipitation, the main factor positively influencing the duration of it. Primary (apical) growth is also reported to be influenced by precipitation; however, in our study, no differences in precipitation sum between the meteorological stations closes to sites were found and the on-site measurements were not available. Hence it was not possible to evaluate the impact of inter-annual variation in precipitation in relation to the height increment.

The observed differences in growth may be caused not only by meteorological conditions, but presumably can be linked to other factors, e.g., soil conditions that have an effect on growth of trees. At the beginning of the season trees were significantly ($P < 0.01$) higher in Rembate than in Auce ($117 \pm 1.6$ cm and $72 \pm 2.1$ cm, respectively). These differences, in turn, affected total length of height increment (it was strongly correlated with initial tree height ($r = 0.78$, $P < 0.05$ and $r = 0.54$, $P < 0.05$ in Rembate and Auce, respectively), and therefore also the growth intensity.
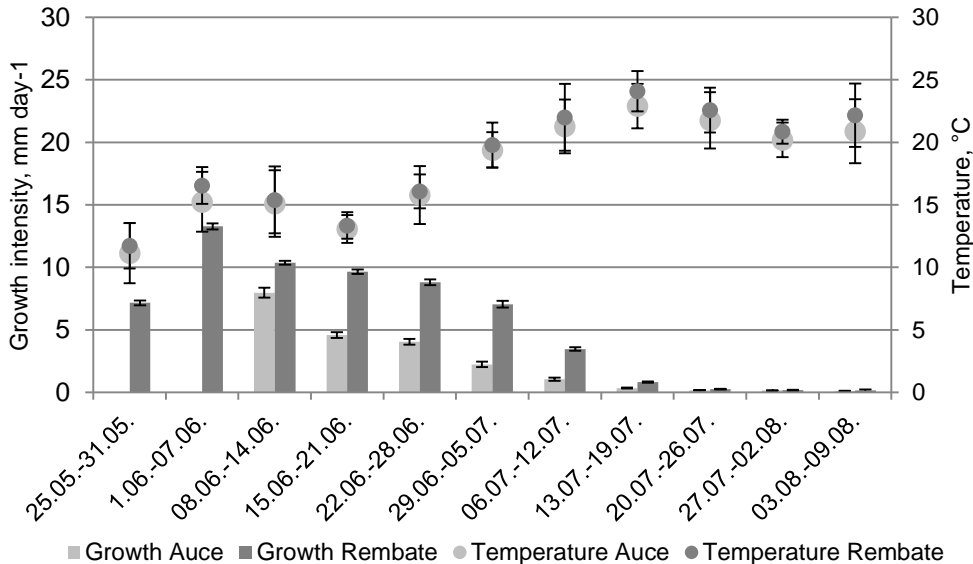


**Figure 1.** Growth intensity and diurnal mean temperature in Rembate and Auce.

Lammas shoots were observed for a relatively high proportion of trees in both sites: 14.0% in Rembate and 22.3% in Auce (Neimane et al, 2015). Trees with lammas shoots had similar trend in changes of growth intensity during the growth period than trees without them (Fig. 2). However, they were growing notably (on average by 23%) and, in most observation periods, also significantly ($P < 0.05$) faster. Consequently, trees with lammas shoots also had longer height increment, both in absolute and relative (as proportion of tree height) terms. As a result, height superiority of trees with lammas shoots, in comparison to those without, increased from 14% at the beginning of the season to 18% at the end of it in Rembate. Similarly, in Auce trees forming lammas shoots at the end of growing period had a 11% higher increment in comparison to trees that didn't and their relative length of height increment was significantly larger, 23% and 19%, respectively. A significant relationship between tree height and presence of lammas shoots was also previously reported in Latvia from an analysis of more than 100 stands (Neimane et al., 2016). Significant cumulative influence of lammas shoots on tree height had been found at the end of the 13th growing season trees with the lammas shoots in Norway spruce progeny trials were 14–20% taller than trees without it (Neimane et al, 2015). We can conclude, that a self-reinforcing loop is formed: larger, stronger trees have higher growth intensity and more frequently form lammas shoots, even further

increasing their height superiority. Genetic link between these traits was similar: proportion of trees with lammas shoots in the family correlated moderately and significantly both with tree height and height increment: $r_{fam} = 0.50$ (Neimane et al., 2015). Overall significant family effect on the proportion of trees showing lammas shoots was found; this was in accordance with the results of previous studies, reporting moderate (Hannerz, 1999) or high (Skrøppa & Steffenrem, 2015) heritability of this trait.
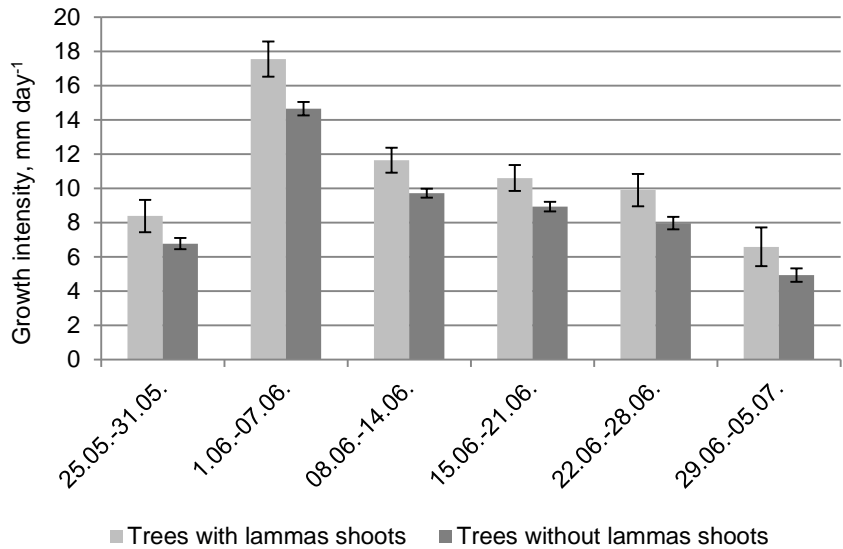


**Figure 2.** Growth intensity for trees with and without lammas shoots in Rembate.

Occurrence of lammas shoots at family level was linked not only to length of height increment, but also to timing of growth. Families that have early growth start and growth cessation were more likely to develop lammas shoots (Skrøppa & Steffenrem, 2015). Similar effect with regards to growth cessation was found also in our analysis.

Time of growth cessation had significant influence on the length of height increment (Fig. 3). Trees that stopped growth later had a 22% longer increment than the ones which stopped at the peak of growth cessation (13th – 26th of July). The largest trees tended to stop growing later in the season, presumably, indicating a cumulative positive impact of such a trait over time. Significant family effect on growth cessation was observed: family mean correlation between proportion of trees that had stopped their growth during last week of July or first week of August (mean $27 \pm 2.7$%, ranging from 0 to 62%) and the total length of height increment was positive, moderate and significant ($r_{fam} = 0.38$, $P < 0.01$). Also, Skrøppa & Steffenrem (2015) found, that families having later growth cessation at the age of 5 years were tallest at the age of 17 years. In this study as well as in studies in Sweden (Ekber et al., 1994) strong correlation between growth initiation and cessation was found. Both of these traits were clearly linked with frost damage, presumably explaining the observed differences in height growth between the families. In contrast, in our trials no frost damages were observed. Therefore, it is more likely, that the correlation observed in Latvias climatic conditions is a results of better (longer) use of the vegetation period.
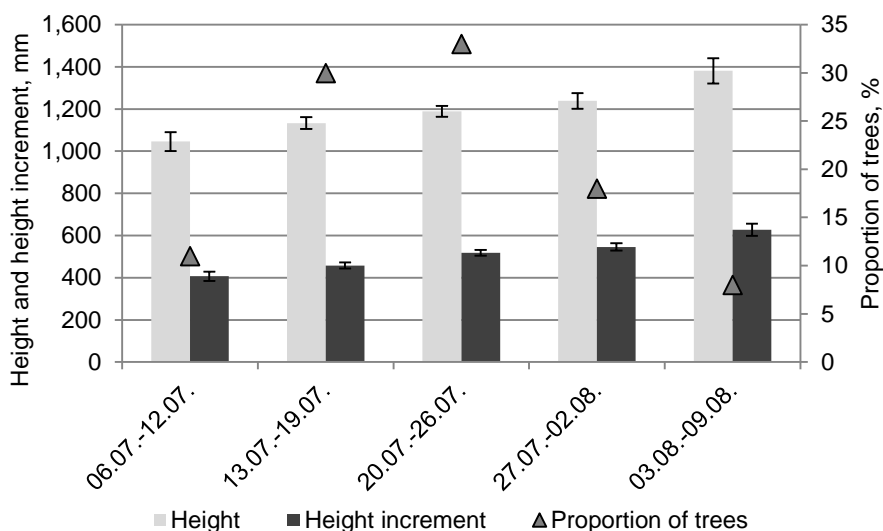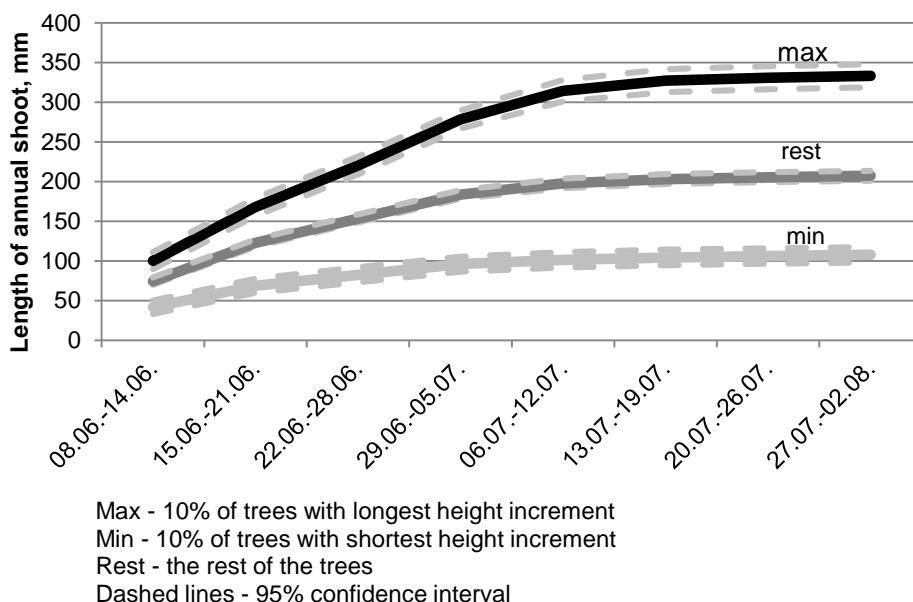
**Figure 3.** Height and height increment (without lammas shoot length) and proportion of trees that stopped growth at the particular period in Rembate.

Not only occurrence of lammas shoots and timing of growth cessation, but also growth intensity was an important factor affecting the length of height increment. Trees with longer height increment also showed higher growth intensity during the period of fastest growth, as well as a longer period of relative fast growth, as demonstrated by results from Auce trial (Fig. 4). This is in agreement with earlier findings by Skrøppa & Magnussen (1993) in the analysis of trials planted in Norway, noting that for spruce provenance from Baltic countries length of growth period and growth intensity were equally important in determining the total length of the annual shoot.

Differences in shoot elongation patterns had been found by numerous studies starting as early as that by Odin (1972) in the analysis of a few coniferous trees in Northern Sweden. To characterize these differences in Rembate (longer period of observations), a non-linear Gompertz model was fitted to height growth intensity data for each tree and family (median).

The models showed that intra-annual growth curves of studied trees and families differed notably. Family effect was significant on all model coefficients, indicating, that not only the intensity of height growth, but also the timing of its end was influenced by genetics even in the trial containing Norway spruce families from such a relatively small geographic area as Latvia. Both tree height and height increment at family mean level correlated strongly with the asymptote parameter ($r_{fam}$ = 0.93, $P<0.01$) and growth rate parameter ($r_{fam}$ = -0.70, $P<0.01$). Growth rate (i.e. rate of cell production) was also noted as a dominant factor in secondary growth, affecting xylem width of Norway spruce (Giagli et al., 2016). Shoot elongation curves in our trials were similar to those observed for other coniferous trees; however, the timing of end of active growth phase differed (Odin, 1972; Skrøppa & Magnussen, 1993; Rossi et al., 2006), presumably due to species differences.

Max - 10% of trees with longest height increment
Min - 10% of trees with shortest height increment
Rest - the rest of the trees
Dashed lines - 95% confidence interval

**Figure 4.** Dynamics of shoot elongation for trees with different annual height increment in Auce.

Results indicate, that selection of faster-growing families will most likely results in choice of genotypes with longer growth period (later cessation), higher growth intensity and higher probability to form lammas shoots. Since the length of vegetation period is expected to increase notably in the future, it is very likely that such genotypes will be capable of better utilization of the improved growing conditions. However, additional tests in growth chambers are needed to evaluate the probability that it might lead to increased frost damages, not observed in the trials currently. Even so it has been suggested that a single trial and year is sufficient for the estimation of breeding values of growth rhythm traits (Ekberg et al., 1991; Skrøppa & Steffenrem, 2015) additional information from trials in frost-prone sites would be important to draw wider conclusions.

## CONCLUSIONS

The trend of Norway spruce height growth intensity was similar at both sites. The length of height increment was significantly affected by both time of growth cessation and lammas shoots; trees with lammas shoots had a similar trend in changes of growth intensity during the growth period to trees lacking lammas, whereas they grew notably and, in most observation periods, significantly faster. Family effect was significant in tree height, height increment, as well as presence of lammas shoots. Significantly different shoot elongation patterns were found between families, indicating a potential for selection of the best-adapted genotypes.

# REFERENCES

Bardulis, A., Jansons, A. & Liepa, I. 2012. Below-ground biomass production in young stands of Scots pine (*Pinus sylvestris* L.). In Gaile, Z. (ed): *Proceedings of the 18th international scientific conference Research for Rural Development*, LLU, Jelgava, Latvia, pp. 49–54.

Bušs, K. 1976. Forest classification in Latvia Latvijas PSR meža tipoloģijas pamati. Zinātnes un ražošanas apvienība 'Silava', Rīga: LRZTIPI. 24 pp.

Danusevicius, D. 1999. Major influence of latitude and longitude on frost hardiness of the Baltic *Picea abies* (L.) Karst. provenances. In: *Early genetic evaluation of growth rhythm and tolerance to frost in Picea abies (L.) Karst.* Doctoral thesis, Swedish University of Agricultural Sciences, Uppsala, Silvestria, 103 pp.

Ekberg, I. Eriksson, G. & Nilsson, C. 1991. Consistency of phenology and growth of intra- and inter provenance families of *Picea abies*. *Scandinavian Journal of Forest Research*, DOI: 10.1080/02827589109382671.

Ekberg, I. Eriksson, G. Namkoong, G. Nilsson, C. & Norell, L. 1994. Genetic correlations for growth rhythm and growth capacity at ages 3–8 years for provenance hybrids of *Picea abies*. *Scandinavian Journal of Forest Research*, DOI: 10.1080/02827589409382809.

Eriksson, G. 2008. *Picea abies*. Recent genetic research. Uppsala, Department of Plant Biology and Forest Genetics, Swedish University of Agricultural Sciences, Sweden, 197p.

Fekedulegn, D., Mac Siurtain, M.P. & Colbert, J.J. 1999. Parameter estimation of nonlinear growth models in forestry. *Silva Fennica* **33**, 327–336.

Giagli, K., Gričar, J., Vavrčik, H. & Gryc, V. 2016. Nine-year monitoring of cambial seasonality and cell production in Norway spruce. *iForest* (early view). – doi: 10.3832/ifor1771-008 [online 2016-01-16] 8 p.

Hannerz, M. 1999. *Early testing of growth rhythm in Picea abies for prediction of frost damage and growth in the field.* Doctoral thesis, Swedish University of Agricultural Sciences, Uppsala, Silvestria, 85 pp.

Irbe, I., Sable, I., Nold, G., Grinfelds, U., Jansons, A., Treimanis, A. & Koch, G. 2015. Wood and tracheid properties of Norway spruce (*Picea abies* [L] Karst.) clones grown on former agricultural land in Latvia. *Baltic Forestry* **21**(1), 114–123.

Jansons, A., Donis, J., Danusevičius, D. & Baumanis, I. 2015a. Differential analysis for next breeding cycle for Norway spruce in Latvia. *Baltic Forestry* **21**(2), 285–297.

Jansons, A., Matisons, R., Baumanis, I. & Purina, L. 2013a. Effect of climatic factors on height increment of Scots pine in experimental plantation in Kalsnava, Latvia. *Forest Ecology and Management* **306**, 185–191.

Jansons, Ā., Matisons, R., Krišāns, O., Džeriņa, B. & Zeps, M. 2016. Effect of initial fertilization on 34-year increment and wood properties of Norway spruce in Latvia. *Silva Fennica* **50**(1), id 1346, 8 p.

Jansons, A., Matisons, R., Libiete-Zālīte, Z., Baders, E. & Rieksts-Riekstiņš, J. 2013b. Relationships of height growth of lodgepole pine (*Pinus contorta* var. *latifolia*) and Scots pine (*Pinus sylvestris*) with climatic factors in Zvirgzde, Latvia. *Baltic Forestry* **19**(2), 236–244.

Jansons, Ā., Matisons, R., Zadiņa, M., Sisenis, L. & Jansons, J. 2015b. The effect of climatic factors on height increment of Scots pine in sites differing by continentality in Latvia. *Silva Fennica* **49**(3), id 1262, 14 p.

Jansons, Ā., Zeps, M., Rieksts-Riekstiņš, J., Matisons, R. & Krišāns, O. 2014. Height increment of hybrid aspen *Populus tremuloides × P. tremula* as a function of weather conditions in south-western part of Latvia. *Silva Fennica* **48**(5), id 1124, 13 p.

Jansson, G. Danusevicius, D. Grotehusman, H. Kowalczyk, J. Krajmerova, D. Skrøppa, T. & Wolf, H. 2013. Norway spruce (Picea abies (L.) H. Karst.). In: Pâques L.E, editor. Forest tree breeding in Europe: current state-of-the-art and perspectives. *Managing forest ecosystems* **25**. Dordrecht: Springer Science+Business Media; p. 123–176.

Kaleja, S., Grinfelds, A. & Lazdins, A. 2013. Economic value of wood chips prepared from young stand tending. In Gaile, Z. (ed): *Proceedings of the 19th international scientific conference Research for Rural Development*, LLU, Jelgava, Latvia, pp. 66–72.

Körner, C. 2003. Carbon limitation in trees. *Journal of Ecology* **91**, 4–17.

Kroon, J., Ericsson, T., Jansson, G. & Andersson, B. 2011. Patterns of genetic parameters for height in field genetic tests of *Picea abies* and *Pinus sylvestris* in Sweden. *Tree Genetics & Genomes* **7**(6), 1099–1111.

Krutzsch, P. 1974. The IUFRO 1964/68 provenance test with Norway spruce (*Picea abies* (L.) Karst.). *Silvae Genetica* **23**, 58–62.

Lazdins, A. & Zimelis, A. 2012. System analysis of productivity and cost of stump extraction for biofuel using MCR 500 excavat or head. In Gaile, Z. (ed): *Proceedings of the 18th international scientific conference Research for Rural Development*, LLU, Jelgava, Latvia, pp. 62–68.

Libiete-Zalite, Z. & Jansons, A. 2011. Influence of genetic factors on Norway spruce (*Picea abies* (L.) Karst.) aboveground biomass and its distribution. In Gaile, Z. (ed): *Proceedings of the 17th international scientific conference Research for Rural Development*, LLU, Jelgava, Latvia, pp. 39–45.

Libiete-Zalite, Z., Matisons, R., Rieksts-Riekstins, J., Prieditis, A., Jansons, J., Smilga, J., Aizupiete, G. & Jansons, A. 2016. Aboveground biomass equations of 40 year old Norway spruce in Latvia. *Baltic Forestry* (accepted).

Mäkinen, H., Nojd, P. & Saranpaa, P. 2003. Seasonal changes in stem radius and production of new tracheids in Norway spruce. *Tree Physiology* **23**, 959–968.

Neimane, U., Zadina, M., Jansons, J. & Jansons, A. 2016. Environmental factors affecting formation of lammas shoots in young stands of Norway spruce in Latvia. *Baltic Forestry* (accepted).

Neimane, U., Zadina, M., Sisenis, L., Dzerina, B. & Pobiarzens, A. 2015. Influence of lammas shoots on productivity of Norway spruce in Latvia. *Agronomy Research* **13**, 354–360.

Nikodemus, O. Kasparinskis, R. & Tabors, G. 2008. Soil mapping in Latvia according to the international FAO WRB 2006 soil classification. Problems and solutions. *Vagos,* **80,** 68–74.

Odin, H. 1972. Studies of increment rhythm of Scots pine and Norway spruce. *Studia Forestalia Suecica* **97**, 32 p.

Persson, B. & Persson, A. 1992. Survival and quality of Norway spruce (*Picea abies* (L.) Karst.) provenances at the three Swedish sites of the IUFRO 1964/68 *Picea abies* provenance experiment. *Report*, **29**, Dept For Yield Research, SLU, Sweden. 67 p.

Pollard, D.F.W. & Logan, K.T. 1974. The role of free growth in the differentiation of provenances of black spruce *Picea mariana* (Mill.) B.S.P. *Canadian Journal of Forest Research* **4**(3), 308–311.

R Core Team. 2013. *R: A language and environment for statistical computing*. R Foundation for Statistical Computing, Vienna, Austria. URL http://www.R-project.org/.

Rossi, S., Deslauriers, A., Anfodillo, T., Morin, H., Saracino, A., Motta, R. & Borghetti, M. 2006. Conifers in cold environments synchronize maximum growth rate of tree-ring formation with day length. *New Phytologist* **170**, 301–310.

Skrøppa, T. & Magnussen, S. 1993. Provenance variation in shoot growth components of Norway spruce. *Silvae Genetica* **42**, 111–120.

Skrøppa, T. & Steffenrem, A. 2015. Selection in a provenance trial of Norway spruce (*Picea abies* L. Karst) produced a land race with desirable properties. *Scandinavian Journal of Forest Research*, DOI: 10.1080/02827581.2015.1081983.

Zimelis, A., Lazdans, V. & Lazdiņa, D. 2012. Evaluation of forest regeneration results after stump extraction in joint stock company 'Latvian state forests'. In Gaile, Z. (ed): *Proceedings of the 18th international scientific conference Research for Rural Development*, LLU, Jelgava, Latvia, pp. 69–72.

# Optimization of vehicles' trajectories by means of interpolation and approximation methods

D. Novák[1,*], J. Pavlovkin[1], J. Volf[2] and V. Novák[2]

[1]Matej Bel University, Faculty of Natural Sciences, Department of Technology, Tajovského 40, SK 974 01 Banská Bystrica, Slovakia
[2]Czech University of Life Sciences Prague, Faculty of Engineering, Department of Electrical Engineering and Automation, Kamýcká 129, CZ 16521 Prague 6, Czech Republic
*Correspondence: daniel.novak@umb.sk

**Abstract.** The need to optimize the trajectory of vehicles is still highly topical, regardless weather the means of transport are robots, forklifts or road vehicles. It is not only important the safety by passing obstacles, but also the energy balance, i.e. the energy expended on the movement of the vehicle and on the change of its direction. This paper presents a mathematical approach to solving this problem through interpolation and approximation curves.

**Key words:** means of transport, trajectory optimization, interpolation curves, approximation curves.

## INTRODUCTION

Movement of vehicles only rarely proceeds in a straight line. On the contrary – regardless weather transporting material or people into smaller or larger distances, it is almost always necessary to deal with obstacles on the path. This includes both safe avoiding obstacles and selecting the best possible trajectory from several possible options. Choosing the optimal trajectory makes thus the movement safer, may reduce the transportation costs and last but not least it may also save time.

Mathematically it is possible to perform an interpolation or an approximation of the trajectory. These mathematical procedures are used in this case as generating principles, which allow to model continuous arcs of the line. While by an interpolation the curve always passes all the associated points, by an approximation the curve passes only the first and last point, and does not have to include necessarily other associated points, which depends particularly on the given approximation function. From the mathematical point of view, it does not matter weather it is about a movement of a mobile robot in a production hall, a forklift in a storehouse or a road vehicle on a street (Kvasnová, 2008).

## MATERIALS AND METHODS

### Ferguson interpolation curve
Ferguson interpolation curve of third degree allows an easy following of individual sections. The mathematical description of Ferguson curve bases on the position vectors

$\vec{G}$ a $\vec{H}$, respective points G and H, as well as on the tangent vectors $\vec{g}$ and $\vec{h}$ of the curve at these points. Ferguson curve is then given by equation (1) (Farin, 1993),

$$P(v) = \vec{m}.v^3 + \vec{n}.v^2 + \vec{p}.v + \vec{q},$$ (1)

where: $\vec{P}(v)$ – position vector of a point of the curve; $\vec{m}$, $\vec{n}$, $\vec{p}$, $\vec{q}$ – coefficients' vectors; v – a parameter, for which is true that $\vec{P}(0) = \vec{G}$ a $\vec{P}(1) = \vec{H}$.

Performing the corresponding calculation, we obtain the vectors $\vec{m}$, $\vec{n}$, $\vec{p}$, $\vec{q}$, expressed by four equations (2), (3), (4) a (5)

$$\vec{m} = 2\vec{G} - 2\vec{H} + \vec{g} + \vec{h}$$ (2)

$$\vec{n} = -3\vec{G} + 3\vec{H} - 2\vec{g} - \vec{h}$$ (3)

$$\vec{p} = \vec{g}$$ (4)

$$\vec{g} = \vec{G}$$ (5)

Ferguson curve can also be expressed in form:

$$\vec{P}(v) = A(v)\vec{G} + B(v)\vec{H} + C(v)\vec{g} + D(v)\vec{H}$$ (6)

where: $A(v)$, $B(v)$, $C(v)$ a $D(v)$ are third degree polynomial, for which is true:

$$A(v) = 2v^3 - 3v^2 + 1$$ (7)

$$B(v) = -2v^3 + 3v^2$$ (8)

$$C(v) = v^3 - 2v^2 + v$$ (9)

$$D(v) = v^3 - v^2$$ (10)

If we select in equation (7), (8), (9) and (10) the parameter $v$ of the interval {0,1}, then we obtain a smooth curve that starts at point G and ends at point H. This type of curves is relatively suitable for modeling the trajectory of vehicles, since it ensures – due to appropriate choice of control points – safe passing of obstacles, although the length of the trajectory may increase.

**Bezier interpolation curve**

Bezier interpolation curves allow simple networking of following segments because the first two and the last two control points define a tangent to the curve at the endpoints. The touch vectors at the endpoints are determined by equations (11) and (12) (Pavlovkin & Jurišica, 2003a):

$$C'(0) = n(B_1 - B_0) \tag{11}$$

$$C'(1) = n(B_n - B_{n-1}), \tag{12}$$

where: $n$ is the degree of the curve.

On the other hand, Bezier interpolation curve may cause – by selecting identical control points as by Ferguson curve – a risk of collision with an obstacle, moreover, the length of the trajectory increases.

**Interpolation B-Spline curve**

B-Spline curves exhibit many useful properties, in particular the parametric continuity $C^2$ of third degree curves, so that they can also be used as interpolation curves. The parametric continuity $C^i$ defines in which way are the respective curves connected; the index of the continuity indicates the equality of respective $i$-derivates of the end-points of the individual curves; i.e. the continuity $C^0$ indicates that the curves are connected with an edge (the first derivatives are not equal), the continuity $C^1$ enables a smoother connection of the curves (as the first derivatives are equal) but with different convexity or concavity and thus with an abrupt change of centripetal acceleration. The continuity $C^2$ ensures that the connected curves have the same convexity (concavity), as the both second derivates are equal.

The computation can be performed by means of two methods – matrix inversion or searching for Bezier's control points.

Matrix inversion is a general method which can be used for all curves. If we can – based on the control points – calculate the coordinates of some points on the curve, then it is possible by the inverse procedure to determine the control points from known curve's points, too. The point, where the respective segments are continuing, lies in the anti-centroid of the triangle, defined by three consecutive control points.

Searching for Bezier's control points is basically an extension of Cardinal curves method, allowing to obtain a continuous $C^2$ curve. Bezier's control points $V_i$ are located at the distance $d_i$ from the interpolation points $P_i$; this ensures $C^1$ continuity. If the curve $C^2$ is to be continuous, it must be satisfied (13):

$$P_1 - 2(P_1 - d_1) + (P_0 + d_0) = (P_2 - d_2) - 2(P_1 + d_1) + P_1 \tag{13}$$

The sections $d_0$ and $d_n$ we have to choose. Subsequently, we calculate the coefficients $A_i$ and $B_i$ and then we recursively calculate also the remaining sections $d_{i-1} = A_{i-1} + B_{i-1}.d_i$, thus obtaining the Bezier's control points. The possibility to choose the tangential vectors at the endpoints is a great advantage by vehicles, since the initial vector should have the same direction, as the vehicle is oriented. Thus it will not be necessary to turn the vehicle before starting the movement along the trajectory.

B-Spline curves obtained by both of these methods are almost the same (as we are looking for the same control points), and they differ only at the edges (different choice of tangential vectors at the endpoints). However, the method of searching for Bezier's control points is more preferred, as it is significantly faster than the matrix inversion method. Additionally, interpolation B-Spline curves are like Bezier curves susceptible to creating "loops" and therefore they are used only where the development of such drawbacks does not mind or is excluded (Demidov, 2003; Pavlovkin & Jurišica, 2003a; Boonporm, 2012).

**Bezier approximation curves**

General Bezier curves allow an approximation of $n+1$ given points by an *n-degree* curve. The curve is described by the equation (14):

$$C(t) = \sum_{i=0}^{n} B_i^n(t) P_i \qquad t \in\, <0,1>$$
(14)

The basis functions of Bezier curves $B_i^n(t)$ constitute Bernstein base polynomials:

$$B_i^n(t) = \binom{n}{i}^i (1-t)^{n-1}$$
(15)

General Bezier curves have a relatively high smoothening ability, so that they are only marginally nearing to the individual control points. This is considerably disadvantageous in some applications, but elsewhere it may be useful; it depends on the specific conditions in which the vehicle is moving.

The general disadvantage of Bezier curves is the non-locality of changes – each point of the curve is influenced by all control points; i.e. changing an individual control point changes the shape of the whole curve. Therefore Bezier curves often consist of shorter segments. This way it is possible to obtain the locality of changes and to simplify the difficulty of the calculation, while maintaining all the advantages of the curves. To connecting individual sections, Bezier curves of third degree are mostly used. Basis functions can be determined in advance, since the order of the curve is always known at the beginning (Hwang et al., 2003).

**B-Spline**

Classic B-Spline curve is formed by linking Coons curves in such a way that the last three control points of one segment are identical to the first three points of the next section. In most cases there are used Coons curves of the third degree. The first segment is then determined by the points $P_0$, $P_1$, $P_2$ and $P_3$, the second segment by the points $P_1$, $P_2$, $P_3$ and $P_4$. The last point of the first segment and the first point of the second segment are identical, as they lie in the anti-centroid of the same triangle; thus the $C^0$ continuity is ensured (Demidov, 2003).

Joining of the individual sections is very smooth. B-Spline curves ensure the continuity $C^{k-1}$ in the joint point, where $k$ means the degree of the curve; i.e. B-Spline curve of the third degree guaranties a $C^2$ continuity. Using a Bezier curve, only the $C^1$ continuity is ensured. B-Spline curve therefore retains all the advantages of Bezier curves and it is a lot smoother when connecting the individual sections. B-Spline curve,

however, has one major disadvantage – it does not pass the outermost points of the control polynomial. It can be removed by any of the control points will be multiple (Demidov, 2003).

If one control point is double, then the curve is significantly closing to that control point, and in a certain section it may even overlap the control polynomial. If the control point is triple, then the curve passes directly through this control point and it in the surroundings of such point it is identical with the control polynomial; however, this feature is useful only for the endpoints. So if the endpoints of the control polynomial are triple, the curve will interpolate the endpoints. The disadvantage is that near the endpoints the curve degenerates into line segments and it loses its smoothness. Another, more efficient method is to use different basis functions for the first two and the last two sections of the curve so that the curve passes through the endpoints. However, this method requires at least seven control points, so it cannot be used for simpler trajectories (Elbanhawi et al., 2015).

**Interpolation by Ferguson curve**

The interpolation by Ferguson curve, which is depicted in Fig. 1, is a suitable method for optimizing specific vehicles' trajectory, but it must be expected that the length of the trajectory gets extended compared to the direct path. The vehicle does not have to stop at the edges of the control polynomial; it has only to slow down sufficiently respected to the radius of turn. With this option of control points, the trajectory passes in a safe distance from individual obstacles and thus the risk of collision with one of the obstacles is eliminated.
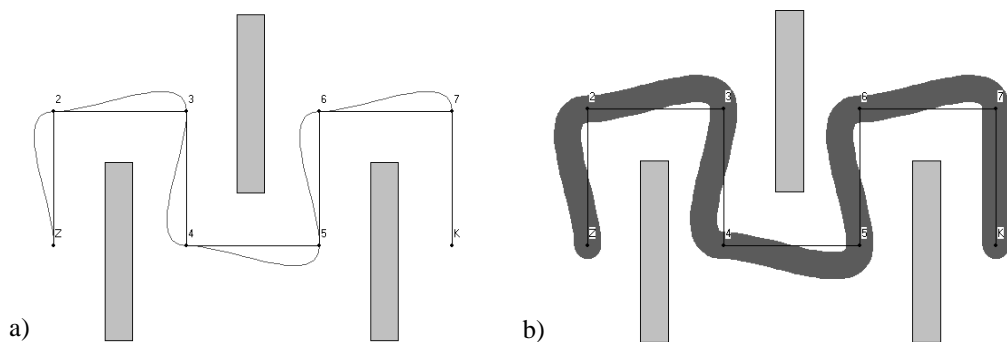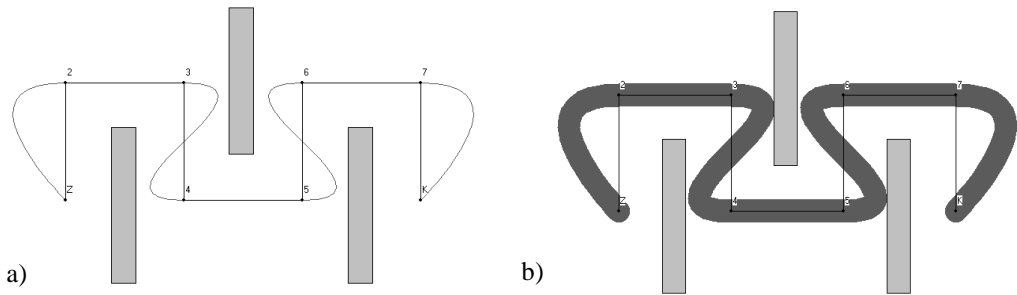


**Figure 1.** Interpolation by Ferguson curve. a) for a pointwise vehicle; b) for a real vehicle.

The calculation of the interpolation is always performed every second point. An element of the array has the coordinates of the point (x, y); an empty element of the array has the coordinates (-1, -1). The drawing of the interpolation curve is solved by means of the C++ graphics program Borland Delphi 2.0. This program draws the Ferguson curve basing on two given points and respective direction vectors at these points.

**Interpolation by Bezier curve**

Interpolation by Bezier curve, shown in Fig. 2, is by the specified setup of control points inappropriate for generating the trajectory of a vehicle, as it causes collisions with obstacles. Total length of the path is also substantially greater than by the interpolation by Ferguson curve. For use in a real environment, it would be necessary to the change are the coordinates of points 3, 4, 5 and 6 to achieve the desired path. The collision-free path of the vehicle for this way changed points is demonstrated in Fig. 3. From the comparison of trajectories in Fig. 2 and Fig. 3 it is apparent that the selection of the supporting points affects significantly the length and the shape of the trajectory. However, a suitable arrangement of the individual control points enables creating a usable trajectory, provided it is possible in respect to the location of the obstacles.



**Figure 2.** Interpolation by Bezier curve. a) for a pointwise vehicle; b) for a real vehicle.
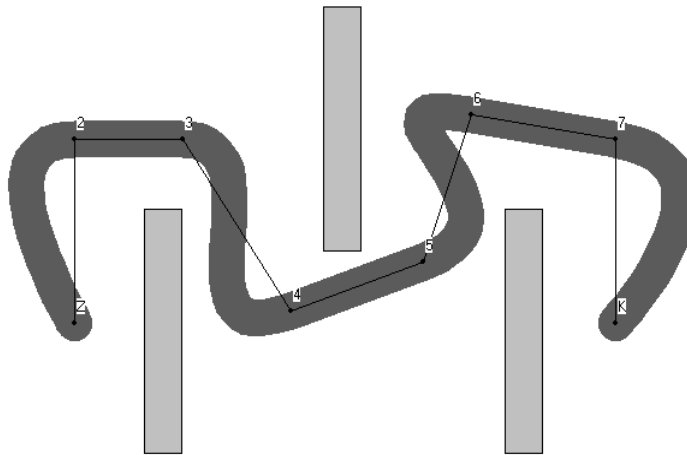


**Figure 3.** Interpolation by Bezier curve after changing the coordinates of the control points.

**Approximation by Ferguson curve**

Unlike the preceding interpolation cases, by an approximation the trajectory does not necessarily include the control points along the path. Approximation by Bezier curve, which is depicted in Fig. 4, is more convenient and shorter than the preceding two cases, but a large-size vehicle may interfere with an obstacle, as shown in Fig. 4b. The possibility of such a conflict can be avoided by changing the coordinates of the control

point 4; the subsequent change in trajectory is demonstrated in Fig. 5. In such setup of control points, it is also possible by an appropriate shifting of the point 6 to shorten the overall length of the trajectory.



a)                                                                    b)
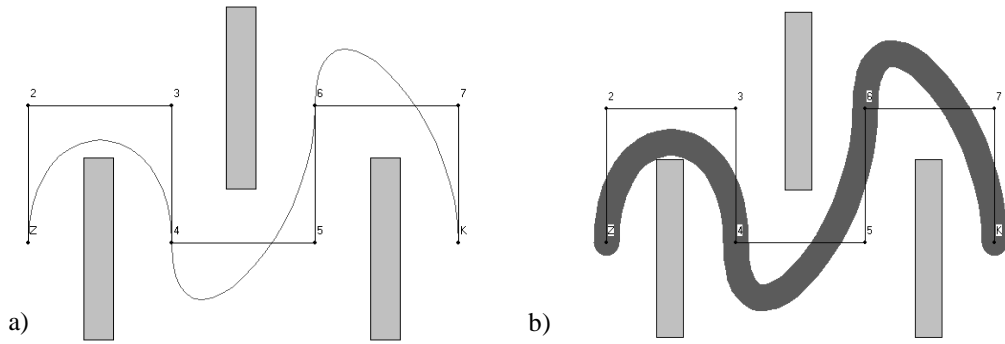
**Figure 4.** Approximation by Ferguson curve. a) for a pointwise vehicle; b) for a real vehicle.
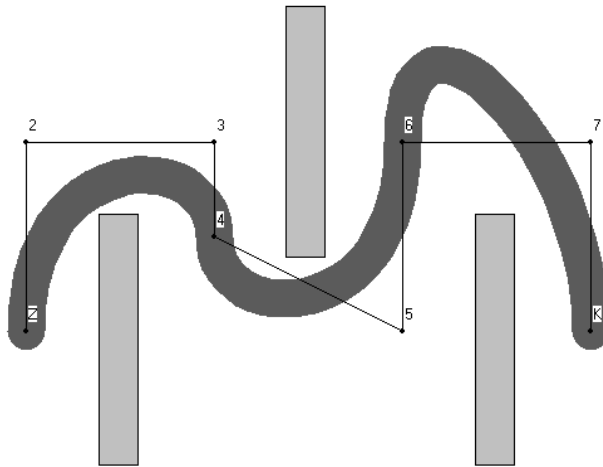


**Figure 5.** Approximation by Ferguson curve after changing the control point 4.

### Approximation by Cubic B-Spline

By approximation of a piecewise linear trajectory by means of Cubic B-Spline curve we obtain a trajectory, which is shorter and smoother, and thus less time- and energy-consuming. The vehicle moves smoothly along such trajectory, i.e. with a smooth change of direction and speed of its movement, as depicted in Fig. 6 (Pavlovkin & Sudolský, 1999; Demidov, 2003).

The basic principle of generation of B-Spline curves is that we define Bezier curves of degree $n$ at intervals $(u_i, u_{i+1})$; where $n$ is the degree of the polynomial of the respective B-Spline curve and $L$ is the number of segments of the B-Spline. So we create a sequence of points, namely the sequence $u_0 \ldots u_{L+2n-2}$. Not all points $u_i$, however, are different; if $u_i = u_{i+1}$ then it is a multiple point.
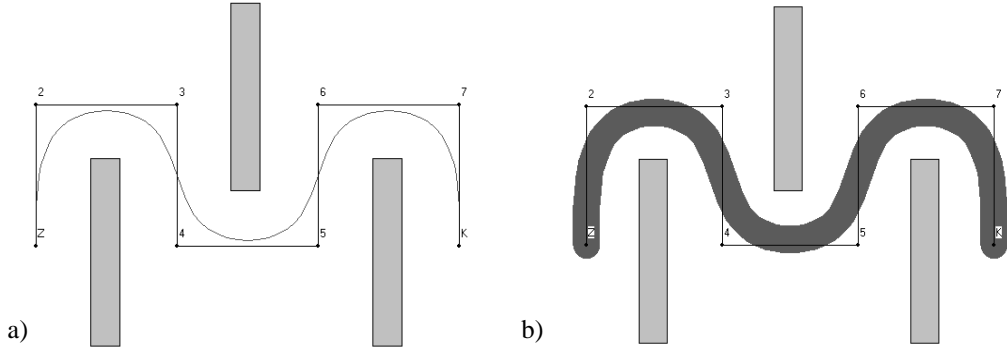
**Figure 6.** Approximation by Cubic B-Spline. a) for a pointwise vehicle; b) for a real vehicle.

To define B-Spline we use the interval $(u_{n-1}, u_{n+L-1})$ as its domain, these points are called domain points, while $L$ means the potential number of segments of the curve. If all domain points are simple, then $L$ is also the number of domain intervals. For every multiplicity of a domain point, the number of domain intervals reduces by one. The sum of multiplicity of all domain points corresponds with $L$, as it true that:

$$\sum_{i=n-1}^{L+n-1} r_i = L+1,\tag{16}$$

where: $r_i$ means the multiplicity of domain points $u_i$.

For generating the B-Splines we used De Boor's algorithm. Let's true that: $u \in [u_I, u_{I+1}] \subset [u_{n-1}, u_{L+n-1}]$. We define:

$$d_i^k(u) = \frac{u_{i+n-k} - u}{u_{i+n-k} - u_{i-1}} d_{i-1}^{k-1}(u) + \frac{u - u_{i-1}}{u_{i+n-k} - u_{i-1}} d_i^{k-1}(u)\tag{17}$$

where $k = 1,...,n-r$ and $i = I-n+k-1,...,I+1$
which is the degree of B-Spline given the parametr $u$.

$$s(u) = d_{I+1}^{n-r}(u),\tag{18}$$

while $d_i^0(u) = d_i C.$

## RESULTS AND DISCUSSION

To analyze the wide range of described approximation and interpolation curves, we used our self-created computer program 'VD' (abbreviation for "path draw" in Slovakian language). The graphical interface of this program and a comparison of some generated curves are depicted in Fig. 7. Within this program, we defined the known position of the obstacles as well as the control points of the trajectory. Then we selected a mathematical model of the trajectory by a preset approximation or interpolation curve formula, we

obtained a graphical and a numerical result. The results were subsequently analyzed graphically and numerically.
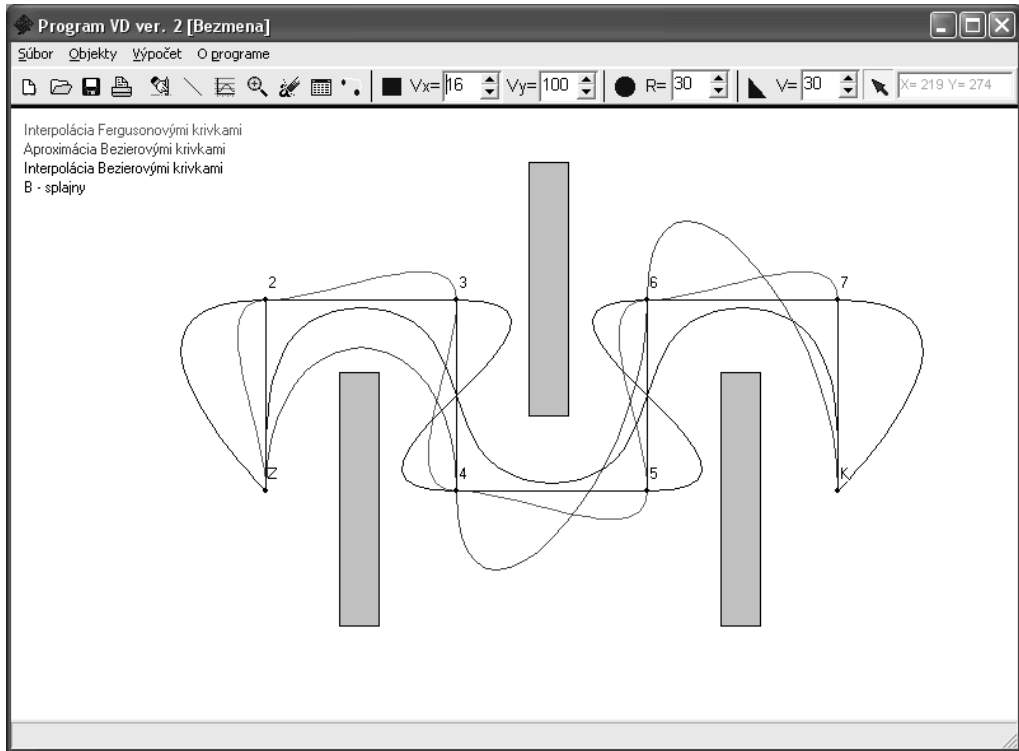


**Figure 7.** Graphical interface of the program VD with examples of trajectories.

The overall length of the trajectory between points $P_0$ and $P_n$ is defined by equation (19):

$$d(P_0, P_n) = \sum_{i=0}^{n} \int_{a_i}^{a_{i+1}} \sqrt{1 + \left(f_i^I(x)\right)^2}\, dx \qquad (19)$$

where: $P_0$ , $P_n$ – start and end point of the trajectory; $a_i$ – individual section of the trajectory; $f_i(x)$ is the respective mathematical function formula of the curve.

To investigate the radius of turn for a selected point of the trajectory – which may be necessary due the specific limitations of the vehicles, the formula (20) is used:

$$R^2 = \frac{\left(1 + \left(f^I(x)\right)^2\right)^3}{\left(f^{II}(x)\right)^2} \qquad (20)$$

where: $R$ means the radius of curvature of the trajectory at a specicic point and; $f(x)$ is the mathematical function formula of the curve.

Basing on the graphical analysis of the curves and on calculations using the preceding formulas, an overall comparison of the various options optimizing of the vehicles' movement between obstacles gave the best results for the approximation based

on Cubic B-Spline. The mathematical model of such trajectory exhibits fluency, both in terms of necessary speed changes, and regarding the smoothness of the change of direction. Important is also the fact that of all the analyzed trajectories this one is the shortest, which yields energy saves. Although the shortening of the trajectory need not be regarded as considerable, compared to other options, the total saving of energy may be high, in particularly over a longer period of time or if the same trajectory repeats regularly several times (stock houses, factories, agricultural activities) (Pavlovkin & Jurišica, 2003b). Finally, it has to be pointed out that the trajectory approximated by Cubic B-Spline exhibits relative high level of safety, as it passes all the obstacles – unlike some other trajectories – with sufficient distance and virtually eliminates any possibility of collision of the vehicle with an obstacle (Kvasnová, 2014).

## CONCLUSIONS

We analyzed the trajectory of a vehicle along a defined path between obstacles. We used mathematical simulations of various approximation and interpolation curves by means of our own program 'VD'. Based on the results, we concluded the most convenient method – considering the smoothness of the trajectory, its length, shape and obstacle clearance – using the approximation by Cubic B-Spline curve.

The current development of defining and optimizing vehicles' trajectories prefers a direct control through a system of sensors placed directly on vehicles. Sensors provide information about possible obstacles along the path; the information is evaluated by a computer installed in the vehicle, which controls the vehicle to change flexibly its trajectory (Fu et al., 2013). Although the technical level of sensors has considerably improved and their price has sunk, this method is, however, still technically more complicated, which poses an enhanced risk of malfunctions and increases acquisition and maintenance costs. Therefore, if the layout of obstacles is permanent, the approximation and interpolation methods described in the article to define its trajectory are still useful. In such a layout, vehicles may be equipped only with a simple 'emergency stop sensor' to increase safety and to avoid unpredicted collisions.

## REFERENCES

Boonporm, P. 2012. Online path replanning of autonomous mobile robot with Spline based algorithm. In: *IPCSIT*. IACSIT Press, Singapore, Vol. 23. http://www.ipcsit.com/vol23/11-ICSMO2012-W0022.pdf. Accessed 25.3.2015.

Demidov, E. 2003. *An Interactive Introduction to Splines*. http://www.people.nnov.ru/fractal/Splines/Intro.htm. Accessed 8.8.2015.

Elbanhawi, M., Simic, M. & Jazar, R.N. 2015. Continuous Path Smoothing for Car-Like Robots Using B-Spline Curves. *Journal of Intelligent & Robotic Systems* **80**(1), 23–56.

Farin, G. 1993. *Curves and Surfaces for Computer Aided Geometric Design. A Practical Guide*. Academic Press, Inc.

Fu, W., Hadj-Abdelkader, H. & Colle, E. 2013. Reactive collision avoidance using B-spline representation: Application for mobile robot navigation. In: *European Conference on Mobile Robots (ECMR) 2013*, Barcelona, pp. 319–324.

Hwang, J.H., Arkin, R.C. & Kwon, D.S. 2003. Mobile robots at your fingertip: Bezier curve on-line trajectory generation for supervisory control. In: *Intelligent Robots and Systems* **2**, 1444–1449.

Kvasnová, P. 2008. Universal loader and the possibilities of its use / Univerzálny nakladač a možnosti jeho využitia. In: *Technika odpadového hospodárstva*. Technická univerzita vo Zvolenu, Zvolen, Slovakia, pp. 70–76 (in Slovak).

Kvasnová P. 2014. Evaluation of risk factors / Posudzovanie rizikových faktorov. In: *Bezpečná práca: dvojmesačník pre teóriu a prax bezpečnosti práce* **45**(5), 3–9 (in Slovak).

Pavlovkin, J. & Jurišica, L. 2003a. Mobile robot navigation (1) / Navigácia mobilného robota (1). In: *AT&P JOURNAL* **2**, 72–73 (in Slovak).

Pavlovkin, J. & Jurišica, L. 2003b. Mobile robot navigation (2) / Navigácia mobilného robota (2). In: *AT&P JOURNAL* **3**, 100 (in Slovak).

Pavlovkin, J. & Sudolský, M. 1999. Aplikácie B-splajnov na plánovanie lokálnych ciest mobilného robota. In: *ROBTEP `99 Automatizacion – Robotics in Theory and Practice*. Strojná fakulta Technickej univerzity v Košiciach, Košice, Slovakia, pp. 215–220 (in Slovak).

# Comparison of methods for fuel consumption measuring of vehicles

J. Pavlu[*], V. Jurca, Z. Ales and M. Pexa

Czech University of Life Sciences Prague, Faculty of Engineering, Department for Quality and Dependability of Machines, Kamycka 129, 165 21 Prague 6, Czech Republic
[*]Correspondence: jindrichpavlu@seznam.cz

**Abstract.** Essential task for companies in these days is to reduce operating costs and optimization of workflow processes of machines, in order to increase the competitiveness and productivity. Telematics systems is relatively widespread and utilized for fleet management and enables collecting a wide range of operating parameters. One of the monitored parameters of operating costs is fuel consumption of machines. The collection of data on fuel consumption can be realized using various methods. By default, the fuel consumption data is transmitted from CAN–BUS which does not always coincide with the value of the real fuel consumption. Another possible way of fuel consumption monitoring is realized via installation of capacitance probe mounted directly into the fuel tank. The principle of measurement of these two methods is different, and each method has its own specifics. For instance, a capacitive probe enables detection of non-standard decreases of fuel level in the fuel tank. The aim of this paper is to compare the methods of fuel consumption measuring via the CAN–BUS and utilization of capacitive fuel probe. Measuring unit Gcom was used for collecting data which sends data of fuel consumption to the server in real–time. The purpose of this paper is to prove or disprove the hypothesis that measured fuel consumption is statistically significant between measuring via CAN-BUS compared to capacitance probe.

**Key words:** Fuel consumption, capacitance probe, CAN-BUS, telematics system.

## INTRODUCTION

There are various methods for measuring fuel consumption, which are based on detection of the fuel level in fuel tank. These methods for example include measurements using mechanical floats, ultrasonic sensors, digital rulers with mechanical float, pressure sensors, relay floats. Mentioned methods of measuring fuel level have a number of disadvantages. Mechanical floats are often unreliable due to the use of mechanical components. Ultrasonic sensors may have difficulty with obtaining a proper signal at wavy surface of fuel level and are also more expensive. Pressure sensors have problems with the accuracy of measurement when overpressure occurs in the fuel tank due to temperature changes. Measuring accuracy of relay floats is relatively low (Partner mb, 2010).

Nowadays transport companies routinely use mainly two ways of measuring fuel consumption with respect to the acquisition price, reliability, accuracy of measuring and control of unfair methods of treating fuels.

By default, the fuel consumption data is transmitted from CAN–BUS which does not always coincide with the value of the real fuel consumption. Another possible way of fuel consumption monitoring is realized via installation of capacitance probe mounted directly into the fuel tank (Li & Fan, 2007). The principle of measurement of these two methods is different, and each method has its own specifics. For instance, a capacitive probe enables detection of non-standard decreases of fuel level in the fuel tank.

The data from both of these methods are transferred telematics systems and via web interface are available in real time (Daniel et al., 2011).

The purpose of this paper is to prove or disprove the hypothesis that measured fuel consumption is statistically significant between these two methods. Whether, there is the difference between fuel consumption measured via CAN–BUS compared to capacitance probe.

## MATERIALS AND METHODS

Telematics system is an eminent technology which merges telecommunications and informatics. This blending of wireless telecommunication technologies along with computers is done ostensibly with the goal of conveying information over vast networks to handle vehicle information. The entire system consists of TeCU (Telematics Control Unit) which is called Gcom, server and webpage application to monitor and to sense ample information's received from vehicle. Telematics Control Unit (TeCU) has to be designed and developed, which could be used in real time and off time monitoring, tracking and reporting system (Dhivyasri et al., 2015).

Data about fuel level in the tank were transmitted each 120 s from capacitance probe CAP04. From the CAN–BUS were transmitted data with the same period, but fuel rate was recorded by Gcom each 1 s.

Observed vehicles for experiment were chosen from a transport company, which has a vehicle fleet of 150 vehicles. From the total number of vehicles were selected vehicles with operating time of more than 60,000 km over a period of six months.

Records from vehicle re–fueling were compared with data measured by capacitance probe. The differences were up to ± 1% which is not statistically significant.

Vehicle brands were not compared among each other because of different variation of driving style of individual drivers, difficultness of route (highway, urban condition, etc.) and differing amounts of cargo transported.

### Principle of measuring fuel consumption via CAN-BUS
It seems as a convenient solution is obtaining information about fuel consumption via CAN–BUS. This information is contained in the messages of engine diagnostic interface or in the messages of on–board bus of vehicles.
Currently, majority of truck manufacturers voluntarily comply the standardization in field CAN–BUS according to the standard SAE J1939 or standardized format FMS (Fleet Management System) gateway. These standards contain information about the instantaneous fuel rate to the engine (ACEA Working Group HDEI/BCEI, 2012).

Before using these data, it is necessary to be aware of how these data are collected in the truck. Instantaneous fuel rate depends on the designers of engine control system. Usually instantaneous fuel rate is measured by length of the injection and it is conversion to fuel rate.

CAN protocol uses two types of data messages. The first type is defined by specifications 2.0A (Standard Frame), while 2.0B specification defines Extended Frame (J1939). The only significant difference between the two these formats is the length of the message identifier which is 11 bits for a Standard Frame and 29 bits for the Extended Frame.

The data link layer describes the general characteristics of the CAN–BUS as a structure of data frame identification, transport protocol for transmitting messages that contain more than 8 bytes and encoding parameter groups.

Standard SAE J1939–71 (Vehicle Application Layer) defines groups of parameters and contained therein signals, for example engine coolant temperature, engine oil temperature, fuel rate etc. Groups of current parameters are transmitted in the data message. Each group of parameters is defined by a unique PGN (Parameter Group Numbers) (Fig. 1). This number consists of two parts in the message identifier. The first part is the PDU format and the second is a specific PDU.

| 0x00FEF2 | | | | | PGN Hex |
|----------|---|---|---|---|---------|
| 65,266 | | | | | PGN |
| 100 ms | | | | | Rep. Rate |
| **Data Byte 1** | **Data Byte 2** | **Data Byte 3** | **Data Byte 4** | **Data Byte 5-8** | Byte No. |
| 8 7 6 5 4 3 2 1 | 8 7 6 5 4 3 2 1 | 8 7 6 5 4 3 2 1 | 8 7 6 5 4 3 2 1 | | Bit No. |
| Fuel Rate | Fuel Rate | Instantaneous Fuel Economy | Instantaneous Fuel Economy | | Name |
| | | | | | Name |
| $0.05 \ l \ h^{-1}$ per bit | $0.05 \ l \ h^{-1}$ per bit | $1 \ 512^{-1} \ km \ l^{-1}$ per bit | $1 \ 512^{-1} \ km \ l^{-1}$ per bit | Not used for (BUS) FMS standard | Values |
| 0 offset | 0 offset | 0 offset | 0 offset | | Values |
| 0 to 3,212.75 $l \ h^{-1}$ | 0 to 3,212.75 $l \ h^{-1}$ | 0 to 125.5 $km \ l^{-1}$ | 0 to 125.5 $km \ l^{-1}$ | | Values |
| SPN 183 | SPN 183 | SPN 184 | SPN 184 | | SPN |

**Figure 1.** Parameters CAN-BUS according SAE J1939 (ACEA Working Group HDEI/BCEI, 2012).

**Principle of measuring of fuel level in the tank by the capacitance probe CAP04**

The principle of measuring of fuel level by the capacitance fuel level sensor is based on the fact that diesel is electrically non–conductive liquid. Capacitive probe CAP04 consists of two tubes of different diameter, which are the electrodes of capacitor. The dielectric is composed of electrically non-conductive material, specifically with a fuel and air. The relative permittivity of air is $\varepsilon_r = 1$, during refuelling the air is replaced with diesel which has relative permittivity $\varepsilon_r = 2$ and due to this fact the capacity of the

capacitor increases. The capacitive sensor measures the position of the boundary between air and diesel fuel (Fig. 2). (Partner mb, 2010)
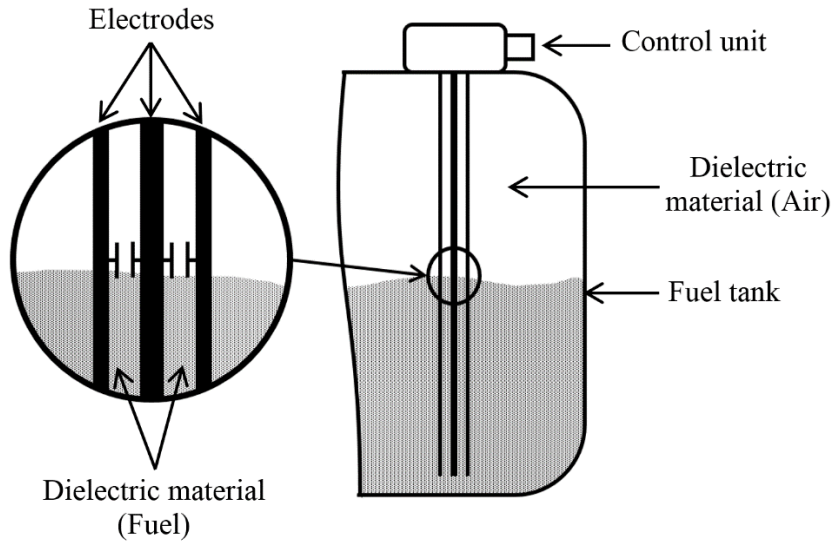


**Figure 2.** Principle of measuring of fuel level in the tank by the capacitance probe.

The probe is also equipped with thermometers to sense temperature of fuel and the surface temperature of the fuel tank. The processor evaluates data according to the actual capacity of the probe to match the measured volume of diesel at a reference temperature 15 °C. This method ensures that the reported amounts of fuel are not distorted by thermal expansion of diesel. Furthermore, the probe measures the tilt of the tank in two axes. While driving terrain when the level of diesel fluctuates rapidly and strongly, the probe indicates stable signal by means of appropriate filters of the signal.

Before installing the fuel probes the accuracy of measurement of the probe was tested at temperatures from -15 °C to +55 °C. Samples of diesel from three different fuel suppliers (Shell, Slovnaft, OMV) were used for testing. The highest deviation of measurement was measured on a sample from Shell at 13 °C – deviation was 0.21%. (Pavlu et al., 2013; Ales et al., 2015).

Experiment involved five brands of truck manufacturers (Scania R 440 Volvo FH 460, MAN TGX 480, DAF XF 460, Renault Kerax 420). Each brand was represented by fifteen trucks. Vehicles were operated primarily in companies focused on road transport and freight forwarding in Central and Eastern Europe. The observation period of operation of trucks was determined for the second half of year 2015. Average distance travelled of one truck was around 80,000 kilometres. The observation period truck traffic was relatively short, and therefore effects of wear on the fuel system was neglected.

# RESULTS AND DISCUSSION

Collected data from telematics system must always be properly processed. VBA code was used to process the raw data. Data were sorted out and filtered under specific conditions. Proceed data show cumulative fuel consumption. Raw data of one vehicle (6 months period) had approximately 50,000 records. Data on fuel consumption measured via CAN–BUS are in incremental format and do not include information about refuelling. Calculation of cumulative trend of consumption is simple (dotted line in Fig. 3). In terms of capacitance probe each user has continuous information about consumption and refuelling (referenced to the distance travelled). This data represents a saw–tooth pattern in (Fig. 3). Such data must be converted into cumulative form. For this purpose, a code in Visual Basic for Applications was created. Program code can reliably distinguish between consumption and refuelling or other factors as may be fuel tank tilting or fuel theft. The linear trend of cumulative consumption with linear equation (Fig. 3). Slope of linear equation represents consumption of a heavy truck for 1 kilometre. Multiplying slope of linear equation of the line 100 times, it is possible to obtain a commonly used form of fuel consumption in litres per 100 kilometres.
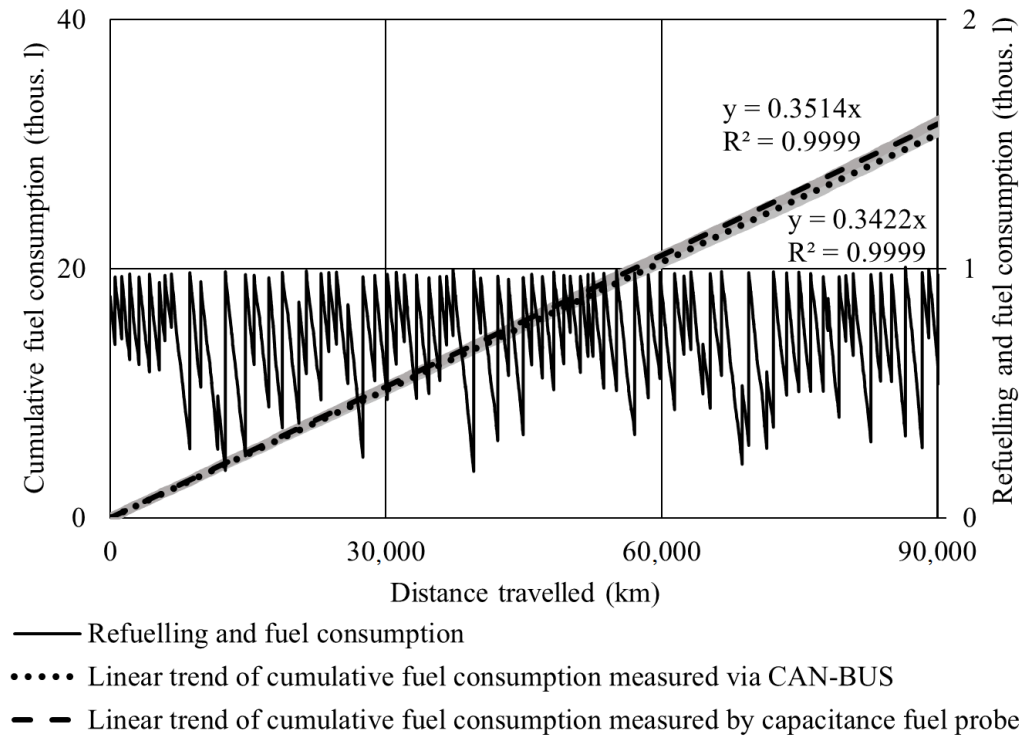


**Figure 3.** Measured and calculated data of fuel consumption - Scania R 440 No. 1.

Results calculated from obtained data are for each brand of vehicles (Tables 1–5). Results show the specific values of fuel consumption, both from the CAN–BUS and capacitance probe. The last column shows the difference between the fuel consumption compared methods in the tables.

**Table 1.** Results of calculated data from telematics system– Scania R 440

| Number of vehicle | Distance travelled (km) | Fuel consumption CAN-BUS (l 100 km$^{-1}$) | Fuel consumption capacitance probe (l 1,00 km$^{-1}$) | Difference of fuel consumption (l 100 km$^{-1}$) |
|---|---|---|---|---|
| **1*** | **90,089** | **34.215** | **35.141** | **0.9262** |
| 2 | 78,144 | 34.335 | 35.151 | 0.8160 |
| 3 | 80,359 | 33.102 | 34.030 | 0.9280 |
| 4 | 66,486 | 36.746 | 37.553 | 0.8070 |
| 5 | 75,745 | 34.200 | 35.053 | 0.8526 |
| 6 | 92,316 | 33.709 | 34.377 | 0.6677 |
| 7 | 86,849 | 33.876 | 34.339 | 0.4630 |
| 8 | 75,802 | 33.723 | 34.515 | 0.7916 |
| 9 | 66,061 | 35.835 | 36.532 | 0.6965 |
| 10 | 94,989 | 34.186 | 34.760 | 0.5743 |
| 11 | 76,393 | 35.887 | 36.639 | 0.7521 |
| 12 | 89,742 | 36.067 | 36.933 | 0.8660 |
| 13 | 65,732 | 33.435 | 34.074 | 0.6394 |
| 14 | 86,561 | 35.658 | 36.386 | 0.7275 |
| 15 | 74,248 | 35.310 | 35.737 | 0.4272 |

* - measured and calculated data of fuel consumption (Fig. 2).

**Table 2.** Results of calculated data from telematics system – VOLVO FH 460

| Number of vehicle | Distance travelled (km) | Fuel consumption CAN-BUS (l 100 km$^{-1}$) | Fuel consumption capacitance probe (l 100 km$^{-1}$) | Difference of fuel consumption (l 100 km$^{-1}$) |
|---|---|---|---|---|
| 1 | 63,510 | 36.824 | 37.487 | 0.663 |
| 2 | 66,250 | 35.587 | 36.152 | 0.565 |
| 3 | 62,837 | 33.370 | 33.837 | 0.467 |
| 4 | 63,332 | 35.397 | 36.402 | 1.005 |
| 5 | 64,789 | 34.647 | 34.852 | 0.205 |
| 6 | 70,234 | 37.466 | 38.203 | 0.737 |
| 7 | 84,443 | 37.048 | 37.593 | 0.545 |
| 8 | 95,294 | 32.077 | 32.954 | 0.877 |
| 9 | 71,327 | 35.453 | 36.319 | 0.866 |
| 10 | 62,633 | 32.450 | 33.369 | 0.919 |
| 11 | 63,665 | 37.147 | 37.670 | 0.523 |
| 12 | 84,338 | 33.804 | 34.530 | 0.726 |
| 13 | 93,061 | 34.390 | 34.896 | 0.506 |
| 14 | 86,843 | 37.968 | 38.736 | 0.768 |
| 15 | 64,758 | 33.457 | 34.334 | 0.877 |

**Table 3.** Results of calculated data from telematics system – MAN TGX 480

| Number of vehicle | Distance travelled (km) | Fuel consumption CAN-BUS (l 100 km$^{-1}$) | Fuel consumption capacitance probe (l 100 km$^{-1}$) | Difference of fuel consumption (l 100 km$^{-1}$) |
|---|---|---|---|---|
| 1 | 77,851 | 37.080 | 37.264 | 0.1839 |
| 2 | 65,719 | 35.652 | 36.147 | 0.4948 |
| 3 | 63,104 | 37.184 | 37.954 | 0.7697 |
| 4 | 68,936 | 34.539 | 35.526 | 0.9873 |
| 5 | 63,756 | 33.149 | 33.824 | 0.6745 |
| 6 | 63,413 | 35.001 | 35.705 | 0.7039 |
| 7 | 77,878 | 37.717 | 38.360 | 0.6431 |
| 8 | 62,754 | 37.838 | 38.764 | 0.9257 |
| 9 | 63,182 | 33.926 | 34.616 | 0.6903 |
| 10 | 64,080 | 35.486 | 36.009 | 0.5228 |
| 11 | 93,819 | 35.117 | 35.630 | 0.5133 |
| 12 | 71,457 | 33.241 | 33.799 | 0.5580 |
| 13 | 84,717 | 36.605 | 37.466 | 0.8614 |
| 14 | 70,055 | 36.324 | 37.316 | 0.9919 |
| 15 | 69,348 | 36.510 | 37.120 | 0.6096 |

**Table 4.** Results of calculated data from telematics system – DAF XF 460

| Number of vehicle | Distance travelled (km) | Fuel consumption CAN-BUS (l 100 km$^{-1}$) | Fuel consumption capacitance probe (l 100 km$^{-1}$) | Difference of fuel consumption (l 100 km$^{-1}$) |
|---|---|---|---|---|
| 1 | 84,010 | 33.475 | 34.181 | 0.7062 |
| 2 | 74,061 | 34.854 | 35.442 | 0.5882 |
| 3 | 80,967 | 32.964 | 33.911 | 0.9465 |
| 4 | 63,184 | 37.894 | 38.651 | 0.7567 |
| 5 | 83,840 | 34.537 | 35.122 | 0.5854 |
| 6 | 71,348 | 37.954 | 38.553 | 0.5986 |
| 7 | 95,672 | 32.934 | 33.718 | 0.7839 |
| 8 | 67,330 | 37.895 | 38.776 | 0.8806 |
| 9 | 94,342 | 35.049 | 35.635 | 0.5864 |
| 10 | 70,258 | 37.684 | 38.471 | 0.7873 |
| 11 | 63,179 | 32.570 | 33.223 | 0.6532 |
| 12 | 97,545 | 35.949 | 36.543 | 0.5942 |
| 13 | 89,319 | 36.318 | 37.135 | 0.8167 |
| 14 | 86,689 | 34.286 | 34.931 | 0.6453 |
| 15 | 81,650 | 36.515 | 37.085 | 0.5697 |

**Table 5.** Results of calculated data from telematics system – Renault Kerax 420

| Number of vehicle | Distance travelled (km) | Fuel consumption CAN-BUS (l 100 km$^{-1}$) | Fuel consumption capacitance probe (l 100 km$^{-1}$) | Difference of fuel consumption (l 100 km$^{-1}$) |
|---|---|---|---|---|
| 1 | 77,187 | 32.260 | 32.989 | 0.7286 |
| 2 | 91,602 | 38.181 | 39.146 | 0.9647 |
| 3 | 63,225 | 32.133 | 32.748 | 0.6146 |
| 4 | 85,157 | 36.544 | 37.414 | 0.8698 |
| 5 | 91,953 | 35.289 | 35.874 | 0.5845 |
| 6 | 84,998 | 33.098 | 33.885 | 0.7865 |
| 7 | 93,115 | 35.468 | 35.879 | 0.4112 |
| 8 | 96,863 | 35.236 | 35.894 | 0.6580 |
| 9 | 79,693 | 33.807 | 34.548 | 0.7410 |
| 10 | 94,249 | 33.812 | 34.649 | 0.8371 |
| 11 | 82,134 | 37.496 | 38.465 | 0.9689 |
| 12 | 96,707 | 33.552 | 34.110 | 0.5583 |
| 13 | 93,037 | 33.378 | 34.209 | 0.8312 |
| 14 | 85,378 | 35.406 | 36.291 | 0.8848 |
| 15 | 94,704 | 34.844 | 35.325 | 0.4809 |

From the calculated data can be determined null hypothesis $H_0$: there is no statistically significant difference between consumption measured via CAN–BUS and capacitance probe. Wilcoxon Signed–Rank non-parametric test (Equation 1–2) was used to verify this hypothesis (Mosna, 2015). Significance level was set at $\alpha = 0.05$ and two-tailed hypothesis was chosen.

$$Z = \frac{\min\left(W^+;W^-\right)-\frac{1}{4}n\cdot(n+1)}{\sqrt{\frac{1}{24}n\cdot(n+1)\cdot(2n+1)}} \tag{1}$$

$$Z = \frac{\min(2,850;0)-\frac{1}{4}75\cdot(75+1)}{\sqrt{\frac{1}{24}75\cdot(75+1)\cdot(2\cdot75+1)}} = -7.52479 \tag{2}$$

where: $W$ – sum of the signed ranks ($^+$positive, $^-$ negative); $n$ – sample size.

The Z-value is -7.52479. The p-value is 0. The result is significant at $P \leq 0.05$. That can be concluded that null hypothesis $H_0$ is rejected. Therefore, there is statistically significant difference between consumption measured via CAN-BUS and capacitance probe.

All results of difference between fuel consumption measured via CAN-BUS and capacitance probe are shown in box plot in Fig. 3. The average difference between compared methods for all trucks under consideration was $0.7\,l\,100\,km^{-1}$ of fuel consumption.
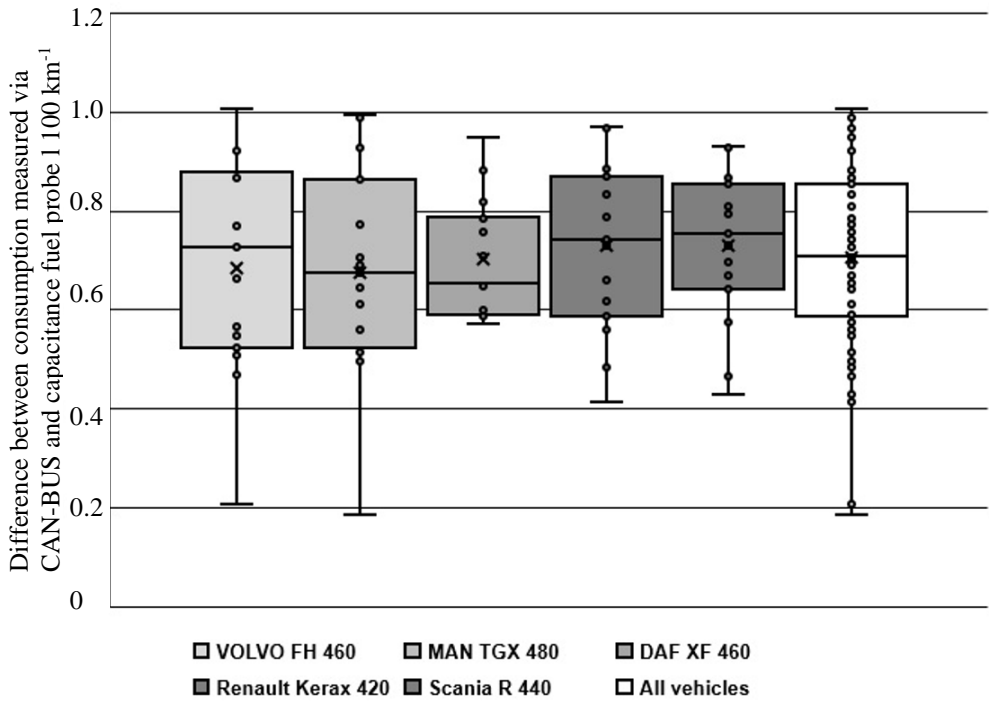


**Figure 3.** Box plot representing measured Difference between consumption measured by capacitance probe and CAN–BUS.


# CONCLUSIONS

The aim of the paper was to prove or disprove the hypothesis, if there is statistically significant difference between described methods of measuring fuel consumption.

Designed experiment involved 75 trucks. Trucks were operated primarily in companies focused on road transport and freight forwarding in Central and Eastern Europe. The observation period of operation of trucks was determined for 6 months. Average distance travelled of one truck was around 80,000 kilometers. Fuel consumption was monitored for each truck using two methods via CAN–BUS compared to capacitance probe. Collected data was transmitted through telematics system and then processed based on an algorithm created in Visual Basic for Applications. Results were statistically processed in order to accept or reject the hypothesis. Null hypothesis $H_0$ was rejected, it means, there is statistically significant difference between consumption measured via CAN–BUS compared to capacitance probe. Created box plot shows that average difference between compared methods for all trucks under consideration was

0.7 l 100 km$^{-1}$ of fuel consumption. The results confirm that the fuel consumption measured via CAN–BUS shows lower values compared to real fuel consumption.

## REFERENCES

ACEA Working Group HDEI/BCEI. 2012. http://www.fms-standard.com/Truck/down_load/ fms_document_ver03_vers_14_09_2012.pdf. Accessed 2.1.2016.

Ales, Z., Pavlu, J. & Jurca, V. 2015. Maintenance interval optimization based on fuel consumption data via GPS monitoring. *Agronomy Research* **13**, 17–24.

Daniel, O.G., Dayo, O., & Anne, O.O. 2011. Monitoring and controlling fuel level of remote tanks using aplicom 12 GSM module. *ARPN Journal of Engineering and Applied Sciences* **6**, 56–60.

Dhivyasri, G., Mariappan, R., & Sathya, R. 2015. Telematic unit for advanced fuel level monitoring system. *Proceedings of 2015 IEEE 9th International Conference on Intelligent Systems and Control, ISCO 2015*, DOI: 10.1109/ISCO.2015.7282260

Li, X., & Fan, Y., 2007. Study on high precision capacitance sensor of the fuel level. Yi Qi Yi Biao Xue Bao/Chinese. *Journal of Scientific Instrument* **28**, 32–35.

Mosna, F. 2015. Riemann integral-possibilities of definition. *APLIMAT 2015 – 14th Conference on Applied Mathematics*, Proceedings, 602–607.

Partner mb, s.r.o. 2010. Zařízení pro měření hladiny kapaliny v zásobníku. Česká republika. 2009–21834. Přihlášeno 20.10.2009. Zapsáno 15.02.2010. http://spisy.upv.cz/UtilityModels/FullDocuments/FDUM0020/uv020522.pdf. Accessed 2.1.2016.

Pavlu, J., Ales, Z., & Jurca, V. 2013. Utilization of satellite monitoring for determination of optimal maintenance interval. *Scientia Agriculturae Bohemica* **3**, 159–166.

# Efficient use of arable land for energy: Comparison of cropping natural fibre plants and energy plants

R. Pecenka[*], H.-J. Gusovius, J. Budde and T. Hoffmann

Leibniz Institute for Agricultural Engineering Potsdam-Bornim (ATB), Max-Eyth-Allee 100, DE 14469 Potsdam, Germany
[*]Correspondence: rpecenka@atb-potsdam.de

**Abstract.** With focus on renewable energy from agriculture governments can either support the growing production of energy crops or it can invest in technology or measures to reduce the energy consumption. But what is more efficient with regard to the use of the limited resource arable land: to insulate a building with fibre material grown on arable land to reduce the heating demand or to use such land for growing energy plants for the sustainable energy supply of a building? To answer this question, a long term balance calculation under consideration of numerous framework parameters is necessary.

Based on traditional fibre plants like hemp, flax, and woody fibre crops (e.g. poplar), these agricultural plants and their processing to insulation material were examined. Based on available data for the typical building structure of detached and semi-detached houses in Germany, models of buildings were developed and the accessible potentials for heating energy savings by using suitable insulation measures with natural fibre materials were determined. As a comparable system for the supply of renewable energy, bio-methane from silage maize was chosen, since it can be used efficiently in conventional gas boilers for heat generation. The different levels of consideration allow the following interpretations of results: in a balance calculation period of 30 years, the required acreage for heating supply with methane can be reduced by approx. 20%, when at the beginning of the use period fibre plants for the insulation of the houses are grown on the arable acreage. Contrariwise, to compensate only the existing loss in heating energy due to inadequate insulation of older detached and semi-detached houses (build prior to 1979) an annual acreage of approx. 3 million ha silage maize for bio-methane would be required in Germany. Therefore, from the land use perspective the production of biogas plants in agriculture for heating should be accompanied by the production of fibre plants for a reasonable improvement of the heat insulation of houses.

**Key words:** natural fibre plants, fibre, bioenergy, biogas, heat insulation, heating.

## INTRODUCTION

Due to an increasing awareness for global warming and a simultaneously increasing worldwide demand of energy, the interest in alternative energy resources from agricultural production is growing continuously. The EU's Renewable energy directive sets a binding target of 20% final energy consumption from renewable sources as an average of all members states by 2020 (Directive 2009/28/EC). To achieve this, EU countries have committed to reaching their own national renewables targets ranging from 10% in Malta to 49% in Sweden. According to the individual national action plans

of the EU countries biomass from forestry and agriculture plays an important role for the majority of all member states to reach the targets for renewable energy and reduction of $CO_2$ emissions (National action plans 2016). Hence, the acreage for cropping energy plants for bioheat, bioelectricity and biofuels has increased in the last years (European Commission, 2016). For example, in Germany the acreage for energy plants has about tripled in the past 10 years (FNR, 2015). With a total of 2.07 million ha, energy plants have covered approx. 12% of the total arable area in Germany in 2014 (Statistisches Bundesamt, 2015). Therefore, the annual increase of the required crop area for silage maize for biogas production and the relation with regard to the competition for acreage of other field crop, the high expense for fertilizers, and the effects on the humus balance are discussed controversially (AEE, 2010; Willms, 2013; Scholz et. al, 2010). An important driver for the increasing share of renewable energy in the German total energy mix is the long term regulation of remuneration for renewable energies (EEG, 2011 and EEG, 2014). Thus, the share of renewable energy in the final energy mix for electric power could be increased to currently approx. 27% (BMWI, 2015) and for the total consumption of end-use energy to approx. 13.7% for the year 2014 in Germany. Although at present an area of 1.27 million ha (approx. 60% of total energy plant area) is required for biogas generation alone, the energy generated from biogas covers only 1.2% of the end energy demand, or respectively 4.9% of the electric power consumption (BMWI, 2015; BMWI, 2016). The acreage for fibre plants in Germany has significantly been decreased in the past 10 years and presently only 500 ha are cultivated with fibre plants (FNR, 2015). Main reason for that is, besides certain process technological problems at the beginning (Pecenka et al., 2009a), the increasing competition to other field crop, not least the competition to energy plants, since in energy production numerous additional subsidies have their effects. Thus, growing of energy plants is substantially more attractive for farmers in Germany (Carus, 2008). From the aspects of sustainable energy supply this is certainly correct; however, it raises the question regarding the efficient use of available acreage and the related costs for the national economy on the whole.

A significant share of energy from renewable sources is used for the supply to households. The total demand of private households in 2013 was at approx. 2,603 PJ and thus represents approx. 28% of the final energy demand in Germany (UBA, 2016). About 69% of the total demand of private households is required for heating alone (year 2012). Besides the use of renewable sources, the reduction of the absolute consumption is a substantial factor for sustainable resource management. Thus various statutory incentive implements are available, particularly for the reduction of demanded heating energy of residential buildings, e.g. by insulation of building substance. However, various studies about age and structure of existing buildings have shown that 70 to 75% of detached and semidetached houses in Germany build prior to 1979 do not feature any heat insulation in addition to the conventional brickwork (Diefenbach et al, 2010a; Diefenbach et al., 2010b; Weiß & Dunkelberg, 2010).

At present the annual progress of insulation activities in old buildings is only about 1%. Considering this level, it can be expected that a period of 65 to 70 years will be required before all buildings feature sufficient insulation. The cultivation of fibre plants and their consecutive processing into insulation material for subsequent insulation of resident buildings could tap this potential of lasting energy savings (Krüger, 2011). Simultaneously, not only substantial emission of $CO_2$ could be avoided, but also carbon

would be bound long term as a substantial compound of natural insulation material. Moreover, natural insulation materials provide significant advantages compared to the mainly synthetic materials applied at present. The production of natural fibre insulation requires up to 20 times less energy (Tscheutschler, 1999; UBA, 2011) and allows for resource-neutral disposal by thermal recycling, simultaneously delivering renewable energy.

To answer the question, what is more efficient with regard to the use of the limited resource arable land: to insulate a house with fibre material grown on arable land to reduce the heating demand or to use this land for growing energy plants for the sustainable supply of heating energy, several sub-questions have to be answered. For a long term balance analysis some of the most important points are:

− What is the typical heating energy demand of common detached and semi-detached houses typical for rural areas?
− What is the share of houses with inadequate heat insulation?
− What is the acreage of agricultural land required to cover the heating energy demand of a common detached or semi-detached house with bioenergy?
− How much insulation material is necessary to improve the heat insulation of older houses to meet current standards?
− What is the acreage of agricultural land required to crop fibre plants for an upgrade of the heat insulation of a house to current standard using natural fibre insulation materials?

All research and balance calculations required to answer these questions were made exemplarily for Germany, since a good data base is available due to up-to-date inquiries. However, the results are also interesting for other European countries in particular for countries with similar climate conditions and a comparable state of the building stock.
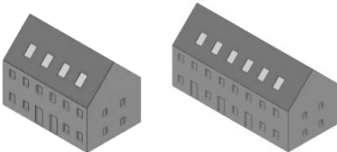
## MATERIALS AND METHODS

Fig. 1 shows the relation between age and heating energy demand of detached and semi-detached houses according to Weiß & Dunkelberg (2010), which has been used to determine saving potentials for heating. These types of houses represent 59% of the entire inventory of residential buildings in Germany (Destatis, 2011).

Characteristic model houses were designed for this study based the analyses on building inventory as well as on heating requirements of different residential buildings carried out by Weiß & Dunkelberg (2010) and Diefenbach et al. (2010a). To analyse the possible savings of heating energy as well as the required amount of insulation material to realise these savings, the model houses H1 – H5 have been investigated in detail (Table 1). Based on the model houses, the balance could be calculated about the demand and effects of different insulation measures on the exterior walls. Beside the shape of the building, the structural-physical properties of the used building materials have also an important impact. Therefore, the different properties of the basic structure of existing buildings, e.g. different wall structures and their impact on heating energy demand had to be considered in the model calculations (Table 2).
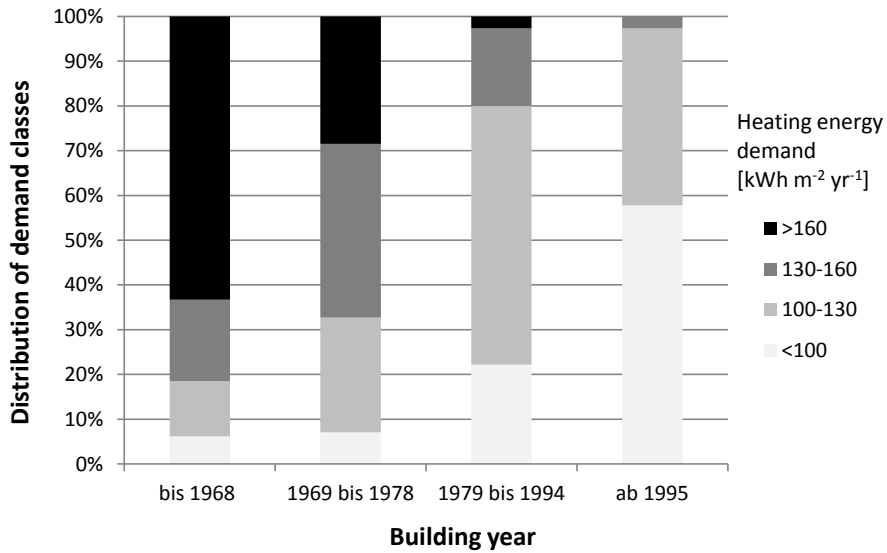
**Figure 1.** Classes of heating energy demand of detached and semi-detached houses in Germany, dependent on year of construction (Weiß & Dunkelberg, 2010).

**Table 1.** Building concepts

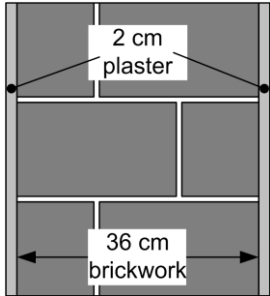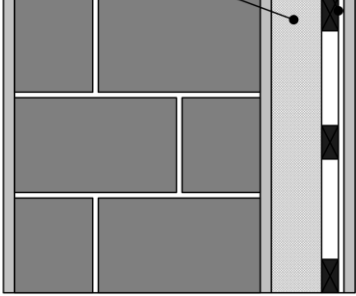| Model code | Model buildings | Living space [m²] | Exterior wall area [m²] |
|---|---|---|---|
| | Detached houses | | |
| H1 – H3 | | 139 to 163 | 142 to 162 |
| | Semi-detached and three-family houses | | |
| H4 – H5 | | 238 to 357 | 246 to 311 |

The building-specific insulation properties relevant for the calculation of heating energy demand were implemented in the calculation as U-values. On basis of the heat transmission coefficient (U-value) of an individual bounding surface of a house (roof, exterior wall, window, door and floor plate) the heat flow through this specific surface can be calculated according to Equation 1.

$$\dot{Q} = -U \, A \, \Delta T \qquad (1)$$

where: $\dot{Q}$ – Heat flow in Wh; U – Coefficient of heat transmission in W m$^{-2}$ K$^{-1}$; $\Delta T$ - Temperature difference between inner and outer wall surface in K.

To calculate the total heating energy demand of a house the complex structure of the whole house has to be considered taking the heat flows through all bounding surfaces into account. For this purpose the software Energieberater 7 (Hottgenroth, 2011) was used to calculate the heating energy demand for all combinations of different model houses (Table 1, H1 – H5), wall types and insulation thicknesses (Table 2) based on the climate conditions of Braunschweig (middle Germany, 52°19'N 10°33'O). For the roof, windows, doors, and floor plate typical values for houses built prior 1979 have been chosen from the database provided by the software Energieberater 7 in accordance with the analysis of Weiß & Dunkelberg, 2010.

**Table 2.** U-values of various typical wall building materials (Hottgenroth 2011)

| Non-insulated wall | | Insulated wall | |
|---|---|---|---|



| | U-value [W m$^{-2}$ K$^{-1}$] | insulated 5 to 20 cm | U-value [W m$^{-2}$ K$^{-1}$] |
|---|---|---|---|
| Poroton (P) | 0.41 | Poroton | 0.27 to 0.14 |
| Perforated brick (PB) | 0.77 | Perforated brick | 0.39 to 0.17 |
| Solid brick (SB) | 1.01 | Solid bricks | 0.45 to 0.18 |
| Heavy solid brick (HSB) | 1.28 | Heavy solid bricks | 0.49 to 0.19 |

Results from long-term crop measurements on ATB's raw material plantation (Fig. 2) as well as data from the German agriculture statistic (Destatis, 2011) were used for research on supply of energy as well as fibre materials. The harvested fibre crop needs to be mechanically decorticated and processed into insulation mats or insulation boards for its use in building industry. Substantial for the material balance is the achievable fibre yield in this process for the different raw materials. Based on own research in a pilot plant and several production plants (Munder et al., 2004; Pecenka, 2009b; Scholz et al., 2010), crop data and yields shown in Table 3 were used for further calculations. Fast growing poplar was used for the comparison of fibre production from wood on agricultural land.
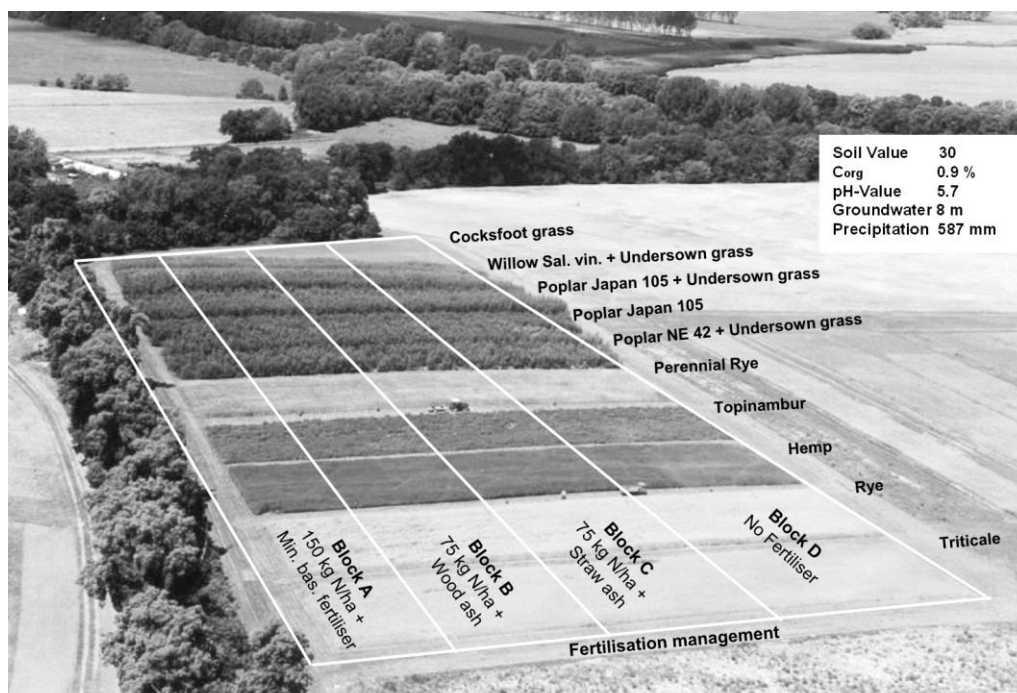
**Figure 2.** Raw material and energy plantation (ATB).

**Table 3.** Crop data used for the calculations of yields of energy and insulation materials

*Material use*

|  | biomass yield $t_{DM}$ ha$^{-1}$ yr$^{-1}$ | fibre yield t ha$^{-1}$ | insulation material density kg m$^{-3}$ | yield of insulation material m³ ha$^{-1}$ |
|---|---|---|---|---|
| Maize | 17.5 | - | - | - |
| Hemp | 7 | 1.75 | 100 | 17.5 |
| Flax | 5.5 | 1.4 | 80 | 17.2 |
| Poplar | 10 | 7.2 | 180 | 40 |

*Energetic use*

|  | biomass yield $t_{DM}$ ha$^{-1}$ yr$^{-1}$ | methane yield $m_N^3$ ha$^{-1}$ yr$^{-1}$ | processing loss % | energy yield GJ ha$^{-1}$ yr$^{-1}$ |
|---|---|---|---|---|
| Maize | 17.5 | 4997 | 28 | 116.5 |
| Hemp | 7 | - | - | 136.0 |
| Flax | 5.5 | - | - | 9.89 |
| Poplar | 10 | - | - | 177.1 |

DM – dry mass, poplar yields data based on 20 years averages from own measurements at the ATB energy plantation (county Brandenburg, Germany), all other yields based on averages for sandy soils under the growing conditions in the county Brandenburg (Germany), (Munder et al., 2004; Pecenka, 2009b; Scholz et al., 2010; Destatis, 2011).

Not considered in the point balance were energy yields for natural fibre insulation materials from their thermal recycling when being disposed of at the end of their life (poplar fibre approx. 120 GJ ha$^{-1}$, hemp fibre 24 GJ ha$^{-1}$). Poplar from short rotation plantations were estimated to achieve 72% fibre yield at considered storage loss of 20%

dry matter, and hemp and flax were estimated to achieve fibre yields of 25% (Pecenka et al., 2014; Lenz et al., 2015). The generation of biogas or bio-methane (processed biogas, fit for feed into domestic gas network) from silage maize were used as reference for energy plant production. Silage maize yield of 50 t with 35% dry mass content per hectare and year were considered for the calculation of the bio-methane yield. 12% storage loss and 28% loss due to processing of biogas into bio-methane were taken into account (KTBL 2009; KTBL 2010; Mühlenhoff & Dittrich, 2011).

## RESULTS AND DISCUSSION

Contingent saving potential for heating energy demand of detached and semi-detached houses were investigated based on the data for building inventory in Germany (see Fig. 1). The most economically accessible potentials are present in houses build prior to 1979, as shown in Fig. 3.
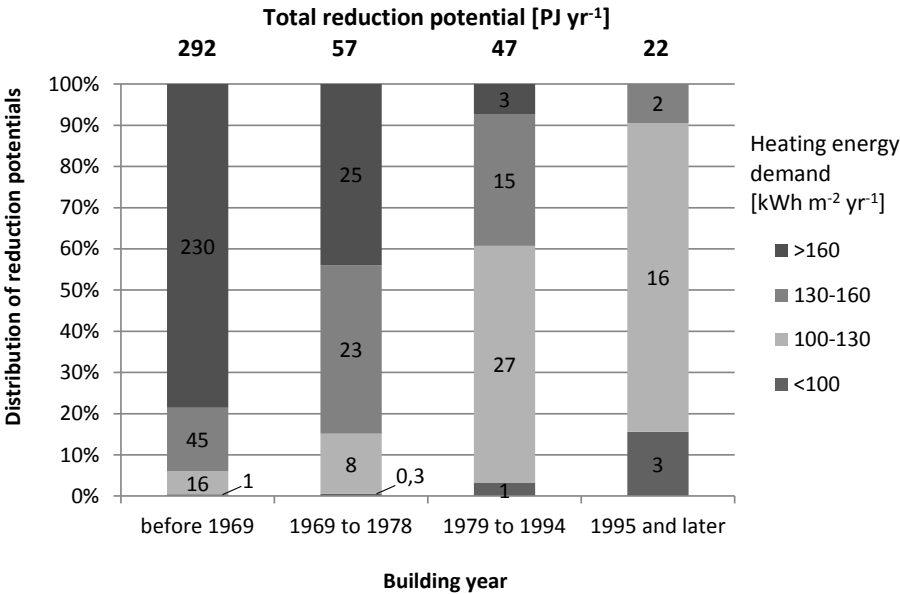


**Figure 3.** Saving potentials for heating energy for detached and semi-detached houses in Germany (target for specific heating energy demand: 80 kWh m$^{-2}$ yr$^{-1}$).

Total annual energy savings of approx. 349 PJ could be achieved by implementing suitable insulation measures for houses built prior to 1979, targeting on a reduction of the specific heating energy demand to 80 kWh (m² a)$^{-1}$ which represents an average of the current standards for newly build houses in Germany. With regard to the final energy demand of households in Germany in 2013 of approx. 2,603 PJ this equals savings of 13%.

To answer the question how many hectares of fibre plants have to be cultivated to use the calculated saving potential, the specific demand of insulation material has to be investigated for houses built prior 1979. Firstly, the impact of different building concepts on heating energy demand was determined dependent on the type of model house,

insulation thickness, and wall material. As shown in Fig. 4a, the choice of wall material for non-insulated walls has a substantial impact on the heating energy demand. Whereas a single house (type H1) with common heavy solid brick (HSB) walls has a specific heating energy demand of 144 kWh m² yr$^{-1}$, the same house with Poroton (porous clay brick) walls requires 75 kWh m$^{-2}$ yr$^{-1}$ only. These differences are already reduced by applying an insulation thickness of 5 cm to a heating energy demand of 82 resp. 65 kWh m$^{-2}$ yr$^{-1}$ and at 10 cm insulation thickness they are only at 68 resp. 60 kWh m$^{-2}$ yr$^{-1}$.



a) influence of wall types, house type H1          b) influence of house types, wall type PB
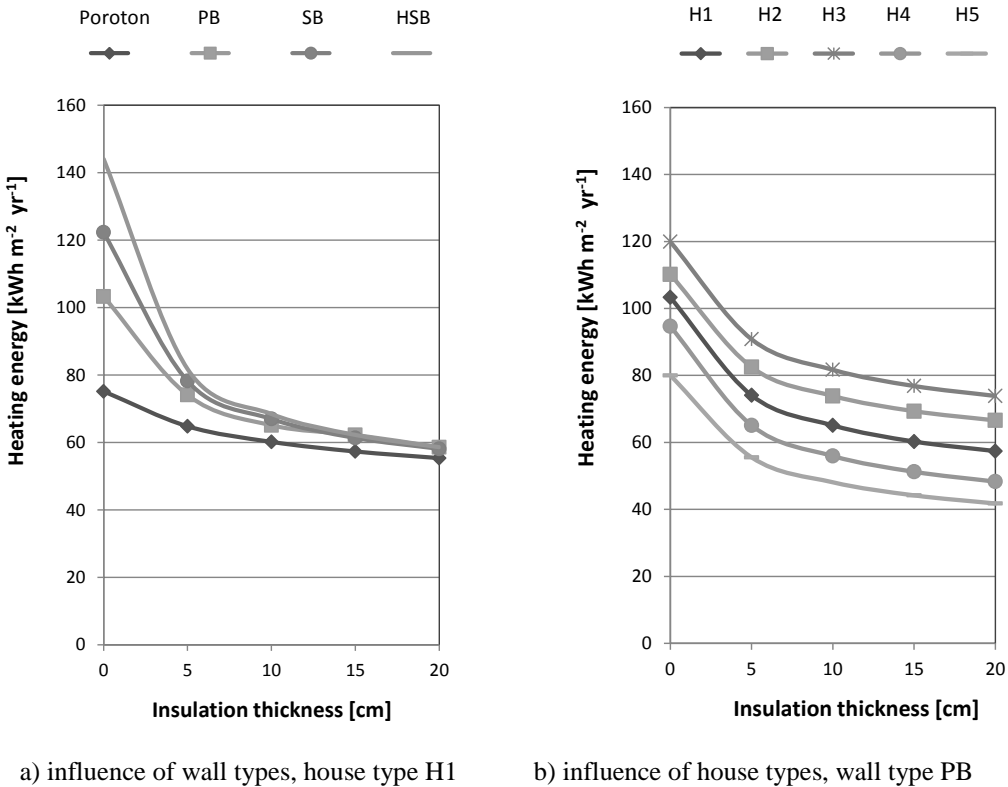
**Figure 4.** Impact of different model house concepts and insulation material thicknesses on heating energy demand for subsequent exterior wall insulation in old buildings
(Poroton – Porous clay brick, PB – Perforated brick, SB – Solid brick, HSB – Heavy solid brick H1…H5 – model house type 1…5).

Similar results are shown in Fig. 4b for the impact of the chosen type of model house on the heating energy demand. The well-known energetic disadvantages of detached houses (H1 to H3) compared to semi-detached and three family houses (H4 and H5) become clear. In general, a heat insulation of 5 to 10 cm on the exterior walls showed to be already quite efficient to use the most of the available saving potentials. Further common refurbishment measures, e.g. additional insulation of the roof, insulation of the basement ceiling, or heating modernization were not considered at this stage of evaluation.

A large-scale cultivation of fibre plants is required for the utilization of these potentials if natural fibres should be used as heat insulation material. A potential 10 cm exterior building insulation with natural fibre material of all detached and semi-detached houses (built prior to 1979) within 1 year would theoretically require cultivation of 7.5 million ha of hemp or 3.3 million ha of short rotation plantations with poplar (Fig. 5, column A). On the other hand, a lasting coverage of the so far unused potential for savings of 349 PJ yr$^{-1}$ in heating energy by using renewable energies in form of bio-methane would require the cultivation of approx. 3 million ha maize every year.

A substantial reduction of annual required arable land for cultivation of fibre plants is possible when considering more realistic plans for refurbishing houses in a period of 10 to 20 years. If wood fibre (poplar) should be used in the coming 10 years, an annual cultivation area of 329,000 ha will be required (column B). For a balance period of 20 years the required area would decrease to 165,000 ha respectively (column C). Hemp cultivation would require much larger cultivation areas due to a lower fibre yield (factor 2.3). However, when evaluating hemp cultivation the use of hemp shives as by-product is not taken into consideration. Hemp shives are subsequent building insulation as well (Bevan & Woolley, 2008) and represent approx. 60% of the overall mass flow of hemp processing.
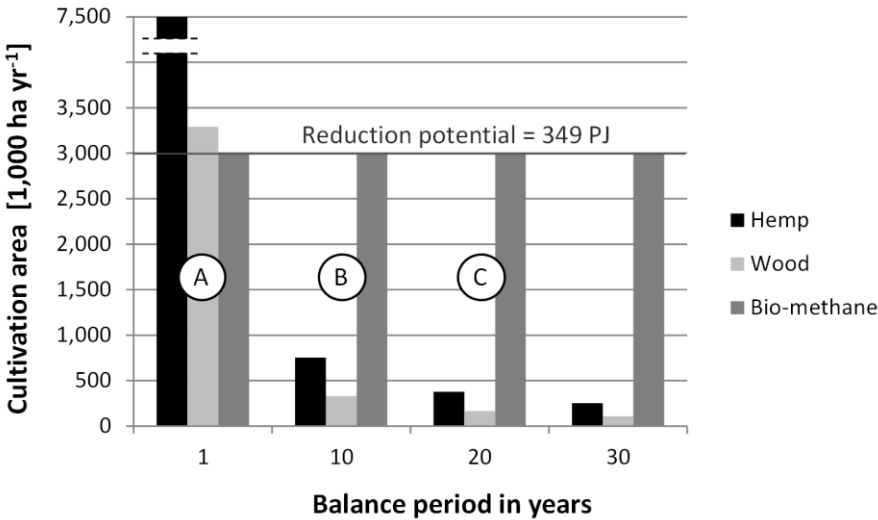


**Figure 5.** Area requirements for production of insulation material and respectively for generation of bio-methane for heating (required heating energy = saving potential of 349 PJ)
A: Required acreage for fibre plants in order to achieve the energy savings potential of 349 PJ within one year by providing the insulation for the facade.
B/C: Required acreage for fibre plants in order to achieve the energy savings potential of 349 PJ within 10 resp. 20 years through insulation of the house facade.

The amount of saved heating energy increases proportional to the length of the useful life of exterior wall insulation. Considering the potential energy savings over the usual depreciation period for buildings of 50 years, it can be calculated that in the case of model house H1, by making an exterior wall insulation from natural fibre with a

thicknesses of 10 to 20 cm it can be saved a total of 950 to 1,150 GJ in heating energy during the evaluated time of 50 years. This is equivalent to the annual energy generated from cultivation of silage maize and the subsequent generation of biomethane from 8 to 10 ha of acreage.

Balancing the achievable energy savings for a house (model H1, wall material: perforated brick – PB), the demand in arable land for agricultural supply of raw material and energy are as shown in Fig. 6. Applying exterior wall insulation from natural fibre at thicknesses of 10 to 20 cm, the demanded acreage for bio-methane production for heating energy supply can be reduced by 19 to 22% over a balance period of 30 years.
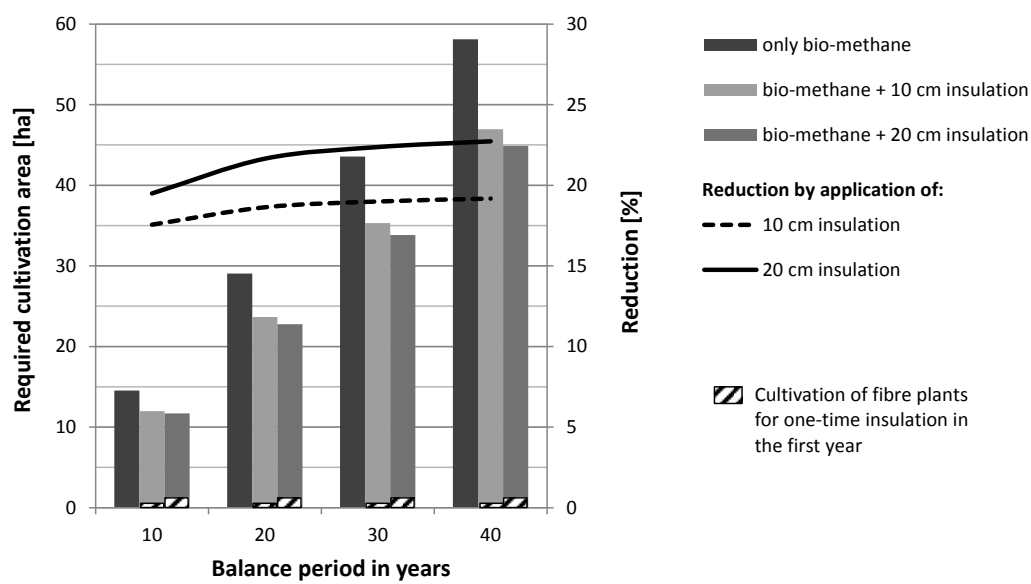


**Figure 6.** Acreage demand for heating energy supply of a detached house (model H1) with bio-methane (with and without exterior wall insulation).

Further positive environmental effects of using natural fibre insulation materials lie in their potential for long term $CO_2$ storage and the possibility of thermal utilization when being disposed at the end of their useful life. Furnishing the model house H1 with 10 cm or 20 cm exterior wall insulation respectively requires 1.2 to 4.5 t natural insulation material. Thus, 2.1 to 7.8 t $CO_2$ equivalent are sequestrated in such wall insulation. Looking at the overall potential of older detached and semi-detached houses (built prior to 1979 – comp. Fig. 5) for $CO_2$-sequestration, 22 million tons of $CO_2$ equivalent could be sequestrated long term by using hemp fibre insulation, or 41 million tons of $CO_2$ equivalent respectively by using wood fibre insulation. Energy yields of thermal utilisation on disposal would be at approx. 200 PJ for hemp fibre insulation, or approx. 360 PJ for wood fibre insulation respectively (KTBL 2006). However, additional $CO_2$-sequestration potentials of the cultivation of fibre plants were not taken into account in this analysis. According to Scholz et al. (2010) for the cultivation of poplar in short rotation an annual sequestration of carbon in the soil between 880 to 1,600 kg ha$^{-1}$ respectively 3.2 to 5.9 t ha$^{-1}$ $CO_2$ can be assumed. Whereas for the cultivation of maize for bio-methane a reduction in the soil carbon content between -560

to -800 kg ha$^{-1}$ have to be assumed and compensated by organic fertilisation (Willms, 2013). Furthermore, the required application of mineral fertiliser, which is required for efficient cropping maize, hemp and flax leads to high emissions of nitrous oxide. Cropping poplar for the production of fibres for insulation materials requires no or only minimal fertilisation. Therefore, nitrous oxide emission can be reduced from 2 to 4 kg N ha$^{-1}$ yr$^{-1}$ common for maize and hemp cultivation to approx. 0.5 kg N ha$^{-1}$ yr$^{-1}$ for poplar (Dambreville et al., 2008; Scholz et al., 2010, Willms, 2013,). These additional environmental effects should be taken into account as well if a life cycle assessment is undertaken for a more comprehensive comparison of the discussed different supply scenarios.

## CONCLUSIONS

Besides the use of renewable energy sources, the reduction of the absolute consumption is an essential factor for sustainable resource management. Economically relevant energy savings are potentially possible by cultivating fibre plants and processing them into insulation material for subsequent heat insulation of residential buildings. Compared to energy plant cultivation only, the existing acreage can be used much more efficiently. In addition to that, the emission of considerable volume of $CO_2$ can be avoided, while substantial amounts of carbon as an essential compound of natural fibre insulation could be long term sequestrated.

The biggest savings with respect to the required acreage for renewable raw materials and energy sources can be achieved with the cultivation of poplar on short rotation plantations and its use for insulation materials. Hemp cultivation would require larger cultivation areas due to lower fibre yield. Besides the efficient material use of shives in building materials, the woody shives can be used as energy resource as well.

Due to the high demand for agricultural land to produce bio-energy and natural insulation materials public incentives should focus on the continuous modernisation of detached houses over a longer balance period of 10 or more years, starting with houses built prior 1979 for the German case. Already a natural fibre insulation with a thickness of 10 cm proved to be very efficient to use 90% and more of the calculated energy saving potential. An insulation of 20 cm thickness needs the double of raw material as well as agricultural land for fibre plant production, whereas the additional energy savings are lower than 10% compared to an insulation of 10 cm thickness.

## REFERENCES

AEE. 2011. Agentur für Erneuerbare Energien e.V. (Hrsg.): Der volle Durchblick in Sachen Energiepflanzen. Daten & Fakten zur Debatte um eine wichtige Energiequelle. Berlin 2011. (in German).

Bevan, R. & Woolley, T. 2008. Hemp Lime Construction. Bracknell IHS/BRE Press.

BMWI. 2015. Bundesministerium für Wirtschaft und Energie: Erneuerbare Energie in Zahlen. Nationale und international Entwicklung. Berlin, 84 pp. (in German).

BMWI. 2016. Bundesministerium für Wirtschaft und Technologie: Energiedaten: Gesamtausgabe. Stand Januar 2016. Berlin, 76 pp. (in German).

Carus, M. 2008. Raw Material Shift. International Congress 'Raw Material Shift and Biomaterials', 3.–4. December 2008, Cologne Germany.

Dambreville, C., Morvan, T. & Germon, J.-C. 2008. $N_2O$ emission in maize-crops fertilized with pig slurry, matured pig manure or ammonium nitrate in Brittany. *Agriculture, Ecosystems & Environment* **123**, 201–210

Destatis 2011. Statistisches Bundesamt: Statistisches Jahrbuch 2011. Wiesbaden. (in German).

Diefenbach, N., Cischinsky, H., Rodenfels, M. & Clausnitzer, K.-D. 2010. Summary of the Research Project 'Data Base of the Building Stock – Data Survey of the State and the Trends of Energy Saving Measures in the German Residential Building Stock'. Institut Wohnen und Umwelt, Darmstadt. (in German).

Diefenbach, N., Cischinsky, H., Rodenfels, M. & Clausnitzer, K.-D. 2010a. Datenbasis Gebäudebestand. Institut Wohnen und Umwelt, Darmstadt. (in German).

Directive 2009/28/EC of the European Parliament and of the Council of 23 April 2009 on the promotion of the use of energy from renewable sources and amending and subsequently repealing Directives 2001/77/EC and 2003/30/EC. *Official Journal of the European Union*, L140/16

EEG. 2011. Gesetz zur Neuregelung des Rechtsrahmens für die Förderung der Stromerzeugung aus erneuerbarer Energien. Bundesgesetzblatt Jahrgang 2011 Teil I Nr. 42. Bonn 4. August 2011.(in German).

EEG. 2014. Gesetz zur grundlegenden Reform des Erneuerbare-Energien-Gesetzes und zur Änderung weiterer Bestimmungen des Energiewirtschaftsrechts. Bundesgesetzblatt Jahrgang 2014 Teil I Nr. 33. Bonn 24. Juli 2014. (in German).

European Commission 2016. State of play on the sustainability of solid and gaseous biomass used for electricity, heating and cooling in the EU. http://ec.europa.eu/energy/node/70. Accessed 15.1.2016

FNR. 2016. *https://mediathek.fnr.de/grafiken/daten-und-fakten/bioenergie. html.* Accessed 15.1.2016.

Hottgenroth. 2011. Hottgenroth Sofware: Energieberater Plus Version 18599, Köln 2011.

Krüger, K. 2011. Bewertung des Anbaus von nachwachsenden Rohstoffe, Bachelor Thesis, Universität Rostock. (in German).

KTBL. 2006. Kuratorium für Technik und Bauwesen in der Landwirtschaft (Hrsg.) (2006): Energiepflanzen. Darmstadt. (in German).

KTBL. 2009. Kuratorium für Technik und Bauwesen in der Landwirtschaft (Hrsg.): Faustzahlen Biogas. Darmstadt. (in German).

KTBL. 2010. Kuratorium für Technik und Bauwesen in der Landwirtschaft (Hrsg.): Gasausbeute in landwirtschaftlichen Biogasanlagen. Darmstadt. (in German).

Lenz, H., Idler, C., Hartung, E. & Pecenka, R. 2015. Open-air storage of fine and coarse wood chips of poplar from short rotation coppice in covered piles. *Biomass and Bioenergy* **83**, 269–277.

Munder, F., Fürll, C. & Hempel, H. 2004. Advanced Decortication Technology for not retted Bast Fibres. *Journal of Natural Fibers* **1**, 49–65.

Mühlenhoff, J. & Dittrich, K. 2011. Biogas-Nutzungspfade im Vergleich. Agentur für Erneuerbare Energien e.V., Berlin. (in German).

National action plans 2016. *https://ec.europa.eu/energy/node/71.* Accessed 22.3.2016.

Pecenka, R., Fürll, C., Gusovius, H.-J. & Hoffmann, T. 2009a. Optimal plant lay-out for profitable bast fiber production in Europe with a novel processing technology. *Journal of Biobased Materials and Bioenergy* **3**, 282–285.

Pecenka, R., Fürll, C., Idler, C., Grundmann, P. & Radosavljevic, L. 2009b. Fibre boards and composites from wet preserved hemp. *Int. Journal of Materials and Product Technology* **36**, 208–220.

Pecenka, R., Lenz, H., Idler, C., Daries, W. & Ehlert, D. 2015. Development of bio-physical properties during storage of poplar chips from 15 ha test fields. *Biomass and Bioenergy* **65**, 13–19.

Statistisches Bundesamt 2015. Kap. 19: Land- und Forstwirtschaft. Wiesbaden (in German).

Scholz, V., Heiermann, M. & Kaulfuß, P. 2010. Sustainability of energy crop cultivation in Central Europe. In: Sociology, Organic Farming, Climate Change and Soil Science. *Sustainable Agriculture Reviews* **3**, 109–145.

Tzscheutschler, P. 1999. Ganzheitliche Bilanzierung von Grundstoffen und Halbzeugen, Teil IV Kunststoffe. Forschungsstelle für Energiewirtschaft, München. (in German)

UBA. 2011. Kumulierter Energieaufwand von Materialien und Produkten *http://www.probas.umweltbundesamt.de/php/index.php*. Accessed 12.06.2011

UBA. 2016. Energieverbrauch der privaten Haushalte. *https://www. umweltbundesamt.de/daten/private-haushalte-konsum/energieverbrauch-der-privaten-haushalte*. Accessed 15.1.2016

Weiß, J. & Dunkelberg, E. 2010. Erschließbare Energieeinsparpotenziale im Ein- und Zweifamilienhausbestand. Institut für ökologische Wirtschaftsforschung (IÖW), Berlin. (in German).

Willms, M. 2013. Humusbilanzen im Energiepflanzenanbau: Gärreste gezielt rückführen und Fruchtfolgen anpassen. *Mais* **40**, 64–68. (in German)

# Quality labels in Estonian food market. Do the labels matter?

I. Riivits-Arkonsuo[*], A. Leppiman and J. Hartšenko

Tallinn University of Technology, Faculty of Economics, Institute of Business Administration, Ehitajate tee5, EE 19086 Tallinn, Estonia
[*]Correspondence: Iivi.riivits@ttu.ee

**Abstract.** The current study investigates the consumers' perception of quality labels for Estonian food. Based on empirical findings from a representative population survey, this paper analyzes and discusses consumers' attitudes and the behavioural consequences towards two quality labels and related campaigns: *the best Estonian foodstuff and the sign of national flag.* The representative survey was fielded annually, at first in 2009 following in the years 2011−2015. Every wave comprises the answers of 1,000 Estonian inhabitants. Employing the same methodology over the time the current study achieves an understanding of development in consumer awareness the quality labels and the impact of those labels on the purchasing behaviour. The paper enables to estimate the effectiveness of launching quality labels for foodstuffs and concludes that the labels serve their purposes.

**Key words:** quality food labels, consumer behaviour, hierarchy-of-effects (HOE), consumer decision-making.

## INTRODUCTION

Both in the European Union in general, and as well the Estonian producers, can incorporate a variety of food quality labels. Labels may provide information on the origin of the food or the quality of the product, refer to the long tradition-based production method, and indicate the specific features of the product. Such labels have a potential direct impact on consumer decision-making (Verbeke, 2005) and in turn, food producers discuss whether a use of the labels would be a useful tool in their overall marketing mix (Grunert & Aachmann, 2016).

Past research has examined how the food quality labels affect consumers. A literature review compiled by Grunert & Aachmann (2016) identifies 35 studies, published between 1999–2014 focuing on topic how EU promotes food quality labels. Based on a hierarchy of effects framework Grunert & Aachmann investigate what impact the labels have on consumer purchasing intention. They suggest that quality labels can have the function only to the extent that consumers are aware of them, understand them and use them in their decision-making. There is a solid body of research concerning region-of-origin labeling (Botonaki & Tsakiridou, 2004; Verbeke & Roosen, 2009; Deselnieu et al., 2013; Bryla, 2015; Lorenz et al., 2015) and labels of organic foods (Krystallis et al., 2006; Hughner et al., 2007; Larceneux et al., 2012; Jannsen & Hamm, 2014; Müller & Gaus, 2015).

On the other hand, there is a lack of the studies examining how quickly quality labels launched in the food market will achieve awareness, understanding, and behavioral consequence among consumers. Such studies would enable to determine whether the quality labels fulfill its' objectives of strengthening the domestic food sector. This study aims to fill the research gap in literature by taking the retrospective view of the consumers' responses concerning quality labels in Estonian food market focusing on two of them – *the best Estonian foodstuff* and the *sign of national flag.*

The quality label *the best Estonian foodstuff* refers to a new Estonian product that has passed and is awarded in the annual competition in its category. The product has to be manufactured in Estonia. The competition aims to encourage the food industry to carry out product development, introduce new foods to the consumers and retailers, and develop a positive attitude to food processing and food. Such competitions have been held since 1994. (Estonian Food Industry Association, 2016)

In June 2009, began the Estonian Food Industry Association in cooperation with the number the retail food chains, the campaigns intended to provide clear information to consumers of food products in the domestic origin. National flag sign in a product's price tag indicates that the Estonian food industry makes this product for people who appreciate the Estonian cuisine traditions and taste. The food industries that join the campaign for domestic products can be identified by the national flag label in the store price tags. With the sign of national flag, is labelled the products with the country origin, either produced or manufactured in Estonia. (Ministry of Rural Affairs, 2016) Thus, the aim of the aforementioned campaign is to meet the consumers' expectation to get accurate information concerning the domestic origin of food.

Since September 2009 began the Estonian Food Industry Association to measure the effects of those two labels (see Fig. 1) on consumer behaviour. The awareness and attitude, likewise the behavioural consequences are examined annually.

The authors of the current study utilise the data of the nationwide surveys and use the hierarchy-of-effects (HOE) framework to examine the effectiveness of those two quality labels in Estonian food market.



**Figure 1.** The labels of *national flag sign* and the *best Estonian foodstuff.*

HOE model explains a mental process that consumers go through while forming awareness, attitudes and making buying decisions. The information moves through a cognitive (learning, knowing), affective (thinking, feeling), and conative (intending, doing) sequence steps (Verbeke, 2005).

In HOE model, the consumer begins with no awareness of the brand (Smith et al., 2008) The following stage of consumer response involves learning and remembering the cues made in the marketing communications (Weilbacher, 2001). Awareness of the quality labels results from perception. Referring Grunert & Aachmann (2016) awareness can be regarded as a proxy of perception. Creating awareness through attention and interest is the key goal of marketing communications in HOE model. Once the consumers have the knowledge about quality labels, then they can develop the liking and preference. The affective component of the model contains the feelings and emotions, attitudes and attitudinal changes (Clow & Baack, 2004). The final stage in HOE model is the conation or purchasing intention stage (Smith et al., 2008)

There has been a long debate in behavioural sciences about the sequence and inter-distance of these hierarchical steps. For instance, sometimes the consumers first make a purchase following by develop knowledge, liking, and preference (Weilbacher, 2001; Clow & Baack, 2004; Verbeke, 2005). We considered that HOE model with the cognitive, affective and conative components fitted the best into the framework of the current study. The sequence and inter-distance of these hierarchical steps is out of scope of current study. The applying HOE model principles enable us to answer the research questions how the awareness of quality labels has changed over the time and what impacts have the labels to the purchasing intention.

## MATERIAL AND METHODS

This study utilizes data from a probability-based representative survey carried out by the research agency Turu-uuringute AS (Estonian Surveys Ltd.). A representative sample from a population stands for a scaled-down version of the entire population, where all different characteristics of the population are presented (Grafström & Schelin, 2014). All population members have a probability $p > 0$ of being in the sample (Aaker et al., 2004).

### Sampling procedure and study design

Respondents were recruited on a random sample basis to ensure the proportional representation of all Estonian counties and habitat types in the sample. The territorial model of the sample has been compiled by the population statistics database of the Estonian Statistical Office. In the first stage of random sampling, 100 sampling points were determined all over Estonia and the second step then yielded particular interviewees at every sampling point. Address selection relied on the source address method where every interviewer is given a randomly selected address to conduct the first interview. The interviewer will then move on according to a specific interval to ensure the randomness of domiciles in the sample. The respondent selection was subject to the so-called youngest male rule where the interviewer first requests to speak with the most immature man (at least 17 years old) currently at home. If no men are at home, the youngest female is the next preferred candidate. This sampling method ensures an increased probability of representation for those categories least likely to be found at home (predominantly young respondents or men). Aforementioned is done to provide the better coverage of genders and different age groups in the sample. The interviews were conducted in the respondents' homes in Estonian and Russian.

Due to the representative sample regarding major demographic criteria, the results can be extrapolated to the universe that is, all the Estonian population considering the margin of error.

Table 1 depicts the period when the nationwide surveys were conducted, the number of respondents, age of target group, and data collection methods. In 2014, Turu-uuringute AS renewed the data collection method introducing the computer-assisted personal interviews (CAPI) instead of previous paper and pencil personal interviews (PAPI). In the same year, the agency changed the scope of age the respondents, withdrawing the upper age limit 74 years.

**Survey instrument**

Asking awareness, dichotomous yes/no measures were used. Measuring the attitude toward the labels either single or multiple choice nominal scales were used. Impact on decision making was measured either by 4-points Likert scale or by multiple choice scale. In current study, the survey instrument and collected data are used post-hoc. That is, the instrument is not created for specific scientific purpose but based on the monitoring needs of Estonian Food Industry Association.

**Table 1.** Study methodology

| Time | n = respondents | Age | Data collection |
| --- | --- | --- | --- |
| 2009 September | 1,004 | 15–74 | PAPI |
| 2011 August | 1,000 | 15–74 | PAPI |
| 2012 September | 1,001 | 15–74 | PAPI |
| 2013 September | 998 | 15–74 | PAPI |
| 2014 September | 1,007 | 15+ | CAPI |
| 2015 September | 1,003 | 15+ | CAPI |

**Statistical analyses**

Analyses were conducted with SPSS version 21.0. In the analysis we have different type data: qualitative and quantitative. Descriptive statistics such as frequency and percentage distributions as well as parameters describing location and standard deviation were used in the analysis. Some statistical tests require that our data are normally distributed and therefore we use the Shapiro-Wilk test to check if this assumption is violated. The p-value is 0.000. We can't reject the alternative hypothesis and conclude that the data comes from a not normal distribution. As the dimension of data did not meet the assumption of normality, we used the Mann–Whitney, Chi square and Kruskal–Wallis tests to examine associations.

## RESULTS AND DISCUSSION

**Cognitive stage – awareness**

Implementing the HOE model to the context of the current study, the consumers begin with no awareness of the quality labels. Marketing communications create awareness through attention and interest.

Fig. 2 presents how the consumers have perceived the presence of the label *the national flag* on price tags when shopping.

Based on Fig. 2 above, we conclude relating the linear regression that there is on average the increase in awareness of 9 every year. In 2009, after launching the label the awareness was 34 while on last year already 81.
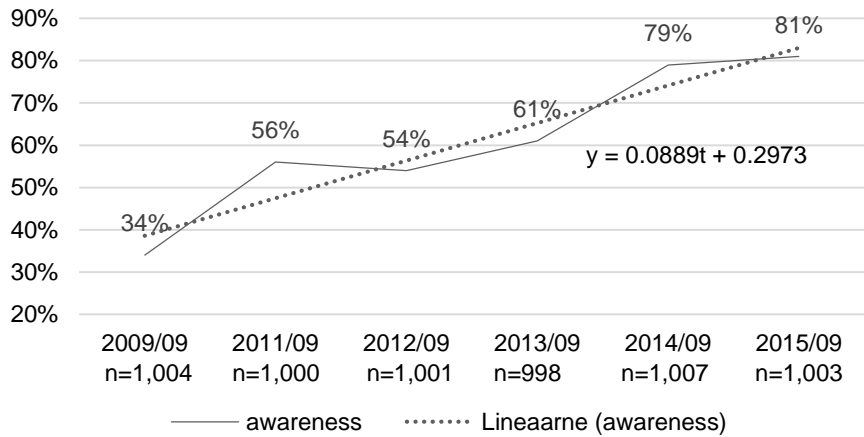


**Figure 2.** The dynamics of awareness the quality label (the sign of national flag) from launching to hitherto.

Fig. 3 compares in the run of last five years how the consumers have perceived the presence of the label the *best Estonian foodstuff* and the label *the national flag* on price tags when shopping. The awareness had been during the first three years when surveys carried out quite similar. The results of the studies in 2014 and 2015 show the increasing awareness.
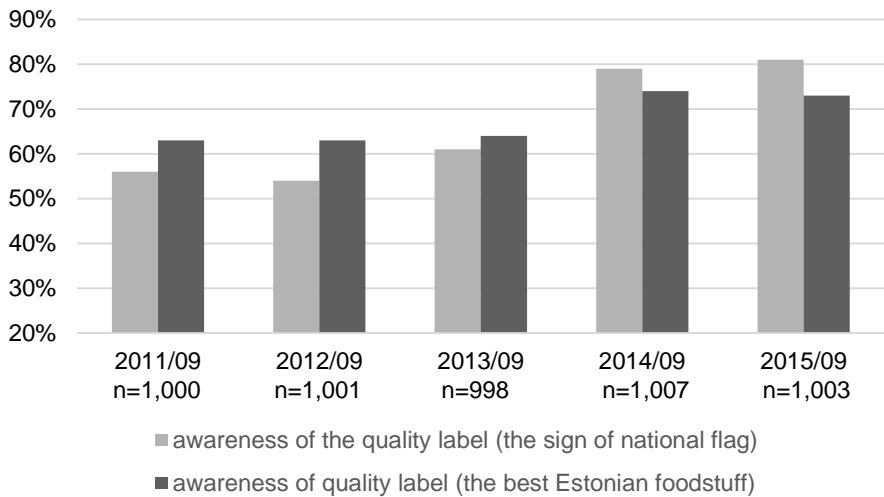


**Figure 3.** The dynamics of awareness the quality labels.

Compared to results the surveys of awareness European food quality certification schemes such as protected destination of origin (PDO, awareness 68%), protected geographical indication (PGI, awareness 36%), and traditional speciality guaranteed (TSG, awareness 25%) carried out in European countries (Verbeke et al. 2012) the awareness of local labels in Estonia is much higher when it comes to *national flag sign* and somewhat higher when it is the label *best Estonian foodstuff*. On the other hand, that comparison is not entirely correct because the characteristics of European food quality certification schemes mentioned above differ.

That is, PDO covers agricultural products and foodstuffs that are produced, processed, and prepared in a given geographical area while PGI refers to agricultural products and foodstuffs closely linked to the geographical area. Both schemes promoted by EU aim to protect product names from misuse and imitation. Estonian food quality labels *national flag sign* and *the best Estonian foodstuff*, in turn, are intended to propagate consuming and purchasing the food of Estonian origin. Common to PDO, PGI, and Estonian labels is that they help the consumers in the decision making.

The study by Verbeke and others (2012) analyses European consumers' awareness and determinants of use of PDO, PGI and TSG labels in six European countries (Italy, Spain, France, Belgium, Norway and Poland) using data from a cross-sectional survey with 4,828 participants. It is interesting to mention that awareness is higher among men and people aged above 50 years while the both quality labels in Estonia over the years are better known for women and individuals less than 50 years old.

Table 2 presents the results of analyzes related to awareness of quality label *the best Estonian foodstuff* and presents the socio-demographical variables of the respondents.

Thus, we can report a statistically highly significant difference between all background variables and awareness of the label *the best Estonian foodstuff*. The level of statistical significance was set at p-value is 0.05. Exception is the place of residence.

**Affective stage – attitude**
The affective component of the HOE model contains the attitudes and feelings. Beginning from the year 2013 the question 'Is the label *national flag sign* important to you?' was asked. When in 2013 (54.8%) respondents said that this label helped them recognize the food manufactured or produced in Estonia, then in the next 2014 year has the rate increased to 69.8% being in 2015 similar (57.5%) to the year 2013. Thus, we can conclude that quality label serves its purpose – for more than half respondents the label is relevant. On the other side, such relevance can explain with a normative preference for regional products, related to the concept of ethnocentrism (Lorenz et al. 2015).

26% of respondents in 2013, 14.5% in 2014, and 21.2% in 2015 reported that their habits and preferences are more important than the flag sign in price tags. Importance was measured by single choice nominal scale.

**Tabel 2.** Awareness of the quality label *the best Estonian foodstuff* between 2011 and 2013 by demography (%). *P-value used: Chi square association test

| Variable | Awareness 2011 | | p value* | Awareness 2012 | | p value* | Awareness 2013 | | p value* |
|---|---|---|---|---|---|---|---|---|---|
| | Yes | No | | Yes | No | | Yes | No | |
| **Age** 15–24 | 15.0 | 17.3 | 0.000 | 12.9 | 13.9 | 0.000 | 11.9 | 11.3 | 0.000 |
| 25–34 | 20.4 | 12.5 | | 22.7 | 11.0 | | 20.0 | 11.0 | |
| 35–49 | 29.8 | 16.7 | | 28.5 | 15.7 | | 29.4 | 19.9 | |
| 50–64 | 25.0 | 33.4 | | 24.5 | 37.1 | | 30.0 | 36.8 | |
| 65–74 | 9.8 | 20.1 | | 11.4 | 22.3 | | 8.8 | 21.0 | |
| **Gender** female | 61.6 | 49.5 | 0.000 | 59.4 | 47.2 | 0.000 | 59.8 | 43.0 | 0.000 |
| male | 38.4 | 50.5 | | 40.6 | 52.8 | | 40.2 | 57.0 | |
| **Household monthly net income** | | | | | | | | | |
| kuni 300 € | 9.6 | 22.3 | 0.000 | 12.7 | 16.9 | 0.001 | 7.7 | 13.9 | 0.000 |
| 301–400 € | 9.2 | 13.5 | | 15.5 | 20.5 | | 8.9 | 11.4 | |
| 401–500 € | 6.4 | 11.2 | | 16.3 | 17.5 | | 5.3 | 10.4 | |
| 501–800 € | 24.0 | 30.7 | | 19.6 | 12.8 | | 20.4 | 26.2 | |
| 801–1.300 € | 30.5 | 17.1 | | 12.7 | 6.5 | | 30.2 | 25.2 | |
| 1.301+ € | 20.2 | 5.2 | | 23.2 | 25.8 | | 27.4 | 12.9 | |
| **Education** | | | | | | | | | |
| Lower secondary | 16.2 | 28.0 | 0.000 | 11.0 | 22.0 | 0.000 | 9.2 | 16.5 | 0.000 |
| Upper secondary | 53.8 | 57.1 | | 60.1 | 59.6 | | 60.5 | 65.3 | |
| Higher education | 30.0 | 14.9 | | 29.0 | 18.4 | | 30.3 | 18.2 | |
| **Social status** | | | | | | | | | |
| Entrepreneur. manager | 17.6 | 6.7 | 0.000 | 19.0 | 10.4 | 0.000 | 23.3 | 23.3 | 0.000 |
| Office worker | 28.1 | 16.1 | | 23.0 | 12.8 | | 26.9 | 26.9 | |
| Tradesman | 14.2 | 20.1 | | 17.1 | 18.4 | | 13.8 | 13.8 | |
| Other employed | 5.1 | 7.9 | | 3.7 | 4.5 | | 5.6 | 5.6 | |
| Student | 7.2 | 8.8 | | 7.9 | 9.8 | | 6.4 | 6.4 | |
| Retired person | 15.4 | 29.5 | | 17.6 | 31.5 | | 14.2 | 14.2 | |
| **Language** Estonian | 82.4 | 52.9 | 0.000 | 82.8 | 58.8 | 0.000 | 79.8 | 44.3 | 0.000 |
| Other | 17.6 | 47.1 | | 17.2 | 41.2 | | 20.2 | 55.7 | |
| **Residence of living** | | | | | | | | | |
| Capital | 31.2 | 27.1 | 0.006 | 30.3 | 30.3 | 0.157 | 31.7 | 27.8 | 0.186 |
| City | 16.5 | 24.6 | | 20.8 | 19.3 | | 15.9 | 21.6 | |
| Regional center | 30.4 | 32.2 | | 26.9 | 32.9 | | 18.6 | 18.2 | |
| Country | 21.8 | 16.1 | | 22.1 | 17.5 | | 33.8 | 32.3 | |

Measuring the attitude towards label *the best Estonian foodstuff* the multiple choice scale was used. The results are presented in Fig. 4.
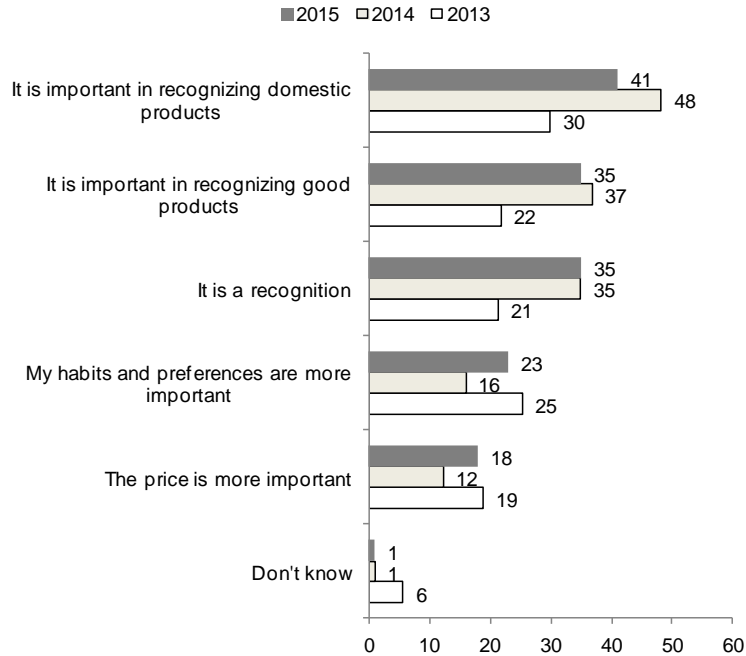


**Figure 4.** Importance the label *the best Estonian foodstuff*.

Comparing the results of three-year run can see that in last two year the importance of quality label has increased. Roughly saying almost a half part of respondents agree that the label is important in recognizing domestic foodstuff. One-third of respondents agree that those products represent an excellent quality, and one-third understands the label being the recognition.

**Conative stage - purchasing intention**

Next we show what impact has food quality label on consumer choices, in other words, does it influence the purchasing decision. In the HOE model, the last stage refers to the consumers' decision making.

The question asked was worded as follows: 'Does the label the best Estonian foodstuff have an impact on your buying decision?' A 4-point, Likert-type measurement scale was used, where 1 referred to 'No', 2 'rather no', 3 'rather yes', and 4 'yes'.

For analyzing the data set Kruskal-Wallis Test p-value was applied. The results (Table 3) provide the confirmation that the label has impact on buying decision when it comes to gender, age (in 2011 and 2013), education, social status (in 2011), place of residence (divided into the following variables: capital, cities and county centers, other town and rural), and region. Languages spoken in Estonia are Estonian and Russian. Language had an impact on the buying decision in 2013.

No significant differences in the purchasing intentions were found between people with different household monthly net income as well the social status in 2012 and 2013.

**Table 3.** Determinants of consumer's bying decision of the quality label (the best Estonian foodstuff)

|  | p-value* 2011 | p-value * 2012 | p-value* 2013 |
|---|---|---|---|
| Age | **0.003** | 0.372 | **0.013** |
| Gender | **0.045** | **0.000** | **0.006** |
| Household monthly net income | 0.167 | 0.076 | 0.524 |
| Education | **0.000** | **0.006** | **0.000** |
| Social status | **0.000** | 0.322 | 0.251 |
| Place of residence | **0.00** | **0.002** | **0.041** |
| Language | 0.362 | 0.071 | **0.048** |
| Region | **0.00** | **0.001** | **0.029** |

Note: * Kruskall-Wallis test was used.

Female consumers were significantly more to make a decision buying the product with the quality label. Furthermore, consumers with higher education were significantly associated with the purchasing intentions on products with the quality label.

## CONCLUSIONS

In the line with the study by Grunert & Aachemann (2016) presenting the reviews of 35 published research on how EU quality labels affect consumers, we highlight that quality labels can have the function only to the extent that consumers are aware of them, understand them and use them in their decision-making. Employing the same methodology over the time the current study achieves an understanding of development in consumer awareness regarding two Estonian food quality labels and their impact on the purchasing behaviour. Applying the HOE framework as the analytical model we come up with the following conclusions:

First, the general level of awareness of Estonian food quality labels is relatively high; suggesting that mainly consumers will perceive the presence of the label.

Second, beginning the year 2009 while the label *national flag sign* was launched its awareness increased from 34% to 81%. Thus, on average the increase in awareness has been near 9% every year.

Third, we can report a statistically highly significant difference between respondents' background variable (such as gender, age, household monthly net income, social status, and language) and awareness of the label *the best Estonian foodstuff*.

Fourth, quality label national flag sign serves its purpose – for more than half respondents the label is relevant. Moreover, our work provides evidence for manufacturers' and marketers' expectation that quality label *the best Estonian foodstuff* indluences consumers' purchasing decisions.

The authors of this study address the scales used for the survey instrument be the subject to statistical limitations. For instance, the attitudes towards quality labels were measured either by single or multiple choice nominal scales. It is a reason the reporting of results in the basic level. Furthermore, the survey started from 2009 is monitoring via the tracking studies. However, the survey instrument is not consistent. That is, the

questions and variables have been changed, removed, and added. Thus, comparability of the results between years suffers.

It would be desirable to investigate more the role of quality labels in actual decision-making. Additional studies are suggested how ethnocentrism will influence the perception of quality labels and particularly their purchasing behaviour.

# REFERENCES

Aaker, D.A., Kumar, V. & Day, G.S. 2004. Marketing Research. Eight Edition, John Wiley & Sons, Inc.

Botonaki, A. & Tsakiridou, E. 2004. Consumer response evaluation of a Greek quality wine. Acta Agriculturae Scandinavica Section C, *Food Economics* **1**(2), 91–98.

Bryla, P. 2015. The role of appeals to tradition in origin food marketing. A survey among Polish consumers. *Appetite* **91**, 302–210.

Clow, K.E. & Baack, D. 2004. Integrated Advertising, Promotion, and Marketing Communications. Second Edition. Upper Saddle River (N.J.): Pearson Prentice Hall.

Deselnieu, O.C., Constanigro, M., Souza-Monteiro, D.M. & McFadden, D.T. 2013. A meta-analysis if geographical indication food valuation studies: What drives the premium for origin-based labels? *Journal of Agricultural and Resource Economics* **38**(2), 204–219.

Estonian Food Industry Association 2016. http://toiduliit.ee/index.php. Accessed 7.1.2016

Grafström, A. & Schelin, L. 2012. How to Select Representative Samples. *Scandinavian Journal of Statistics* **41**, 277 –290.

Grunert, K.G. & Aachmann, K. 2016. Consumer reactions to use of EU labels on food products: A review of the literature. *Food Control* **59**, 178–187.

Hughner, R.S., McDonagh, P., Prothero, A., Shultz, C.J. & Stanton, J. 2007. Who are the organic food consumers? A compilation and review of why people purchase organic food. *Journal of Consumer Behaviour* **6**(2–3), 94–110.

Jannsen, M. & Hamm, U. 2014. Governmental and private certification labels for organic food: Consumer attitudes and preferences in Germany. *Food Policy* **49**, 437–448.

Krystallis, A., Fotopoulus, C. & Zotos, Y. 2006. Organic Consumers' Profile andTheir Willingness to Pay (WTP) for Selected Organic Food Products in Greece. *Journal of International Consumer Marketing* **19** (1), 81–106.

Larceneux, F., Benoit-Moreau, F. & Renaudin, V. 2012. Why Might Organic Labels Fail to Influence Consumer Choices? Marginal Labelling and Brand Equity Effects. *Journal of Consumer Policy* **35**(1), 85–104.

Lorenz, B.A., Hartmann, M. & Simons, J. 2015. Impacts from region-of-origin labeling on consumer product perception and purchasing intention – Causal relationships in a TPB based model. *Food Quality and Preference* **45**, 149–157.

Ministry of Rural Affairs 2016. http://www.agri.ee/et/eesmargid-tegevused/pollumajandus-ja-toiduturg/kvaliteedimargid#eesti. Accessed 7.1.2016

Müller, C.E. & Gaus, H. 2015. Consumer Response to Negative Media Information about Certified Organic Food Products. *Journal of Consumer Policy* **38**, 387–409.

Smith, R.E., Chen, J. & Yang, X. 2008. The Impact of Advertising Creativity on the Hierarchy-of-Effects. *Journal of Advertising* **37**(4) 47–61.

Verbeke, W. & Roosen, J. 2009. Market differentiation potential of country-of-origin, quality, and traceability labeling. The Estey Centre Journal of International Law and Trade Policy, **10**(1), 20–35.

Verbeke, W. 2005. Agriculture and the food industry in the information age. *European Review of Agricultural Economics* **32**(3), 347–368.

Verbeke, W., Pieniak, Z., Guerrero, L. & Hersleth, M. 2012. Consumers' awareness and attitudinal determinants of European Union quality label use on traditional foods. *Bio-based and Applied Economics* **1**(2), 213–229.

Weilbacher, W.M. 2001. Point of View: Does Advertising Cause a Hierarchy of Effects? *Journal of Advertising Research* **41**(6), 19–26.

# Small- and medium-scale biogas plants in Sri Lanka: Case study on flue gas analysis of biogas cookers

H. Roubík[*] and J. Mazancová

Czech University of Life Sciences Prague, Faculty of Tropical AgriSciences, Department of Sustainable Technologies, Kamýcká 129, CZ-165 00 Prague, Czech Republic; [*]Correspondence: roubik@ftz.czu.cz

**Abstract.** Biogas technology has received attention in Sri Lanka already from the initial days of the energy crisis in 1973. Biogas production by anaerobic fermentation is a promising method of producing energy while achieving multiple environmental benefits. The study was carried out in the different areas of Sri Lanka at the level of biogas plants owners (n = 51) and local consultants (n = 4) in August 2014. Methods of data collection included semi-structured personal interviews and questionnaire survey. Further, at 51 biogas plants flue gas analysis was done through the portable device TESTO 330-2, which is capable of capturing the gas concentration of CO and NO; consequently by recalculating the concentration of $CO_2$ and $NO_2$. Surprisingly, the quite high concentration of CO was detected $c(CO) = 1,008.92$ mg m$^{-3}$, which might be caused by one and/or various combinations of the following factors such as insufficient burning, inappropriate biogas cookers and inappropriate maintenance. The concentration of NO is under the value of 0.046 mg m$^{-3}$, which is under the permissible exposure limit of nitric oxide. Average temperature of flue gas is within the typical flue gas exit temperature for burning in biogas cookers (TS = 449.16 °C) and flue gas excess air (4.0%), however the air/gas efficiency (54.0%) was recognized at lower value than the optimal one for small- and medium-scale biogas plants. Easy energy access is a trigger for development, especially in terms of human, social and economic development and biogas plants represents a boon for farmers and rural people to meet their energy needs. However, further factors must be also examined and evaluated, such as exploration of gas composition and its microbiological content, emission analysis exploring particle size distribution, emission rates and potential harmful exposures.

**Key words:** biogas technology, biogas cookers, Sri Lanka, flue gas analysis.

## INTRODUCTION

Sri Lanka (officially the Democratic Socialist Republic of Sri Lanka) is an island country with abundant sun-light year-round in the northern Indian Ocean off the southern coast of the Indian subcontinent in South Asia (Kolhe et al., 2015). It has a total land area of 65.610 km$^2$ and an estimated population of 20.33 million (Department of Census and Statistics, 2013). There have been large increases in fossil fuels emissions (Mattsson et al., 2012), so further emission reduction potential should be considered.

In 2002 energy consumption was 4 GJ annual per capita showing a low level of industrial development in Sri Lanka. Biomass provided about 52% of total energy used, petroleum accounted for about 40% and electricity only for around 8%. The household energy consumption accounted for about 65% of total energy consumption and industry

for about 13%, transportation for further 13% and the rest for other purposes (de Alwis, 2002). These days Sri Lanka is still very reliant on the agricultural sector. Currently, the electricity generation system comprises 40.5% of hydropower, 49.0% of thermal power and 10.5% of renewable energy. However, in dry seasons the thermal power stations based on fossil fuels increase their share up to the 70% (Kolhe et al., 2015). Furthermore, Sri Lanka is currently dependent on imported fossil fuels, making the country vulnerable to the disruptions. The energy sector of Sri Lanka is expected to show further rapid growth in the coming decades, leading to higher $CO_2$ emissions (Selvakkumaran & Limmeechokchai, 2015). Therefore the low carbon activities and activities with beneficial impact in reducing the $CO_2$ emissions have to be designed and implemented.

The biogas technology was first introduced to Sri Lanka in 1970s (mainly on the research basis). In 2011 it was believed to be up to 5,000 biogas plants in use (de Alwis, 2002; Bond & Templeton, 2011); however, only one third of these BGPs functioned properly. Through the Sri Lanka Domestic Biogas Programme it was built further 3,150 biogas plants from 2011 to 2014[2]; however, the exact number of biogas plants in Sri Lanka remains unknown as well as information about distribution of different BGPs models. However, the most common types in Sri Lanka are the following: BGPs based on the Chinese fixed dome model (various sizes) and currently rising up model of Arpico based on floating drum models (1 $m^3$ and 5 $m^3$) and SiriLak Umaga model.

The small-scale BGPs are predominant in the target area where input material is commonly composited from one or various combinations of kitchen organic waste, kitchen waste water, market organic waste, and human waste without chemicals. The most common size of these small-scale BGPs is 8 $m^3$ with expected feedstock load of 25 kg of organic materials producing around 30 $m^3$ of biogas monthly. Medium-scale BGPs are mainly connected with the developing industrial sector (such as hotels, factories, farms, hospitals, religious places, training centres and prisons and force camps) in Sri Lanka.

Furthermore, community scale biogas plants are rising as well. Majority of above mentioned BGPs use standard two-flame biogas cookers from various manufacturers.

The Ministry proposal also highlights the objective of increasing the share of nonconventional renewable energy from 4.1% in 2007 to 20% in 2020 including BGPs (Anonymous, 2013a). To promote the expansion of feasible biogas production, optimisation of the whole process chain is essential (Mann et al., 2009). Biogas technology has already received attention in Sri Lanka from the initial days of the energy crisis in 1973, including 'Colombo Declaration', which was calling for regional development of biogas technology (de Alwis, 2002). The penetration of cleaner and energy efficient technologies in small power systems such as the case of Sri Lanka has encountered many problems, such as: high initial costs, unclear government policy, lack of financing instruments, lack of awareness about the usable technology and others (Priyantha et al., 2006).

The use of renewable energy sources is often suggested as a possible solution to reduce a nation´s contribution to climate change and its dependency on fossil fuels (Liu et al., 2010), but there is need for further evaluation (Zhang et al., 2013). Global

---

[2]Currently there is running The SWITCH-Asia joint partnership Project called Sri Lankan Renewable Energy focused on up-scaling of biogas technology in Sri Lanka.

warming, caused by increasing emissions of $CO_2$ and other greenhouse gases (GHGs) as a result of human activities, is one of the major threats currently confronting the environment (Fan et al., 2007). $CO_2$ accounts for the largest share of GHGs globally (Fan et al., 2007), for agricultural activities it is estimated to account for about 13.5% of the total GHG emissions (Phan et al., 2012) and if emissions are allowed to increase without limits, the greenhouse effect can possibly destroy the environment for humans and other living creatures, even threatening the existence of humankind (Fan et al., 2007).

Biogas production by anaerobic fermentation is a promising method of producing energy while achieving multiple environmental benefit e.g. fossil energy substitution, carbon emission reduction, pollution abatement, welfare improvement (Contreas et al., 2009; Zhang et al., 2013) and it was evaluated as one of the most energy-efficient and environmentally friendly forms and technologies for renewable energy production (Weiland, 2010). According to Pehme & Veroman (2015) technology of biogas production shows great environmental benefit in comparison with conventional technologies in terms of global warming potential. However, there are still some unscrutinised factors of biogas technology (Roubik et al., 2016) waiting for examination. One of such is a flue gas analysis of biogas cookers, as it can show the quality of combustion (Skanderová et al., 2015) having direct effect on service life of such a device (Roubik et al., 2016).

Household biogas cookers, although individually small in size, are numerous and thus have the potential to contribute significantly to inventories of GHGs (Obada et al., 2014). Biogas cookers are common in use in developing countries, where biogas technology is exploited. However, these biogas cookers do not achieve high and stabile combustion efficiency (SNV, 2001; Obada et al., 2014). Thereby, emitting a substantial amount of fuel carbon as product of incomplete combustion (such as carbon monoxide, methane and total non-methane organic compounds as well as carbon dioxide) can be expected (Ramana, 1991).

The major objective of this paper is to fill in the gap around flue gas of biogas cookers, to find out the quality and efficiency of combustion, because the inefficient combustion process can lead to the high emissions of carbon monoxide and nitrogen oxides (Skanderová et al., 2015). Therefore the flue gas analysis was conducted. This survey intends to provide in-depth understanding about the issue with taking into accounts possible risks. Investigating such a topic is within continuing concern about biogas technology in rural areas of developing countries.

## MATERIALS AND METHODS

### Target area, data collection methods and statistical analysis

The survey was carried out in the different areas of Sri Lanka: Ampara, Anuradhapura, Akkaraipathu, Arugambay, Batticaloa, Colombo, Galle, Kandy, Kegalle, Karuwalagaswewa, Galle, Puttlam, Nochchiyagama (Fig. 1), at the level of BGPs and BGP owners (*n = 51*) and local consultants (*n = 4*), in August 2014. Methods of data collection included semi-structured personal interviews, questionnaire survey at the level of BGP owners and local consultants and observation; and flue gas analyses at the level of biogas technology.

A semi-structured personal interviews and questionnaire survey were used to obtain information about biogas technology owners, time spent on maintenance of biogas technology, funding and economic aspects of the technology, and types of inputs, hours of cooking, digestate practices and information about biogas cookers. Small- and medium-scale biogas plants were chosen according to the list of the Czech NGO People in Need implementing the project: '*Promoting Renewable Energy as a Driver for Sustainable Development and Mitigation of Climate Change in Sri Lanka*' and local project partners from Janathakshan (GTE) Limited. Collected data were categorized, coded and analysed in a statistical programme Statistica 10. Due to the nature of data Spearmen's correlation coefficient ($\rho$) was used to detect possible relations between time spent on maintenance of biogas technology and its recalculated concentration of $CO_2$ from flue gas analysis and age of biogas cooker and recalculated amounts of $CO_2$ from flue gas analysis. Student´s *t*-test was used to determine if there are variances among flue gas analysis through categories of biogas plants.
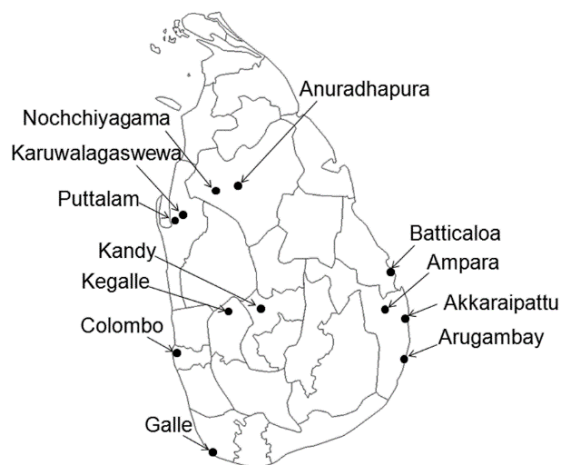


**Figure 1.** Map of visited areas (Sri Lanka).

### Biogas yield calculations
Minimal biogas yield from various biodegradable wastes (resulting from survey results of the most common input material) was calculated for an average biogas plant according to the typical yields in mesophilic conditions (*i.e.* 20–45 °C) according to IAEA (2008).

### Biogas plants categorization
For purposes of data representation, the categorization of biogas plants according to their size was chosen (Table 1).

**Table 1.** BGPs categorization

|  | No of analysed BGPs | Size of BGPs (m³)* |
|---|---|---|
| Community scale biogas plant | 4 | More than 60 |
| Medium-scale biogas plants | 16 | 12–60 |
| Small-scale biogas plants | 31 | Less than 12 |

*The size is showing the total volume of the biogas plant digester

**The flue gas analysis**

The flue gas analysis was done through the portable device TESTO 330-2 (Testo AG, Germany), which is capable of capturing the gas concentration of CO and NO; consequently by recalculating concentrations of $CO_2$ and $NO_2$. As specified by the manufacturer (Testo AG, Germany), the recommended minimum measurement time for obtaining accurate values covers 3 minutes for 90% response. After every measurement, the flushing of the device was done, according to recommended flushing times (automatically set up by the device according to the ppm concentrations).

Principle of recalculation of the mass concentration of $CO_2$ is following:

$$CO_2 \left[\frac{mg}{m^3}\right] = \frac{[CO_{2max} \cdot (O_{2ref} - O_2)]}{O_{2ref}} \tag{1}$$

where: $CO_{2max}$ – maximal concentration of $CO_2$; $O_{2ref}$ – referential oxygen value (21%); $O_2$ – measured concentration in %.

Principle of recalculation of the mass concentration of CO is following:

$$CO \left[\frac{mg}{m^3}\right] = \left[\frac{O_2 - O_{2refer}}{O_{2ref} - O_2}\right] \cdot CO_{ppm} \cdot 1.25 \tag{2}$$

where: $O_{2refer}$ – cross-referential oxygen value (3%, according to the manual-Testo AG, Germany).

Principle of recalculation of the mass concentration of NOx is following:

$$NO_x \left[\frac{mg}{m^3}\right] = \left[\frac{O_2 - O_{2refer}}{O_{2ref} - O_2}\right] \cdot CO_{ppm} \cdot 2.05 \tag{3}$$

The conversion factors (1.25 and 2.05 for the concentrations of CO and $NO_x$, respectively) are applied in above formulas 2 and 3 corresponding to the standard density in mg m⁻³ of the gas concerned. For $NO_x$ the standard density of $NO_2$ is used, because only $NO_2$ is a stabile compound and NO reacts very fast with oxygen to $NO_2$ (Testo, 2011).

## RESULTS AND DISCUSSION

With relatively stable thermal efficiency, biogas might be of a high heat value and is also convenient to use, making it appropriate for technological economy. Although, the structure of rural energy consumption has changed in Sri Lanka, cooking still plays the leading role in energy consumption in rural household and examined BGPs.

From the examined BGPs majority were fixed dome models (72.55%), followed by SiriLak Dahara models (21.57%) and Arpico models (5.88%). Majority of surveyed BGPs use standard two-flame biogas cookers (in case of larger BGPs multiple two-flame biogas cookers were in use) from various manufacturers. Commonly, biogas cookers were initially set within the implementation of BGP and fixed. For the small-scale BGPs various feedstock materials and their mixtures are used. Most common input material was kitchen waste (74.19%), followed by toilet waste (22.58%), pig manure (12.90%), cow dong (6.45%) and quail manure (3.22%). In case of medium-scale biogas plants, major input material was also kitchen waste (68.75%), followed by wastewater (37.5%) and pig manure (12.50%). In case of community scale BGPs majority of input material were market leftovers (vegetable mainly) in 50% and wastewater (also 50%), followed by rice starch in 25%.

If considered almost 20 m$^3$ as the average size of surveyed BGPs and average time of biogas cookers on active use: 6.03 hours/day (+/-3.98), with minimum 1 hour/day up to 12 hours/day – cooking during the full day without cease (counting with stabile feedstock), 600–700 m$^3$ of biogas generation per year can be expected (considering the fact that users use biogas until its end).

Table 2 shows average values of flue gas analysis calculated for all 51 BGPs. Interesting results are related to the high concentration of CO (mg m$^{-3}$) detected. This might be caused by the one and/or various combinations of the following factors such as insufficient burning, inappropriate biogas cookers and inappropriate maintenance. Table 2 shows also measured difference from concentration of CO in its diluted and undiluted form (37.59% in diluted form). The concentration of unavoidable produced NO equals $c(NO) = 0.05$ mg m$^{-3}$, which is showing still acceptable value for transformation of biodegradable wastes into biogas and its consequent burning. According to the Occupational Safety and Health Administration (OSHA) the permissible exposure limit for nitric oxide (NO) exposure is as (30 mg m$^{-3}$) over an 8-hour workday (NIOSH, 2015). As the typical flue gas exit temperature is in the range from 440 °C to 500 °C (Anonymous, 2013b). Average temperature of flue gas (TS) with almost 450 °C seems to be appropriate for average use of biogas cooker. However, the respondents reported occasional use of high temperatures to accelerate the process (*i.e.* cooking, water boiling). Such a practice can lead to the malfunction of biogas cooker (Roubík et al., 2016).

As the optimal air/gas efficiency is expected to be over 55% and if considered measured air/gas efficiency 54%, the further potential of a cooker could be maximised by improving air/gas regulation systems (KEBS, 2013) and maintenance habits of the users (Roubík & Mazancová, 2014).

If the biogas flame has too much fuel, then it will burn incompletely, giving unwanted CO, carbon particles and is less efficient (Fulford, 1996). Biogas cookers should run with a small excess of air to avoid the danger of flame have too much fuel (Fulford, 1996), however when the excess of air is too high it cools the flame resulting

also into lowering the efficiency. Our results of excess air (4%) in average, if compared with results of Obada et al. (2014) (1% among two types of biogas cookers), show slightly different values which might be caused also by the higher amount of inlet air jets.

**Table 2.** Average values from flue gas analysis (N = 51)

| $O_2$ (%) | $CO_2$ (%) | $CO_2$ max (%) | CO (mg m$^{-3}$) | CO (undiluted/ (mg m$^{-3}$)) | NO (mg m$^{-3}$) | TS* (°C) | Efficiency of flow (%) | Excess air (%) | Flow (l min$^{-1}$) |
|---|---|---|---|---|---|---|---|---|---|
| 13.30 | 4.95 | 13.6 | 1,008.92 | 2,683.99 | 0.046 | 449.16 | 53.96 | 3.99 | 0.66 |

*Average temperature of flue gas measured from biogas cooker outlet

The recalculated average concentrations of $CO_2$, CO and $NO_X$ s for all examined BGPs are shown in Table 3. A quite high dispersion of values of CO is obvious, which we assume are caused by the combination of several factors: variability of burning of biogas cookers during flue gas analysis, various input materials for BGPs and divergent maintenance of biogas cookers. These values are in accordance with values described in Obada et al. (2014) for similar biogas systems. However, interesting results were found out in following biogas systems: lower flue gas analysis results of the hotel medium-scale biogas plants (N = 6), which is expected to be caused by proper maintenance and proper BGP feeding. Similar results were found out in the case of tea farms (medium scale BGPs with higher reported time spent on maintenance of technology; N = 2). On the other hand, rice mills BGPs and pig farm BGPs (medium scale biogas plants, N = 6) showed higher flue gas analysis. In case of rice mill BGPs, we assume poor maintenance and composition of biogas feedstock can be main reasons.

**Table 3.** Recalculated values of essential compound from flue gas analysis (N = 51)

|  | $CO_2$ (mg m$^{-3}$) | CO (mg m$^{-3}$) | NOx (mg m$^{-3}$) |
|---|---|---|---|
| Average | 4.98 | 2,9495.60 | 0.02 |
| Min | 0.78 | 59.34 | 0 |
| max | 12.69 | 19,3500 | 0.65 |

There were no significant differences (using *t*-test) in results of flue gas analysis among size categories of biogas plants; as also mentioned in the study by Obada et al. (2014); showing so that the size of BGPs is not a crucial factor influencing the amount of flue gas of the biogas cookers. The factors *time spent on maintenance of biogas technology* and its *recalculated concentration of $CO_2$ from flue gas* analysis were analysed using Spearmen´s correlation. The results show that with higher time assigned to the maintenance, the flue gas analysis of $CO_2$ was slightly lower (Table 4). This implies the importance of proper maintenance and adequate time which need to be stipulated for the technology maintenance (Roubík & Mazancová, 2014). Furthermore, the age of biogas cookers and recalculated concentrations of $CO_2$ from flue gas analysis were contrasted by Spearmen's correlation coefficient. Results imply ($\rho = 0.286$, $\alpha = 0.05$) that with age of the biogas cookers the concentrations of $CO_2$ growth. This can be also caused by adherence of dirt on the biogas cookers, as well as the decreasing condition of the device.

**Table 4.** Relationship between maintenance of biogas technology and concentration of $CO_2$

| Category of biogas plants | Spearmen´s correlation coefficient |
|---|---|
| Community biogas plants | $\rho = -0.102$, $\alpha = 0.05$ |
| Medium-scale biogas plants | $\rho = -0.125$, $\alpha = 0.05$ |
| Small-scale biogas plants | $\rho = -0.091$, $\alpha = 0.05$ |

Also further consideration should be given to exploration of gas itself and its microbiological content. For example Vinneras et al. (2006) were trying to identify microbiological community in biogas systems. Low risks of spreading disease via biogas system were evaluated; however, wide variety of fungi, spore-forming and non-spore-forming bacteria was recognized in biogas. According to our survey bad smell was identified in 28% of cases signalling the possible presence of $H_2S$. However, this can be easily removed by the use of a $H_2S$ absorbent (Roubik et al., 2016). Further research should be done in characterization and analysis of emissions from biogas cookers, as similarly was done in study of Fan & Zhang (2001), with taking into account also particle size distribution, emission rates and potential exposures. Also further research focusing on effects of use of different biogas cookers on the flue gas during the time is needed.

## CONCLUSIONS

The technology of biogas production has multiple advantages: to reduce waste and transform it into valuable energy. Biogas plants in Sri Lanka offer environmental, health and socio-economic benefits for local, regional and even national level. However, further factors must be also taken into account, such as combustion of biogas and its consequent effects. Due to this reason this study provided view into the flue gas analysis connected to the biogas cookers. Flue gas analysis was done through the portable device TESTO 330-2, which is capable of capturing the gas concentration of CO, NO; consequently by recalculating concentrations of $CO_2$ and $NO_2$. In our case reflecting almost 20 $m^3$ as the average size of surveyed BGPs and average time of biogas cookers on use: 6.03 hours/day (+/- 3.98), with minimum 1 hour/day up to 12 hours/day (counting with stabile feedstock), 600–700 $m^3$ of biogas generation per year can be expected. Quite high concentration of CO was detected c(CO) = 1,008.92 mg $m^{-3}$), which might be caused by combination of the following factors such as: burning, inappropriate biogas cookers and inappropriate maintenance. The concentration of NO was c(NO) = 0.046 mg $m^{-3}$. Average temperature of flue gas was within the typical flue gas exit temperature for burning in biogas cookers (TS = 450 °C). Air/gas efficiency was slightly under the adequate value of 55% (54%), therefore further potential should be maximised by improving of air/gas regulation systems and maintenance habits of the users. Furthermore, excess air (4%) was analysed. Also bad odour was identified in 28% of cases signalling the possible presence of $H_2S$.

Easy energy access is a trigger for development, especially in form of human, social and economic development and biogas plants represents a boon for farmers and rural people to meet their energy needs. This study implies that it is important to explore further factors such as exploration of gas itself and its microbiological content with its effects on flue gas analysis, as well as exploring particle size distribution, emission rates and potential human harmful exposures. It is essential to minimize the potential conflict

among the environment, sustainable development and further use of biogas technology in rural areas of developing countries.

## REFERENCES

Anonymous. 2013a. Performance 2013 and Programmes for 2014. Ministry of Power and Energy, 2013.

Anonymous. 2013b. Producing and using biogas. FM BioEnergy. Available online: *http://adbioresources.org/wp-content/uploads/2013/06/59-80_chapter5_v41.pdf*

Alwis. A. 2002. Biogas – a review of Sri Lanka´s performance with a renewable energy technology. *Energy for Sustainable Development* **6**(1), 30–37.

Bond, T. & Templeton, M.R. 2011. History and future of domestic biogas plants in the developing world. *Energy for Sustainable Development* **15**, 347–354.

Contreas, A.M., Rosa, E., Perez, M., Langenhove, H.V. & Dewulf, J. 2009. Comparative life cycle assesment of four alternatives for using by-products of cane sugar production. *Journal of Cleaner Production* **17**, 772–779.

Department of Census and Statistics. 2013. National Accounts of Sri Lanka 2012. Available at: *http://www.statistics.gov.lk/national_accounts/National%20Accounts%20of%20Sri%20Lanka.pdf* (retrieved 2014-01-08).

Fan, Ch. & Zhang, J. 2001. Characterization of emissions from portable household combustion devices: particle size distribution, emission rates and factors, and potential exposures. *Atmospheric Environment* **35**, 1281–1290.

Fan, Y., Yiang, Q-M., Wei, Y-M. & Okada, N. 2007. A model for China´s energy requirements and $CO_2$ emission analysis. *Environmental Modelling and Software* **22**, 378–393.

Fulford, D., 1996. Biogas Stove Design – A short course. Available online: *http://www.kingdombio.com/BiogasBurner1.pdf*

IAEA. 2008. International Atomic Energy Agency: Guidelines for Sustainable Manure Management in Asian Livestock Production Systems. ISBN 978-92-0-111607-9

KEBS. 2013. Domestic biogas stoves – Specification. First edition. Kenya Bureau of Standards. KS 2520:2013.

Kolhe, M.L., Ranaweera, K.M.I.U. & Gunawardana, A.G.B.S. 2015. Techno-economic sizing off-grid hybrid renewable energy system for rural electrification in Sri Lanka. Sustainable *Energy Technologies and Assessments* **11**, 53–64.

Liu, Y.X., Langer, V., Jensen, H.H. & Egelyng, H. 2010. Life cycle assessment of fossil energy use and greenhouse gas in Chinese pear production. *Journal of Cleaner Production* **18**, 1423–1430.

Mann, G., Schlegel, M., Schumann, R. & Sakalauskas, A. 2009. Biogas-conditioning with microalgae. *Agronomy Research* **7**, 33–38.

Mattsson, E., Persson, U.M., Ostwald, M. & Nissanka, N. 2012. REDD+ readiness implications for Sri Lanka in terms of reducing deforestation. *Journal of Environmental Management* **100**, 29–40.

NIOSH. 2015. NIOSH Pocket Guide to Chemical Hazards. Available online: *http://www.cdc.gov/niosh/npg/npgd0448.html*

Obada, D.O., Dauda, M., Anafi, O.F., Samotu, I.A. & Chira, Ch.V. 2014. Production of biogas and greenhouse implication of its combustion device. *Advances in Applied Science Research* **5**(2), 279–285.

Pehme, S. & Veroman, E. 2015. Environmental consequences of anaerobic digestion of manure with different co-substrates to produce bioenergy: A review of life cycle assessments. *Agronomy Research* **13**(2), 372–381.

Phan, N-T., Kim, K-H., Parker, D., Jeon, E-Ch., SA, J-H., Cho & Ch-S. 2012. Effect of beef cattle application rate on CH4 and $CO_2$ emissions. *Atmospheric environment* **63**, 327–336.

Priyantha, D.C.W., Siriwardena, K., Fernando, W.J.L.S., Shrestha, R.M. & Attalage, R.A. 2006. Strategies to overcome barriers for cleaner generation technologies in small developing power systems: Sri Lanka case study. *Energy Conversion and Management* **47**, 1179–1191.

Ramana, V. 1991. Biogas Programme in India, 1(3), 1–12.

Roubík, H., Mazancová, J. 2014. Identification of context specific knowledge as tool for facilitators and their quality involvement. *11th International Conference on Efficiency and Responsibility in Education*. Prague, 664–670.

Roubík, H., Mazancová, J., Banout, J. & Verner, V. 2016. Addressing problems at small-scale biogas plants: a case study from central Vietnam. *Journal of Cleaner Production* **112**(4), 2784–2792.

Selvakkumaran, S. & Limmeechokchai, B. 2015. Low Carbon Scenario for An Energy Import-Dependent Asian Country: The Case Study of Sri Lanka. *Energy Procedia* **79**, 1033–1038.

Skanderová, K., Maľák, J. & Bradna, J. 2015. Energy use of compost pellets for small combustion plants. *Agronomy Research* **13**(2), 413–419.

SNV. 2001. A study report on Efficiency Measurement of Biogas, Kerosene and LPG stoves: *http://www.snvworld.org/files/publications/efficiency_measurement_of_biogas_kerosene_and_lpg_stoves_nepal_2001.pdf*

Testo. 2011. Flue Gas Analysis in Industry. Practical guide for Emission and Process Measurements. 2nd edition. Available online: *http://www.testo350.com/downloads/Flue_Gas_in_Industry_0981_2773.pdf*

Vinneras, B., Schonning, C. & Nordin, A. 2006. Identification of the microbiological community in biogas systems and evaluation of microbial risks from gas usage. *Science of the Total Environment* **367**, 606–615.

Weiland, P. 2010. Biogas productions: current state and perspectives. *Application of Microbiology and Biotechnology* **2010**, 849–860.

Zhang, L.X., Wang, C.B. & Song, B. 2013. Carbon emission reduction potential of a typical household biogas system in rural China. *Journal of Cleaner Production* **47**, 415–421.

# Development of belt sorters smoothly adjustable belt drums

K. Soots[*], T. Leemet, K. Tops and J. Olt

Institute of Technology, Estonian University of Life Sciences, Fr.R. Kreutzwaldi 56, EE51014 Tartu, Estonia; [*]Correspondence: kaarel.soots@emu.ee

**Abstract.** Belt sorters are used to sort different type of objects according by their size. Making belt sorter easily and quickly adjustable in desired range has positive influence on it's functionality and productivity. One solution for that is to use one or more adjustable belt drums. This option allows to change the distance between belts evenly and through this change the mesh size so to speak. Greater benefits will be obtained if belt drum is smoothly adjustable. The aim of this research paper is to compare technical peculiarities of two patented technical solutions for smoothly adjustable drum and identify if the newer has benefits compared with the older one. In this study comparative tests are performed using real prototypes. Both prototypes have key structure that determine the range of their adjustability. Prototype with older technical solution contains CNC milled key structure and prototype with improved solution contains 3D printed key structure. Prototype's mechanical parameters like belt pulleys backlash relative to the fixing point, backlash between two neighboring belt pulleys and required torque to regulate slot width between belt pulleys are studied. Also, it is considered how both technical solutions influence the sorting quality. During this study different measuring instruments are used included laser scanner. Obtained results are used to develop better and more reliable technical solution for belt sorters that can be used in berry processing lines.

**Key words:** agricultural engineering, post–harvest treatment, berry sorter, blueberry, product development.
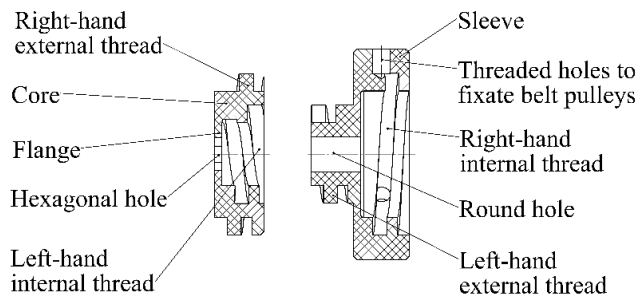
## INTRODUCTION

Belt sorter with adjustable fractioning slot has wider utilisation range than belt sorter without that function. For example, when sorting berries then it is possible to use adjustable sorter for different berry varieties or to adjust berry fraction size by customer needs. Thus, it will increase utilisation possibilities of berries' post–harvest processing lines with belt sorters like Lakewood Process Machinery (2014) produces (Olt, 2015; Soots & Olt, 2016). Belt sorter sorting area is formed by belts that are placed on drums. Drums should have rabbets on their sides to fixate belts in the right position thus determining fractioning slot width between belts. The idea of making belt sorter adjustable is to distribute belt pulleys' rabbets evenly along the axis of drum. This can be done using one or more smoothly adjustable drums. For the belt sorter to be applicable in practice, the adjusting process should be fast, easy and uniform.

According to our previous research (Soots et al., 2014) technical solution, that is described in patent EE05642 B1 (hereinafter referred to as 1st generation), has problems with belt pulleys' backlash relative to the fixing point in a work situation. It causes changes in fractioning slot width between belts and that affects uniformity of sorted

fractions (Soots et al., 2014). 1st generation has a technical flaw which may cause this problem. More precisely, the key structure in 1st generation is steering shaft (patent EE05642 B1, 2013). Steering shaft moves and fixes belt pulleys on pipe–shaped casing. Steering shaft has right–hand and left–hand guiding grooves with variable step. Every belt pulley is connected to the steering shaft through the longitudinal opening in pipe–shaped casing with a single bolt in such a way that the tip of the bolt reaches inside the guiding groove of the steering shaft (patent EE05642 B1, 2013; Soots et al., 2014). The problem of the backlash comes from the fact that every belt pulley is connected to the steering shaft by only one bolt. This problem could be solved by adding extra fixing points to each pulley. Unfortunately, it cannot be done in the case of 1st generation because guiding grooves will overlap each other and that may cause malfunctions during adjustment.

To solve this problem, new and improved technical solution was developed. This 2nd generation technical construction is described in patent application P201400049 (in press). If the key structure in the 1st generation construction is a single-piece steering shaft with guiding grooves to move and fix belt pulleys, then the key structure in the 2nd generation construction contains whole set of cores and sleeves (see Fig. 1) that allow to adjust distance between belt pulleys evenly.



**Figure 1.** 2nd generation core and sleeve cross-section view.

Beside the need to improve how belt pulleys move and fix, the pipe–shaped casing production technology needs improvement too. The pipe–shaped casing with one longitudinal opening of the 1st generation construction is made of welded cold drawn cylinder steel tube. Reason for using this kind of tube is that the tube's inner and outer surface must be smooth and dimensionally accurate. When the longitudinal opening was milled in the tube, the diameter of the tube increased in the middle of tube probably due to internal stress. This causes a need to remove extra material with turning to ensure accurate and even outer diameter of the tube.

The aim of this research is to compare technical differences of the two patented technical solutions for smoothly adjustable drum and identify if the newer construction has any benefits compared to the older one. To accomplish this, following steps were taken and measurements done:

1. Prototyping 2nd generation core and sleeve.
2. Performing stress relieving annealing for pipe–shaped casing before milling longitudinal openings and determining outer diameter change.
3. Measuring backlash between two neighboring belt pulleys.

4. Measuring belt pulleys backlash relative to the fixing point when belt pulleys are fixed at one point.

5. Measuring the torque that is required to regulate slot width between belt pulleys.

## MATERIALS AND METHODS

For tests, prototypes of both generations are required. 1st generation remained from our previous research (Soots et al., 2014), but 2nd generation prototype was specifically manufactured for the purposes of this research.

### Prototyping core and sleeve for 2nd generation

2nd generation core and sleeve given in Fig. 1 were manufactured by 3D printing. 3D printing is widely used for this kind of rapid prototyping (Wu et al., 2015). 3D printing has many different technologies but in this case fused deposit modelling (FDM) 3D printing was used. This technology was chosen due to its ability to manufacture complex parts quickly and easily with modest costs. The idea of FDM technology is to create details layer by layer with thermoplastic filament (Palermo, 2013; Wu et al., 2015; Stratasys Ltd., 2016). In this research Stratasys uPrint SE Plus was used and the printing layer height was 0.254 mm (Stratasys Ltd., 2016). Reason why this 3D printer was chosen is that it allows to print soluble support material in addition to the basic material. 3D printing doesn't allow to print in the air and protruding parts of the details need to be supported from below. Many FDM technology 3D printers print the parts and required supports using the same material and after printing, supports are removed mechanically thus, the detail surface quality may decrease. With Stratasys uPrint SE Plus 3D printer the supports are printed with soluble material that are later removed in a special cleaning machine. In this research Stratasys WaveWash support cleaning system was used to remove supports from core and sleeve. To ensure core rotational movement in the sleeves, clearance of 0.25 mm between the printed parts was chosen for 3D printing (Peets, 2016).

### Pipe–shaped casing manufacturing

2nd generation pipe–shaped casing is made of welded cold drawn cylinder tube that is made of steel E355 (Novero S.P.A., 2016). Inner diameter of the used tube is 70 mm and outer diameter 80 mm, according to manufacturer's certificate (Novero S.P.A., 2016). While 1st generation pipe–shaped casing has just one longitudinal opening, 2nd generation casing has three openings in order to add the extra belt pulleys' fixing points to the regulating element. Before milling the longitudinal openings in pipe–shaped casing, the stress relieving annealing was performed. According to material certificate, this must be done at temperature 580–630 °C and holding time of 1–2 min per mm of plate thickness, but holding time must be at least 30 min (Fischer et al, 2010; ThyssenKrupp, 2016). The thermal treatment was done at the local aluminium casting workshop at 450 °C with duration of 4.5 hours. After the thermal treatment and milling, the pipe–shaped casing's outer diameter was measured with Nikon measuring arm MCAx20 combined with laser scanner MMDx50. According to Nikon Metrology NV, 2016, accuracy of this laser scanning system is 50 μm. Obtained results were processed with Nikon Focus software. Outer diameter was measured in five places on the tube.

First measurement was taken 3 mm from the beginning of the tube, following four measurements with 130 mm increments.

In addition to thermal treatment of the pipe–shaped casing, changes in the construction of longitudinal openings were also made. Compared to 1st generation, the 2nd generation pipe–shaped casing has two small bridges in between each longitudinal opening as it is shown in Fig. 2.
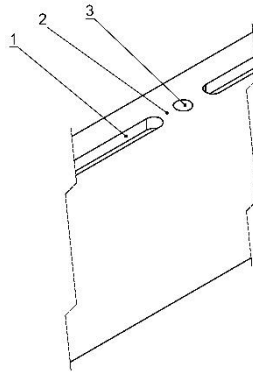


**Figure 2.** Bridges in between longitudinal openings (1 – longitudinal openings; 2 – bridges; 3 – opening for middle belt pulley fixing element).

This improvement in construction of the longitudinal opening should guarnatee that the outer diameter remains constant after milling longitudinal openings even if the thermal treatment has not fully relieved the inner stress of the casing.

### Backlash between two neighboring belt pulleys

Backlash between two neighboring belt pulleys was measured with Mitutoyo Absolut AOS Digimatic Caliper (code no 500–161–30) with accuracy ± 0.02 mm (Mitutoyo, 2016). Measurements were made at minimum, medium and maximum slot width (0, 6 and 10 mm, respectively) with both generations. 1st generation prototype has 23 belt pulleys and 2nd generation prototype has 17 belt pulleys.

### Belt pulleys' backlash relative to the fixing point

Belt pulleys' backlash relative to the fixing point when belt pulleys are fixed at one point was measured. This is the biggest problem with 1st generation construction (Soots et al., 2014). Measurements were made using Mitutoyo Absolut AOS Digimatic Caliper (code no 500–161–30) with accuracy ± 0.02 mm (Mitutoyo, 2016). Measurements were taken in medium slot width, where slot width between belt pulleys is 6 mm. In case of 1st generation construction, each belt pulley has one fixing point to the steering shaft and measurements were taken at the opposite side of fixing points. In case of 2nd generation construction, each belt pulley has three fixing points to the sleeve and measurements were taken at the opposite side of each fixing point.

**Required torque to regulate slot width between belt pulleys**

Required torque to regulate the slot width between belt pulleys must be determined in such a way that torque, rotational speed of the regulating lever, and angle of rotation can be measured continuously at the same time. Tests were carried out with tensile testing system Instron 5969, 1 kN load cell was used. Picture of the test setup to measure required torque to regulate slot width between belt pulleys is shown in Fig. 3.
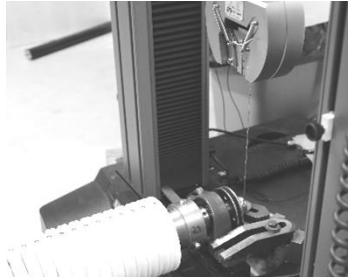


**Figure 3.** Picture of the test setup to measure required torque to regulate slot width between belt pulleys.

As it is shown in Fig. 3, smoothly adjustable drum is fixed to the base of tensile testing system. Regulating lever of drum is connected via grip to steel hawser. Diameter of the regulating lever is 29.90 mm for 1$^{st}$ generation and 30.09 mm for 2$^{nd}$ generation construction. For tests, tensile speeds of 30 mm min$^{-1}$ and 130 mm min$^{-1}$ were used. When converted to the rotational speeds of the handle, 1$^{st}$ generation handle rotational speeds are 0.32 min$^{-1}$ and 1.384 min$^{-1}$ and 2$^{nd}$ generation handle rotational speeds are 0.318 min$^{-1}$ and 1.376 min$^{-1}$. Handle rotation scope for 1$^{st}$ generation is 340 deg and for 2$^{nd}$ generation is 215 deg. All tests were performed without belts and without any force on belt pulleys.

## RESULTS AND DISCUSSION

**Prototyping core and sleeve for 2$^{nd}$ generation**

2$^{nd}$ generation 3D printed core and sleeve are shown in Fig. 4. In the figure also support material (white) can be seen.



**Figure 4.** 2$^{nd}$ generation 3D printed core and sleeve.

Results show that used 3D printing technology is suitable for function testing. With used FDM technology, parts are printed layer by layer and threads' surfaces are not smooth. They remind little steps as can be seen in Fig. 4. The smaller is thickness of the printed layer - the smaller are the steps. The used 3D printer allows to use minimal layer thickness of 0.254 mm, so the steps are 0.254 mm high. This affects parts surface roughness and thereby core movement inside the sleeves.

Chosen clearance between the printed parts was sufficient to obtain movement between them and only minor mechanical polishing and oil lubrication was required.

### Pipe–shaped casing manufacturing

The results of outer diameter measurements of the pipe–shaped casing are shown in Fig. 5.
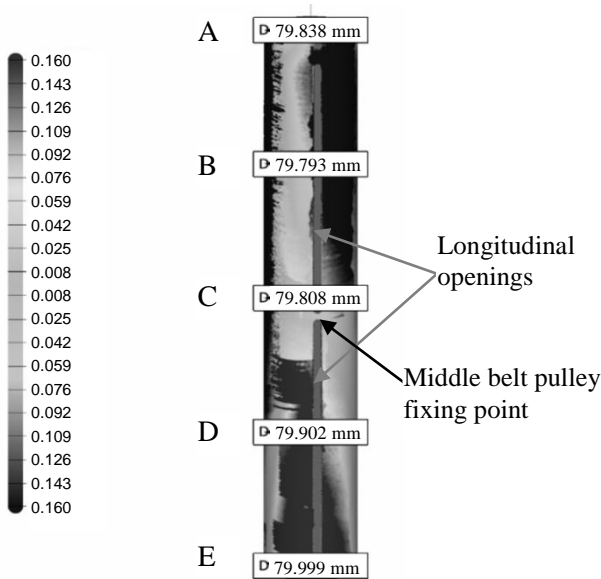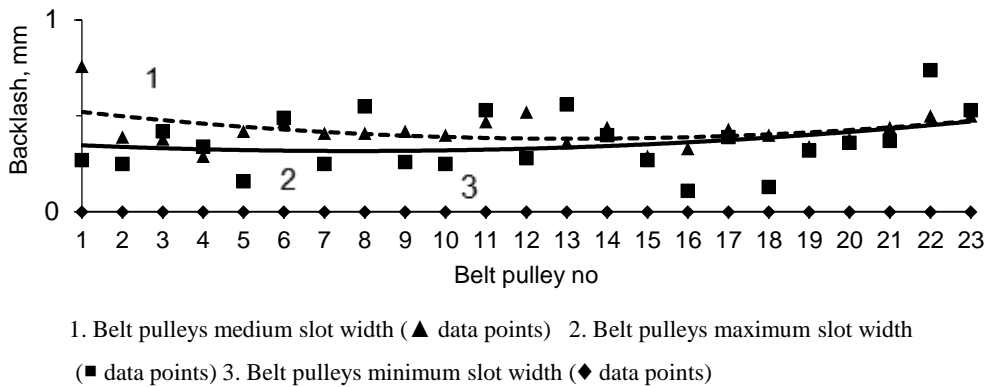


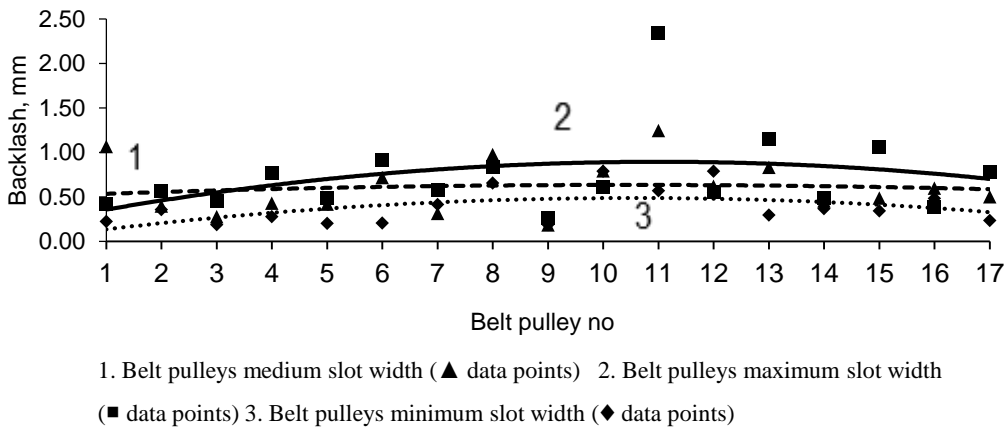**Figure 5.** Determination of outer diameter of the pipe–shaped casing.

According to the pipe manufacturer's certificate nominal outer diameter of the pipe is 80 mm, tolerances are not given. All the obtained results stayed below that value and did not show any increase of outer diameter in the middle of longitudinal openings (Fig. 5 measurements in points B and D) compared to the middle and ends of pipe-shaped casing.

### Backlash between two neighboring belt pulleys

Results of the tests where backlash between two neighboring belt pulleys was measured are shown in Figs 6 and 7.

1. Belt pulleys medium slot width (▲ data points)  2. Belt pulleys maximum slot width

(■ data points) 3. Belt pulleys minimum slot width (♦ data points)

**Figure 6.** 1st generation backlash between two neighboring belt pulleys.



1. Belt pulleys medium slot width (▲ data points)  2. Belt pulleys maximum slot width

(■ data points) 3. Belt pulleys minimum slot width (♦ data points)

**Figure 7.** 2nd generation backlash between two neighboring belt pulleys.

Results of tests where backlash between two neighboring belt pulleys where measured shows that:

1. 1st generation backlash between two neighboring belt pulleys is smaller than that of 2nd generation.

    a.   at minimum slot width between belt pulleys, 1st generation average backlash between two neighboring belt pulleys is 0 mm. In case of 2nd generation, average backlash is 0.40 mm at the same conditions.

    b.   at average slot width between belt pulleys, 1st generation average backlash between two neighboring belt pulleys is 0.42 mm. In case of 2nd generation, average backlash is 0.61 mm at the same conditions.

    c.   at maximum slot width between belt pulleys, 1st generation average backlash between two neighboring belt pulleys is 0.36 mm. In case of 2nd generation, average backlash is 0.74 mm at the same conditions.

2. 2nd generation the outermost belt pulley's backlash relative to the middle one depends on the backlashes of other belt pulleys that are between them. This is due to the

constructional peculiarities of II generation. Particularly, that outermost sleeve is connected to the middle sleeve through all cores and sleeves between them and the clearances of all the threads accumulate.

3. 1st generation outermost belt pulley backlash relative to the middle one doesn't depend on backlash of other belt pulleys because every thread is independent on a single solid steering shaft.

4. In case of both generations, average backlashes between two neighboring belt pulleys depend on the slot width between belt pulleys.

**Belt pulleys backlash relative to the fixing point**

Test results for belt pulleys backlash relative to the fixing point are given in the Figs 8 and 9.
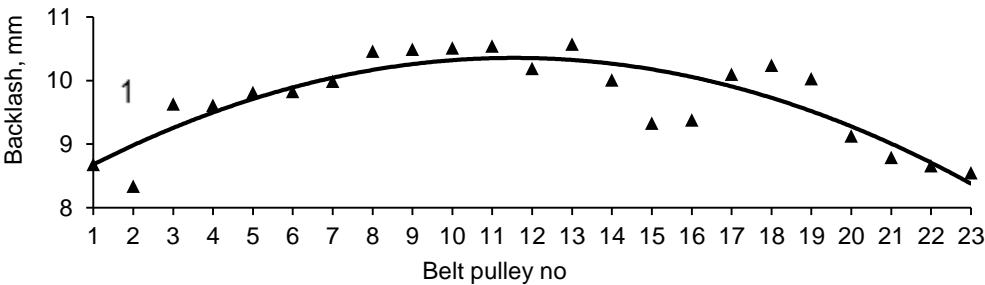


**Figure 8.** 1st generation belt pulleys backlash with medium slot width, measured at the opposite side of belt pulley fixing point.
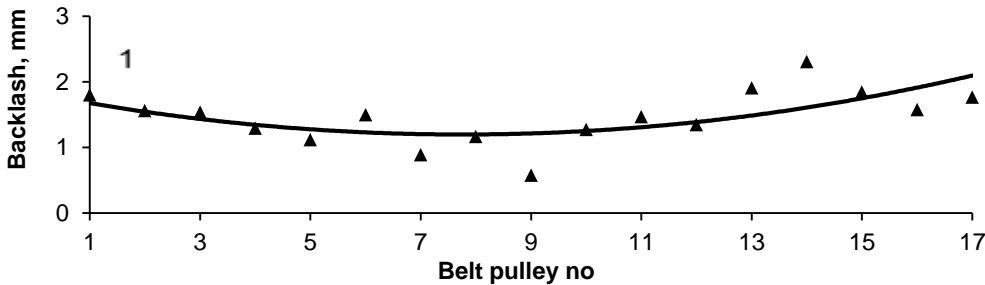


**Figure 9.** 2nd generation belt pulleys backlash with medium slot width, measured at three opposite sides of belt pulleys fixing points.

Obtained test results about belt pulleys backlash relative to the fixing point show that:
1. 1st generation belt pulleys' backlash (maximum 10.57 mm) is greater than 2nd generation (maximum 2.31 mm).
2. 1st generation belt pulleys' backlash decreases away from the middle of pipe–shaped casing where the middle belt pulley is fixed.
3. 2nd generation belt pulleys' backlash increases away from the middle of pipe–shaped casing where the middle belt pulley is fixed.

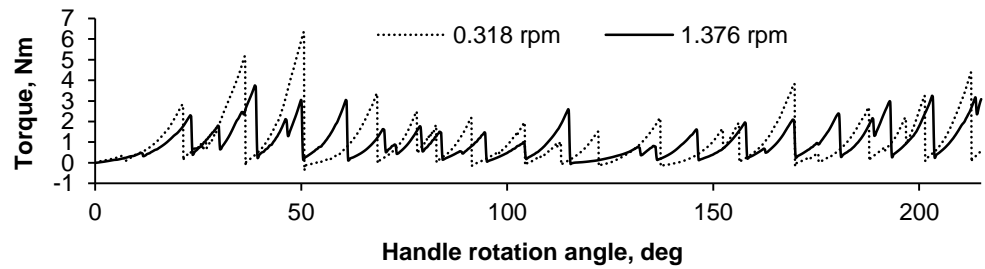**Required torque to regulate slot width between belt pulleys**

Test results for required torque to regulate slot width between belt pulleys are shown in Figs 10–13. Handle position of 0 deg in Figs 10 and 12 indicates minimum slot width between belt pulleys. In Figs 11 and 13 the 0 deg indicates maximum slot width between belt pulleys. While Figs 10–13 show the shape of curves, Fig. 14 shows the summarized results from tests.
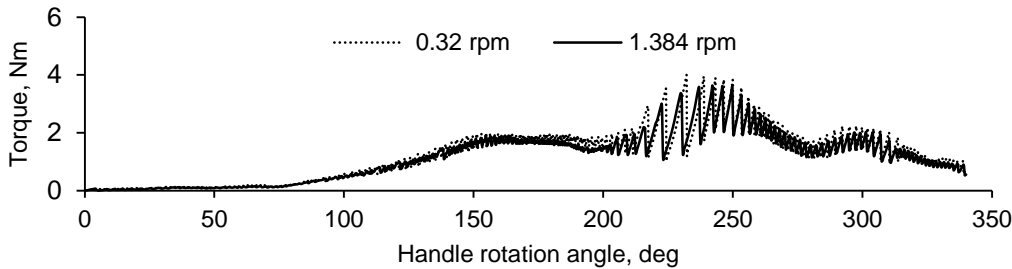


**Figure 10.** Required torque to increase the slot width between belt pulleys for 1$^{st}$ generation with two regulating speeds.
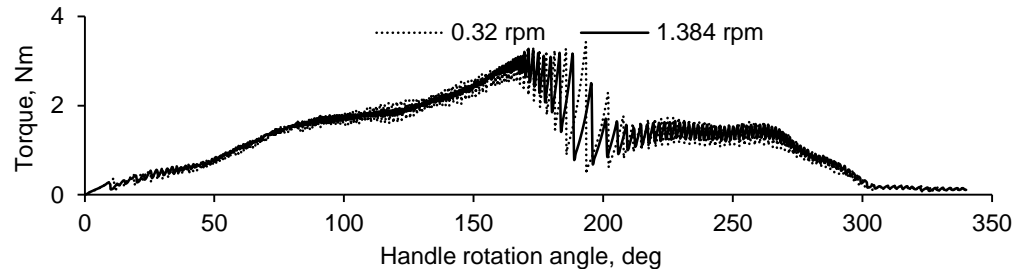


**Figure 11.** Required torque to decrease the slot width between belt pulleys for 1$^{st}$ generation with two regulating speeds.
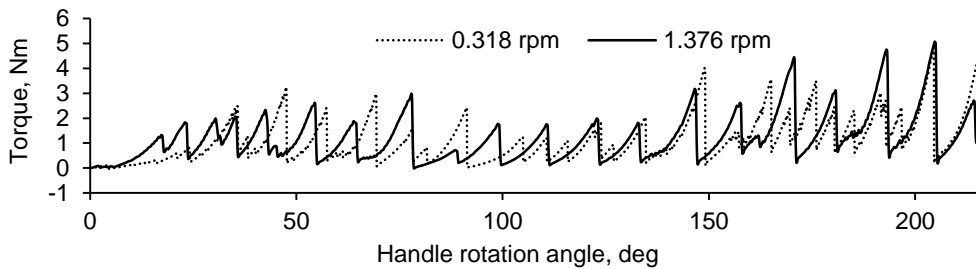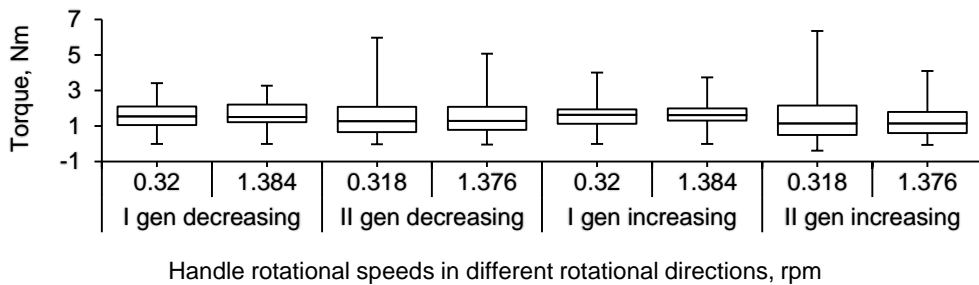


**Figure 12.** Required torque to increase the slot width between belt pulleys for 2$^{nd}$ generation with two regulating speeds.

**Figure 13.** Required torque to decrease the distance between belt pulleys for 2nd generation with two regulating speeds.



**Figure 14.** Summarized results for required torque to regulate the slot width between belt pulleys.

Obtained test results for required torque to regulate slot width between belt pulleys show that:

1. With 1st generation the required torque to regulate is maximum at the medium slot width when decreasing or increasing the slot width between belt pulleys.

2. With 2nd generation the required torque to regulate is stepped because the thread surfaces of 3D printed parts are also stepped, not smooth. Every step starts with smooth rise and ends with rapid decrease.

3. According to test results the 2nd generation maximum required torque for regulate is higher than 1st generation. With 2nd generation 6.35 Nm is required when increasing slot width at rotational speed 0.318 rpm but with 1st generation 4.01 Nm is required when increasing slot width at rotational speed 0.32 rpm.

4. Mean required torque to regulate is smaller with 2nd generation in both regulating directions and with both rotational speeds.

5. 2nd generation required torque to regulate dispersion is bigger than it is with 1st generation with both regulating speeds and direction as it is presented in Table 1 (raw-data is obtained from Instron tensile testing system and standard deviation is calculated in MS Excel).

6. For both generation faster regulating speed decreases required torque to regulate dispersion and it's maximum value.

**Table 1.** Standard deviations of required torque for regulating distance between belt pulleys at different regulating speeds for 1st and 2nd generation

| | 1st gen decreasing | | 2nd gen decreasing | | 1st gen increasing | | 2nd gen increasing | |
|---|---|---|---|---|---|---|---|---|
| | 0.32 rpm | 1.384 rpm | 0.318 rpm | 1.376 rpm | 0.32 rpm | 1.384 rpm | 0.318 rpm | 1.376 rpm |
| Standard deviation, σ | 0.79 | 0.75 | 1.04 | 1.00 | 0.84 | 0.72 | 1.23 | 0.82 |

In conclusion, it can be said that 2nd generation fixes the biggest problem that 1st generation has. 1st generation belt pulleys' backlash relative to the fixing point is a maximum of 10.57 mm but 2nd generation has a maximum belt pulleys' backlash relative to the fixing point of 2.31 mm. Desired backlash relative to the fixing point should be maximum of 0.5 mm at all slot widths. But on the other hand 2nd generation has some new problems. Test results show that the technology that is used to prototype core and sleeve for 2nd generation don't suit very well in this case and more suitable technology must be used. It is essential to ensure smooth thread surface finish and smaller clearance between core and sleeve threads to avoid the accumulating backlash between two neighboring belt pulleys and ensure more even and lower required torque to regulate slot width between belt pulleys. Because of required clearance between 3D printed parts, backlash between two neighboring belt pulleys is bigger than it's should be and it depends on slot width between belt pulleys. Desired backlash between two neighboring belt pulleys should be maximum of 0.5 mm and it should not be dependent on slot width between belt pulleys. Decreasing clearance between core and sleeve will have positive affect on belt pulleys backlash relative to the fixing point and especially on backlash between two neighboring belt pulleys. Overall 2nd generation technical solution showed promising results and has more potential than 1st generation.

## CONCLUSION

This paper compares technical characteristics of two patented technical solutions of smoothly adjustable drum and brings out their pros and cons. Main constructional differences are:

1. 1st generation key structure is single one-piece steering shaft with right–hand and left–hand guiding grooves with variable step while 2nd generation has multiple sets of cores and sleeves to regulate distance between belt pulleys.

2. 2nd generation has improved pipe-shaped casing construction and preparation method.

Named 2nd generation developments has following effects:

1. Two extra fixing points to every 2nd generation belt pulley to the key structure is added compared to 1st generation.

2. The outer diameter of 2nd generation pipe–shaped casing's is constant across it's length.

3. Belt pulleys' average backlash relative to the fixing point of 2nd generation is smaller. Maximum belt pulleys' backlash relative to the fixing point decreased by 8.26 mm.

4. Backlash between two neighboring belt pulleys of 2nd generation is greater than that of 1st generation and it depends on slot width between belt pulleys.

5. Required torque to regulate slot width between belt pulleys of 2$^{nd}$ generation is greater and stepped.

Results show that the last two negative effects of the 2$^{nd}$ generation are caused by the peculiarities of the chosen prototyping method for the key structure and these can be solved by using more suitable manufacturing method. Further research with 2$^{nd}$ generation is necessary to study if these arguments are true.

## REFERENCES

Fischer, U., Gomeringer, R., Heinzler, M., Kilgus, R., Näher, F., Oesterle, S., Paetzold, H. & Stephan, A. 2010. *Mechanical and Metal Trades Handbook*, (2nd English edition). Verlag Europa Lehrmittel, Germany, 428 pp (in English).

Lakewood Process Machinery 2016. (February 26) URL: http://lakewoodpm.com

Mitutoyo 2016. (March 3). URL: http://dl.mitutoyo.eu/HE/eBook/en_us/index.html?page=180.

Nikon Metrology NV. 2016. (March 3) URL: http://www.nikonmetrology.com/en_EU/Products/Laser-Scanning/Handheld-scanning/ModelMaker-MMDx/(specifications).

Novero, S.P.A. 2016. (February 19). URL: http://www.noverotubi.com

Olt, J. 2015. *Põllumajandustehnika I. Põllundusmasinad*. Kuma Print, Paide, 208 pp. (in Estonian).

Olt, J. & Soots, K. 2013. Patent EE 05642 B1. 2013. *Berry sorter*, B07B13/065.

Palermo, E. 2013. *Fused Deposition Modeling: Most Common 3D Printing Method*. Livescience. URL: http://www.livescience.com/39810-fused-deposition-modeling.html.

Peets, A. 2016. (February 26). *Vabavaraline 3D printimine õppematerjal*. URL: https://moodle.hitsa.ee/course/view.php?id=14120. (in Estonian).

Soots, K., Maksarov, V. & Olt, J. 2014. Continuously adjustable berry sorter. *Agronomy Research* **12**(1), 161–170.

Soots, K., Olt, J. 2016. Non-stationary processing center for small and medium sized blueberry farms. *Research in Agricultural Engineering*. (in press).

Soots, K. & Olt, J. 2014. Patent application P201400049. *Belt sorter*. (in press).

Stratasys Ltd. 2016. (February 26). URL: http://www.stratasys.com.

ThyssenKrupp Materials International 2016. (February 22). URL: http://www.s-k-h.com/media/de/Service/Werkstoffblaetter_englisch/Dickwand__Hohlprofile/E355R_engl.pdf.

Wu, W., Geng, P., Li, G., Zhao, D., Zhang, H. & Zhao, J. 2015. Influence of Layer Thickness and Raster Angle on the Mechanical Properties of 3D-Printed PEEK and a Comparative Mechanical Study between PEEK and ABS. *Materials* **8**, 5834–5846.

# Freshwater sapropel (gyttja): its description, properties and opportunities of use in contemporary agriculture

K. Stankevica, Z. Vincevica-Gaile and M. Klavins[*]

University of Latvia, Faculty of Geography and Earth Sciences, Department of Environmental Science, Jelgavas street 1, LV-1004, Riga
[*]Correspondence: maris.klavins@lu.lv

**Abstract.** Sapropel (gyttja or dy) is a type of fine-grained and loose sediments, rich in organic matter, deposited in freshwater bodies. Properties of sapropel and quite wide possibilities of extraction makes it as an important natural resource that can be used predominantly in agriculture, horticulture, forestry, farming. Sapropel and its processing products are environmentally friendly, non-toxic, with a definite content of nutrients. The aim of the current paper was to gather the available information about the sapropel properties and its application in agriculture as soil fertilizer or soil amendment, indicating the efficiency and possible ways amounts of application. Another reason why the investigation of sapropel is important in the Baltic States and northern Europe is its wide distribution and availability in freshwater bodies that leads to find out new ways of extraction and bioeconomically-effective utilization of this highly valuable natural resource, obtainable in economically significant amounts, with high opportunities of its use in agriculture. Contemporary agriculture strongly desiderates in new products of high effectivity enhancing soil and crop productivity and quality hand in hand with sustainable development and careful attitude to the nature and surrounding environment.

**Key words:** lake sediments, humic substances, organic fertilizer, soil amendment, natural resources.

## INTRODUCTION

Sapropel, also called as 'gyttja' or 'dy', is a renewable natural resource, which can be found as the quaternary freshwater organic sediments that accumulate due to the deposition of remains of aquatic plants and animals, mixed with mineral components. Sapropel is a unique geological formation occurring at the bottom of a waterbody throughout its existence (Lopotko, 1974; Lopatin, 1983; Bambalov, 2013). Sapropel formation is highly dependent on the processes in the lake, and the sapropel sediment formation can take place only due to the disruption of the substances and energy circulation, which is a process widely observed in eutrophic lakes (Kurzo, 2005).

Various freshwater sediments, including sapropel, are widely distributed in many waterbodies of the world. The most intensive formation and accumulation of sapropel is characteristic to the temperate zones of Asia and Europe (Russia, Scandinavian Peninsula, France, Germany, Poland, the Baltic States, Belarus and Ukraine), and the continent of America in the Great Lakes region (Canada and USA) (Shtin, 2005).

Sapropel deposits in waterbodies appeared after the glacier retreat. In the Baltic countries it happened 12–15 thousand years ago (Braks, 1971). Massive sapropel formation in this region took place in the Holocene (12 000 yr BP – present), and because of that, it is not only a valuable natural resource, but also a material evidence for studies of the past climate changes (Yu & McAndrews, 1994; Axford et al., 2009; Stančikaitė et al., 2009; Heikkilä & Seppä, 2010; Ozola et al., 2010; Grimm et al., 2011; Klavins et al., 2011; Stankevica et al., 2015).

Sapropel can be of autochthonous origin, if its accumulation takes place due to the lake biomass deposits; and also of allochthonous origin, where sediments accumulate a large amount of humic substances, which enter the lake from the surrounding areas and marshes (Cranwell, 1975; Largin, 1991; Golterman, 2004). Sapropel of autochthonous origin with maximum organic matter content is considered to be more valuable, since the initial biomass, its biochemical degradation and transformation into sapropel organic substances does not create polycyclic aromatic hydrocarbons, such as benzopyrene, which is characteristic to soil, peat and particularly coal humic substances (Dmitriyeva, 2003).

Basic composition of sapropel consists of three components: minerals of allochthonous origin, inorganic components of biogenic origin, and organic matter arising from remains of plants and animals existing in the lake and its surroundings (Stankeviča, 2011).

Wide distribution of sapropel and versatility of application possibilities makes these organic sediments as an important strategic natural resource. It is used in agriculture, horticulture and forestry as an organic fertilizer and soil conditioner, in farming, for example, as an additive in farm animal feeds. Besides that, sapropel is a suitable raw material for the chemical and construction industry as well as it is applicable in medicine or cosmetology as a therapeutic mud and can be used as a raw material for the production of coagulants.

The aim of the current paper was to gather the available information about the sapropel properties and its application in agriculture as soil fertilizer and soil filler in recultivated or eroded areas, indicating the effectivity and possible ways and amounts of application. Another reason why the investigation of sapropel is important in the Baltic States and northern Europe is its wide distribution and availability in freshwater bodies that leads to find out new ways of extraction and bioeconomical utilization of this highly valuable natural resource. Until now, peat is the main natural resource widely applicable in agriculture as a growth medium, substrate and soil additive (atsauce); however, the use of peat in many countries will be restricted in near future, thus giving a way for development of new soil amendments using alternative resources among whitch sapropel can be mentioned.

It should be noted that intensive investigation of sapropel was performed during the middle of 20th century, especially in the countries of eastern Europe (e.g., Russia, Belarus, Latvia, Lithuania). Thus the current paper summarizes historical data and scientific information that has been published locally, but which is valuable for the sapropel research and economic efficiency evaluation nowadays in larger scale.

# CHARACTERISTICS AND CLASSIFICATION OF SAPROPEL

Sapropel is a type of fine-grained and loose sediments, rich in organic matter, deposited in waterbodies. In petrology, the term 'sapropelic coal' denotes the sediments that are formed in the aquatic environment from the remains of macrophytes. The term 'sapropel' is often used to designate mainly dark-coloured sediments, rich in organic carbon (Emeis, 2009).

In a narrower sense 'sapropel' (from Greek, *'sapros'* rotten + *'pelos'* mud) denotes contemporary or subfossil, colloidal sediments of continental waterbodies characteristic with a fine structure, that contains significant quantities of organic matter and remains of microscopic water organisms with a small amount of inorganic biogenic component content and admixture of mineral ingredients, which may include sand, clay, calcium carbonate and other minerals (Korde, 1960; Lācis, 2003).

Usually sapropel is formed in a relatively anoxic environment, as a result of physicochemical and biochemical transformations of lake hydrobionts with the participation of various mineral and organic substances in terrigenous (from Latin, *'terrigenus'* created by land) runoff. The sapropel composition and properties in various fields of deposit are very various, and these differences are determined by the productivity of the particular waterbody, surface runoff characteristics and climatic conditions at the area. In general, sapropel is considered to be the specific freshwater sediments with the organic matter content greater than 15%, otherwise, if organic matter content is lower, such deposits are considered to be the mineral lake sediments (Korde, 1960; Kurzo, 2005).

Peat is a natural resource widely applicable in agriculture as a growth medium, substrate and soil additive (Bohne, 2007); however, the use of peat in many countries, e.g., Switzerland and United Kingdom, will be restricted in near future (Waller & Temple-Heald, 2003), thus giving a way for development of new soil amendments using alternative resources among whitch sapropel can be mentioned. Sapropel differs from peat, as summed up in Table 1, with its fine structure, reaction, quantity of organic matter, the remains of organisms forming it and the amount of humic substances (Korde, 1960; Lishtvan et al., 1989; Bambalov, 2013).

**Table 1.** The main differences between natural resources such as peat and sapropel

| Indicators | Natural resource | |
| --- | --- | --- |
| | Sapropel | Peat |
| Environment of formation | Relatively anoxic | Anoxic |
| Place of formation | Lakes, estuaries, rivers | Marshes, bogs |
| Organic matter content, % | 15–85 | < 50 |
| Sources forming the organic matter | Aquatic organisms: phytoplankton, zooplankton, vascular water and coastal plants | Marsh plants: deciduous and coniferous trees, bushes, grasses, moss |

Formation of a uniform terminology and classification of lake sediments is burdensome, because each interested science field has developed its own classification and lists of terms, which corresponds to the direction, objectives and certain aims of an individual research (Lundquist, 1927; Titov, 1950; Kireycheva & Khokhlova, 1998; Schnurrenberger et al., 2003). According to the origin of sediments, they can be divided

into two large groups: 'gyttja' attributed to autochthonous sediments and 'dy' – to allochthonous sediments. Later the German scientist R. Lauterborn extended this classification by adding the term 'sapropel' describing sediments characteristic with hydrogen sulphide odour (Hansen, 1959; Kurzo, 1988). The modern understanding of the term 'sapropel' has been introduced by H. Potonie. Classifying lake sediments, H. Potonie singled out two groups: 'sapropel' – viscous, finely dispersed residue, containing 25–90% organic matter, and mineralized sediments – 'sapropelite', which further can be split according to their mineral components: diatomite, lime, iron and sand (Kurzo et al., 2012).

A more detailed and most often used classification of sapropel has been provided by Pidoplichko & Grishchuk. According to their suggestion, lake sediments can be subdivided into seven types (Pidoplichko & Grishchuk, 1962):

- **Clayey sapropel** is highly mineral; usually it is deposited in lakes naturally; it is pasty, heavy, in grey or grey-blue colour;
- **Calcareous sapropel** characteristic with ash content higher than 35% (including 50–65% CaO); deposits are formed in calcium rich groundwater outflow locations; it is of a grey-green colour, after drying out it forms unbound, whitish-grey mass;
- • **Silicate sapropel** has a high ash content – greater than 30% (including $SiO_2 >30\%$ and CaO <10%); it is grey-green or green with sand grains and dark-coloured, dense dykes;
- **Mixed sapropel** has very high ash content (about 70–80%); it can contain a large amount of calcium and silicates, silicate and clay or clayey particles and calcium; such mixed lake sediments are formed from plankton organisms. Mineral supply source for this type of sapropel can be ground or surface waters; t can be greyish, dark green, blue-green or greyish-brown;
- **Organic (fine detritus) sapropel** has a low ash content not exceeding 30%. It is green, and with an admixture of humus – greenish-brown. Organic sapropel is formed in waterbodies that do not have large mineral matter inflow;
- **Coarse detritus sapropel** has low ash content. It accumulates in lakes, where in addition to planktonic organisms there are many vascular aquatic plants, whose residues in large quantities remains in sapropel. This sapropel is usually dark green in colour and the higher aquatic plant trace inclusions can be observed therein. It is usually deposited on the other sapropel types and does not form thick layers;
- **Peaty sapropel** is formed when the peat deposits come into a contact with a lake, or results from overgrowing of eutrophic waterbodies littoral. This is the intermediate formation between sapropel and peat, brown in colour and containing a variety of thelmatic plants – residues of reeds, sedges, horsetails and other plants. When pulverized, peat sapropel does not smear, nor stain; it is characterized by a very low ash content (8–10%) and high decomposition (around 25–30%). This type of sapropel is deposited in layers between peat and sapropel deposits.

During the 70s of the 20th century, Belarusian scientists developed sapropel classification (Table 2), taking into account the requirements of industry and the principles of sapropel genesis (Yevdokimova et al., 1980). This classification is based on quantitative analysis of seven indicators describing the chemical structure of sediments; each isolated type of sapropel is defined as a raw material for a specific direction of use – this is the most complex sapropel classification. Nowadays this

classification is practically adopted as the Governmental Standards of the Republic of Belarus (BSSCI, 2010).

According to the ratio between the organic and mineral part, the authors classify sapropel as low ashy (ash content less than 30%) and high ashy (ash content of 31–85%) sapropel. Low ashy sapropel is divided in four types, according to the ratio of humic substances and easily hydrolysable substances associated with the genesis of the proteins in sediments. The first type of sediments contains larger amounts of allochthonous humic material. The other three types of organic sapropel contain humic substances formed of autochthonous material. The sapropel group with high ash content is further categorized into three subtypes based on the chemical analysis of the mineral part: sapropel containing silicon dioxide, carbonate sapropel and mixed sapropel. Taking into account the sapropel composition and properties, the given classification determines the most rational use of sapropel (Braks et al., 1967).

D. Nikolayev's states that the sapropelic organic matter consists of the aquatic organisms, e.g., algae, phytoplankton, zooplankton, higher aquatic animals and plants (Nikolayev, 2003). The proportion of these remains (green algae, cyanobacteria, zooplankton, vascular plants) in sapropel determines the characteristics and quantity of sapropel's organic matter, as well as the fields of its use. For example, sheaths of green algae mainly consist of cellulose (Horne & Goldman, 1994), which is poorly degradable over time, subsequently, sapropel which organic mass proportion consists of green algae is rich in cellulose, but poor in humic substances and minerals. Consequently, this type of sapropel can be rationally used as an adhesive or binder in production of various ecological building materials.

N. Braks definition of sapropel's organic substances can be used when reviewing sapropel from the aspect of chemical technology, in which the organic mass elemental composition is reflected: content of carbon, hydrogen, oxygen, nitrogen and sulphur. The average composition of these elements in sapropelic organic substances is (normalized %): C = 55%; H = 6.7%; N = 2.5%; O = 35.0%, C/H ratio ≈ 7.0–8.9 (Braks, 1971).

Studies of sapropel derived from 130 localities in Belarus determined that fluctuations of C, H and N in one type of sapropel depend on its constituent components. Elevated C, but lowered H and N content is characteristic of sediments, which contain 40–60% humic substances and are mainly formed from vascular plants. H and N content increases in sapropel with more zoogenic residues, while C content decreases (Yevdokimova et al., 1980).

Scientists in Latvia revealed that nitrogen content is not directly related to the sapropel mineralization degree, because sapropel with a different ash content has approximately the same amount of nitrogen, but distribution of nitrogen content (also the ash content) in vertical cross-sections of the sediments in different localities differs due to its nature (Braks et al., 1967; Braks, 1971).

Lopotko believes that the maximum concentration of nitrogen is in the pelogenous layer (7.0–7.5% of organic matter) – the layer where active microbiological and biochemical processes take place and large amounts of microorganism protein and nitrogen fixed from the air by cyanobacteria are accumulated (Lopotko & Kislov, 1990).

**Table 2.** Industrially genetic classification of sapropel (after Yevdokimova et al., 1980)

| Type | Form | Label | $A_c$, % | Biological composition and oxides, % | | Utilization | Diagnostic indicators |
|---|---|---|---|---|---|---|---|
| Organic | Peaty | $Орг_1$ | <30 | Thelmatic plants | >70 | Growth promoters, HS products, fertilizers, production of construction materials | $A_c^*$ |
| | Organic, with a high HS content | $Орг_2$ | <30 | Thelmatic and vascular aquatic plants | 50–70 | Therapeutic mud, biologically active substances, fertilizers | |
| | Organic, with a medium HS content | $Орг_3$ | <30 | Diatoms and cyanobacteria | – | Fillers, drilling solutions, therapeutic mud, fertilizers | |
| | Organic, with a low HS content | $Орг_4$ | <30 | Green algae | – | Binder substances, drilling fluids, therapeutic mud, fertilizers | |
| Containing silicon dioxide | Silicate (low ash content) | $Кр_1$ | 30–50 | Diatoms $SiO_2/CaO$ $Fe_2O_3$ | >90 >2 <10 | Fertilizers, drilling fluids, production of construction materials, therapeutic mud | $A_c$ $SiO_2/CaO$ $Fe_2O_3$ |
| | Silicate (high ash content) | $Кр_2$ | 50–85 | Diatoms $SiO_2/CaO$ $Fe_2O_3$ | >90 >10 <10 | Soil colmation, tamponage solutions, fertilizers | |
| | Autogenous silicate | $Кр_3$ | 30–50 | Diatoms $SiO_2/CaO$ $Fe_2O_3$ | >90 >2 <10 | Growth promoters, therapeutic mud | |
| | Silicate ferruginous | $Кр_4$ | >30 | Diatoms $SiO_2/CaO$ $Fe_2O_3$ | >90 >2 >10 | Therapeutic mud | |
| Carbonate | Carbonate | $Карб_1$ | >30 | $SiO_2/CaO$ $Fe_2O_3$ | <0.4 <5 | Animal feed additives rich in minerals and vitamins, therapeutic mud, soil liming | $A_c$ $SiO_2/CaO$ $Fe_2O_3$ Minerals = $= A_c+CO_2$ |
| | Carbonate ferruginous | $Карб_2$ | >30 | $SiO_2/CaO$ $Fe_2O_3$ | 0.4–0.7 >5 | Soil liming, tamponage solutions, therapeutic mud | |
| Mixed | Mixed organic silicate carbonate | $См_1$ | >30 | $SiO_2/CaO$ $SiO_2/Fe_2O_3$ $CaO/Fe_2O_3$ $SO_3$ | 0.7–2.0 >4 >3 >10 | Fertilizers, construction material production, therapeutic mud | $A_c$ $SiO_2/CaO$ $SiO_2/Fe_2O_3$ $CaO/Fe_2O_3$ $SO_3$ |
| | Mixed silicate carbonate ferruginous | $См_2$ | >30 | $SiO_2/CaO$ $SiO_2/Fe_2O_3$ $CaO/Fe_2O_3$ $SO_3$ | 0.7–2.0 1.0–4.0 0.4–3.0 <10 | Drilling solutions, construction material production, therapeutic mud | |
| | Mixed organic silicate ferruginous | $См_3$ | >30 | $SiO_2/CaO$ $SiO_2/Fe_2O_3$ $CaO/Fe_2O_3$ $SO_3$ | 0.7–2.0 <1 <0.4 <10 | Therapeutic mud | |
| | Mixed organic carbonate sulphate | $См_4$ | >30 | $SiO_2/CaO$ $SiO_2/Fe_2O_3$ $SO_3$ | 0.7–2.0 >1 >10 | Therapeutic mud | |

$^*A_c$ – ash content, %

Changes of nitrogen content in vertical sections of sediments as well as other chemical indicators can be used for sapropel layer splitting in certain stratigraphic horizons.

Content of nitrogen in various types of sapropel ranges from 2.7% to 6% of organic substances and 0.5 to 4.0% dry weight. Organic substances of sapropel, which include animal residues, contain more nitrogen (4.4–4.8%) than algae (3.0–4.2%) or peat forming plant residue (2,6–3.5%) (Ponomareva, 2002).

Content of sulphur in sapropelic organic matter ranges from 0.1% to 1.8%, not exceeding 3% in the dry mass, but while industrially preparing and storing sapropel, sulphur compounds are oxidized, thus the acidity increases (Kazakov & Pronina, 1941; Yevdokimova et al., 1980; Lopotko et al., 1983). The highest sulphur concentrations in organic substances are present in the carbonate sapropel (Kireycheva & Khokhlova, 1998).

According to the elemental composition the freshwater sapropel is similar to humus. The sediments of saline lakes contains smaller amount of organic substances (approximately ≥10%); flora and fauna is poorer in these lakes and mineralization processes are faster (Lishtvan & Lopotko, 1976; Shtin, 2005).

It should be noted that the total content of organic substance in various sapropel types is different: in organic sapropel 70–93% in silicate and carbonate sapropel – 15–70%, in mixed sapropel – 15–70% (Lopotko, 1974; Pidoplichko, 1975; Yevdokimova et al., 1980; Kireycheva & Khokhlova, 1998).

## ORGANIC SUBSTANCES OF SAPROPEL

Organic substances of sapropel can be defined in various ways:
- Undissolved remains of hydrobionts and autochthonous colloidal substances, as terrigenous input through runoff. It is the sum of biological and organic components (Baksheyev, 1998; Nikolayev, 2003);
- A complex of low molecular weight organic compounds and biopolymers, and adsorption complexes with minerals (Lopotko et al., 1983).

Sapropel can be defined as an underwater form of humus while the classifying the biolites of organic matter – the sedimentary rocks composed primarily of extinct animals, plants and their life product remnants (Hansen, 1959), but other scientists distinguish soil, peat and sapropel humus, considering them as accumulation forms of organic matter with various origins (Filippov et al., 1969).

Any carbon containing fossil sediments consist of various groups of chemical compounds (Poznyak & Rakovskiy, 1962). Identification of different compound groups extracted from the organic mass of sapropel is based on fractionation methods; therefore, according to these methods several composition variations of individual components have arisen. Poznyak and Rakovskiy (1962) identified following compounds within the sapropelic organic mass:
- Bitumens;
- Water-soluble substances;
- Easily hydrolysable substances (including humic and fulvic acids);
- Cellulose;
- Non-hydrolysable substances.

Similarly Baksheyev (1998) isolated such sapropelic organic substances as bitumens, hydrocarbons, sapropel acids and the non-hydrolysable substances. Comparing the group of chemical compounds in various sapropel samples, it was established that the groups of substances (e.g., humic acids, non-hydrolysable substances), according to their chemical nature from different sites, are not identical and in great extent are dependent on the properties of sapropel forming organisms (e.g., plankton, vascular plants, humic substances) and their transformation conditions (Braks, 1971).

Kireycheva & Khokhlova (1998) in their study of sapropel isolated bitumens and lipids (extracted with non-polar solvents such as benzene, diethyl ether etc.), humic substances (extracted with alkaline solutions), easily hydrolysable substances (extracted after hydrolysis using 2% HCl), difficult hydrolysable substances (extracted after hydrolysis using 80% $H_2SO_4$) and non-hydrolysable substances (remaining after the sequential extraction of all fractions). Bitumens extracted from sapropel have a larger molecular weight of fatty acids than peat bitumens, and sapropel storage on the field for two months, increases concentration of bitumen in sapropel by 1.5 times (Karpukhin, 1998). Bitumens are organic substances (lipids) that can be extracted from sapropel with a variety of organic solvents. Bitumen composition is characterized by fatty acids, steroids, carotenoids, paraffin, wax and glycerol content (Orlov et al., 1996). Sapropel bitumen components attract particular attention because they have a high bactericidal, bacteriostatic and antioxidant activity. Several studies have focused on the easy and efficient methods to obtain these substances from sapropel (Kireycheva & Khokhlova, 1998; Šīre, 2010). Organic substances that have been only slightly altered are composed of peloid bitumen (therapeutic mud), which contain a large number of double bonds and functional groups – carotene, phospholipids, unsaturated fatty acids and alcohols (Fillipov et al., 1969).

Lopotko with colleagues (1992) in their studies determined that sapropel has a low bitumen content of 2–7% of the organic mass, but Poznyak & Rakovskiy (1962), extracting bitumens with gasoline and alcohol-benzene mixture, obtained them in amount 4.3–9.9%. In low ash and medium ash sediments bitumen quantities usually do not exceed 5%, rarely they can reach 6.0–8.1% of the organic mass (Ponomareva, 2002). Bitumen content in sapropel is lower than in peat; sapropel bitumens predominantly consist of saturated compounds. Sapropel bitumens differ from the peat bitumens with lower acidity level and lower saponification that indicates a content of neutral character compounds – hydrocarbons (Kazakov & Pronina, 1941).

Sapropel is characterized by low carbohydrate amount, because during the sapropel formation there is an active decomposition of the carbohydrates to carbon dioxide and humification (formation of the humic substances in the reactions of amino acid condensation). An average quantity of hemicellulose in organic matter of sapropel is 6–25%, but cellulose – 1–8% (Pidoplichko & Grishchuk, 1962). Sapropel components contain 1–2% of cellulose. Sapropel carbohydrate complex consists of ≥80% of hemicellulose; therefore it can be used in production of animal feed additives and fertilizers applicable in agriculture and horticulture (Lopotko et al., 1992).

Composition and properties of sapropel humic substances are determined by their most important features such as biological activity, biochemical stability, binding ability etc. Depending on the content and the specific relationship of humic substances, sapropel that is brought into soil may variously affect biochemical processes, soil structure

formation resulting in quality of agricultural products. Sapropel humic substances differ from the soil humic substances with a higher carbon/hydrogen ratio and absence of saturated aromatic rings (Orlov et al., 1996). Humic substances of sapropel are more reduced and possess a greater activity than soil humic substances. Humic substances of sapropel consist from humic acids, fulvic acids and humine. Eextraction of humic substances from sapropel minerals and organic compounds is usually performed according to the classical scheme of Tyurin, which is used for studying the chemical composition of soils (Orlov et al., 1996). Investigated sapropel samples are decalcified to remove carbonates. Although this method is simple, natural polymer dissolution and deposition do not enable a complete elimination of all low molecular weight components (carbohydrates, alcohols, amino acids), therefore, depending on the investigated object and purposes, this scheme is often modified (Karpukhin, 1998; Kireycheva & Khokhlova, 1998).

Humic acids is the largest group of organic substances. They are usually extracted from the sediments with alkaline solvents and precipitated into an acid environment (pH 1–2). The dark brown colour is characteristic to humic acids. In humic acids of fen and raised peat the amount of carbon ranges from 57.7% to 64.2%, while hydrogen from 4.3% to 5.4% (Kazakov & Pronina, 1941). Humic acids of sapropel differ from the peat in the sense of elemental composition as follows: the hydrogen content is higher than that of peat humic acids, which indicates the presence of fatty acids. Y. Kazakov (1950) stated that higher content of nitrogen in sapropel humic acids testifies to humin like compounds – melanoids, generated by the condensation of protein decomposition substances (amino acids and substances formed as a result of carbohydrates destruction). Types of sapropel humic substances vary in elemental composition, content of functional groups and fragments, which are determined by sapropel forming substances, and the humification conditions of the particular reservoir (Stepanova, 1996).

Valuable finding indicates the presence of water-soluble vitamins in sapropel: ascorbic acid (C), B group vitamins – thiamine (B1), riboflavin (B2), pantothenic acid (B5), pyridoxine (B6), folic acid (B9) and cyanocobalamin (B12). Large quantities of fat-soluble vitamins – tocopherol (E), vitamins D and P were also found (Shtin, 2005). Sapropel containing cyanocobalamin (vitamin B12), which is concentrated in the upper layer (up to 1 m) of sediments, has a high value to be applied as a livestock feed additive. Experimental studies show that vitamin B12 is synthesized by many microorganisms in mud sediments, it plays an important role in protein exchange and other processes, but as many vitamins are not stable substances, refrigeration or long storage of sapropel reduces the cyanocobalamin content (Letunova, 1958).

## CHEMICAL COMPOSITION OF MINERAL SUBSTANCES IN SAPROPEL

Mineral components of sapropel are important for the characteristics of sediment type and application potential in agriculture. Formation process of mineral components in the bottom sediments is associated with sedimentation of terrigenous runoff minerals as well as organic and chemical deposition of mineral ions dissolved in a lake waterbody. Usually terrigenous runoff minerals are quartz ($SiO_2$), dolomite ($CaMg(CO_3)_2$), silicates and aluminosilicates (e.g., feldspar, hydromica, chlorites, kaolinite). Biochemical processes lead to the accumulation of calcite and aragonite (carbonates of Mg, Ca, Sr, Ba, Fe, Mn), pyrite ($FeS_2$), gypsum ($CaSO_4 \cdot 2H_2O$), hematite ($Fe_2O_3$), marcasite ($FeS_2$)

and vivianite into the sapropel of a watercourse (Korde, 1960; Krasov et al., 1986; Lopotko & Yevdokimova, 1986; Wetzel, 2001).

Among the iron minerals the brown oxides are prevalent – iron(III) oxyhydroxides, hydrogoethite (FeOOH), more rarely – iron pyrite and phosphates, rarely – siderite ($FeCO_3$). Iron heptahydrate minerals are typical of the lower part of the sapropel layer, where siderite and part of the iron phosphates are formed. This happens due to the decomposition of organic matter and any reduction conditions resulting thereof. Iron phosphates, as well as the brown iron oxides are common in all genetic types of sapropel – content of iron phosphate increases with the decrease of carbonates. Content of these phosphates in carbonate sapropel is about 0.4%, in mixed sapropel – 0.8%, but in sapropel containing silica – 1.4%. Calcium phosphates in sapropel occur in the form of apatite, iron phosphates – in the form of vivianite (Krasov et al., 1986). The total amount of iron in sapropel constitutes 2–18%, rarely as much as >25%. The iron generally enters the sediments in the form of colloidal organo-mineral compounds together with the clay particles. $Fe_2O_3$ in organic sapropel typically constitutes 4.9%, in sapropel containing silicon dioxide – 5.6%, carbonate – 4.7%, mixed sapropel – 8.4%, but sometimes this figure may reach 30–50% of the ash volume (Shtin, 2005). Large quantities of iron, especially in mobile forms, have suppressing influence on the plants (Yevdokimova et al., 1980). Intensive mineral depletion takes place in aquatic environment, and thereby the quantity of iron mobile forms increases, and may represent up to 80% of the total iron mass (Lopotko et al., 1983). Iron compound reduction and mobility decreases in the process of drying and ventilating in the air, and a part of hydrated forms transit into crystals. Mobile iron compounds do not exceed 1% in air-dry samples (Yevdokimova et al., 1980; Lopotko & Yevdokimova, 1986).

At the integrated level the mineral composition of sapropel is evaluated according to the ashiness (composition/content of ash). The greatest part of the ash is made up by iron and calcium phosphates – within the ash composition in the form of the stable oxide there are not less than one 1% of the following compounds: $SiO_2$, $Fe_2O_3$, $Al_2O_3$, CaO, MgO, $Na_2O$, $K_2O$, $P_2O_5$ (Yevdokimova et al., 1980). Russian, Lithuanian and Latvian scientists consider sediments with ash content greater than 85% to be the lake sediments with a high ash content (Nikolayev, 2003).

The correlations of silicon component accumulation in various types of sapropel showed that the silicon enters sapropel in form of suspension from the remains of diatoms and accumulate in bacteria; the major component of the ash characteristic to organic sapropel is $SiO_2$, while other silicon compounds are present in very small quantities. Significant differences of silicon compounds in the ash of organic sapropel were not determined (Lopotko & Yevdokimova, 1986; Kireycheva & Khokhlova, 1998). Mixed sapropel contains a slightly larger quantity of ash, but its content is identical to that of the organic sapropel when $SiO_2$ dominates in ash. If the mixed sapropel contains carbonates, then CaO+MgO content is 7.9% to 16.6%, but the ash content of such sapropel can reach 60%. Silicate sapropel contains silicon oxide in free form – quartz and quartz in the form of various silicates and aluminosilicates, and the content ranges from 30.3% to 70% (Kurzo, 1988). Diatoms sapropel contains amorphous silicic acids, which are more available to plants (Lopotko, 1974), but the abundance of silicon does not have a toxic effect on plants (Nikolayev, 2003).

The main mineral component of carbonate sapropel is calcium carbonate. The mineral form of calcium is dolomite, clayey-ferruginous carbonate aggregates and

biogenic calcite. Carbonates (about 20–50% of the total content) are present as amorphous and colloidal compounds, which have an organic origin and a high degree of mobility (Yevdokimova et al., 1980). CaO content of carbonate sapropel may reach 90%, but in organic sapropel – 0.4% to 5.25% of ash. Mixed sapropel contain 0.9–12.5% of CaO, but silicate sapropel – 1.2–12.3% of dry matter, on average in different sapropel types CaO content ranges from 0.7% to 37% of dry matter.

Calcite precipitation in eutrophic waterbodies is promoted by the photosynthesis of plants, which bind $CO_2$, and organisms (molluscs, small barnacles) that during their lifetime accumulate calcium in the cells. As the amount of sulphate in water increases, reduction of sulphate may occur, resulting in calcareous sediments. The presence of calcium in the watercourse accelerates the decomposition of organic matter and increases the calcium content of the sediments (Stable, 1986). Due to increased acidity which is caused by larger $CO_2$ content in the organic matter degradation process, carbonates may also fail to deposit (Nikolayev, 2003).

Aluminium content of sapropel changes within the range from 0.3% to 11%, usually it is within 2–4% range and its higher concentrations can be found in silicate sapropel, as it contains clay minerals. The studies of sapropel in Belarus did not reveal the presence of amorphous forms of aluminium, which are highly toxic to plants (Kurzo, 1988; Wetzel, 2001).

## LIVING ORGANISMS IN SAPROPEL AND THEIR ROLE IN BIOLOGICAL ACTIVITY

Biological components of freshwater ecosystems consist of many hydrobionts, which life cycle is a part of the life cycle of a whole waterbody, and that leads to the accumulation of organic matter as sediments in the ecosystem.

Prokaryotes are among the most important contributors to the transformation of complex organic compounds and minerals in freshwater sediments, besides, they can be assessed as important components of benthic food chain as well as of nutrient cycling (Tamaki et al., 2005). Lake sapropel is richly populated by microorganisms – depending on the type of sapropel colony forming units (CFU) varied from $5.20\ 10^3$ to $6.88\ 10^6$ CFU per g of dry matter (Stankevica et al., 2014). It is characteristic that the number of microorganisms decreases with the depth of sediments (Kuznetsov, 1970). There is an evidence that microorganisms able to produce antibiotics can be found in sapropel. Such microorganisms are antagonistic to the series of pathogen saprophytic microorganisms. This finding is important for safe use of sapropel in medicine, cosmetology, balneology (Platonov et al., 2014). Antibiotics and sulphonamides are synthesized in sapropel by fungi and actinomycetes, while vitamins – by bacteria and algae. Azobacteria promote nitrogen transfer to the form available to plants. Various bacteria and groups of water fungi are specific decomposers of organic substances (decomposes dead hydrobionts, splitting them into individual fragments) and are involved in the biochemical processes – sapropel secondary organic matter synthesis (humification) (Nikolayev, 2003).

Regarding living organisms in sapropel, range of substances transformation are carried out, not only formation of sapropel sediments, but also regeneration and preservation of sediment properties over time. Microorganisms are involved in the mineralization and synthesis of organic substances in sapropel; it determines the

presence of various gases (e.g., hydrogen sulphide, ammonia, methane) and their quantity in sediments. Biochemical substances formed by microorganisms in biological processes also determine some physically chemical properties of sapropel. Sediments like sapropel are tended to accumulate biologically active and antibacterial substances, which are of a great importance in balneology, as well as in agriculture and soil recultivation perspectives.

## USE OF SAPROPEL IN AGRICULTURE

Sapropel has a very wide range of possible application ways in broad spectrum of fields of national economics (Fig. 1), among which agriculture currently takes the greatest part. Sapropel can be applied widely, from a raw material to production of processed products, but until now its wide variety and fragmented research data rarely have driven sapropel extraction and utilization to cost-effective, sustainable and well-grounded perspective market niche development.
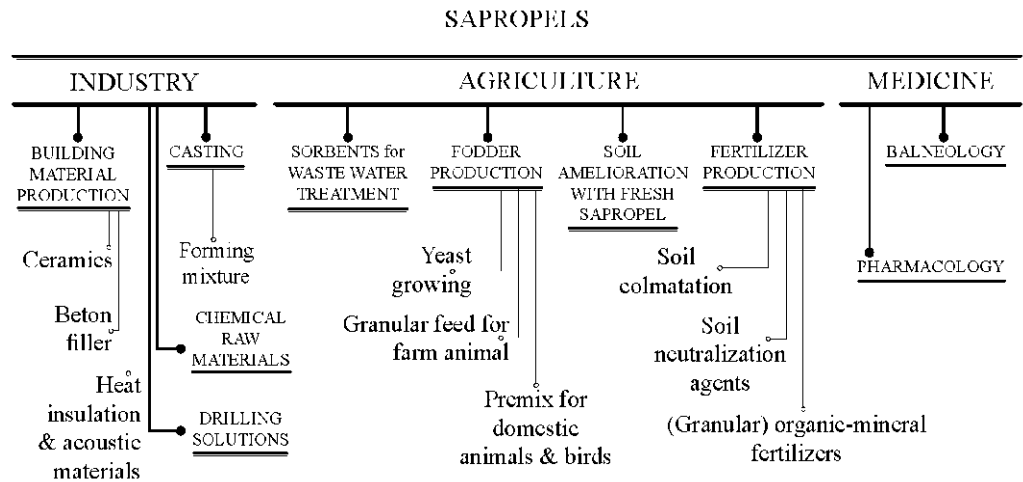


**Figure 1.** Application options of sapropel in fields of national economics (authors' workout, according to Kurzo, 2005).

Among the possible applications of sapropel, animal feed production already is an existing field. Sapropel alkali extracts, similarly to lignite and peat extracts, contain 40% humic substances. Improvement of animal feed mixtures' efficiency using sapropel has been extensively studied in Lithuania and Belarus during the second half of the 20th century. Sapropelic feed additives improve operation of animal liver and stomach, blood formation and circulation, reduces the occurrence of diseases and increases resistance of animal health to adverse environmental conditions (Lishtvan & Lopotko, 1976; Soldatenkov, 1976; Yevdokimova et al., 1980; Shtin, 2005). The most valuable type of sapropel for use in feed additives is deemed to be the organic sapropel, because it contains enough high concentration of proteins, vitamins, enzymes and other biologically active substances, but studies conducted in Lithuania have showed that

almost all types of sapropel can be used in a production of feed additive (Soldatenkov, 1976; Kurzo, 2005).

Currently increasing popularity is attributed to feed additives of sapropelic humus such as sodium humate. These humic formulations enhance the oxidation processes in animal body, i.e., helps to increase and accumulate proteins in blood and body mass, increases the formation of erythrocytes in the red bone marrow, improves synthesis of vitamin A and other vitamins, normalizes metabolism and is effective in the treatment of toxicities (Shtin, 2005).

Another highly important application way of sapropel in agriculture is its use for preparation of soil substrates or growth media. Major criteria in this respect is content of organic matter and balance of pH in sediments (Semakina et al., 2001). Sapropel as soil substrate can be used in form of mixtures with peat, sludge and any kinds of composted biowaste (Kurzo, 2005; Yongoing et al., 2010). Some authors suggest also supply of mineral fertilisers to improve the application potential of sapropel (Skromanis et al., 1989). Most widely the possibilities of sapropel application in soil substrates or soil amendments have been tested in Belarus, where actual applications of sapropel in agriculture reached 1.5 million tons per year (Kurzo, 2005).

According to the data provided by Kurmysheva (1988), keeping sapropel on the field for two months the quantity of bitumen increases twice, but storing the sapropel in settling tanks for one year the amount reduces by 1.5–2 times. However, in case of sapropel stored in the settling tanks the analysis of samples from upper layer revealed the increase of bitumen quantity 6.0–7.6%, and these changes are analogous to the sapropel that is stored on the field and where over time appropriate microflora developed as well. Storing sapropel in settling tanks for five years, the amount of bitumen increased, but did not reach the initial scores. Multiple freezing and refreezing of sapropel did not significantly influence the quantity of bitumen fractions (Kireycheva & Khokhlova, 1998).

Another field of recently developed sapropel application is a production of liquid sapropel-based fertilisers and sapropel extracts containing a complex of biologically active substances, predominantly taking into account content and specifics of humic substances (Diskovska et al., 2011; Ferdman et al., 2011). Sapropel extracts and mixtures containing humic substances can be obtained using extraction with alkaline solutions and dispersion technologies. Recent studies have demonstrated high efficiency of such formulations for various crop cultures and extension of application options (Pastukh & Popov, 2007; Ferdman et al., 2011; Bunere et al., 2014). For example, laboratory tests implemented at the Department of Environmental science in the University of Latvia involved cultivation of radish in hydroponics where liquid fertilizer of humic acids derived from sapropel was tested. Investigating the efficiency of liquid fertilizer at various concentrations, it was detected that humic acids in concentration of 5 mg $L^{-1}$ lead to increase of radish root dry mass by 94%, but dry mass of foliage increased by 1.5 times, in addition with double increase of total chlorophile content in comparison to the control samples. Parallel experiments were performed using suspension of raw sapropel and water at various concentrations, recalculating to the amount of humic substances. Obtained results revealed lower efficiency, i.e., dry mass of radish roots increased only by 62% (Bunere et al., 2014). Efficiency of raw sapropel application can be influenced by several factors such as chemical state of humic substances as they might present in other forms than salts, as well as a defficiency of $K^+$

ions that stimutlat seed germination and plant development (Ponomareva, 2002). Ponamoreva (2002) conducted two years long field experiment cultivating crops and fertilizing them only three times during a vegetation period using a liquid containing 0.01% potassium sapropel humates. Results indicated an increase in a crop yield for tomato cultivars (30–35%), potato (20–25%), cucumber (45–50%), sweet pepper (25–35%), sugar beet (25–45%), wheat (30–35%). Besides the crop yield increase, applicationd of potassium sapropel humates elevated crop resistance against several plant diseases such as peronosporosis, *Botrytis cinerea*, bacteriosis and verticilosis (Ponomareva, 2002).

In general, all types of sapropel are applicable as soil fertilizing agents, and regarding this application, sapropel conditionally can be divided into three groups (Shtin, 2005):

Group 1 – sapropel with organic matter content above 50% is used to produce organic mineral fertilizers. Composting this type of sapropel, it does not require addition of different organic materials (such as peat or other);

Group 2 – sapropel with organic matter content from 10% to 50% is used for production of complex mineral fertilizers, which are rich in lime, phosphoric acid, total nitrogen and organic matter;

Group 3 – mineralized sediments with organic matter content up to 10% are mainly used to improve soil texture and mechanical content. If such sediments have high concentrations of CaO, field application of them reduce soil acidity.

Notable results in practical performance of soil fertilization using sapropel were achieved in 1954–1955 in Latvia at the Bulduri Horticultural Technical College (Vimba, 1956). Comparable field experiments were accomplished using sapropel, manure and sapropelite as fertilizers in light sandy soil for cultivation of potatoes, cabbages and carrots. Results indicated increase of crop yield in favour of sapropel (Table 3).

**Table 3.** Impact of sapropel, sapropelite and manure application as fertilizers on crop yield (Vimba, 1956)

| Crop | Fertilizer[*] | Yield, (cnt ha$^{-1}$) | Yield, (%) |
|------|-----------|------------------|----------|
| Potatoes | Control | 207 | 100 |
| | Manure | 255 | 123 |
| | Sapropel | 334 | 160 |
| | Sapropelite | 292 | 141 |
| Cabbage | Control | 360 | 100 |
| | Manure | 580 | 160 |
| | Sapropel | 630 | 175 |
| Carrots | Control | 441 | 100 |
| | Manure | 595 | 135 |
| | Sapropel | 618 | 140 |
| | Sapropelite | 618 | 140 |

[*]*Fertilizer was applied at concentration 30 t ha$^{-1}$; control – without fertilizer*

Experiments showed that using sapropel in humic soil pots, and replacing the humic soil with sapropel, early cabbage seedlings in sapropel pots developed much better and were stronger than the seedlings in the usual humus pots. Besides sapropel, in tests also

sapropelite (containing about 25% of organic matter) derived from the Lielupe River (Latvia) was used. Compared with control, applications of sapropelite increased the carrot yield by 40%, potatoes yield by 41% and cucumber yield by 60% (Vimba, 1956).

Another, ten years long, study done by Lithuanian scientist using carbonate sapropel revealed that sapropel addition to soil may change not only soil acidity but also can increase moisture level of soil as well as total porosity, independently from meteorological conditions. After all fertilizer treatments was not detected changes in soil density. Use of carbonate sapropel as soil fertilizer can improve soil physical properties better than limestone applications. Data analysis of crop productivity changing season by season increased in higher level after applications of carbonate sapropel applications in comparison with limestone due to sapropel's mineral content and plant nutrition potential (Daugvilienė, 2014).

The most rational use of sapropel would be distribution within the industry and agriculture. Economic value of this natural resource can increase by applying more valuable types of sapropel in the chemical industry, but those with higher rate of mineralization in subfields of agriculture.

## CONCLUDING REMARKS

Agriculture, including forestry, horticulture, conventional and organic, domestic and industrial, food and feed crop cultivation, urban gardening, and also animal breeding and soil recultivation after intensive exploitation are among the most important and perspective spheres of sapropel application potential. Contemporary agriculture strongly desiderates in new products of high effectivity enhancing soil and crop productivity and quality hand in hand with sustainable development and careful attitude to the nature and surrounding environment. Sapropel is a natural resource obtainable in economically significant amounts, and in this time of shortage of resourses worldwide, it has to be exploited at utmost appropriate way, giving benefits for both, economics and environment.

## REFERENCES

Axford, Y., Briner, J.P., Cooke, C.A., Francis, D.R., Michelutti, N., Miller, G.H., Smol, J.P., Thomas E.K., Wilson, C.R. & Wolfe, A.P. 2009. Recent changes in a remote Arctic Lake are unique within the past 200,000 years *Proceedings of the National Academy of Sciences of the United States of America* **106**(44), 18443–18446.

Baksheyev, V.N. 1998. *Sapropel yesterday, today and tomorrow,* Regional News Agency, Tyumen, 80 pp. (in Russian).

Bambalov, N.N. 2013. Relationships between biotic and abiotic processes in peat and sapropel sediments formation. *Biospera* **5**(1), 154–165 (in Russian).

Braks, N., Dubava, L., Braks, I. & Logina, K. 1967. *Sapropel deposits in water basins of Latvian SSR,* Zinatne, Riga, 80 pp. (in Russian).

Braks, N.A. 1971. *Sapropel sediments and application possibilities,* Zinatne, Riga, 282 pp. (in Russian).

Bunere, S., Stankeviča, K. & Klavins, M. 2014. *Effects of sapropel on the growth of radish (Raphanus sativus L.)*. The 56th International Scientific Conference of Daugavpils University, Saule, Daugzvpils, pp. 16–24.

BSSCI 2010. Sapropel: industrial-genetic classification. *Environmental protection and nature use.* Nedra, Minsk, 9 pp. (in Russian).

Bohne, H. 2007. Influence of a peat-free substrate and kind of fertilizer on the nitrogen- and water balance and on plant growth. *European Journal of Horticultural Science* **72**, 53–59.

Cranwell, P.A. 1975. Environmental organic chemistry of rivers and lakes, both water and sediments. *In:* Eglinton, G. (ed.) *Environmental chemistry.* Royal society of chemistry, Belfast, 22–54.

Daugvilienė, D., Burba, A. & Bakšienė, E. 2014. Changes of sandy loam Cambisol properties at application for calcareous sapropel and limestone. *Food, Agriculture and Environment* **12**, 491–495.

Diskovska, T.P., Merlenko, I.M., Havryliuk, V.A. & Melnychuk, E.V. 2011. *Process for the production of pastelike fertilizer from sapropel by the dispergation method.* UA patent 58139.

Dmitriyeva, Y.D. 2003. *Chemical composition and biological activity of Belgorod region sapropel.* Doctoral Thesis, Tula State Pedagogical University, St. Petersburg, 233 pp. (in Russian).

Dodds, W. & Whiles, M. 2010. *Freshwater ecology: Concepts & environmental application of limnology,* Academic Press, San Diego, 809 pp.

Emeis, K.-C. 2009. Sapropels. *In:* Gornitz, V. (ed.) *Encyclopedia of paleoclimatology and ancient environments.* Springer, Dordrecht, 876–877.

Ferdman, V.M., Gabbasova, I.M., Garipov, T.T., Sagitov, I.O. & Tomilova, A.A. 2011. *Method of producing water-soluble humic acids.* RU patent 2463282.

Filippov, Y.N., Taraskina, D.V. & Zhuravlev, A.I. 1969. An antioxidative mode of some therapeutic peloid's organic fractions. *Problems of Resort Treatment* **1,** 17–21 (in Russian).

Forel, F.A. 1895. La limnologie, branche de la geographie. Comptes Rendue Du Sixième Congres International de Geographie, 1895. pp. 1–4.

Golterman, H.L. 1975. Energy and mass transport through food chains. *Physiological limnology: An approach to the physiology of lake ecosystems.* Elsevier Scientific Publishing, Amsterdam, pp. 275–324.

Golterman, H.L. 2004. Chemical composition of freshwater. *The chemistry of phosphate and nitrogen compounds in sediments.* Springer Netherlands, Dordrecht, pp. 25–50.

Grimm, E.,C., Donovan, J.J. & Brown, K.J. 2011. A high-resolution record of climate variability and landscape response from Kettle Lake, northern Great Plains, North America. *Quaternary Science Reviews,* **30**(20), 2626–2650.

Hansen, K. 1959. The terms gyttja and dy. *Hydrobiologia* **13**(4), 309–315.

Heikkilä, M. & Seppä, H. 2010. Holocene climate dynamics in Latvia, eastern Baltic region: a pollen-based summer temperature reconstruction and regional comparison. *Boreas* **39**(4), 705–719.

Horne, A.J. & Goldman, C.R. 1994. *Limnology,* McGraw-Hill, New York, 576 pp.

Juday, C. 1942. The summer standing crop of plants and animals in four Wisconsin lakes. *Transactions of the Wisconsin Academy of Sciences, Arts and Letters* **34**, 103–135.

Karpukhin, A.I. 1998. Complex compounds of humic substances with heavy metals. *Eurasian Soil Science* **31**(7), 764–771.

Kazakov, Y. 1950. Genesis and the chemical nature of freshwater sapropel. *Proceedings of the Institute of Fossil Fuels* **2**, 253–266 (in Russian).

Kazakov, Y. & Pronina, M. 1941. The chemical composition of the various forms of plankton and benthos. *Proceedings of the Laboratory of sapropel genesis* **2**, 49–57 (in Russian).

Kireycheva, L.V. & Khokhlova, O.B. 1998. *Sapropels: composition, properties, application,* Roma, Moscow, 120 pp. (in Russian).

Klavins, M., Kokorite, I., Jankevica, M., Rodinovs, V. & Dreijalte, L. 2011. Reconstruction of anthropogenic impact intensity changes during last 300 years in Lake Engure using analysis of sedimentary records. *Environmental and Climate Technologies* **7,** 66–71.

Korde, N.V. 1960. *Biostratification and typology of Russian sapropels,* USSR Academy of Science, Moscow, 220 pp. (in Russian).

Krasov, D.D., Davydova, N.N. & Rumyantsev, V.A. (eds.) 1986. *General patterns of occurrence and development of lakes: Methods of studying the history of the lakes,* Science, Leningrad, 254 pp. (in Russian).

Kurmysheva, N.A. 1988. *Effect of sapropel fertilizers on humus state in sodgley and sodpodzolic soils.* Summary of Doctoral Thesis, MSU, Moscow, 20 pp.

Kurzo, B.V. 1988. Aquatic animal ecology as factor of low ash content sapropel formation. *Peat industry* **2**, 120–126 (in Russian).

Kurzo, B.V. 2005. *Sapropel formation regularity and problems of application,* Belarusian Science, Minsk, 224 pp. (in Russian).

Kurzo, B.V., Gajdukevich, O.M. & Zhukov, V.K. 2012. Researches in the field of genesis, resources and development of sapropel deposits in Belarus. *Nature management* **22**, 57–66 (in Russian).

Kuznetsov, S. 1970. *Microflora of lakes and its geochemical activity,* Science, Leningrad, 439 pp. (in Russian).

Lācis, A. 2003. *Sapropelis Latvijā / Sapropel in Latvia.* Thesis of the 61st Conference of University of Latvia, LU, Riga, 161–163 (in Latvian).

Largin, I.F. 1991. *Properties and research methods of peat and sapropel deposits,* TPI, Tver, 27–53 pp. (in Russian).

Leinerte, M. 1988. *Ezeri deg! / Fire on lakes!* Zinātne, Riga, 94 pp. (in Latvian).

Letunova, S.V. 1958. Formation of vitamin B12 by different types of actinomycetes and bacteria isolated from sedimentos formed in cobalt biochemical provinces. *Microbiology* **27**(4), 2–27 (in Russian).

Lippmann, F. 1973. *Sedimentary carbonate minerals,* Springer Berlin Heidelberg, New York, 229 pp.

Lishtvan, I.I., Bazin, E.T., Gemayunov, N.I. & Terentyev, A.A. 1989. *Chemistry and physics of peat,* Nedra, Moscow, 304 pp. (in Russian).

Lishtvan, M. & Lopotko, M. 1976. The use of sapropel in the national economy. *Problems of sapropel application in the national economy* 5–13, (in Russian).

Lopatin, N.V. 1983. *Formation of fossil fuels,* Science, Moscow, 192 pp. (in Russian).

Lopotko, M. & Kislov, N. 1990. *Sapropel application in the national economy of USSR and abroad,* Ministry of Fuel Industry of the RSFSR, Moscow, 85 pp. (in Russian).

Lopotko, M. & Yevdokimova, G. 1986. *Sapropels and products based on them,* Academy of Science of the Belarussian SSR, Minsk, 61 pp. (in Russian).

Lopotko, M., Yevdokimova, G. & Bukach, O. 1983. *Cadastre of Byelorussian SSR sapropel deposits,* Science and Technology, Minsk, 118 pp. (in Russian).

Lopotko, M., Yevdokimova, G. & Kuzmitskiy, P. 1992. *Sapropelits in agriculture,* Science and Technology, Minks, 215 pp. (in Russian).

Lopotko, M.Z. 1974. *Sapropels of Byelorussian SSR, their production and application,* Science and Technology, Minsk, 208 pp. (in Russian).

Lundquist, G. 1927. Bodenablagerungen und Entwicklungstypen der Seen. *Die Binnengewässer.* E. Schweizerbartsche Verlag, Stuttgart, 124.

Nikolayev, D. 2003. *Carbonate - chara sapropel: chemical structure and biological activity.* Doctoral Thesis, MSU, Moscow, 161 pp. (in Russian).

Orlov, D., Biryukova, O. & Sukhanova, N. 1996. *Soil organic matter of Russia,* Science, Moskow, 258 pp. (in Russian).

Ozola, I., Ceriņa, A. & Kalniņa, L. 2010. Reconstruction of palaeovegetation and sedimentation conditions in the area of ancient Lake Burtnieks, northern Latvia *Estonian Journal of Earth Sciences* **59**(2), 164–179.

Pastukh, O.M. & Popov, V.D. 2007. *Method for production of complex humin fertilizer from sapropel.* UA patent 21128.

Perfilyev, B. 1972. Microzonal structure of lacustrine silty deposits and methods of studying them. *Science*, 6–16 (in Russian).

Pidoplichko, A.P. 1975. *Lacustrine deposits of the Byelorussian SSR,* Science and Technology, Minsk, 120 pp. (in Russian).

Pidoplichko, A.P. & Grishchuk, R.I. 1962. Certain results of research of Belarus SSR sapropel deposits. *Chemistry and genesis of peat and sapropel.* Academy of Science of the Belarussian SSR, Minsk, pp. 258–274 (in Russian).

Platonov, V.V., Khadartsev, A.A., Chunosov, S.N. & Fridzon, K.Y. 2014. The biological effect of sapropel. *The Fundamental Researches* **9**(11), 2474–2480 (in Russian).

Ponomareva, M.A. 2002. *Chemical composition and application possibilities of Tatarstan sapropel,* Ph.D. Candidate Thesis, Tula State L.N. Tolstoy Pedagogical University, Tula, 245 pp. (in Russian).

Potonie, H. 1915. *Die rezenten Kaustobiolithe und ihre Lagerstätten,* Königlichen Geologischen Landesanstalt, Berlin, 100 pp.

Poznyak, V. & Rakovskiy, V. 1962. The chemical composition of the organic mass of Byelorussian SSR sapropel. *Chemistry and genesis of peat and sapropel.* Academy of Science of the Belarussian SSR, Minsk, pp. 298–308 (in Russian).

Pullin, R.S.V. 1987. General dimmion on detritus and microbial ecology in aquaculture In Moriarty, D.J.W. & Pullin, R.S.V. (eds): *Detritus and microbial ecology in aquaculture* International Center for Living Aquatic Resources Management, Manila, pp. 368–381.

Semakina, O.K., Khudinova, N.V., Babenko, S.A. & Bokutsova, K.P. 2001. *Method of preparing uncaking organomineral fertilizers of prolonged activity.* RU patent 2162832.

Schnurrenberger, D., Russell, J. & Kelts, K. 2003. Classification of lacustrine sediments based on sedimentary components. *Journal of Paleolimnology* **29**(2), 141–154.

Shtin, S.M. 2005. *Lake sapropels and those complex cultivation,* Moscow State Mining University, Moscow, 373 pp. (in Russian).

Šīre, J. 2010. *Composition and properties of rised bog peat humic acids.* Doctoral Thesis, University of Latvia, Riga, 105 pp.

Skromanis, A., Anspoks, P., Grīnbergs, V., Asars, A., Iermacāns, E. & Kronbergs, E. 1989. *Sapropeļa ieguve un izmantošana kultūraugu mēslošanā Latvijas PSR: pagaidu ieteikumi Extraction and use of sapropel for crop fertilization in Latvian SSR: temporary recommendations.* Scientific-Technical Information and Propaganda Center of Agroindustrial Committee of Latvian SSR, Riga, 16 pp. (in Latvian).

Soldatenkov, P.F. 1976. *Influence of sapropel on physiological processes in the animal organism,* Science, Leningrad, 171pp. (in Russian).

Stable, H.-H. 1986. Calcite precipitation in Lake Constance: Chemical equilibrium, sedimentation, and nucleation by algae. *Limnology and Oceanography* **31**(5), 1081–1093.

Stančikaitė, M., Kisielienė, D., Moe, D. & Vaikutienė, G. 2009. Lateglacial and early Holocene environmental changes in northeastern Lithuania. *Quaternary International* **207**(1–2), 80–92.

Stankeviča, K. 2011. *Sapropeļa īpašības un tā izmantošanas iespējas / Properties of sapropel and its utilization opportunities.* Master Thesis, University of Latvia, Riga, 109 pp. (in Latvian).

Stankevica, K., Kalnina, L., Klavins, M., Cerina, A., Ustupe, L. & Kaup, E. 2015. Reconstruction of the Holocene palaeoenvironmental conditions accordingly to the

multiproxy sedimentary records from Lake Pilvelis, Latvia. *Quaternary International,* **386**, 102–115.

Stankevica, K., Vincevica-Gaile, Z. & Muter, O. 2014. Microbial community analysis of sapropel (gyttja) derived from small overgrowing lakes in the eastern Latvia. *In:* Truu, J. & Kalnenieks, U., eds. *The 2nd Conference of Baltic Microbiologists*, Tartu, Estonia. University of Tartu Press, pp. 66–82.

Stepanova, Y. 1996. *Chemical properties and structure of sapropel humic acids.* Doctoral Thesis, MSU, Moscow, 101 pp. (in Russian).

Stumm, W. & Morgan, J.J. 1996. Regulation of the chemical composition of natural waters *Aquatic chemistry: Chemical equilibria and rates in natural waters.* Wiley, New York, pp. 818–867.

Tamaki, H., Sekiguchi, Y., Hanada, S., Nakamura, K., Nomura, N., Matsumura, M. & Kamagata, Y. 2005. Comparative analysis of bacterial diversity in freshwater sediment of a shallow eutrophic lake by molecular and improved cultivation-based techniques. *Applied and Environmental Microbiology* **71**(4), 2162–2169.

Titov, Y. 1950. Pigments of Ural sapropels. *Proceedings of the sapropel deposits laboratory* **4**, 114–119 (in Russian).

Vimba, B. 1956. *Sapropeļa termiskā šķīdināšana un iegūto produktu ķīmiskais raksturojums Thermal dissolution of sapropel and chemical characteristics of derived products.* Doctoral Thesis, Latvian Agriculture Academy, Riga, 170 pp. (in Latvian).

Waller, P. & Temple-Heald, N. 2003. Compost and growing media manufacturing in the UK, opportunities for the use of composted materials. *Compost and growing media supply and demand study.* Banbury: The Old Academy, 52 pp.

Wetzel, R. G. 2001. *Limnology: Lake and river ecosystems,* Academic Press, London, 1006 pp.

Yevdokimova, G., Bukach, O., Tyshkovich, A., Lopatko, M., Dudka, A. & Dubovets, A. 1980. Agrochemical value of sapropel's mineral components. *Science* **4**, 38–42 (in Russian).

Yongoing, Q., Hongkai, L., Zhongmin, S. & Hongyan, Z. 2010. *Moisture-preserving nutritious soil for growing herbaceous flower seedlings and preparation method thereof.* CN patent 101715714.

Yu, Z. & McAndrews, J.H. 1994. Holocene water levels at Rice Lake, Ontario, Canada: sedement, pollen and plant macrofossil evidence. *The Holocene* **4**(2), 141–152.

# Soil physical characteristics and soil-tillage implement draft assessment for different variants of soil amendments

P. Šařec[*] and N. Žemličková

Czech University of Life Sciences Prague, Faculty of Engineering, Department of Machinery Utilization, Kamycka 129, CZ 165 21 Prague 6 – Suchdol, Czech Republic
[*]Correspondence: psarec@tf.czu.cz

**Abstract.** The article discusses the results of measurement of soil physical properties and implement draft that has been done within field trial established at Sloveč in the year 2014. Different variants of treatment with substances for soil (PRP Sol) and manure (PRP Fix) amendment with organic fertilisers of various origins have been examined in terms of their influence on several parameters including energy demand for soil tillage. In the first stage, soil physical properties, i.e. soil bulk density and cone index, were measured. The results indicate that at soil upper layer, cone index of all the trial variants dropped relative to control regardless of the manure origin, manure treatment with PRP Fix, or the application of PRP Sol. Concerning soil bulk density, observed drop in values can be discerned with the application of cattle manure, and with majority of variants using pig manure where there are high dosage rates, but the drop was found also with PRP Sol alone. Subsequently, draft of chosen tillage implements was measured in order to assess potential decrease in energy demand of treated variants. There was almost 3% drop in aggregate unit draft after manure, and soil and manure activators' application compared to the control. The decrease was attained in all variants except three. Two of them were the variants of untreated manure (cattle and poultry origin) application and the third was the variant of poultry manure treated with PRP Fix with additional application of PRP Sol. Here though, the difference was minor only.

**Key words:** draft, activator of organic matter, manure application, soil properties.

## INTRODUCTION

Since 2014, field trials have been carried out in order to verify the influence of application of fermented farmyard manures and substances for soil amendment (activators of organic matter) on the changes of physical, physical-chemical and biological soil characteristics, organic matter fixation, improvement of parameters of infiltration and water retention, decrease of soil erosion risks, and decrease of energy demand for soil tillage.

Soil compaction is one of the soil properties in question. It leads to loss in crop yield, since the compaction prevents plants' root system to penetrate through to deeper soil layers to reach water / nutrients. Soil compaction has also negative impact on the environment (Ball et al., 1999; Chyba et al., 2014) due to the reduced ability of the soil to absorb water. Chyba et al. (2014) verified significantly higher water infiltration rate in the non-compacted soil than in the compacted soil.

Soil compaction primarily affects the physical properties of soil, either in the short or long term. For example at higher soil moisture levels, passes of farm machinery can lead to excessive soil compaction. The results of Vero et al. (2012) indicate that higher soil moisture deficits (SMD) at the time of machinery trafficking resulted in smaller changes to soil characteristics and more rapid recovery from surface deformation than when trafficking occurred at lower SMD. According to the results of Ahmadi & Ghaur (2015), gradual increase in soil water content generally resulted in an increase in soil bulk density after tractor wheeling. The negative effect of soil compaction is manifested through increased bulk density, soil cone index, and other variables. This all leads to reduction in porosity, hydraulic soil properties, stability and other variables (Alakukku, 1996). All these parameters are connected together and influence crop yields. Celik et al. (2010) confirmed organic applications to significantly lower the soil bulk density and penetration resistance.

Effect of the use of substances for soil amendment (activators) on soil properties is a relatively unexplored phenomenon. Impact can be mainly expected on the physical and chemical properties of soil. Kroulík et al. (2011) suggested a beneficial effect of incorporation of organic matter on the physical properties of soil, on water infiltration into the soil and on partial elimination of the consequences of soil compaction beneath the tracks. It can be also assumed that changes in soil properties will be reflected in the long term rather than immediately after application. According to Podhrázská et al. (2012), repeated conventional tillage and application of PRP Sol did not demonstrate any improvement in soil physical properties (density, porosity, soil compaction, reduced water content in soil).

Another factor that influences the variables mentioned is soil structure and soil aeration. If the soil is loosened, water capacity is higher compared to the untilled soil (Ekwue & Harrilal, 2010). Each soil structure has its own typical values of bulk density, porosity, hydraulic characteristics and other variables. For example, sandy-loam soils have higher cumulative infiltration rate than clay-loam soils, the lowest values are observed in turn with clay soils (Ekwue & Harrilal, 2010).

For the evaluation of soil compaction, values of soil density and penetration measurements are commonly used. Penetration measurement is also known as the cone index, i.e. the value of soil resistance against a cone of known dimensions (angle and area). Measurement of cone index has advantages over measurements of density in a simple data acquisition from the entire soil depth (limited by penetrometer depth range), the process of penetration measurements can also be automated (Raper, 2005).

In terms of economy and operation, energy demand of soil tillage is one of the crucial elements. Tillage is the base operation in agricultural systems and its energy consumption represents a considerable portion of the energy consumed in crop production (Larson et al., 1995). McLaughlin et al. (2002), Liang et al. (2013) and Peltre et al. (2015) reported manure amendments to have significant effect on reduction in tillage implement draft. Prolonged application and higher rates brought advanced reduction.

The purpose of this study was to verify any changes in draft required for tillage after several years of treatment with substances for soil amendment and with fermented farmyard manure.

## MATERIALS AND METHODS

In 2014, field trials examining effects of substances for soil amendment and fermented manure were established. In 2014, the measurements were done on 2nd October straightway after the barley harvest. Silage maize was grown in the field afterwards, and the measurements were completed on 1st September 2015 after its harvest. The trial field is located near Sloveč in the Central Bohemia (GPS: N 50°14.256', E 15°20.705', altitude: 273 m). The topography is gently sloping, facing southwest. Soil texture in the field is very heavy and the soil is thus difficult to cultivate. The content of clay particles under 0.01 mm is 62% of weight at the depth from 0 to 0.3 m. Some selected soil properties at the beginning of the experiment are presented in Table 1.

**Table 1.** Selected physical and chemical properties of soil at Sloveč (13th August, 2014)

|  | Soil depth [m] | |
| --- | --- | --- |
|  | 0.00–0.30 | 0.30–0.60 |
| clay (< 0.002 mm) [%] | 48 | 60 |
| silt (0.002–0.05 mm) [%] | 32 | 39 |
| very fine sand (0.05–0.10 mm) [%] | 2 | 1 |
| fine sand (0.10–0.25 mm) [%] | 18 | 0 |
| texture (USDA) | clay | clay |
| bulk density [g cm$^{-3}$] | 1.46 | 1.48 |
| total porosity [%] | 46.15 | 43.99 |
| volumetric moisture [%] | 35.65 | 40.20 |
| humus content [%] | 3.89 | 1.44 |
| pH (H$_2$O) | 7.50 | 7.82 |
| pH (KCl) | 7.18 | 7.21 |
| CEC – cation exchange capacity [mmol kg$^{-1}$] | 278 | 272 |

The trial plot was a 140 meters wide and 630 meters long rectangle selected to be homogenous and to avoid headland. It was divided crosswise into individual 45 wide and 140 meters long variants where fertilizer application was carried out according to a plan. The plots' spatial distribution had to be simple due to an operational nature of the experiment. The fertilizers used were manures from cattle, pig, and poultry, and NPK 15-15-15 (Lovofert). As the soil activator, PRP Sol (PRP Technologies) was applied during stubble cultivation. PRP Sol is formed by a matrix of calcium and magnesium carbonate, and mineral elements. As the activator of biological transformation of manure, PRP Fix (PRP Technologies) was applied directly into bedding. PRP Fix is a granular mixture of mineral salts and carbonates. Both activators should not be regarded as fertilizers. They are supposed to improve conditions for the transformation of organic matter. Fertilization of individual variants is shown in Table 2. The variants differed by fertilizers used. Dosage of cattle manure was 50 t ha$^{-1}$, of pig manure 40 t ha$^{-1}$, of poultry manure 10 t ha$^{-1}$, of PRP Sol 200 kg ha$^{-1}$, and of NPK 200 kg ha$^{-1}$. The field was ploughed afterwards. In spring, seedbed preparation was carried out.

**Table 2.** Fertilization of individual variants of field trial at Sloveč

| Variant | Fertilization |
|---------|---------------|
| I a | cattle manure with FIX + NPK |
| II a | cattle manure with FIX + SOL+ NPK |
| III a | cattle manure+ NPK |
| IV a | cattle manure + SOL+ NPK |
| V a | SOL + NPK |
| VI a | NPK (Control) |
| I b | pig manure with FIX + NPK |
| II b | pig manure with FIX + SOL+ NPK |
| III b | pig manure+ NPK |
| IV b | pig manure + SOL+ NPK |
| I c | poultry manure with FIX + NPK |
| II c | poultry manure with FIX + SOL+ NPK |
| III c | poultry manure+ NPK |
| IV c | poultry manure + SOL+ NPK |

Selected soil physical properties have been measured in the trial fields. Two basic methods were used. Firstly, undisturbed soil samples were taken using Kopecky's cylinders of a volume of 100 cm$^3$. Secondly, cone index measuring method was used. The registered penetrometer PEN 70 developed at the CULS Prague was employed. Moisture was measured by Theta Probe (Delta-T Devices Ltd, UK). The draft of selected soil tillage implements was measured by means of the method of drawbar dynamometer with strain gauges S-38 /200 kN/ (LUKAS, the Czech Republic) between two tractors (see Fig. 1). Data acquisition system NI CompactRIO (National Instruments Corporation, USA) was employed, and its sample rate was set at 0.1 s. Several machinery passes were carried out for each variant. Firstly, the tillage implement was working at a set-up working depth and at a constant speed in order to measure the overall draft of the pulled tractor and implement working. The working depth was verified by its measurement for each pass. Secondly, the measurement was done with implement not working in order to measure the rolling resistance and the force induced by potential field gradient. These were deduced from the overall draft in order to calculate the implement draft. Direction of passes, i.e. downhill and uphill, was therefore taken into account. Trimble Business Center 2.70 (Trimble, USA) was used to assign acquired data to individual trial variants. Data were then processed by the programmes MS Excel (Microsoft Corp., USA) and Statistica 12 (Statsoft Inc.,USA). Finally, the measured draft values were compared to the values calculated using ASAE D497.7 standard (ASABE Standards 2011). This standard uses a simplified draft prediction equation:

$$D = F_i \cdot (A + B \cdot S + C \cdot S^2) \cdot W \cdot T \quad [N] \tag{1}$$

where D is the implement draft force; $F_i$ is a dimensionless soil texture adjustment parameter with different values for fine, medium and coarse textured soils; A, B and C are machine-specific parameters; S is field speed; W is implement width; and T is tillage depth.

**Figure 1.** Photo of draft measurement of chisel plough Strom Terraland TN 3000 at Sloveč in autumn 2014.

## RESULTS AND DISCUSSION

Table 3 shows the overall average values of the basic physical properties of soils. There is a clear difference in volumetric soil moisture between the two years due to exceptionally dry weather over the whole vegetative period of the year 2015. Fig. 2 shows lower precipitation and higher temperatures of the year 2015 compared to the year 2014 during the periods preceding the measurements. This clearly increased the values of cone index which dependants on soil moisture. Illustrative aggregate values at three different depths are presented in the Table 3.

**Table 3.** The overall averages of soil moisture and bulk density, and operating conditions and overall results of measurement of soil tillage implement drafts at Sloveč in autumn of 2014 and 2015

|  | Fall 2014 | Fall 2015 |
|---|---|---|
| Soil properties |  |  |
| vol. moisture at 0.00–0.05 m [%] | 35.16 | 15.24 |
| cone index at 0.08 m [$10^6$ Pa] | 1.124 | 1.186 |
| cone index at 0.12 m [$10^6$ Pa] | 1.326 | 1.850 |
| cone index at 0.16 m [$10^6$ Pa] | 1.571 | 2.500 |
| bulk density at 0.05–0.10 m [g cm$^{-3}$] | 1.763 | 1.547 |
| red. bulk density at 0.05–0.10 m [g cm$^{-3}$] | 1.367 | 1.291 |
| Draft measurement |  |  |
| tractor | NH TG285 | JD 9560 RT |
| engine power [HP] | 285 | 570 |
| implement | chisel plough | tine cultivator |
| implement type | Strom Terraland TN 3000 | Köckerling Vario 480 |
| working width [m] | 3 | 4.8 |
| working depth [m] | 0.117 | 0.080 |
| working speed [km.hour$^{-1}$] | 7.81 | 8.04 |
| overall implement draft [N] | 37 594 | 42 511 |
| ASAE predicted draft [N] | 23 929 | 32 260 |
| unit draft [N m$^{-2}$] | 107 187 | 110 707 |
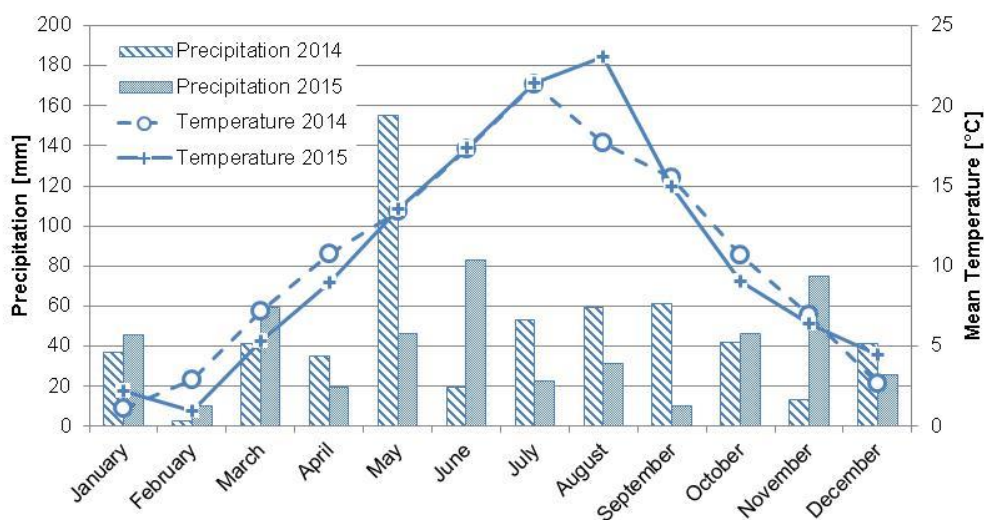
**Figure 2.** Graph of monthly precipitation and mean temperatures at Sloveč in the years 2014 and 2015.

Since the climatic conditions were drastically different in both years, more interesting than the absolute values are the relative differences to the control variant VIa.

Year-on-year changes in relative cone index values at upper soil layer are presented in Fig. 3 and 4. Cone index of all the trial variants dropped relative to control regardless of the manure origin, manure treatment with PRP Fix, or the application of PRP Sol.
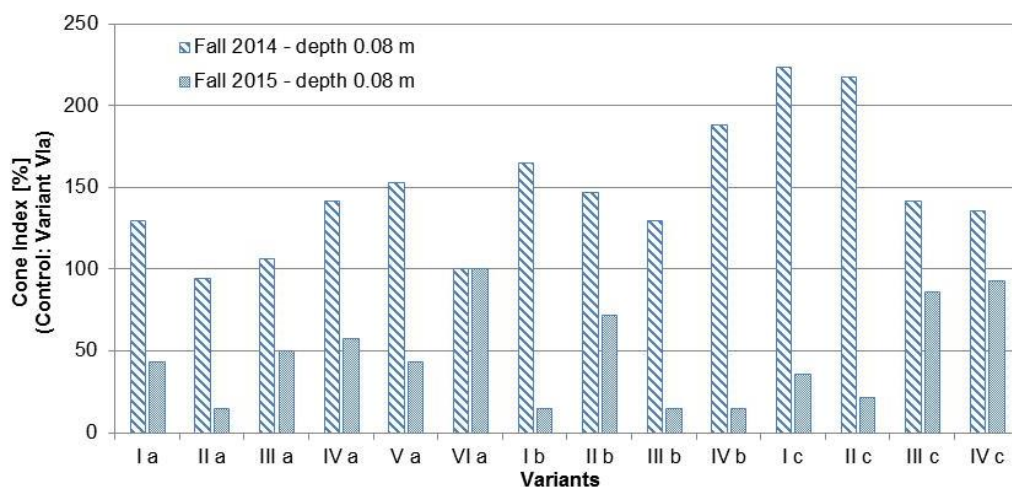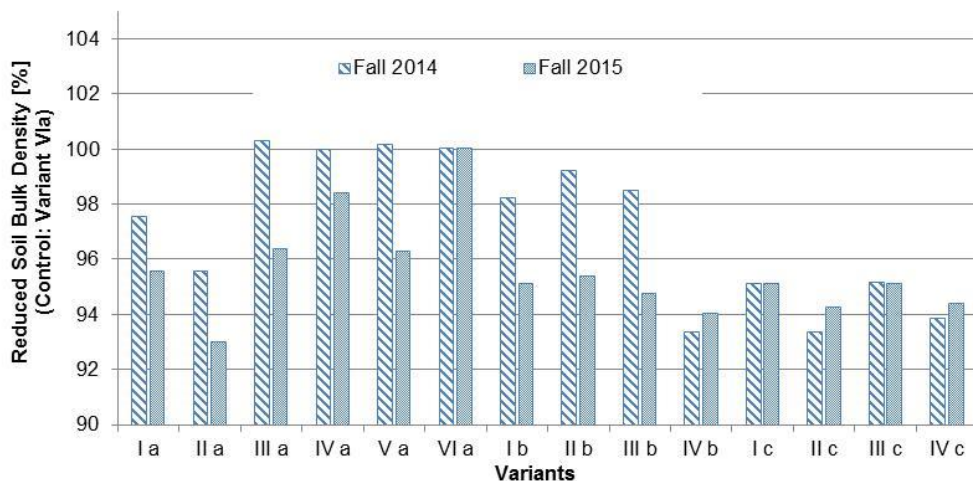


**Figure 3.** Graph comparing relative differences of soil cone index values at the depth of 0.08 m at Sloveč in autumn 2014 and 2015 (Variant VIa – 100%).

953
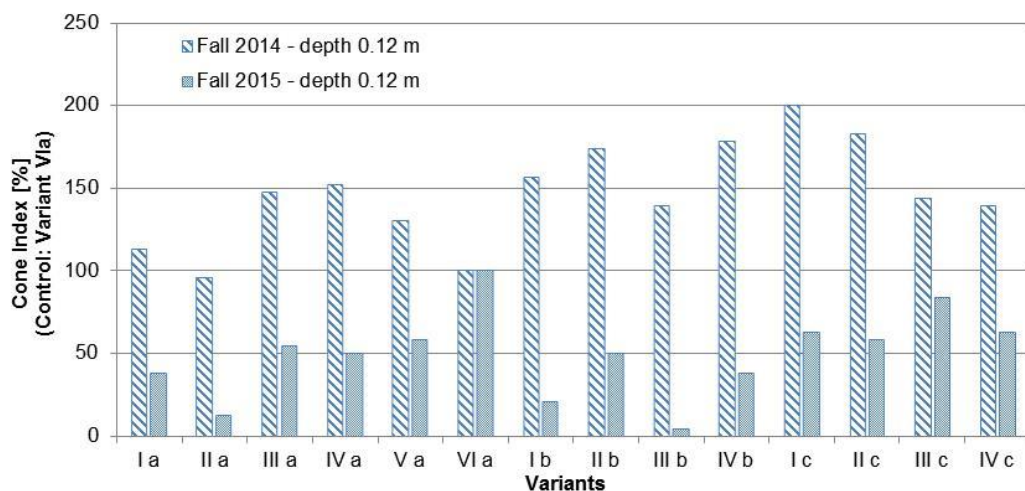
**Figure 4.** Graph comparing relative differences of soil cone index values at the depth of 0.12 m at Sloveč in autumn 2014 and 2015 (Variant VIa – 100%).

On the other hand, overall soil bulk density values decreased, although moderately only. Fig. 5 demonstrates relative comparison to the control variant. A drop can be discerned with the application of cattle manure, and with majority of variants using pig manure. No major differences can be recognized after the application of poultry manure. Bulk density of these variants had been lower than the control even before the manure application. Lower dosage rate of poultry manure could be another reason.



**Figure 5.** Graph comparing relative differences of reduced soil bulk density at Sloveč in autumn 2014 and 2015 (Variant VIa – 100%).

When measuring draft force (Table 3), two different implements were engaged. Both overall implement draft values were rather high and surpassed predictions (ASAE D497.7 MAR2011 standard) by 33% in the case of the chisel plough, and by 24% in the case of the tine cultivator. Very heavy soil at Sloveč probably falls outside the soil texture adjustment parameter range. Nevertheless, the difference still fits within the ±50% range allowed for by the ASAE standard. Overall implement draft was recalculated to unit draft in order to allow for working width and depth of tillage. Values of unit draft of both implements are rather similar.

Fig. 6 presents aggregate unit draft values compared to the control. Due to the different climatic conditions and soil tillage implements used, absolute values cannot be considered. The ratio of individual measured unit draft values to the average value of the control variant is therefore used for evaluation. There is almost 3% drop in unit draft after manure and soil and manure activators. The difference is statistically highly significant (p = 0.000000000661).
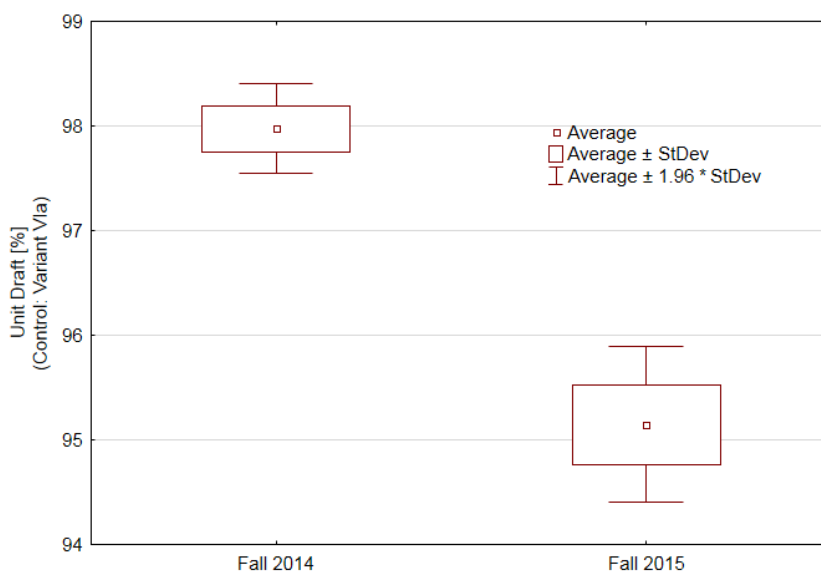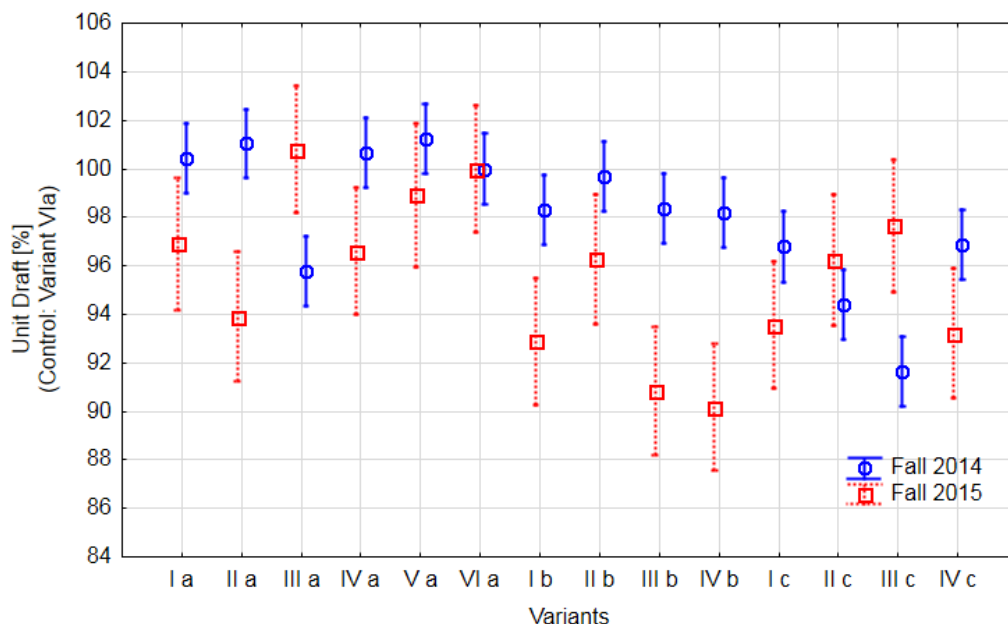


**Figure 6.** Graph comparing relative differences of implement unit draft related to control at Sloveč in autumn 2014 and 2015 (control variant VIa excluded).

When taking into account relative differences of individual variants (Fig. 7), the decrease was attained in all cases except three. Two of them were the variants of untreated manure (cattle and poultry origin) application and the third was the variant of poultry manure treated with PRP Fix, and with additional application of PRP Sol. Here though, the difference was minor only.

Initial research assumptions were mostly confirmed. As Celik et al. (2010) suggested, cone index values decreased largely compared to the control. With higher application rates of manure, soil bulk density decreased as well. This is consistent with Schjønning et al. (1994) who reported that long term without fertiliser application lead to greater soil strength and soil bulk density than manure or inorganic fertilizer

treatments. To date, application of PRP Sol brought improvements as well. Findings of Podhrázská et al. (2012) were thus not confirmed so far.



**Figure 7.** Graph comparing relative differences of implement unit draft with respect to individual variants at Sloveč in autumn 2014 and 2015 (Variant VIa – 100%; vertical lines depict 0.95 confidence intervals).

Conclusions of McLaughlin et al. (2002), Liang et al. (2013) and Peltre et al. (2015) on manure application influence on implement draft reduction are consistent with the trial results. The effects of activators of organic matter are among the less explored topics. In connection with changing composition of organic fertilizer (fewer manure and slurry but more compost and waste from biogas plants), the increased importance of activators of organic matter can be expected. Measurements were certainly affected by a short duration of the experiment. It can be assumed that the effect is going to be gradual and the verification should be carried out also in following trial years, when there will be enough data to carry out thorough statistical analysis.

## CONCLUSIONS

So far, the work has demonstrated the beneficial effect of substances for soil (PRP Sol) and manure amendment (PRP Fix) and of organic fertilisers of various origins on soil bulk density, cone index and on implement draft force reduction. A longer duration of the experiment would though enable to draw more detailed conclusions. At soil upper layer, cone index of all the trial variants dropped relative to control regardless of the manure origin, manure treatment with PRP Fix, or the application of PRP Sol. Concerning soil bulk density, a drop in values can be discerned with the application of cattle manure, and with majority of variants using pig manure where there are high dosage rates, but the drop was found also with PRP Sol alone.

Subsequently, draft of chosen tillage implements was measured. There was almost 3% drop in aggregate unit draft after manure, and soil and manure activators' application compared to the control. The decrease was attained in all variants except three. Two of them were the variants of untreated manure (cattle and poultry origin) application and the third was the variant of poultry manure treated with PRP Fix with additional application of PRP Sol. Here though, the difference was minor only.

The necessity of long-term examination of the effects of activators of organic matter should be emphasized. Research needs to be validated in more locations in order to eliminate the influence of the local environment.

## REFERENCES

Ahmadi, I. & Ghaur, H. 2015. Effects of soil moisture content and tractor wheeling intensity on traffic-induced soil compaction. *Journal of Central European Agriculture* **16**(4), 489–502.

Alakukku, L. 1996. Persistence of soil compaction due to high axle load traffic. I. Short-term effects on the properties of clay and organic soils. *Soil and Tillage Research* **37**, 211–222.

ASABE Standards 2011. ASAE D497.7 MAR2011, *Agricultural Machinery Management Data*. ASABE, St. Joseph, MI, USA.

Ball, B.C., Parker, J.P & Scott, A. 1999. Soil and residue management effects on cropping conditions and nitrous oxide fluxes under controlled traffic in Scotland. *Soil & Tillage Research* **52**, 191–201.

Celik, I, Gunal, H., Budak, M. & Akpinar, C. 2010. Effects of long-term organic and mineral fertilizers on bulk density and penetration resistance in semi-arid Mediterranean soil conditions. *Geoderma* **160**, 236–263.

Chyba, J., Kroulík, M., Krištof, K., Misiewicz, P. & Chaney, K. 2014. Influence of soil compaction by farm machinery and livestock on water infiltration rate on grassland. *Agronomy Research* **12**, 59–64.

Ekwue, E.I. & Harrilal, A. 2010. Effect of soil type, peat, slope, compaction effort and their interactions on infiltration, runoff and raindrop erosion of some Trinidadian soils. *Biosystems Engineering* **105**, 112–118.

Kroulík, M., Kvíz, Z., Kumhála, F., Hůla, J. & Loch, T. 2011. Procedures of soil farming allowing reduction of compaction. *Precision Agriculture* **12**, 317–333.

Larson, D.L. & Clyma, H.E. 1995. Electro-osmosis effectiveness in reducing tillage draft force and energy forces. *Transactions of ASAE* **38**, 1281–1288.

Liang, A., McLaughlin, N.B., Ma, B.L., Gregorich, E.G., Morrison, M.J., Burtt, S.D., Patterson, B.S. & Evenson, L.I. 2013. Changes in mouldboard plough draught and tractor fuel consumption on continuous corn after 18 years of organic and inorganic N amendments. *Energy* **52**, 89–95.

McLaughlin, N.B., Gregorich, E.G., Dwyer, L.M. & Ma, B.L. 2002. Effect of organic and inorganic soil nitrogen amendments on mouldboard plow draft. *Soil & tillage research* **64**, 211–219.

Peltre, C., Nyord, T., Bruun, S., Jensen, L.S. & Magid, J. 2015. Repeated soil application of organic waste amendments reduces draught force and fuel consumption for soil tillage. *Agriculture, Ecosystems and Environment* **211**, 94–101.

Podhrázská, J., Konečná, J., Kameníčková, I. & Dumbrovský, M. 2012. Survey of the impact of PRP SOL subsidiary substance on the hydrophysical properties of soil at cultivation of sugar beet. *Listy cukrovarnické a řepařské* **128**, 128–133.

Raper, R.L. 2005. Agricultural traffic impacts on soil. *Journal of Terramechanics* **42**, 259–280.

Schjønning, P., Christensen, B.T. & Carstensen, B. 1994. Physical and chemical-properties of a sandy loam receiving animal manure, mineral fertilizer or No fertilizer for 90 years. *European Journal of Soil Science* **45**, 257–268.

Vero, S.E., Antille, D.L., Lalor, S.T.J. & Holden, N.M. 2012. The effect of soil moisture deficit on the susceptibility of soil to compaction as a result of vehicle traffic. In: *American Society of Agricultural and Biological Engineers Annual International Meeting 2012*. Dallas, TX, United States, ASABE 7, 5419–5434.

# Mapping of some soil properties due to precision irrigation in agriculture

K.E. Temizel

University of Ondokuz Mayıs, Faculty of Agriculture, Department of Agricultural Structures and Irrigation, Samsun, Turkey; e-mail: ersint@omu.edu.tr

**Abstract.** Precision Agriculture (PA) is a whole-farm management approach using information technology, satellite positioning (GNSS) data, remote sensing and proximal data gathering. These technologies have the goal of optimizing returns on inputs whilst potentially reducing environmental impacts. This study was conducted out to determine the acidity, salinity, field capacity, permanent wilting point and water holding capacity in precision agriculture by analyzing soil samples taken from the field in 32 points. Maps were drawn by obtaining data from the field. The purpose of this research is to use the geographic information system for comparing the obtained data from soil more quickly and easily than before and also the water amount in order to make precise decisions for agriculture progress and applying the appropriate inputs which is related to water. The present results also indicated that water holding capacity maps. These maps are usage for the irrigation management and the information from different points of the field. These data obtained the field has an important role in the management of precision agriculture.

**Key words:** Precision Agriculture, Precision Irrigation, Field capacity, Wilting point.

## INTRODUCTION

Precision agriculture has mostly emphasized variable-rate nutrients, seeding, and pesticide application, but at several research sites, variable-rate irrigation equipment has been developed to explore the potential for managing irrigation spatially. One goal of precision agriculture is to apply only the optimum amount of an input. While conditions could exist for which the entire field's optimum input is greater than the amount usually applied in a conventional, whole-field mode, most participants expect a reduction in input use on at least parts of fields, if not a reduction in the value aggregated over entire fields (Sadler et al., 2005).

Its meaning in the irrigation industry connotes a precise amount of water applied at the correct time, but uniformly across the field (Evans et al., 2000).

While giving more water than necessary to the field increases leaked water or runoff, giving less water than calculated is defined as deficit irrigation. Both condition is wrong fort the right irrigation. Runoff leaving the field represents waste of water. Either way, the field is also subject to sediment and nutrients moving with the runoff. Precision irrigation, an existing aspect of precision agriculture just beginning to be explored, means applying water in the right place with the right amount. The use of precision agriculture for irrigation water management is still in the development stage and requires a lot of investigation and experimental work to determine its feasibility and

applicability (Al-Karadsheh et al., 2001). The last issue of the operation phase of Precision agriculture is variable rate application technology which finds maximum application widely used in Fertilizers, pesticides, irrigation and tillage practices variable rate application technology (Güler & Kara, 2005). A study was conducted to present the benefits and advantages brought by combined use of Factor Analysis and GIS in planning and management of precision agriculture implementations. Precision agriculture represents the approaches allowing the implementation of environment-friendly methods and techniques in agricultural production activities. Parallel to developments in global positioning systems (GPS), farmers have started to be aware of the advantages brought by the implementations carried out in agriculture through considering the spatial differences (Temizel et al., 2015).

A study in Nitra in Slovak Republic, about the effects of precision agriculture was investigated. As compared to conventional water application, precision irrigation contributed to water saving in the amount of 478.56 $m^3$ $ha^{-1}$. The electric power saving reached 249.68 kWh.$ha^{-1}$. The cost saving was characterized by the value of 9.1 EUR $ha^{-1}$ and this represented 23.8%. The results have shown that precision irrigation is a fully effective system of precision farming (Jobbágy et al., 2011).

Precision irrigation as an aspect of precision agriculture, is a relatively new concept in irrigation farming worldwide (Temizel & Koç, 2015). It involves the application of irrigation water in optimum quantities over an area of land which are not uniform and has variations in soil type, soil water capacity, potential yield and topography. Precision irrigation provides a sustainable agricultural system which uses resources efficiently and develops and maintains the actual water demands (Temizel et al., 2014). Precision agriculture is a knowledge-based technical management system which should optimise farm profit and minimise the impact of agriculture on the environment (Dennis & Nell, 2002).

This study aims to show how to save a limited amount of available water through precision agriculture.

## MATERIALS AND METHODS

**Material**
**Land and Climate Policy**
This study was carried out in Samsun 19 May University, Faculty of Agriculture experiment area. Workspace is approximately 5.5 hectares. Samsun prevails 'type of humid temperate climate'. February is the lowest monthly average temperature month as 6.6 °C and the warmest month is August as 23 °C. Average annual rainfall of 721.4 mm; most rainy month is October (86.1) and the least rainy months of July (30.4) (Bahadır, 2013) The position of the field under investigation is shown in Fig. 1, with the surface area of 5.5 ha and with 33 monitoring points.
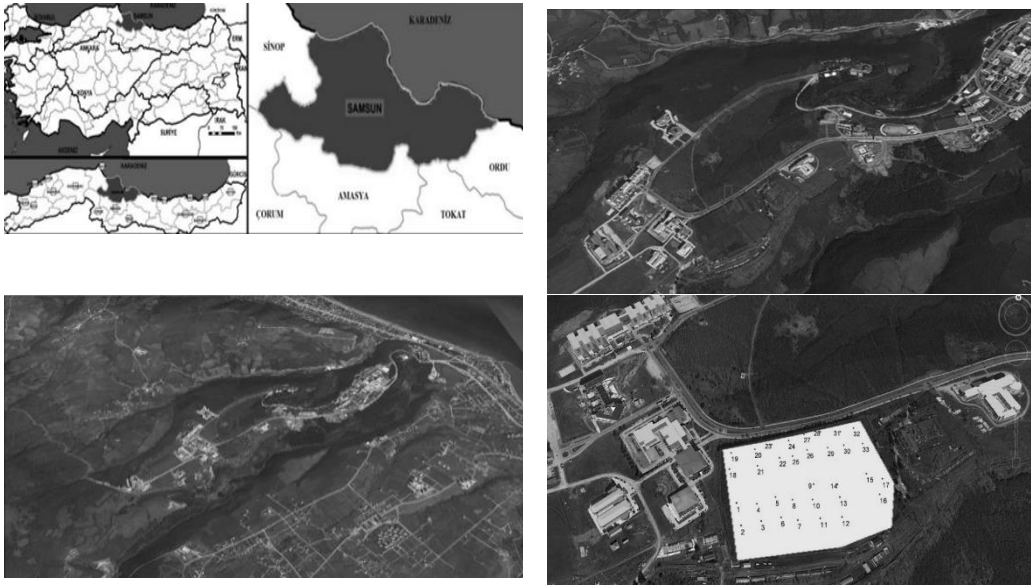
**Figure 1.** Study area and monitoring points.

### Tools and equipment of the study

In this study, GPS, soil auger, test sieves, precision scales, EC and pH meters, pressure vessels and the oven are used for obtaining the necessary data (Fig. 2).



**Figure 2.** The tools and equipments used in the experiment.

**Method**
**Analysis of Soil samples**
With new advances in agriculture and the availability of global positioning satellites, it is now possible to divide a field into smaller units or grid cells that can be sampled individually. Soil test results from each grid can be used to prepare various maps of fields (Thom et al., 2003). pH analysis was performed in soil samples with pH meter. The choice of a proper method to measure pH in soils is a contentious issue (Anon, 2015). In this study pH is measured with pH meter. EC meter values in soil samples were measured with EC meter according to (Rhoadesa, 1990). Field capacity and Permanent wilting point values are mesured pressure plate apparatus, and water holding capacity is found subtracting from each ohter (Günay & Ul, 2001; Temizel & Apan, 2010).

**Drawing Maps**
Geographic information systems are used in the preparation of the spatial distribution of the data obtained from the field specific point. In order to determine the spatial distribution of the soil properties in the study area were utilized widely used geographic information system . For this purpose map ArcGIS 9.3 software has been chosen for each parameter of ordinary Kriging method (Arslan, 2012; Arslan, 2014).

## RESULTS AND DISCUSSION

Soil samples were randomly taken from 33 different location points to depts of 30 cm. Table 1 shows several descriptive statistical parameters belong to general results such as EC, pH, Field capacity (Pw FC), Permanent wilting point (Pw WP), bulk density ($\gamma_t$), and Water holding capacity (WHC) of the trial area.

**Table 1.** Descriptive statistics for studied soil properties

|          | EC(micromhos cm$^{-1}$) | ph   | Pw FC | Pw WP | $\gamma_t$ | WHC (mm) |
|----------|--------------------------|------|-------|-------|------------|----------|
| Max      | 1813.00                  | 8.27 | 0.59  | 0.39  | 1.46       | 61.58    |
| Min      | 832.00                   | 6.88 | 0.35  | 0.20  | 1.30       | 52.74    |
| Mean     | 1278.52                  | 7.56 | 0.47  | 0.31  | 1.38       | 57.54    |
| Std.dev. | 244.981                  | 0.330| 0.051 | 0.039 | 0.048      | 2.639    |
| CV       | 19.2                     | 4.4  | 10.8  | 12.4  | 3.4        | 4.6      |

**pH Mapping**
The pH values ranged between 6.88 and 8.27 (Ave. 7.56). The resulting map of the pH is shown in Fig. 3.

Across the land can be seen from Fig. 3, it is seen that pH values between 7.50 to 7.80. pH values between 7.10 and 6.88 on the map are equal to approximately 0.8% (0.45 da) of all areas of the field. The Area between 7.10 and 7.50 pH values, which is equal to 36.2% (19.90da) of the entire area. Areas having a pH between 7.50 and 7.80 is equal to 57% (31.60 da) of the entire area. Rest area having between 7.80 and 8.27 pH value is equal to 6% (3.44 da) of all areas with pH. It is explicit that every point in map has different pH value.

## EC (salinity) Mapping

EC map was plotted by obtaining the data from the field. EC values ranged between 0.832 and 1.813 dS m$^{-1}$ (ave.1.278). EC map shown in Fig. 4 was drawn taking into account the EC data for the study area.
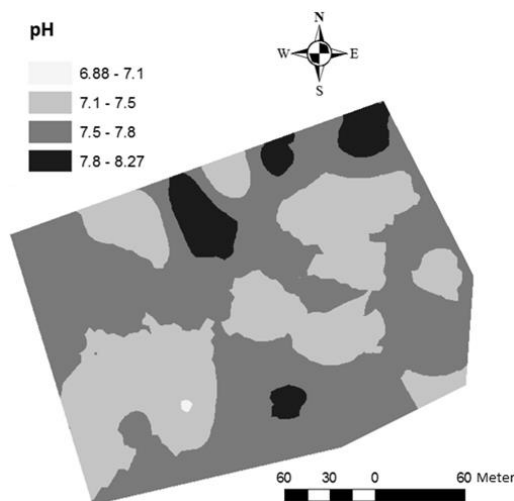


**Figure 3.** PH maps relating to field.
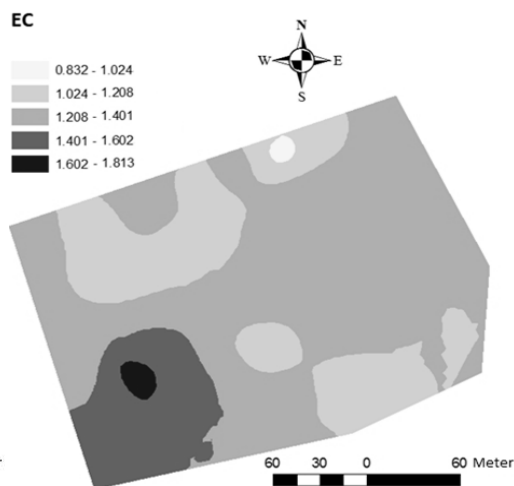


**Figure 4.** EC map for the area.

As seen in Fig. 4, EC values are shown in four parts. EC values classified between 0.832 and 1.024, 1.024 and 1.208, 1.208 and 1.401, 1.401 and 1.602, and 1.602 and 1.813. Their area ratios are 0.4% (0.23da), 26% (13.74 da), 60% (33.48da), 12.8% (7.09da) and 0.8% (0.45da) respectively.

## Soil Bulk Density

Soil bulk density ($\gamma_t$) obtained from the soil samples taking the field were plotted shown in Fig. 5.

As seen in Fig. 5, soil density values are ranged 1.30 and 1.46 g cm$^{-3}$. The area has different soil bulk density. This condition should be taken into account during irrigation.
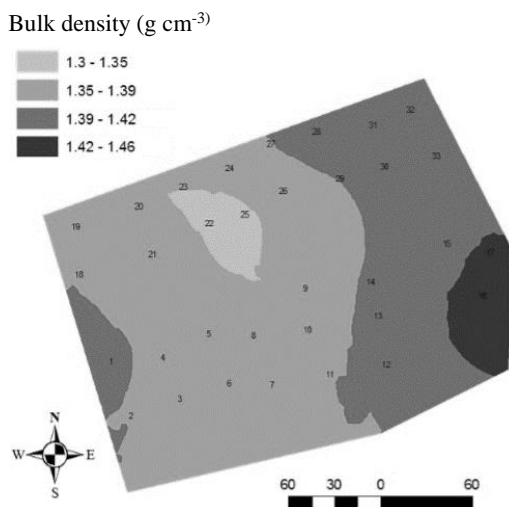


**Figure 5.** Soil bulk density map.

## Field Capacity and Permanent Wilting Point Mapping

The field capacity ranged between 28.12% and 41.56% (Ave. 34.8%) by weight, and the wilting point was in the interval between 16.08% and 25.78% (Ave. 20.9) by weight. The resulting map of the field capacity (FC) and Permanent wilting point are shown in Fig. 6.

As seen in Fig. 6 these values classified in to four group in maps. Their range threshold for FC are 28.12, 32, 35, 37, 41.56 respectively and for the PWP are 16.08, 18, 20, 22, 25.78% by weight respectively. This shows every point in area need different inputs.
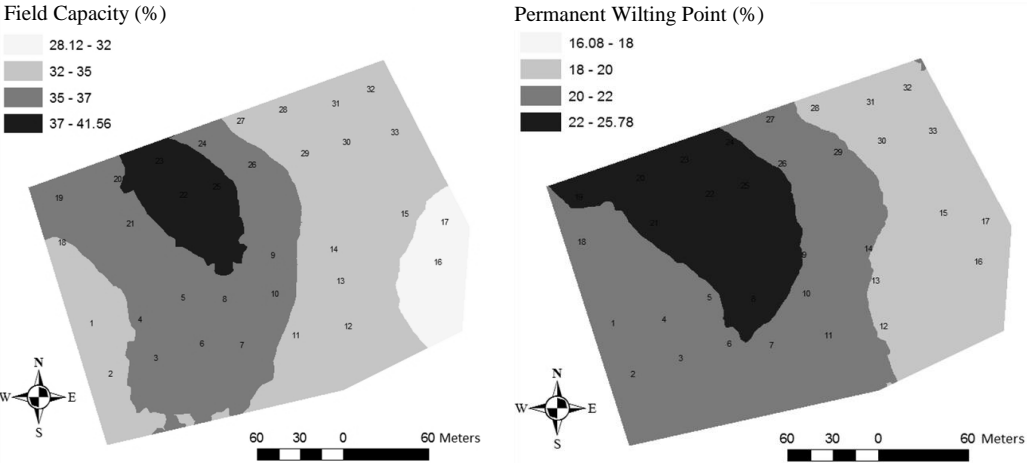


**Figure 6.** Field capacity (FC) and Permanent wilting point (PWP) maps.
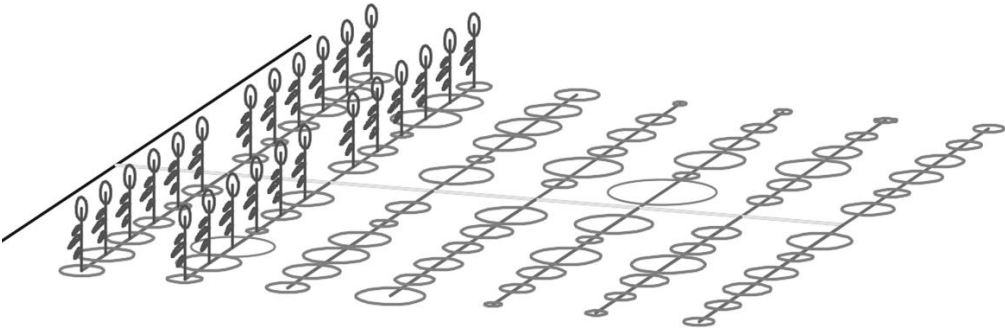
## Water Holding Capacity Map

Water holding capacity (WHC) is between field capacity and wilting point. Therefore, water holding capacities are found by subtracting from field capacity to wilting point. Water holding capacities for the field were plotted spatially shown in Fig. 7.

As seen in Fig. 7, Water holding capacities belog to field were classified four group. These groups are between 52–55, 55–57, 57–59, 59–61 mm respectively. It is obvious that most point in area have different value of water holding capacity.
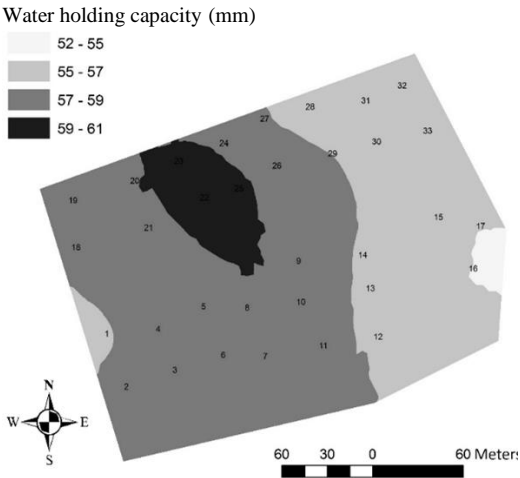


**Figure 7.** Water holding capacity map.

Drippers flow can be adjusted by on-line emitters for the precision irrigation due to get good distribution uniformity. This condition can be seen in Fig. 8.



**Figure 8.** Aspects of different flow of emitters according to water holding capacity.

In drip irrigation Management Allowable Depletion (MAD) can be chosen as about 30% of the water holding capacity (Orta, 2007). When irrigation time is 3.75 h and MAD is 30%, plotted map for the emitter flow (L h⁻¹) shown in Fig. 9.

As seen in Fig. 9, every point in the field have different properties according to irrigation. Therefore, farmers should adjust the dripper flow on emitters respect to the map of precission irrigation.
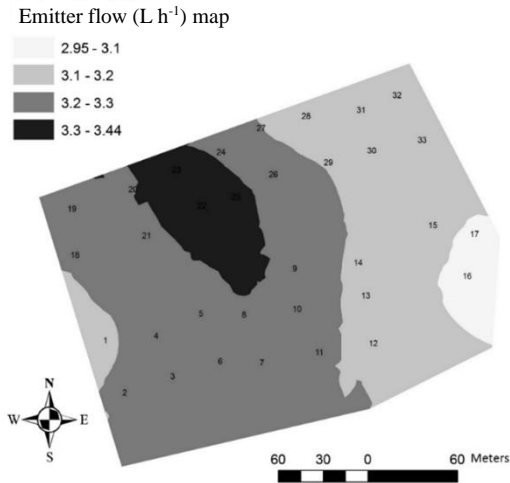


**Figure 9.** Emitter flow map.

## CONCLUSIONS

Precision irrigation used soil parameters for irrigation need some parameters as pH, EC, $\gamma_t$, FC, PWP, WHC. One of the aim of precision farming is to send inputs to the points as they need, not too much and not too less. Precision irrigation supply required emitter flow with calculating its value. Conventional irrigation even use drip irrigation, farmers needn't chose emitter flow because of unknowing properties of parameters for irrigation together. While some region of the study area need more water, other side need less water than average. If the farmers use standard flow for the emitters, some region having high water holding capacity gets 18,563 L less water than average. Likewise, some region having low water holding capacity gets 18,563 L more water than its hold.

It means runoff or deep percolation can be seen on the surface resulting erosion. In other words, some region has low water holding capacity, some region has high water holding capacity. If the user irrigate the field according to water holding capacity, user have to decide only one water depth that may higher or lower than mean. This problem can be solve with precision irrigation.

## REFERENCES

Al-Karadsheh, E., Sourell, H. & Krause, R. 2001. Precision Irrigation: New strategy irrigation water management. Witzenhausen, October 9–11, Conference on International Agricultural Research for Development.

Anon. 2015. Test Method for the Determination of pH Value Of Water or Soil by pH meter.

Available at: https://www.dot.ny.gov/divisions/engineering/technical-services/technical-services-repository/GTM-24b.pdf

Arslan, H. 2012. Spatial and temporal mapping of groundwater salinity using ordinary kriging and indicator kriging: The case of Bafra Plain, Turkey. *Agricultural Water Management, Cilt* **113**, 57–63.

Arslan, H. 2014. Spatial and Temporal Distribution of Areas with Drainage Problems as Estimated by Different Interpolation Techniques. *Water and Environmental Journal* **28**(2), 6.

Bahadır, M. 2013. Samsun İli İklim Özelliklerinin Enterpolasyon Teknikleri ile Analizi. *Journal of Anatolian Natural Sciences* **4**(1), 28–46.

Dennis, H.J. & Nell, W.T. 2002. Precision Irrigation in South Africa. Wageningen, The Netherlands., 13th International Farm Management Congress, July 7–12.

Evans, R. 2000. Controls for precision irrigation with self-propelled systems. Proceedings of the 4th Decennial National Irrigation Symposium, American Society of Agricultural Engineers, St. Joseph, Michigan., pp. 322–331.

Güler, M. & Kara, T. 2005. Hassas Uygulamali Tarim Teknolojisine Genel Bir bakiş. *J. of Fac. of Agric. OMU* **20**(3), 110–117.

Günay, A. & Ul, M. 2001. Irrigation of greenhouses. Ege Üniv. İzmir.

Jobbágy, J., Simoník, J. & Findura, P., 2011. Evaluation of efficiency of precision irrigation for potatoes. *Res. Agr. Eng.* **57**(Special Issue), 14–S23.

Orta, H., 2007. Peyzaj Alanlarında Sulama. Tekirdağ: yazarı bilinmiyor

Rhoadesa, J.D. 1990. Determining soil salinity from measurements of electrical conductivity. *Communications in Soil Science and Plant Analysis* **13–16**(Volume 21, Issue 13–16), 1887–1926.

Sadler, E., Evans, R., Stone, K. & Camp, C. 2005. Opportunities for conservation with precision irrigation. *Journal of Soil and Water Conservation* **60**(6), 371–379.

Temizel, K.E. & Apan, M. 2010. Determining the Appropriate Furrow Length in Bafra Plain Land Conditions. *Anadolu J. Agric. Sci.* **25**(2), 84–88.

Temizel, K.E., Arslan, H. & Sağlam, M. 2015. Applications of Factor Analysis and Geographical Informatıon Systems for Precision Agriculture Over Alluvial Lands. Fresenius *Environmental Bulletin* **24**(7), 2374–2383.

Temizel, K.E., Arslan, H. & Koç, Y. 2014. The effects of soil water holding capacity on the water usage with geostatistical mapping methods. 12. Ulusal Kültürteknik Sempozyumu. Tekirdağ

Temizel, K. & Koç, Y. 2015. Benefits of geographic information system in precision agriculture: The case of. *Anadolu J. Agr. Sci.* **30**(2), 130–135.

Thom, W., Schwab, G., Murdock, L. & Sikora, F. 2003. Taking Soil Test Samples. [Çevrimiçi]

Available at: http://www2.ca.uky.edu/agc/pubs/agr/agr16/agr16.pdf [Erişildi: 11 01 2016].

**INSTRUCTIONS TO AUTHORS**

Papers must be in English (British spelling). English will be revised by a proofreader, but authors are strongly urged to have their manuscripts reviewed linguistically prior to submission. Contributions should be sent electronically. Papers are considered by referees before acceptance. The manuscript should follow the instructions below.

**Structure:** Title, Authors (initials & surname; an asterisk indicates the corresponding author), Authors' affiliation with postal address (each on a separate line) and e-mail of the corresponding author, Abstract (up to 250 words), Key words (not repeating words in the title), Introduction, Materials and methods, Results and discussion, Conclusions, Acknowledgements (optional), References.

**Layout, page size and font**
- Use preferably the latest version of **Microsoft Word**, doc., docx. format.
- Set page size to **B5 Envelope or ISO B5 (17.6 x 25 cm)**, all margins at 2 cm.
- Use single line spacing and justify the text. Do not use page numbering. Use indent 0.8 cm (do not use tab or spaces instead).
- Use font Times New Roman, point size for the title of article **14 (Bold)**, author's names 12, core text 11; Abstract, Key words, Acknowledgements, References, tables and figure captions 10.
- Use *italics* for Latin biological names, mathematical variables and statistical terms.
- Use single ('…') instead of double quotation marks ("…").

**Tables**
- All tables must be referred to in the text (Table 1; Tables 1, 3; Tables 2–3).
- Use font Times New Roman, regular, 10 pt. Insert tables by Word's 'Insert' menu.
- Do not use vertical lines as dividers; only horizontal lines (1/2 pt) are allowed. Primary column and row headings should start with an initial capital.

**Figures**
- All figures must be referred to in the text (Fig. 1; Fig. 1 A; Figs 1, 3; Figs 1–3). Use only black and white or greyscale for figures. Avoid 3D charts, background shading, gridlines and excessive symbols. Use font **Arial** within the figures. Make sure that thickness of the lines is greater than 0.3 pt.
- Do not put caption in the frame of the figure.
- The preferred graphic format is EPS; for half-tones please use TIFF. MS Office files are also acceptable. Please include these files in your submission.
- Check and double-check spelling in figures and graphs. Proof-readers may not be able to change mistakes in a different program.

**References**

- **Within the text**

In case of two authors, use '&', if more than two authors, provide first author 'et al.':
    Smith & Jones (1996); (Smith & Jones, 1996);
    Brown et al. (1997); (Brown et al., 1997)

When referring to more than one publication, arrange them by following keys: 1. year of publication (ascending), 2. alphabetical order for the same year of publication:

(Smith & Jones, 1996; Brown et al., 1997; Adams, 1998; Smith, 1998)

- **For whole books**

Name(s) and initials of the author(s). Year of publication. *Title of the book* (*in italics*). Publisher, place of publication, number of pages.

Shiyatov, S.G. 1986. *Dendrochronology of the upper timberline in the Urals*. Nauka, Moscow, 350 pp. (in Russian).

- **For articles in a journal**

Name(s) and initials of the author(s). Year of publication. Title of the article. *Abbreviated journal title* (*in italic*) volume (in bold), page numbers.

Titles of papers published in languages other than English, German, French, Italian, Spanish, and Portuguese should be replaced by an English translation, with an explanatory note at the end, e.g., (in Russian, English abstr.).

Karube, I. & Tamiyra, M.Y. 1987. Biosensors for environmental control. *Pure Appl. Chem.* **59**, 545–554.

Frey, R. 1958. Zur Kenntnis der Diptera brachycera p.p. der Kapverdischen Inseln. *Commentat.Biol.* **18**(4), 1–61.

Danielyan, S.G. & Nabaldiyan, K.M. 1971. The causal agents of meloids in bees. *Veterinariya* **8**, 64–65 (in Russian).

- **For articles in collections:**

Name(s) and initials of the author(s). Year of publication. Title of the article. Name(s) and initials of the editor(s) (preceded by In:) *Title of the collection (in italics)*, publisher, place of publication, page numbers.

Yurtsev, B.A., Tolmachev, A.I. & Rebristaya, O.V. 1978. The floristic delimitation and subdivisions of the Arctic. In: Yurtsev, B. A. (ed.) *The Arctic Floristic Region*. Nauka, Leningrad, pp. 9–104 (in Russian).

- **For conference proceedings:**

Name(s) and initials of the author(s). Year of publication. Name(s) and initials of the editor(s) (preceded by In:) *Proceedings name (in italics)*, publisher, place of publishing, page numbers.

Ritchie, M.E. & Olff, H. 1999. Herbivore diversity and plant dynamics: compensatory and additive effects. In: Olff, H., Brown, V.K. & Drent R.H. (eds) *Herbivores between plants and predators. Proc. Int. Conf. The 38<sup>th</sup> Symposium of the British Ecological Society*, Blackwell Science, Oxford, UK, pp. 175–204.

.....................................................................................................………

**Please note**

- Use '.' ( not ',') for decimal point: $0.6 \pm 0.2$; Use ',' for thousands – 1,230.4;
- Use '–' (not '-') and without space: pp. 27–36, 1998–2000, 4–6 min, 3–5 kg
- With spaces: 5 h, 5 kg, 5 m, 5°C, C : D = $0.6 \pm 0.2$; $p < 0.001$
- Without space: 55°, 5% (not 55 °, 5 %)
- Use 'kg ha$^{-1}$' (not 'kg/ha');
- Use degree sign ' ° ' : 5 °C (not 5 $^{O}$ C).